CZECH TECHNICAL
UNIVERSITY
IN PRAGUE

FACULTY OF CIVIL
ENGINEERING

HABILITATION THESIS

2025

DANA
KOŇÁKOVÁ

FACULTY OF CIVIL
ENGINEERING
CTU IN PRAGUE

Prague 2025

Calcium Aluminate Cement-Based Composites and Their Future Perspective

HABILITATION THESIS

Collection of selected research papers

Branch: Theory of Building Structures and Materials (NAU-157/2022-8)

DECLARATION and ACKNOWLEDGEMENT

Applicant name: Ing. Dana Koňáková, Ph.D.

Title of the habilitation thesis: Calcium Aluminate Cement-Based Composites and Their Future Prospects

I hereby declare that I am the author of this habilitation thesis, which has been prepared as a collection of scientific papers. I confirm that I made a significant contribution to the conception, experimental work, analysis, and/or interpretation of results in each of these papers, and that the thesis as a whole represents the outcome of my own research activities.

I would like to express my sincere gratitude to my mentor and great friend, prof. Ing. Eva Vejmelková, Ph.D., for her continuous support since the beginning of my studies, for her help, kindness and motivation. I would also like to thank my colleagues, especially prof. Martin Keppert, Ph.D. and Ing. Vojtěch Pommer, Ph.D., for their advice, assistance, helpfulness and confidence. Without these great people, this thesis would hardly have been possible.

My sincere thanks also go to my husband, my sons and my whole family and friends for all the patience and understanding during my studies, my work and my life. Last but not least, I would like to dedicate this thesis to my father to express my deepest gratitude for the encouragement and strength that had guided me throughout my life.

In Prague on .....

.....
signature

Abstrakt:

Tato habilitační práce představuje ucelenou studii kompozitů na bázi hlinitanového cementu (CAC) se zaměřením na jeho hydrataci, vývoj mikrostruktury, tepelné vlastnosti a udržitelnost. CAC je známý svou výjimečnou chemickou odolností, rychlým nárůstem pevnosti a vynikající stabilitou při vystavení vysokým teplotám, což z něj činí vhodnou alternativu portlandského cementu pro extrémní podmínky. Jeho širší použití však bylo historicky omezeno obavami souvisejícími s fázovou přeměnou způsobující výraznou ztrátu pevnosti. Výzkum shrnuje několik let experimentálního výzkumu systémů CAC vylepšených reaktivními příměsemi (SCM) a vláknovou výztuží. Pokud jde o SCM, byla zkoumána široká škála materiálů, přičemž jako nejperspektivnější alternativy se jevily kalcinovaná břidlice a odpadní cihelný prach. V kombinaci s přísadami bohatými na oxid hlinitý byly navržené ternární pojivové systémy, které prokázaly synergické účinky jak při vlastní hydrataci, tak z pohledu zhutnění mikrostruktury a dlouhodobé trvanlivosti, přičemž umožnily významné snížení obsahu slínku, a tím zmírnění dopadu na životní prostředí. Co se týče vláknové výztuže, čedičová a hlinitokřemičitanová vlákna byla vyhodnocena jako vhodná alternativa, neboť nabízejí rovnováhu mezi mechanickými vlastnostmi, tepelnou odolností a kompatibilitou s matricí CAC. Jejich přidání zlepšilo odolnost vůči tepelnému zatížení, omezilo šíření trhlin a přispělo k mechanické stabilitě i po vystavení teplotám přesahujícím 1000 °C. Dosažené výsledky prokazují, že kompozity na bázi CAC jsou při optimálním složení schopny splňovat požadavky na užitné vlastnosti i udržitelnost v konstrukčních a žáruvzdorných aplikacích.

Klíčová slova: *Hlinitanový cement, vláknová výztuž, reaktivní příměsi, tepelná odolnost*

Abstract:

This habilitation thesis presents a comprehensive study on calcium aluminate cement (CAC)-based composites, with a focus on their hydration, microstructural development, thermal performance, and environmental sustainability. CAC is known for its exceptional chemical resistance, rapid strength gain, and superior high-temperature stability, making it a viable alternative to Portland cement in demanding environments. However, its broader application has been historically limited by concerns related to long-term phase conversion and associated strength loss. The research consolidates several years of experimental investigations into CAC systems enhanced by supplementary cementitious materials (SCMs) and fibre reinforcement. Concerning SCMs, a wide range of materials has been examined, with calcined shale and waste ceramic powder emerging as the most promising alternatives. When combined with alumina-rich admixtures in ternary binder systems, these materials demonstrated synergistic effects on hydration reactions, microstructural densification, and long-term durability, while enabling significant clinker reduction and environmental impact mitigation. Regarding fibre reinforcement, basalt and aluminium silicate fibres have been identified as particularly effective, offering a balance between mechanical enhancement, thermal resistance, and chemical compatibility with the CAC matrix. Their inclusion improved resistance to thermal loading, limited crack propagation, and contributed to mechanical stability even after exposure to temperatures exceeding 1000 °C. Altogether, the thesis confirms that CAC-based composites, with optimally formulated composition, are capable of meeting both performance and sustainability demands in structural and refractory applications.

Keywords*: Calcium aluminate cement, fibre reinforcement, supplementary cementitious materials, thermal resistance*

Content

1 Introduction

Cementitious materials belong among the most widely used construction materials worldwide, with Portland cement (PC) having a dominant role in the building industry. However, in applications requiring enhanced chemical resistance, fast setting times, or superior performance under extreme temperatures, alternative binders are needed. One such alternative is calcium aluminate cement (CAC), whose distinct mineralogical composition and hydration mechanisms provide properties unattainable by conventional cements.

The historical development of CAC dates back to the early 20th century, initially driven by the need for rapid-setting, sulphate-resistant binders suitable for harsh environments such as marine structures and sewer systems. Despite its advantages, the early widespread use of CAC was curtailed by concerns about the long-term stability of its hydration products. Particularly, the issue of mineralogical conversion leading to the strength loss over time. This challenge led to a global reassessment of CAC's use in structural applications, restricting its employment primarily to non-load-bearing components and refractory environments.

In recent decades, renewed interest in CAC has emerged, driven by advances in material characterisation and a deeper understanding of its hydration chemistry. Modern CAC formulations offer enhanced durability, thermal resistance, and mechanical stability, making them attractive candidates for high-performance composites in extreme service conditions. From an environmental perspective, CAC-based systems offer several advantages. They can be produced with lower limestone content, reducing carbon emissions from calcination. Their superior performance in aggressive environments and at elevated temperatures also extends the service life of structures, contributing to lower maintenance demands and resource consumption over time.

1.1 Motivation and main aim of the thesis

The motivation behind this thesis arises not only from the need for durable and high-performance materials for extreme environments but also from the imperative to develop environmentally responsible construction composites. Calcium aluminate cement composites, particularly when enhanced with recycled or industrial by-products, present an opportunity to balance performance with sustainability.

The primary goal of this work is to advance the understanding of CAC-based composites, examining their hydration chemistry, mechanical performance, and high-temperature behaviour. Special emphasis is placed on the use of appropriate fibre reinforcement and supplementary cementitious materials (SCMs) to optimise the microstructure, durability, and environmental footprint. The thesis consolidates several years of experimental research, offering both scientific insights and practical formulations for industrial applications.

The thesis aims to contribute to the development of sustainable composites, supporting the transition towards low-carbon, resource-efficient building practices and, of course, enhanced functional properties. These qualities make CAC-based systems an excellent choice for demanding structural and refractory applications, where conventional cementitious materials fall short.

1.2 Structure of the habilitation thesis

The thesis is structured as a collection of research studies framed by a comprehensive contextual introduction. It begins with an overview of the production processes, chemical composition, and hydration mechanisms of calcium aluminate cements, followed by an exploration of their essential material characteristics and practical performance benefits.

Subsequent chapters present detailed investigations along three distinct research areas concerning CAC composites. The first section focuses on the use of chemical additives, with particular emphasis on the selection and suitability of plasticisers. The second research area examines the incorporation of supplementary cementitious materials, with special attention given to their ability to enhance composite performance while significantly reducing environmental impacts by replacing up to 60% of the CAC clinker content. The final section addresses the role of fibre reinforcement in enhancing thermal resistance, aiming to improve both mechanical performance and durability of CAC-based composites.

2 Calcium aluminate cement

The first investigation dealing with calcium aluminates dates back to the 1850s when Louis Vicat and Jacques-Joseph Ebelmen explored the alumina and marble reactivity [1]. However, the invention of Calcium aluminate cement (CAC) or high-aluminate cement, as such, was attributed to Jules Bied, an engineer at Lafarge [1,2]. The initial purpose for its preparation was the need for a quick-setting cement with high sulphate-resistant cement for marine and underground construction. J. Bied experimented with the combination of bauxite, limestone and clays, which proposed the cement with a higher content of calcium aluminates, namely CA and CA_2. Later, with further investigation of other properties, CAC was found to have great overall chemical resistance, high initial strengths and, in particular, excellent temperature resistance [3]. In 1908, this high-alumina cement was patented under the brand name “Cement Fondu” [4]. Afterwards, CAC became extensively used in the 1920s, particularly in environments where its beneficial properties were essential, such as sewerage systems, chemical plants or military constructions. Another employment consisted of emergency repairs and also as a binder for a concrete cast during the winter seasons.

The widespread use of CAC for load-bearing structures was interrupted in the 1970s due to the numerous construction defects and failures. Concerns about the long-term durability of CAC promoted further investigation. It was discovered that calcium aluminate hydrates are metastable. Over time, they undergo inevitable mineralogical conversion and consequently, the CAC cement loses its initial high strengths [5]. This issue limited the use of calcium aluminate cement in structural applications, and later it was banned in load-bearing structures globally. In the Czech Republic, this prohibition came in 1984 following the collapse of a factory building in Uherské Hradiště [6]. However, its use as a binder for refractory concrete, as well as in sewage systems or self-levelling floors, remains viable and offers many advantages. In addition, with a deeper understanding and further research, modern CAC formulations have better control over the conversion process and are more applicable. In general, to mitigate the negative effects of conversion, it is recommended to use a higher proportion of calcium aluminate cement (more than 400 $kg.m^3$) while keeping the water-cement ratio below 0.40 [3,5].

2.1 Production process

Similar to the production of standard Portland cement, the production process of CAC also involves several key stages: raw materials selection and their preparation, clinker production and grinding. These stages influenced the final product, its quality and further applicability of calcium aluminate cement.

2.1.1 Raw-materials

The primary raw materials for the CAC production are bauxite and limestone. Bauxite provides a source of alumina (Al_2O_3); in general, it contains about 45-60% of Al_2O_3 [7]. It is a residual rock formed by a lateralisation, soil-forming process in subtropical climates when parent rocks or clays are hydrolysed and oxidised. Due to the leaching of silica in the hydrated form, the content of alumina in the rock is enriched. Bauxite is composed of aluminate minerals, usually gibbsite ($Al(OH)_3$), boehmite (γ-AlO(OH)) and diaspore (α-AlO(OH)). It usually also contains iron oxides such as hematite (Fe_2O_3) or goethite (α-$Fe^{3+}O(OH)$), quartz (SiO_2), clay minerals or anatase (TiO_2). It is usually reddish-brown with a density of about 2 700 kg m^{-3} [8]. Owing to the mining process, the bauxite ore is usually found near the surface, and it is usually extracted using the open-pit mining method. The main localities are Australia (the largest global producer), Guinea, Brazil, China, India and Jamaica. Because deposits of bauxite are limited, sometimes alumina-rich secondary materials can be used. From this field, it can be named industrial byproducts such as alumina refinery waste, some kinds of fly ashes or slag. Another possibility is the employment of synthetic alumina, such as calcined, tabular or reactive alumina or alumina hydrates.

Limestone, which contributes calcium (CaO), is a sedimentary rock with a biogenic or chemical origin. Specifically, it is formed when calcium carbonates precipitate out of water containing dissolved calcium, which can take place through both biological and nonbiological processes. It is composed of varying forms of calcium carbonate ($CaCO_3$), but mainly of calcite, accompanied by aragonite in an amount of about 95% [8]. Another common component is magnesium carbonate, e.g.in form of dolomite ($CaMg(CO_3)_2$). Eventual minor constituents include silica, feldspars, clay minerals or pyrite. Limestone is commonly white to grey. Its mining, similar to that of bauxite, is performed in open-pit quarries, but sometimes also in underground mines. It is a more common material compared to bauxite, with extensive deposits worldwide, but the biggest producers are the United States, China, India and Brazil.

Regarding the quality of the raw materials, a high purity is required, meaning those materials containing only alumina and calcium oxides. The content of silica (SiO_2) must be minimal (lower than 8% [5]) if one wants to prevent the formation of unfavourable phases, such as gehlenite (C_2AS) or dicalcium silicate (C_2S), during the production. There are also limits to the content of iron oxide (Fe_2O_3) because it can influence the colour of the cement, as well as its refractoriness or its chemical resistance. The limit depends on the type of final product (as it is visible in Table 1), for refractory CAC, it should be 1-2% [2].

Table 1 Oxide composition [% by mass] for calcium aluminate cements [9]

	Al_2O_3	CaO	SiO_2	Fe_2O_3	MgO	TiO_2	SO_3
Low Alumina Cement	20-35	50-55	7-12	5-10	1-2	<1	<0.5
Standard CAC	35-40	36-42	3-8	8-15	1-3	1-2	<0.5
High Alumina Cement	40-55	30-40	3-7	5-10	1-2	<2	<0.5
Refractory grade of CAC	50-70	25-35	<1-3	<1-2	<1	<1	<0.5

2.1.2 Specific production process

Raw materials are first crushed in jaw, gyratory, or cone crushers to have a uniform particle size of about 10-50 mm [2]. Afterwards, these particles are ground in the mill for fine powder with particles less than 200 μm [2]. Such fine particles ensure proper chemical reactions in the calcination process in the kiln. Another aspect which has to be respected is the homogeneity of the fine powder. On that account, the finely ground raw materials are often sent to blending silos, where they are thoroughly mixed to achieve a uniform chemical composition before being fed into the kiln. After the first treatments of the raw materials, the calculation of their appropriate ratio in the batch has to be done, taking into account the desired final product (as represented table in Table 1). In general, it can be simplified that the limestone to bauxite is mixed in a ratio of 1:1 [5]. The last step of the raw-material preparation is optional, and it is the preheating of the prepared batch before feeding the kiln. In the preheater (usually a series of cyclone preheaters), the batch is exposed to hot gases from the kiln, which provide energy (and consequently, fuel savings) and initiate the reaction process leading to the production of higher-quality clinker.

A variety of methods have been employed to manufacture calcium aluminate cements. However, there are two main production processes: the melting procedure and the sintering procedure. Melting cement is manufactured in an electric-arc furnace

at temperatures of about 1600 °C, and coarser grains of raw materials can be used. The sintering process is performed in a rotary kiln at temperatures of around 1350 °C. The rotary kiln is a long, cylindrical, rotating furnace. It is inclined slightly so that the raw mix gradually moves towards the hotter end. Sintering results in the formation of more pure cement with a higher aluminate content [5]. Regardless of the production processes, the reactions are similar. Firstly, calcium carbonates ($CaCO_3$) are decomposed at temperatures of about 700-900 °C. It gives rise to lime (CaO) and carbon dioxide (CO_2). Afterwards, at higher temperatures, the reactions between the calcium oxide and alumina begin according to the particular ratio of these oxides; there are a lot of possible reaction products in this system, what is clearly illustrated by the phase diagram in Figure 1. However, a summary of chemical reactions which take place during the sintering process is as follows [10]:

$$CaCO_3 \rightarrow CaO + CO_2 \tag{1}$$

$$CaO + Al_2O_3 \rightarrow CaO.Al_2O_3 \qquad (C + A \rightarrow CA) \tag{2}$$

$$CaO + 2Al_2O_3 \rightarrow CaO.2Al_2O_3 \qquad (C + 2A \rightarrow CA_2) \tag{3}$$

$$12CaO + 7Al_2O_3 \rightarrow 12CaO.7Al_2O_3 \qquad (12C + 7A \rightarrow C_{12}A_7) \tag{4}$$

$$12CaO.7Al_2O_3 + 5Al_2O_3 \rightarrow 12\,CaO.Al_2O_3 \qquad (C_{12}A_7 + 5A \rightarrow 12CA) \tag{5}$$

$$CaO.Al_2O_3 + Al_2O_3 \rightarrow CaO.2Al_2O_3 \qquad (CA + A \rightarrow CA_2) \tag{6}$$

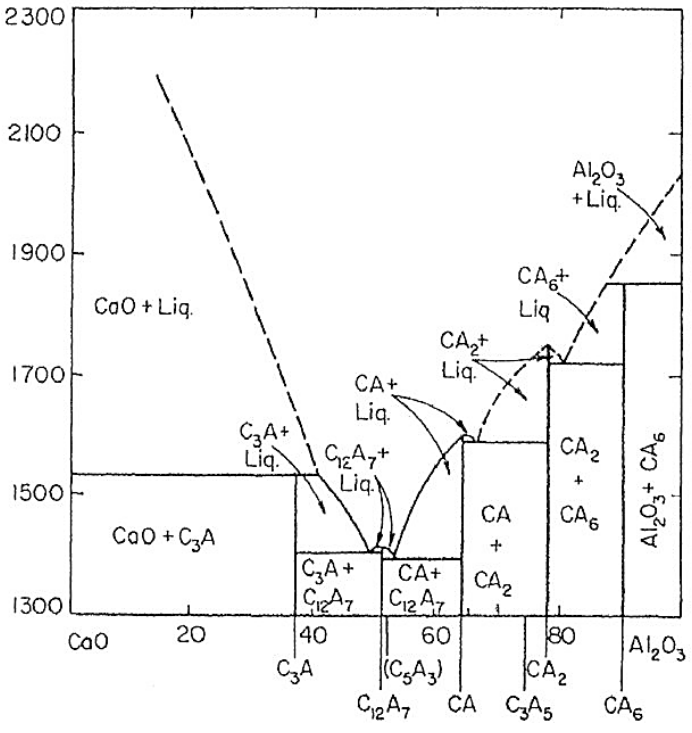

Figure 1 Phase diagram of the CaO – Al_2O_3 system [11]

Once a desired composition of clinker is reached, more precisely at the end of the rotary kiln, the material exits the kiln at a very high temperature. This hot material must be rapidly cooled to ensure the proper composition of the calcium aluminate phases. Specifically, the reactive monocalcium aluminate (CA) and calcium dialuminate (CA_2) are the desired phases. On the other hand, slow cooling can lead to the formation of thermodynamically more stable but less reactive phases such as dodecacalcium heptaaluminate ($C_{12}A_7$). Wrong cooling can therefore reduce the performance characteristics of the calcium aluminate cement, as in the case of Portland cement. Cooling systems, such as grate coolers or rotary coolers, are usually used, and the cooling rate has to be carefully controlled to avoid thermal shock, which could cause microcracks in the clinker, potentially leading to issues during grinding and again a reduction in cement quality.

The last step of calcium aluminate cement production is grinding lumps of the clinker into a fine powder. The grinding process is carefully controlled to achieve a specific particle size (as can be seen in Figure 2), which influences the cement's hydration rate and final properties. A finer grind generally leads to higher early strength but can also result in rapid setting times. In general, median particle size (D50) falls within the range of 5 to 15μm, and Blain-specific surface area typically reaches values from 300 to 400 $m^2.kg^{-1}$ [1, 5]. For proper and efficient grinding, it is usually necessary to add some grinding intensifiers, also known as grinding aids or intensificators. There have been developed many types of them, but the most common representatives are glycols (ethylene glycol, diethylene glycol), amines (triethanolamine, diethanolamine) and alkanolamines (triisopropanolamine) [12]. They can reduce the agglomeration of particles and promote a more uniform particle size distribution, consequently reducing energy consumption and improving the overall properties of the final product.

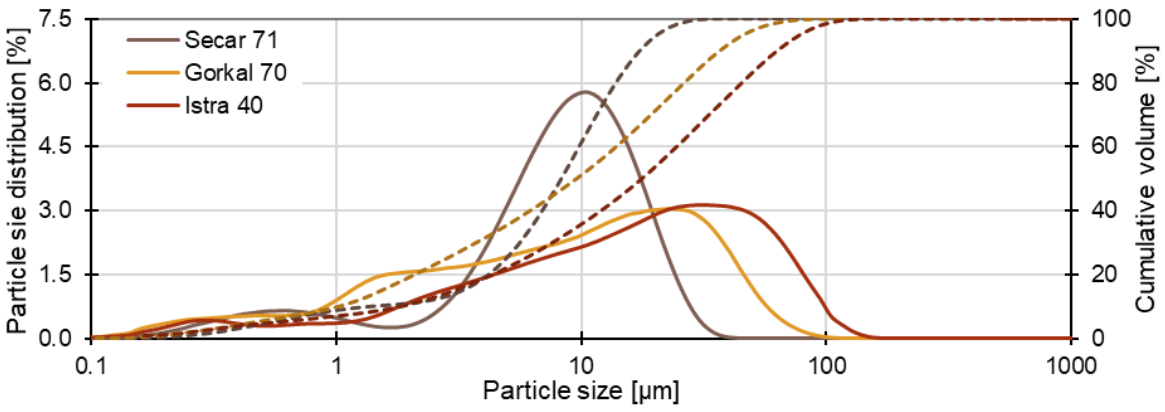

Figure 2 Particle size distribution curves of CAC

2.1.3 Global production and market

The global production of calcium aluminate cement (CAC) is a niche but significant market within the broader cement industry. However, the global market for CAC was valued at around $1.4 billion in 2022, with expectations to grow to approximately $2.2 billion by 2031 [13]. Regarding the producers of calcium aluminate cement, currently, several major companies manufacture this binder. Kerneos (in France) is one of the largest and oldest producers of calcium aluminate cement. The company specialises in providing high-quality CAC for use in refractories, building chemistry, and various other sectors. Kerneos operates globally, with multiple laboratories and production sites. Almatis (in Germany) is a global leader in the production of premium alumina and alumina-based products, including calcium aluminate cements. With a history spanning over 100 years, Almatis operates numerous manufacturing and research facilities worldwide, focusing on high-performance products for various industrial applications. Calucem (Germany/USA) is the second-largest producer of calcium aluminate cements. The company has a strong focus on innovation and sustainability, with manufacturing facilities in Germany, Croatia, and a newly established plant in the United States. Among other companies, it can be named Kerui Refractory (in China), specialising in a wide range of high-temperature applications for varying industries worldwide, including iron-steel, aluminium, power, glass, boiler, non-ferrous, and cement industries. Elfusa (in Brazil) is a prominent Brazilian producer of refractory materials, including calcium aluminate cement, while Cimsa (in Turkey) belongs to the cement producers, whose production portfolio includes calcium aluminate cement as well. Concerning Central Europe, Górkacement company based in Trzebinia, Poland, is an active producer of several kinds of CAC with 40 – 80% of Al_2O_3 content. Historically (30^{th} to 60^{th} of 20^{th} century), CAC was produced in Ladce, Slovakia, under the trademark Bauximent.

2.1.4 Economic and ecological aspects

The production of CAC is, similarly to Portland cement (PC), economically and ecologically demanding. Regarding raw-material depletion, bauxite is more costly and less abundant when compared to limestone, clays and sands needed for the production of PC. Regarding the energy consumption, cement clinker production is extremely energy-intensive due to the high operation temperature (about 1300 – 1400 °C), extremely energy-intensive regardless of the cement type.

However, for the production of CAC, slightly lower temperatures are needed than in the case of PC (about 1450 °C). The energy demand for CAC production is typically around 3.5 to 4.2 GJ per ton of cement, while in the case of PC, the demands usually range from 4.5 to 5.5 GJ per ton of cement [14]. The biggest issue connected with the production process is, however carbon footprint. The overall cement industry is responsible for 7% of global carbon dioxide emissions. These emissions are partially inevitable as they originate not only in fuel combustion but especially in the calcination of limestone. Nevertheless, from this point of view, CAC production is more economically friendly because a somewhat lower temperature is required, and also a lower amount of limestone is used. Regarding the particular data, depending on the particular production process, carbon emissions of CAC range from 600 to 750 kg of CO_2 per ton of cement, while in the case of PC, it oscillates from 800-900 kg of CO_2 per ton [14]. On the other hand, CAC is used for special applications, and its production is less broadened, leading to higher market prices and more volatility compared to PC. Another economic aspect is the higher transportation costs of CAC, connected precisely with regional or local production.

2.2 Composition and properties of CAC

As it was indicated in the previous chapter, calcium aluminate cement is composed primarily of calcium aluminates (as visible in Figure 3, where is an example of CAC composition measured by XRD). The most common representatives are shown in Figure 4. The primary phase is monocalcium aluminate ($CaO.Al_2O_3$, CA), which typically accounts for about 40-65% of CAC [1,2]. This phase crystallises in a monoclinic system with a space group P21/n, and it is known as krotite. It is quite a hard mineral with a hardness of 6.5, and it has a specific gravity of 2 944 $kg.m^{-3}$ [8]. It's highly reactive calcium aluminate, which is responsible for a high early strength development.

Another phase, which can be present in CAC, is calcium dialuminate ($CaO.2Al_2O_3$, CA_2). Its presence depends on a particular type of CAC. In the case of standard and low alumina CAC, it is presented in minor amounts up to 5-10%. With increasing content of alumina, the amount of CA_2 goes up, and it can reach up to 40% in the case of high alumina cement [1, 2]. Similarly to krotite, it also has a monoclinic crystal structure but with space group $P2_1/c$. Its mineralogical name is grossite, and

the specific gravity is about 2 880 kg.m^{-3} [8]. Regarding its reactivity, it is less reactive than krotite, and it contributes more to the long-term strengths.

The last major calcium aluminate phase is dodecacalcium heptaaluminate ($12CaO.7Al_2O_3$, $C_{12}A_7$). Again, its presence depends on the type of cement; generally, it accounts for 10-30% [1,5], but in the case of high alumina cement, it is present in trace amounts. It has a cubic crystal structure with the I-43 space group [15]. Its mineralogical name is mayenite, and it has a specific gravity of about 2680 kg.m^{-3}. This mineral is special for having two oxide ions O^{2-}, OH^-, or even electrons trapped within its framework, leading to its electrical (ionic) conductivity. Regarding the properties of CAC, it is the most reactive phase among calcium aluminates; it significantly accelerates the setting of cement and contributes to early strength.

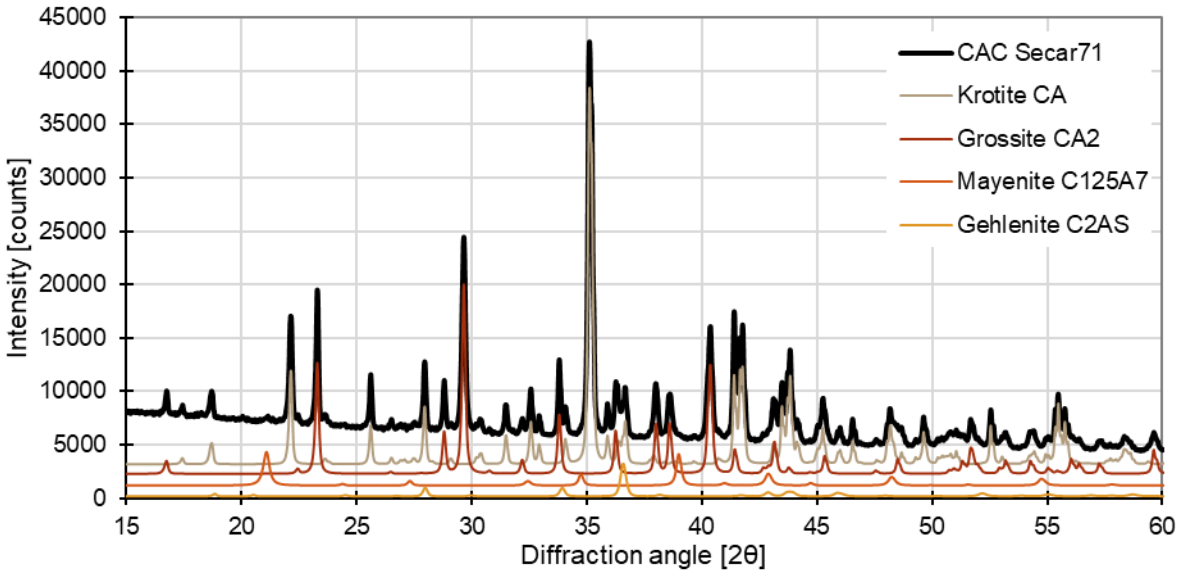

Figure 3 X-ray diffractogram of high alumina CAC

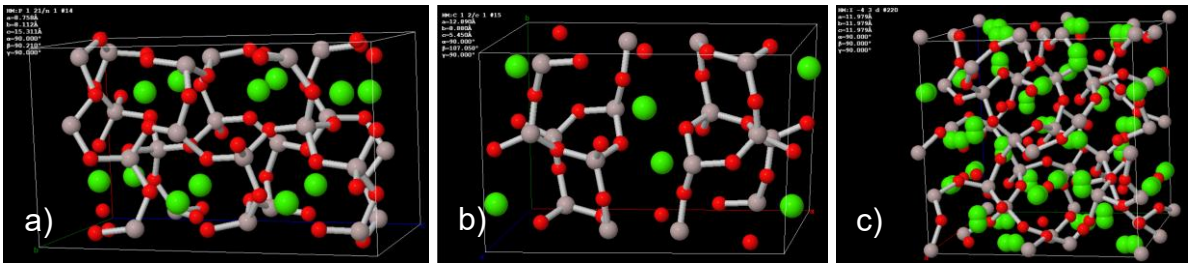

Figure 4 Crystal structure of C-A: a) krotite CA, b) grossite CA_2, c) mayenite $C_{12}A_7$ [8]

Minor phases that CAC may contain are gehlenite ($2CaO{\cdot}Al_2O_3{\cdot}SiO_2$, C_2AS), dicalcium silicate ($CaO.SiO_2$, C_2S), ferrite phases ($C_2(A,F)$) or perovskite ($CaTiO_3$). Gehlenite (C_2AS) is present when the raw materials contain more silica. It is less

reactive than the main calcium aluminate phases, and it influences the durability and high-temperature resistance of CAC. A higher content of silica can also give rise to dicalcium silicate (C_2S). This phase hydrates more slowly than the aluminate phases and contributes to the later stages of strength. On the other hand, it again deteriorates the refractoriness of CAC. Regarding the ferrite components, they are represented as a part of calcium aluminoferrites, and the most common representative is tetracalcium aluminoferrite ($4CaO.Al_2O_3.Fe_2O_3$, C_4AF). They somehow contribute to strength development, but mainly influence the colour of CAC, which is in the presence of ferrite phases, remarkably darker. Concerning the perovskite, it may appear as a minor phase when titanium is present in the raw materials. It is relatively inert and does not significantly influence the hydration behaviour of CAC.

2.3 Hydration of CAC

The hydration of CAC is remarkably different from that observed in the case of PC. The biggest difference is that the course of the hydration process is significantly influenced by curing temperature. The hydration of calcium silicate compounds in the case of PC remains relatively stable over time and at temperatures up to approximately 100 °C (the rate of hydration is influenced by temperature, indeed, but phase composition remains). In contrast, the nature of hydration products in CAC is highly temperature-dependent even at ambient temperature.

In Table 2, the main hydration reactions, depending on particular temperatures, are summarised [1,5,16–18]. The dominant reaction is always listed at the top, while the coexisting reaction of the particular calcium aluminate (if present) is shown in italics below. Monocalcium aluminate (CA) is the most sensitive phase to varying temperature ranges, but its hydration is fast. On the contrary, the hydration of calcium dialuminate (CA_2) is slower but less dependent on temperature variation [5,16]. Hydration of dodecacalcium heptaaluminate ($C_{12}A_7$) is extremely fast, but it is also not as dependent on the temperature. However, it should be mentioned that the observed calcium aluminate hydrates are not stable; specifically, CAH_{10} and C_2AH_8 undergo conversion (which will be described in the subsequent chapter). Consequently, the identification and characterisation of specific hydration products may be influenced by the unstable nature and potential phase transitions of these metastable hydrates. Another aspect is the substantial hydration heat evolved during the reactions, which can contribute to the higher temperature during hydration than is anticipated.

Table 2 Hydration reaction of monocalcium aluminate CA depending on temperature

Temperature range [°C]	**Hydration reaction (dominant / *coexisting*)**	**Product of hydration (dominant / *coexisting*)**
< 15	CA + 10H	CAH_{10}
	$2CA_2$ + 17H	$C_2AH_8 + 3AH_3^{(amorph.)}$
	$C_{12}A_7$ + 51H *$C_{12}A_7$ + 60H*	$6C_2AH_8 + AH_3^{(amorph.)}$ *$2CAH_{10} + 5C_2AH_8$*
15 – 25	2CA + 11H *CA + 10H*	$C_2AH_8 + AH_3^{(amorph.)}$ *CAH_{10}*
	$2CA_2$ + 17H	$C_2AH_8 + 3AH_3^{(amorph.)}$
	$C_{12}A_7$ + 51H *$C_{12}A_7$ + 60H*	$6C_2AH_8 + AH_3^{(amorph.)}$ *$2CAH_{10} + 5C_2AH_8$*
25 – 30	2CA + 11H *3CA + 12H*	$C_2AH_8 + AH_3^{(amorph.)}$ *$C_3AH_6 + 2AH_3^{(amorph)}$*
	$3CA_2$ + 21H	$C_3AH_6 + 5AH_3^{(cryst.)}$
	$C_{12}A_7$ + 51H	$6C_2AH_8 + AH_3^{(amorph.)}$
30 – 35	3CA + 12H *2CA + 11H*	$C_3AH_6 + 2AH_3^{(cryst./amorph)}$ *$C_2AH_8 + AH_3^{(cryst/amorph)}$*
	$3CA_2$ + 21H	$C_3AH_6 + 5AH_3^{(cryst.)}$
	$C_{12}A_7$ + 51H *$C_{12}A_7$ + 51H*	$6C_2AH_8 + AH_3^{(amorph.)}$ *$4C_3AH_6 + 3AH_3^{(cryst.)}$*
> 35	3CA + 12H	$C_3AH_6 + 2AH_3^{(cryst.)}$
	$3CA_2$ + 21H	$C_3AH_6 + 5AH_3^{(cryst.)}$
	$C_{12}A_7$ + 51H	$4C_3AH_6 + 3AH_3^{(cryst.)}$

Regardless of the particular reactions, the mechanism of calcium aluminate hydration can be divided into three phases. In the initial phase, upon contact with water, the calcium aluminate grains immediately begin to dissolve, firstly dissolving CA and later also CA_2. This process, known as hydrolysis, results in the formation of calcium ions (Ca^{2+}) and aluminate ions, specifically in the form of aluminate tetrahydroxide complexes ($Al(OH)_4^-$), within the solution. The dissolution of calcium aluminates is a distinctively exothermic reaction, meaning it releases heat, which can cause a noticeable increase in the temperature of the cement paste. During this phase, a small amount of aluminium oxide (Al_2O_3) precipitates out of the solution. As the concentration of the ions increases, the conductivity and pH of the solution also

rise. The solution continues to absorb ions until it reaches a state of supersaturation. At this point, the system is primed for the next phase of hydration.

Following this, the process enters the latent or nucleation phase. After the solution becomes supersaturated, the rate of dissolution of calcium aluminates slows down significantly. Despite the slowdown in dissolution, the formation of hydrate phases begins, though it progresses very slowly during this stage. The solution remains highly concentrated with calcium and aluminate ions ($Ca^{2+}$and $Al(OH)_4^-$). This phase can last from several minutes to a few hours, depending on the environmental conditions, such as temperature and the presence of additives.

Finally, in the main hydration phase, there is a massive precipitation of these ions, leading to the formation of the main hydration products, depending on temperature, the concentration of available ions of Ca^{2+} and $Al(OH)_4^-$ and their respective ratio. The arising hydration products are initially semi-crystalline, but then gradually grow and merge as the hydration process continues. As the ions are rapidly depleted due to the precipitation, additional calcium aluminates begin to dissolve, which in turn accelerates the overall hydration reaction. This phase is characterised by an immense heat release and a noticeable decrease in conductivity and ions' concentration.

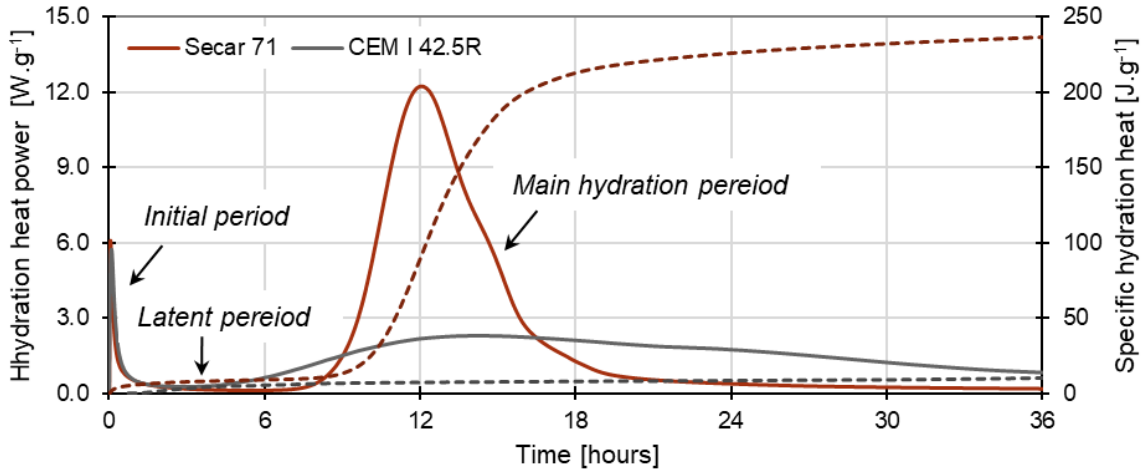

Figure 5 Comparison of the hydration heat of CAC and PC

The hydration in CAC occurs rapidly (in comparison with PC, Figure 5), generally leading to a noticeably shorter setting time. The average initial setting time ranges from 45 minutes to 2.5 hours, while the final setting time usually occurs within 3 to 6 hours [1,19]. The accelerated hydration is also associated with a higher heat of hydration. Specifically, the total heat released during the hydration of CACs ranges between 545 $J.g^{-1}$ and 650 $J.g^{-1}$, which is substantially higher than the hydration heat of PC (typically falls within the range of 375 $J.g^{-1}$ – 525 $J.g^{-1}$) [5, 9]. The combination of faster

setting and higher thermal output makes CAC distinct in their performance, particularly in applications where rapid strength gain and higher thermal resilience are required. Despite this being particularly advantageous in cold climates or applications requiring quick setting (e.g. repair mortars and refractories), in hot environments or mass structures, this rapid heat evolution must be carefully managed.

2.4 Hardened cement matrix

The hardened cement matrix plays a crucial role in determining the material's properties, such as mechanical strengths, durability, thermal resistance, etc. Unlike PC, CAC undergoes a unique hydration process (as was described in the previous chapter), resulting in the formation of distinct phases. These phases consequently influence the matrix stability and overall performance of CAC-based composites.

2.4.1 Phase composition

The hardened cement matrix comprises several phases that can be divided into several groups. As it is described herein-above, the main hydration products are calcium aluminate hydrates (C-A-H), followed by aluminate hydrates (A-H). In addition, in the case of low alumina cement, the matrix can also contain a remarkable amount of calcium aluminate silicate hydrate (C-A-S-H) or a trace amount of calcium silicate hydrate (C-S-H). Of course, as not all cement grains undergo hydration, unreacted calcium aluminates (C-A) are usually present in the hardened matrix as well. The basic properties of hydration products are summarised in Table 3, and in Figure 6, there are delineated diffractograms of fundamental hydration products.

Table 3 Properties of crystal hydration products of CAC

Hydrates	**Chemical composition [%]**			**Structure**	**Specific gravity [kg.m^{-3}]**
	CaO	**Al_2O_3**	**H_2O**		
CAH_{10}	16.6	30.1	53.3	Hexagonal	1743
C_2AH_8	31.3	28.4	40.3	Hexagonal	1950
C_3AH_6 - Katoite	44.4	27.0	28.6	Cubic	2520
C_4AH_{13}	40.0	18.2	41.8	Hexagonal	2046
AH_3 - Gibbsite	-	65.4	34.6	Hexagonal	2420
AH_3 - Bayerite	-	65.4	34.6	Monoclinic	2530
AH_3 - Norstrandite	-	65.4	34.6	Triclinic	2420
C_2ASH_8 - Strätlingite	27.4	24.9	33.0	Hexagonal	1936

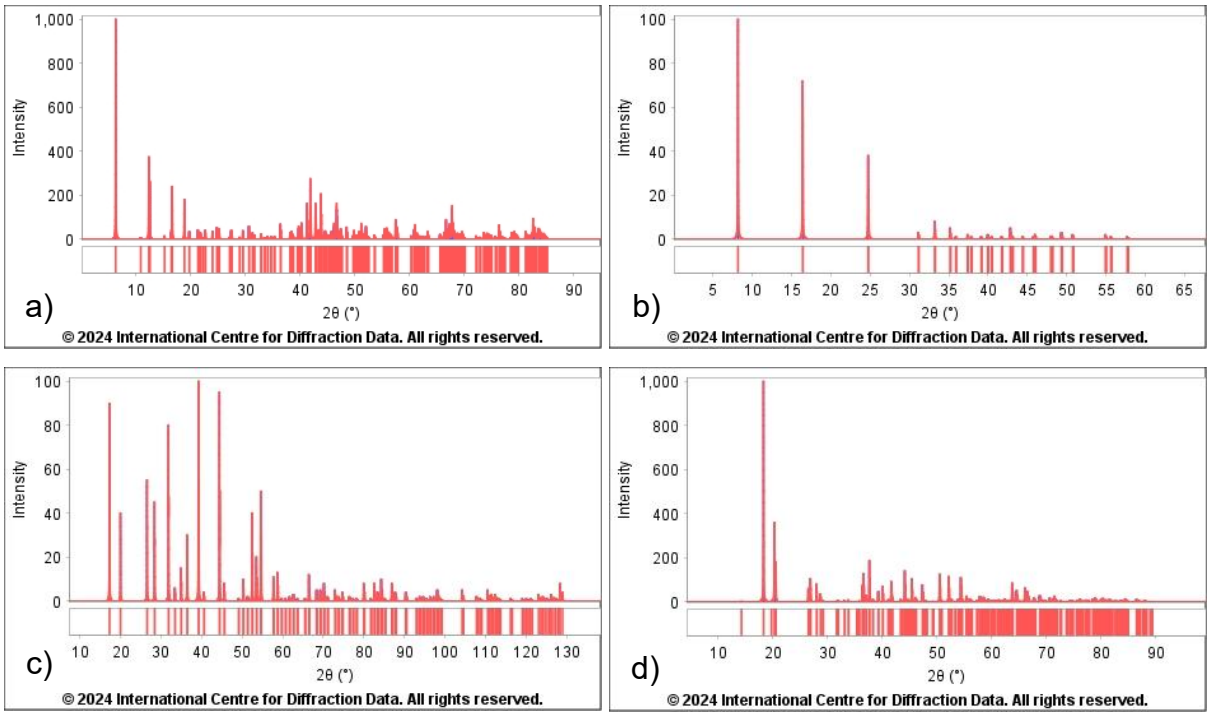

Figure 6 Diffractograms of hydration products (from PDF-5+ database): a) CAH_{10}, b) C_2AH_8, c) katoite - C_3AH_6 and d) gibbsite - AH_3

There are three main C-A-H products (Figure 7). The CAH_{10} ($CaO.Al_2O_3.10H_2O$) is usually created at lower temperatures and in the excess presence of water. Its creation is quite fast, and it is responsible for high initial strengths. It crystallises in small hexagonal prisms, and in SEM images, it looks like needles. Regarding its crystal structure, it is layered, with calcium ions (Ca^{2+}) coordinated with aluminate ions ($Al(OH)_4^-$) and surrounded by ten water molecules. These water molecules are interspersed between the layers and are bound both through hydrogen bonding and ionic interactions with calcium. The second C-A-H is C_2AH_8 ($2CaO.Al_2O_3.8H_2O$), typically crystallising at moderate temperatures. It creates layered plate-like hexagonal crystals, which create clusters. Its crystal structure consists of alternating layers of calcium and aluminate ions, coordinated by hydroxyl ions and water molecules. In C_2AH_8, two calcium ions are bound to aluminate units and eight water molecules. Unfortunately, both later phases are metastable. In addition, their structures have not yet been properly described, making their credible quantification by Rietveld refinement (XRD) difficult or rather impossible. The last major representative of C-A-H is katoite C_3AH_6 ($3CaO.Al_2O_3.6H_2O$). This phase generates dense cubic crystals, and it is usually created at higher temperatures or at a later age of hydration. Katoite is thermodynamically the most stable C-A-H. Crystals consist of three calcium ions

coordinated with aluminate ions and six water molecules. They form a stable and highly ordered structure. This phase contributes to the long-term strength and durability of the matrix. The last-mentioned phase C_4AH_{13} or C_4AH_{19}, can form as well, but usually at lower temperatures below 20 °C and in minor amounts. It is also metastable and undergoes conversion. It should also be mentioned that present phases are the most common and recognised representative, but the stoichiometric coefficients can vary slightly according to particular hydration conditions and cement composition (e.g. CAH_9, $C_2AH_{7.5}$, or C_4AH_{12}).

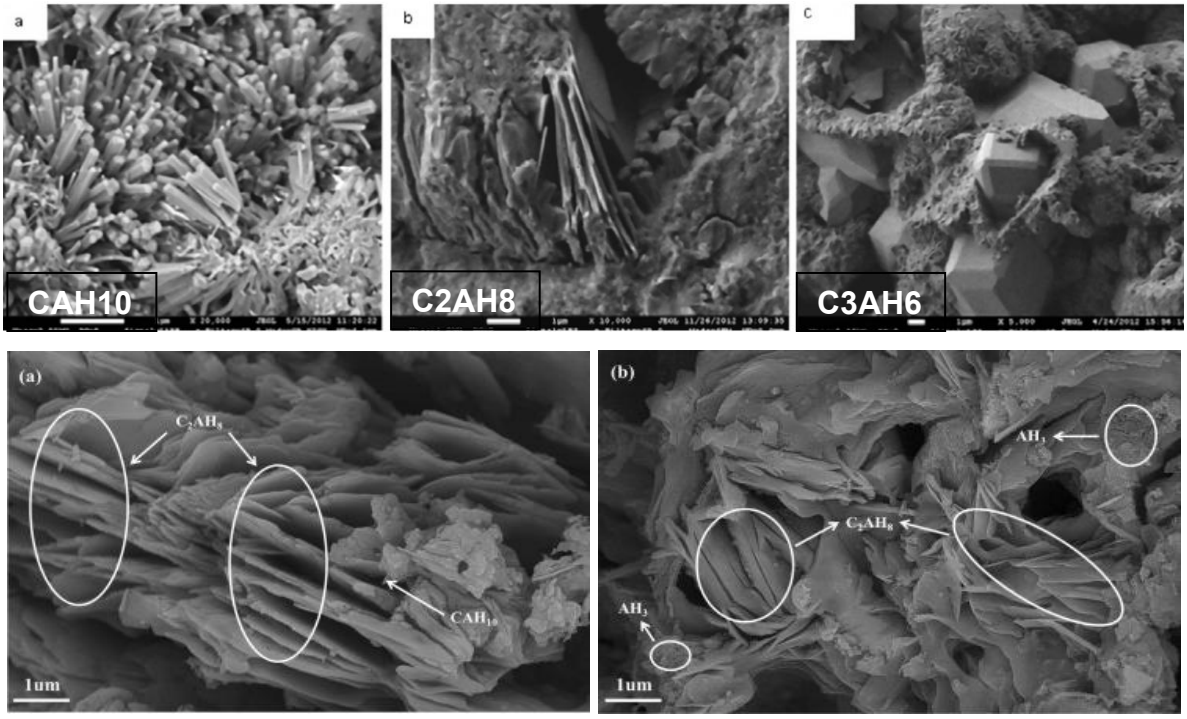

Figure 7 Examples of SEM images of C-A-H [17,20]

Regarding the A-H or aluminium hydroxide, respectively, there are also several types of these compounds. At lower and moderate temperatures, amorphous matter of AH_3 ($Al_2O_3.3H_2O$) is generated. This gel-like substance usually fills the pores and increases the overall strength and durability of the matrix. At higher temperatures or due to the conversion process, gibbsite AH_3 ($Al_2O_3.3H_2O$), the crystalline representative of A-H, arises. It has a layered crystal structure, with aluminium ions (Al^{3+}) at the centre of an octahedral coordination surrounded by hydroxide ions. This phase significantly contributes not only to the strength but also to the chemical resistance of cement. Other polymorphs of A-H are bayerite or nordstrandite. However, they are less common and are present only in minor amounts or in specific conditions.

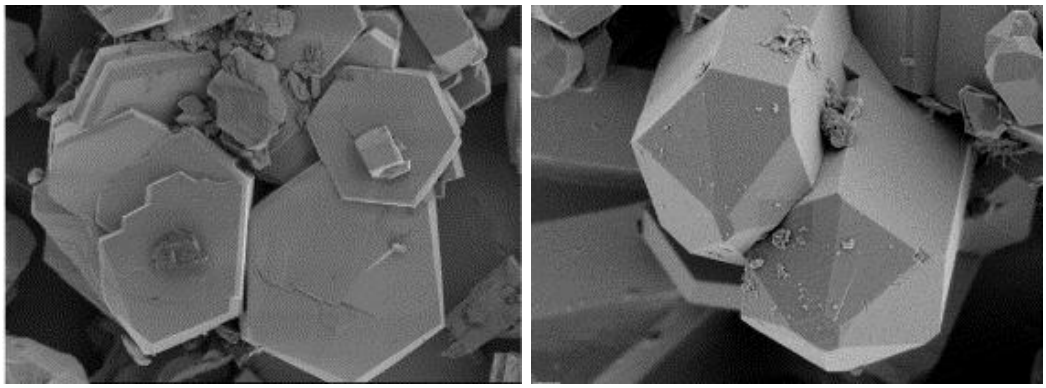

Figure 8 Examples of gibbsite SEM images [21]

2.4.2 Conversion of metastable phases

The biggest problem of CAC is the thermodynamic metastability of the main hydration products (in particular CAH_{10} and C_2AH_8). Over time, these phases are continuously converted into a stable form (specifically into katoite C_3AH_6). Unfortunately, this is an inevitable process, and its rate depends on many factors such as temperature, humidity, w/c ratio of mix, etc [5,9,22]. Due to the strong impact of temperature and high hydration heat, the conversion process can appear even during the hydration process due to the self-heating of larger concrete elements [23]. However, in general, it takes from hours (in the case of higher temperatures) to years (at lower temperatures or lower humidity). The conversion process can be described by the following equations:

$$2CAH_{10} \rightarrow C_2AH_8 + AH_3 + 9H \quad (7)$$

$$3C_2AH_8 \rightarrow 2C_3AH_6 + AH_3 + 9H \quad (8)$$

The recrystallisation itself would not be a problem, as katoite (C_3AH_6) also has suitable properties. The problem is that this stable phase is significantly denser (by 45% compared to CAH_{10} and 30% compared to C_2AH_8). On that account, the conversion is accompanied by a significant porosity increase and, consequently mechanical strength fall. However, the performance of strength development is not as simple. Metastable hydrates are formed at the early state of hydration, and they are responsible for high values of initial strengths. Due to the conversion, the high initial strength falls up to a certain point when the structure is stabilised and the material shows the long-term stable strength. The high initial strength has to be, therefore, considered simply as a transient. On the contrary, the long-term strength is derived from the formation of stable hydrates. It is usually lower compared to the initial

(transient) state. But in the case of higher temperatures or bigger elements, the stable hydrates can form straight away, and such materials are therefore stable directly. Another aspect is the presence of the unhydrated portion of CAC. As can be derived from the equations of conversion processes, a significant amount of water is released during the transformation. This water can then participate in the hydration of unhydrated CAC. As a result, the strength of the cement matrix can further increase. Typical curves of strength development are delineated in the following Figure 9.

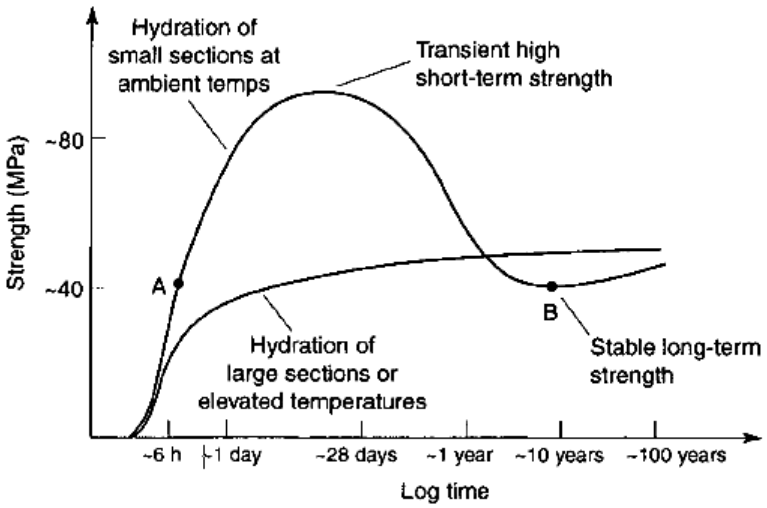

Figure 9 Curves of strength development of CAC-based concrete [5]

2.4.3 Thermal resistance of CAC

One of the most profound applications of calcium aluminate cement-based composites is dedicated to high-temperature environments, as this binder has great thermal resistance. According to the purity of cement, it can withstand temperatures of about 1600 °C and it is also resistant to cyclic thermal loading. For comparison, Portland cement-based materials can hardly withstand temperatures of 1000 °C. However, calcium aluminate cement also undergoes substantial changes in structure and phase composition when heated. The main reactions are summarised in Table 4, while in Figure 10, examples of DSC curves of CAC-based paste over time can be found. In the figure, the continuous conversion of the paste is visible. Nevertheless, the temperature-dependent processes in the CAC can be divided into three or four areas respectively.

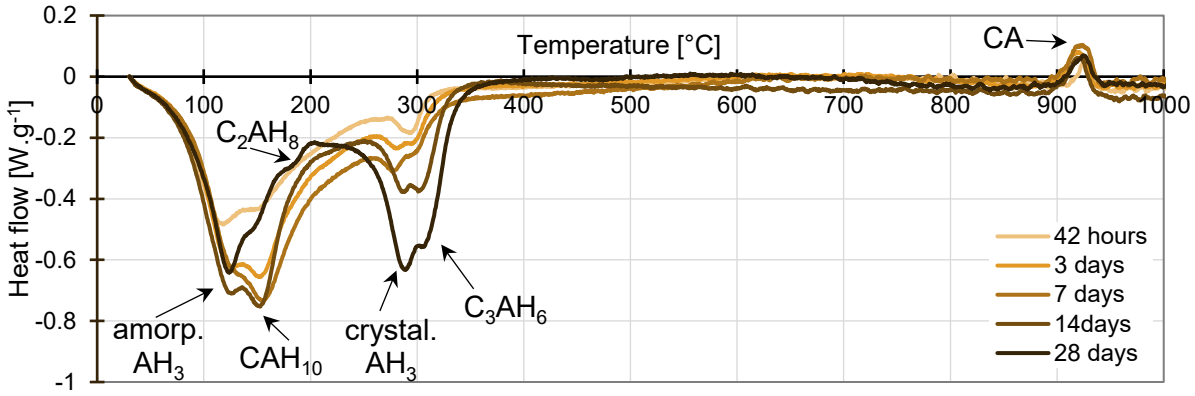

Figure 10 Examples of DSC curves of CAC pastes over time

Table 4 Summary of reactions in CAC due to the temperature exposure [5, 17, 24–26]

Temperature range [°C]	**Reactant**	**Reaction**
Up to 120		Evaporation of free water
60 – 120	$Al(OH)_3$ gel	$2Al(OH)_3 \rightarrow \beta\ Al_2O_3 + 3H_2O$
100 – 160	CAH_{10} ($CaO.Al_2O_3.10H_2O$)	$2CAH_{10} \rightarrow C_2AH_8 + AH_3 + 9H$
140 – 240	C_2AH_8 ($2CaO.Al_2O_3.8H_2O$)	$3C_2AH_8 \rightarrow 2C_3AH_6 + AH_3 + 9H$
210 – 320	$Al(OH)_3$ Gibbsite	$Al(OH)_3 \rightarrow AlOOH + H_2O$
240 – 370	C_3AH_6 ($3CaO.Al_2O_3.6H_2O$) Katoite	$7C_3AH_6 \rightarrow C_{12}A_7H + 9CH + 32H$
		$3C_3AH_6 \rightarrow C_4A_3H_3 + 5CH + 10H$
475 – 550	AlOOH Boehmite	$AlOOH \rightarrow Al_2O_3 + H_2O$
450	$Ca(OH)_2$	$Ca(OH)_2 \rightarrow CaO + H_2O$
440 – 620	$C_4A_3H_3$	$3C_4A_3H_3 \rightarrow C_{12}A_7 + 2A + 9H$
690 – 750	$C_{12}A_7H$	$C_{12}A_7H \rightarrow C_{12}A_7 + H$
900	$C_{12}A_7$ ($12CaO.7Al_2O_3$) Mayenite	$C_{12}A_7 + 5\ Al_2O_3 \rightarrow 12CA$
800 – 1000	$CaO + Al_2O_3$	$CaO + Al_2O_3 \rightarrow CaO.Al_2O_3$
1000 – 1300	CA ($CaO.Al_2O_3$) Krotite	$CA + Al_2O_3 \rightarrow CA2$
1400 – 1600	CA2 ($CaO.Al_2O_3$) Grossite	$CA_2 + Al_2O_3 \rightarrow$ CA6 Hibonite

The first area involves the evaporation of physically bounded water, but the main process is the dehydration of the hydrated calcium aluminate phases. Regarding the first two unstable hydrates, CAH_{10} and C_2AH_8, their transformation is well known, and the reactions are coherently described in the literature. On the contrary, in the case of katoite (C_3AH_6), the dehydration process can vary, but there are often presented two varying courses. The first is partial dehydration to $C_{12}A_7H$, while in the second, there is reported creation of $C_4A_3H_3$. Despite these differences, both progressions result in mayenite ($C_{12}A_7$) as the final dehydration product, and the dehydration of these partially dehydrated forms of katoite is more continuous and

is not connected with distinctive STA peaks. The dehydration takes place from ambient temperature to approximately 400 °C. It is accompanied by substantial mass changes (about 20% mass loss according to particular composition and hydration degree), caused by the water release. Consequently, small microcracks and further thicker cracks occur in the material structure. These cracks further impact the mechanical properties, typically resulting in an average reduction of compressive strengths by 10% [27]. In some cases, a partial increase in strength can be observed after exposure to lower temperatures (up to around 200 °C). This phenomenon is usually attributed to additional hydration, more precisely to the reaction of unreacted calcium aluminates grains with released water. On the other hand, at the second part of the dehydration range (usually from 200 to 400 °C), explosive spalling can occur. It is a dangerous and harmful act in which material from the surface of concrete or refractory structures suddenly and violently fractures and detaches. This usually happens during rapid heating, when internal pore pressure, generated by the rapid vaporisation of water, exceeds the tensile strength of the material.

The second area could be called a steady state, taking place from 400 °C to about 900 °C. Although some reactions are documented within this temperature range (Table 4), no significant changes in material occur (as is visible in Figure 10). In the case of boehmite (AlOOH) and portlandite ($Ca(OH)_2$) dehydration, the impact is minimal due to their lower content in the hydrated pastes. In contrast, the high content of Portlandite in the case of Portland cement is responsible for the lower temperature stability of this binder. Regarding the partially dehydrated hydrogarnets, it is visible that $C_4A_3H_3$ dehydrates slowly in a wider temperature range, while the $C_{12}A_7H$ releases only one molecule of water during the process. Despite minimal changes in phase composition, the gradual development of microcracks continues, further contributing to the continuous decline in mechanical properties. In general, at about 900 °C, CAC-based composites show the lowest compressive strength.

The third area is typical of recrystallisation of new or more precisely re-new phases of calcium aluminates as mayenite ($C_{12}A_7$), krotite (CA), grossite (CA_2) and hibonite (CA_6). These phases exhibit high-temperature stability, significantly contributing to the material's enhanced mechanical strength and durability. In addition, at temperatures above 1200°C, sintering begins to take place, further transforming the structure of a material (Figure 11). Sintering can be considered as a separate fourth area, as it is a different process. Specifically, it is a physical process driven by atomic

diffusion when the structure is compacted and bonded together, resulting in a dense, usually pore-free or low-porosity structure. The combination of phase recrystallisations and structure sintering leads to the development of so-called ceramic bonds – robust interparticle connections that significantly enhance compressive strength and thermal resistance. These bonds contribute to the material's ability to withstand extreme temperatures and mechanical stress, making it suitable for refractory applications and environments involving high thermal loads.

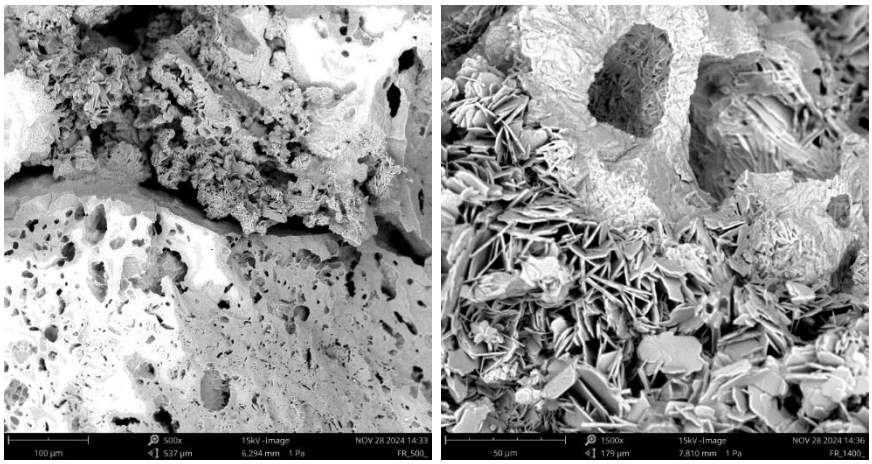

Figure 11 Examples of the structure of CAC paste exposed to 1400 °C

2.4.4 Other degradation processes

Similarly to PC, in the case of CAC, carbonation is also an important process affecting the performance and durability of the cement-based material. The mechanism is similar; carbon dioxide (CO_2) from the atmosphere penetrates the material and reacts with a cement matrix. Contrary to the PC, where the main reactant for carbonation is Portlandite, in the case of CAC, all calcium aluminate hydrates (C-A-H phases) can undergo carbonation, resulting in the formation of calcium carbonate ($CaCO_3$), alumina hydroxide (AH_3), and the release of water. It begins at the exposed surfaces of the material and progresses inward over time. Initially, the reaction leads to the formation of metastable calcium carbonate polymorphs such as vaterite or aragonite. As the carbonation process continues, these carbonates gradually recrystallise into calcite. Regarding the structure of alumina hydroxide (AH_3), it is, in most cases, gibbsite; rarely, bayerite or norstrandite can occur [28]. The rate and extent of carbonation are influenced by several factors, mainly by moisture content, porosity, environmental CO_2 level, and temperature. The carbonation reactions can be summarised by the following equations [5]:

$$CAH_{10} + CO_2 \rightarrow CaCO_3 + AH_3 + 7H \quad (9)$$

$$C_2AH_8 + 2CO_2 \rightarrow CaCO_3 + AH_3 + 5H \quad (10)$$

$$C_3AH_6 + 3CO_2 \rightarrow 3CaCO_3 + AH_3 + 3H \quad (11)$$

As in the case of PC, carbonation of CAC initially leads to densification of the matrix, reducing porosity and enhancing surface hardness, which improves resistance to chemical attack and limits further degradation by restricting water ingress. In fact, controlled carbonation curing can serve as a prevention for the conversion, because the metastable hydrates are transformed during carbonation and thus no changes and porosity increase further occur [29,30]; however, the formation of calcium carbonate ($CaCO_3$) is not beneficial from the point of thermal resistance.

In the presence of alkalis, the decomposition of calcium aluminate hydrates occurs at a significantly accelerated rate. This phenomenon, known as alkaline hydrolysis, results in a substantial reduction in mechanical strength [5]. Among calcium aluminate hydrates, katoite (C_3AH_6) is particularly prone to decomposition, while calcium aluminate decahydrate (CAH_{10}) demonstrates relatively higher resistance to this process [31]. For instance, the reactions with potassium carbonate serve as a notable example of alkaline hydrolysis.

$$CaO.Al_2O_3.10H_2O + K_2CO_3 \rightarrow CaCO_3 + K_2O.Al_2O_3 + 10H_2O \quad (12)$$

$$3 * 3CaO.Al_2O_3.6H_2O + K_2CO_3 \rightarrow 3CaCO_3 + K_2O.Al_2O_3 + 6H_2O \quad (13)$$

$$K_2O.Al_2O_3 + CO_2 \rightarrow K_2CO_3 + Al_2O_3 \quad (14)$$

When compared to conversion, alkaline hydrolysis is a much faster process, with noticeable effects often observed within just one week. Furthermore, these two processes (conversion and alkaline hydrolysis) exhibit a synergistic relationship. Conversion leads to an increase in porosity, which, in turn, enhances the material's permeability. This higher permeability facilitates alkaline hydrolysis, creating a feedback loop that accelerates degradation. Conversely, the progression of alkaline hydrolysis significantly reduces the quantity of katoite (C_3AH_6) in the system. This shift alters the equilibrium, further driving the conversion process [31]. Other factors affecting the rate of alkaline hydrolysis are alkali concentration, temperature, porosity or permeability, more precisely, and of course phase composition of cement. Regarding the alkali, not only concentration but also the type of alkaline is important, e.g. NaOH is more deteriorating than KOH.

3 Suitable additives for CAC

Calcium aluminate cement, such as every other cement, can be enhanced with additives to improve its performance and adapt it to specific applications. These substances are usually liquid materials introduced into the concrete mix (during the mixing) in lower amounts, up to 5% of the cement mass. Additives can influence the hydration kinetics, mechanical strength, durability, and resistance to environmental factors.

3.1 Cement additives

The vast majority of commercially available chemical additives have been developed and optimised primarily for ordinary Portland cement. The hydration chemistry of OPC, dominated by silicate and aluminate phases such as tricalcium silicate (C_3S) and tricalcium aluminate (C_3A), is well understood and has shaped the evolution of additives formulations over the past decades. In contrast, calcium aluminate cements (CAC) present a distinct mineralogical and chemical system, characterised by rapid hydration of calcium aluminate phases and the risk of conversion of metastable hydrates over time. Despite these unique features, the research and development of additives specifically tailored to CACs remains limited. Most available data on additive performance derive from studies on Portland cement systems, leaving a knowledge gap regarding their effectiveness, compatibility, and optimisation in CAC-based materials. Therefore, the following chapter summarises the state of the art of commonly used chemical additives, with an emphasis on their mechanisms and applications in Portland cement. This review serves as a necessary foundation before addressing the more specialised and less-explored topic of additives suitable for calcium aluminate cement systems.

3.1.1 Plasticisers and superplasticisers

Plasticisers are the most frequently used type of additive in concrete production. Their addition improves cement mix workability, reduces water content, and modifies rheological properties. Consequently, they improve the mechanical properties and durability of the final hardened concretes. These substances play a crucial role in enhancing the properties of cement and the final concrete product. The development of high-performance concrete relied significantly on the incorporation of plasticisers and superplasticisers.

Plasticisers, also known as water reducers, facilitate a higher degree of dispersion of cement particles, reducing porosity and mitigating microcracks. This is achieved through their surface-active properties, where polymer molecules are adsorbed onto the surface of cement particles, creating a negative charge (measured in millivolts). This electrostatic repulsion between the particles leads to their dispersion, freeing water bound within the cement structure and consequently increasing the fluidity of the mix. The water-cement ratio can be reduced significantly, sometimes to as low as 0.3, without compromising workability. The common representatives are lignosulfonic and hydroxycarboxylic acids and their salts.

Despite their advantages, plasticisers are not without drawbacks. Their chemical composition often contains impurities, which can introduce variability in performance. Additionally, they may delay the setting time and induce air entrainment due to bubble formation. However, targeted modifications and optimisation of these compounds can address such challenges. This optimisation led to the development of superplasticisers, also referred to as "high-range water reducers,". These synthetic compounds are more effective in achieving superior fluidity and workability while maintaining a lower water-cement ratio, even about 0.16. Compared to conventional plasticisers, superplasticisers provide a higher primary effect without adverse secondary phenomena. The mechanism of superplasticisers' action is based on electrostatic repulsion, similar to plasticisers, but also provides a steric hindrance, depending on the type. This spatial effect is derived from long polymer chains of superplasticisers that extend into the surrounding solution. These chains physically block particles from coming close to one another, creating a "protective shield" and further enhancing the dispersion of cement grains. The most common representatives are summarised in the following Table 5.

Plasticising additives are typically dosed 1–2 minutes after mixing cement with water to maximise their effectiveness. However, their effect is time-limited, which can pose challenges during the transportation of concrete. Solutions include the addition of hydration retarders or delaying the introduction of superplasticisers until the concrete reaches the construction site. The critical factor in the use of superplasticisers is achieving the saturation point. Above this concentration, additional amounts of the plasticiser do not result in further increases in fluidity. This highlights the importance of precise dosing to balance performance and cost efficiency.

Table 5 List of commonly used superplasticisers

Chemical base	Modified Lignosulfonates	Sulfonated Naphthalene Formaldehyde	Sulfonated Melamine Formaldehyde	Polycarboxylates
Abbreviation	MLS	SNF	SMF	PC
Developed	1960s – 1970s	1960s	1970s	1980s – 1990s
Primary Mechanism	Electrostatic repulsion	Electrostatic repulsion	Electrostatic repulsion	Electrostatic repulsion + steric hindrance
Dosage	0.2 – 0.6%	0.5 – 1.5%	0.5 – 1.5%	0.2 – 1.0%
Effectivity	Moderate	High	High	Very High
Water Reduction	8 – 15%	15 – 25%	15 – 25%	20 – 30% or more
Limitations	Limited water reduction, impurities	Time-limited, minimal steric hindrance	Expensive, time-limited action	Expensive, sensitive to dosage

3.1.2 Accelerators

Accelerators are additives used in concrete to speed up the rate of cement hydration, resulting in faster setting and strength development. They are useful in casting in cold weather conditions or when higher early strength is required for construction processes like formwork removal or early load application. Another application lay in the precast concrete and repair works. The primary mechanism of their action is increasing the dissolution of cement particles, providing more ions for faster reactions and also providing nucleation sites for the faster generation of hydration products. This way, they reduce the induction period of hydration. However, they also affect the structural formation and rheological behaviour of cement pastes.

According to the chemical basis, accelerators can be divided into inorganic and organic groups. From the inorganic represents it can be named, for example, calcium chloride ($CaCl_2$), which belongs to the oldest used and most effective accelerator. However, its use is limited because chloride ions promote the corrosion of steel reinforcement through electrochemical processes. As a result, calcium chloride-based accelerators are not suitable for steel-reinforced or prestressed concrete. On that account, non-chloride accelerators have been developed based on calcium nitrate ($Ca(NO_3)_2$) or sodium carbonate (Na_2CO_3). They typically exhibit slightly lower acceleration efficiency for silicate hydration, meaning that their early strength development may be somewhat slower. Later, other representatives of inorganic accelerators include thiocyanate-based compounds. They do not introduce chloride

ions, making them suitable for reinforced concrete; however, their use is limited by cost, potential toxicity, and environmental concerns. Regarding the organic group of accelerators, formates have gained popularity, particularly for use in cold-weather concreting. A more recent development in acceleration chemistry involves the use of alkanolamines. They are particularly useful in combination with other additives, such as superplasticisers, and in blended cement systems. Table 6 provides a summary of commonly used accelerators and together with their properties.

Table 6 List of commonly used accelerators [32–34]

Chemical base	**Calcium/ sodium chloride**	**Nitrates/ carbonates**	**Thio-cyanates**	**Formates**	**Alkano-lamines**
Primary component	$CaCl_2$,NaCl	$Ca(NO_3)_2$, Na_2CO_3	NaSCN, KSCN	$Ca(HCOO)_2$	DEA, TEA, TIPA, DEIPA
Developed	Early 20th century	Mid 20th century	1970s–1980s	1980s–1990s	2000s
Target phase	C_3S and C_3A	C_3A and gypsum	C_3S and C_3A	C_3S and C_3A	C_3A, C_4AF
Dosage	0.5 – 2%	1.0 – 3.0%	0.2 – 1.0%	0.5 – 2.0%	0.1 – 0.3%
Effectivity	Highest	Considerable	Moderate	High	Moderate
Advantages	Cost-effective, rapid hydration	Effective in cold, Nitrates – corrosion inhibitors	Fast setting	Effective in cold, compatible with various cements	Enhance workability
Limitations	Steel reinforcement corrosion	Moderate cost, risk of higher porosity	Higher cost, toxicity, and potential AAR	Higher cost, risk of flash setting	Risk of flash setting

3.1.3 Retarders

Contrary to the accelerators, retarders are chemical additives designed to delay the hydration reactions of cement, extending setting times and slowing early strength development. They are critical in hot-weather concreting, where high ambient temperatures accelerate hydration excessively, as well as in complex concrete pours, mass concrete structures, and oil well cementing, where longer working times are needed to ensure proper placement and finishing.

The use of retarders in cementitious systems dates back to the early 20th century, coinciding with the industrial expansion of concrete as a structural material. The first retarders were organic substances, often discovered accidentally when sugar-contaminated water or molasses-contaminated aggregates delayed cement setting.

Early empirical observations highlighted that certain natural products, particularly sugars and organic acids, could profoundly influence setting times. Later studies led to the industrial use of lignosulfonates, by-products of the wood pulping industry, as the first standardised retarding and water-reducing additives. These were followed by the development of inorganic retarders such as phosphates and borates, particularly suited for high-temperature applications, including oilwell cementing. These compounds typically interact with cement hydration by adsorbing onto clinker grain surfaces or forming insoluble complexes with calcium or aluminium ions, thus delaying the nucleation of hydration products. With the advancements in coordination chemistry, the role of ion complexation in retarder performance leads to fine-tuning of organic retarders such as citric acid. In recent decades, research has focused on refining retarder formulations for specialised cement systems, including high-performance concrete, self-compacting concrete, and 3D-printed materials, where precise hydration control is essential. Basic information about commonly used retarders is summarised in Table 7.

Table 7 List of commonly used retarders [35–37]

Chemical base	**Sugar**	**Ligno-sulfonates**	**Phosphates**	**Citrates / Glauconate**	**Borates**
Developed	Early 20th century	1940s–1950s	Mid 20th century	1960s–1970s	1950s–1960s
Mechanism	Inhibit dissolution and nucleation; chelate Ca^{2+}	Disperse particles, retard ion dissolution	Form insoluble calcium phosphate layers	Chelate Ca^{2+},	Form calcium borate complexes
Target phase	C_3S	C_3S and C_3A	C_3A	C_3S	C_3A
Dosage	0.01 – 0.1%	0.1 – 0.5%	0.2 – 1.0%	0.1 – 0.5%	0.2 – 1.0%
Effectivity	High	Moderate	High	Moderate	High
Advantages	Natural origin	Water reducer	Effective at high temperatures	Compatible with blended cements	Effective at high temperatures
Limitations	Sensitive to overdose	Variability in purity	Risk of strength reduction	High cost, week at high temperature	Risk of brittle structure formation

3.1.4 Other additives

In addition to the most utilised above-described additives, modern concrete technology employs a wide range of other chemical substances to optimise specific

properties of cement-based materials. These additives are designed to enhance durability, improve workability retention, control air content, reduce shrinkage, or provide specialised functional properties like corrosion inhibitors or alkali-resistance additives. Their role has become increasingly important with the growing use of high-performance concretes and blended cements.

Air-entraining agents are used to introduce and stabilise microscopic air bubbles within the concrete matrix. These fine, uniformly distributed air voids enhance freeze-thaw durability by providing space for ice expansion. Air-entraining agents are typically based on synthetic surfactants, wood resins, or fatty acid salts, which lower the surface tension of mixing water and stabilise air during mixing. Their careful dosage is essential, as excessive air can reduce strength.

Shrinkage-reducing additives aim to minimise drying shrinkage, one of the main causes of cracking in hardened concrete. These additives function by reducing the capillary stresses within the pore solution during moisture loss. Common shrinkage-reducing additives are based on polyethene glycol derivatives or propylene glycol, which alter the liquid's surface tension and evaporation behaviour. By mitigating shrinkage, they help preserve structural integrity in exposed slabs, precast components, and large-volume pours.

Corrosion inhibitors are used in reinforced concrete to protect steel rebar from corrosion, especially in chloride-rich environments like coastal areas or roadways and bridges exposed to de-icing salts. They work either by forming a protective film on steel surfaces (organic inhibitors like amines) or by modifying the electrolyte chemistry (calcium nitrite). These additives extend the service life of concrete structures by delaying the onset of corrosion-induced cracking.

Viscosity-modifying additives have gained considerable attention in recent years, driven by the development of self-compacting concrete, 3D-printed concrete, and other advanced placement technologies where precise rheological control is essential. Additives, based on cellulose ethers, polysaccharides, or synthetic polymers, increase the viscosity of the mix, preventing segregation and bleeding while maintaining flowability. This is essential for complex placements where consistent workability and shape retention are required.

3.2 Author contribution – selected paper

Due to the unique hydration pathways of calcium aluminate cement, conventional additives designed for PC are often ineffective or incompatible with CAC. Unfortunately, these aspects are somewhat ignored in current research. Consequently, recent research has focused on the assessment of chemical additives suitable for CAC systems, aiming to optimise setting behaviour, rheology, and durability without triggering adverse hydration phase transitions.

3.2.1 Impact of plasticiser' types on the performance of calcium aluminate cement

D. Koňáková, V. Pommer, K. Šádková, M. Keppert, R. Černý, E. Vejmelková, Journal of Material Research and Technology 20 (2022) 1512–1523. [38] https://doi.org/10.1016/j.jmrt.2022.07.155

The selected paper represents a significant contribution to the understanding of chemical additives in calcium aluminate cement (CAC) systems, specifically focusing on plasticisers and their influence on hydration, microstructure, and thermo-mechanical performance. Recognising the gap in existing literature, where most plasticiser research is tailored for ordinary Portland cement, there are systematically studied the performance of four distinct plasticiser types: melamine-formaldehyde resin, lignosulfonate, polycarboxylates, and modified polycarboxylates.

The research demonstrated that these plasticisers significantly influence the hydration kinetics and phase assemblage of CAC. Detailed mineralogical analyses (XRD, STA) confirmed that plasticisers modify the balance between metastable and stable calcium aluminate hydrates (CAH_{10}, C_2AH_8, C_3AH_6, AH_3). Among them, modified polycarboxylates were identified as the most promising additive, offering a balance between workability enhancement and mechanical performance, while minimising adverse effects such as excessive retardation or porosity increase. In contrast, melamine-formaldehyde resins were found to be unsuitable, as they resulted in high porosity and poor mechanical performance.

Beyond hydration chemistry, the study also addressed the temperature-dependent performance of CAC composites. By analysing the porosity, mechanical strength, and dynamic modulus up to 1400 °C, the author demonstrated how selected additives influence the thermal stability of CAC systems, a topic scarcely addressed in prior

literature. Importantly, the research provided practical recommendations for dosage optimisation, highlighting the susceptibility of CAC to bleeding and rapid setting when additives are misapplied.

Key findings include:

- Additives - cement phase compatibility
- Thermal stability of CAC composites with plasticisers
- Practical guidelines for formulating high-performance CAC-based materials for refractory and structural applications.

These findings form a basis for future research into tailored additive formulations for non-Portland systems, contributing both to academic understanding and industrial practice.

Available online at www.sciencedirect.com

jmr&t Journal of Materials Research and Technology

journal homepage: www.elsevier.com/locate/jmrt

Original Article

Impact of plasticizers' types on the performance of calcium aluminate cement

*Dana Koňáková**, *Vojtěch Pommer*, *Kateřina Šádková*, *Martin Keppert*, *Robert Černý*, *Eva Vejmelková*

Department of Materials Engineering and Chemistry, Faculty of Civil Engineering, Czech Technical University in Prague, Thákurova 7, 166 29 Prague 6, Czech Republic

ARTICLE INFO

Article history:
Received 21 April 2022
Accepted 26 July 2022
Available online 10 August 2022

Keywords:
Calcium aluminate cement
Plasticizers
Simultaneous thermal analysis
X ray diffraction
Mechanical properties
Thermal strain

ABSTRACT

Nowadays it is almost impossible to design a cement based mixture without the application of some plasticizing additives. There have been developed many types of plasticizers, but they are mostly directed for Portland cement applications. In the case of calcium aluminate cement (CAC), they are also widely employed, but their impact has not been properly studied yet. In this paper, four different bases of plasticizers are investigated through the view of their impact on the composition of hardened CAC paste and on the physical properties of CAC composites as well. The most convenient additive for refractories was found to be plasticizer based on modified polycarboxylates. For the application of CAC at ambient temperature the best solution was the polycarboxylates. However, the dosage of latter have to be performed carefully, because these mixtures are susceptible to bleeding. On the other hand, the melamine formaldehyde resin was assessed as an unsuitable plasticiser for CAC.

© 2022 The Author(s). Published by Elsevier B.V. This is an open access article under the CC BY license (http://creativecommons.org/licenses/by/4.0/).

1. Introduction

Nowadays it is almost impossible to design cement based mixtures without the application of some chemical additives, such as accelerators, retarders, foamers, and extenders. The most crucial additive for the development of modern kinds of concrete is indisputable plasticizing respectively dispersant additives [1,2]. Many types of plasticizers have been developed, but they have been mostly dedicated to ordinary Portland cement (OPC) based composites [3,4]. However, they are commonly used also in the case of other binders, usually unfortunately without proper assessment of the plasticizer's application impact. One of the binders is calcium aluminate cement (CAC). It is a crucial binder for castable refractories. Despite its several limitations, its employment is almost irreplaceable [5].

One of CAC's disadvantages is that its hydration is highly influenced by many factors, such as temperature, the molar ratio of calcium oxide and aluminium oxide, curing condition, and water/cement ratio. The most crucial is the impact of curing temperature. Nowadays it is assumed, that the hydration products depending on curing temperature are as follows [6–9]: Below 15 °C, the metastable CAH_{10} is the only C A H which

* Corresponding author.
E mail address: dana.konakova@fsv.cvut.cz (D. Koňáková).
https://doi.org/10.1016/j.jmrt.2022.07.155
2238 7854/© 2022 The Author(s). Published by Elsevier B.V. This is an open access article under the CC BY license (http://creativecommons.org/licenses/by/4.0/).

arises. In the temperature range between 15 and 27 °C, the main product is metastable C_2AH_8, which is continuously replaced by stable katoite C_3AH_6 in higher temperatures. Over 35 °C katoite C_3AH_6 is the only arising phase among C A H. However, this phenomenon should not be significant, but metastable hydrates are during time converted to stable katoite C_3AH_6 [10–12]. This conversion is due to the higher specific gravity of katoite C_3AH_6 (compared to metastable CAH_{10} and C_2AH_8), accompanied by porosity growth and thus a significant fall of compressive strength. Not only the curing temperature but also the hygric environment has an important influence on the hydration of CAC. Contrary to the OPC, it seems to be more appropriate to cure CAC based materials in the air than submerged in the water. Another important factor influencing the performance of hardened CAC based composite is the water/cement (w/c) ratio. Similar to the OPC, as the water dosage grows, compressive strength goes noticeably down [13]. On the other hand, a higher w/c ratio is recommended to prevent the negative impact of the conversion process.

It is evident, that performance of CAC is much more complicated than in the case of an OPC. On that account, it seems to be crucial to carefully assess the impact of any other raw materials used in combination with CAC. Especially, the impact of chemical additives can be of great importance, as they somehow influence the hydration process of CAC in their nature. However, only a few studies dealing with this theme can be found. It can be named the work of Engbert et al. [9], who studied the effect of alginates on CAC's hydration and examined also the combination of the alginates with polycarboxylates based plasticizer. They reported beneficial performance of these mixtures, as the polycarboxylates improved workability, and retarded the hydration, which was accelerated by alginates application. On the other hand, Met wali et al. [14] reported intercalation of polycarboxylates based superplasticizers into hydrates of CAC. This was confirmed by Alonso et al. [15]. Moreover, they presented, that polycarboxylate not only retard hydration but also strongly decreases the total amount of generated hydrates. Oliveira and Pandolfelli [16] dealt with anhydrous citric acid and two kinds of polycarboxylates ethers in combination with medium aluminate cement. They presented, that used plasticizers served not only as dispersant additives but had an impact also on the formation of a hydrated structure and their decompo sition due to the temperature exposure as well. According to their study, the polycarboxylates ether was found to be the most efficient dispersant for CAC. Its application induced the formation of AH_3 at ambient temperature and favoured the creation of CA_2 and CA_6 at a higher temperature. Wang et al. [17] studied the impact of sulfonate formaldehyde conden sate, sodium tripolyphosphate and propionic acid used as dispersants for spinel containing calcium aluminate cement. They reported that the application of dispersants has a sub stantial impact on the morphology of formed hydrates. Plas ticizers also influenced values of compressive strengths and cold modulus of rupture. Propionic acid was found to be the most efficient and proposed the highest compressive strength. Unfortunately, both studies of Oliveira and Pandofelli [16] as well as Wang et al. [17] did not contain reference materials without any plasticizing additives, and thus the evaluation of the additives' impact cannot be used for further credible comparison. On the contrary, in the study performed by Kri voborodov et al. [18], the reference material has been consid ered. They focused on technical calcium aluminates and studied the impact of two plasticizers. The first contained sulfonated polycondensates and sodium sulphate, while the second was based on sulfosalicylic acid. The improving impact of plasticizers was indisputable. They reported that their application substantially reduced the loss of concretes' strength after heating up to 900 °C. Idrees et al. [19] studied the possi bilities of varying mineral admixtures for CAC mortars. How ever, in the case of reference pastes, they used powder super plasticizing additive. They reported beneficial performance, as the material based on CAC with superplasticizer showed the highest compressive strength among studied mortars. But on the other hand, the hydration was retarded (by about 2 h) and specific hydration heat power decreased as well.

Contrary, there can be found in several studies, where some kind of dispersants were used, but without an assessment of their impact on CAC performance. Lee et al. [20] investigated the microstructural performance of calcium aluminate cement based UHPC and used a superplasticizer (unknown type) in each case of their mixtures. As well as Salomao et al. [21] used dispersant ad ditives (specifically modified polycarboxylates based) in all mix tures when they studied the formation of hibonite in the castable alumina. Roig Flores et al. [22] investigated thermo mechanical properties of CAC based concrete with varying aggregates and used lignosulphonate based plasticizer in all cases of studied mixtures. Similarly, in the study performed by Wan et al. [23] polycarboxylate based superplasticizer was used for workability improvement in all studied aluminate cement adhesives for por celain insulators, regardless of the possible impact of the additive. It can be named also a study by Abolhasani et al. [24], who used polycarboxylates based plasticizers and dealt with CAC based material at elevated temperatures.

As it was mentioned here in above, plasticizers are often used in the case of CAC based cement. It is evident from the literature review, that plasticizers could propose beneficial improvements not only in workability but in the overall per formance of final composites. However, their impact has to be properly assessed, to be able to consider all possible issues connected with their unappropriated utilization. For those reasons, commonly used plasticizers with different chemical bases were studied in this article. Their impact on rheological properties was assessed through the flow of fresh mixtures, more precisely through the varying w/c ratio necessary for equal consistency. However, the main attention was paid to the performance of hardened materials. The impact of the varying additives and their appropriateness for CAC was assessed through the view of cement stone characterization and mainly through the view of basic physical, mechanical and thermomechanical properties of hardened materials at ambient and high temperature conditions.

2. Experimental methods

2.1. *Technological properties*

Consistency of fresh pastes was measured by Vicat apparatus with penetration plunge, the method according to standard

[25] was adopted, and the reached values of penetration depth were read after the stabilization of the plunge.

Consistency of fresh mixture was described by the employment of flow. For the determination, the standard method for mortars [26] was used, since it is applicable also for those mixtures with fine aggregate. The fresh mixture was put in the special mould with the shape of a truncated cone. After its compacting, the mould was given away and the flow table was lifted and dropped 15 times. Two orthogonal diameters of flowed mixtures characterize the mixture flow.

For determination of setting times, the automatic Vicat needle device from FORM + TEST Seidner&Co. GmbH was used. This equipment automatically performs plunges in predefined intervals and records depths of needle penetration. Final initial and setting times were determined in accordance with the standard [25].

2.2. Material characterization

For a determination of granulometry of fine components, the laser diffraction method was employed (Bettersizer S3 Plus device). Granulometric curves of aggregates were determined by grading tests according to standards [27].

The phase composition of raw materials as well as of prepared composites was studied by X ray diffraction (XRD) using a PANalytical Aeris system with a $Co_{K\alpha}$ tube. The qualification of phases was performed by using HighScore, while for the quantification the Profex software [28] (which employed Rietveld analysis with internal standard (20% of ZnO)) was employed.

Simultaneous thermal analysis (STA), consisting of differential scanning calorimetry (DSC) and thermogravimetry (TG), was carried out using a Labsys EVO TG/DSC from Setaram Inc. The experiments were done in the temperature range from 30 to 500 °C with a heating rate of 5 °C min^{-1} and in an argon atmosphere with a flow rate of 40 ml min^{-1}.

2.3. Basic physical properties

Matrix density, bulk density and open porosity were measured by the following methods: Matrix density was determined by helium pycnometer (Pycnomatic ATC, Thermo Fisher Scientific Inc.). Bulk density was determined by the gravimetric method. Consequently, the values of porosity were counted based on the known values of matrix density and bulk density.

Characterization of a pore structure was performed by mercury intrusion porosimetry. Measurement was conducted using instruments Pascal 140 + 440 made by Thermo Fisher Scientific Inc. The range of an applied pressure corresponded to the pore radius from 10 nm to 100 μm.

2.4. Mechanical parameters

Mechanical properties, specifically compressive strength and bending strength, were measured according to the standard [29]. Determination of bending strength was performed on three samples (40 × 40 × 160 mm) using the loading device MTS 100. The arrangement of the experiment was a classical three point bending with a 100 mm span length. Compressive strength was then measured on fragments from the bending strength experiments. The loading device EU40 was used.

Dynamic modulus of elasticity was measured by ultra sound testing [30] before actual loading of specimens used for determination of mechanical strengths. Specifically, The Proceq PunditLab+ ultrasonic velocity instrument with the 54 kHz pulse transducer was used to determine the ultrasound speed. The one dimensional adjustment was employed and the ambient dimensionality coefficient was assumed to be 1.

2.5. Thermomechanical analysis

Thermal strain depending on temperature was measured by a linear thermal horizontal dilatometer [31]. The device utilizes a comparative method when the real thermal expansion is determined by comparing the analysed specimen with a reference corundum rod. Three specimens with the dimensions of 15 × 15 × 160 mm were used for a particular measurement. The maximal temperature of measurement was 1000 °C and the heating rate was set as 1 °C per min.

3. Studied materials

3.1. Raw materials and their characterization

Four kinds of plasticizers were chosen for the need of this study. As was already mentioned, such kinds of additives are commonly used in the concrete industry, more precisely in the production of cement based composites. In general, they can have a different chemical base, dosage, colour, and properties. Chosen additives belonged to the commonly used plasticizers in the field of OPC based composites. They were also several times used in combination with CAC (but without further assessment of their impact). The list of chosen materials can be found in Table 1. All of them were commercially available products. The first three were produced by Stachema CZ,s.r.o. and the last one by Sika CZ, s.r.o. Specifically, commercial products were used as follows: Stachement MM was melamine formaldehyde resin, Stacheplast 17 was lignosulfonate, Stachement 508 was polycarboxylates and ViscoCrete® 2700 was modified polycarboxylates. It is visible that

Table 1 – Studied plasticizers.

Chemical base	Label	Colour	Density [kg m^{-3}]	pH	Max. alkali content	Dry matter content
Melamine formaldehyde resin	F	bright	1250	9 11	8%	40%
Lignosulfonate	L	deep brown	1210	8 11.5	8%	40%
Polycarboxylates	P	reddish brown	1070	5 7	2%	30%
Modified polycarboxylates	M	yellowish	1060	1 4.5	1%	30%

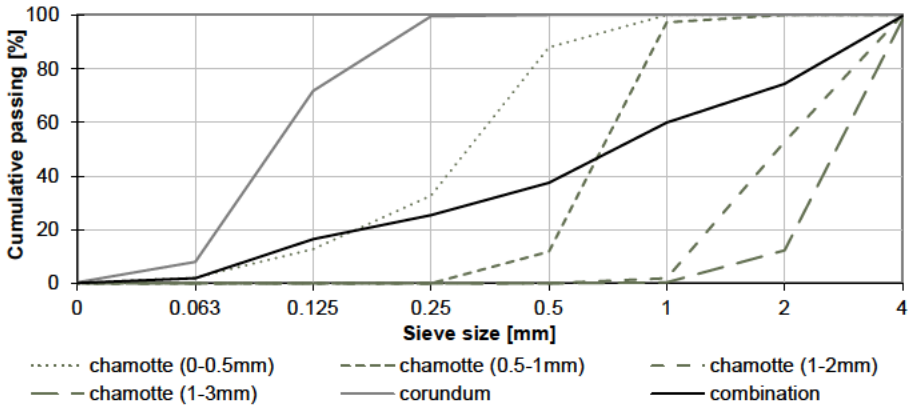

Fig. 1 – Granulometric curves of used aggregates.

they differ not only in chemical base, but also in the density and pH varied widely. Also, alkali content (Na_2O equivalent) showed different values, especially in the case of poly carboxylates and modified polycarboxylates.

The binder used for the need of this study was medium aluminate cement, specifically Secar71 produced by Kerneos Inc. It contained 70.7% of Al_2O_3, 28.2% of CaO and its main phase composition was 35.8% grossite ($CaO.2Al_2O_3$) and 55.1% krotite ($CaO.Al_2O_3$). The specific surface area was 381 m^2 kg^{-1} and D_{50} was 7.7 μm. The initial setting time of the binder was 255 min and its final setting time was 285 min.

The used aggregate was of two kinds. Primarily four gra dins of chamotte (suplied by České lupkové závody, a.s) par ticles were chosen and complemented by one grade of fine corundum. According to XRD measurements, chamotte is composed of 64.7% mullite, 3.6% quartz and 2.9% cristobalite, while corundum with a purity of 92% was complemented by 8% of β alumina ($Na_2O{\cdot}11Al_2O_3$). Designed granulometric curves can be found in Fig. 1

3.2. *Composition and production process of studied mixtures*

The evaluation of varying plasticizers' impact on the perfor mance of CAC was divided into two parts. Firstly, cement pastes were prepared. They were studied through the virtue of phase composition and basic physical properties at ambient temper ature. Particular compositions of mixtures can be found in Table 2. For all plasticizer types, cement pastes with two varying ad ditives' amounts were prepared. Specifically, the minimal and maximal amount of recommended dosages for PC was employed. Pure cement paste R was produced as well and served as the reference material. Regarding the w/c ratio, it was different in all cases. The main aim was to produce pastes with a comparable consistency. Therefore, the w/c ratio was set experimentally based on the performed measurement of stan dard consistency. All designed materials were produced with the penetration depth in the range of standard requirements [25]; specifically, 6 ± 2 mm from the bottom of the mould. It is worth mentioning, that the melamine formaldehyde resin and lignosulphonate based plasticizers caused only minor de creases in water consumption, while in the case of poly carboxylates and especially modified polycarboxylates, the water dosage requirements were significantly lowered.

Moreover, the initial and final setting times were measured as well. Reached values are also included in Table 2. Except for the modified polycarboxylates, all plasticizing additives caused delays in the initial setting times. The lowest changes were observed in the case of polycarboxylate based plasti cizer, and the biggest in the case of lignosulphonates. Mean while, the final setting times were significantly extended in all cases of studied additives, especially in the case of ligno sulphonate the extension was extreme. Contrary, the lowest impact on the final setting times was observed in the case of melamine formaldehyde resin, which also showed the lowest changes in the overall setting times.

In the second part of the work, CAC based composites with aggregates were designed. Their composition is presented in Table 3. The main aim was to assess the impact of plasticizers on the properties of composites, specifically on pore structure and mechanical properties. The dosage of plasticizers was this time set equal for all cases, specifically 1%, which is the approximate average value of recommended dosages. Con cerning the water dosage, the w/c ratios were different for all

Table 2 – Composition of cement pastes.

	R	F1	F2	L1	L2	P1	P2	M1	M2
Calcium aluminate cement [g]	600	600	600	600	600	600	600	600	600
Plasticizer [%]		0.4	1.4	0.6	1.3	0.4	1.4	0.2	2.5
w/c ratio	0.30	0.30	0.28	0.25	0.23	0.17	0.15	0.22	0.15
Initial setting time [min]	205	240	280	300	330	210	210	180	180
Final setting time [min]	280	330	435	800	870	570	630	360	450

Table 3 – Composition of cement composites [kg m ^{3}].

	R	F	L	P	M
Calcium aluminate cement	500	500	500	500	500
Chamotte (0 0.5 mm)	250	250	250	250	250
Chamotte (0.5 1 mm)	350	350	350	350	350
Chamotte (1 2 mm)	350	350	350	350	350
Chamotte (1 3 mm)	300	300	300	300	300
White corundum	250	250	250	250	250
Plasticizer	0	5	5	5	5
w/c	0.514	0.500	0.510	0.455	0.400

cases of studied composites. Similar to previous cases, the main aim was to produce comparable composites with the same workability. As the comparative property, the flow of the fresh mixture was employed. The reference composite R showed the flow of 140/140 mm and the others with plasti cizing additives were designed to show equal value. On that account, the w/c ratio differed.

Three cubes with the edge of 50 mm of particular pastes and twelve prismatic specimens with dimensions of 40 × 40 × 40 mm of particular composites were prepared (see Fig. 2). Specimens were prepared in laboratory conditions (20 ± 1 °C and relative humidity 25–30%). Primarily the dry components were properly mixed. Then third of the expected water dosage mixed with plasticizers was poured in. After wards, the water was continuously added up to the reaching desired consistency (flow of 140/140 mm). The prepared mix was then put into the plastic mould and compacted on the vibration table. Final compacted specimens were covered by plastic film. After one day they were demoulded and put into the climatic chamber with a controlled temperature of 20 °C and RH 50%. It is worth mentioning, that both polycarboxylate based and modified polycarboxylates based plasticizers significantly changed the performance of fresh mixtures. Such mixes were extremely flowable, but hard. They were also susceptible to bleeding, thus the water dosage had to be set carefully.

Experimental measurements were done after 28 days of curing. Before actual experiments, nine specimens of cement composites were exposed to temperature loadings (see Fig. 3). These specimens were initially dried in the oven at 105 °C. Then three of them were heated to the temperature of 400, 1000 or 1400 °C respectively. The heating rate was 1 °C min ^{1} and the exposure duration was 3 h. Samples were then left to spontaneous cooling.

4. Achieved results and discussion

4.1. *Cement pastes*

4.1.1. *Composition of hardened cement paste*

In the following graphs, results of hardened cement pastes characterizations are presented. Specifically, in Fig. 4 there are X ray diffractograms, in Fig. 5 results of X ray quantitative analysis are shown, Fig. 6 contains results of thermal analysis and in Fig. 7 thermogravimetry can be found. To be able to accurately describe the composition of hardened cement stone, it seems to be more accurate to combine these methods. There are several issues, which complicated the phase quantification in CAC hydrated systems. The first problem is an unknown structure of C_2AH_8, which make quantification of this phase by Rietveld refinement impos sible. Regarding the results of DSC, the overlapped ranges of temperature decomposition complicate the phase quantifi cation as well. Moreover, by combining the used experimental methods, the presented results can be verified [32]. For the assessment of hydration degree, the average percentual

Fig. 2 – Production process of cement composites.

Fig. 3 – Thermal loading of cement composites.

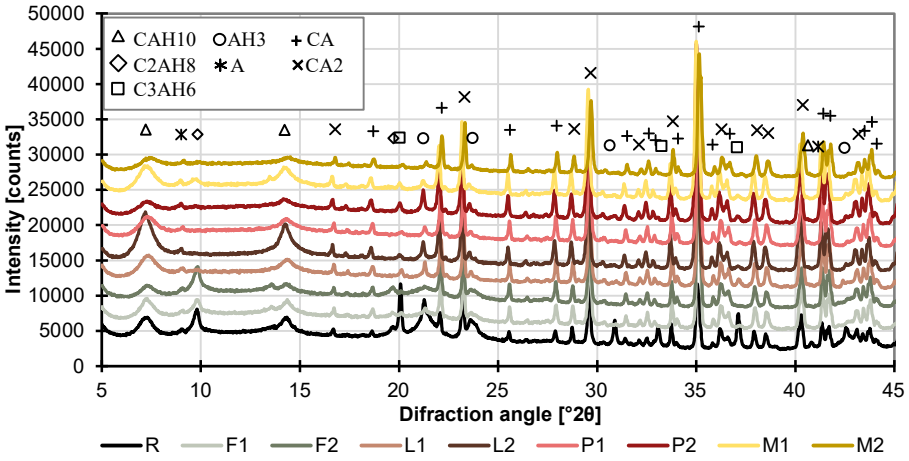

Fig. 4 – X-ray diffractograms of cement pastes.

decrease of krotite and grossite content in the hardened pastes related to the amount of the latter mineral in the fresh mixture (more precisely in the raw cement) was counted.

Reference paste R with no plasticizers showed the highest hydration degree, about 69% of CAC was hydrated. Regarding its composition, this paste was the only one with converted composition. Thus, it contained a much higher amount of katoite C_3AH_6 and crystalline AH_3 (primarily in the form of gibbsite). Regarding other hydrated phases, C_2AH_8, as well as CAH10, were observed in minor amounts.

The impact of melamine formaldehyde resin on cement paste hydration was the lowest among the studied additives. The most noticeable change was a decrease in hydration de gree; it was about 53% and 52% for paste F1 and F2 respec tively. Regarding the hydrates' composition, the amount of metastable hydrates CAH_{10} and C_2AH_8 seemed to be un changed. In contrast with reference paste, only a minor amount of C_3AH_6 was observed. Simultaneously, the amount of crystal AH_3 was decreased by 61% and 50% for F1 and F2 respectively. Nevertheless, the difference between the two dosages of the plasticizer was not considerable.

Lignosulphonate based plasticizer caused a further decrease in hydration degree; in the case of L1, it was about 46% and 45% for paste L2. This time, the composition of CAH was significantly different. The main phase was CAH_{10}, which was presented in the highest amount of studied cement pastes. The amount of amorphous AH_3 was substantially higher in the case of lignosulphonate as well. Contrary to previous cases no C_2AH_8 and only marginal C_3AH_6 were observed. In accordance with not converted composition, also the amount of crystal AH_3 was quite small, by 76% and 69% lower compared to the reference paste R.

Polycarboxylate based plasticizer had the most retarding impact on the hydration reaction; the hydration degree reached the lowest values, 42% for P1 and even 40% for P2. Regarding the phase composition, the amount of hydrated crystal phases was really small. The lower dosage gave rise primarily to CAH_{10}, while in the case of a higher amount C_3AH_6 seemed to be dominant. C_2AH_8 was not observed. Regarding the AH_3, the lowest amount of amorphous AH_3 was present. Crystal AH_3 was decreased by 78% for P1 and by 67% for P2.

The Impact of modified polycarboxylate did not show such retarding impact on hydration reaction as lignosulphonate and polycarboxylate based plasticizers. The hydration degree of cement pastes M1 and M2 was 49% and 47%. When focused on the composition of hydrates, CAH_{10} seemed to be the main hydration product. It was accompanied by a minor amount of C_2AH_8 and C_3AH_6. The amount of crystalline AH_3 was the lowest from studied pastes; by 77% and 82% lower than pure cement paste R.

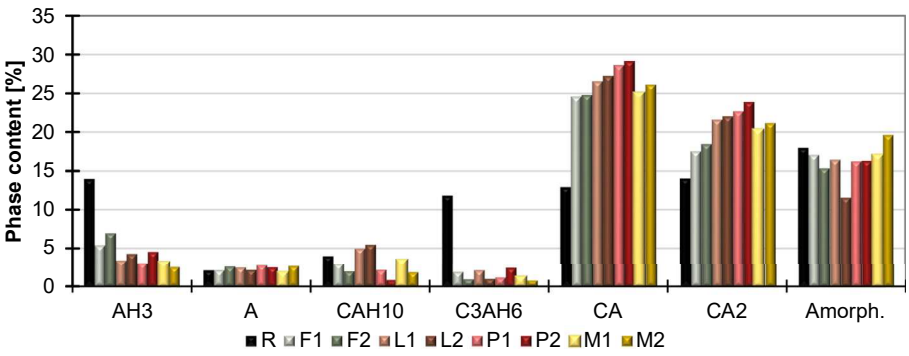

Fig. 5 – Phase composition of cement pastes.

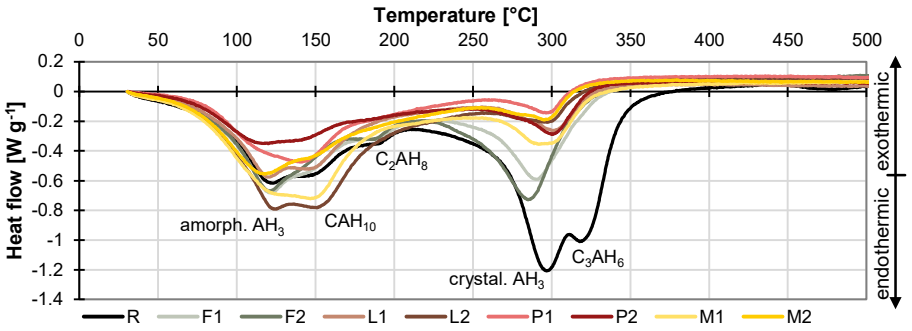

Fig. 6 – Differential scanning calorimetry of cement pastes.

The hydration rate was decreased in all cases of studied plasticizers, but it is in a relatively good correlation with the decreasing w/c ratio. The more important is varying miner alogical composition, and especially not converted composi tion. In the study by Krivoborodov et al. [18], the reversed tendency was observed, higher hydration degree with plasti cizers applications. However, they used an equal w/c ratio for all cases. On the other hand, Alonso et al. [15] were in rela tively good correlation with this study, as they reported, that application of polycarboxylates reduced the amount of generated hydrates by 45%.

4.1.2. Basic physical properties of cement pastes

Measured values of matrix density of cement paste are sum marized in Table 4. It is visible that the impact of plasticizer application was noticeable primarily at ambient temperature. Reference material R showed the highest matrix density of the studied pastes. These results well corresponded to the sub stantially higher amount of katoite C_3AH_6, which had a significantly higher specific density (2520 kg m ^{3}). When plasticizers were used, the matrix density went down. These falls were influenced primarily by different mineralogical compositions, when the metastable hydrates showed lower densities (CAH_{10}–1743 kg m ^{3}, C_2AH_8–1950 kg m ^{3}). The hy dration degree also took part in the decreasing tendency of the matrix density; the original minerals had a bigger specific density (CA–2940 kg m ^{3}, CA_2–2880 kg m ^{3}) and by their hy dration, the value of matrix density went down. Melamine formaldehyde resin caused the biggest fall in matrix density; compared to the reference material by 11% and 13% for paste F1 and F2. Contrary, polycarboxylates and modified polycarboxylate based plasticizers in higher dosages caused the lowest decrease, by 2% and 4% for P2 and M2. After exposure to 400 °C, the differences between particular pastes were reduced significantly. After higher temperature loading, there were observed no remarkable differences between particular cement pastes. This can be attributed to the varying compositions of thermally loaded pastes and different specific densities of observed minerals. During the thermal loading, more precisely during the dehydration process, the denser products arose; calcium aluminate hydrates CAH_{10}, C_2AH_8 and C_3AH_6 were successively transformed into denser CA and CA_2.

In Table 4, there can be found also values of cement pastes' porosity. At ambient temperature, the reference paste R reached the highest value of porosity. This can be explained not only by a slightly higher w/c ratio but especially by con verted composition when the stable katoite C_3AH_6 was formed. The biggest difference was observed in the case of polycarboxylates and modified polycarboxylate based plasti cizers, their porosity was by 48%, 50%, 45% and 55% lower for pastes P1, P2, M1 and M2 respectively. Contrary to that, lignosulphonate based plasticizer caused the lowest fall of porosity, specifically by 12% and 6% for L1 and L2 respectively. When focused on the performance after the temperature exposure, the porosity tendency was increasing up to 1000 °C. After 1400 °C the values went down due to the sintering pro cess. This time, the differences between particular mixtures were remarkable also after the temperature exposure. While the melamine formaldehyde resin and lignosulphonate showed comparable residual values as the reference

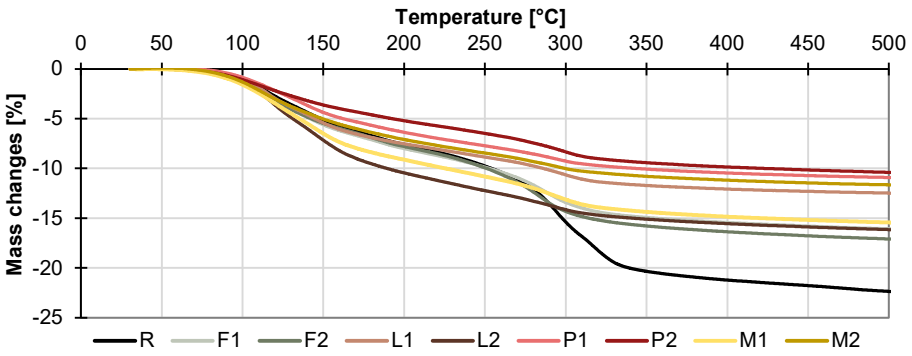

Fig. 7 – Thermogravimetry of cement pastes.

Table 4 – Basic physical properties of cement pastes.

	Matrix density [kg m ^{3}]				Porosity [%]			
	20 °C	400 °C	1000 °C	1400 °C	20 °C	400 °C	1000 °C	1400 °C
R	2592	2712	2777	2748	24.8	34.1	41.1	30.0
F1	2304	2579	2868	2884	15.3	30.4	43.4	32.9
F2	2269	2669	2888	2830	14.9	32.7	43.5	28.8
L1	2498	2623	2848	2860	21.8	32.8	40.9	29.0
L2	2395	2683	2876	2859	23.4	34.1	42.6	33.9
P1	2318	2686	2889	2839	12.4	26.6	36.0	25.2
P2	2539	2708	2887	2853	12.5	21.1	30.3	24.3
M1	2371	2607	2872	2817	13.7	26.5	38.1	27.5
M2	2501	2728	2888	2863	11.2	26.9	36.6	26.1

materials, the two remaining plasticizers caused significant lower porosity also after the temperature exposure.

The porosity of cement pastes (more precisely of pastes based on varying calcium aluminates) was presented in the study by Krivoborov et al. [18]. Despite their pastes being cured under the water, the results of porosity were equal to the ones in this work; about 27.8% for reference materials, 14% for materials with the mix of sulfonated polycondensates and sodium sulphate and 13% in the case of sulfosalicylic acid application. In comparison, polycarboxylates and modified polycarboxylates seemed to have a more densifying effect.

4.2. *Cement composites*

4.2.1. *Basic physical properties of cement composites*

Values of matrix density are presented in Table 5. Similar to the case of cement pastes, the highest values at ambient temperature, were observed for reference material R. How ever, this time the difference between the studied materials was not so significant. Composites with plasticizers had on average by 2% lower matrix densities. Because the difference between particular plasticizers was less than the accuracy of the used measurement method, particular plasticizers can be considered as having minimal impact on the matrix density of cement composites This can be explained by the higher amount of aggregates in cement composites, and thus the varying densities of cement pastes had a lower impact on total matrix density.

Regarding the impact of temperature, the matrix density went continuously up with increasing temperature up to 1000 °C, and afterwards slightly decreased up to 1400 °C. The changes were also comparable for all cases of studied plas ticizers. The increase was on average by 8% after 400 °C, by 13% after 1000 °C and by 8% after exposure to 1400 °C. Con trary, reference paste R showed a lower increase of residual matrix density; by 4%, 8% and 7% for particular temperature exposure.

The porosity of studied composites is also in Table 5. The impact of the used plasticizers at ambient temperature was substantial. While formaldehyde resin caused the increase of porosity by 6%, lignosulphonate based plasticizer showed similar performance as reference composite. In accordance with substantially lower w/c ratio and hardened paste composition, polycarboxylate based plasticizer reached by 30% lower porosity, and modified polycarboxylate caused a decrease by even by 35%. These performances remain alike also after the temperature exposure. Similar results of porosity fall due to the polycarboxylate based dispersant were observed also in the work of Oliveira et Pandolfelli [16].

More important than a value of porosity for the overall durability of cement composites is pore system structure. On that account pore, size distribution curves were measured (Fig. 8). The biggest difference between particular materials was found to be at ambient temperature. It is visible that plasticizer application has a substantial impact also on the pore structure. Reference paste R has the biggest amount of pores with the diameter of about 0.1 μm. The application of melamine formaldehyde resin caused a significant growth of porosity in general, without any significant change in pore size distribution. Contrary, the lignosulphonate based plasti cizer decreased the number of pores with the diameter of about 0.1 μm, but significantly increase pores amount with a diameter of about 20 μm. In accordance with the lowest value of porosity, polycarboxylate based additives showed the lowest values or relative pore volume as well. Moreover, the pore structure was the finest among studied composites. Modified polycarboxylate application led to a similar perfor mance of fluent pore size distribution as polycarboxylates, but the particular values were slightly higher. When focused on temperature exposure, it is visible that with increasing

Table 5 – Basic physical properties of cement composites.

	Matrix density [kg m ^{3}]				Porosity [%]			
	20 °C	400 °C	1000 °C	1400 °C	20 °C	400 °C	1000 °C	1400 °C
R	2701	2799	2907	2884	14.6	26.8	29.9	29.8
F	2665	2830	3025	2837	16.2	27.0	31.2	27.6
L	2637	2836	2929	2846	14.3	25.7	29.9	30.4
P	2625	2817	2934	2863	10.2	20.9	24.4	25.0
M	2654	2871	3004	2870	12.8	21.5	26.1	25.9

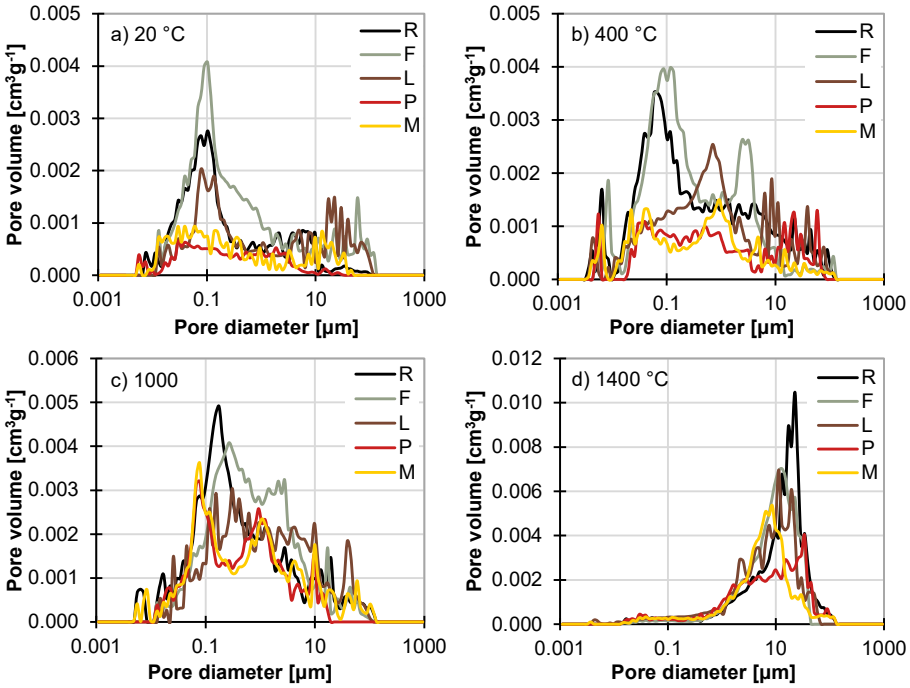

Fig. 8 – Pore size distribution curves of cement composites. a) 20 °C. b) 400 °C. c) 1000 °C. d) 1400 °C.

temperature to 400 °C not only overall pore volume grew, but a big amount of micropores with a diameter of about 0.0085 μm gave rise. However, further temperature increase to 1000 °C caused the elimination of mentioned micropores, and the pore distribution showed maximal values at the pore diameter from 0.1 to 1 μm. The biggest change was observed after the exposure to 1400 °C. Due to the sintering, the small pores disappeared, and the structure contained only bigger pores with a diameter of about 10 μm.

4.2.2. *Mechanical parameters of cement composites*

The obtained results of compressive strengths depending on the temperature exposure are delineated in Fig. 9. Similar to the previously described characteristics, also mechanical strength is significantly influenced by different plasticizers. At ambient temperature, melamine formaldehyde resin caused a minor fall of compressive strength, by 11% compared to reference material R. Contrary, the application of three remaining additives led to substantial growth of compressive strength at ambient temperature. Lignosulphonate caused growth by 38%, polycarboxylate even by 107% and modified polycarboxylate by 60%. The overall performance seemed to be mostly influenced by pore structure variation, which was in accordance with the observed performance of compressive strengths. When focused on the impact of temperature exposure, the compressive strengths decreased with increasing temperature in all cases. However, there were substantial differences between particular composites. While those containing melamine formaldehyde resin F and ligno sulphonate L showed similar values as reference composite R, polycarboxylate P and modified polycarboxylate M plasticizer reached considerably higher values of residual compressive strengths.

Values of bending strength are summarized in Fig. 9. This characteristic was improved by the application of all plasti cizers. However, the melamine formaldehyde resin had the

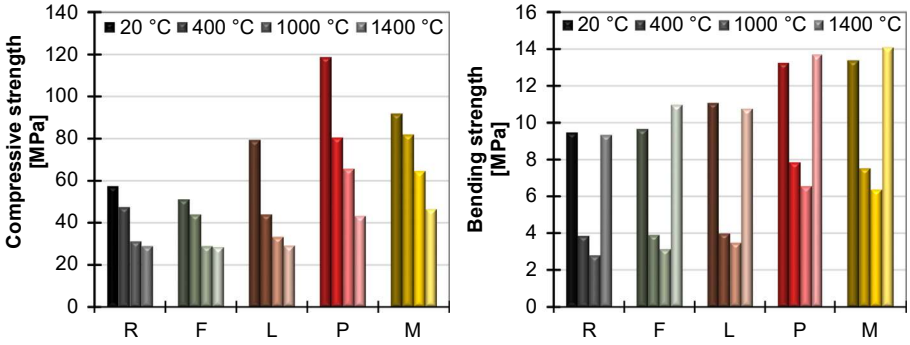

Fig. 9 – Compressive and bending strength of cement composites.

Table 6 – Dynamic modulus of elasticity of cement composites.

	Dynamic modulus of elasticity [GPa]			
	20 °C	400 °C	1000 °C	1400 °C
R	41.8	11.6	7.8	26.6
F	48.7	17.3	10.6	31.5
L	55.4	16.6	12.7	30.4
P	68.1	34.1	25.3	40.2
M	71.4	33.3	23.0	38.9

lowest impact, as bending strength was increased only by 2% at ambient temperature. Lignosulphonate based plasticizer caused the higher improvement, by 17%. Two other polycarboxylates and modified polycarboxylates based additives caused an increase by 40% and 41% for composites P and M respectively. Regarding the impact of temperatures, the residual bending strengths went down up to 1000 °C, and afterwards, up to 1400 °C, they grew up at approximately original values. Similar to the previous case of compressive strengths, melamine formaldehyde resin and lignosulphonate application led to comparable residual values as reached by reference material. Polycarboxylate and modified carboxylates showed on average twice time higher residual bending strength up to 1000 °C.

The last measured mechanical property was the dynamic modulus of elasticity. Reached values are summarized in Table 6. The improving impact of varying plasticizers was more distinctive. Melamine formaldehyde resin caused by 17% better value of dynamic modulus of elasticity at ambient temperature, lignosulphonates by 33%, polycarboxylates by 63% and modified polycarboxylates even by 71%. The improvement was considerable also after exposure to high temperature loadings in all cases of studied plasticizers.

4.2.3. *Thermomechanical analysis*

The thermal expansion coefficient depending on temperature loading is shown in Fig. 10. Also in this case, the immense impact of plasticizers is visible. Significant peaks did correspond to the phase changes in the binder. Reference material showed from 60 °C decrease in thermal expansion coefficient. Up to 120 °C it corresponded to the dehydration of amorphous AH_3. Simultaneously also metastable CAH_{10} was dehydrated, but this reaction continued up to 160 °C. Afterwards, the straight tendency at about 180 °C was influenced by C_2AH_8 decomposition, which causing the fall of the thermal expansion coefficient also. The biggest decrease in the temperature ranges from 210 to 370 °C corresponded to katoite C_3AH_6 and gibbsite AH_3 dehydration. From 400 to 850 °C no remarkable changes occurred in the calcium aluminate cement, and thus the coefficient remains constant. The last drop is caused by the recrystallization of krotite CA. As in the previous cases, melamine formaldehyde resin caused a minimal difference in the performance of the reference composite. The only noticeable variation was observed at about 300 °C. Lower values of thermal expansion coefficient in this range signalized a lower amount of the gibbsite AH_3 and katoite C_3AH_6 in the binder (regardless of whether they originated in the hydration process or decomposition of metastable hydrates). Contrary, lignosulfonate based plasticizer application led to somehow different performance compared to the two previous cases. Composite L showed a more significant fall of thermal expansion coefficient at temperatures above 120 °C. This can be attributed to the higher amount of amorphous AH_3 and CAH_{10} in the cement structure. Whereas the increase of thermal expansion at about 180 °C can be explained by the absence of C_2AH_8. Regarding the polycarboxylates based plasticizer, the course was comparable to the latter, but the values were slightly lower. Then it can be concluded that composite P had a similar composition as composite L (higher amount of AH_3, no C_2AH_8 and lower amount of C_3AH_6). Modified polycarboxylates reached the most linear course of thermal expansion coefficient. This can signify a lower hydration degree of composite with modified polycarboxylates. On the other hand, it also corresponds to the lowest changes of other properties due to the temperature exposure.

The thermal strain was measured by Oliveire end Pandolfelli [16], despite that, there were no reference materials. It can be concluded that their plasticizers (polycarboxylates and anhydrous citric acid) caused more linear but substantially steeper performance of thermal strains, thus thermal expansion coefficient would reach about twice time higher values.

5. Conclusions

In this article, the applicability of four different plasticizing additives in combination with calcium aluminate cement is assessed. Chosen plasticizers differ primarily in their chemical basis; specifically, melamine formaldehyde resin, lignosulphonate, polycarboxylates and modified polycarboxylates

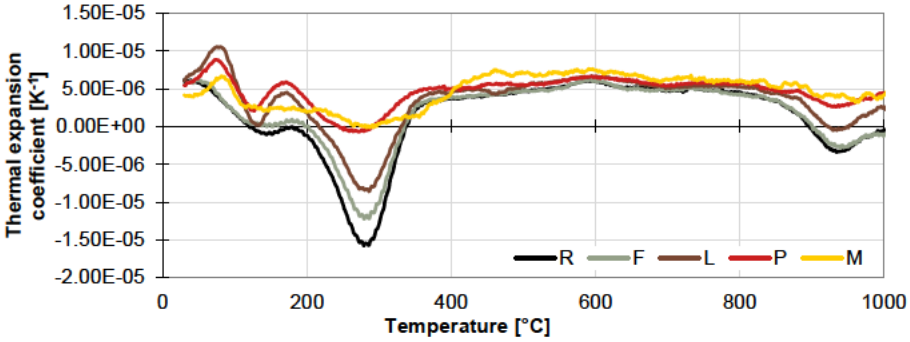

Fig. 10 – Thermal strain of cement composites.

were studied. Their applicability was assessed through the view of the mineralogical composition of cement stone as well as of the performance of calcium aluminate cemented based pastes and composites in the temperature range up to 1400 °C. The main findings can be outlined as follows:

Studied plasticizers decreased the hydration degree and reduced the porosity and matrix density of cement stone. On the other hand, they improved the porosity structure of composite materials and increased their flexural strengths and dynamic modulus of elasticity.

Melamine formaldehyde resin had the lowest impact on the cement stone composition. It showed the lowest decrease in hydration degree among studied pastes. On the other hand, the composite based on the melamine formaldehyde resin reached the highest porosities and lowest compressive strengths. On that account, it was assessed as an unsuitable plasticizer for calcium aluminate cement.

Lignosulphonate based plasticizers performed better. In the cement stone, the highest amount of CAH_{10} was observed. The cement pastes showed only slightly lower values of porosity compared to the reference material. Similarly cement composite showed a bit lower porosity. Regarding the me chanical performance, lignosulphonate caused better perfor mance compared to the reference, but only at ambient temperature. Thus, lignosulphonates are not really beneficial for the calcium aluminate cement.

Polycarboxylates based additives had the most retarding impact on cement hydration. The hydration degree was the lowest, as well as the amount of bonded water. Despite that, those CAC based paste and composites showed the lowest porosity and the highest compressive strength at ambient temperature.

Modified polycarboxylates seemed to have bigger potential than the previous additives. The hydration degree was the second highest among studied plasticizers, despite that these materials required substantially lower water dosage. Modified polycarboxylates showed the highest values of residua me chanical properties, their lowest changes and the most linear performance of the thermal expansion coefficient.

Considering the common applications of CAC based ma terials, modified polycarboxylates were chosen as the most suitable plasticizing additives, however, its dosage should al ways be carefully set up and verified for all particular applications.

Data availability

All measured data and images are available upon request. As well as any other detailed information about particular mea surement processes.

Declaration of Competing Interest

The authors declare the following financial interests/personal relationships which may be considered as potential competing interests.

Acknowledgement

This research has been supported by the Czech Science Foundation [project No. 20 00653S] and by the Grant Agency of the Czech Technical University in Prague [grant No. SGS22/137/OHK1/3T/11].

REFERENCES

[1] Topçu İB, Ateşin Ö. Effect of high dosage lignosulphonate and naphthalene sulphonate based plasticizer usage on micro concrete properties. Construct Build Mater 2016;120:189 97.
[2] Nkinamubanzi PC, Mantellato S, Flatt RJ. 16 superplasticizers in practice. In: Science and technology of concrete admixtures. Woodhead Publishing; 2016. p. 353 77.
[3] Akhlaghi O, Menceloglu YZ, Akbulut O. Poly(carboxylate ether) based superplasticizer achieves workability retention in calcium aluminate cement. Sci Rep 2017;7:41743.
[4] Aïtcin PC, Eberhardt AB. Historical background of the development of concrete admixtures. In: Science and technology of concrete admixtures. Woodhead Publishing; 2016. xli lii.
[5] Ideker JH, Scrivener KL, Fryda H. Calcium aluminate cements. In: Lea's chemistry of cement and concrete. Butterworth Heinemann; 2019. p. 537 84.
[6] Antonovič V, Kerien J, Boris R, Aleknevičius M. The effect of temperature on the formation of the hydrated calcium aluminate cement structure. Procedia Eng 2013;57:99 106.
[7] Smith A, Chotard T, Gimet Breart N, Fargeout D. Correlation between hydration mechanism and ultrasonic measurements in an aluminous cement: effect of setting time and temperature on the early hydration. J Eur Ceram Soc 2002;22:1947 58.
[8] Lapyote P, Issara S. Dissolution, nucleation, and crystal growth mechanism of calcium aluminate cement. J Sustain Cement Based Mat 2019;8(3):180 97.
[9] Engbert A, Gruber S, Plank J. The effect of alginates on the hydration of calcium aluminate cement. Carbohydr Polym 2020;236:116038.
[10] Pacewska B, Nowacka M. Studies of conversion progress of calcium aluminate cement hydrates by thermal analysis method. J Therm Anal Calorim 2014;117(2):653 60.
[11] Midgley HG, Midgley A. The conversion of high alumina cement. Mag Concr Res 1975;27(91):59 77.
[12] Falzone G, Balonis M, Sant G. X AFm stabilization as a mechanism of bypassing conversion phenomena in calcium aluminate cements. Cement Concr Res 2015;72:54 68.
[13] Scrivener KL, Campas A. 13 calcium aluminate cements. In: Lea's chemistry of cemnet and concrete. Oxford: Elsevier Butterworth Heinemann; 2003. p. 713 82.
[14] Ng S, Metwali E, Müller Buschbaum P, Plank J. Occurrence of intercalation of PCE superplasticizers in calcium aluminate cement under actual application conditions, as evidenced by SAXS analysis. Cement Concr Res 2013;54:191 8.
[15] Alonso MdM, Placios M, Puertas F. Effect of polycarboxylate ether admixtures on calcium aluminate cement pastes. Part 2: hydration studies. Ind Eng Chem Res 2013;52(49):17330 40.
[16] Oliveira IR, Pandolfelli VC. Does a tiny amount of dispersant make any change to refractory castable properties? Ceram Int 2010;36:79 85.

[17] Wang Y, Zhu B, Li X, Chen P. Effect ofdispersants on the hydrate morphologies of spinel containing calcium aluminate cement and on the properties of refractory castables. Ceram Int 2016;42:711 20.
[18] Krivoborodov YR, Samchenko SV, Kuznetsova TV. Structural changes in refractory calcium aluminate cement concrete. Refract Ind Ceram 2018;59(2):45 9.
[19] Idrees M, Ekincioglu O, Sonyal MS. Hydration behavior of calcium aluminate cement mortars with mineral admixtures at different curing temperatures. Construct Build Mater 2021;285:122839.
[20] Lee NK, Koh KT, Park SH, Ryu GS. Microstructural investigation of calcium aluminate cement based ultra high performance concrete (UHPC) exposed to high temperatures. Cement Concr Res 2017;102:109 18.
[21] Salomão R, Kawamura MA, Emilio ABV, Sakihama J, Segadães AM. Calcium aluminate cement in castable alumina: from hydrate bonding to the in situ formation of calcium hexaluminate. Ceram Int 2021;47(11):15082 93.
[22] Roig Flores M, Lucio Martin T, Alonso MA, Guerreiro L. Evolution of thermo mechanical properties of concrete with calcium aluminate cement and special aggregates for energy storage. Cement Concr Res 2021;141:106323.
[23] Wan H, Zhangyin H, Liu G, Xiao J, Wang Y. Study of the electrical properties of aluminate cement adhesives for porcelain insulators. Materials 2021;14(9):2232.
[24] Abolhasani A, Samali B, Aslani F. Physicochemical, mineralogical, and mechanical properties of calcium aluminate cement concrete exposed to elevated temperatures. Materials 2021;14(14):3855.
[25] ČSN EN 196 3 (722100). Methods of testing cement Part 3: determination of setting times and soundness. Prague: Czech Standardization Agency; 2017.
[26] ČSN EN 72 2400. Methods of test of mortar for masonry Part 3: determination of consistence of fresh mortar (by flow table). Prague: Czech Standardization Agency; 2000.
[27] ČSN EN 933 1 (721193). Test for geometrical properties of aggregates Part 1: determination of particle size distribution sieving method. Prague: Czech Standardization Agency; 2012.
[28] Döbelin N, Kleeberg R. Profex: a graphical user interface for the Rietveld refinement program BGMN. J Appl Crystallogr 2015;48:157 8.
[29] ČSN EN 1015. Methods of test for mortar for masonry Part 11: determination of flexural and compressive strength of hardened mortar. Prague: Czech Standardization Institute; 2000.
[30] ČSN EN 12504 4. Testing concrete Part 4: determination of ultrasonic pulse velocity. Prague: Czech standardization agency; 2005.
[31] Trník A, Medveď I, Černý R. Measurement of linear thermal expansion coefficient of concrete at high temperatures: a comparison of isothermal and non isothermal method. Cement Wapno Beton 2012;79:363 72.
[32] Koňáková D, Pommer V, Jerman M, Keppert M, Černý R, Vejmelková E. Utilization of ceramic powder, calcined shale and sintered mullite as partial replacements of calcium aluminate cement. Construct Build Mater 2022;326:126824.

4 Supplementary cementitious materials

The combination of calcium aluminate cement with supplementary cementitious materials (SCMs) represents a strategy for modifying and enhancing the performance of cement-based composites. While CAC alone is valued for its rapid strength development, chemical resistance, and thermal stability, it is also characterised by phase instability. Incorporating SCMs modifies the hydration process and can lead to the creation of a stable product. In addition, these materials can refine the pore structure and improve long-term durability, as in the case of PC. Last but not least, SCMs' application also helps reduce environmental impacts by lowering clinker content. Despite these advantages, the interactions between CAC hydrates and pozzolanic or latent hydraulic SCMs differ from those observed in PC systems, requiring careful investigation to avoid undesirable reactions or strength loss at ambient temperatures, but especially after temperature loading.

4.1 Impact on hydration mechanisms and phase evolution

As was described in Chapter 2.3, hydration of CAC follows a distinct pathway dominated by the rapid formation of metastable hydrates (CAH_{10}, C_2AH_8), which later convert into the stable phase (C_3AH_6). The addition of SCMs affects both the hydration course and the reaction kinetics. Due to the dilution of calcium aluminates, the onset of solution supersaturation can be delayed. On the other hand, they also introduce additional ions. So, more precisely, SCM alter the ionic balance of the solution. As a result, they significantly modify the initial period of hydration as well as the specific heat released during the first minutes. Afterwards, the grains of SCM can serve as the nucleation sites, promoting the precipitation of hydration products, and therefore shortening the duration of the latent period. As the relative concentration of reactive calcium aluminates is reduced and diluted in the presence of SCMs, the rapid hydration of metastable hydrates is usually slowed, which often promotes the formation of more thermodynamically stable and compositionally varied phases, depending on the specific composition of the SCM.

The most favourable element in commonly used SCMs is silicon, typically present in the form of amorphous silica. Its incorporation into the CAC alters the composition of the hydration products. In contrast to pure cement, the hydration pathway promotes the direct formation of stable hydrates. Specifically, the phase assemblage is dominated by katoite (C_3AH_6) and gibbsite (AH_3). Alongside, the formation of calcium

aluminosilicate hydrates (C-A-S-H) occurs either in an amorphous state, crystalline hydrogarnets or strätlingite (C_2ASH_8) or gismondine (CAS_2H_4). In the case of a higher amount of Si^{4+}, for example, in the form of microsilica, calcium silicate hydrate (C-S-H) can also be formed. Although the early-age mechanical strengths of these modified systems tend to be somewhat lower, the long-term performance is significantly improved as the elimination of the conversion process results in a stable microstructure with refined porosity. Regarding the modification under high-temperature exposure, the presence of siliceous components significantly alters the phase evolution as well, forming calcium aluminosilicate phases apart from calcium aluminates. One of the primary high-temperature phases is gehlenite (C_2AS), a stable calcium aluminosilicate that crystallises in the temperature range of 800 – 1000 °C with a melting temperature of 1593 °C. Additionally, the presence of silica favours the formation of anorthite (CAS_2) at higher temperatures above 1100 °C. This mineral also has quite a high melting point at about 1550 °C.

Contrary, the addition of aluminium element to CAC influences the hydration mechanism but does not introduce new hydration products. It rather affects the phase assemblage of the hardened matrix. Some aluminium-bearing compounds act as a reactive component that increases the availability of aluminate ions in the pore solution during the initial hydration phase, promoting faster supersaturation. It favours the precipitation of pure aluminate hydrates (AH_3), but usually in varying crystal forms (i.e. nordstrandite and bayerite). Regarding calcium aluminate hydrates (C-A-H), the higher concentration of Al^{3+} should intuitively support the formation of alumina-rich hydrates CAH_{10}. In practice, the excess alumina does not drive the stabilisation of CAH_{10} but instead precipitates as mentioned aluminium hydroxide (AH_3). The dominant calcium aluminate hydrate phase is still controlled primarily by water availability and temperature, not solely by the aluminium concentration. On the contrary, the increased alumina content significantly influences the high-temperature phase composition. The system often shifts towards the formation of aluminate-rich refractory phases, particularly hibonite (CA_6), which recrystallise much earlier than in pure CAC. Hibonite with a high melting point of around 1875 °C offers improved refractoriness and chemical resistance, but also a significant increase in porosity.

Regarding another common element in cement systems, calcium content promotes the fast hydration of CAC. The higher presence of Ca^{2+} ions in the solution

causes the modification of Ca/Al balance. Contrary to PC, where ions of Ca^{2+} are abundant, leading to crystallisation of portlandite ($Ca(OH)_2$), in the case of CAC, there is a lack of these ions and thus the balancing product is $Al(OH)_3$. Therefore, when the amount of calcium is increased, the nucleation of C-A-H is accelerated, which noticeably shortens the latent period. Concerning the particular calcium aluminate hydrate, the increased calcium availability shifts the equilibrium toward the direct formation of stable katoite (C_3AH_6). However, its precipitation may occur already during the initial or latent hydration phases, meaning that the overall hydration kinetics are noticeably accelerated. In excessive amounts of calcium (e.g. from calcium hydroxide), the hydration is extremely fast and exothermic, leading to almost immediate setting. On that account, the content of calcium in SCMs must be carefully controlled.

4.2 Possible admixtures for CAC

Microsilica, a by-product of silicon or ferrosilicon alloy production, represents one of the most effective pozzolanic materials used in high-performance cementitious composites. Composed predominantly of amorphous silicon dioxide (SiO_2) with particle sizes approximately 100 times smaller than cement grains, it significantly enhances the microstructure of CAC-based materials. When incorporated into CAC matrices, microsilica serves both as a physical filler, reducing porosity and refining the pore structure, and as a reactive agent, participating in secondary hydration reactions that improve long-term strength and durability [52]. Specifically, the addition of microsilica has been reported to stabilise the hydration products by promoting the formation of hydrogarnet phases, thereby mitigating the adverse effects of the conversion of calcium aluminate hydrates [53]. Furthermore, microsilica can promote the formation of strätlingite (C_2ASH_8), together with porosity refinement (about 6% increase in pores below 10μm), resulting in denser and more durable matrices [54]. Studies have shown that optimal microsilica additions typically range from 5–20%.

Fly ash, a by-product from coal combustion, is also an effective supplementary cementitious material for enhancing the performance of CAC composites. It contains high amounts of reactive silica and alumina, which enable it to participate in pozzolanic reactions and modify the hydration behaviour accordingly [55]. However, as there are two main kinds of coal fly ash, it is necessary to distinguish them. Class C, with high calcium content, significantly enhances reactivity and promotes the formation of more C-A-S-H and also C-S-H. Consequently, it gives rise to a denser structure with about

5% higher compressive strength than in the case of Class F (with low calcium content) [56]. In addition, it was proven that 20% of fly ash (Class C) led to workability improvement and to a 64% reduction in porosity. The most efficient impact was, however, observed in the case of compressive strength. Although at 1 day the values were 28% lower compared to pure CAC, after 56 days the blend with fly ash reached by 30.5% higher value, confirming the positive impact of fly ash utilisation on conversion prevention [57]. The typical dosage ranges between 15–30% according to the specific composition of the used fly ash.

Ground granulated blast furnace slag (GGBS) has also gained attention as a valuable SCM in CAC-based systems. It is a by-product of the iron and steel industry, formed when molten slag from blast furnaces is rapidly quenched in water to produce a glassy, granular material. This material is then dried and finely ground to a Blaine specific surface area typically between 400 – 600 $m^2.kg^{-1}$. The rapid cooling preserves the amorphous phase, making GGBS a highly reactive latent hydraulic material that hardens in the presence of water and calcium hydroxide or under alkaline activation. As in the previous cases, the impact of the GGBS on the performance of CAC covers phase modification towards calcium aluminate silicate hydrates, specifically to strätlingite (C_2ASH_8) formation. 10% of GGBS lead to the faster development of mechanical strength compared to fly ash and silica fume, reaching the highest compressive strength after 90 days [58]. However, compared to the pure CAC, GGBS caused a decrease in hydration heat and a prolonged latent period [60]. 10% of GGBS increase not only compressive strength, split-tensile strength, and thermal conductivity properties of CAC blended concrete but also its residual properties under high-temperature cyclic load (290°C–550°C) [59]. According to the studies, the dosage of the GGBS falls within quite a wide range, from 10% to 45%.

4.3 Author contribution – selected papers

The development of SCMs for CAC systems remains an evolving research area, particularly concerning not only their hydration behaviour and phase stability, but especially high-temperature performance. Prior studies have explored primarily common industrial by-products and pozzolanic materials at ambient temperatures. Gaps remain in involving less conventional materials and optimising binder compositions for refractory applications, including ternary systems. These studies provide new insights into the design of low-cement, heat-resistant composites.

4.3.1 Utilisation of ceramic powder, calcined shale and sintered mullite as partial replacements of calcium aluminate cement

D. Koňáková, V. Pommer, M. Jerman, M. Keppert, R. Černý, E. Vejmelková
Construction and Building Materials 326 (2022) 126824 [61]
https://doi.org/10.1016/j.conbuildmat.2022.126824

This paper contributes to the field of refractory and high-temperature-resistant cementitious systems by evaluating non-conventional SCMs. Specifically, ceramic powder, calcined shale, and sintered mullite were examined as partial replacements for CAC in amounts of 5% and 15% in order to extends the scope to industrial waste and refractory-grade materials.

The research systematically assessed the hydration behaviour, phase composition, and mechanical performance of CAC pastes. Ceramic powder significantly accelerated hydration kinetics due to its amorphous CaO content, promoting early formation of metastable hydrates (CAH_{10}, C_2AH_8) and enhancing early compressive strength. However, it also increased porosity, particularly after high-temperature exposure. Calcined shale improved the degree of hydration without drastically altering the phase composition, enhancing mechanical strength while maintaining moderate porosity. Sintered mullite led to the formation of stable katoite (C_3AH_6) and reduced metastable hydrates, enhancing phase stability and thermal resistance. After high-temperature exposure (up to 1400 °C), the modified CAC systems demonstrated improved thermal stability, with the formation of gehlenite (C_2AS), grossite (CA_2), and hibonite (CA_6) depending on the specific SCM.

This work advances the state of the art by:

- Introducing new kinds of SCMs for CAC
- Demonstrating that SCM selection strongly influences hydration kinetics, phase stability, and high-temperature performance
- Providing insights into the performance of non-conventional SCM in terms of early mechanical strength, porosity, and thermal durability.

In summary, the study broadens the understanding of SCMs in CAC systems, identifying non-traditional, cost-effective, and thermally stable replacements that enhance performance in high-temperature and refractory applications.

Construction and Building Materials 326 (2022) 126824

Contents lists available at ScienceDirect

Construction and Building Materials

journal homepage: www.elsevier.com/locate/conbuildmat

Utilization of ceramic powder, calcined shale and sintered mullite as partial replacements of calcium aluminate cement

Dana Koňáková *, Vojtěch Pommer, Miloš Jerman, Martin Keppert, Robert Černý, Eva Vejmelková

Department of Materials Engineering and Chemistry, Faculty of Civil Engineering, Czech Technical University in Prague, Thákurova 7, 166 29 Prague 6, Czech Republic

ARTICLE INFO

Keywords:
Calcium Aluminate Cement
Blended Cement
Thermal Treatment
Characterization
Physical Properties

ABSTRACT

Supplementary cementitious materials (SCMs) are widely used with Portland cement. Similar approach was applied for calcium aluminium cement in this paper. Potential SCMs were ceramic powder, calcined shale and sintered mullite. Cement pastes with 5% or 15% of SCM were prepared and their phase compositions and basic physical and mechanical properties were studied. The analysed blended cements showed an advantageous performance not only at the ambient temperature, but also after high-temperature exposure up to 1400 °C. Ceramic powder had the most significant impact on the hydration process. Calcined shale caused a higher hydration degree, sintered mullite primarily affected the formed C-A-S-H phases.

1. Introduction

Calcium aluminate cement (CAC) belongs to the most important binders in the castable refractories production. The utilization of CAC based refractories in numerous manufacturing devices (e.g., non-ferrous metallurgy, steel production, pre-heaters of incinerators and cement kilns, furnace lining in general, industrials floor, or waste sewer lining) is almost irreplaceable, because of its excellent high temperature resistance (more than 1600 °C), as well as great chemical resistance. Moreover, concrete based on CAC shows high early-strength development and quick setting, which predestines this material for repair purposes and everywhere, where the fast strength increase is required. It also has a fairly high heat of hydration, which is evolved more rapidly than in other cements [1,2]. Therefore, its application is possible even at lower temperatures.

However, to be comprehensive, CAC also has several disadvantages. In contrast to ordinary Portland cement (OPC), hydration of CAC distinctively depends on temperature. The main active mineral in CAC cements is krotite (CA), which is accompanied by less reactive grossite (CA_2) [3]. According to the current knowledge, the hydration products are as follows [4,5]: Below 15 °C the CAH_{10} is formed almost exclusively from possible calcium aluminate hydrates (CAH). The main product in the range between 15 °C and 27 °C is C_2AH_8, which is up to 30 °C accompanied by lower amount of katoite C_3AH_6. This phase becomes dominant at higher temperatures up to 35 °C. Then, above 35 °C, C_3AH_6 presents the only CAH phase. Gibbsite ($Al(OH)_3$; AH_3) is formed in the hydration process in addition to the Ca-containing phases. However, the most crucial disadvantage of CAC is the conversion of metastable hexagonal hydrates (CAH_{10}, C_2AH_8) in stable hydrates [6–8]. Stable cubic hydrate C_3AH_6 shows a higher specific gravity (i.e., lower specific volume), and on that account the porosity grows during the conversion process. This consequently leads to lower compressive strength of the converted material. This problematic transformation was the reason for the limitation of CAC application in load bearing structures in the 1970 s. Other issues are a higher production cost compared to OPC, mainly the need for pure raw materials (bauxite and limestone with a limited amount of SiO_2) and a higher production temperature (1600 °C in an electric-arc furnace or 1350 °C in rotary kilns), which negatively influences the fairly high price of CAC [1,9].

The global cement consumption (regardless the kind) is currently more than 4.4 billion tons per year. The production of such amount of cement is extremely demanding from both economic and ecological point of view, due to the fairly high kiln temperature, as well as the consumption of not-renewable resources. However, the most problematic issue is indisputably the high emission of CO_2 during the production process. In average it is about 0.6 tons CO_2 for one ton of the produced cement [10,11]. This makes cement production responsible for about 7% of worldwide emissions of CO_2 [10,11]. Taking to the account that the highest consumer is structure production, the need for cement usage reduction in this branch is of great importance. One of the promising

* Corresponding author.
E-mail address: dana.konakova@fsv.cvut.cz (D. Koňáková).

https://doi.org/10.1016/j.conbuildmat.2022.126824
Received 20 October 2021; Received in revised form 29 December 2021; Accepted 8 February 2022
Available online 21 February 2022
0950-0618/© 2022 Elsevier Ltd. All rights reserved.

ways to help with such reduction is the partial replacement of cement with another material. In the case of OPC, the application of mineral admixtures as supplementary cementitious materials (SCMs) has not only been widely studied, but currently it is very frequent. The utilization of SCMs brings many benefits. Except for the desired cement (clinker) consumption, they are able to improve the overall performance of final concrete. SCMs are primarily able to increase mechanical strength. Despite the prolonged strength development due to the delayed pozzolanic reaction, the final strengths are higher in general. Moreover, SCMs improve workability of fresh mixture, reduce permeability of hardened concrete, and thus increase the overall durability of concrete based on OPC. The most common representatives of the used admixtures are either industrial by-products or waste materials, and therefore their application provides other advantages from not only ecological but also economic point of view. Microsilica or silica fume [12,13], fly ash [14], and blast-furnace slag [15] can be considered as the most common representatives of SCMs. Besides these industrial by-products, also natural pozzolans [16], agricultural wastes [17], and artificial materials, such as calcined shale [18] or calcined clays [19], can be used as SCMs.

Regarding CAC, the SCMs application was studied relatively rarely. Such researches were focused primarily on SCMs commonly used for OPC. The most frequently discussed admixtures were microsilica, silica fume, fly ash, and blast-furnace slag. In the Lea's Chemistry of Cement and Concrete [1] it was presented that the hydration of CAC with reactive siliceous materials leads to the formation of stratlingite C_2ASH_8, and slower strength development. Mercury et al. [20], who studied hydration of calcium aluminates (synthetic C_3A, $C_{12}A_7$ and CA) with amorphous SiO_2, reported a direct formation of stable hydration products (katoite C_3AH_6 and gibbsite AH_3) when microsilica was used. Also, C-S-H and C-A-S-H phases were found in [20], but contrary to Lea's Chemistry primarily in the amorphous phase. Lee et al. [21] used silica fume for the production of CAC based UHPC. However, they used the same amount in all studied mixtures, and the type of cement was the variable. Nevertheless, they reported a high strength capability of CAC based UHPC up to 800 °C. Collepardi et al. [22] studied silica fume as well. Moreover, they used fly ash as another admixture to CAC pastes. Silica fume was able to reduce the negative conversion of metastable hydrates by stratlingite C_2ASH_8 formation in their mixes. Using fly ash was though not found advantageous, as its application reduced the strength. A similar study was presented by Hidalgo et al. [23] who analyzed the conversion of CAC paste in the presence of silica fume or fly ash, but they were focused on microstructural analysis. They reported a decelerating effect on the conversion process of CAC due to both admixtures' application. Moreover, they observed also isomorphous replacement of alumina by silica in hydrogarnets and the formation of laumontite. A more complex study was presented by Idrees et al. [24] who dealt with the impact of silica fume, fly ash and ground granulated blast furnace slag (GGBFS) on low-aluminate CAC based mortars and identified 10% of fly ash and GGBFS as the optimum dosage. However, contrary to the approach used in this work, they replaced sand by mineral admixture and the cement amount was fixed. They also compared the blended mortar with the CAC based mortar with superplasticizer. Thus, due to the different experimental procedures, the results obtained could not be adequately compared. GGBFS was studied also by Kirca et al. [25], who prepared blended mortars and examined primarily compressive strength at different curing temperatures. They reported a positive impact of GGBFS, especially in higher dosage, on the elimination of the conversion process by stratlingite formation, at lower temperatures in particular. Cheng et al. [26] confirmed the positive impact of GGBFS on mechanical properties as well. Furthermore, they studied also the pore size distribution and thermal conductivity and observed an improvement in both cases. Metakaolin and zeolites belong to less frequently used SCMs. They have been studied, e.g., by Nowacka et al. [27] who analyzed their impact on the early hydration of CAC. Metakaolin was found to accelerate setting and hardening times, while zeolite behaved differently at different hardening temperatures (6, 25, 40 and 60° C).

As it follows from the literature review, SCMs application was in the case of CAC focused almost entirely on conventional admixtures. Nevertheless, they proved their advantageous applicability. This paper is focused on the study of nonconventional admixtures used as SCMs for calcium aluminate cement. Based on the performed market survey aimed at accessible materials, three possible candidates were selected. Specifically, waste ceramic powder from brick block production, calcined shale and sintered mullite were applied as potential supplementary cementitious materials. Their usability was assessed primarily by their impact on the composition of hydrated cement pastes. Selected promising mixtures were then subjected to a high temperature exposure up to 1400 °C. Basic physical properties, mechanical parameters, and thermal strain of blended calcium aluminate cement pastes served as the main criteria for the evaluation of applicability of studied nonconventional SCMs.

2. Experimental methods

2.1. Material characterization

The hydration heat power was measured by a TAM Air isothermal calorimeter (TA instruments) which is based on the differential measurement of heat flow. Specimens with a mass of 4 g were used for the measurement. According to the ČSN EN 196–11 standard [28], the water/binder (w/b) ratio is supposed to be 0.4. In the experiments in this paper, the w/b ratio was slightly higher than the recommended value in order to achieve a good homogeneity of the mixture during the initial preparative part of hydration heat measurement. The temperature was set on 20 °C. After temperature stabilization the water and solid component were mixed for 30 s. Each experiment was performed for 120 h.

The phase composition of studied materials was analyzed by X-ray diffraction (XRD) using a PANalytical Aeris system with $Co_{K\alpha}$ tube. The quantification of the present phases was performed by Rietveld analysis with internal standard (20% of ZnO); the evaluation is done by the HighScore and Profex software [29].

Simultaneous thermal analysis (STA), consisting of differential scanning calorimetry (DSC) and thermogravimetry (TG), was carried out using a LABSYS EVO DTA/DSC device (SETARAM Inc.). The experiments were done in the temperature range from 30 °C to 1000 °C with a heating rate of 5 °C min^{-1} and in an argon atmosphere with a flow rate of 40 mL min^{-1}. A part of DSC measurements was performed with a DSC 404 F3 device (Netzsch, Germany). The experiments were done in the temperature range from 30 °C to 1400 °C with a heating rate of 5 °C·min^{-1} and in argon atmosphere with a flow rate of 40 mL·min^{-1}. The powder samples with a mass of ~ 50 mg were placed in an alumina crucible with a lid.

For the determination of granulometry of fine components, the laser diffraction method was used (Bettersizer S3 Plus device). The samples were dispersed in ethanol in order to prevent hydration and sonicated 3 min prior to the analysis.

The SEM micrographs were acquired using a Phenom XL desktop device equipped with BSE detector and CeB6 source. The voltage was set as 15 kV or 10 kV, the magnification was from 1000x to 12000x. The phases in the SEM images were derived based on the spectral analysis in a combination with the known crystal morphology.

2.2. Thermomechanical analysis

The measurement of thermal strain in dependence on temperature was performed by a linear thermal horizontal dilatometer [30] for three samples with the dimensions of 15 × 15 × 160 mm. The device utilizes a comparative method; the real thermal expansion is determined by comparing the analyzed specimen with a reference corundum rod. The

heating rate of the dilatometer was set as 1 °C per min and the maximal temperature of measurement was 1000 °C.

2.3. Basic physical properties

Matrix density, bulk density, and open porosity were the basic physical properties investigated. The matrix density was determined by helium pycnometry. This experiment was carried out using a Pycnomatic ATC device (Thermo Fisher Scientific Inc.). The bulk density was determined by the gravimetric method. The values of porosity were calculated based on the known values of matrix density and bulk density.

2.4. Mechanical parameters

The mechanical properties, specifically compressive strength and bending strength, were measured on cement pastes and the experiments were performed according to the EN standard [31]. Determination of the bending strength was performed on three samples (40 × 40 × 160 mm) using an MTS 100 loading device. The arrangement of the measurement was a three-point bending test with 100 mm span length. The compressive strength was then determined on fragment samples from the bending strength measurement. A EU40 loading device was employed and in the actual experiment the samples were put between two steel pressure plates with the dimensions of 40 × 40 mm.

3. Raw materials and their characterization

The main binder used in this study was calcium aluminate cement (CAC). It contained about 70% of alumina (Tab. 1), and thus belonged to medium aluminate cements. Three different raw materials were chosen as possible supplementary cementitious materials. The first one was ceramic powder with a density of 2590 kg m^{-3}. This was waste material originating in the grinding process of thermal insulating bricks. It showed a good pozzolanic activity and was already successfully used as SCM for Portland cement-based concrete [32]. The second raw material was calcined shale with a density of 2475 kg m^{-3}. This was a material similar to metakaolin, but in this case the shale was used as the raw material. From the petrological point of view, it was layered claystone, specifically consolidated sedimentary rock with kaolinite as a dominant component. Calcined shale also belongs to the proved SCMs for Portland cement [19]. The third studied material was sintered mullite with a density of 2800 kg m^{-3}, which has a great thermal resistance. The chemical composition (as determined by XRF) of raw materials is summarized in Table 1. It is apparent that ceramic powder had quite a high content of CaO, which could have negative impact on the high temperature resistance. The sintered mullite, with the highest content of Al_2O_3, could provide a better performance in that respect. However, also the mineralogical composition is of great importance. It is presented in Table 2. As it can be seen, the used materials contained a high amount of amorphous phase, which could have crucial impact on their reactivity. It can be assumed that calcined shale together with ceramic powder would be more reactive compared to the mullite. The approximate composition of amorphous phases was calculated as well, and it is shown in Table 3. From that point of view calcined shale with the highest content of amorphous Al_2O_3 and SiO_2 seemed to have the highest potential as supplementary cementitious material for calcium aluminate cement. For comprehensiveness of the material characterization, DSC and TG curves of raw materials are delineated in Fig. 1 and Fig. 2. Another important factor is the granulometry, the grain size distribution curves are shown in Fig. 3. Studied materials differed widely also in this aspect. Calcined shale was the finest one, ceramic powder has similar granularity as calcium aluminate cement and mullite showed the coarsest grains. Although it could be more adequate to mill materials to similar grain-size, it was decided to study firstly their applicability in their original nature.

4. Cement paste preparation and thermal loading

The composition of the analyzed cement pastes is summarized in Table 4. The reference material R contained only calcium aluminate cement. Its w/b ratio was 0.3 and its flow was (as determined by flow table experiments) 180/180. Then the other cement pastes were prepared. Specifically, 5% and 15% of calcium aluminate cement were always replaced by an SCM. Potable water was added gradually with the aim of obtaining the same consistency as the reference paste (flow 180/180). Therefore, the w/b ratio was different for the individual pastes. It is quite interesting, that 5% replacement usually led to the somewhat lower water content, while for 15% a higher water amount was demanded.

The samples were made and cured in the laboratory conditions (temperature 20 ± 1 °C and relative humidity 50%). After 28 days, they were exposed to four different thermal treatments. The first set of samples was not exposed to the temperature loading and was examined at the ambient temperature. The other three sets were thermally loaded by 400 °C, 1000 °C and 1400 °C. The temperature exposure took place in an electrical top-cover furnace. Before the actual loading, the specimens had been dried in an oven at 105 °C for 24 h. The main aim was the evaporation of free water from the inner structure in order to prevent the samples from explosive spalling during the thermal load. The thermal loading was performed continuously with a temperature increase rate of 1 °C min^{-1}. After reaching the chosen temperature, the time of temperature exposure was 3 h. Then the specimens were left to spontaneous cooling. In Fig. 4, there can be found images of prepared and treated specimens.

5. Results and discussion

5.1. Hydration heat

The specific hydration heat power of blended cement pastes is shown in Fig. 5. The main hydration stages were completed within 16 h. Therefore, in Fig. 6 the hydration heat development is presented in this time range. The first maximum (observed at about 5 min) reflected the first contact of the blended mixture with water. The magnitude of this peak was influenced by the wetting and dissolving heat. Regarding the impact of particular admixtures, the most decisive in this period was the granulometry of used materials. Calcined shale with the finest grains caused the highest increase of the specific hydration heat power. The application of ceramic powder with slightly smaller grains (as compared to the CAC) led to a substantial growth as well. The utilization of sintered mullite had almost no effect or caused a minor decrease, what was in accordance with the bigger grains of this material.

The second peak was already connected with the hydration process.

Table 1
Chemical composition of raw materials [%]

	Al_2O_3	SiO_2	Fe_2O_3	CaO	MgO	TiO_2	K_2O	Na_2O
Calcium aluminate cement	70.7	0.4	0.1	28.2	0.1	–	0.1	–
Ceramic powder	20.0	51.3	6	11.5	4.5	0.8	3.2	1.3
Calcined shale	47.3	49.1	0.9	0.2	0.1	1.6	0.5	–
Sintered mullite	72.0	26.0	0.3	0.1	0.1	0.2	0.6	0.2

Table 2
Mineralogical composition of raw materials [%]

Calcium aluminate cement		Ceramic powder		Calcined shale		Sintered mullite	
Amorphous	16.4	**Amorphous**	32.6	**Amorphous**	49.0	**Amorphous**	17.4
Krotite	48.8	**Quartz**	34.0	**Kaolinite**	27.0	**Mullite**	76.2
Grossite	33.5	**Illite**	10.5	**Illite**	9.3	**Sillimanite**	3.1
Mayenite	0.3	**Orthoclase**	5.1	**Quartz**	4.3	**Corundum**	2.1
Corundum	0.8	**Mullite**	3.5	**Muscovite**	3.3	**Gibbsite**	1.2
β-alumina	0.1	**Calcite**	3.2	**Mullite**	3.0		
Katoite	0.1	**Biotite**	2.8	**Anatase**	3.0		
		Microcline	2.5	**Biotite**	0.8		
		Albite	2.4				
		Hematite	2.2				
		Akermanite	1.2				

Table 3
Chemical composition of amorphous phase [%]

	Al_2O_3	SiO_2	Fe_2O_3	CaO	Na_2O
Calcium aluminate cement	11.4	0.1	3.0	–	–
Ceramic powder	9.6	4.8	3.4	9.0	–
Calcined shale	28.1	26.8	0.9	–	0.5
Sintered mullite	8.0	7.8	–	–	–

In the case of CAC, the maximum occurred after about 8.2 h and its magnitude was 20.6 mW g^{-1}. After the fall after about 16 h, the hydration heat was evolved continuously and after 120 h the total specific hydration heat reached 332 J g^{-1} (Fig. 6).

The presence of ceramic powder led to a steep acceleration and caused also higher maximum of the main hydration peak. Specifically, the paste with 5% of ceramic powder reached the maximum after 6 h, and in the case of higher dosage even after 4.4 h. The acceleration was caused primarily by the higher amount of amorphous CaO in ceramic powder. The growth of specific hydration heat power was more conspicuous in the case of lower replacement level, compared to pure CAC it was by 11%. The C15 paste with 15% replacement level showed an only 3% increase. However, the total hydration heat after 120 h was in this case lower compared to the pure CAC. The value of specific hydration heat was by 11% lower for C5, 9% for C15.

The effect of calcined shale was less distinct. The lower dosage of 5% caused a noticeable growth of specific hydration heat power by 15% but almost no shift of the time. The higher dosage (S15 paste) led to an only 8% increase, but the acceleration was comparable to the utilization of 5% of ceramic powder. It is worth mentioning that similarly to the ceramic powder, in the case of calcined shale the first parts of the specific hydration heat power curves were steeper. This can be explained by the improving effect on the hydrate's nucleation caused by finer grains of used admixtures. Regarding the total evolved specific hydration heat, calcined shale also showed a lower value after 120 h. Nevertheless, the difference was less considerable, 5% caused fall by 1% and the decrease for higher dosage was 5%.

A minimal effect on the development of hydration heat was found for sintered mullite. The maximum of specific hydration heat power of the M5 paste with lower admixture dosage was similar to reference alumina cement, with respect to both time and the particular value. When higher

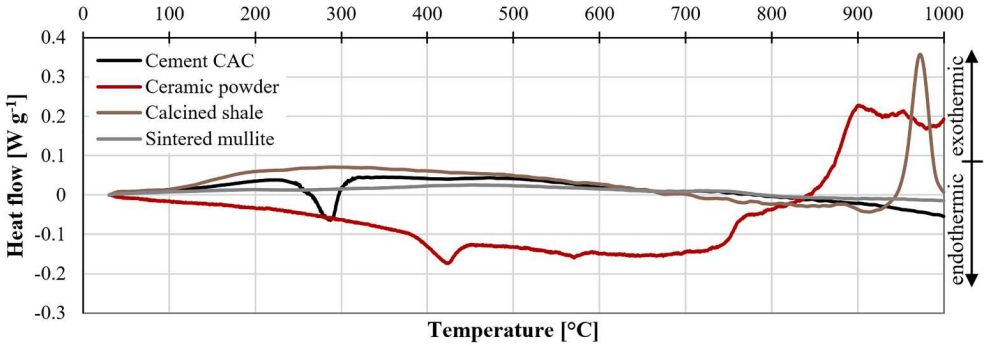

Fig. 1. DSC curves of raw materials.

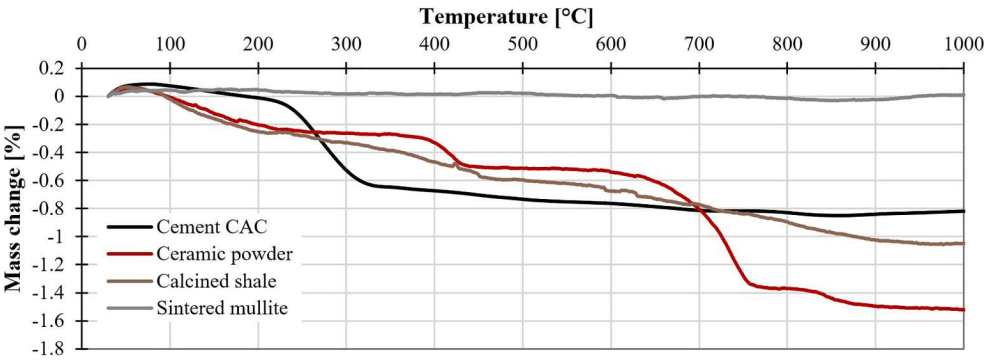

Fig. 2. TG curves of raw materials.

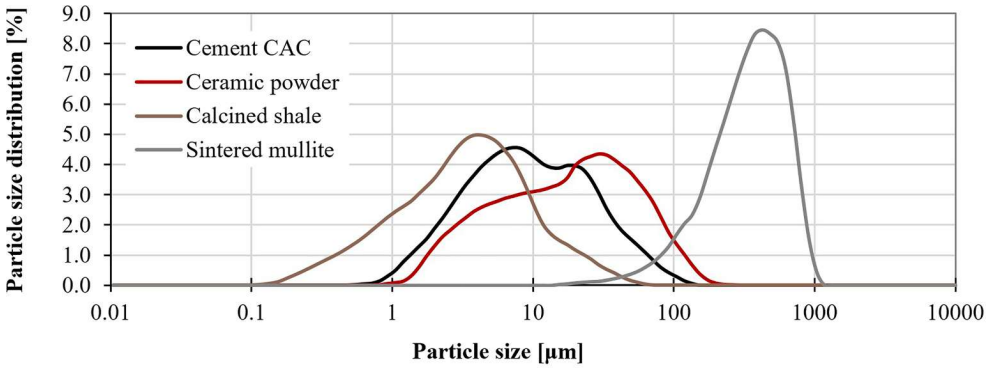

Fig. 3. Granulometric curves of raw materials.

Table 4
Composition of studied cement pastes [g]

	Calcium aluminate cement	Ceramic powder	Calcined shale	Sintered mullite	w/b
R	3000	–	–	–	0.300
C5	2850	150	–	–	0.296
C15	2550	450	–	–	0.338
S5	2850	–	150	–	0.280
S15	2550	–	450	–	0.318
M5	2850	–	–	150	0.301
M15	2550	–	–	450	0.312

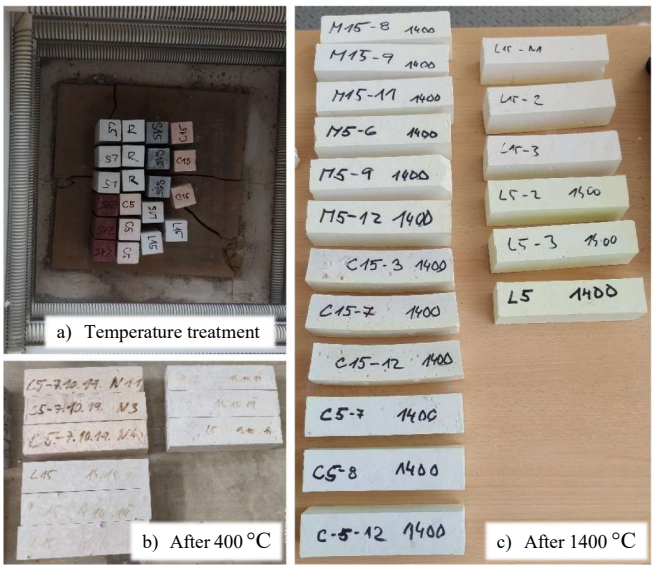

Fig. 4. Photos of measured materials: a) specimens in the electric oven, b) specimens after the exposure to 400 °C, c) specimens after the exposure to 1400 °C.

dosage was employed, the only noticeable change was observed in the time delay. The maximum was reached by about 0.4 h later compared to pure CAC paste R. Also, from the point of view of specific hydration heat, the impact of sintered mullite was the least among the studied admixtures. It caused a minor decrease, specifically by less than 1% for 5% dosage of sintered mullite and by 4% for higher percentage of that admixture.

The hydration kinetics of calcium aluminate cement containing brick powder, calcined shale or sintered mullite as an addition have not been studied yet. A similar course of hydration heat development of pure calcium aluminate cement was observed by B. Zhu [33]. They reported also only two hydration peaks and the second main peak occurred approximately 8 h after mixing. Mineral admixtures studied in the work of Idrees [24] also caused accelerating of hydration, as the maximum of hydration peak was fairly higher for silica fume, fly ash, as well as GGBFS blended mortars. The time of its occurrence was also much shorter. As it was mentioned in the Introduction, the application of 15% metakaolin studied by Nowacka et al. [27] led to the accelerating of hydration. Despite the varying curing condition, metakaolin and calcined shale are on the similar basis, and thus their impact should be similar, and the obtained results were in conformity with their study. Several varying studies dealing with hydration heat of CAC with different additives were found. For example, the effect of alginates on the hydration of calcium aluminate cement was studied by Engbert et al. [34]. It was shown that alginate accelerates the hydration heat. The early hydration of CAC with different kinds of zinc was studied by Wang et al. [35]. It was found that zinc salt delayed the hydration heat development, on the other hand the total hydration heat was higher than for reference CAC.

5.2. Cement stone characterization

The characterization of the cement stones was performed using XRD in a combination with DSC analysis (Fig. 7). The CAC phases are generally of crystalline structure, and thus XRD should be sufficient for the phase determination. However, the crystal structure of C_2AH_8 has not been described yet, in the case of CAH_{10} there were several attempts, but it seems to be more appropriate to combine both methods. Therefore, a thorough description of DSC curves was given in the following sections dealing with cement stone's composition after particular temperature treatment. Besides that, SEM images and their analysis were employed at the ambient temperature as well, on the account of presented results confirmation. Measured diffractograms as well as more SEM images can be found in Supplementary materials.

5.2.1. Ambient temperature

At the ambient temperature (Fig. 8) the reference cement paste R showed a common composition, with only minor difference – no CAH_{10} content. Despite the monitored temperature of 20 °C during the hydration, it seems, that the evolved hydration heat caused samples warming, which led to the primarily katoite C_3AH_6 formation. Based on the DSC it can be assumed, that C_2AH_8 arose as well, but the peak is quite small, and on the XRD diffractogram this phase was not observed. On that account it can be assumed that this phase is present in a minor amount. This was confirmed also by SEM observation (Fig. 9, supplementary materials), where only minor crystals of C_2AH_8 were found. Regarding the aluminum hydroxide $Al(OH)_3$, its crystal structure was primarily in the form of gibbsite, accompanied by smaller amounts of nordstrandite and bayerite. However, a relatively high amorphous content was found. Other observed phases included unreacted krotite

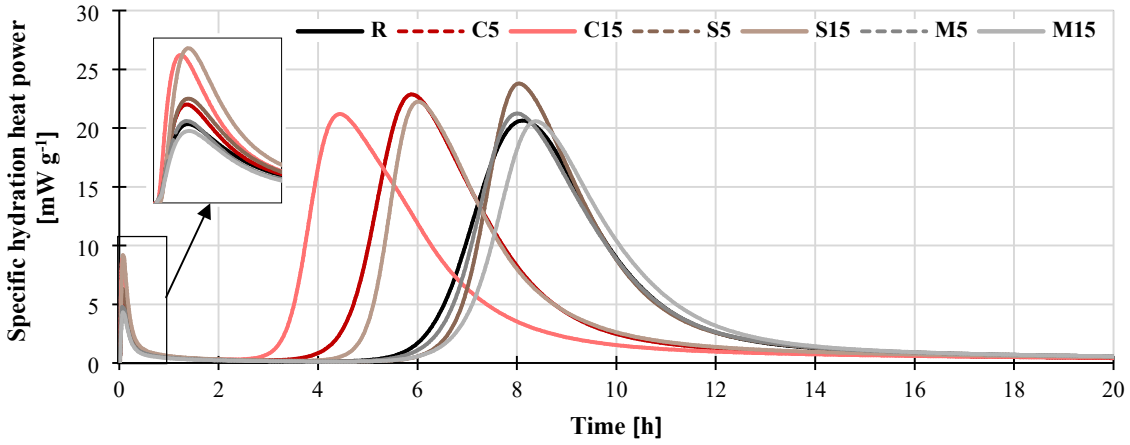

Fig. 5. Specific hydration heat power of studied pastes.

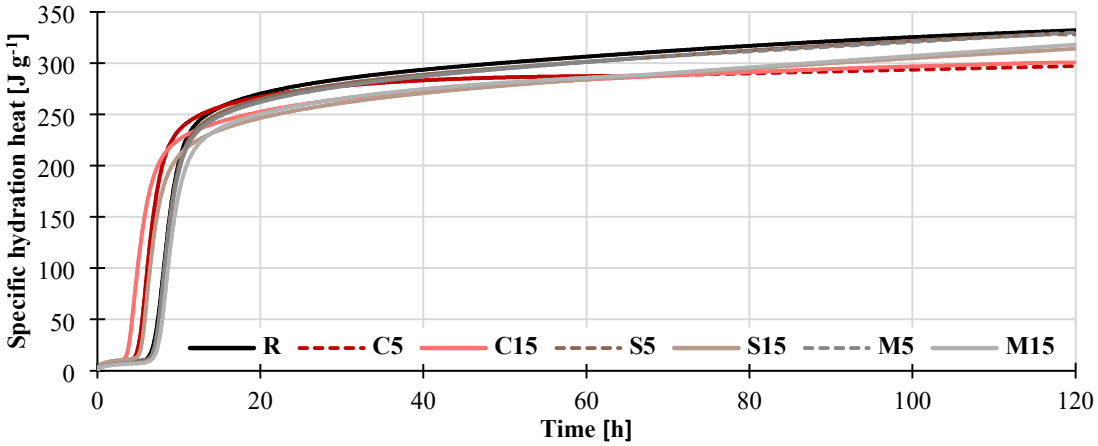

Fig. 6. Specific hydration heat of studied pastes.

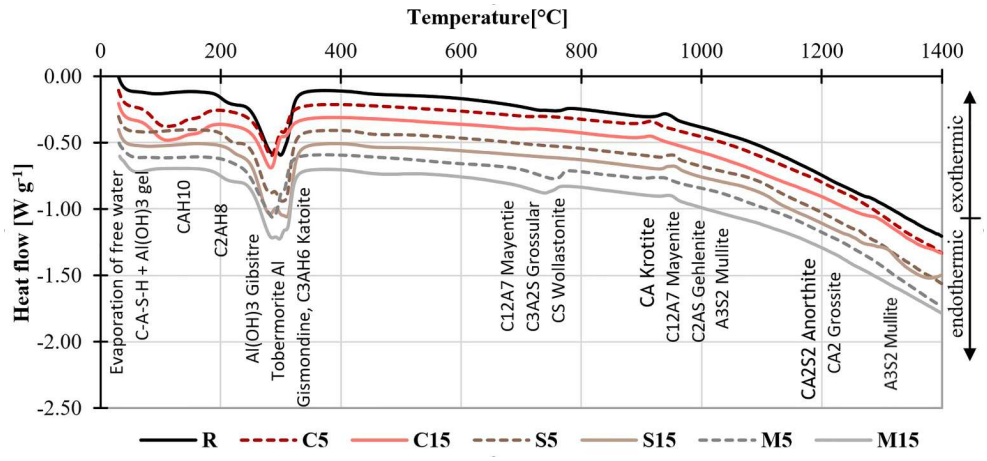

Fig. 7. DSC of studied cement stones.

CA and grossite CA_2 grains. Their amounts give some sight of hydration degree of cement paste.

The biggest impact on hydration was observed in the case of ceramic powder utilization. The SEM images (Fig. 9, supplementary materials) are distinctively different as the structure was composed primarily of needle shaped crystals. It was the only material with proved CAH_{10} and C_2AH_8 content (Fig. 7, supplementary materials). The amount of C_2AH_8 was not determined, but it is covered in the amorphous and not identified phase, which values were in the case of C5 and C15 sharply bigger. Regarding the katoite C_3AH_6, this hydrate was present in lower amount as well as crystalline aluminum hydroxide $Al(OH)_3$. Such phenomenon of metastable hydrates formation can be attributed to lower hydration degree of krotite CA, which during hydration released a high amount of heat at once. On the contrary, grossite CA_2 released heat continuously

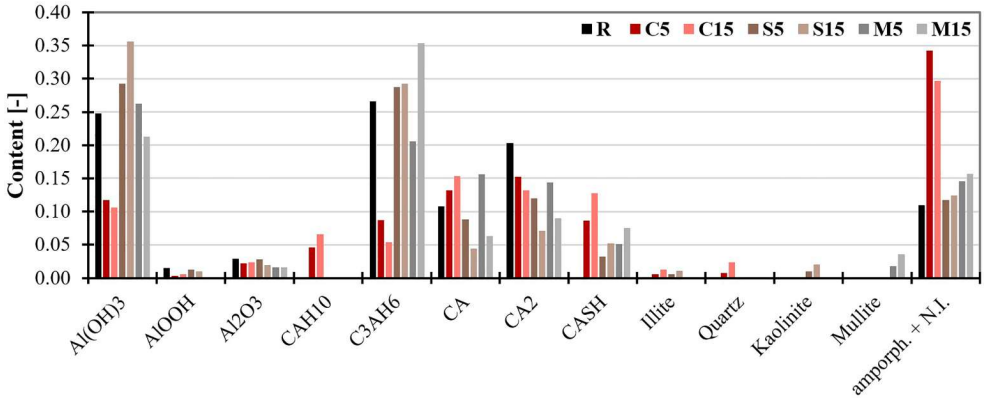

Fig. 8. Phase composition of studied cement stones at ambient temperature.

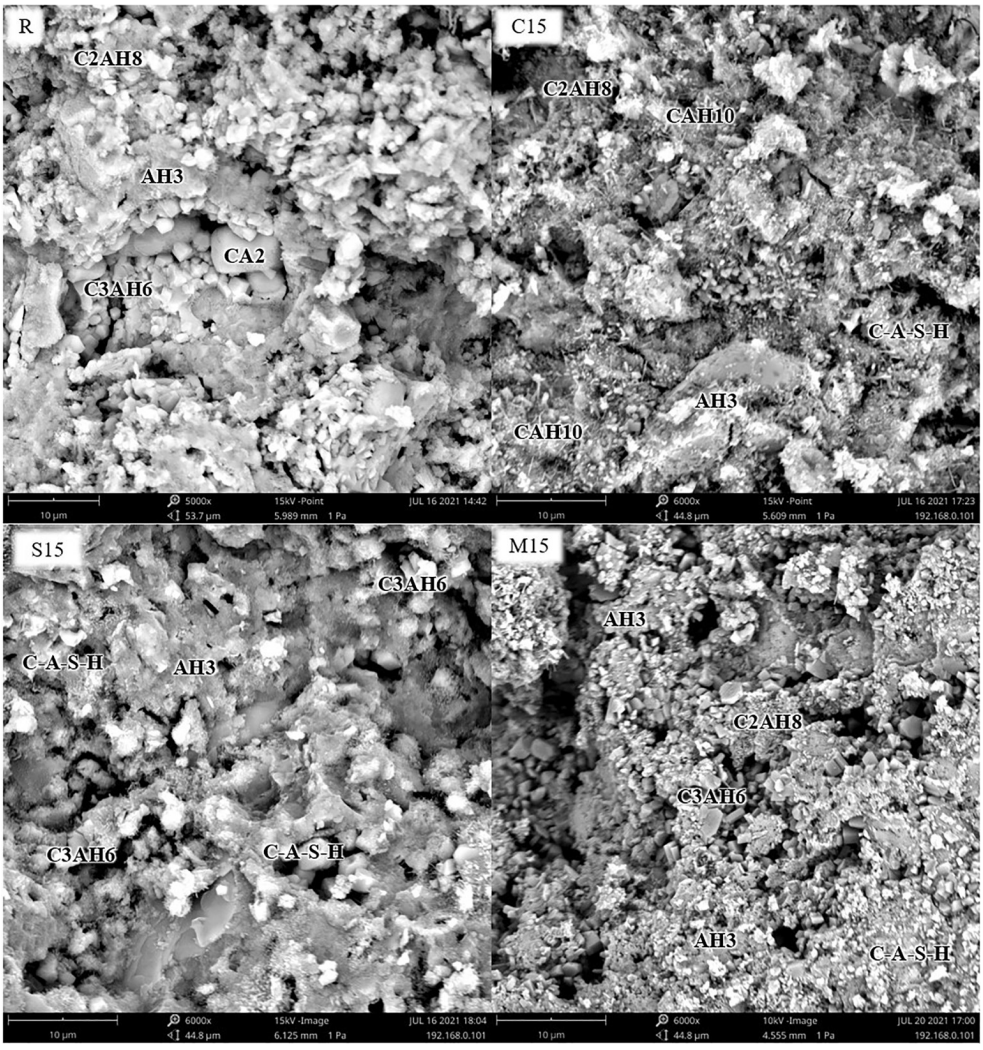

Fig. 9. SEM images of cement stones at ambient temperature at the age of 28 days.

for a longer time [2]. Thus, the overheating of the samples did not have to be so severe. Another issue was probably higher reactivity of ceramic powder, which gave rise to the higher amounts of C-A-S-H phases. Consequently, the exothermic hydration reaction of calcium aluminates could be somewhat mitigated. A substantial role could also play similar granulometry of CAC and ceramic powder, which contributed to the hydration mitigation. Contrary to the common assumptions, the main structure of C-A-S-H phases observed in this work was not stratlingite C_2ASH_8, but gismondine CAS_2H_4, accompanied by Al rich tobermorite, and hibschite. It is attributed to the poor crystallization rate of stratlingite or its metastability in combination with CAC, as it was already reported elsewhere [2,36,37].

The calcined shale has the biggest amorphous content, and thus it had been assumed to be the most reactive. Despite that fact, the

hydration products were not as much changed (both DSC and XRD curves showed almost the same performance). The amounts of CA and CA_2 in cement stone of S5 and S15 were distinctively decreased, simultaneously the amount of $Al(OH)_3$ and C_3AH_6 grew up. It seemed that calcined shale application led primarily to the higher hydration degree. The lowest amount of varying crystalline C-A-S-H phases was observed in this case. Therefore, it was concluded that calcined shale grains served more as an improving element for hydrates' nucleation and contributed to the formation of amorphous phase.

The performance of the last studied admixture – sintered mullite - varied significantly with the different dosage. In the case of M5, where 5% of mullite was used, the performance was comparable to the ceramic powder application, but in this case stable hydrate katoite C_3AH_6 was formed instead of the metastable ones. This can be attributed especially to lower amount of mullite's amorphous phase, which was in this case confirmed also by lower amounts of C-A-S-H phases. When one is focused on the cement stones with higher admixture dosage, it is obvious that 15% of mullite led to the higher hydration degree as both krotite CA and grossite CA_2 amounts were significantly decreased (Fig. 7). However, also in this case the heating of a sample seemed to have a crucial impact, because no CAH_{10} and only minor amount of C_2AH_8 were observed. In accordance, the SEM images (Fig. 9, supplementary materials) revealed the highest amount of katoite C_3AH_6, and minor amount of C_2AH_8. Moreover, the hydration of another different phases was confirmed as well, as the higher amount of crystalline C-A-S-H was determined, together with the bigger peak around 60 °C which was attributed to the dehydration of mentioned C-A-S-H phases (regardless of the structure type).

To make a description of reached results complete, it is worth to mention, that unreacted crystalline phases of original admixtures were observed in minor amounts as well; illite and quartz for ceramic powder, illite and kaolinite for calcined shale, and mullite for sintered mullite.

Comparing the obtained results with the impact of other admixtures, a higher amount of arising amorphous phase was reported also in the case of microsilica. According to the Mercury et al. [20] the C-A-S-H was primarily in the amorphous phase, and the presence of stratlingite was reported only in the higher dosage of microsilica and hydration temperature of 65 °C. Similar results were presented by Lee et al. [21] who observed C-A-S-H primarily in amorphous phase. In the work of Hidalog [23] different hydration products were observed when silica fume and fly ash were used. They observed not only hydrogarnet and stratlingite C_2ASH_8, but also laumontite CAS_4H_4. However, this mineral was present only in the case of the higher admixture dosage, more precisely when the higher amount of amorphous silica was used. In this paper, calcined shale with the highest content of amorphous silica among the studied admixtures still showed its by about 50% lower amount than fly ash. Thus, in conformity with their results this mineral was not observed. Another issue of stratlingite C_2ASH_8 presence was reported by Idrees [24] and Kirca [25]. According to their observation, this mineral was not formed as a product of hydration, but it raised during the conversion process of C_2AH_8, when stratlingite C_2ASH_8 was the stable product of conversion instead of katoite C_3AH_6. Regarding the GGBFS, Cheng et al. [26] reported a similar impact as in the case of microsilica [20]. The presence of stratlingite C_2ASH_8 was observed only in the case of the higher replacement level, specifically when the dosage of GGBFS was higher than 20%.

5.2.2. *Cement stones at 400 °C*

The phase composition of specimens exposed to 400 °C is summarized in Fig. 10. As it was expected the amount of krotite CA and grossite CA_2 remained unchanged, compared to the results at the ambient temperature (Fig. 8). Also, the amount of unreacted crystalline phases of admixtures (specifically illite, quartz, kaolinite, mullite) remained constant.

Regarding the other changes, after exposure to 400 °C the main process was (at it is delineated in Fig. 7) dehydration of hydrated phases. Successively, the evaporation of free water, jointly with the dehydration of amorphous $Al(OH)_3$ and C-A-S-H phases took places. Then at the temperature between 100 and 240 °C, several processes could occur: Dehydration of CAH_{10} (100–160 °C [3]) and stratlingite (100–240 °C [38]), partial dehydration of gismondine (105–155 °C [39]), and finally dehydration of C_2AH_8 (140–240 °C [3]). Afterwards, the biggest group of peaks was observed in the temperature range between 210 and 370 °C. Similarly to the previous temperature range, also in this case more processes could be identified: primarily the gibbsite AH_3 decomposition (210–320 °C [3]), followed by the dehydration of katoite C_3AH_6 (240–370 °C [3]). However, besides these main transformations, also Al-rich tobermorite (300 °C [40]) and gismondine (350 °C [39]) recrystallizations took place. As a final product of the mentioned processes, boehmite γAlOOH, partially dehydrated hydrogarnets (specifically $C_4A_3H_3$, $C_{12}A_7H$ and $C_{12}A_7H_{15}$), and new let's say "dehydrated" C-A-S-H phases (specifically rivesideite and Ca-feldspar structures) were observed.

When focused on the particular admixtures, the varying amount of mentioned dehydrated phases corresponded to the differences at ambient temperature. The biggest quotable change was observed in the case of amorphous and not identified phases of pastes containing ceramic powder. That was caused by the high amount of C_2AH_8, which was included in this value. After 400 °C, the C_2AH_8 was dehydrated, and consequently the amount of amorphous phase of specimens with ceramic powder C5 and C15 phase was slightly lower than of reference stone R.

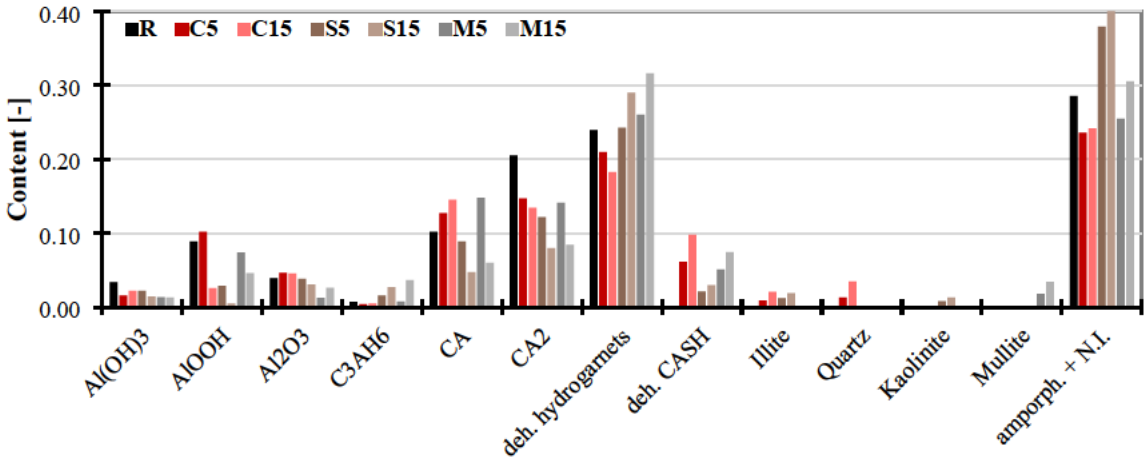

Fig. 10. Phase composition of studied pastes after exposure to 400 °C.

5.2.3. Cement stone at 1000 °C

In Fig. 11 the phase compositions of studied cement stones after temperature loading by 1000 °C can be found. In contrast to the range up to 400 °C, the dehydration of phases continued much more gradually between 400 °C and 1000 °C. The observed peaks were much smaller (see Fig. 2). The first endothermic peak in this interval can be generally attributed to the dehydration of varying phases, when the final products were wollastonite CS (700 °C [40]), grossular C_3AS_3 (700 °C [41]), or mayenite $C_{12}A_7$ (stepwise 620 °C, 690–750 °C [39]). In confrontation with the phase composition of the reference material and those with sintered mullite, it was concluded, that this peak signified mayenite occurrence. Another peak was observed around 900 °C, this time in all cases of studied cement stones. The exothermic peak can also signify several processes: crystallization of krotite CA (800–1000 °C [3]), corundum αAl_2O_3 (940–1050 °C [3]), or gehlenite C_2AS (930 °C [38]). Besides those processes, also recrystallization of grossite CA_2 had to begin, as its amount significantly grew. In general, this transformation should take place at higher temperatures (1000 – 1300 °C), but the growth of grossite CA_2 amount in cement stones was undisputable. The dehydration should be supposedly completed at 1000 °C but it was obvious that minor amounts of dehydrated hydrogarnets remained. Specifically, it was $C_4A_3H_3$, which can be present up to 1100 °C, when its complete transformation to mayenite $C_{12}A_7$ takes place [41].

Regarding the impact of studied admixtures, their application led to the crystallization of new CAS phases, specifically to the formation of gehlenite C_2AS which was the dominant phase in all cases of studied admixtures. Grossular C_3AS_3 and anorthite CAS_2 were also found, but just in minor amounts. In the case of ceramic powder and calcined shale application, another new phase was found. Minor amount of mullite was observed, as a consequence of recrystallization of dehydroxylated kaolinite and illite. This phase of transformation occurred at about 980 °C [42] and besides mullite also a diminutive amount of silica SiO_2 arose.

5.2.4. Cement stones at 1400 °C

The last studied loading temperature was 1400 °C. The results are presented in Fig. 12, where the phase compositions of studied cement stones exposed to the highest temperature can be found. The main difference compared to 1000 °C is in the amount of calcium aluminate phases. As it was described above, the transformation of grossite CA_2 from krotite CA took place, and thus amount of krotite CA was significantly reduced. The content of hibonite CA_6 also begun to arise. This material originates from grossite CA_2, generally at temperatures from 1400 to 1600 °C [43]. The second highest change was observed in the case of CAS phases. This time it was not any new phases occurrence, but a significant growth of gehlenite C_2AS amount, especially in the case of 15% dosage.

The application of ceramic powder and calcined shale had a significant impact on krotite CA transformation. Especially the 15% dosage caused a remarkable acceleration of this reaction, as the amount of krotite was lower than 4%. Moreover, these higher dosages also showed some deflections in DSC at the temperatures above 1300 °C (Fig. 7), this was attributed to the further recrystallization of mullite, which can occur up to 1400 °C [42]. In contrast, sintered mullite showed a different behavior; the highest amount of alumina Al_2O_3 and hibonite CA_6 was present, while the amount of mullite remained unchanged. Sintered mullite utilization also led to the modification of CAS phases, as the higher amount of anorthite was observed.

5.3. Thermomechanical analysis

The thermal strains of the studied pastes up to 1000 °C are presented in Fig. 13, while their thermal expansion coefficients can be found in Fig. 14. Up to about 100 °C, all pastes showed a minor expansion. The maximal values of thermal expansion coefficients were observed at about 75 °C. As it was described hereinabove, the evaporation of free water together with dehydration of amorphous $Al(OH)_3$ and C-A-S-H took place in this temperature range. However, these changes caused no shrinkage of the analyzed materials. It is quite important that in this temperature range the application of ceramic powder, as well as calcined shale caused only a minor growth of the thermal strain and the thermal expansion coefficient, whereas sintered mullite somewhat reduced it.

The decrease of thermal strain began after about 100 °C, where the dehydration of CAH_{10}, stratlingite C_2ASH_8 and gismondine CAS_2H_4 was proved to take place. The reference paste R did not contain such components, and thus its thermal strain decrease was the lowest and its thermal expansion coefficient showed the lowest value as well. On the contrary, ceramic powder showed the highest decrease and the highest thermal expansion coefficient among the studied pastes, what was in accordance with its composition (the highest amount of mentioned phases).

The deepest fall of the thermal strain was observed in the temperature range from about 210 °C to 370 °C where the main dehydration processes took place. The reference paste R also in this range showed the lowest fall, in conformity with its composition. Regarding the impact of the studied admixtures, the higher dosage was used, the higher fall of thermal strain was observed. When focused on particular admixtures, calcined shale showed the biggest impact, closely followed by ceramic powder. Sintered mullite proved to have a much lower effect, however also its application caused a fall of thermal strain.

In the temperature range up to about 700 °C all studied materials

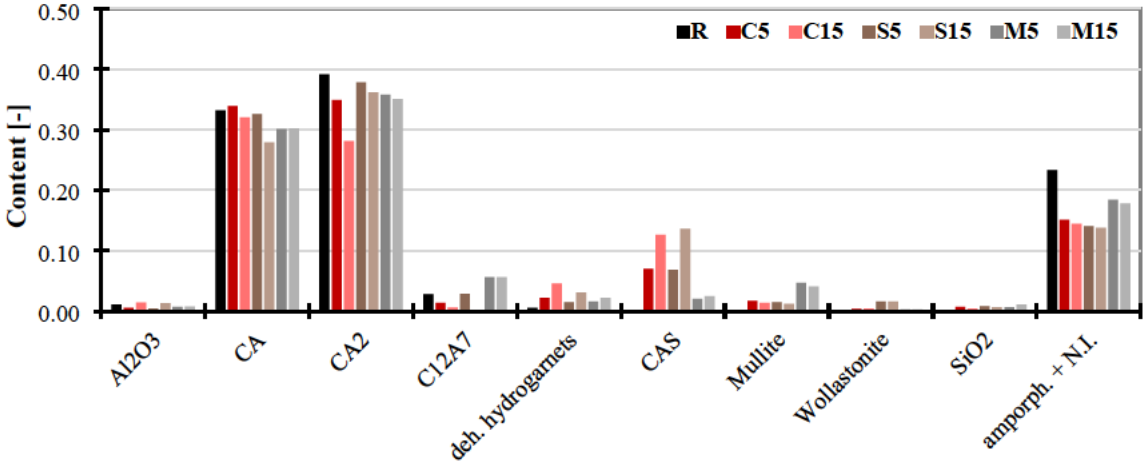

Fig. 11. Phase composition of studied cement stones after exposure to 1000 °C.

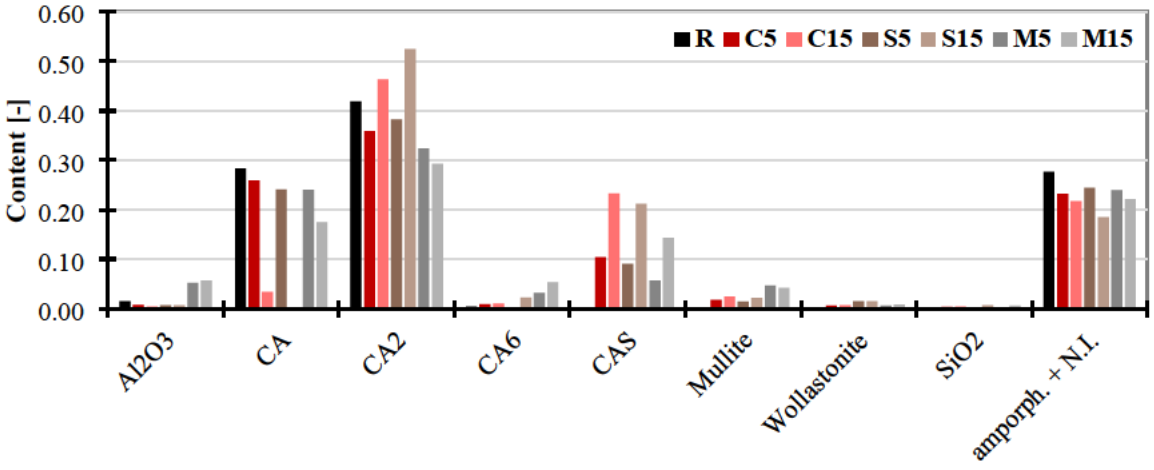

Fig. 12. Phase composition of studied cement stones after exposure to 1400 °C.

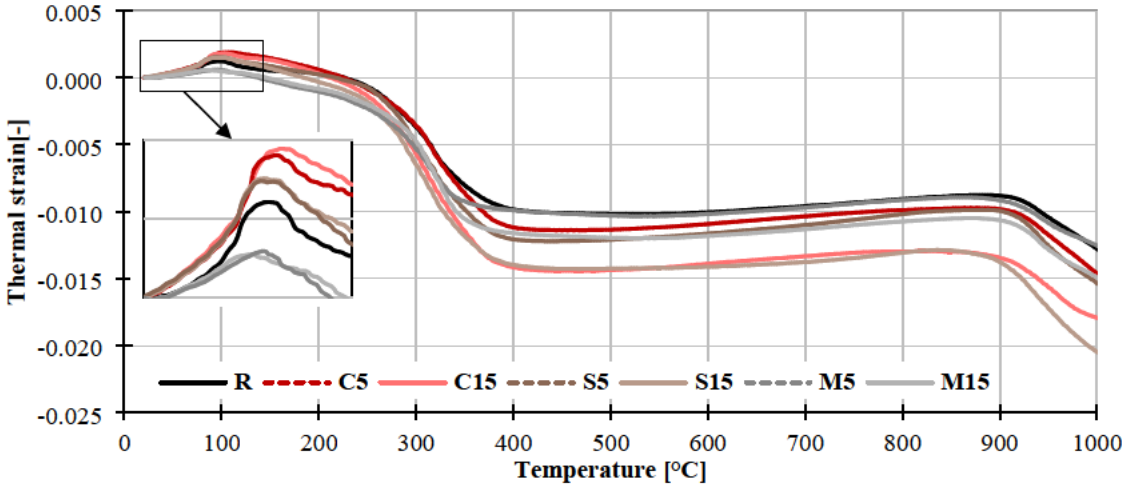

Fig. 13. Thermal strain of studied pastes up to 1000 °C.

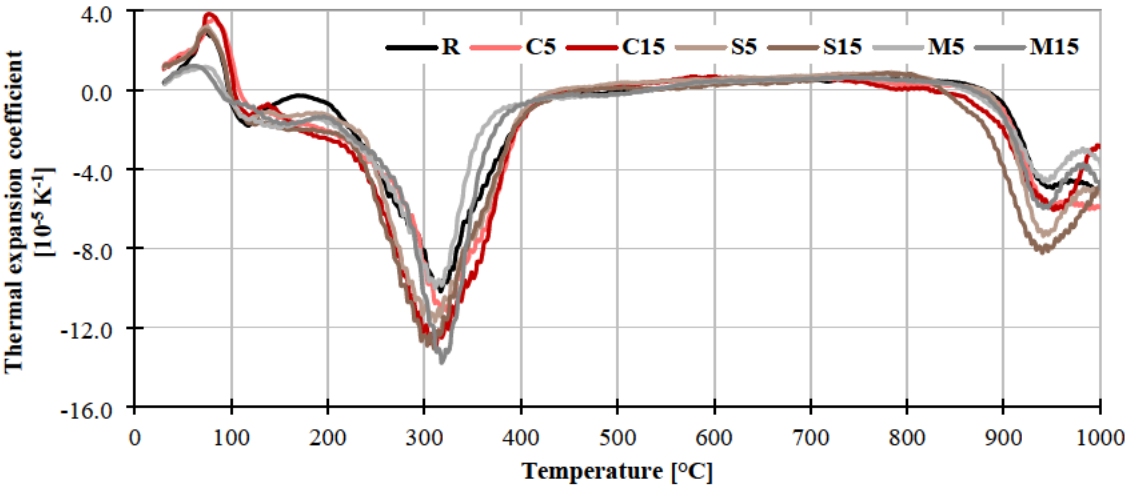

Fig. 14. Thermal expansion coefficient of studied pastes up to 1000 °C.

showed linear thermal strains and equal values of thermal expansion coefficient. No important phase transformation occurred and thus thermal strain continuously increased. Krotite CA and gehlenite C_2AS recrystallized between 800 and 850 °C, which led to a substantial fall of thermal strain, as well as of thermal expansion coefficient. The reference material showed the lowest decrease, followed by mullite, ceramic

powder. The highest difference caused calcined shale.

5.4. Basic physical properties

The basic physical properties were measured at the ambient temperature and after exposure to temperature loading by 400 °C, 1000 °C and 1400 °C. The values of matrix densities are presented in Fig. 15. The maximal difference of matrix densities at the ambient temperature was about ± 3% compared to the reference paste R. Ceramic powder as the only admixture caused the matrix density to fall, the C5 and C15 blended pastes were also the only materials with a higher amount of metastable hydrates CAH_{10} and C_2AH_8 and the biggest amount of C-A-S-H phases. The mentioned phases had lower values of specific gravity compared to katoite C_3AH_6, which was dominant in the case of reference paste R. In accordance with this conclusion, the calcined shale and sintered mullite aplication led to the matrix density growth. In the case of calcined shale, the growth was continuous, and thus it could be concluded, that with the increasing amount of this admixutre the hydration degree was increased and as a consequence also the matrix density went up. In the case of sintered mullite, the performance was reverse, the 5% dosage led to the matrix density growth, while 15% caused an additional reduction. This phenomena could be also linked to the phase composition; the M5 paste with 5% of sintered mullite showed the lowest hydration degree, and thus was composed of denser unhydrated phases. In the case of M15 with 15% od admixture dosage, the more important role played higher amount of C-A-S-H phases, which have much lower specific gravity.

In all cases of high-temperature pretreatment, the matrix density went up as a consequence of dehydration resulting in later hydration of denser phases. When focused primarily on 400 °C, the highest growth showed the paste with ceramic powder, specifically by 13% and 18% (compared to the ambient temperature) for 5% and 15% of admixture dosage, respectively. The reference paste showed a growth by 8% and the two other admixtures, calcined shale and sintered mullite, reached a similar increase by 5%. The further temperature loading by 1000 °C caused a consecutive growth of matrix densities. . However, the residual values of blended pastes were by up to 2% higher compared to the reference paste R. This performance was atributed to the higher amount of gehlenite C_2AS in these pastes, as this phase shows a higher specific gravity compared to korite CA and grossite CA_2. However, as the differences of residual matrix density were quite small, no specific impact of admixtures' aplication could be derived. The exposure to 1400 °C caused almost no differneces as well. Moreover, no noticeable changes were observed compared to the previous temperature.

The measured values of bulk densities are presented in Fig. 16. Generally, this property is related to matrix density and porosity, thus the specific explanations of bulk density performance can be found in previous or following paragraphs where behaviors of mentioned basic properties are described in detail. However, it is worth mentioning that at the ambient temperature the application of all studied admixtures led to the bulk density decrease. The maximum fall was observed in the case of 15% dosage of ceramic powder and calcined shale.

The exposure to 400 °C led to the decrease of residual bulk densities, by 11% in average. The fall continued up to 1000 °C, when the values were, in average, by 15% lower compared to the ambient temperature. The last loading temperature of 1400 °C caused the biggest changes. The residual values, influenced by sintering process, went up sharply. The highest growth was observed in the case of 15% of calcined shale (S15); compared to the ambient temperature the residual bulk density was by 15% higher and compared to 1000 °C even by 30%.

The last analyzed basic physical property was the porosity. The achieved results can be found in Fig. 17. At the ambient temperature all studied admixtures caused a distinguishable growth of porosity. Both ceramic powder and calcined shale showed a gradual increasing tendency; as the dosage grew, the porosity went up; for ceramic powder C5 and C15 by 10% and 18%, respectively, and for calcined shale S5 and S15 by 10% and 38%, as compared to the reference paste R. A different behavior was observed for sintered mullite. M5 with 5% dosage caused a growth of porosity even by 29%, but when 15% was used, the increase was only 9% compared to the reference paste R. This varying performance could be attributed to the different granulometry, specifically to the bigger grains of sintered mullite, which could affect the pore distribution.

As a result of cement pastes dehydration, the porosity was significantly increased after the exposure to 400 °C. However, the increasing impact of admixture application remained identical. In accordance with the observed phase composition, specifically the highest amount of unstable hydrates CAH_{10} and C_2AH_8, the ceramic powder application led to the biggest growth of residual porosity; by 80% and 101% for C5 and C15. On the contrary, despite the higher hydration degree, the application of two other admixtures (calcined shale and sintered mullite) led to a smaller growth of porosity, as compared with the reference pastes R. After the exposure to 1000 °C the studied pastes showed the highest values of porosity among the studied conditions. However, the difference between particular materials was lower than 3% (except for the paste C15 with 15% of ceramic powder), which was two times lower than the accuracy of the used method. On that account, no conclusion of admixture impact could be deduced in this case.

The residual porosity after the exposure to 1400 °C was significantly influenced by the sintering process. Its values went down by 31% in average as compared to 1000 °C. Ceramic powder showed a similar performance as the reference paste R, calcined shale application led to a higher fall and in the case of sintered mullite a lower decrease was observed. Some explanation of this performance could be probably found in different granulometry of used admixtures: ceramic powder showed equal grain size distribution as the calcium aluminate cement, calcined shale had smaller grains, while sintered mullite bigger ones.

The porosity, more precisely the pore structure, was measured by Cheng et. al [26], who presented a similar porosity increase due to the supplementary cementitious material application. However, they used MIP for determining the pore structure and found that GGBFS affected only pores with the diameter in the range of 0.001 to 0.1 μm. Regarding the impact of the high temperature exposure, they reported a substantial porosity increase up to 800 °C

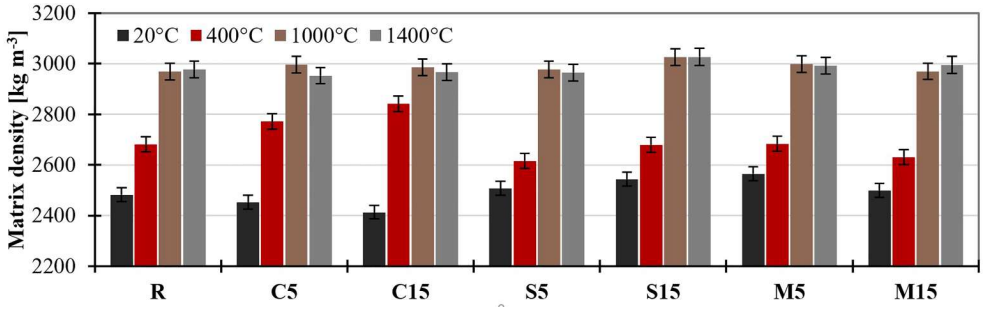

Fig. 15. Matrix density of studied pastes.

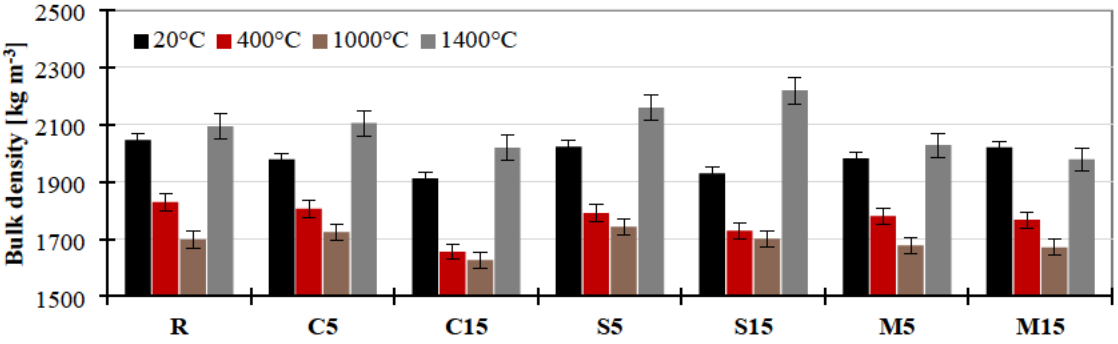

Fig. 16. Bulk density of studied pastes.

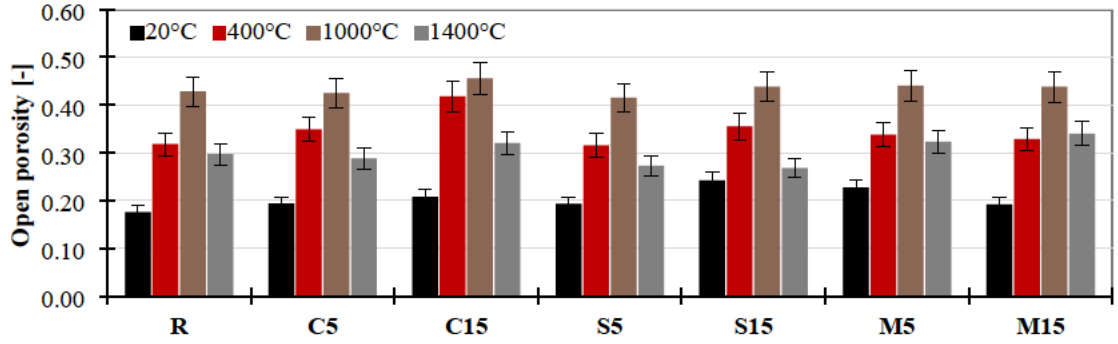

Fig. 17. Porosity of studied pastes.

5.5. Mechanical parameters

The residual mechanical parameters were determined in the four different thermal-load based states. One of the most important characteristics for practical applications is compressive strength. The results obtained for the studied cement pastes are summarized in Fig. 18. At the ambient temperature the utilization of the analyzed admixtures caused generally a growth of compressive strength. In the case of ceramic powder, the increase was the highest; by 29% for 5% dosage and even by 42% when 15% was used. This behavior was in line with the phase compositions. The samples with ceramic powder contained metastable hydrates (CAH_{10} and C_2AH_8), as well as the biggest amount of C-A-S-H, which resulted in the highest mechanical strengths. In the case of calcined shale, the positive impact was observed only in the case of 5% dosage, when the growth of compressive strength was by 30%. On the contrary, despite the higher hydration degree, and thus higher amounts of hydrated phases, the 15% dosage led to a minor fall by about 5%. The most decisive factor was the porosity (Fig. 17), which was in the case of paste with 15% of calcined shale fairly higher. The sintered mullite, similarly to the ceramic powder, caused a compressive strength increase; specifically, by 20% for 5% dosage and 33% for 15%. When linking that result to the phase composition, it seems to be accurate, because these materials based on sintered mullite showed a higher hydration degree, and thus bigger amounts of strength-bearing katoite C_3AH_6 and C-A-S-H phases, but no CAH_{10} and C_2AH_8.

Regarding the impact of temperature up to 1000 °C, the compressive strength was primarily influenced by hydrate phases' dehydration, and simultaneously by the porosity growth. In general, the obtained values for blended pastes were (with two exceptions) somewhat higher compared to the reference CAC. However, compared to the ambient temperature, the decrease of residual compressive strength was the most significant in the case of ceramic powder application, in conformity with the highest amount of metastable phases C-A-H, as well as C-A-S-H phases at ambient temperature. Due to the exposure to 400 °C, the fall of

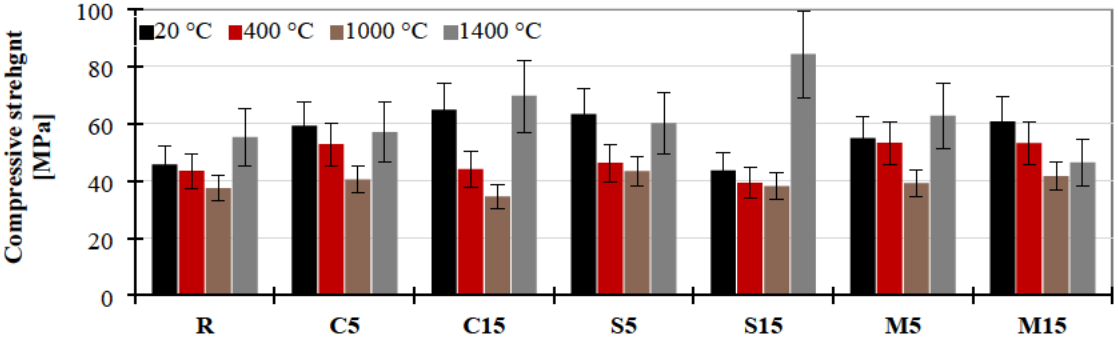

Fig. 18. Compressive strength of studied pastes.

residual compressive strength was by 11% and 32% for C5 and C15, respectively. For 1000 °C it was even by 32% and 47% for 5% and 15% dosage of ceramic powder. Calcined shale proposed a better performance, as the decrease was only by 7% and 10% for particular dosages at 400 °C. After exposure to 1000 °C, the paste with 5% of calcined shale showed a higher fall of residual compressive strength, by 27%. However, 15% dosage remained indisputably positive, when the decrease of compressive strength was only 13%. The composition of the pastes with calcined shale was the most similar among studied admixtures to the reference paste R. Thus, their performance was also the closest to the behavior of the CAC paste, of which residual compressive strength went down by 5% and 18% for the exposure to 400 °C and 1000 °C. Sintered mullite likewise reached a good performance after the exposure to 400 °C, the fall was by 3% for 5% dosage and 13% when 15% was used. However, after the loading by 1000 °C, the residual compressive strength went down more distinctively, by 29% and 31% for the particular dosages. This phenomenon of higher fall could be attributed to the highest presence of mayenite $C_{12}A_7$, which was decomposed in this temperature range.

After the exposure to 1400 °C the compressive strengths were significantly increased, and particular results reached the highest values. This was in accordance with the porosity changes, particularly with the sintering of studied pastes which occurred after reaching approximately 1200 °C. Except for the M15 paste with 15% of sintered mullite, the compressive strengths of blended pastes were always higher as compared to the CAC. The highest growth was observed in the case of S15 with 15% of calcined shale, what is in accordance with the lowest residual porosity of this paste. Another significant impact could have the phase composition. The recrystallization of krotite CA was in the case of S15 complete. Similarly, the second highest residual compressive strength was shown by the C15 paste with 15% of ceramic powder, when only minor amount of krotite CA was observed. Thus, it could be concluded, that recrystallization of krotite CA to grossite CA_2 led to a significant increase of residual compressive strength.

For a comparison with the effect of other admixtures, the results of Collepardi et al. [22], who reported a decreasing effect of silica fume on the compressive strength of blended CAC pastes, were used. A detailed specific comparison could not be done in this case as they studied low-alumina cement. However, the systematic lowering impact of the silica fume was indisputable. A more deteriorating impact was observed for fly ash, which they concluded to be unsuitable for CAC. Contrary to that, all admixtures used in this paper exhibited a positive effect and a better performance. Compressive strength of a material with GGBSF was analyzed in [25]. Its value for mortar with 20% cement replacement at 28 days and cured at 20 °C decreased by 14% when compared to the reference material. On that account, it can be concluded that the non-convectional admixtures used in this study performed better, as the biggest decrease of compressive strength was only 5% (the S15 paste with calcined clay). Con the other hand, Cheng et al. [26] observed a positive impact of GGBSF on the compressive strength of blended paste up to the replacement level of 40%. However, they used low-alumina cement, and curing condition was 50 °C.

The values of bending strengths are presented in Fig. 19. It can be seen that this parameter was significantly impaired by the application of ceramic waste, especially by its higher dosage. The bending strengths were reduced by 9% and 21% for 5% and 15% of ceramic powder, respectively. On the contrary, the two other admixtures had a positive impact, as the bending strength was increased. In the case of calcined shale, the improvement was lower, the bending strength values went up by 7% and 14% for S5 and S15, respectively. The best results were observed when sintered mullite was used. This time, the growth was by 10% when 5% of mullite was used, and even by 43% when the higher dosage was used. An explanation for the varying bending strengths can be found in the different amounts of amorphous phases of the studied materials, as well as in the varying granulometry of used raw materials. It seems that the higher amorphous phase a particular paste contained, the higher bending strength the material showed.

In general, the high-temperature loading caused similar changes of bending strength as in the case of compressive strength. However, the alteration was much more distinctive. The reference paste R showed after exposure to 400 °C by 39% lower residual bending strength than at the ambient temperature. When 5% of admixtures was used, the fall was somewhat reduced. Specifically, the residual bending strength was lowered by 34%, 38% and 37% for C5, S5 and M5 pastes. On the other hand, the higher dosage showed a worsening impact, the biggest change was observed in the case of 15% of ceramic powder. The C15 paste after the exposure to 400 °C had by 68% lower residual bending strength compared to the ambient temperature. The remaining admixtures also caused a bending strength decrease, but it was less distinct. The application of 15% of calcined shale led to the decrease by 41%, while sintered mullite caused in this dosage a fall by 47%. The blended pastes showed a better performance after exposure to 1000 °C, as compared with the reference paste R. The CAC paste showed by 87% lower value of residual bending strength, while with the application of studied admixtures the fall was decreased by about 79%, in average.

Similarly to the compressive strength, the sintering process had also a crucial impact on the residual bending strength behavior after the exposure to 1400 °C. However, the final values of residual bending strengths were not always higher compared to the ambient temperature. The reference paste R showed by 35% lower bending strength value, which was the worst deterioration. On the contrary, the ceramic powder had the best results, as its residual bending strength was by 37% higher than at the ambient temperature. When calcined shale was used, the residual bending strength was also higher, this time by 2% and 16% for particular dosages. The paste with sintered mullite showed, similarly to the reference R, lower residual bending strengths, but the decrease was lower, by 23% when 5% was used and by 19% in the case of 15% dosage.

6. Conclusions

This paper was focused on the study of nonconventional supplementary cementitious materials applicable for calcium aluminate

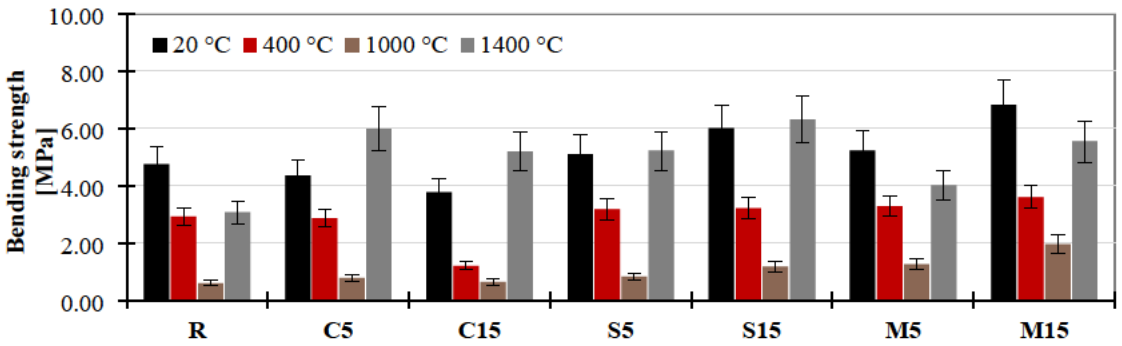

Fig. 19. Bending strength of studied pastes.

cement. Specifically, waste ceramic powder, calcined shale, and sintered mullite were tested as the possible candidates. As a reference material, medium alumina cement paste was employed. Then, 5% and 15% of cement amount was replaced by particular admixtures. The samples were cured at 20 °C and tested at the age of 28 days. The main findings can be summarized as follows:

- Ceramic powder exhibited the highest impact on CAC hydration. Not only different phases were formed but the hydration rate was significantly accelerated. This led to a minor porosity increase of blended cement pastes but simultaneously also to significantly higher compressive strength. The more convenient dosage was 5%.
- The application of calcined shale caused the least alteration of hydration products compared to the reference paste but it significantly increased the hydration degree. Moreover, the hydration rate was accelerated, particularly in the case of higher dosage. Regarding the porosity, it was increased distinctively, but on the other hand, compressive strength grew as well. In the case of calcined shale, both 5% and 15% dosage could be considered as appropriate amounts.
- Despite the lower content of amorphous phase, sintered mullite significantly influenced the amounts of C-A-S-H phases. Its application showed the highest diversity according to varying dosage. However, its impact on hydration rate was negligible, the hydration heat power was almost unchanged. Similarly to the other studied SCMs, the values of porosity and compressive strength of blended pastes were fairly increased. The cement with 15% of sintered mullite showed a better performance.
- The analyzed pastes based on blended cements showed an improved performance not only at ambient temperature. Their properties were significantly enhanced also in high temperature conditions up to 1400 °C.
- Based on the presented results, all three analyzed nonconventional supplementary cementitious materials could be considered as promising, as for the partial calcium aluminate cement replacement, but a more detailed research would be necessary to confirm their real potential in practical applications.

Data availability

All measured data and images are available upon request as well as any other detailed information about particular measurement's processes.

CRediT authorship contribution statement

Dana Koňáková: Conceptualization, Writing – original draft, Data curation, Investigation. **Vojtěch Pommer:** Investigation, Data curation. **Miloš Jerman:** Investigation. **Martin Keppert:** Validation, Writing – review & editing. **Robert Černý:** Funding acquisition, Writing – review & editing. **Eva Vejmelková:** Resources, Investigation, Writing – review & editing.

Declaration of Competing Interest

The authors declare that they have no known competing financial interests or personal relationships that could have appeared to influence the work reported in this paper.

Acknowledgment

This research has been supported by the Czech Science , under project No. 20-00653S and by the Grant Agency of the Czech Technical University in Prague, grant No. SGS19/143/OHK1/3T/11.

Appendix A. Supplementary data

Supplementary data to this article can be found online at https://doi.org/10.1016/j.conbuildmat.2022.126824.

References

[1] K.L. Scrivener, A. Capmas, 13 Calcium Aluminate Cements, Oxford, Elsevier Butterworth-Heinemann, Lea's Chemistry of Cement and Concrete, 2003, pp. 713–782.
[2] S.R. Klaus, J. Neubauer, F. Goetz-neunhoeffer, Hydration kinetics of CA2 and CA—Investigations performed on a synthetic calcium aluminate cement, Cem. Concr. Res. 43 (2013) 62–69.
[3] E. Vejmelková, D. Koňáková, L. Scheinherrová, M. Doleželová, M. Keppert, R. Černý, High temperature durability of fiber reinforced high alumina cement composites, Constr. Build. Mater. 162 (2018) 881–891.
[4] V. Antonovič, J. Keriene, R. Boris, M. Aleknevičius, The effect of temperature on the formation of the hydrated calcium aluminate cement structure, Procedia Eng. 57 (2013) 99–106.
[5] A. Smith, T. Chotard, N. Gimet-Breart, D. Fargeot, Correlation between hydration mechanism and ultrasonic measurements in an aluminous cement: effect of setting time and temperature on the early hydration, J. Eur. Ceram. Soc. 22 (2002) 1947–1958.
[6] H.G. Midgley, A. Midgley, The conversion of high alumina cement, Mag. Concr. Res. 27 (91) (1975) 59–77.
[7] B. Pacewska, M. Nowacka, Studies of conversion progress of calcium aluminate cement hydrates by thermal analysis method, J. Therm. Anal. Calorim. 117 (2) (2014) 653–660.
[8] W. Khaliq, H.A. Khan, High temperature material properties of calcium aluminate cement concrete, Constr. Build. Mater. 94 (2015) 475–487.
[9] J.E. Kopanda, G. MacZura, Processes, Properties and Applications for Calcium Aluminate Cements. *Alumina Chemicals Science and Technology Handbook*, American Ceramic Society, 1990, pp. 171–181.
[10] Q. Tushar, M.A. Bhuiyan, G. Zhang, T. Mawqood, T. Tasmin, Application of a harmonized life cycle assessment method for supplementary cementitious materials in structural concrete, Constr. Build. Mater. 316 (17) (2022), 125850.
[11] T. Vass, P. Levi, A. Gouy, H. Mandová, Cement, International Energy Agency, Paris, 2021 https://www.iea.org/reports/cement.
[12] M.I. Khan, 14-Nanosilica/silica fume. *Waste and Supplementary Cementitious Materials in Concrete*, Woodhead Publishig (2018) 461–491.
[13] R. Lewis, The role of microsilica in sustainable concrete, MATEC Web of Conferences 120 (2017) 02011.
[14] P.R. da Silva, J. de Brito, Experimental study of the porosity and microstructure of self-compacting concrete (SBP) with binary and ternary mixes of fly ash and limestone filler, Constr. Build. Mater. 86 (2015) 101–112.
[15] A.C.P. Martins, J.M.F. de Carvalho, L.C.B. Costa, H.D. Andrade, T.V. de Melo, J.C. L. Ribeiro, L.G. Redroti, R.A.F. Peixoto, Steel slags in cement-based composites: An ultimate review on characterization, applications and performance, Constr. Build. Mater. 291 (2021), 123265.
[16] E. Vejmelková, D. Koňáková, T. Kulovaná, M. Keppert, J. Žumár, P. Rovnaníková, Z. Keršner, M. Sedlmajer, R. Černý, Engineering properties of concrete containing natural zeolite as supplementary cementitious material: Strength, toughness, durability, and hygrothermal performance, Cem. Concr. Compos. 55 (2015) 259–267.
[17] K. Wi, H.-S. Lee, S. Lim, H. Song, M.W. Hussin, M.A. Ismail, Use of an agricultural by-product, nano sized Palm Oil Fuel Ash as a supplementary cementitious material, Cem. Concr. Compos. 183 (2018) 139–149.
[18] R. Siddique, J. Klaus, Influence of calcined shale on the properties of mortar and concrete: A review, Appl. Clay Sci. 43 (3–4) (2009) 392–400.
[19] E. Vejmelková, D. Koňáková, M. Doleželová, L. Scheinherrová, P. Svora, M. Keppert, P. Reiterman, R. Černý, Effect of calcined Czech claystone on the properties of high-performance concrete: Microstructure, strength and durability, Constr. Build. Mater. 168 (2018) 966–974.
[20] J.M.R. Mercury, X. Turrillas, A.H. de Aza, P. Pena, Calcium aluminates hydration in presence of amorphous SiO_2 at temperatures below 90 °C, J. Solid State Chem. 179 (2006) 2988–2997.
[21] N.K. Lee, K.T. Koh, S.H. Park, G.S. Ryu, Microstructural investigation of calcium aluminate cement-based ultra-high performance concrete (UHPC) exposed to high temperatures, Cem. Concr. Res. 102 (2017) 109–118.
[22] M. Collepardi, S. Monosi, P. Piccioli, The influence of pozzolanic materials on the mechanical stability of aluminous cement, Cement Concrete Research 25 (5) (1995) 961–968.
[23] A. Hidalgo, J.L. García, M.C. Alonso, L. Fernández, C. Andrade, Microstructure development in mixes of calcium aluminate cement with silica fume or fly ash, Journal of *Thermal Analysis and Calorimetry* 96 (2) (2009) 335–345.
[24] M. Idrees, O. Ekincioglu, M.S. Sonyal, Hydration behavior of calcium aluminate cement mortars with mineral admixtures at different curing temperatures, Constr. Build. Mater. 285 (2021), 122839.
[25] O. Kirca, I.O. Yaman, M. Tokyay, Compressive strength development of calcium aluminate cement–GGBFS blends, Cem. Concr. Compos. 35 (2013) 163–170.
[26] X. Cheng, Q. Dong, Y. Ma, C.h. Zhang, Y. Gao, Y. Yu, Z. Wen, C.h. Zhang, X. Guo, Mechanical and thermal properties of aluminate cement paste with blast furnace slag at high temperatures, Constr. Build. Mater. 228 (2019), 116747.
[27] M. Nowacka, B. Pacewska, Effect of structurally different aluminosilicates on early-age hydration of calcium aluminate cement depending on temperature, Constr. Build. Mater. 235 (2020), 117404.

[28] Č.S.N. En, *196–11*: Methods of testing cement - Part 11: Heat of hydration – Isothermal Conduction Calorimetry method, Czech Standardization Institute. Prague (2019).
[29] N. Dobelin, R. Kleeberg, Profex: a graphical user interface for the Rietveld refinement program BGMN, J. Appl. Crystallogr. 48 (2015) 1573–1580.
[30] A. Trník, I. Medveď, R. Černý, Measurement of linear thermal expansion coefficient of concrete at high temperatures: A comparison of isothermal and non-isothermal method, Cement Wapno Beton 79 (2012) 363–372.
[31] Č.S.N. En, *196–1*: Methods of testing cement – Part 1: Determination of strength, Czech Standardization Institute. Prague (2005).
[32] E. Vejmelková, D. Koňáková, M. Čáchová, M. Záleská, P. Svora, M. Keppert, P. Rovnaníková, R. Černý, High-strength concrete based on ternary binder with high pozzolan content, Structural Concrete 19 (5) (2018) 1258–1267.
[33] B. Zhu, Y. Song, X. Li, P. Chen, Z. Ma, Synthesis and hydration kinetics of calcium aluminate cement with micro $MgAl_2O_4$ spinels, Mater. Chem. Phys. 154 (2015) 158–163.
[34] A. Engbert, S. Gruber, H. Plank, The effect of alginates on the hydration of calcium aluminate cement, Carbohydr. Polym. 236 (2020), 116038.
[35] J. Wang, J. Zhang, H. Tan, B. Ma, Effect of Different Kinds of Zinc (II) on Early Hydration of Calcium Aluminate Cement, J. Wuhan University of Technology (2020) 925–929.
[36] F. Wang, P. Chen, X. Li, B. Zhu, Effect of colloidal silica on the hydration behaviour of calcium aluminate cement, Materials 11 (2018) 1849.
[37] J.M.R. Mercury, X. Turrillas, A.H. de Aza, P. Pena, Calcium aluminates hydration in presence of amorphous SiO2 at temperatures below 90 °C, J. Solid State Chem. 179 (10) (2006) 2988–2997.
[38] M.U. Okoronkwo, F.P. Glasser, Stability of stratlingite in the C-A-S-H system, Mater. Struct. 49 (2016) 4305–4318.
[39] M.U. Okoronkwo, S.K. Mondal, B. Wang, H. Ma, A. Kumar, Formation and stability of gismondine-type zeolite in cementitious systems, J. Am. Ceram. Soc. 104 (3) (2021) 1513–1525.
[40] C. Biagioni, E. Bonaccorsi, M. Lezzerini, S. Merlino, Thermal behaviour of Al-rich tobermorite, Eur. J. Mineral. 28 (1) (2016) 23–32.
[41] J.E. Burke, Progress in Ceramic Science, Elsevier Science 1 (2013) 240.
[42] H.M. Zhou, X.C. Qiao, J.G. Yu, Influences of quartz and muscovite on the formation of mullite from kaolinite, Appl. Clay Sci. 80–81 (2013) 176–181.
[43] J. Khajornboon, K. Ota, K. Washijima, T. Shiono, Control of hexagonal plate-like microstructure of in-situ calcium hexaluminate in monolithic refractories, J. Asian Ceram. Soc. 6 (3) (2018) 196–204.

4.3.2 Application of secondary calcined shale in the design of low-cement binder for thermal-resistant composites

K. Šádková, D. Koňáková, V. Pommer, R. Černý, E. Vejmelková
Ceramic International 49 (2023) 13452–13468 [62]
https://doi.org/10.1016/j.ceramint.2022.12.220

This study advances the development of low-cement refractory composites by investigating secondary calcined shale (waste metashale) as a partial replacement for CAC, addressing the ecological and economic challenges of CAC production. It highlights the potential of waste material to be valorised as a functional SCM, promoting a circular economy approach where industrial waste is redirected from landfilling towards high-performance thermal-resistant binders.

The research systematically evaluated binders composed of waste metashale, super-reactive alumina, and boehmite powder, replacing CAC in various ratios, by means of hydration behaviour, microstructure and phase development, and mechanical performance up to 1400 °C. Waste metashale contributed silica and alumina, promoting the formation of calcium aluminosilicate hydrates (C-A-S-H) and reducing metastable hydrates. Despite increased porosity at ambient temperatures, these blends showed improved thermal performance. After thermal exposure, the modified binders contained gehlenite (C_2AS), anorthite ($CaAl_2Si_2O_8$), and hibonite (CA_6), enhancing refractoriness and dimensional stability. Optimal performance was observed in mixtures containing 60% waste metashale and 40% CAC, balancing porosity and high-temperature strength. These binders showed superior compressive strength and reduced porosity growth after 1400 °C.

Key contributions include:

- Demonstrating the applicability of industrial waste calcined shale as an effective SCM in refractory CAC binders
- Providing a detailed thermal and phase analysis of the blended systems
- Designing low-cement, thermally stable composites

In summary, this study expands the material basis for thermal-resistant cement composites by introducing secondary calcined shale as a sustainable, effective component for reducing CAC content while enhancing high-temperature performance.

Ceramics International 49 (2023) 13452–13468

Contents lists available at ScienceDirect

Ceramics International

journal homepage: www.elsevier.com/locate/ceramint

Application of secondary calcined shale in the design of low-cement binder for thermal-resistant composites

Kateřina Šádková, Dana Koňáková *, Vojtěch Pommer, Robert Černý, Eva Vejmelková

Department of Materials Engineering and Chemistry, Faculty of Civil Engineering, Czech Technical University in Prague, Thákurova 7, 166 29, Prague 6, Czech Republic

ARTICLE INFO

Handling Editor: Dr P. Vincenzini

Keywords:
Composites
Al_2O_3
Clays
Refractories

ABSTRACT

This paper deals with the possibility of partial replacement of aluminate cement in refractory concretes with waste material from calcined shale production. The waste "metashale" was combined with super-reactive alumina and boehmite powder in order to design a low-cement binder for high-temperature-resistant composites. Designed binders were studied at ambient temperature as well as after exposures to temperatures of 400 °C, 1000 °C and 1400 °C. Firstly, blended binder-based pastes were observed in an electron microscope to determine structural changes in the material, while XRD and DSC characterization was performed as well for determining phase compositions and their changes. Metashale application lead to the creation of different C-A-S-H phases, which were found to be contributing to the higher temperature resistance of designed binders. The further monitored parameters were basic physical and mechanical properties and thermal strain. Despite that the application of metashale caused an increase of porosity at an ambient temperature, the designed low cement binder showed more stable properties during the temperature exposures. Considering the reached properties and the environmental aspects, the most promising mixture was found to be the one, with metashale and cement in a 60:40 ratio. This binder was used to prepare refractory. Because it reached substantially better performance compared to the pure calcium aluminate-based composite, the designed binder proved its applicability.

1. Introduction

Today, refractory binders are most often a mixture of aluminate oxidizes accompanied by calcium oxides and their compounds. It is caused by their suitable properties and as well relative accessibility. These composites should withstand temperatures above 1400 °C without melting or some threatening changes of the properties. The most common and most frequently used binder is indisputably calcium aluminate cement (CAC), which is able to withstand temperatures of about 1600 °C.

Hydration of aluminate cement produces various types of calcium aluminates hydrates (C-A-H) such as $CaO{\cdot}Al_2O_3{\cdot}10H_2O$ (CAH_{10}), $2CaO{\cdot}Al_2O_3{\cdot}8H_2O$ (C_2AH_8), $3CaO{\cdot}Al_2O_3{\cdot}6H_2O$ (C_3AH_6) and $Al_2O_3{\cdot}3H_2O$ (AH_3) [1–3]. Research shows that CAH_{10} forms primarily at lower temperatures (below 15 °C), the main thermodynamically metastable hydration products (C_2AH_8 and AH_3) between 15 °C and 25 °C, and at temperatures above 40 °C (especially above 60 °C), the thermodynamically stable C_3AH_6 and gibbsite AH_3 are formed solely [2–5]. However, over time the unstable hydrates CAH_{10} and C_2AH_8 are transformed into thermodynamically stable C_3AH_6 and AH_3 phases, this is the so-called conversion. The speed of conversion depends on the temperature acting on the structure. At a temperature of 20 °C, it takes several years, while at 50 °C it takes only a few hours. During the conversion process, the existing hydrates CAH_{10} and C_2AH_8 release water which fills the voids and thus products with smaller molar volumes and higher matrix density are formed. As a result of the reduction in molar volume, porosity and permeability increase significantly, leading to a significant reduction in strengths [6]. This process is the reason why aluminate cement cannot be used in load-bearing structures. At the same time, however, increased porosity creates channels through which the water resulting from the decomposition of hydrates can flow [2,7–9]. The risk of explosive spalling is then reduced. Despite the complication of conversion, aluminate cement is still one of the most suitable binders for refractory concrete.

When a structure with aluminate cement is subjected to high temperatures, significant changes in structure and consequently the properties variations appear. In general, the process can be divided into five stages. The first stage up to 400 °C involves the dehydration of basic

* Corresponding author.
E-mail addresses: katerina.sadkova@fsv.cvut.cz (K. Šádková), dana.konakova@fsv.cvut.cz (D. Koňáková), vojtech.pommer@fsv.cvut.cz (V. Pommer), cernyr@fsv.cvut.cz (R. Černý), eva.vejmelkova@fsv.cvut.cz (E. Vejmelková).

https://doi.org/10.1016/j.ceramint.2022.12.220
Received 7 September 2022; Received in revised form 15 December 2022; Accepted 23 December 2022
Available online 26 December 2022
0272-8842/© 2022 Elsevier Ltd and Techna Group S.r.l. All rights reserved.

hydration products. It can be further divided into four overlapping sections. In the first one, up to about 105 °C, evaporation of free and physically bounded water in capillary pores and dehydration of amorphous AH_3 take place. Consequently, decomposition of the crystal hydrates CAH_{10} occurs in the temperature range between 100 °C and 160 °C. It primarily gives rise to C_2AH_8 and crystal AH_3 (in the form of Gibbsite). The third part from 140 °C to 240 °C involves the dehydration of C_2AH_8, with the dehydration product of katoite C_3AH_6 and again crystal AH_3. In the last section from 210 °C, the decomposition of the cubic C_3AH_6 and crystal AH_3 arises. In the case of katoite C_3AH_6, the dehydration products can vary, but it is usually assumed to be $C_{12}A_7H$, $C_{12}A_7H_{15}$ or C_4A_3H. Regarding the decomposition of Gibbsite AH_3, it gives rise to the boehmite AlOOH. As the dehydration process continues, denser minerals are formed and the porosity of the matrix increases, as a consequence mechanical properties are significantly decreased. Also, explosive spalling can take place at this temperature range, it occurs generally at temperatures up to 300 °C, however as it was mentioned herein above, in the case of CAC the explosive spalling hazard is somehow lower. The second stage from 400 °C to about 700 °C can be the so-called resting stage. The dehydration of the remaining hydrate phases continues slowly and no significant changes occur. Regarding the mechanical performance, there are expected to decrease only slightly, as a consequence of several cracks which can occur in this stage. However, it should be mentioned that aluminate cement shows quite poor mechanical properties in this range, but it is not unusual for materials with hydraulic binders [10–12]. Afterwards, the third stage from 700 °C to 1000 °C can be characterized by the recrystallization of re-new phases. Similar to the first stage, it can be named several minerals. Mayenite $12CaO{\cdot}7Al_2O_3$ ($C_{12}A_7$) recrystallizes at the temperature range from 690 °C to 750 °C, krotite $CaO{\cdot}Al_2O_3$ (CA) at about 900 °C and grossite $CaO{\cdot}2Al_2O_3$ (CA_2) up to 1200 °C [13,14]. Speaking about mechanical performance, the strengths reach the lowest values but elastic properties can go up. As is known from the literature, crystallization phenomena generally involve an increase in elastic properties because atomic bonds are stiffer in crystals than in amorphous structures [15]. At temperatures of about 1200 °C sintering of material occurs, this process can be classified as the fourth section. It is caused by forming liquid phases in the material, which increases the viscoelastic character. Due to the diffusion and viscosity, the material starts to agglomerate and consequently, the porosity sharply decreases. The whole process is campaigned by considerable volumetric changes. The created so-called ceramic bond is characterized by great mechanical properties, which can reach even much higher values than at ambient temperatures [16]. If the material is exposed to a temperature greater than 1400 °C and there is enough alumina, the hibonite $CaO{\cdot}6Al_2O_3$ (CA_6) can also form [17–19]. The last stage is the cooling stage. During the cooling of the material, the liquid phase changes to different crystalline phases with high elastic properties. The minor decrease in the mechanical properties between 900 °C and room temperature is due to microcracks caused by thermal expansion mismatch [17].

Although calcium aluminate cement appears to be a good binder for refractory concrete, its production is very demanding in terms of ecology and economics. Similarly to Portland cement, its production involves immense fuel and electricity consumption and the production of large amounts of emissions CO2, and also extraction and consumption of non-renewable resources (limestone, bauxite) [20]. In the case of Portland cement (PC), there are commonly used supplementary cementitious materials (SCM) to reduce the Portland clinker consumption in composites [21–23]. They provide not only price reduction, but their application usually also contributes to better durability of final concrete. The manner of SCM application can be advantageously used also in the field of castable CAC products. However, the choice of appropriate materials is in the case of CAC more difficult. Their impact not only on hydraulic processes (more precisely pozzolanic reaction) and physical properties but also on the influence on the thermal resistance of the final matrix has to be taken into account. Moreover, the conversion process can be somehow affected as well. Thus the solution of low-cement-heat-resistant composites is an important issue to be addressed.

Several attempts in the field of supplementary cementitious materials for CAC have been performed, but they were focused primarily on the convectional materials usually applied for Portland cement. If blast furnace slag processed at 20 °C–60 °C is used, the conversion of hexagonal hydrates is slowed and a continuous increase in compressive strength appears. Silica retarded the formation of C_2AH_8 and C_3AH_6 and, in turn, promoted the formation of stratlingite $2CaO{\cdot}Al_2O_3{\cdot}SiO_2{\cdot}8H_2O$ (C_2ASH_8), making the structure of the material denser and more stable [24]. Also, metakaolin promotes the formation of hydration products such as stratlingite C_2ASH_8 and thus limits the conversion process [25]. Furthermore, metakaolin develops pozzolanic properties (formed calcium hydro silicates) and accelerates the hardening of concrete (especially in its initial phase), it reduces the shrinkage of concrete and the number of cracks [26,27]. However, particle crystallization occurs earlier in metakaolin-containing concretes and therefore this concrete is also slightly stronger than micro silica-containing concrete [28]. The concrete mix with added metakaolin behaves linearly elastic during heating to a temperature of 800 °C. After this temperature is exceeded, the material started to behave viscoplastically. At the same time, at this temperature, sintering occurred. Microscopic observations suggest a mechanism of intergranular creep [29]. This progression corresponds to what several authors have reported in their papers about alumina silicate refractories [30,31], namely that there are two basic types of behaviour of concrete after exposures to high temperatures. At lower temperatures (20 °C–800 °C), the quasi-linear behaviour is observed and at higher temperatures (900 °C–1000 °C) it is viscoplastic behaviour. At lower temperatures (20 °C–800 °C), the material has a low elasticity deformation before the stress peak. At the peak, diffusion damage occurs, including decohesion and microcracks. This leads to a coalition of microcracks that produce a typically brittle fracture. After reaching the peak, the stress level drops sharply. At higher temperatures (900 °C–1000 °C) a linear to quasi-linear evolution up to 35–80% of the maximum can be seen. Then a non-linear behaviour until the maximum stress is reached, and afterwards, a significant decrease in stress is observed [30,32]. At 1000 °C, there is a significant increase in plastic strain due to the viscosity of the glassy phase. Very good properties were also achieved when the cement was replaced by a combination of micro silica and metakaolin [33].

Similarly, to metakaolin, metashale is a product of firing clay materials. The original material is shale, a clastic sedimentary rock based on aluminosilicates with a grain size of up to 0.02 mm. By its firing, a product that shows good pozzolanic properties arises. Its pozzolanic activity measured by the modified Chapelle test is 911 $mg(Ca(OH)_2)g^{-1}$ [34]. Metashale was primarily investigated as a Portland cement replacement. In this work by Vejmelková et al. [34], six different mixtures of UHPC with varying proportions of calcined shale were investigated. There was presented the positive impact of this replacement on the microstructure of studied concrete. In the case of the 30% replacement level, the porosity was significantly decreased and finessed, which caused a more compacted structure. Thus the beneficial effect on mechanical properties was observed as well. Moreover, when 40% of Portland cement is substituted by calcined shale, such concrete shows due to the lower porosity also less permeable structure for water vapour and water liquid transport [35,36]. Furthermore, it can be deduced that the more metashale the mix contains, the more pores with a smaller radius [35–38]. On the other hand, in this replacement range of up to 40%, thermal properties, more precisely thermal conductivity showed a little bit higher values [37,38]. However, calcined shale seems to be suitable also for CAC application [39]. According to research carried out, it appears that if 20–25% of aluminate cement is replaced by metashale, the resulting composite will have a higher strength than the reference sample. In the study performed by Koňáková et al. [14], the impact of metashale on the performance of CAC pastes was investigated

more from the point of view of its impact on the hydration process and not only based on mechanical properties. Two varying dosages were investigated, namely replacement by 5% and 15%. Results revealed that the application of metashale caused a significant increase in the hydration degree of calcium aluminates C-A. Moreover, the hydration rate in the case of these blended cement pastes was significantly accelerated. The resulting hydration products were not only calcium-aluminate-hydrates C-A-H, and aluminate-hydrates A-H, but also calcium-aluminate-silicate hydrates C-A-S-H. When focused on the properties, it was shown that despite the application of calcined shale causing an increase in porosity, mechanical properties went up as well.

Nevertheless, during the production of commercially available metashale, waste by-products arise. Such waste metashale does not contain such a high amount of amorphous content, and it is less reactive because its firing is not appropriate. Because of its composition, it is not possible to sell this product as properly calcined shale. Detailed chemical composition of such waste will be revealed here-in-follows. However, this waste contains insufficiently fired clays as well as let's say over-burned material. Due to the over-burned part, it is not possible to recycle such waste as a new batch during calcined shale production. On that account, it is primarily landfilled and it searches for a new possible application.

The application of supplementary cementitious materials, in general, is a perspective possibility from ecological and economic points of view. However, an application of waste material, which has no further application, will propose even more advantages. Because it was proven before [14,39] that properly calcined shale is applicable as a partial CAC replacement, this study aims to investigate the effect of waste metashale. Moreover, contrary to previous cases, this study aimed higher, as one of the partial goals is to develop a low-cement-binder. On that account, five different mixtures with varying amounts of waste metashale are designed. Afterwards, by means of the phase composition of hardened cement pastes, its microstructure, thermomechanical performance, basic physical properties and mechanical parameters at ambient temperature as well as after temperature exposure up to 1400 °C, the impact and applicability of waste metashale are assessed. Finally, the chosen binder is used for the production of castable refractories, which performance is evaluated through the view of its mechanical parameters.

2. Experimental methods

In high-temperature applications, the service life of refractory concrete passes through three main stages. During commissioning, the temperature of the concrete rises and causes damage such as cracks and/or failures due to dehydration, microstructural changes, and shrinkage. During cyclic operation, a second stage occurs, the formation or propagation of cracks due to thermal shocks [40]. In the last stage, after the material has been completely cooled, its structure and degree of damage are controlled. Based on this inspection, an adequate repair or total replacement of the construction is then proposed. Based on that manner, a similar approach was adopted in this study. Specimens were investigated at an ambient temperature of 20 °C as well as after several temperature loadings, specifically after 400 °C 1000 °C and 1400 °C. The heating regime was 1 °C/min and after reaching the particular temperature the duration of its exposure was always 3 h. Samples were then left to cool spontaneously. For better clarity of the experimental program, a frame diagram describing the overall work performed in this work can be found in Fig. 2.

2.1. Technological properties

The granulometry of raw materials was determined using a laser diffraction method (Bettersizer S3 Plus device). This instrument combines laser diffraction and dynamic image analysis, and it is able to measure the size of the particles from 0.01 μm to 3500 μm.

The consistency of the fresh mixture was described using a flow. For its determination, the standard method for mortars [41] was used. A fresh mixture was put in the special mould with the shape of a truncated cone. After de-moulding, the flow table was dropped 15 times. Two orthogonal diameters (of flowed mixtures) characterize the mixture flow.

2.2. Characterization properties

The composition and microstructure of each material were investigated by differential scanning calorimetry (DSC), thermogravimetry (TG), X-ray diffraction analysis (XRD), and scanning electron microscopy (SEM).

Simultaneous thermal analysis (STA), consisting of DSC and TG measurements, was carried out using a LABSYS EVO DTA/DSC device (SETARAM Inc.). The heating rate was 5 °C/min and the experiment was performed in an argon atmosphere with a flow rate of 40 ml min^{-1}.

XRD analysis was performed using a PANalytical Aeris diffractometer equipped with a conventional X-ray tube (CoKα radiation, 40 kV, 30 mA, line focus). For the determination of the amorphous phase amount, zincite was used as a standard. Evaluation of reached diffractograms was done with the employment of HighScore software (for qualitative analysis) and Profex [42] software (quantitative analysis).

Microscopic images were taken with a Phenom XL electron microscope desktop device equipped with a BSE detector and CeB6 source. The voltage was set at 15 kV, and the magnification was from 1000× to 10,000x. The sample was placed on a double-sided carbon tape glued on an aluminium substrate. A thin layer of gold was sputtered onto the sample before it was placed in the microscope. For the determination of phase composition, two approaches were combined. The spectral analysis was performed. Based on the results of the determined chemical composition and together with considering the known structure of minerals, phase identification was performed.

2.3. Basic physical properties

Bulk density was measured using the gravimetric method. Specifically, specimens for further investigation of mechanical properties were primarily measured and weighted and then the bulk density was

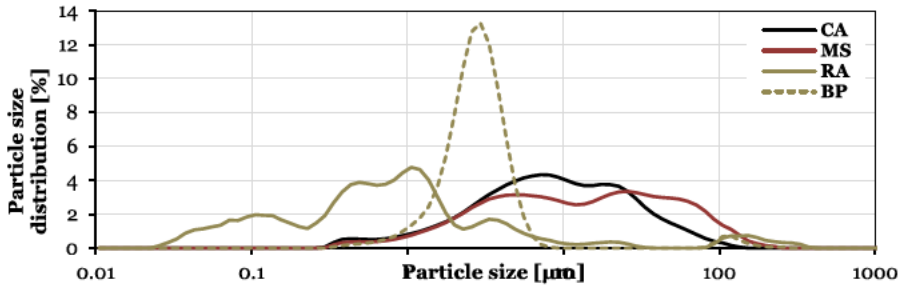

Fig. 1. Particle size distribution of raw-materials.

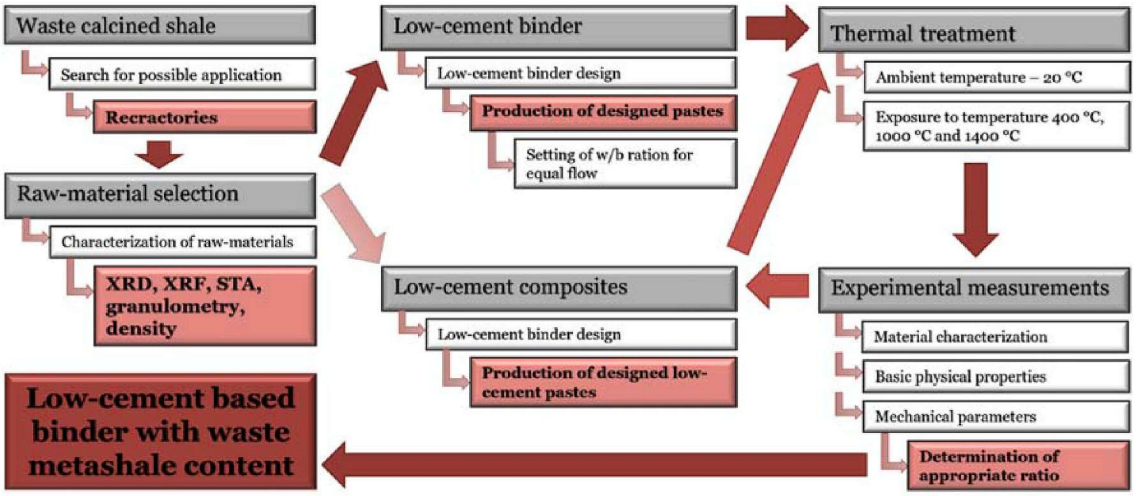

Fig. 2. Frame diagram of experimental program.

counted. Whereas matrix density was determined by a helium pycnometer using a Pycnomatic ATC instrument. Based on the known values of bulk density and matrix density, the value of total porosity was counted as well.

Furthermore, at ambient temperature, a mercury intrusion porosimeter was used, specifically, the PASCAL 140 + 440 porosimeter (Thermo Scientific), to obtain a detailed description of pore structure, more precisely the pore size distribution curves.

2.4. Thermomechanical analysis

The measurement of thermal strain depending on temperature was performed by a linear thermal horizontal dilatometer. Three specimens with dimensions of 20 × 20 × 100 mm were measured. The device utilizes a comparative method; the real thermal expansion is determined by comparing the analysed specimen with a standard. For that purpose, corundum having standardized properties was employed. Length changes during the temperature exposure were recorded by the computer program "Dilatometer 1.3" from CLASIC CZ s. r. o.

2.5. Mechanical properties

Compressive strength and bending strength were determined according to the standard [43,44] on the three beams (40 × 40 × 160 mm). The bending strength was measured using an MTS 100 loading device. The arrangement of the measurement was a four-point bending test with a span length of 150 mm. The resulting fragments of the original beams were then inserted into the EU40 loading device between two 40 × 40 mm steel plates and the compressive strength was measured on them.

The dynamic modulus of elasticity was measured on the same beams as the mechanical strengths, before the actual loading at destructive testing. This quantity was determined using the ultrasonic pulse method according to EN standards [45]. For this purpose, a Proceq instrument was used. A direct (counter-rotating) sounding method was used for the measurements.

3. Studied materials

The foundation for all binders was calcium aluminate cement. In addition to the reference sample, the cement was replaced in varying proportions with waste metashale, super-reactive alumina and boehmite powder. The test specimens were prepared as a cement paste without aggregate. The chemical composition of all materials and their densities are given in Table 1 and their granulometry is given in Fig. 1.

Calcium aluminate cement (CAC), specifically Secar 71, is manufactured in North America (Kerneos Inc.). It is an aluminate cement that has a minimum guaranteed compressive strength of 31.7 MPa after 24 h. As can be seen in Table 1, this CAC contains 71% alumina and therefore it belongs to a medium aluminate cement. Regarding its mineralogical composition, it is primarily composed of krotite (CA) and grossite (CA_2).

The main substitute for cement was the waste metashale, which originated in České lupkové závody a.s. This company produced chamotte and calcined shale, which is a material similar to metakaolin, but as a raw-material shale is employed instead of kaolinitic clay. Shale is a sedimentary rock with clay-sized particles less than 0.02 mm, which is not laminated or easily split. During the manufacturing of chamotte and calcined metashale, the imperfectly fired materials give rise as well. Such soft waste is formed during thermal and granulometric treatment of shale in the rotary furnace passage area at temperatures of 500–950 °C (the highest percentage of particles are formed at about 550 °C). Rising waste is a fine dust with D50 of 12.53 μm and the specific surface area of 6460 cm^2g^{-1}. However, because the firing is not perfect it contains a larger amount of unfired kaolinite as well as a higher amount of overdoing mullite, as can be seen in Table 2 where the phase composition of shale at raw state, properly calcined and of the waste can be found. Such imperfectly fired metashale cannot be sold together with

Table 1
Characterization of raw materials.

Materials	Density [kg.m ^{3}]	Chemical composition [%]						
		Al_2O_3	SiO_2	Fe_2O_3	CaO	MgO	TiO_2	Na_2O
Calcium alum. cement (CA)	2903	70.70	0.40	0.10	28.20	0.10	–	–
Waste metashale (MS)	2619	37.00	56.70	2.50	–	0.23	1.70	0.80
Super reactive alumina (RA)	3884	99.70	0.05	0.03	–	–	–	0.10
Boehmite powder (BP)	2998	99.00	–	–	–	–	–	–
Chamotte (CH)	2549	41.73	53.95	1.25	0.13	0.18	1.54	0.05
White corundum (WC)	1728	99.70	0.03	0.04	0.01	–	–	0.02

Table 2
The phase composition of shale [%].

Phase	Raw shale	Properly calcined shale	Waste metashale
Quartz	5.77%	5.14%	4.30%
Illite	7.31%	–	3.24%
Kaolinite	71.54%	15.48%	32.81%
Mullite	–	1.68%	13.43%
Anatase	2.02%	1.94%	1.80%
Amporph. and n.i.	13.36%	75.76%	44.42%

sufficiently calcined shale and thus sought alternative uses.

Another substitute for the above-mentioned cement was the super reactive alumina NABALOX NO 713 (Nabaltec AG). This material was added to the mixture mainly because of its high reactivity, homogeneous microstructure, and low sodium oxide content. Table 1 shows that this material contains more than 99% alumina. The mineralogical phase is mainly corundum. This admixture has very fine particles, which can be seen in Fig. 1. Another alternative for CAC was the boehmite powder Apyral AOH 40 (Nabaltec AG). This is a flame-retardant mineral with excellent resistance to acids and alkalis. This admixture also contains more than 99% alumina but it has particles slightly larger than those of super-reactive alumina.

A total of 5 different formulations of low-cement-based binders and a reference one containing only CAC were designed. The compositions of particular mixes are shown in Table 3. Designed mixes always contained 40% CAC and the rest of the binder was replaced with alternative materials in different proportions. The water binder ratio (w/b) was determined by experimental measurements before the production of the samples. It ranged from 0.2 to 0.4. The reason for varying w/b ratios was that it was desired to achieve equal consistency for all binders. On that account, the requirement of an equal flow of 180/180 mm was set. The P-LN5 mixture required the largest amount of water to achieve the desired consistency.

To confirm the applicability of metashale replacement in castable refractories and also to show how such composite would behave, two additional mixtures were made. A combination of white corundum (WC) and chamotte (CH) was used as an aggregate. Alumina also predominates in the corundum. In contrast, the chamotte aggregate contains a larger amount of silica. The reference mix without metashale contained 25% aluminium cement. In the second mix, 15% of the cement was replaced with waste metashale. This time the equal w/b ratio was employed, but the mixture with metashale was too dry and it was not possible to properly mix it. On that account, 1% of the Sika ViscoCrete 2700 Plasticizer was used in this mix to reach applicable consistency, which was set to be 160/160. The detailed compositions of all investigated mixtures are shown in Table 3.

Regarding the production process, it was as follows: the appropriate amounts of cement and alternative binders were first weighed with an accuracy of ±2 g. These dry ingredients were thoroughly mixed in an electric mixer with a mortar attachment and water was gradually added to the mixture after about 3 min. Wet mixing took at least another 3 min. If, after this mixing phase, the mixture showed no signs of lumps, impurities or unwetted parts of cement or other admixture, the consistency of the mixture was tested by the flow (Fig. 3). According to the reached results, the w/b ratio was subsequently adjusted. Once the optimal consistency was reached, the mixture was placed in pre-cleaned and greased test beam moulds. After being filled, the moulds were shaken on a vibrating table to remove possible air bubbles. Finally, the samples were aligned along the edges of the moulds and stored at room temperature (20 °C). After one day the samples were demoulded and placed in a climate chamber. The samples were aged at a controlled temperature of 20 °C and a relative humidity of 50%. After 28 days of curing, experiments were performed on 3 beams of each set. The other beams were exposed to temperatures of 400 °C, 1000 °C, and 1400 °C before further testing.

4. Results and discussion of pastes

4.1. STA and XRD analysis

Results of the simultaneous thermal analysis are presented in Figs. 4 and 5. Concrete containing aluminate cement has already been mentioned to exhibit the C-A-H transformation when exposed to temperatures up to 400 °C [1,10]. According to current knowledge, the first peak of the DSC analysis (Fig. 4) was assumed to symbolize the dehydration of amorphous AH_3 together with the loss of water and CAH_{10}. In the same way, it can be deduced that the second peak of the DSC analysis referred to the dehydration of C_2AH_8. However, the designed ternary binder-based materials showed slightly different performances at the first two main peaks. It is also probable that at these two peaks dehydration of calcium aluminate silicate hydrates (C-A-S-H) was involved. Nevertheless, the third peak corresponded to the gibbsite (crystal AH_3) decomposition and the fourth one to the dehydration of katoite C_3AH_6. Binders with a higher amount of alumina content showed a remarkable peak at a temperature of about 560 °C. On the contrary, such a peak occurred earlier and had a significantly lower value for the reference mixture and the P-LN5 mixture. This peak signified the boehmite decomposition, and it is visible that with the lowering content of boehmite in the mixtures, these peaks went down. Unlike the previous changes, the subsequent crystallizations were not as evident in Fig. 5, which shows the mass changes for each sample. This is because water evaporation and other significant mass changes no longer took place during further recrystallization. They only varied in structure as the individual crystals were transformed. At temperatures slightly under 1000 °C recrystallization of krotite CA was visible. Grossite CA_2 seemed to recrystallize more fluently as there was no significant peak in the corresponding temperature range, but the thermal flow continuously increased. It is assumed, that the last exothermal peaks at about 1350 °C signified the formation of hibonite CA_6. In addition, varying forms of C-A-S could be created, but this should be revealed in XRD analysis. For example, the low-cement binders with a higher amount of metashale showed the shift of the peak under 1000 °C, which can be caused by gehlenite $Ca_2Al_2SiO_7$ (C_2AS) formation. Another variation was observed at the higher abundance of heat flow at about 1200 °C, which can be attributed to anorthite $CaAl_2Si_2O_8$ (CAS_2) crystallization.

Fig. 6 summarizes the results of XRD quantification at ambient temperature, more precisely at 20 °C. The percentages of chemical compounds corresponded to the compositions of the individual

Table 3
Composition of cement mixtures.

Mixture	CA	MS	RA	BP	CH	WC	Plast.	Water	w/b ratio	Flow [mm/mm]
P-LNR	1700	–	–	–	–	–	–	400	0.24	180/181
P-LN1	680	170	212.5	637.5	–	–	–	488	0.29	178/180
P-LN2	680	340	170	510	–	–	–	525	0.31	179/179
P-LN3	680	510	127.5	382.5	–	–	–	500	0.29	180/181
P-LN4	680	680	85	255	–	–	–	525	0.31	181/180
P-LN5	680	1020	–	–	–	–	–	625	0.37	180/179
K-LNR	500	–	–	–	1250	250	–	150	0.3	159/160
K-LN5	200	300	–	–	1250	250	12.5	150	0.3	159/158

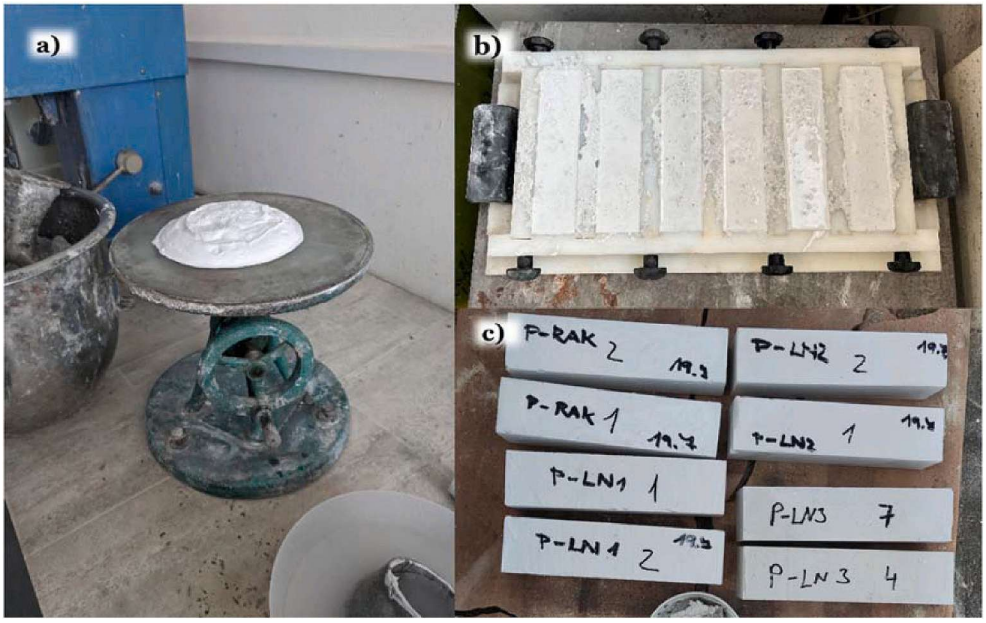

Fig. 3. Samples production: a) measurement of the flow, b) fresh samples in moulds, c) samples in furnace before temperature exposure.

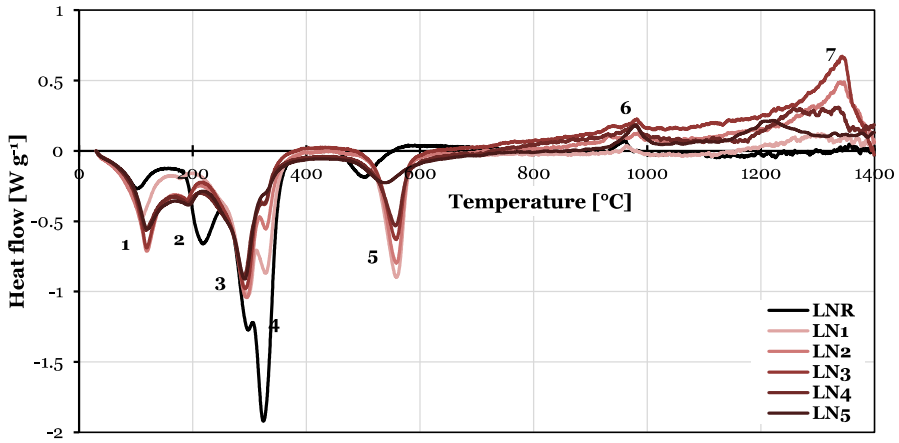

Fig. 4. Differential scanning calorimetry of studied pastes.

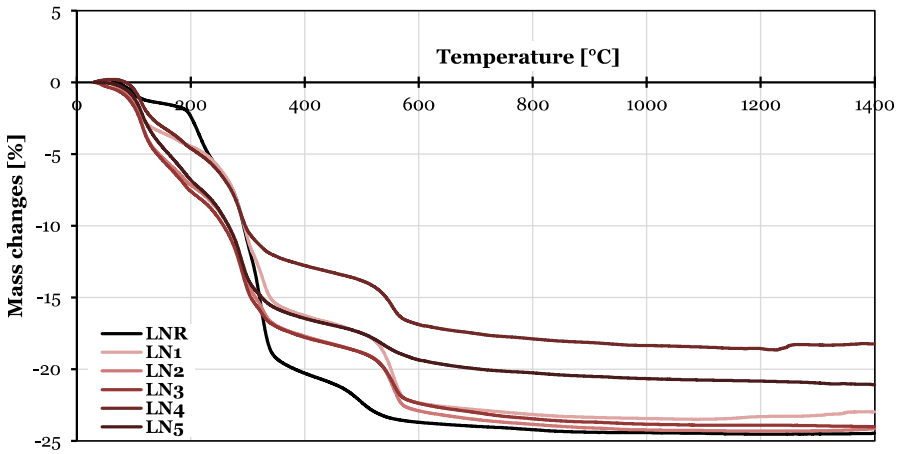

Fig. 5. Thermogravimetry of studied pastes.

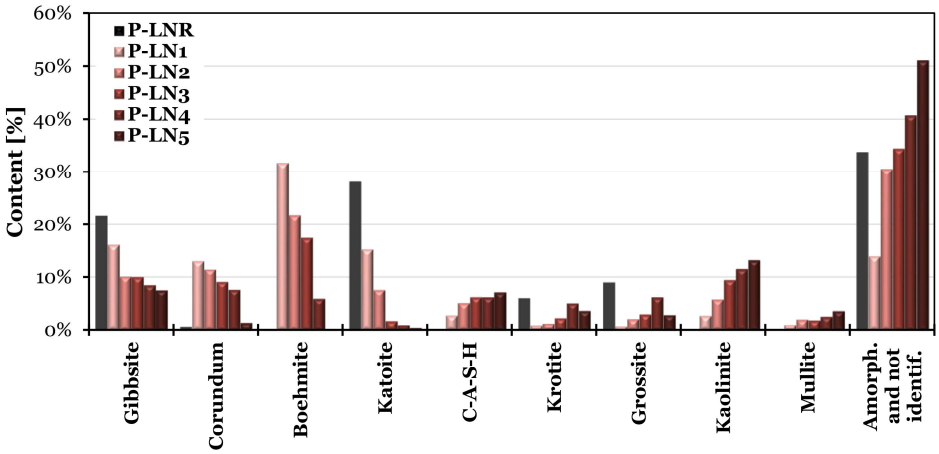

Fig. 6. Phases composition of studied pastes at ambient temperature - 20 °C.

mixtures. Almost no representation of corundum Al_2O_3 was found in the reference mixture, and its amount varied according to the amount of super-reactive alumina added. The same was true for boehmite AlOOH. Regarding the hydration product, the reference paste containing only aluminate cement produced a substantially higher amount of katoite C_3AH_6. This went against expectations of hydration at a controlled temperature of 20 °C. The reference mixture should contain the most CAH_{10}. Due to a large amount of hydration heat released during the hydration of CAC [46–48], the mixture had been probably overheated, and therefore more katoite C_3AH_6 was formed. Another reason might also be the fast conversion of the mixture. Regarding the second metastable hydrate C_2AH_8, it was presented as well (taking into account a substantial peak observed at about 200 °C R Fig. 4). Unfortunately, the structure of this metastable mineral has not been well described yet, and thus their presence can be derived only by the application of different methods than XRD quantification. In this work, STA and SEM were employed. In the XRD quantification, its amounts were covered in the amorphous and unidentified phases. When focused on the impact of waste calcined shale, its application led to the C-A-S-H creation. Metashale contained silicon, which enabled the formation of these compounds. By qualitative XRD analysis of studied materials, primarily stratlingite (C_2ASH_8), and gismondine $CaAl_2Si_2O_8{\cdot}4H_2O$ (CAS_2H_4) were detected as the main C-A-S-H phases. A minor amount of lawsonite $CaAl_2Si_2O_7(OH)_2{\cdot}H_2O$ (CAS_2H_2) was observed as well. To make the description of the studied binder complete, it should be mentioned that the addition of the alumina components led to a substantially higher hydration degree of calcium aluminate cement. The amount of the non-hydrated Krotite CA and Grossite CA_2 was significantly lower in the case of P-LN1 and P-LN2. On the contrary, waste metashale seemed to have a negative effect on the hydration rate of calcium aluminate cement, as the amount of mentioned minerals was somehow higher in materials P-LN4 and P-LN5. Regarding the remaining components, there can be seen minerals of unreacted waste metashale, namely kaolinite and mullite.

Fig. 7 summarizes the mineralogical composition of the studied pastes after the temperature exposure to 400 °C. In conformity with the described performance of STA (Figs. 4 and 5), the hydrated alumina AH_3 (amorphous and in form of gibbsite) decomposed, and its remnants could be present in the form of boehmite ALOOH, the amount of which had increased compared to 20 °C. Regarding the other hydration products, it is obvious that they dehydrated and gave rise to the new components, which are together so-called dehydrated C-A-H and dehydrated C-A-S-H. Specifically, C_4A_3H and $C_{12}A_7H$ belonged to the observed partially dehydrated C-A-H, while C-A-S-H were represented by partially dehydrated gismondine and lawsonite. The representative or original aluminate cement (krotite CA and grossite CA_2) and waste metashale (kaolinite and mullite) remained unchanged.

In Fig. 8, there can be found the summary of the XRD analysis after

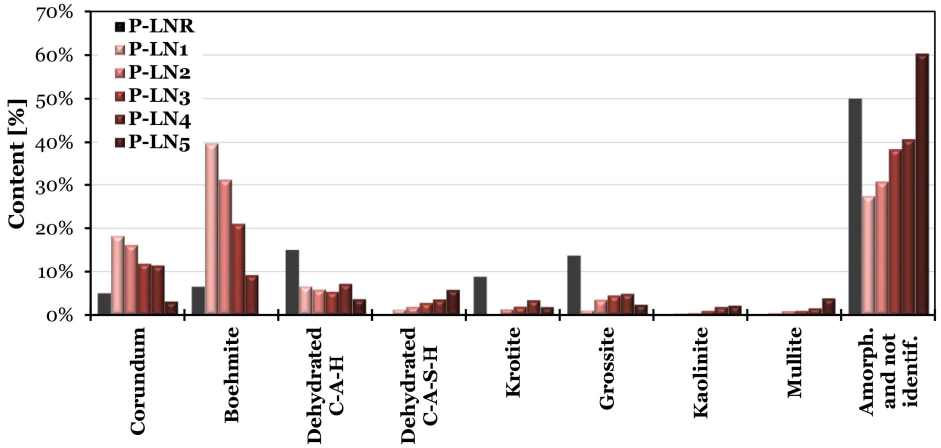

Fig. 7. Phases composition of studied pastes exposed to 400 °C.

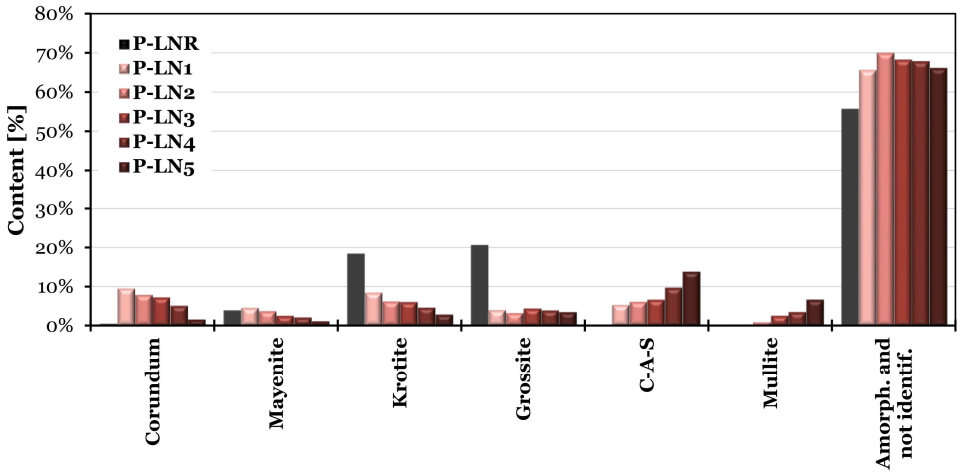

Fig. 8. Phases composition of studied pastes exposed to 1000 °C.

the exposure to 1000 °C. In accordance with the statement on boehmite AlOOH dehydration at temperatures of about 560 °C, this mineral disappeared and was not present in any of the studied pastes. Concerning corundum, the amount of alumina went down substantially, as a consequence of pronounced recrystallization of the new phases, most probably in the varying forms of calcium-aluminates (C-A), but also in the phases of calcium-aluminate-silicates (C-A-S). In the paste compositions, there has also been found a new component mayenite $C_{12}A_7$, which was formed by the final dehydration of C-A-H. Furthermore, it can be seen from Fig. 8 that all the water from C-A-S-H evaporated, resulting in the formation of calcium-aluminium-silicate phases (C-A-S). Namely gehlenite ($Ca_2Al[AlSiO_7]$) (C_2AS), grossular $Ca_3Al_2(SiO_4)_3$ (C_3A_2S), and anorthite $Ca(Al_2Si_2O_8)$ (CA_2S_2) were detected by qualitative analysis. Other elements of the metashale had also experienced significant alteration. Due to dehydroxylation, which takes place in the temperature range of 450 °C–700 °C, kaolin was converted to metakaolin. Afterwards, at temperatures ranging from 1100 °C to 1300 °C [49] metakaolin recrystallizes in the form of mullite. However, as the amount of mullite slightly increased even at 1000 °C, it seemed that this reaction began at lower temperatures. Due to the high-temperature exposure, krotite (CA) and grossite (CA_2) started to crystallize and their abundance increased. This change corresponded to the results of STA (Fig. 4) where other peaks appeared on the curve for all mixtures, just before reaching 1000 °C. It is also worth mentioning, that after the exposure to a temperature of 1000 °C, the largest amount of amorphous and unidentified phases occurred in the mixtures. This signified a substantially higher amount of the liquid phase, which could be further recrystallized or melted.

After the exposure to a temperature of 1400 °C, the internal structure of the material was sintered. Except for this physical process, structural changes were also observed. The phase composition of residual pastes is presented in Fig. 9. When focused on calcium-aluminate phases (C-A), as it is mentioned here-in above, at a temperature of 900 °C–1000 °C, mayenite $C_{12}A_7$ recrystallized to krotite CA, and further at 1000 °C–1300 °C to grossite CA_2. In the reference paste, there was therefore a remarkable increase of these latter minerals. On the contrary, in the ternary binder-based pastes, instead of mayenite $C_{12}A_7$, there was hibonite $CaAl_{12}O_{19}$ (CA_6) by successive alteration. It was the most abundant in the mixtures in which the greatest amount of calcium aluminate cement was replaced by aluminas. Despite that, it should occur somewhat later in the temperature range from 1400 °C to 1600 °C [50]. It confirms the assumption that the last exothermic peak at STA was the recrystallization of the hibonite CA_6. Further krotite CA and grossite CA_2 were observed as well in the ternary binder-based mixtures, but only in trace amounts. Regarding the amount of C-A-S, it increased radically as a result of its crystallization. Again, it can be seen, that an upward increase of this component in the mixtures depended on how much metashale they contained. The particular phases of C-A-S formed

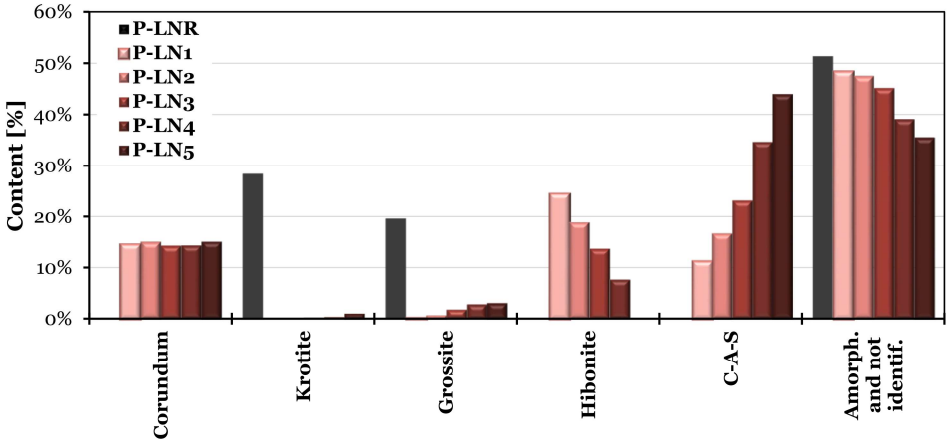

Fig. 9. Phases composition of studied pastes exposed to 1400 °C.

after exposing the sample to the highest temperature do not differ much from the previous stage. Gehlenite (C_2AS), grossular (C_3A_2S) and anorthite (CA_2S_2) were observed. However, it is worth mentioning that the amount of anorthite (CA_2S_2) significantly increased, and this mineral became dominant among the observed C-A-S structures. This could be supported also by the vanishing of mullite, which decomposition, more precisely transformation could give rise to another amount of anorthite (CA_2S_2) [51].

4.2. SEM analysis

For this analysis only four materials were chosen; namely, reference paste P-LNR, P-LN1, P-LN3 and P-LN5. Scanning electron microscopy images confirmed the results of XRD and DSC analysis. At ambient temperature, the small needle shape crystals of CAH_{10} and the larger cubic crystals of katoite C_3AH_6 were clearly visible in the reference sample (Fig. 10 a). The mixture of P-LN1 and P-LN3 (Fig. 10 b, c) also contained square slices of corundum Al_2O_3, while this compound was not detectable in the mixture of P-LN5 (Fig. 10 d). The P-LN3 and P-LN5 mixtures were richer in kaolinite, which was observed in both images of those materials. Amorphous AH_3 was then present in all cases of studied mixtures.

After the exposure to 400 °C, only C-A and dehydrated C-A-H were visible in the reference sample (Fig. 11 a). In contrast, many corundum Al_2O_3 and boehmite crystals AlOOH could be found in the mixtures P-LN1 and P-LN3 (Fig. 11 b, c). For the sample made from the P-LN5 mixture, it was almost impossible to find any particular crystal because the amorphous phase was dominated after the exposure to 400 °C (Fig. 11 d).

The increase of the liquid, more precisely the amorphous phase, was already visible under the electron microscope in samples exposed to 1000 °C. Except for that, the first signs of sintering were observed even at this temperature loading. The most obvious sintering was observed in the reference sample (Fig. 12 a). In the other mixtures, it was sporadic. Consistent with the XRD and DSC analysis, only krotite CA and grossite CA_2 could be seen in the reference sample. For samples P-LN1 and P-LN3, corundum Al_2O_3 crystals were still visible (Fig. 12 b,c). In samples with more metashale, more C-A-S was also formed, as can be seen in Fig. 12 b, c.

When the samples were exposed to a temperature of 1400 °C, a high degree of sintering was already visible in all of them. However, the reference sample was the most sintered, as shown in Fig. 13 a. No separate crystals were found; only one large continuous sintered area and several cracks were found, probably caused by large volume changes. At this point, the reference paste contained only krotite CA and grossite CA_2 in addition to the amorphous phase. A distinct difference can be seen in the P-LN1 and P-LN3 samples. In these, a hibonite CA_6 was formed, which had a regular hexagonal structure (Fig. 13 b, c). In the P-LN5 binder, in accordance with the lower amount of alumina in the mixture composition, hibonite was no longer found. Here, C-A-S

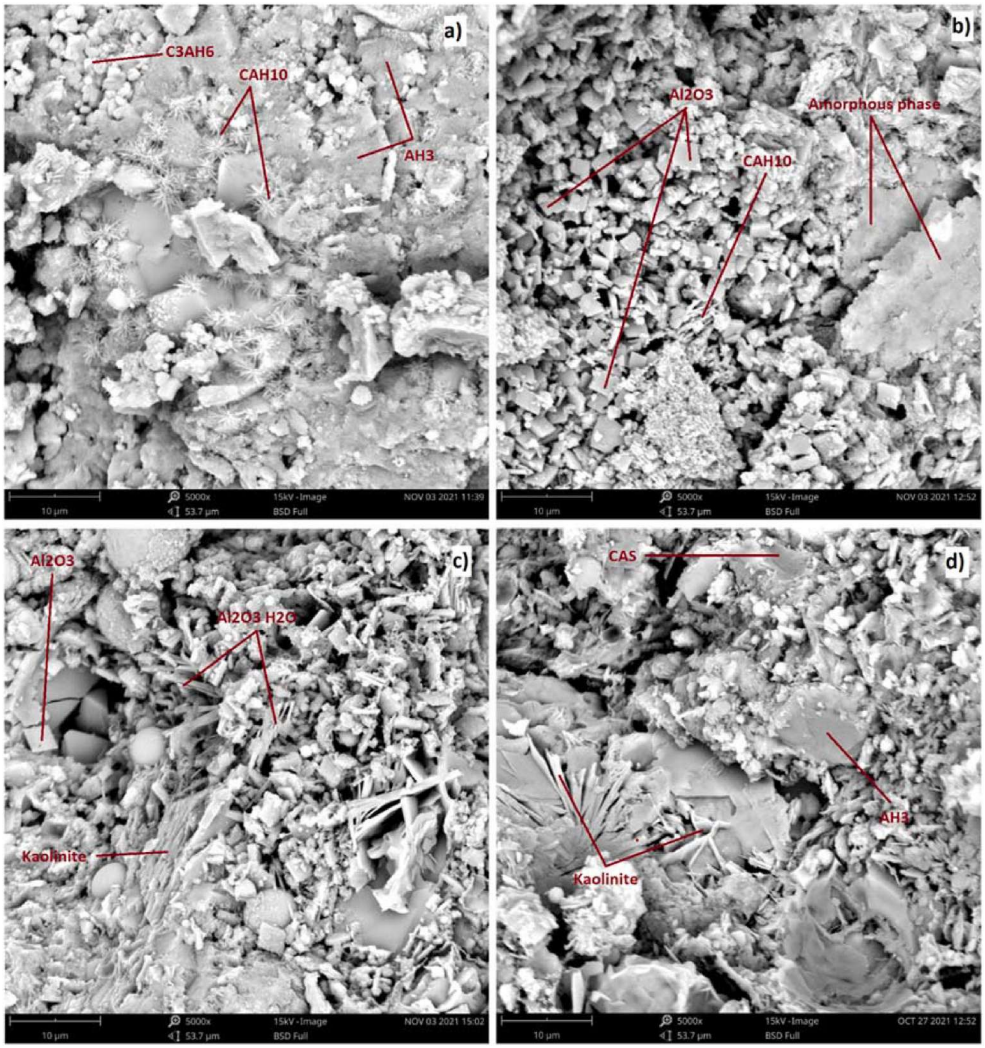

Fig. 10. SEM images of pastes exposed to 20 °C (a) P- LNR, (b) P-LN1, (c) P-LN3, (d) P-LN5.

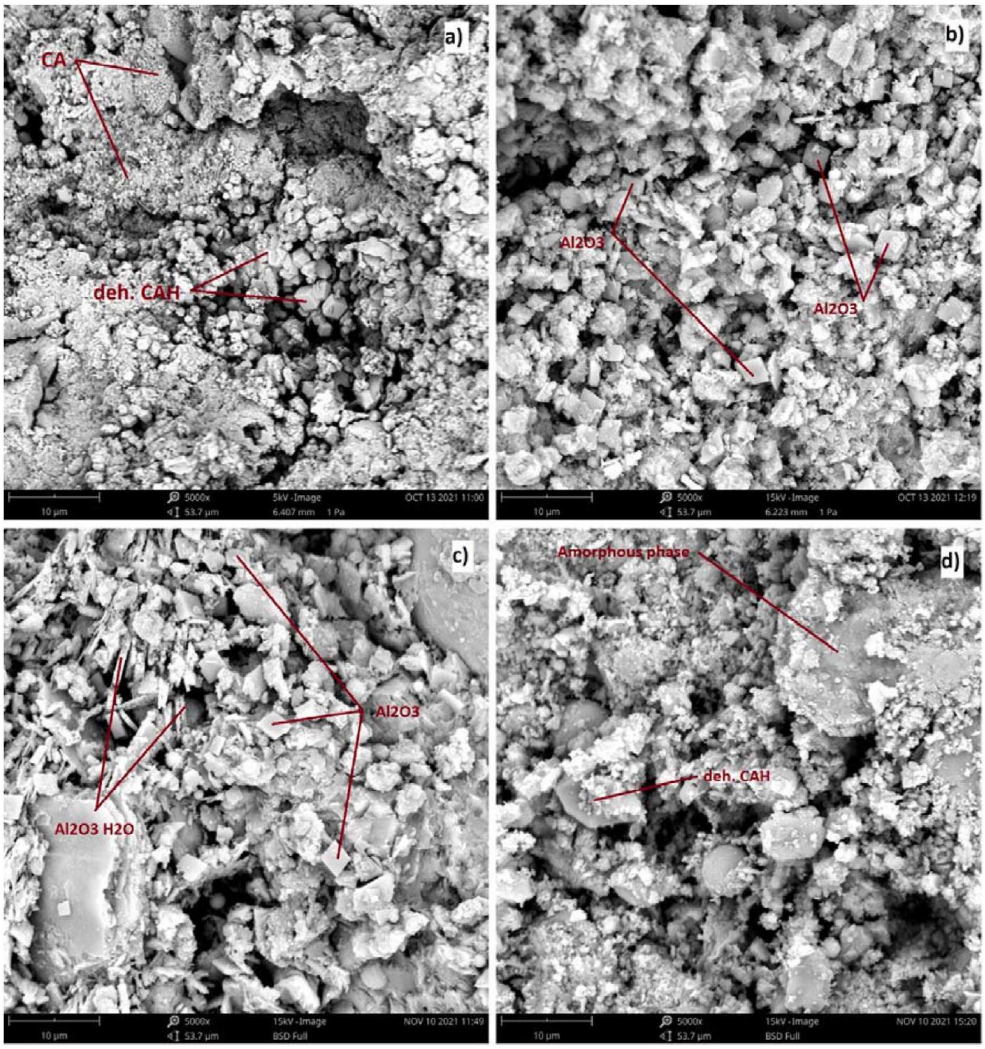

Fig. 11. SEM images of pastes exposed to 400 °C (a) P-LNR, (b) P-LN1, (c) P-LN3, (d) P-LN5.

predominated.

4.3. Thermomechanical analysis

The results of the thermal strain are consistent with the results of the DSC and XRD analysis. The large fluctuations in values were found in both Figs. 14 and 15 before 400 °C and before 600 °C. This corresponded to the katoite C_3AH_6 and boehmite AlOOH dehydration. It is interesting, that while the dehydration of C-A-H led to the shrinkage, the boehmite decomposition caused prolongation. Another visible drop of thermal strain was found at a temperature of about 900 °C. This shrinkage can be attributed to the two varying processes, mayenite $C_{12}A_7$ recrystallization and gehlenite C_2AS formation. However, both transformations showed a shrinkage effect, as the thermal strain went down for all studied specimens. The thermal strain performance also revealed that the sintering of the studied materials occurred at around 1200 °C. After the sintering, there was a sharp shrinkage of the samples P-LN1, P-LN2 and P-LN3 at around 1350 °C, this was attributed to the recrystallization of the hibonite CA_6. The reference and P-LN5 mixtures showed the lowest shrinkage, followed by binders P-LN5 and P-LN4. On the contrary, the mixtures P-LN1, P-LN2, and P-LN3 showed the highest shrinkage.

The thermal expansion coefficient was almost constant up to 1200 °C, except for minor fluctuations before 400 °C and 600 °C, which are related to the dehydration of the here-in-above described elements. More fluctuations occurred after the sintering of the material. The most stable coefficient was measured for the pastes P-LN4 and P-LN5, while due to the hibonite CA_6 creation, paste P-LN1, P-LN2 and P-LN3 showed almost inapplicable values.

4.4. Basic physical properties

The bulk density measured by the gravimetric method is shown in Table 4. Interestingly, all pastes with alternative replacement of CAC had very similar values of around 1700 kg m^{-3}, which is approximately 15% less than the bulk density of the reference sample. Regarding the ternary binders, the highest bulk density was measured for the P-LN1 mixture with the lowest proportion of waste metashale, and, in contrast, the lowest bulk density showed samples P-LN5 with the highest proportion of waste metashale. From this it can be deduced that the more waste metashale is added to the concrete mix, the lower the bulk density will be. The exposures of the pastes to high temperatures did not cause large changes in bulk density. It should be mentioned, that the bulk density is strictly dependent on matrix density and open porosity. With increasing matrix density, the matrix density increases as well, while the dependence on porosity is reversed, the increase in porosity caused a decrease in bulk density. On that account, bulk density was not as much affected by the temperature exposure, as both matrix density and porosity went up.

The second presented basic physical quantity, obtained by the

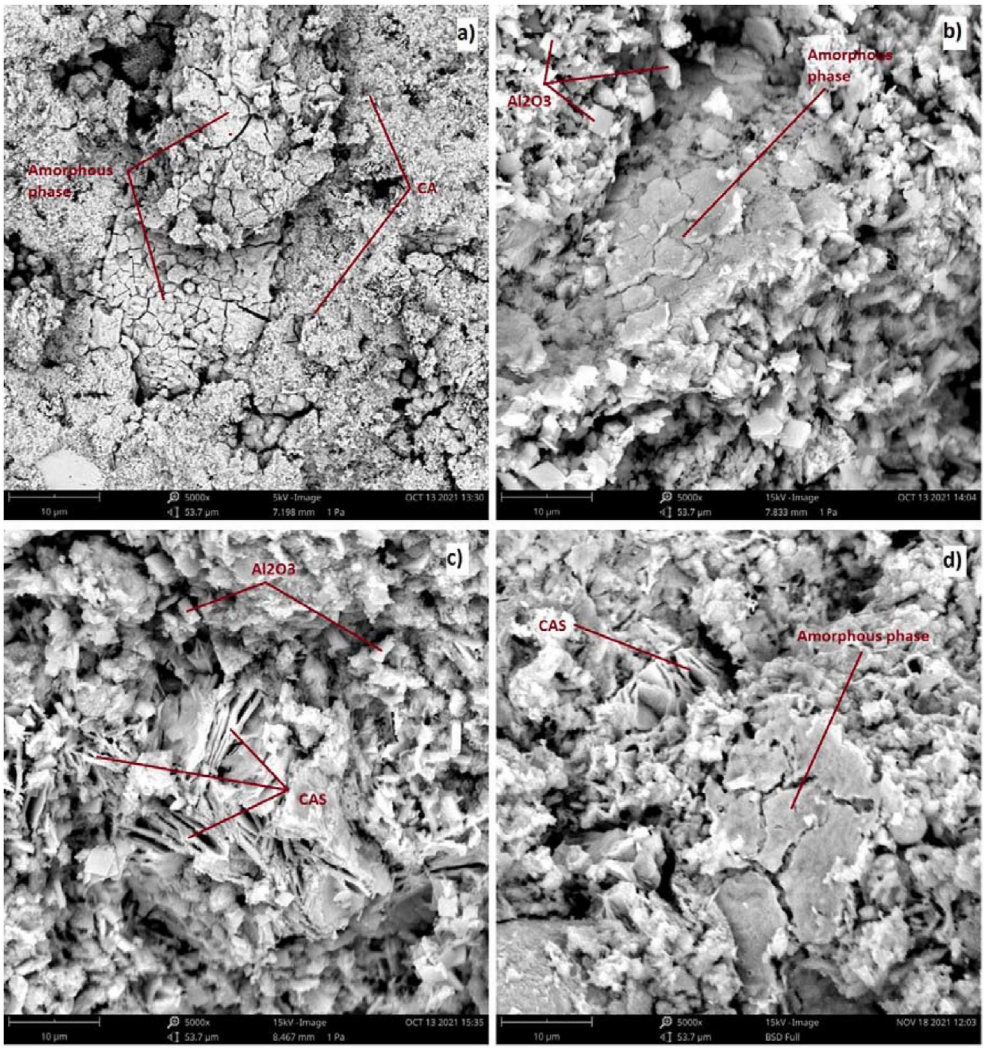

Fig. 12. SEM images of pastes exposed to 1000 °C (a) P-LNR, (b) P-LN1, (c) P-LN3, (d) P-LN5.

helium pycnometer, was the matrix density. The results are shown in Table 4 as well. The highest value of matrix density was again achieved by the P-LN1 mixture with the smallest metashale dosage. At room temperature, this difference from the reference sample was 7%. This decrease in matrix density can be linked to the phase composition. Despite that the density of amorphous and not identified phase is not determined, specific gravities of observed minerals are in accordance with the observed performance of matrix densities. The paste P-LN1 contained a higher amount of Stratlingite C_2ASH_8 with the lowest specific gravity (1936 kg m^{-3} [52]) among observed phases. In the case of reference paste P-LNR, the main phases were Katoite C_3AH_6 with a specific density of 2520 kg m^{-3} [52] and Gibbsite AH_3 2520 kg m^{-3} [52]. While with an increasing amount of aluminates in the binders the boehmite and corundum were observed as well, the latter showed noticeably higher specific gravity (3030 kg m^{-3} [52] for boehmite AlOOH and 3980 kg m^{-3} [52] for corundum Al_2O_3). The matrix density increased with the increasing temperature to which the sample was exposed. This was due to the transformation of the material caused by exposure to high temperatures. The chemical components (namely C-A-H, A-H, C-A-S-H) were dehydrated, resulting in denser, water-free minerals (C-A and C-A-S), as it was described in chapter 4.1. However, when the matrix density value was compared after the exposure to 1400 °C, the highest value was observed for binder PLN1, 21% higher compared to the reference material P-LNR. Such a high difference was predictable due to the highest amount of hibonite CA_6 observed. Compared to the other minerals, this one showed the highest specific gravity (3840 kg m^{-3}) [52]. On the other hand, paste P-LN5 showed by 1% lower residual matrix density than the reference. Again this performance can be linked to the phase composition, specifically to the low specific density of Anorthite CAS_2 (2730 kg m^{-3} [52]). As with the bulk density, it can be deduced that as the proportion of waste metashale in the mixture increases, the matrix density of the resulting mixture decreases.

The last property in Table 4 is total porosity. At first sight, it can be seen that the pastes with the alternative CAC replacement had a porosity of an order of magnitude higher. The porosity of these samples was increased on average by 112% compared to the reference paste. This can be attributed to the higher water dosage, which had been necessary for the equal consistency of fresh mixtures. Although all samples with alternative binders showed quite bigger porosity than the reference sample, it can be seen the beneficial effect of the metashale application. Despite the higher water demand, the more waste the mixture contained, the lower the resulting porosity was. After the exposure to 1400 °C, the highest porosity was measured in the case of P-LN1. Compared to room temperature, its porosity increased by 53.4%. On the contrary, reference paste P-LNR reached the lowest value of residual porosity, but on the other hand, the increase was more significant. The residual porosity of reference paste P-LNR increased by 99.3%. Therefore, it can be expected that the reference sample will contain more cracks due to the abrupt change in porosity. This assumption was

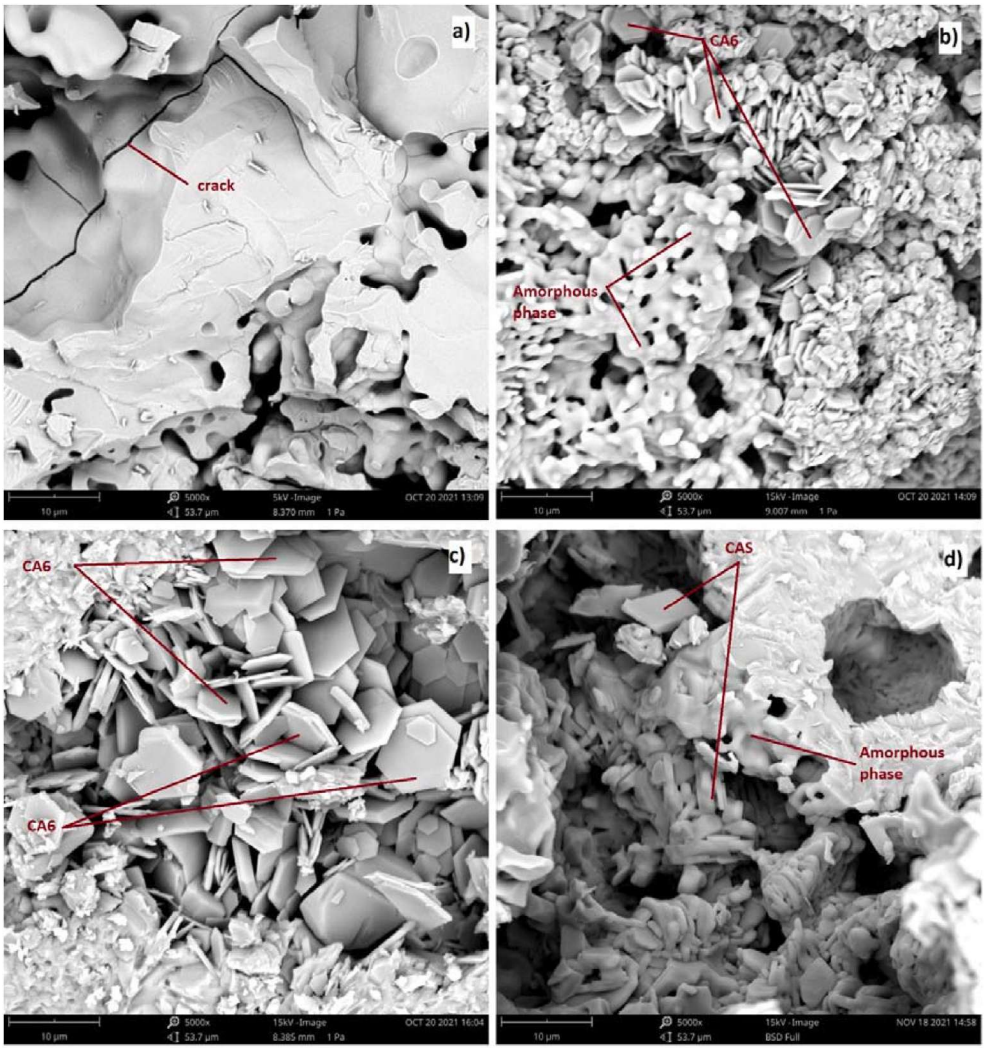

Fig. 13. SEM images of pastes exposed to 1400 °C (a) P-LNR, (b) P-LN1, (c) P-LN3, (d) P-LN5.

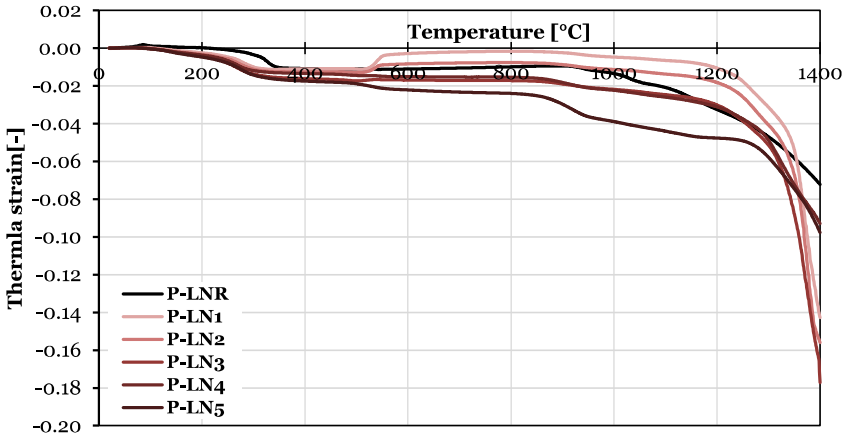

Fig. 14. Thermal strains of studied pastes.

confirmed by electron microscope images, which showed relatively wide cracks in the reference sample after the exposure to 1400 °C.

When comparing the open porosity of the studied pastes with composites from other studies measured at room temperature [35,38], a similar trend can be seen. Samples with 60% replacement of Portland cement with metashale, natural zeolite or brick dust were measured to have almost twice the open porosity. An even more accurate comparison can be made with the research by Koňáková et al. [14], where calcium aluminate cement-based pastes exposed to temperatures of 400 °C, 1000 °C and 1400 °C were investigated. That study includes a

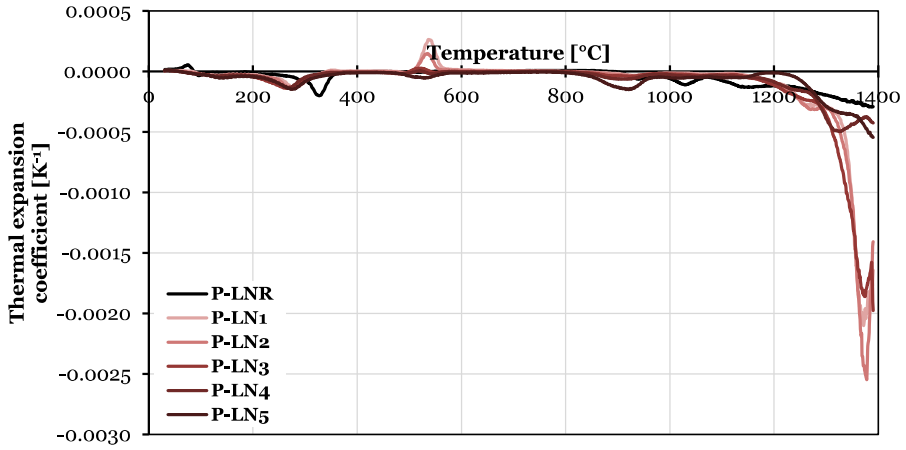

Fig. 15. Thermal expansion coefficients of studied pastes.

Table 4
Basic physical properties of studied pastes.

	Temperature	P-LNR	P-LN1	P-LN2	P-LN3	P-LN4	P-LN5
Bulk density [kg m^{-3}]	20 °C	2051	1741	1676	1678	1701	1617
	400 °C	2055	1724	1677	1696	1708	1624
	1000 °C	2044	1719	1747	1695	1685	1602
	1400 °C	2038	1748	1700	1694	1679	1637
Matrix density [kg m^{-3}]	20 °C	2387	2561	2427	2377	2284	2174
	400 °C	2506	2676	2804	2770	2632	2557
	1000 °C	2868	3017	2989	2930	2825	2757
	1400 °C	2833	3436	3141	3059	3018	2796
Porosity [%]	20 °C	14%	32%	31%	29%	26%	26%
	400 °C	18%	36%	40%	39%	35%	36%
	1000 °C	29%	43%	42%	42%	40%	42%
	1400 °C	28%	49%	46%	45%	44%	41%

replacement of cement with 5% and 15% of metashale, ceramic dust and sintered mullite. At room temperature, the open porosity increased significantly less than for the mixtures investigated in this study. The increase was 10% for the mixture with 5% metashale and 38% for the mixture with 15% metashale. Nevertheless, as in this study, the replacement level was much higher, it can be concluded, that the higher the dosage of sintered shale is used, the higher porosity the hardened matrix shows. After the exposure to 400 °C, a further increase in open porosity occurred due to the dehydration of the cement pastes. However, in accordance with this study, the increase in residual porosity for the metashale mixture was not as significant as for the reference mixture. In contrast to the pastes presented in this paper, the greatest increase in porosity was reported after to 1000 °C. Afterwards, there was a slight decrease after the exposure to 1400 °C due to sintering. Thus, in this case, sintering had a greater effect on the porosity of the structure of the resulting material.

The pore size distribution curves at ambient temperature in Fig. 16 show an even more noticeable difference between the reference mixture containing only aluminate cement and the other blended binders. The reference sample had the largest pore volume at a diameter of about 0.1 μm, while the most abundant pore diameter of the other mixtures was close to 0.4 μm. There was a significant effect of metashale on the porosity of the resulting mixture. While the curves of the mixtures with fewer metashale had one significant peak at a pore diameter close to 0.4 μm, the curves of the mixtures P-LN4 and P-LN5 had the other large peak at a pore size around 0.01 μm. From this, it can be concluded that the metashale content caused the appearance of pores of a smaller radius in the material structure. Furthermore, reached results conform with the SEM images, which showed that the reference mixture was the least porous, whereas the mixtures with the alternative replacement of CAC contained much more pores (see Fig. 10).

This hypothesis can be confirmed by the measurement of pore size distribution using a mercury porosimeter by Koňáková et al. [35]. In that research, composites in which silica sand and micro silica were used

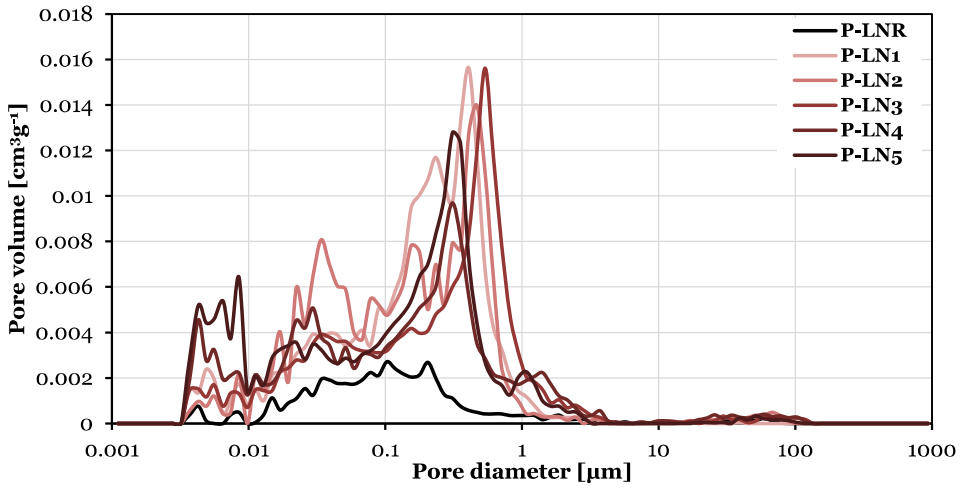

Fig. 16. Pore structure at ambient temperature - 20 °C.

as fillers and Portland cement was replaced in varying proportions by metashale were investigated. Despite that the samples were not exposed to high temperatures and a different cement was used, a similar trend can be observed. The number of larger pores with a radius of 0.1 μm decreased with increasing amounts of metashale and, conversely, the number of smaller pores with a radius of 0.02 μm increased. Similar results of mercury porosimetry were reported by Čáchová et al. [36], who replaced cement in composites with brick dust and natural zeolite in addition to metashale. These samples were also measured only at room temperature. For all these alternative admixtures, the largest number of pores had a radius of 0.01–0.1 μm. Again, the metashale composites contained the smallest pores. Thus, the more pozzolanic admixtures a given compound contains, the smaller pores it can be expected to have.

4.5. Mechanical properties

Measured values of mechanical properties are summarized in Table 5. Bending strength shows that all mixtures performed somehow worse than the reference sample in most cases. The worst bending strength was achieved by the P-LN1 mixture with the least replacement of the aluminate cement by metashale. After exposing the paste of this composition to 1400 °C, the sample was damaged so much that the bending strength could not even be measured. This is consistent with its high porosity (49%). Very low values can also be seen for the P-LN2 mixture. However, the other three mixtures showed applicable values of bending strengths. Based on this outcome, it can be deduced that the metashale application, despite that it didn't reach as high values as the reference, showed a beneficial impact on bending strength compared to the alumina admixtures. Especially after the exposure to 1400 °C, they reached even higher bending strengths. When comparing the bending strength of the reference sample after 1400 °C (1.9 MPa) and the bending strength of the sample with the highest replacement of aluminate cement by metashale after 1400 °C (8.4 MPa), the value was more than 300% higher. Concerning the measured results, the best values were achieved by the P-LN5 mixture, which contained more metashale than aluminate cement and no other alternative binders.

Although the mixes with a higher metashale content achieved strength values lower than those of the reference mix, the change in strength affected by exposure to a large temperature change was much lower. The reference specimen showed a 26.2% decrease in strength when heated from 20 °C to 400 °C, while the P-LN4 mixture showed only a 6.7% decrease in strength after the same heating, and the P-LN5 mixture even showed a 5.8% decrease. Therefore, it can be said that, like the increase in porosity, the decrease in strength is more gradual for mixtures with the alternative replacement of aluminate cement.

The compressive strength of the pastes with the replacement of the aluminate cement by alternative materials, shown in Table 5, was again lower than that of the reference sample at room temperature and after the exposure to temperatures of 400 °C–1000 °C. The binder that performed the worst was again P-LN1, as its compressive strength was more than 50% worse than that of the reference sample. On the other hand, these low strengths were not as unexpected because all the mixes tested contained only 40% aluminate cement. However, there was a rapid increase in compressive strength values when the samples were exposed to 1400 °C. Most pastes with alternative replacement of aluminate cement showed a threefold increase in strength after sintering compared to the reference sample at room temperature. The best results, in this case, were achieved by the P-LN4 mixture, whose compressive strength was more than 100% higher than the compressive strength of the reference mixture after the highest temperature exposure. This mixture contained equal amounts of aluminate cement and metashale and other alternative binders.

Similar to the performance of bending strength, more gradual changes in strengths were observed for mixes with the alternative replacement. The strengths of the mixtures P-LN3, P-LN4 and P-LN5 were almost the same at room temperature and after 400 °C. Moreover, the binder based only on waste metashale and aluminate cement had almost the same strength at room temperature and even after the exposure to 1000 °C.

When the results of compressive strength are compared with those of other samples containing metashale, a similar trend can be seen. In both studies mentioned above by Koňáková et al. [14,35], the compressive strength at room temperature was improved when the mixture under investigation contains up to 20% metashale. When looking in more detail at the development of the strength after an exposure to high temperatures [14], there was always the largest decrease in strength for the samples at about 1000 °C and then a substantial increase after loading by 1400 °C due to sintering. Thanks to the paper by Jogl et al. [39], the positive effect of adding an aluminate admixture other than metashale alone to the mixture can be seen. For composites with cement replacement by metashale alone, there was a continuous decrease in compressive strength until the temperature reached 1000 °C, whereas, in the results presented in this paper, the compressive strength after an exposure to 400 °C was higher, very similar or only a few percent lower than at room temperature. Compressive strength increased up to 400 °C was reported also by Mohamed et al. [33], who investigated Portland cement pastes with different ratios of metakaolin and silica fume. They showed a decreasing trend of compressive strength from 400 °C to 800 °C. Other composites for comparison were offered by Stonis et al. [28], who replaced aluminate cement with micro silica and metakaolin and exposed the samples to temperatures up to 1200 °C. The strengths showed a decreasing trend, but the metakaolin mixture performed better, with values approximately 5–10% higher than the micro silica mixtures. Pundene [53] also came up with the idea of using the substitution of aluminate cement by the waste material in combination with other pozzolanic admixtures in refractory concrete. In his research, he used spent catalyst waste, micro silica, reactive alumina and fireclay aggregate. He exposed individual samples to temperatures up to 1250 °C. The compressive strength values are very similar to those of the metashale mixtures. Also, a decreasing trend could be seen up to 1000 °C, but at higher temperatures, the strength increased again due to

Table 5
Mechanical properties of studied pastes.

	Temperature	P-LNR	P-LN1	P-LN2	P-LN3	P-LN4	P-LN5
Bending strength [MPa]	20 °C	4.2	2.1	2.3	2.9	3.0	3.5
	400 °C	3.1	1.4	1.9	2.8	2.8	3.3
	1000 °C	2.8	0.8	0.2	0.9	1.8	2.2
	1400 °C	1.9	0.0	1.1	6.7	7.9	8.4
Compressive strength [MPa]	20 °C	36.5	14.9	19.0	26.4	29.3	29.7
	400 °C	32.0	20.7	21.9	24.5	28.6	28.3
	1000 °C	30.6	8.9	12.4	14.4	18.8	28.3
	1400 °C	46.2	0.0	73.8	92.4	105.4	93.8
Dynamic modulus of elasticity [GPa]	20 °C	33.4	14.0	14.0	16.1	16.3	14.2
	400 °C	11.0	6.5	6.6	8.6	9.2	9.4
	1000 °C	7.7	1.0	3.2	4.8	6.7	9.3
	1400 °C	24.3	0.4	42.8	53.7	44.5	42.1

sintering. Waste material had noticeably improved the properties of composites. The best results were achieved by mixing the mixtures with a combination of waste material and both aluminate admixtures. Therefore, it can be seen that it makes sense to partially replace expensive aluminate admixtures with waste material having suitable properties.

The results of the dynamic modulus in Table 5 show a trend similar to that of the bending strength and compressive strength. All mixtures showed a worse dynamic modulus than the reference sample at room temperature and after the exposure to temperatures of 400 °C–1000 °C. Again, the worst results were obtained for the P-LN1 paste.

However, after 1400 °C, the dynamic modulus increased and exceeded the values of the reference sample after the exposure to the same magnitude of temperature. All pastes with alternative binders achieved high values, but in this case paste P-LN3, in which metashale represented 34% of the alternative binders, achieved slightly higher values. Its dynamic modulus was 120% higher than that of the reference sample after the exposure to 1400 °C.

Similar to previous properties, the change in dynamic modulus was more stable for samples with alternative materials. As with compressive strength, the smallest change is observed for the P-LN5 mixture. The modulus of elasticity decreased by 34.5% when the temperature increased from 20 °C to 1000 °C, while the modulus of elasticity of the reference, with the same increase in temperature, decreased by 77%.

However, when focused on the overall performance of mechanical properties, it is visible, that at ambient temperature it was primarily dependent on the porosity of studied composites (Table 4 and Fig. 16). The higher the porosity materials showed, the lower the mechanical performance was. However, after temperature exposures, a significant role played not only porosity variation (Table 4), but some linkages between phase variation can be derived as well. It can be deduced that the content of C-A-S phases led to a considerable increase in mechanical properties. On the contrary, due to the hibonite CA_6 creation, significant shrinkage was observed, which caused a further decrease in mechanical properties.

5. Mechanical properties of refractories

From the above results, the binders P-LN4 and P-LN5 can be considered as proving the best overall performance. Taking into the account desired target of waste metashale application, binder P-LN5 was chosen as the most suitable. Therefore, this combination of raw materials was selected for further investigation in the form of a cement composite. Reached results of mechanical properties can be found in Table 6.

The mixture containing the waste metashale achieved even bigger bending strengths than the reference mixture in all investigated temperature states. At room temperature, the K-LN5 mixture had a 10.3% higher bending strength and after the exposure to 1400 °C the difference was 58%. It is interesting to observe the evolution of the strengths as a function of temperature. In the case of reference composite K-LNR, the biggest decrease of bending strength was 68% when the sample was exposed to 1000 °C, and then after the exposure to 1400 °C, it reached the highest value of 8% higher than at ambient temperature. The reason for these significant changes is most likely the sintering process that occurred in these mixtures at around 1200 °C, as demonstrated earlier in the text. On the contrary, the composite K-LN5 with metashale showed a lower decrease at 1000 °C, namely by 24% compared to ambient temperature, and afterwards at 1400 °C increase by 54%.

A similar trend was also observed for compressive strength. Except for the ambient temperature, where the strength of the reference mixture K-LNR showed a 9% higher value, the higher values of compressive strength were observed each time in the case of K-LN5. Regarding the variety of compressive strengths due to the temperature exposures, similar to bending strengths, compressive strengths reached the lowest values at 1000 °C. In the case of reference composite K-LNR, the drop was by 45%. Afterwards, at 1400 °C the value remained almost equal, and no significant difference was observed. On the contrary, composite with waste metashale K-LN5 showed a drop at 1000 °C of only 9%, and then an immense increase of compressive strength was observed. Compared to the ambient temperature, the residual value was 104% higher and exceeded 100 MPa. This shows that again this material reached its highest strength after the exposure to 1400 °C. This strength was nearly 250% higher than the reference mixture.

A similar pattern of values can be found for the dynamic modulus of elasticity. Values with alternative cement replacement were higher at all temperatures, even at 20 °C, where the difference was 27.8%. The lowest values were again measured after 1000 °C, specifically by 81% for K-LNR and by 58% for K-LN5. However, this time the temperature of 1400 °C did not cause such a steep increase. After the highest temperature treatment, both materials reached a residual dynamic modulus of elasticity lower than at the ambient temperature, namely by 36% for K-LNR and by 9% for K-LN5.

Table 6
Mechanical properties of refractories.

	Temperature	K-LNR	K-LN5
Bending strength [MPa]	20 °C	8.7	9.6
	400 °C	3.9	12.1
	1000 °C	2.8	7.2
	1400 °C	9.3	14.7
Compressive strength [MPa]	20 °C	54.7	49.6
	400 °C	45.9	50.6
	1000 °C	30.3	45.3
	1400 °C	29.0	101.3
Dynamic modulus of elasticity [GPa]	20 °C	41.8	53.4
	400 °C	11.6	31.8
	1000 °C	7.8	22.3
	1400 °C	26.6	48.4

6. Conclusions

In this study, five different low-cement binders with refractory applications were designed. The studied materials were composed of varying amounts of reactive alumina, boehmite powder and waste metashale, while always containing a fixed amount of calcium aluminate cement. The main aim was to study the possibility of waste metashale applications in the field of castables. The particular findings presented in this paper can be summarized as follows:

- The binder with 60% of metashale contained significantly less CAH10, which could propose the advantage of being less susceptible to the conversion process. As a result of the silicon content, mixtures with waste metashale contained the most C-A-S-H phases, which were transformed to C-A-S at high temperatures. Therefore, a more crystalline structure with higher strength was formed after temperature exposure.
- The higher alumina content in the mixtures with a higher dosage of reactive alumina and boehmite powder led to the formation of hibonite after 1350 °C, which caused severe shrinkage.
- The pastes with the aluminate cement replacements had a lower bulk density, but a higher matrix density than the reference sample. Even the porosity was significantly greater for the mixes with the designed low-cement binders. However, the increase in porosity after exposures to high temperatures was not as rapid as that of the reference mixture and therefore did not produce as many cracks.
- The mechanical properties at the ambient temperature of the low-cement-based pastes were lower than the reference paste showed. However, after exposures to high temperatures, the strength fall was not as steep as that of the reference, and after the exposure to the extreme 1400 °C, the mechanical strengths were substantially improved in the case of the blended binder. The best overall performance was measured for the 60% of metashale replacement.

The test results proved that the replacement of aluminate cement with waste metashale seemed to be promising for refractory concrete. Although the paste with the highest metashale content was the most demanding in terms of water content, its overall values were closest to those of the reference mix. It is very positive that this particular binder contained more waste metashale than aluminate cement in a 60:40 ratio. Due to the results obtained, this ratio was also applied to the composite mixture. Mechanical testing of this refractory confirmed that the mixture with aluminate cement and waste metashale has great potential. Based on the presented results it was concluded that the designed alternative binder could be used in future applications of refractory structures. The advantage of such an application would be not only financial savings but would have also a positive environmental impact.

Data availability

All measured data and images are available upon request. As well as any other detailed information about particular measurement processes.

Declaration of competing interest

The authors declare that they have no known competing financial interests or personal relationships that could have appeared to influence the work reported in this paper.

Acknowledgement

This research has been supported by the Czech Science Foundation [project No. 20-00653S] and by the Grant Agency of the Czech Technical University in Prague [grant No. SGS22/137/OHK1/3T/11].

References

[1] N. Ukrainczyk, T. Matusinovic, S. Kurajica, B. Zimmermann, J. Sipusic, Dehydration of a layered double hydroxide—C2AH8, Thermochim. Acta 464 (2007) 7–15, https://doi.org/10.1016/J.TCA.2007.07.022.
[2] B. Pacewska, M. Nowacka, Studies of conversion progress of calcium aluminate cement hydrates by thermal analysis method, J. Therm. Anal. Calorim. 117 (2014) 653–660, https://doi.org/10.1007/s10973-014-3804-5.
[3] A.P. Luz, M.A.L. Braulio, V.C. Pandolfelli, Refractory Castable Engineering, first ed., Goller Verlag, Baden-Baden, Germany, 2015.
[4] S.M. Bushnell-Watson, J.H. Sharp, On the cause of the anomalous setting behaviour with respect to temperature of calcium aluminate cements, Cement Concr. Res. 20 (1990) 677–686, https://doi.org/10.1016/0008-8846(90)90002-F.
[5] B. Pacewska, M. Nowacka, I. Wilińska, W. Kubissa, V. Antonovich, Studies on the influence of spent FCC catalyst on hydration of calcium aluminate cements at ambient temperature, J. Therm. Anal. Calorim. 105 (2011) 129–140, https://doi.org/10.1007/s10973-011-1303-5.
[6] Y. Zhang, G. Ye, W. Gu, D. Ding, L. Chen, L. Zhu, Conversion of calcium aluminate cement hydrates at 60°C with and without water, J. Am. Ceram. Soc. 101 (2018) 2712–2717, https://doi.org/10.1111/jace.15505.
[7] A.P. Luz, V.C. Pandolfelli, CaCO 3 addition effect on the hydration and mechanical strength evolution of calcium aluminate cement for endodontic applications, Ceram. Int. 38 (2012) 1417–1425, https://doi.org/10.1016/j.ceramint.2011.09.021.
[8] K.L. Scrivener, J.-L. Cabiron, R. Letourneux, High-performance Concretes from Calcium Aluminate Cements, 1999.
[9] X. Shang, G. Ye, Y. Zhang, H. Li, D. Hou, Effect of micro-sized alumina powder on the hydration products of calcium aluminate cement at 40 °C, Ceram. Int. 42 (2016) 14391–14394, https://doi.org/10.1016/j.ceramint.2016.06.005.
[10] S. Majumdar, R. Sarkar, P. Vajifdar, S. Narayanan, R. Cursetji, A. Chatterjee, User friendly high refractory calcium aluminate cement, in: Calcium Aluminate Cements 2001, Iom Communications Ltd, London, 2001, pp. 467–476.
[11] A. Abolhasani, M. Shakouri, M. Dehestani, B. Samali, S. Banihashemi, A comprehensive evaluation of fracture toughness, fracture energy, flexural strength and microstructure of calcium aluminate cement concrete exposed to high temperatures, Eng. Fract. Mech. 261 (2022), https://doi.org/10.1016/j.engfracmech.2021.108221.
[12] X. Cheng, Q. Dong, Y. Ma, C. Zhang, X. Gao, Y. Yu, Z. Wen, C. Zhang, X. Guo, Mechanical and thermal properties of aluminate cement paste with blast furnace slag at high temperatures, Construct. Build. Mater. 228 (2019), https://doi.org/10.1016/j.conbuildmat.2019.116747.
[13] D. Konakova, E. Vejmelkova, L. Scheinherrova, M. Keppert, A. Cheng, R. Cerny, Basic physical and mechanical properties of cement composites after temperature exposure, MATEC Web of Conferences 322 (2020), 01001, https://doi.org/10.1051/matecconf/202032201001.
[14] D. Koňáková, V. Pommer, M. Jerman, M. Keppert, R. Černý, E. Vejmelková, Utilization of ceramic powder, calcined shale and sintered mullite as partial replacements of calcium aluminate cement, Construct. Build. Mater. 326 (2022), https://doi.org/10.1016/j.conbuildmat.2022.126824.
[15] N. Ukrainczyk, T. Matusinović, Thermal properties of hydrating calcium aluminate cement pastes, Cement Concr. Res. 40 (2010) 128–136, https://doi.org/10.1016/j.cemconres.2009.09.005.
[16] D. Koňáková, E. Vejmelková, V. Pommer, M. Keppert, A. Trník, R. Černý, Physical and chemical characteristics of heat resistant materials based on high alumina cement, in: AIP Conf Proc, American Institute of Physics Inc., 2021, https://doi.org/10.1063/5.0069565.
[17] J. Soro, A. Smith, C. Gault, Thermomechanical characteristics of calcium aluminate cement and sand tapes prepared by tape casting, J. Eur. Ceram. Soc. 26 (2006) 3799–3807, https://doi.org/10.1016/j.jeurceramsoc.2005.11.010.
[18] R. Salomao, M.A. Kawamura, A.B.V. Emilio, J. Sakihama, A.M. Segadaes, Calcium aluminate cement in castable alumina: from hydrate bonding to the in situ formation of calcium hexaluminate, Ceram. Int. 47 (2021) 15082–15093, https://doi.org/10.1016/j.ceramint.2021.02.066.
[19] R. Salomao, V.L. Ferreira, L.M.M. Costa, I.R. de Oliveira, Effects of the initial CaO-Al2O3 ratio on the microstructure development and mechanical properties of porous calcium hexaluminate, Ceram. Int. 44 (2018) 2626–2631, https://doi.org/10.1016/j.ceramint.2017.11.010.
[20] D. Fernández-González, J. Prazuch, I. Ruiz-Bustinza, C. González-Gasca, J. Pinuela-Noval, L.F. Verdeja, Solar synthesis of calcium aluminates, Sol. Energy 171 (2018) 658–666, https://doi.org/10.1016/j.solener.2018.07.012.
[21] M.M. Hossain, M.R. Karim, M. Hasan, M.K. Hossain, M.F.M. Zain, Durability of mortar and concrete made up of pozzolans as a partial replacement of cement: a review, Construct. Build. Mater. 166 (2016) 128–140, https://doi.org/10.1016/j.conbuildmat.2016.04.147.
[22] Z. Li, X. Gao, D. Lu, J. Dong, Early hydration properties and reaction kinetics of multi-composite cement pastes with supplementary cementitious materials (SCMs), Thermochim. Acta 709 (2022), 179157, https://doi.org/10.1016/j.tca.2022.179157.
[23] S. Samad, A. Shah, Role of binary cement including Supplementary Cementitious Material (SCM), in production of environmentally sustainable concrete: a critical review, Int. J. Sustain. Built Environ. 6 (2) (2017) 663–674, https://doi.org/10.1016/j.ijsbe.2017.07.003.
[24] M. Heikal, M.M. Radwan, O.K. Al-Duaij, Physico-mechanical characteristics and durability of calcium aluminate blended cement subject to different aggressive media, Construct. Build. Mater. 78 (2015) 379–385, https://doi.org/10.1016/j.conbuildmat.2015.01.033.
[25] E. Badogiannis, G. Kakali, G. Dimopoulou, E. Chaniotakis, S. Tsivilis, Metakaolin as a main cement constituent. Exploitation of poor Greek kaolins, Cem. Concr. Compos. 27 (2005) 197–203, https://doi.org/10.1016/j.cemconcomp.2004.02.007.
[26] H.S. Wong, H.A. Razak, Efficiency of calcined kaolin and silica fume as cement replacement material for strength performance, Cement Concr. Res. 35 (2005) 696–702, https://doi.org/10.1016/j.cemconres.2004.05.051.
[27] A. Allahverdi, S. Vakilinia, Pooneh Gharabeglu, Effects of Rfcc Spent Catalyst on Some Physicomechanical Properties of Portland Cement Paste, 2011.
[28] R. Stonis, I. Pundiene, V. Antonovič, M. Kligis, E. Spudulis, Study of the Effect of Replacing Microsilica in Heat-Resistant Concrete with Additive Based on Metakaolin, 2013.
[29] F. Benali, M. Hamidouche, H. Belhouchet, N. Bouaouadja, G. Fantozzi, Thermo-mechanical characterization of a silica-alumina refractory concrete based on calcined algerian kaolin, Ceram. Int. 42 (2016) 9703–9711, https://doi.org/10.1016/j.ceramint.2016.03.059.
[30] B. Amrane, E. Ouedraogo, B. Mamen, S. Djaknoun, N. Mesrati, Experimental study of the thermo-mechanical behaviour of alumina-silicate refractory materials based on a mixture of Algerian kaolinitic clays, Ceram. Int. 37 (2011) 3217–3227, https://doi.org/10.1016/j.ceramint.2011.05.095.
[31] F. Benali, Elaboration Et Caracterisation D'un Refractarie Monolithique A Base De Kaolin, Universite Ferhat Abbas-Setifi Ufasi, 2015.
[32] E. Ouedraogo, N. Prompt, High-temperature mechanical characterisation of an alumina refractory concrete for Blast Furnace main trough. PART II. Material behaviour, J. Eur. Ceram. Soc. 28 (2008) 2867–2875, https://doi.org/10.1016/j.jeurceramsoc.2008.04.027.
[33] S.M. Mohamed, S.S. Sayed, Effect of silica fume and metakaoline pozzolana on the performance of blended cement pastes against fire, Ceramics 51 (2007) 40–44.
[34] E. Vejmelková, D. Koňáková, M. Doleželová, L. Scheinherrová, P. Svora, M. Keppert, P. Reiterman, R. Černý, Effect of calcined Czech claystone on the properties of high performance concrete: microstructure, strength and durability, Construct. Build. Mater. 168 (2018) 966–974, https://doi.org/10.1016/j.conbuildmat.2018.02.204.
[35] D. Koňáková, V. Hovorková, E. Vejmelková, M. Keppert, R. Černý, Influence of metashale as cement replacement on the hygric transport properties of concrete, in: Adv Mat Res, Trans Tech Publications Ltd, 2014, pp. 188–193. https://doi.org/10.4028/www.scientific.net/AMR.1054.188.
[36] M. Čáchová, J. Koťátková, M. Doleželová, E. Vejmelková, P. Konvalinka, R. Černý, Porous structure and hygric properties of concrete for radioactive waste repositories, in: Key Eng Mater, Trans Tech Publications Ltd, 2018, pp. 127–131. https://doi.org/10.4028/www.scientific.net/KEM.760.127.

[37] D. Koňáková, E. Vejmelková, Effect of metashaleas SCM on mechanical and thermal properties in concrete production, Appl. Mech. Mater. 763 (2015) 41–46. https://doi.org/10.4028/www.scientific.net/amm.763.41.
[38] J. Koťátková, M. Čáchová, P. Bezdička, E. Vejmelková, P. Konvalinka, L. Zemanová, R. Černý, Influence of supplementary cementitious materials on the properties of concrete for secondary protection barrier in radioactive waste repositories, in: Key Eng Mater, Trans Tech Publications Ltd, 2018, pp. 96–101. https://doi.org/10.4028/www.scientific.net/KEM.760.96.
[39] M. Jogl, P. Reiterman, O. Holčapek, F. Vogel, P. Konvalinka, Refractory composites with mineral additive, in: Materials Science Forum, Trans Tech Publications Ltd, 2015, pp. 49–53. https://doi.org/10.4028/www.scientific.net/MSF.824.49.
[40] J.P. Singh, J.R. Thomas, D.P.H. Haselman, Analysis of effect of heat-transfer variables on thermal stress resistance of brittle ceramics measured by quenching experiments, J. Am. Ceram. Soc. 63 (1980) 140–144.
[41] ČSN EN 72 2400, Methods of Test for Mortar for Masonry - Part 3: Determination of Consistence of Fresh Mortar, 2000 (by flow table).
[42] N. Dobelin, R. Kleeberg, Profex: a graphical user interface for the Rietveld refinement program BGMN, J. Appl. Crystallogr. (2015) 1573–1580.
[43] ČSN EN 12390-3 - Testing of Hardened Concrete - Part 3: Compressive Strength of Test Specimens, 2020.
[44] ČSN EN 12390-5 - Testing of Hardened Concrete - Part 5: Bending Strength of Test Specimens, 2020.
[45] ČSN 73 1371 - Non-destructive Testing of Concrete - Ultrasonic Pulse Method for Testing Concrete, 2011.
[46] H. Taylor, Cement Chemistry, Thomas Telford, London, 1997.
[47] L. Xu, K. Wu, C. Roßler, P. Wang, H.M. Ludwig, Influence of curing temperatures on the hydration of calcium aluminate cement/Portland cement/calcium sulfate blends, Cem. Concr. Compos. 80 (2017) 298–306, https://doi.org/10.1016/j.cemconcomp.2017.03.016.
[48] D. Torréns-Martín, L. Fernández-Carrasco, M.T. Blanco-Varela, Conduction calorimetric studies of ternary binders based on Portland cement, calcium aluminate cement and calcium sulphate, J. Therm. Anal. Calorim. 114 (2013) 799–807, https://doi.org/10.1007/s10973-013-3003-9.
[49] E. Gasparini, S.C. Tarantino, P. Ghigna, M.P. Riccardi, E.I. Cedillo-González, C. Siligardi, M. Zema, Thermal dehydroxylation of kaolinite under isothermal conditions, Appl. Clay Sci. 80–81 (2013) 417–425, https://doi.org/10.1016/j.clay.2013.07.017.
[50] J. Khajornboon, K. Ota, K. Washijima, T. Shiono, Control of hexagonal plate-like microstructure of in-situ calcium hexaluminate in monolithic refractories, Journal of Asian Ceramic Societies 6 (2018) 196–204, https://doi.org/10.1080/21870764.2018.1484621.
[51] X. Wu, Z. Zhang, Y. Chen, T. Zhou, J. Fan, G. Piao, N. Kobayashi, S. Mori, Y. Itaya, Main mineral melting behavior and mineral reaction mechanism at molecular level of blended coal ash under gasification condition, Fuel Process. Technol. 91 (2010) 1591–1600, https://doi.org/10.1016/j.fuproc.2010.06.007.
[52] Mineral Data, (n.d.). http://www.webmineral.com (accessed August 19, 2022).
[53] I. Pundene, S. Goberis, V. Antonovich, R. Stonis, Refractories Abroad A Study of the Applicability of Waste Catalyst in Heat-Resistant Concrete, 2006.

4.3.3 Heat-resistant composites based on ternary binders with a low cement content: Characterisation and performance

D. Koňáková, V. Pommer, K. Šádková, M. Záleská, M. Böhm, M. et. al.
Developments in the Built Environment 18 (2024) 100400 [63]
https://doi.org/10.1016/j.dibe.2024.100400

This work expands the knowledge of heat-resistant cement composites by designing ternary binder systems based on CAC, alumina admixtures, and various SCMs. While previous works mainly addressed binary CAC-SCM systems, this study systematically evaluates the synergistic performance of ternary combinations aiming for reduced cement content and enhanced thermal resistance.

The investigated SCMs were microsilica, ferrite powder, ceramic powder, calcined shale, and sintered mullite. They were assessed in terms of the impact on hydration, phase evolution, and mechanical and thermal properties after exposure to temperatures up to 1400 °C. Calcined shale and ceramic powder emerged as the most promising SCMs, delivering high compressive strength (up to 128 MPa) even after thermal exposure. Their contribution lies in modifying the phase composition by promoting the formation of gehlenite (C_2AS), hibonite (CA_6), and corundum (Al_2O_3), creating a stable, refractory microstructure. After high-temperature loading, the composites showed reduced porosity growth and improved residual strength, compared to pure CAC binders. Thermal strain measurements confirmed lower thermal expansion coefficients in ternary systems, reducing the risk of cracking at high temperatures.

This work advances the state of the art by:

- Demonstrating the synergistic effect of ternary CAC-based binders
- Designing the low-cement, high-performance thermal-resistant composites
- Providing detailed insights into phase transformations and microstructural evolution during high-temperature exposure

In summary, this study establishes ternary CAC-based binders as a usable system for designing sustainable, heat-resistant composites, reducing clinker demand while enhancing performance in extreme thermal environments.

Developments in the Built Environment 18 (2024) 100400

Contents lists available at ScienceDirect

Developments in the Built Environment

journal homepage: www.sciencedirect.com/journal/developments in the built environment

Heat-resistant composites based on ternary binders with a low cement content: Characterization and performance

Dana Koňáková [a,*], Vojtěch Pommer [a], Kateřina Šádková [a], Martina Záleská [a], Martin Böhm [a], Martin Keppert [a], Eva Vejmelková [a]

[a] Department of Materials Engineering and Chemistry, Faculty of Civil Engineering, Czech Technical University in Prague, Thákurova 7, 166 29, Prague 6, Czech Republic

ARTICLE INFO

Keywords:
Heat-resistant composite
Calcium aluminate cement
Supplementary cementitious materials
Ternary binder
Material characterization
Mechanical properties
Thermal expansion

ABSTRACT

A reduction in cement consumption can be achieved through the use of supplementary cementitious materials (SCMs). In addition, the utilization of more than one SCM can show a beneficial synergic performance. In this paper, a combination of calcium aluminate cement, alumina admixtures and one other type of SCM was investigated. Namely: microsilica, ferrite powder, ceramic dust, calcined shale and sintered mullite were employed. The phase compositions of the designed binders were primarily characterized by XRD, XRF, DSC and SEM. Subsequently, the basic physical and mechanical properties as well as thermal expansion of the ternary binder-based composites up to 1400 °C were determined. The results revealed the synergic performance of used components. Calcined shale and ceramic powder were the most promising admixtures, exhibiting compressive strength of 80 MPa at room temperature and 117 and 128 MPa for ceramic powder and calcined shale, respectively, after exposure to 1400 °C.

1. Introduction

Concrete, a common building material, is in general inherently a non-combustible material. However, it is inappropriate to use concrete containing only Portland cement (PC) in structures regularly exposed to high temperatures such as furnace linings, chimneys, flues, factory floors, etc. In concretes based on PC the first cracks occur as early as 300 °C (Sadrmomtazi et al., 2020) and can hardly withstand temperatures of 1000 °C (Yüzer et al., 2004; Arioz, 2007; Bubeník et al., 2023). In contrast, calcium aluminate cement (CAC) based concretes can withstand temperatures up to 1600 °C. In addition to good resistance to high temperatures, they have very good resistance to aggressive environments (salt water, chlorides, etc.) (Scrivener; Klaus et al., 2013), rapid initial strength and a high hydration heat which enables its casting at lower temperatures. On the other hand, a major disadvantage of CAC-containing concrete is the conversion process – a spontaneous recrystallization of the unstable calcium aluminates CAH_{10} and C_2AH_8 to the thermodynamically stable phases C_3AH_6 and AH_3. This process potentially weakened a long-term strength. (Scrivener).

Cement production faces two primary challenges: environmental impact and energy consumption. To reach the high temperature (1450 °C–1550 °C) required for PC production, a large amount of fuel must be burned, leading to a large production of greenhouse gases (Teng et al., 2018; Luhar et al., 2019a, 2019b). Aluminous cement production demands even higher kiln temperatures (1600 °C–1700 °C), making it more energy-intensive than PC production (Popovics, 1992). Another aspect is the carbon footprint. From that point, CAC has a lower carbon footprint due to fewer carbonates in its raw materials (Zapata et al., 2022). Cement production also heavily depletes non-renewable resources, with 1.5 tons of raw materials needed for every ton of cement (Rashad, 2013; Asaad et al., 2018). As global cement demand is projected to double by 2050 (Nejat et al., 2013; Xie and Ozbakkaloglu, 2015), finding sustainable alternatives for raw materials becomes increasingly urgent.

Materials that can be used as a partial replacement for cement are called Supplementary Cementitious Materials (SCM). To be used as an SCM, the material must demonstrate pozzolanic activity. The SCM material must contain such components, that react well with cement or lime and water. These reactions should ideally result in the formation of hydration products similar to those of cement (Massazza, 2003). In addition to reducing emissions and replacing non-renewable materials, SCMs can improve the properties of the resulting cement composite. The most common representatives of SCMs are blast furnace slag (Martins et al., 2021), microsilica or silica fume (Lewis, 2017), and fly ash (Da

* Corresponding author.
E-mail address: dana.konakova@fsv.cvut.cz (D. Koňáková).

https://doi.org/10.1016/j.dibe.2024.100400
Received 14 February 2024; Received in revised form 6 March 2024; Accepted 12 March 2024
Available online 15 March 2024
2666-1659/© 2024 The Authors. Published by Elsevier Ltd. This is an open access article under the CC BY license (http://creativecommons.org/licenses/by/4.0/).

Silva and De Brito, 2015). In addition to these industrial products, there are also natural pozzolans (Vejmelková et al., 2015), agricultural waste (Wi et al., 2018), or artificial materials such as calcined clays or shales (Vejmelková et al., 2018a; Siddique and Klaus, 2009).

In the case of CAC, the applicability of SCMs is more complicated, as an appropriate replacement has to show adequate properties not only at ambient temperature but especially at high-temperature loadings. Despite that the idea of utilising SCMs in the case of CAC would be a promising solution, this issue was less frequently addressed. More precisely, commonly applied SCMs, such as blast furnace slag (Idrees et al., 2021; Kırca et al., 2013), microsilica or fly ash (Zapata et al., 2022; Massazza, 2003; Rivas Mercury et al., 2006; Collepardi et al., 1995) have been studied, but the scope of possible SCMs is much wider. Based on the latter research, it can be concluded that the application of siliceous components led to the variation of hydrated phases. The stable hydrates katoite C_3AH_6 and gibbsite AH_3 were formed directly together with calcium-aluminium-silicate-hydrates CASH in amorphous form, hydrogarnets or as stratlingite C_2ASH_8. As a consequence of the mentioned modifications, the mechanical strengths development was somehow reduced, but on the other hand, the negative conversion process was eliminated.

Considering the composition of calcium aluminate cement, more adequate admixtures seemed to be those based on alumina instead of silica. Such materials would not affect the rising phases as much and therefore do not influence the thermal resistance of final composites. Reactive alumina (Ghose et al., 2013; Koňáková et al., 2021a, 2021b) belongs to one of the most discussed admixtures, nowadays commonly used in the production of heat-resistant composites or refractories (Madej, 2016; Zhang et al., 2018, 2020). Its application as an SCM led to faster hydration and also higher hydration degree. In addition, after the temperature exposure, it gave rise to a higher amount of mullite and corundum phases, and consequently, it increased the hot modulus of rupture and overall mechanical properties. On the other hand, exposure to extreme temperatures above 1350 °C (Šádková et al., 2023; Salomao et al., 2021) can lead to the crystallization of hibonite, which causes a significant porosity increase.

Calcined clays or shales are other representatives of effective SCMs (Šádková et al., 2023; Koňáková et al., 2022a; Claramunt et al., 2018; Nowacka, 2017; Gonzalez-Lopez et al., 2021). This type of artificial pozzolana reduced the workability of the fresh mixture. On the other hand, it contributed to the higher hydration degree when crystal phases remained less affected, but it gave rise to the modified amorphous phases. As a result, the setting times were significantly decreased due to the application of calcined shale. Similarly to ceramic powder, the application of calcined clays and shales led to porosity variations. In contrast, it also led to the growth of compressive strength, especially after exposure to high-temperature loading.

Research can also be found on the replacement of aluminate cement with ceramics (Koňáková et al., 2022a; García-Álvarez et al., 2018). Ceramics contributed to the creation of metastable hydrates CAH_{10} and C_2AH_8, but a significant amount of crystalline C-A-S-H species was formed as well. Moreover, it also modified the composition of amorphous phases of hydrated pastes. Consequently, it accelerated the hydration and despite that it increased the porosity, the final compressive strength was increased as well. However, similarly to the previous case, more research dealing with a combination of ceramic bricks and CAC can be found in the different areas of their applicability. This time the ceramic was more often used as an aggregate (Baradaran-Nasiri and Nematzadeh, 2017; Halicka et al., 2013; Martins et al., 2016) or as a precursor for alkaline activation of ceramic powder-CAC geopolymers (Reig et al., 2016).

Replacing at least part of the aluminous cement with ferrite material is another option to reduce the consumption of bauxite in the production of aluminous cement. Partially replacing Al_2O_3 in cement clinker with Fe_2O_3 results in the so-called ferrite aluminate cement (FAC) (Idrissi et al., 2010; Li et al., 2007; Bullerjahn et al., 2014; Huang et al., 2021; Hertel et al., 2016). FAC reached adequate mechanical properties (Zhang et al., 2021) but also showed fast setting times and extreme hydration rates (Huang et al., 2021; Wang et al., 2014). Nevertheless, the applicability of these materials in high-temperature conditions has not been studied yet. The next possibility is a combination with magnesium, which gives rise to so-called alumina-spinel castables (Madej, 2016; Zhang et al., 2018; Wang et al., 2018; Boquan et al., 2015; Yun-Fei et al., 2017). These materials are well known for good refractoriness, high corrosion resistance and overall great thermo-mechanical properties. However, in both cases, the more frequently used application was their utilization in clinker production than as a further additive in composites production.

All the above-mentioned published researchers were focused on a binary binder-based approach, more precisely only one SCM was used to produce blended cement pastes. However, it has been already proven that the utilization of more SCMs at once can have a synergic effect on the final performance of designed composites based on Portland Cement (Vejmelková et al., 2018a, 2018b; Papatzani and Paine, 2020; Srinivas et al., 2021; Snellings et al., 2022; Dhandapani et al., 2021). On that account, this paper is aimed at the study of ternary binder-based composites. The first component is CAC, which is primarily partially replaced by the mixture of alumina-based materials (reactive alumina with boehmite powder). This combination would increase the temperature resistivity of the final composite, and provide another alumina source to be employed in phase composition. Afterwards, five different SCMs were chosen to be applied in the mixture composition of ternary binder-based composites. The studied SCMs were microsilica, ferrite powder, ceramic powder, calcined shale and sintered mullite. Firstly, their impact was assessed through the view of the phase composition of cement stone at ambient temperature and also after exposure to 1400 °C. Afterwards, ternary-binder-based composites were produced and their mechanical and thermomechanical properties were determined.

2. Experimental methods

2.1. Material characterization

The laser diffraction method was employed for the determination of granulometry of fine components, specifically, the Bettersizer S3 Plus device was used.

Simultaneous thermal analysis, consisting of differential scanning calorimetry (DSC) and thermogravimetry (TG), was performed using a Labsys EVO DTA/DSC from Setaram Inc. The experiments were done in the temperature range from 30 °C to 1400 °C with a heating rate of 5 °C min^{-1} and in an argon atmosphere with a flow rate of 40 ml min^{-1}.

The phase composition was studied by X-ray diffraction (XRD), specifically using a PANalytical Aeris system with a $Co_{K\alpha}$ tube. The qualification of phases was carried out by using HighScore, while for the quantification the Profex software (Doebelin and Kleeberg, 2015) (which employed Rietveld analysis with internal standard (20% of ZnO)) was employed.

The SEM images were acquired with the help of a Phenom XL desktop device equipped with a BSE detector and CeB6 source. Investigated samples were first immersed in isopropanol and afterwards, platinum coated. The voltage was set to be 5 or 10 kV and the magnification ranged from 250x to 5000x.

2.2. Basic physical properties

Matrix density, bulk density and open porosity belonged to the studied basic physical characteristics. Matrix density was determined by helium pycnometer, by the device Pycnomatic ATC from Thermo Fisher Scientific Inc. Bulk density was determined by gravimetric method. Afterwards, the values of total porosity were counted from the known values of matrix density and bulk density.

For a deeper study of pore structure, mercury intrusion porosimetry

was employed. Specifically, the experiments were carried out using instruments PASCAL 140 + 440 made by Thermo Fisher Scientific Inc. The range of an applied pressure corresponds to the pore radius from 0.001 to 100 μm.

2.3. Mechanical parameters

Mechanical properties, specifically compressive strength and flexural strength were measured according to the standard (ČSN EN 1015-11 (722400), 2020). Flexural strength was measured on three samples (40 × 40 × 160 mm) using the loading device MTS 100. The arrangement of the experiment was a classical three-point bending with a 100 mm span length. Compressive strength was then determined using the loading device EU40 on fragments from the flexural strength experiments.

Before the actual loading of specimens used for the determination of mechanical strengths, the dynamic modulus of elasticity was determined by ultrasound testing (ČSN EN 12504-4, 2005). Specifically, The Proceq PunditLab + ultrasonic velocity instrument with the 54 kHz pulse transducer was used to determine the ultrasound speed. The one-dimensional adjustment was used, and the ambient dimensionality coefficient was assumed to be 1.

2.4. Thermomechanical analysis

Thermal strain depending on temperature was measured by a linear thermal horizontal dilatometer (Trnik et al., 2012). This device utilizes a comparative method when the real thermal expansion is determined by comparing the analysed specimen with a reference corundum rod. Three specimens (15 × 15 × 160 mm) were measured with a maximal temperature of 1400 °C and a heating rate of 1 °C per min.

3. Studied materials

3.1. Raw materials and their characterization

All raw materials were primarily characterized; their chemical composition is presented in Table 1 and in Fig. 1 there are presented the granulometric curves. Calcium aluminate cement Secar71 originated from Kerneos S.A. was used as a principal and reference binder. This cement was composed of 55% krotite (CA, $CaO{\cdot}Al_2O_3$) and 36% grossite (CA_2, $CaO{\cdot}2Al_2O_3$). Its average particle size (D_{50}) was 8.6 μm, its specific gravity was 2900 kg m^{-3} and specific surface area (SSA) was 482 m^2kg^{-1}. With more than 70% of alumina content, it belonged to the medium alumina cement. As it is believed that alumina oxide contributes to the high-temperature resistance of the hardened binder, two other components with almost 100% alumina content were employed. Specifically, super reactive alumina Nabalox NO 713 and boehmite powder Apyral AOH 40 from Nabaltec AG were used. Both admixtures were of crystal structure, super reactive alumina was 92% corundum (Al_2O_3), and boehmite (AlOOH) had a purity of 98%. D_{50} of these components were 0.7 μm and 2.6 μm (for reactive alumina and boehmite respectively) and regarding their specific gravities, reactive alumina showed 3950 kg m^{-3}, while boehmite had 3000 kg m^{-3}. Specific surface area was in the case of reactive alumina 6953 m^2kg^{-1}, and 3509 m^2kg^{-1} for boehmite powder.

The other admixtures, potentially investigated as binder components, were of two groups. The first one was pure materials, which were chosen for a similar oxide composition as the main oxides of cement. Except for the here-in-above described alumina, two other materials were examined. Micro silica, which is the common admixture used in the case of Portland cement, was provided by Stachema CZ. Namely, the Stachesil S with D_{50} of 11.7 μm, the specific gravity of 2200 kg m^{-3} and SSA of 13,680 m^2kg^{-1} was used. This material showed a purity of 95% and 99% of it was in an amorphous phase. The second pure material was ferrite powder with a purity of 98%. It was supplied by company Pk chemie, its D_{50} was 24.6 μm, specific gravity 4850 kg m^{-3} and SSA of 4250 m^2kg^{-1}. Regarding the mineralogical composition, it contained 93% of hematite (Fe_2O_3). Slaked lime ($Ca(OH)_2$) was initially considered as a fourth admixture. However, it extremely accelerated the hardening and hydration of calcium aluminate cement. During the sample preparation, the mixture with lime was in few minutes hard and very hot. Thus this combination was not possible to prepare without an application of a higher amount of retardant additives.

The second group of materials was so-called raw materials with medium alumina content. These examined materials already proved their applicability in combination with calcium aluminate cement (Koňáková et al., 2022a). The first one was ceramic powder, which was a waste material that arose during the grinding of thermal insulating bricks. Its D_{50} was 17.5 μm, specific gravity showed 2590 kg m^{-3} and SSA 3518 m^2kg^{-1}. This material had the most complex chemical as well as mineralogical composition. It contained 30% of the amorphous phase, and the observed minerals were quartz (SiO_2), biotite ($K(Mg, Fe)_3AlSi_3O_{10}(OH)_2$), orthoclase ($K(AlSi_3O_8)$), microcline ($K(AlSi_3O_8)$), albite ($Na(AlSi_3O_8)$), muscovite ($KAl_2(AlSi_3O_{10})(OH)_2$) and hematite ($Fe_2O_3$). The next raw material was calcined claystone, specifically calcined shale from České lupkové závody, a.s. This material was similar to metakaolin. It was thermally activated, and therefore it had a quite high content of amorphous phase (67%) while the most abundant crystalline mineral was kaolinite (22%). Its average particle size was 3.3 μm, specific gravity was 2475 kg m^{-3} and SSA was 12,460 m^2kg^{-1}. The last one was sintered mullite, Symulox M72 originating from Nablatec AG was used. Despite the larger grain size (D_{50} of 334 μm and SSA of 189 m^2kg^{-1}), it was decided to use this material in its original granulometry, as it had been examined in the previous work (Koňáková et al., 2022a). When focused on mineralogical composition, it contained 17% of an amorphous phase, and the rest was almost entirely the mullite ($2Al_2O_3{\cdot}SiO_2$, A_2S). The specific gravity was 2800 kg m^{-3}.

The aggregate used for the need of this study was chamotte A114 VHR from České lupkové závody, a.s. Its specific gravity was 2550 kg m^{-3} and four gradings with maximal grains up to 3 mm were mixed to reach the aggregate mixture's optimal granulometry. Namely, 33% of grading 0–0.5 mm, 23% of grading 0.5–1 mm, 23% of grading 1–2 mm and 20% of grading 1–3 were combined.

Table 1
Chemical composition of raw materials (XRF).

Raw materials	Al_2O_3	SiO_2	Fe_2O_3	CaO	MgO	K_2O	Na_2O
Calcium aluminate cement	70.70	0.40	0.10	28.20	0.10	0.06	–
Super reactive alumina	99.70	0.05	0.03	–	–	–	0.10
Boehmite powder	99.00	–	–	–	–	–	–
Micro silica	0.40	94.60	0.50	0.50	0.50	1.60	0.30
Ferrite powder	0.20	0.15	98.00	0.04	0.02	0.02	0.02
Ceramic powder	20.60	49.40	4.60	15.00	2.80	3.40	0.80
Calcined shale	45.90	50.50	0.70	0.20	0.10	0.60	–
Sintered mullite	72.00	26.00	0.30	0.05	0.10	0.60	0.20
Chamotte	41.73	53.95	1.25	0.13	0.18	0.75	0.05

3.2. Composition and production of studied materials

Compositions of studied materials can be found in Table 2. The reference material, labelled LR, contained only calcium aluminate cement. In the first step, 55% of the calcium aluminate cement was replaced by aluminium-based admixtures. Specifically, super reactive alumina and boehmite powder were used in a ratio of 1:1. These two admixtures already proved their applicability as calcium aluminate cement replacement (Koňáková et al., 2021a, 2021b). The designed low-cement composite was labelled as LA and served as the second reference material. The other five materials were composed of 45% calcium aluminate cement, 40% alumina-based admixtures and 15% other materials investigated as potential SCM. Their labels were as

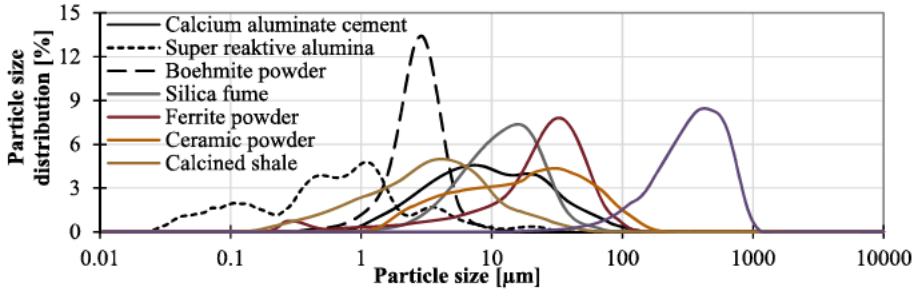

Fig. 1. Granulometric curves of raw-materials.

Table 2
Composition of studied low-cement-based pastes and composites [kg m ^{3}].

Heat-resistant mixtures	LR	LA	LS	LF	LC	LL	LM
Calcium aluminate cement	500	225	225	225	225	225	225
Alumina admixture	–	275	200	200	200	200	200
Micro silica	–	–	75	–	–	–	–
Ferrite powder	–	–	–	75	–	–	–
Ceramic dust	–	–	–	–	75	–	–
Calcined shale	–	–	–	–	–	75	–
Sintered mullite	–	–	–	–	–	–	75
w/b - paste	0.30	0.37	0.38	0.33	0.33	0.34	0.29
Chamotte	1500	1500	1500	1500	1500	1500	1500
Plasticizer	0	5	5	5	5	5	5
w/b - composites	0.30	0.38	0.40	0.36	0.31	0.33	0.32

follows: LS for micro silica, LF for ferrite powder, LC for ceramic dust, LL for calcined shale and LM for sintered mullite.

Although the main aim of this study was to investigate the performance of heat-resistant composites with low cement content, primarily the designed ternary binders had to be properly characterized. On that account, low-cement-based pastes without aggregate (chamotte) and plasticizers were prepared. Those pastes were employed for the performance of XRD, DSC and SEM analysis. Regarding the water/binder ratio, the dosage of water differed. The reference pastes with w/b ratio of 0.3 showed flow (ČSN EN 93 3-1 (721193), 2012) of 180/180 mm. The other pastes were designed with the aim of reaching equal consistency (flow value). It can be noted, that except for sintered mullite, application of all other raw materials led to the growth of w/c ratio requirements.

In the second part of this study, ternary binder-based composites were produced. The mixtures were composed of designed latter binders and four gradings of chamotte aggregates. As for w/b ratios, a similar approach as in the case of cement pastes was employed. This time the desired flow was 140/140, which had been measured for reference paste LR with a w/b ratio of 0.3. However, designed low-cement binder-based mixtures showed substantially higher w/b ratios with this demand. Thus it was chosen to use plasticizing admixture, which would improve the workability of the fresh mixtures, and retain the w/b ratio under 0.4. Based on the previous research (Koňáková et al., 2022b), a superplasticizer based on modified polycarboxylates was chosen. Namely Sika ViscoCrete 2700 from Sika CZ, s.r.o. in the amount of 1% of binder was used in all cases of low-cement binder-based mixtures.

The production process of mixtures was as follows: primarily the dry components of the binders were properly mixed. Afterwards, the aggregate was added. Then after homogenization of the dry mix, approximately one-third of the water mixed with the plasticizer dose was poured in. Subsequently, the remaining water was continuously added up to reach the desired consistency. Fresh mixtures were put into the greased moulds and compacted at the vibration table. The final specimens were covered by plastic film and after one day demoulded. The production took place in laboratory conditions at 20 °C and after the demoulding, specimens were put into a climatic chamber (controlled 20 °C and 50% RH).

After 28 days of curing in monitored conditions, specimens were either directly tested or thermally loaded at the temperature of 1400 °C (Fig. 2). Before actual thermal loading, specimens were for one day dried at the temperature of 105 °C (in order to prevent explosive spalling). Then they were put in the electric furnace and exposed to the 1400 °C. The heating rate was set to 1 °C per minute and the duration of the exposure was 3 h. Afterwards, specimens were left to cool spontaneously.

4. Results and discussion

4.1. Low-cement-based pastes

4.1.1. Phase composition at ambient temperature

The summary of phase composition at the age of 28 days is delineated in Fig. 3. Despite a controlled curing temperature of 20 °C, reference pastes LR showed somehow converted composition with a significant amount of crystals of AH_3 ($Al_2O_3{\cdot}3H_2O$) polymorphs and stable katoite C_3AH_6. Gibbsite was the most abundant polymorph of AH_3, accompanied by a lower amount of nordstrandite and a minor amount of bayerite. However, the highest value was observed in the case of amorphous and not-identified phases. In this number, also the content of hydration product C_2AH_8, whose structure has not been properly described to be quantified by XRD analyses, was included. To be able to somehow characterise the composition of amorphous and not-identified phases, its chemical composition was determined. Firstly, the chemical composition of cement stone was derived from the known chemical composition of raw materials (Table 1), the used composition of studied mixtures (Table 2), and measured thermogravimetry (Fig. 5b), which proposed the information about the water content. Afterwards, the contents of chemical oxides in the observed phases were determined and finally by the subtraction of these later variables the composition of the amorphous phase was calculated. Results can be found in Table 3. In the case of LR, these phases contained a significant amount of aluminium oxide, water and a moderate amount of calcium oxide. Regarding the other component, a significant amount of unreacted cement phase was

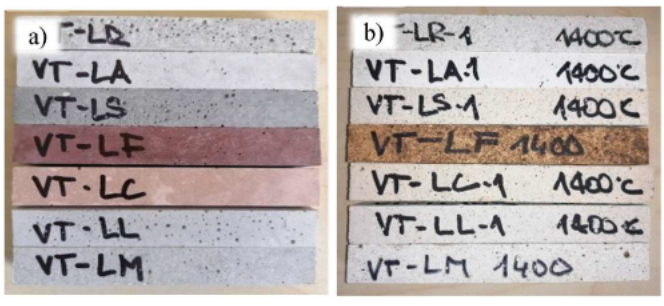

Fig. 2. Studied composites: (a) at ambient temperature (b) after exposure to 1400 °C.

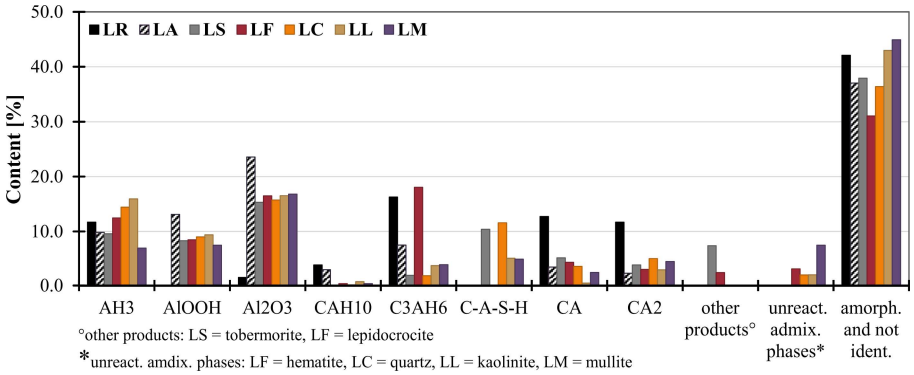

Fig. 3. Phase composition of studied pastes at ambient temperature (20 °C).

Table 3
Chemical composition of amorphous and not identified phases of studied pastes at ambient temperature (20 °C).

Oxides	LR	LA	LS	LF	LC	LL	LM
Al_2O_3	21.4%	19.0%	18.4%	14.2%	18.3%	22.5%	26.4%
CaO	6.5%	3.5%	1.7%	0.3%	6.5%	6.7%	5.9%
SiO_2	–	–	5.4%	–	1.6%	3.8%	–
Fe_2O_3	–	–	–	6.5%	0.6%	–	–
H_2O	13.4%	13.9%	10.8%	11.0%	7.4%	9.2%	12.0%

observed. The hydration degree was determined concerning the ratio between krotite and grossite in the fresh mixture and their amount in the hardened cement stone. In the case of reference material, the hydration degree reached 60%.

When alumina admixtures were used, the composition of LA showed similar performance as in the case of LR. In accordance with a lower amount of used cement, the amount of observed created phases was somehow lowered. In addition, a noticeable amount of unreacted boehmite and corundum were supplemented in the phase composition. From that point of view, the boehmite seemed to be more reactive as its amount decreased more profoundly. On the other hand, assessing the reactivity of corundum would be more complicated, as this phase was observed also in the case of hydrated pure CAC paste LR. Regarding the amorphous and not identified phases, its content was similar to the case of reference material, but it contained a lower amount of calcium oxide. This corresponded to the lower amount of this substance in the mixture composition. On the other hand, a comparable amount of water was observed. Regarding the hydration degree, it seemed that alumina admixtures were beneficial from that point of view, as the paste LA showed a significantly higher hydration degree. It reached 81%, which was remarkably higher than in the case of pure paste LR.

Microsilica utilization led to the most significant modification of created phases. The main hydrates of cement pastes LS were not in the form of C-A-H, which amount decreased significantly, but in the form of C-A-S-H. Specifically, stratlingite and gismondine were observed from crystal phases. In addition, the tobermorite, as a representative of C–S–H was identified as well. When focused on the amorphous and not identified phases, the high content of silica in this nature can signify either the presence of unreacted microsilica but also that the lower amount of C–S–H could have been created during hydration. This assumption was supported by consideration of the amount of water in the observed phases and the hydration degree of LS, which was this time slightly higher than in the case of pure paste LR. Namely, the hydration degree of paste with microsilica LS reached 69%.

When ferrite powder was used the highest amount of crystalline phases were observed. Except for high amounts of crystal AH_3 (in the form of nordstrandite and gibbsite) and katoite C_3AH_6 also a low amount of lepidocrocite FeOOH was identified in the hardened paste LF. A substantial amount of iron oxide remained in the amorphous phases and not identified phases, which can signalize the formation of another kind of poorly crystalline ferrihydrites (Foldvári, 2011). Regarding other components, amorphous and not identified phases contained only a trace amount of calcium oxide. Thus it can be concluded that no C_2AH_8 gave rise and C_3AH_6 was the only one formed C-A-H phase. In addition, also the lowest content of aluminium oxide Al_2O_3 was determined, this can signify the lower amount of amorphous AH_3. The hydration degree of paste with ferrite powder LF was 75%.

The first examined SCM from the field of medium alumina materials was ceramic dust. Its employment contributed to the creation of a higher amount of crystalline AH_3, again in the form of gibbsite and nordstrandite. At first sight, the ceramic powder had a similar impact on crystalline hydration product modification as in the case of microsilica. C-A-H structures were partially replaced by C-A-S-H phases. But when focusing on particular phases, paste LC contained stratlingite and gismondine and no tobermorite. Moreover, from the composition of amorphous and not identified phases, it can be derived that no C–S–H was produced this time as the content of silica oxide was quite low. It is worth noting, that in the case of ceramic powder utilization, the amorphous phase contained the lowest amount of water content. On the other hand, ceramic dust application led to an equal hydration degree as in the case of microsilica, specifically, it showed 69%.

The next studied admixture was calcined shale. In accordance with a higher amount of alumina, its application led to the formation of the highest amount of crystalline AH_3, with the highest gibbsite occurrence. At the same time, the number of formed hydrates C-A-S-H was less than half level compared to the case of ceramic dust, and primarily the phases with lower silica content were created. However, a noticeable amount of silica remained in the amorphous phases, and its composition was quite diverse. When focused on unhydrated cement grains, it is visible that paste with calcined shale LL contained the lowest number of krotite CA and grossite CA_2. The hydration degree reached 86%, which was the highest among the studied materials.

The last admixture was sintered mullite, in accordance with its nature (lower amorphous content and bigger granularity) it seemed to be less reactive. The lesser amount of crystalline AH_3 was formed together with a medium amount of katoite C_3AH_6 and C-A-S-H phases. On the other hand, it reached the highest value of amorphous phases with a significant amount of bounded water in it. As there was no silica oxide presence there, it can be deduced that no amorphous C-A-S-H nor C–S–H were created. Despite the latter described performance, the hydration degree of paste LM was quite high, specifically 75%.

4.1.2. Phase composition after exposure to 1400 °C

The summary of the phase composition of cement pastes after the exposure to 1400 °C can be found in Fig. 4. Similar to the ambient temperature, also this time the chemical (oxide) compositions of amorphous phases (Table 4) were determined considering the chemicals of raw materials, their ratio in the fresh mixture, and the composition of

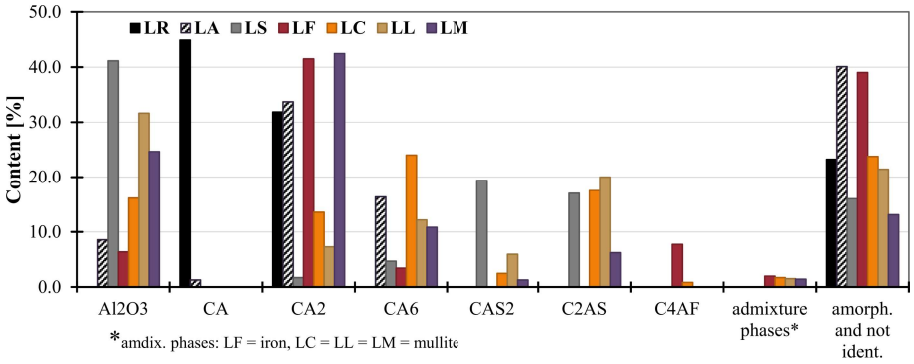

Fig. 4. Phase composition of studied pastes after exposure to 1400 °C.

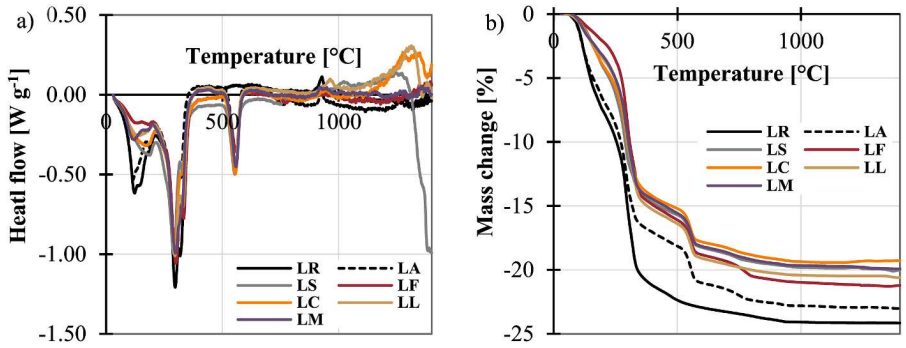

Fig. 5. Simultaneous thermal analysis of studied pastes: (a) DSC, (b) TG.

Table 4
Chemical composition of amorphous and not identified phases of studied pastes after exposure to 1400 °C.

Oxides	LR	LA	LS	LF	LC	LL	LM
Al_2O_3	17.5%	37.3%	11.6%	23.4%	18.0%	19.5%	10.9%
CaO	2.9%	1.4%	1.7%	1.2%	1.4%	0.7%	0.2%
SiO_2	–	–	2.8%	–	0.1%	0.1%	0.4%
Fe_2O_3	–	–	–	12.3%	0.5%	–	–

observed phases. In the case of reference material LR, only two crystalline products after the heat treatment were identified. The high amount of krotite CA was complemented by grossite CA_2 and a substantial amount of amorphous phases. Regarding its composition, the major component was aluminium oxide and only a minor amount of calcium oxide was observed. Despite the high alumina dosage, no other minerals were formed.

When alumina admixtures were used, the composition was different. The amount of krotite CA extremely fell, and a slightly higher number of grossite CA_2 was created. Nevertheless, the biggest difference was the crystallization of a substantial amount of hibonite CA_6 due to the modified aluminium/calcium ratio. In addition, the small dosage of corundum remained unaffected. Regarding the amorphous phase, its content rose remarkably, but similar to the previous case, the biggest portion was aluminium oxide supplemented by a minor amount of calcium oxide.

Microsilica application, as well as utilization of other studied replacements, led to the vanishment of krotite CA. By its recrystallization, further minerals were created. In the case of paste LS, their compositions were more heterogeneous. Due to the high silica content, a considerable amount of C-A-S was formed (specifically in the form of gehlenite C_2AS and anorthite CAS_2 in a similar ratio) supplemented by a low number of hibonite CA_6 and only a minor volume of grossite CA_2. During the heat treatment also a significant amount of corundum was crystallized. Contrary to previous materials, the amorphous phase content was quite low but the composition was similar. The higher amount of aluminium oxide and minor volume of calcium was supplemented by a low amount of silica oxide.

In the case of paste LF with ferrite powder, a higher amount of grossite CA_2 was formed. Other identified calcium and aluminate phases include corundum Al_2O_3 and hibonite CA_6. In accordance with the nature of the used SCMs, a noticeable amount of brownmillerite C_4AF were created as well. A low amount of ferrite created the iron phase, but the biggest portion of the material remained in amorphous phases. This time composed not only of a significant amount of alumina oxide but a remarkable content of ferrite oxide was present as well.

Regarding ceramic dust, its application led to the most diverse composition of thermally treated pastes. The recrystallization of hibonite CA_6 was the most distinctive in the case of paste LC, but a noticeable amount of grossite CA_2 and corundum Al_2O_3 remained as well. Apart from it, a substantial amount of gehlenite C_2AS was created alongside with low content of anorthite CAS_2 and trace content of mullite A_2S brownmillerite C_4AF. When focused on the amorphous and not identified phases, it can be deduced that it contained mainly of aluminium oxide accompanied by calcium oxide. The amount of silica oxide and ferrite oxide was negligible; thus it can be concluded that these chemicals are entirely a part of the crystalline phases.

The phase modification was in the case of calcined shale utilization similar to the case of ceramic dust. However, as the calcined shale had a lower amount of calcium oxide, also a lower amount of grossite CA and hibonite CA_6 were formed (compared to the ceramic powder). On the other hand, a higher number of corundum Al_2O_3 were observed. Regarding the C-A-S phases, their amount was slightly higher, but as in the previous case, gehlenite C_2AS was the dominant form. The performance of the remaining components of paste LL was (except for the absence of brownmillerite C_4AF) equal to the paste with ceramic dust LC: a minor amount of mullite A_2S and moderate content of amorphous phase. On the contrary, this time the amorphous phase was created

almost entirely from aluminium oxide.

The last studied admixture was sintered mullite. The paste LM was composed mainly of grossite CA_2 and corundum Al_2O_3. In accordance with a lower content of silica in this raw material, also the lower content of C-A-S phases was created. Regarding their particular composition, gehlenite C_2AS was again dominant, and only a low amount of anorthite CAS_2 was recrystallized. The further identified phase was again mullite A_2S in a minor amount. The amorphous phase showed the lowest number among the studied pastes. But similar to the calcined shale it was composed almost entirely of alumina oxide.

4.1.3. Phase development during the temperature loading

Results of simultaneous thermal analysis can be found in Fig. 5 where the DSC curves and TG respectively up to 1400 °C were delineated. When focused firstly on the performance of pure cement LR, it showed common behaviour (Koňáková et al., 2022a, 2022b). The first endothermic peak at 124 °C signified the evaporation of physically bounded water together with the dehydration of amorphous AH_3 gel. The next remarkable peak at 145 °C was the dehydration of CAH_{10} followed by dehydration of C_2AH_8 at a temperature of 190 °C. Further two significant peaks were attributed to the dehydration of gibbsite AH_3 at 298 °C and katoite C_3AH_6 at 320 °C. The mass change corresponding to the mentioned dehydration processes was 21%. Taking into the account used w/b ratio, it can be concluded that approximately two-thirds of used water was bounded into the structure and the remaining one-third had a function only for the workability. A slight endothermic peak at 489 °C meant the decomposition of boehmite AlOOH. The last noticeable change was observed at 931 °C, where the recrystallization of krotite CA took place. Considering the noticeable amount of grossite CA_2 in the paste LR after the exposure to 1400 °C, but no other significant peak which could be attributed to its recrystallization, it can be deduced that grossite transformation was more continuous and took place in a wider temperature range.

When alumina admixtures were employed, the course of the studied curves remained almost unchanged. Similar peaks were observed up to 400 °C, but they were somehow lowered. The only exception was the height of C_2AH_8 dehydration, thus it can be concluded that this hydrate was the dominant C-A-H phase. The amount of bounded water was in the case of LA by 20% lower than that of reference material LR. The biggest variation was the slight shift especially the heights of the boehmite peak AlOOH. The endothermic peak at 558 °C related to the mass change corresponded to the boehmite content of 15%. When focused on the phase crystallization at high temperatures, the creation of hibonite CA_6, similar to the reference material LR and grossite CA_2 recrystallization, its formation was more continuous. However, in the case of hibonite CA_6, the transformation can be assigned to the temperature from 1300 °C, where a slight increase of heat flow curve occurred.

The additional replacement of alumina admixtures by potential SCMs led to the further modification of curves. In the case of microsilica application, the noticeable variation is visible up to 223 °C, precisely up to 276 °C. Continuous dehydration at the beginning of the temperature range can be ascribed to the amorphous phases (in the form of AH_3, C-A-S-H and C–S–H), followed by gismondine dehydration at 155 °C (Okoronkwo and Glasser, 2016). As no metastable CAH_{10} was identified in the paste LS, the first peak with a maximum at 188 °C can be attributed primarily to the dehydration of amorphous AH_3, C_2AH_8 but also amorphous C-A-S-H phase and stratlingite C_2ASH_8 (Okoronkwo and Glasser, 2016). A further remarkable new peak at 251 °C can be attributed to the dehydration of the higher amount of tobermorite (Foldvári, 2011; Biagioni et al., 2016). Because of the phase changes in the temperature range up to 400 °C, it is indisputable, that the amount of bounded water went noticeably down, by 30% compared to reference paste LR. Interestingly, this fall was almost equal in all cases of potential SCMs. Taking into account, the results of the composition of amorphous phases (Table 3) and reaching the performance of thermal analysis, it can be concluded that it was primarily the amount of amorphous AH_3 which went down. However, the biggest modification was observed at high temperatures. Initially, at a temperature of around 930 °C, the crystallization peak of krotite CA disappeared. Except for that, visible but more continuous increase, the more precisely exothermic peak from about 988 °C to 1240 °C was observed. This was ascribed to the formation of gehlenite C_2AS. Afterwards, quite a massive endothermic decrease above the temperature of 1276 °C signified the creation of molten phases, which can give rise to anorthite CAS_2 crystallization (Rajabi Mashhadi and Naghizadeh, 2021; Ptáček et al., 2013).

When focused on the ferrite powder application, paste LF reached the lowest endothermic decrease in the first temperature range up to 200 °C. This signified the lowest amount of amorphous phases, which is in accordance with the composition of amorphous and not-identified phases. In addition, an absence of a visible peak was observed at about 188 °C, confirming the assumption of no C_2AH_8. A minor, partially hidden peak at temperatures of about 330 °C (between the gibbsite AH_3 and katoite C_3AH_6 dehydration) can be attributed to the dehydration of ferrihydrites (Foldvári, 2011) and supports the conclusions of their presence in paste LF. The small endothermic peak at 783 °C was also ascribed to the presence of ferrite compounds in the cement paste. However, when focused on the overall amount of bounded water, paste LF showed a similar value of mass change after dehydration as in the case of silica application, specifically by a 30% lower value of mass change compared to paste LR.

The performance of paste LC with ceramic dust was at a lower temperature similar to the one with microsilica. Firstly, amorphous AH_3, C_2AH_8 and also CASH phases were decomposed up to the temperature of 223 °C. Afterwards, by no tobermorite in the hardened cement pastes LC, there were no visible peaks at the temperature of about 251 °C. Nevertheless, in the dehydration temperature range (up to about 400 °C) paste LC showed the lowest mass changes among studied SCMs, the decrease was 33% lower compared to reference paste LR. When focused on the high temperatures, it seemed that recrystallization of new phases became slightly later, after reaching the temperature of 1107 °C. Considering the performance of previously described pastes LR and LA, the growth or exothermic heat flow evolution can be attributed to gehlenite C_2AS crystallization, as the other phases grossite CA_2 and hibonite CA_6 did not cause remarkable changes. The melting phase was, contrary to the microsilica application, significantly lower and it occurred later at 1360 °C. Thus, a lower amount of anorthite CAS_2 was created.

Paste with calcined shale LL showed similar tendencies in the range up to 155 °C as the ones with microsilica LS and ceramic dust LC. However afterwards, their endothermic reaction continuously decreased, and at 187 °C there was no remarkable peak. This indicates the absence of metastable hydrate C_2AH_8 and stratlingite C_2ASH_8. A further performance was similar as in the case of other studied materials; crystalline AH_3 decomposition at about 296 °C, followed by katoite C_3AH_6 dehydration at 329 °C and boehmite AlOOH dissociation at 556 °C. Considering the amount of bounded water, this paste LL reached slightly higher mass changes in the dehydration area, namely the mass decrease was 29% lower compared to the reference paste LR. Regarding the high temperatures, the trend of continuous increase was equal as in the case of ceramic dust, but as the exothermic heat flow was mildly higher, a higher number of gehlenite C_2AS could be formed. On the other hand, a profound fall after 1339 °C signified a higher molten ratio, and thus also bigger space for anorthite recrystallization. These assumptions were in good colouration with the phase composition of cement paste after exposure to 1400 °C.

Paste with sintered mullite LM proved to have a significant amount of amorphous phase as it showed a remarkable peak at a temperature of about 120 °C. Considering its trace amount of stratlingite C_2AH_8, the minor peak at 182 °C can be ascribed to the obvious amount of metastable C_2AH_8. Following double peaks of gibbsite AH_3 and katoite C_3AH_6 dehydration at temperatures between 200 °C and 400 °C was supplemented by a dehydration peak of tobermorite with Al inclusion at about

317 °C (Okoronkwo and Glasser, 2016; Jackson et al., 2013). Regarding the amount of bounded water in the dehydration temperature range, paste LM showed by 32% lower mass change compared to the reference paste LR. The further phase development at high temperatures was similar to reference material LR and the one with alumina admixtures LA with no distinctive heat release. Such performance was in accordance with the lowest number of different C-A-S phases.

4.1.4. Microstructure changes due to the temperature exposure

Microstructural changes were investigated through the SEM analysis. There are always four figures for particular materials. The first two were made at ambient temperature in two different magnifications (a – 1000x, b – 5000x), the second two were after the exposure to 1400 °C and again in two varying magnifications (a – 1000x, b – 5000x). Fig. 6 shows the microstructure of reference pure CAC paste LR. At ambient temperature, the structure was quite porous with a few microcracks. Regarding the phases, in accordance with XRD observation, the visible tiny needle-shaped crystals were identified as CAH_{10}, while the small cubic ones were katoite C_3AH_6 (Koňáková et al., 2022a; Antonovič et al., 2013). Bigger areas of amorphous phases were assumed to be AH_3. When the reference paste was exposed to 1400 °C, the structure was significantly changed. The matrix was much less heterogeneous but with significantly bigger voids. The visible crystals with smooth edges were krotite CA or grossite CA_2 (Zhu et al., 2015). They were supplemented by amorphous phases.

When focused on alumina admixtures application (Fig. 7), the structure contained a much lower amount of voids and was more compacted, however, the number of microcracks was recognizably higher. Contrary to the reference material there were observed small trigonal crystals, which were identified as unreacted corundum Al_2O_3. Thereafter, in Fig. 7b), there are visible plate-like crystals, these were C_2AH_8 (Antonovič et al., 2013). Its presence confirms the STA results (Fig. 5) After the exposure to 1400 °C, the structure became significantly heterogeneous. Areas of amorphous seemingly unchanged structure were alternated with purely crystallines. Such a high amount of amorphous phase was in accordance with XRD analysis (Fig. 4). Apart from a low amount of rounded phases similar to the case of the reference paste, there were noticeably bigger clearly hexagonal plates, which were identified as hibonite CA_6 (Šádková et al., 2023).

At first sight, microsilica addition (Fig. 8) led to the structure comparable as in the case of reference material LR. However, at the higher magnification, the structure of paste LS was more compacted with a significantly different morphology. Rope or string-like amorphous structures were identified as stratlingite C_2ASH_8 (Song et al., 2014), and a noticeable amount of corundum Al_2O_3 was observed as well. Nevertheless, the biggest difference was found after the exposure to 1400 °C. The structure was completely sintered, which is in accordance with DSC (Fig. 5a), and only bigger pores with no voids were present.

Ferrite powder caused further changes in structure, as can be seen in Fig. 9. Bigger pores were observed already at ambient temperature, the microstructure seemed to be more compacted with smaller crystals. Again, the temperature exposure caused significant alteration. The new fibrous phases in Fig. 8c) were identified as brownmillerite C_4A_F (Stutzman, 2004). Nevertheless, the structure after 1400 °C seemed to be one of the most amorphous and highly sintered among studied pastes, which was in quite good correlation with XRD (Fig. 4).

When ceramic powder was used (Fig. 10), the structure of hardened stone was the densest. Observed crystals were considerably grown through and only a few voids were found. This performance was reversed after the exposure to 1400 °C. Nevertheless, the substantial amount of voids was evenly distributed and the structure was quite homogenous compared to reference paste LR and LA. In Fig. 10d), hexagonal plates were observed, these were either hibonite CA_6 or gehlenite C_2AS (Gualtieri et al., 2011; Dovál et al., 2006). They were altered with krotite CA or grossite CA_2.

Calcined shale (Fig. 11) caused at first magnification comparable structure as a reference material, but at a deeper look, there were observed peculiar areas of amorphous matter. This observation was in accordance with XRD results (Fig. 3), where the composite with calcined shale reached one of the highest values of amorphous phases. Temperature exposure led to substantial recrystallization and deepened the heterogeneity of the structure. The amorphous sintered structure was alternated with areas of poorly crystalline phases with small grains and with parts with conglomeration of fully developed hexagonal crystals.

The last studied admixture sintered mullite again significantly modified the structure of the studied composite (Fig. 12). At ambient temperature, the observed appearance was somewhere in the middle between the reference plaster LR and the one with ceramic powder LC. But at a higher magnification, there were observed higher amounts of plate-like foliated crystals of metastable C_2AH_8. After exposure to 1400 °C, the structure contained a noticeably higher amount of cracks compared to the other designed materials.

Despite relatively a low amount of used admixtures, the structures of hardened cement stone were distinctively modified and showed noticeably different performance, especially after exposure to the high temperatures. The most different results were observed in the case of microsilica application.

4.2. Cement composites

4.2.1. Basic physical properties of cement composites

The results of basic physical properties can be found in Table 5. The bulk density of all tested composites was within ±5% of the reference sample at room temperature. The highest values were obtained for the LA mixture containing only alumina admixtures and for the LM mixture containing sintered mullite. After exposure to 1400 °C, all samples with alternative cement replacement showed a decrease in bulk density of 3–7%. In contrast, the bulk density of the reference mixture LR decreased by 11%.

The matrix densities of ternary binder-based composites at room temperature were also very close to the reference LR, namely within the range of ±6%. At a closer look, the reference mixture had the lowest value, the composite LA mixture was almost identical, while the other mixtures reached 2–6% higher values. As it could be assumed due to the

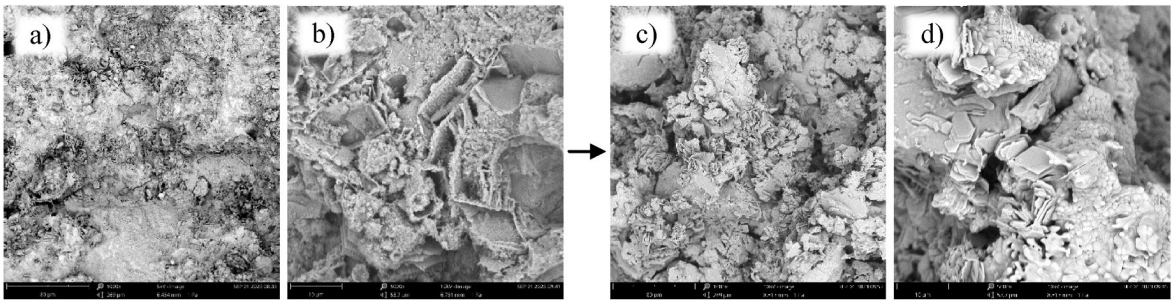

Fig. 6. SEM of LR: (a) 20 °C–1000x, (b) 20 °C–5000x, (c) after 1400 °C–1000x, (d) after 1400 °C–5000x

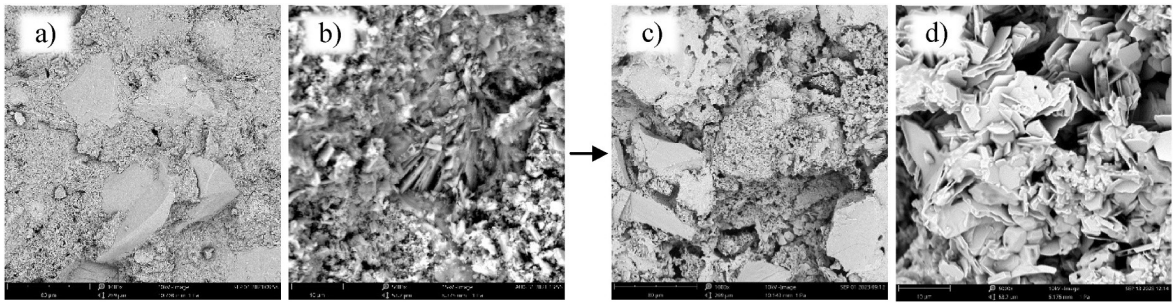

Fig. 7. SEM of LA: (a) 20 °C–1000x, (b) 20 °C–5000x, (c) after 1400 °C–1000x, (d) after 1400 °C–5000x

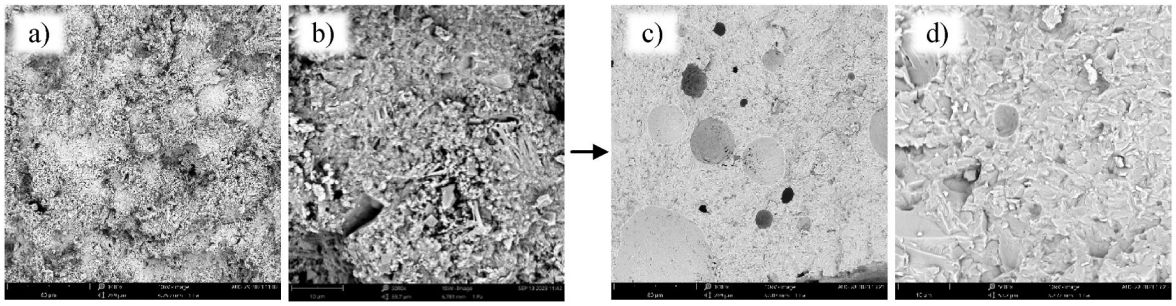

Fig. 8. SEM of LS: (a) 20 °C–1000x, (b) 20 °C–5000x, (c) after 1400 °C–1000x, (d) after 1400 °C–5000x

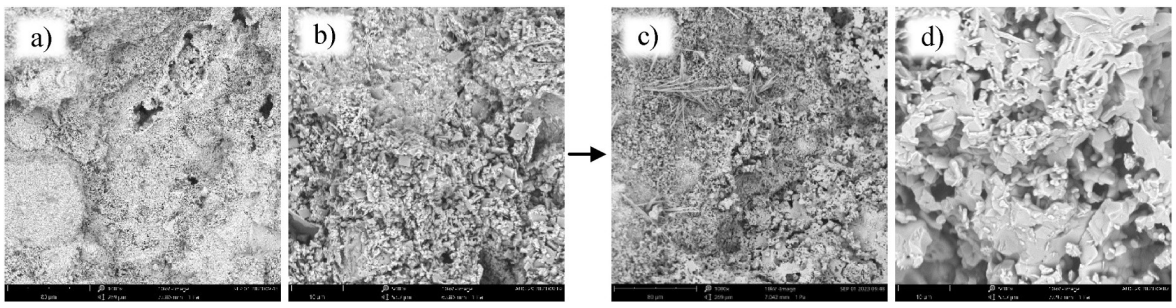

Fig. 9. SEM of LF: (a) 20 °C–1000x, (b) 20 °C–5000x, (c) after 1400 °C–1000x, (d) after 1400 °C–5000x

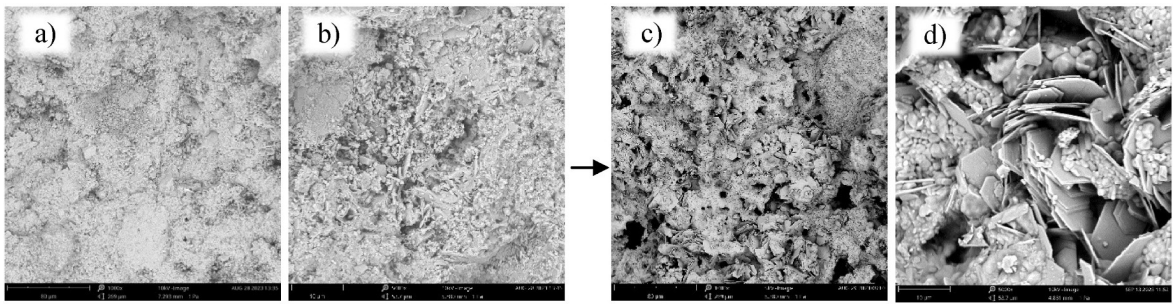

Fig. 10. SEM of LC: (a) 20 °C–1000x, (b) 20 °C–5000x, (c) after 1400 °C–1000x, (d) after 1400 °C–5000x

highest specific gravity of iron compounds, the highest matrix density was measured for the composites with ferrite powder LF. Regarding the impact of temperature, the thermal exposure caused a noticeable increase on average by 7%. This was in accordance with the phase transformations caused by the dehydration and recrystallization process when denser minerals were formed.

Regarding the values of reached porosity, it is visible, that the first replacement of calcium aluminate cement by alumina admixtures led to a significant decrease, specifically by 26%. Because the water/binder was higher, this effect can be attributed primarily to the finesses of used alumina. All other samples had 12–40% higher porosity than the reference composite LR. The biggest increase was observed in the case of the mixture with the addition of sintered mullite LM, which had 40% higher porosity. Again, this is in good correlation with the granulometry of the used SCMs. After exposure to 1400 °C, a large increase in porosity for all samples was observed. The residual porosity of the reference

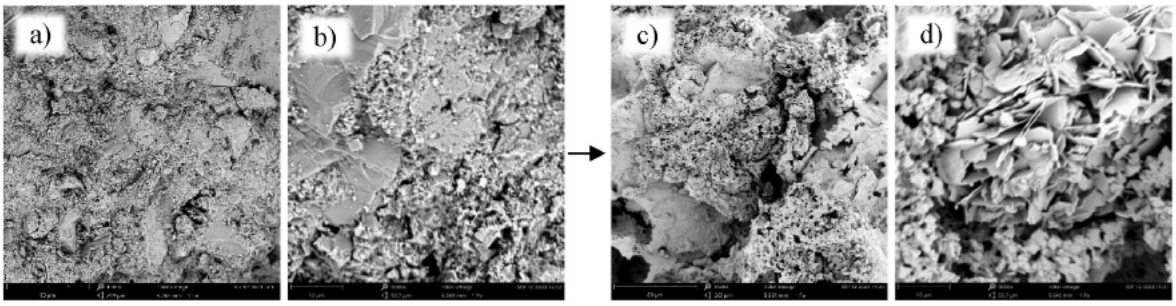

Fig. 11. SEM of LL: (a) 20 °C–1000x, (b) 20 °C–5000x, (c) after 1400 °C–1000x, (d) after 1400 °C–5000x

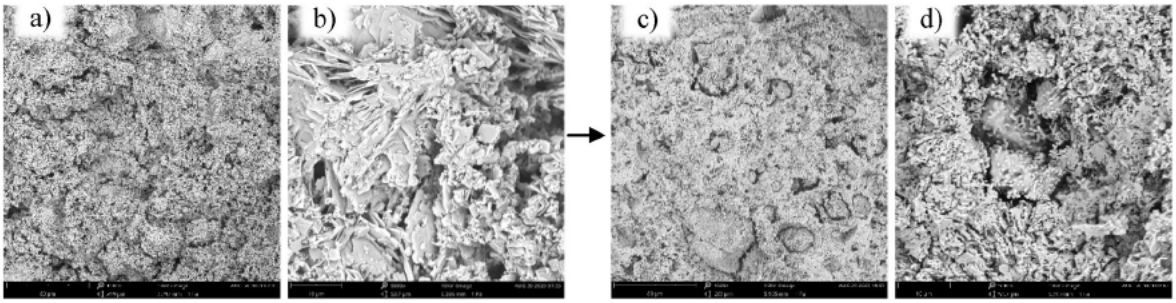

Fig. 12. SEM of LM: (a) 20 °C–1000x, (b) 20 °C–5000x, (c) after 1400 °C–1000x, (d) after 1400 °C–5000x

Table 5
Basic physical properties of studied composites.

Composites	Bulk density [kg m ^{3}]		Matrix density [kg m ^{3}]		Porosity [–]	
	20 °C	1400 °C	20 °C	1400 °C	20 °C	1400 °C
LR	2306	2052	2701	2884	14.6	28.8
LA	2412	2282	2705	2873	10.8	20.6
LS	2298	2170	2792	2957	17.7	26.6
LF	2384	2228	2852	3069	16.4	27.4
LC	2288	2126	2786	2950	17.9	27.9
LL	2287	2208	2805	3025	18.5	27.0
LM	2232	2134	2810	2977	20.5	28.3

mixture LR increased by 97%, becoming the highest porosity of all. Composite with the alumina admixtures LA also showed significant but slightly lower growth by 90%. Additional SCMs employment proved to have a positive impact on the residual porosity variation. Probably due to the sintering, they showed a remarkably lower increase; from 67% in the case of ferrite powder LF to only 38% in the case of sintered mullite LM. However, all ternary binder-based high-temperature resistant composites showed comparable residual porosity within the vary of ±3%.

Not only the value of total porosity is important, the more informative are pore size distribution curves. They can be found in Figs. 13 and 14. It is visible that at ambient temperature, reference composite LR had the main areas of pores with a size of about 0.1 μm. Alumina admixtures caused a slight increase in pore size, as the main peak of pore volume was at about 0.2 μm. The further replacement by other investigated admixtures was characterized by the creation of second dominant areas of pores with sizes in the range of 1–10 μm. This growth was the most distinctive in the case of microsilica application. Due to the temperature exposure to 1400 °C the small pores with a size of about 0.1 disappeared and a higher amount of bigger pores were created. Reference composite LR showed the highest increase in the pore size as the main peak of pore volume reached the maximum at about 22 μm. Contrarily, the alumina admixture significantly eliminated this growth, as the composite LA had the maximum only at a size of 3 μm. From this point, further replacement by other admixtures was not so advantageous, as the main peak was shifted to approximately 10 μm, but still, the pore size was reduced. The only exception was observed in the case of sintered mullite, which showed a maximum of about 19 μm. This was in accordance with the higher amount of cracks observed by SEM.

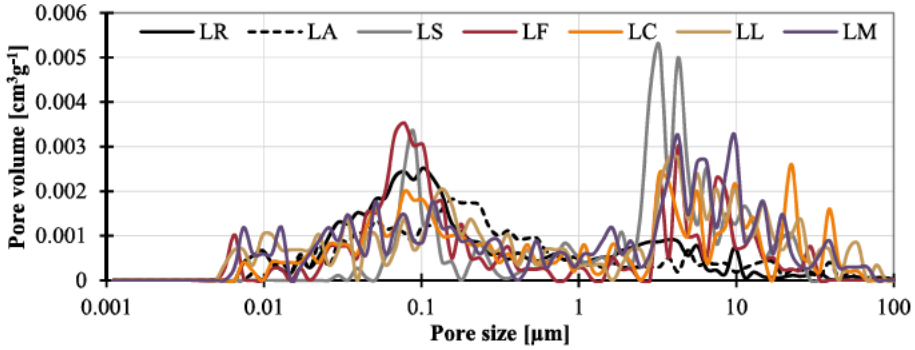

Fig. 13. Pore size distribution curves of studied composites at ambient temperature.

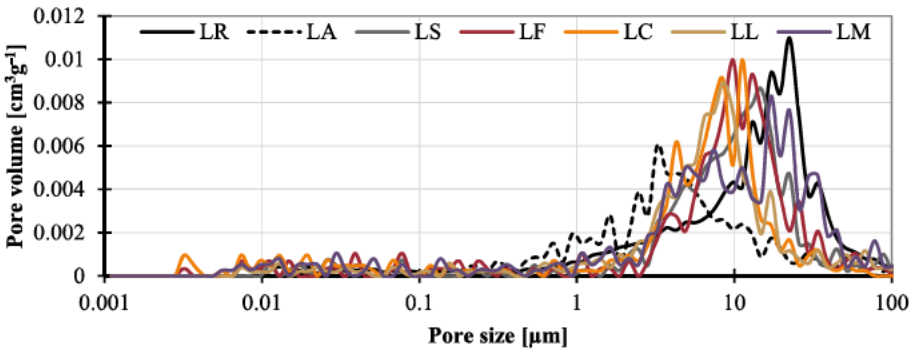

Fig. 14. Pore size distribution curves of studied composites after exposure to 1400 °C.

4.2.2. Mechanical properties of cement composites

Fig. 15 shows that at first sight, the mechanical properties of the resulting composites are very satisfactory. The compressive strengths were higher than those of the reference sample already at room temperature in all cases. The compressive strength after exposure to 1400 °C was even significantly higher in most cases. Nevertheless, at ambient temperature, the utilization of alumina admixtures led to the 21% compressive strength increase, and additional SCM application caused growth even up to 63%. The best compressive strength was achieved by the mixture with ferrite powder LF, followed by medium alumina admixtures LM, LL, and LC. Regarding the residual compressive strengths, the highest value after firing was recorded for the sample with calcined shale LL. When this high-temperature strength was compared with that of a reference material LR subjected to the same temperature loading, it was more than 3 times higher. This extreme increase in strength was not only due to the phase transformation but also due to sintering in the material structure of the composite. In general, most of the composites with alternative cement replacement showed a significant increase in compressive strength after exposure to high temperatures. Only the mixture with mullite LM and ferrite LF had lower differences between the two strengths. Despite that the mixture with sintered mullite LM showed a decrease in residual compressive strength after a temperature of 1400 °C, the drop was not as large; the strength decreased only by 11 %. While in the case of reference composite LR, the fall was by 48%.

Bending strengths results are also summarized in Fig. 15. The values were also higher than the reference compound LR for all designed ternary-binder-based composites. Considering the replacing materials, the lowest value at ambient temperature was measured for the mixture containing only alumina admixtures LA. However, this strength was still 6% higher than that of the reference sample LR. Contrary, the highest bending strength was measured for the mixture with ferrite powder LF. It was 28 % higher compared to the reference sample LR. Nevertheless, it should be mentioned, that the room temperature bending strengths were not significantly different from the reference material LR. On the other hand, the differences after thermal treatment were quite large for all mixes with alternative cement replacement. On average, they reached twice the time higher value than reference composite LR. The largest difference occurred for the composite containing microsilica LS, followed by ceramic dust LC. The worst performance among studied SCMs was observed in the case of sintered mullite LM, which showed the smallest improvement of strength after high-temperature exposure. This can be explained but the significant amount of cracks observed in this structure (Fig. 12). Although its residual bending strength was still 83% higher than that of the reference composite LR.

The last mechanical property, which can be found in Fig. 15 is the dynamic modulus of elasticity. When focused firstly on ambient temperature, it is indisputable, that alumina admixtures LA showed unexpectedly higher values compared to the other materials. The value was 44% higher than the one of reference composite LR. Further utilization of SCMs decreased the dynamic modulus of elasticity, despite that the values were still slightly higher compared to the reference LR. Due to the temperature exposure, the residual dynamic modulus of elasticity of reference composite LR went down by 35%. When alumina admixtures were used, the fall decreased only by 12% and when ternary binder was employed the positive impact was even much better. The highest value of residual dynamic modulus of elasticity, reached by calcined shale LL, was even 34% higher compared to ambient temperature.

4.2.3. Thermal strain of cement composites

Fig. 16 presents the results of the thermomechanical behaviour of studied composites. At ambient temperature, the reference composite showed a slightly higher thermal expansion coefficient, which was further increased at temperatures up to 200 °C. In contrast, the values of ternary binder-based materials showed noticeably lower thermal expansion coefficients. The lowest expansion was observed in the case of microsilica LS. Afterwards, the dehydration of used binders caused remarkable shrinkage. It is visible that from that point of view, microsilica was a less suitable material, as it caused the biggest (absolute) value of the thermal expansion coefficient. Contrary calcined shale LS and ferrite powder LF led to the lowest changes of thermal strains and

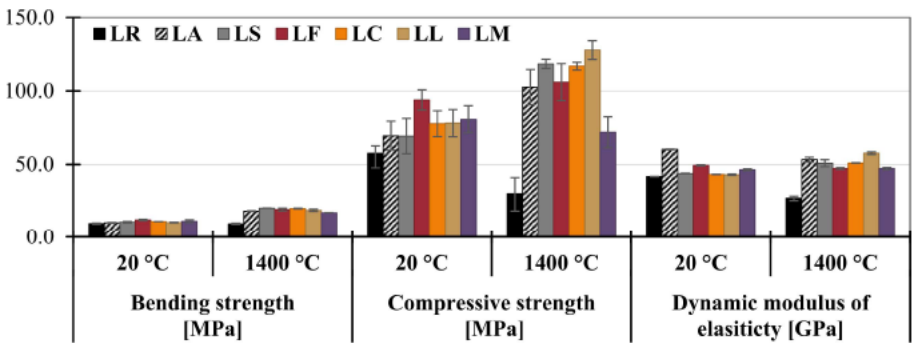

Fig. 15. Mechanical properties of studied composites.

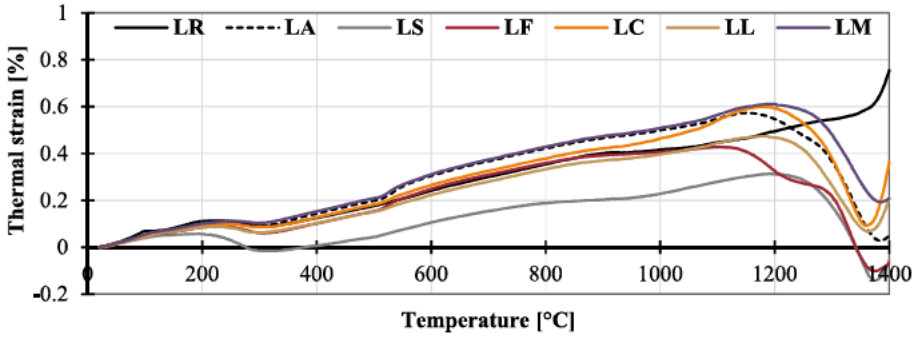

Fig. 16. Thermal strain of studied composites.

thermal expansion coefficients respectively. After the dehydration, the continuous linear expansion of materials was observed up to about 510 °C. In accordance with the here-in-above described phase development, no phase changes took place in this place. At mentioned 510 °C the boehmite AlOOH dehydration occurred. This transformation caused remarkable expansion. In conformity with the composition of studied heat-resistant cement-based composites with alumina admixtures, LA reached the highest thermal expansion coefficient. Next, the development of thermal strain was again linear. At temperatures above 800 °C, further phase recrystallizations occurred and as a consequence, the thermal strain variation was observed. Nevertheless, the biggest variation occurred after 1150 °C. This was not influenced only by the recrystallization of hibonite CA_6, anorthite CAS_2 and other new phases, but sintering also took place in this temperature range. The last steep expansion at above 1380 °C can be attributed to the aggregate strain, as no remarkable expansion was observed in the case of CAC pastes (Šádková et al., 2023).

4.3. Summary of reached results

Alumina admixture improved the hydration degree of calcium aluminate cement but did not significantly modify the phase composition at ambient temperature. But after exposure to 1400 °C, it changed the alumina – calcium oxide ratio and thus it gave rise to the hibonite CA_6 recrystallization and higher amount of amorphous phases. Regarding the impact on the properties, when alumina admixtures were employed, noticeably lower porosity was observed. In addition, the mechanical properties were significantly improved especially after exposure to high temperatures.

Microsilica utilization substantially modified the phase composition of hardened cement stone. Apart from ordinary C-A-H and A-H phases, also C-A-S-H and a minor amount of C–S–H were observed. These modifications were reflected in the phase development after heat treatment, where a substantial amount of gehlenite C_2SA and anorthite CAS_2 were created and the structure was significantly sintered. At ambient temperature high-temperature resistant composites with microsilica showed somewhat higher porosity but comparable mechanical properties as when alumina admixtures were used. However, after the exposure to 1400 °C, porosity went down noticeably and mechanical performance was considerably improved. On the other hand, the thermal expansion coefficient showed the biggest variation among studied SCMs.

The utilization of ferrite powder led to the creation of a converted structure with only one representative of C-A-H. Namely, katoite C_3AH_6 and the lowest amorphous phases were observed. Apart from the latter phases, also a noticeable amount of ferrihydrites were identified. After heat treatment, a substantial amount of grossite CA_2, amorphous phases and a recognizable number of brownmillerite C_4AF were formed. When focused on properties, ferrite powder increased the density of the composite. At ambient temperature, the compressive strength reached the highest value among studied materials. However after exposure to 1400 °C, due to the higher thermal strain, the residual compressive strength was not distinctively increased.

Ceramic dust promoted the hydration of crystalline C-A-S-H phases, whose amount was the highest among studied SCMs. Apart from them also metastable C_2AH_8 and AH_3 were presented in the hardened stone. As a consequence of the most heterogeneous composition of ceramic, it gave rise to the most diverse composition after heat treatment. Despite designed composites with ceramic showed somehow higher porosity at ambient temperature, modified hydrated products had a positive impact on mechanical properties. Even better performance was observed after heat treatment.

Calcined shale application caused the highest hydration degree of calcium aluminate cement. During the hydration, the highest content of AH_3 was formed alongside a moderate number of C-A-S-H (mainly of lower silica content). A distinctive amount of amorphous phase was created as well. Despite that the latter modification did not affect the basic physical properties, a positive impact on mechanical properties was observed. Especially after exposure to 1400 °C, heat-resistant cement-based composites with calcined shale reach the best values of mechanical parameters.

Sintered mullite caused only minor changes in hardened stone composition. It led to the highest amorphous phases composed entirely from calcium and aluminium oxide and water. Silica was presented only in a moderate amount of crystal C-A-S-H. The exposure to 1400 °C led to a remarkable formation of grossite CA_2. Contrary to previously studied SCMs, sintered mullite led to an increase in both ambient as well as residual porosity (including a significant amount of microcracks). Regarding the mechanical properties, its application was beneficial at ambient temperature, but the residual properties showed somehow worsened performance, which was attributed mainly to the observed cracks.

In order to somehow quantify the effect and synergy of the SCMs used in combination with alumina admixtures, the Strength Activity Index (SAI) was applied (ASTM C618, 2003). In the case of the SCM for PC, only the SAI value for compressive strength is usually given. However, in the case of temperature-resistant materials, flexural strength is a crucial factor in their applicability. In addition, the performance after temperature exposure is of greater importance. Therefore, the SAI was counted for both mechanical strengths under both conditions (at ambient temperature as well as after 1400 °C). Finally, the average value was counted to obtain the average SAI. As a reference material, primarily CAC-based composite LR was chosen, and then also the one with the combination of CAC and alumina admixtures LA. The reached values are presented in Table 6. From these results, it is visible that all admixtures were beneficial, as the limit for suitable SCM according to the standard is 0.75. However, it should be mentioned, that this limit is too low, and even a material with low reactivity can meet this requirement. On the other hand, studied materials reached much higher values. In the first column, the SAI of ternary binder-based materials even exceeded the value of 2, with the one exception of composite LM. Considering the second column, it was confirmed that the additional replacement by

Table 6
Average strength activity index of studied composites.

	Average SAI [−]	
	Related to LR	Related to LA
LA	1.9	–
LS	2.1	1.1
LF	2.1	1.2
LC	2.1	1.1
LL	2.2	1.1
LM	1.7	1.0

SMCs resulted in a further synergistic improvement. Reached values of SAI related to alumina admixture composite exceeded the number 1. Again with the one exception of sintered mullite. This material did not degrade the performance of the final composite, nor did it provide any further improvement.

5. Conclusions

This article was focused on ternary-binder-based heat-resistant composites with low calcium aluminate cement content. The reference mixture with a normal dosage of the cement was designed. In the first step, 55% was replaced by alumina-based admixtures (the mix of reactive alumina and boehmite powder in a 1:1 ratio). In the next step the ternary binder, which consisted of 45% calcium aluminate cement, 40% of alumina admixtures and 15% of other potential SCMs was designed. After considering the current state of knowledge, microsilica, ferrite powder, waste ceramic dust, calcined shale and sintered mullite were chosen for the purpose of this study. Designed ternary-binder-based composites were assessed through the view of their composition from ambient temperature up to 1400 °C. Then the basic physical properties, mechanical parameters and thermomechanical performance were studied as well.

In general, all designed heat-resistant composites with low-cement content showed advantageous performance not only at ambient temperature but also after heat treatment. These modified binders showed significantly better mechanical parameters compared to reference calcium aluminate cement. Except for the sintered mullite, ternary binders have even improved performance also compared to blended binder with only alumina admixtures. In addition, due to the modified composition, a lower amount of metastable calcium-aluminate-hydrates was created, and the risk of negative conversion was on that account lowered.

To conclude, it can be stated, that the synergic effect of the application of more than one SCMs for CAC replacement was confirmed. Considering the results, the mixtures with calcined shale and ceramic dust were found to be the most promising while the application of sintered mullite was not useful. On the other hand, it has to be noted, that all the admixtures worsened the workability of fresh mixes, and therefore they required an utilization of plasticizing admixture.

CRediT authorship contribution statement

Dana Koňáková: Writing – original draft, Data curation, Conceptualization. **Vojtěch Pommer:** Investigation, Data curation. **Kateřina Šádková:** Writing – original draft, Investigation. **Martina Záleská:** Investigation. **Martin Bohm:** Investigation, Formal analysis. **Martin Keppert:** Writing – review & editing, Validation. **Eva Vejmelková:** Writing – review & editing, Supervision, Funding acquisition.

Declaration of generative AI and AI-assisted technologies in the writing process

During the preparation of this work, the authors have not used generative AI and AI-assisted technologies. The only tools used during the preparation of the paper were the basic tools for checking grammar, spelling, and reference creation.

Declaration of competing interest

The authors declare that they have no known competing financial interests or personal relationships that could have appeared to influence the work reported in this paper.

Data availability

Data will be made available on request.

Acknowledgement

This research has been supported by the Grant Agency of the Czech Technical University in Prague [grant No. SGS22/137/OHK1/3T/11].

References

Antonovič, V., Keriene, J., Boris, R., Aleknevičius, M., 2013. The effect of temperature on the formation of the hydrated calcium aluminate cement structure. Procedia Eng. 57, 99–106. https://doi.org/10.1016/j.proeng.2013.04.015.
Arioz, O., 2007. Effects of elevated temperatures on properties of concrete. Fire Saf. J. 42, 516–522. https://doi.org/10.1016/j.firesaf.2007.01.003.
Asaad, M.A., Ismail, M., Tahir, M.Md, Huseien, G.F., Raja, P.B., Asmara, Y.P., 2018. Enhanced corrosion resistance of reinforced concrete: role of emerging eco-friendly Elaeis guineensis/silver nanoparticles inhibitor. Construct. Build. Mater. 188, 555–568. https://doi.org/10.1016/j.conbuildmat.2018.08.140.
ASTM C618, 2003. Standard Specification for Fly Ash and Raw or Calcined Natural Pozzolan for Use as a Mineral Admixture in Portland Cement Concrete.
Baradaran-Nasiri, A., Nematzadeh, M., 2017. The effect of elevated temperatures on the mechanical properties of concrete with fine recycled refractory brick aggregate and aluminate cement. Construct. Build. Mater. 147, 865–875. https://doi.org/10.1016/j.conbuildmat.2017.04.138.
Biagioni, C., Bonaccorsi, E., Lezzerini, M., Merlino, S., 2016. Thermal behaviour of Al-rich tobermorite. Ejm 28, 23–32. https://doi.org/10.1127/ejm/2015/0027-2499.
Boquan, Z., Yanan, S., Xiangcheng, L., Ping'an, C., 2015. Hydration process of spinel containing calcium aluminate cement. Rare Met. Mater. Eng. 44, 261–264.
Bubeník, J., Zach, J., Křížová, K., Novák, V., Sedlmajer, M., Žižková, N., 2023. Behavior and properties of ultra-lightweight concrete with foamed glass aggregate and cellulose fibres under high temperature loading. J. Build. Eng. 72, 106677 https://doi.org/10.1016/j.jobe.2023.106677.
Bullerjahn, F., Schmitt, D., Ben Haha, M., 2014. Effect of raw mix design and of clinkering process on the formation and mineralogical composition of (ternesite) belite calcium sulphoaluminate ferrite clinker. Cement Concr. Res. 59, 87–95. https://doi.org/10.1016/j.cemconres.2014.02.004.
Claramunt, J., Ventura, H., Ardanuy, M., 2018. Rheology of CAC-based cement pastes and the relationship to penetrability through nonwoven fabric reinforcements. Cement Concr. Compos. 94, 85–93. https://doi.org/10.1016/j.cemconcomp.2018.08.014.
Collepardi, M., Monosi, S., Piccioli, P., 1995. The influence of pozzolanic materials on the mechanical stability of aluminous cement. Cement Concr. Res. 25, 961–968. https://doi.org/10.1016/0008-8846(95)00091.
ČSN EN 1015-11 (722400), 2020. Methods of Test for Mortar for Masonry - Part 11: Determination of Flexural and Compressive Strength of Hardened Mortar.
ČSN EN 12504-4, 2005. Testing Concrete - Part 4: Determination of Ultrasonic Pulse Velocity.
ČSN EN 933-1 (721193), 2012. Zkoušení Geometrických Vlastností Kameniva - Část 1. Stanovení zrnitosti - Sítový rozbor.
Da Silva, P.R., De Brito, J., 2015. Experimental study of the porosity and microstructure of self-compacting concrete (SCC) with binary and ternary mixes of fly ash and limestone filler. Construct. Build. Mater. 86, 101–112. https://doi.org/10.1016/j.conbuildmat.2015.03.110.
Dhandapani, Y., Santhanam, M., Kaladharan, G., Ramanathan, S., 2021. Towards ternary binders involving limestone additions — a review. Cement Concr. Res. 143, 106396 https://doi.org/10.1016/j.cemconres.2021.106396.
Doebelin, N., Kleeberg, R., 2015. *Profex* : a graphical user interface for the Rietveld refinement program *BGMN*. J. Appl. Crystallogr. 48, 1573–1580. https://doi.org/10.1107/S1600576715014685.
Dovál, M., Palou, M., Kovár, V., 2006. Hydration and microstructure of binder compounds containing C2AS and C2S synthesized by sol-gel method. Ceramics 50, 106–114.
Foldvári, M., 2011. Handbook of Thermogravimetric System of Minerals and its Use in Geological Practice. Geological Inst. of Hungary, Budapest.
García-Álvarez, G., Escobedo-Bocardo, J.C., Cortés-Hernández, D.A., Almanza-Robles, J. M., Sánchez-Escobedo, B.A., 2018. Effect of wollastonite and a bioactive glass-ceramic on the in vitro bioactivity and compressive strength of a calcium aluminate cement. Ceram. Int. 44, 19077–19083. https://doi.org/10.1016/j.ceramint.2018.07.186.

Ghose, S., Saigal, C., Maldhure, A., Kumar Das, S., 2013. Effect of reactive alumina on the physico-mechanical properties of refractory castable. Trans. Indian Ceram. Soc. 72, 113–118. https://doi.org/10.1080/0371750X.2013.794024.
Gonzalez-Lopez, L., Claramunt, J., Haurie, L., Ventura, H., Ardanuy, M., 2021. Study of the fire and thermal behaviour of façade panels made of natural fibre-reinforced cement-based composites. Construct. Build. Mater. 302, 124195 https://doi.org/10.1016/j.conbuildmat.2021.124195.
Gualtieri, A.F., Andreozzi, G.B., Giacobbe, C., Lusvardi, G., Viti, C., 2011. Structural and spectroscopic characterization of anorthite synthesized from secondary raw materials. Period. Mineral. 80, 231–245. https://doi.org/10.2451/2011PM0018.
Halicka, A., Ogrodnik, P., Zegardlo, B., 2013. Using ceramic sanitary ware waste as concrete aggregate. Construct. Build. Mater. 48, 295–305. https://doi.org/10.1016/j.conbuildmat.2013.06.063.
Hertel, T., Neubauer, J., Goetz-Neunhoeffer, F., 2016. Study of hydration potential and kinetics of the ferrite phase in iron-rich CAC. Cement Concr. Res. 83, 79–85. https://doi.org/10.1016/j.cemconres.2016.01.004.
Huang, C., Cheng, Z., Zhao, J., Wang, Y., Pang, J., 2021. The influence of water reducing agents on early hydration property of ferrite aluminate cement paste. Crystals 11, 731. https://doi.org/10.3390/cryst11070731.
Idrees, M., Ekincioglu, O., Sonyal, M.S., 2021. Hydration behavior of calcium aluminate cement mortars with mineral admixtures at different curing temperatures. Construct. Build. Mater. 285, 122839 https://doi.org/10.1016/j.conbuildmat.2021.122839.
Idrissi, M., Diouri, A., Damidot, D., Greneche, J.M., Talbi, M.A., Taibi, M., 2010. Characterisation of iron inclusion during the formation of calcium sulfoaluminate phase. Cement Concr. Res. 40, 1314–1319. https://doi.org/10.1016/j.cemconres.2010.02.009.
Jackson, M.D., Moon, J., Gotti, E., Taylor, R., Chae, S.R., Kunz, M., Emwas, A.-H., Meral, C., Guttmann, P., Levitz, P., Wenk, H.-R., Monteiro, P.J.M., 2013. Material and elastic properties of Al-tobermorite in Ancient Roman Seawater concrete. J. Am. Ceram. Soc. 96, 2598–2606. https://doi.org/10.1111/jace.12407.
Kırca, O., Ozgür Yaman, I., Tokyay, M., 2013. Compressive strength development of calcium aluminate cement–GGBFS blends. Cement Concr. Compos. 35, 163–170. https://doi.org/10.1016/j.cemconcomp.2012.08.016.
Klaus, S.R., Neubauer, J., Goetz-Neunhoeffer, F., 2013. Hydration kinetics of CA2 and CA—investigations performed on a synthetic calcium aluminate cement. Cement Concr. Res. 43, 62–69. https://doi.org/10.1016/j.cemconres.2012.09.005.
Koňáková, D., Vejmelková, E., Pommer, V., Černý, R., 2021a. Properties of CAC Paste with Varying Alumina Based Admixtures. Kazimierz Dolny, Poland, 020017. https://doi.org/10.1063/5.0070338.
Koňáková, D., Vejmelková, E., Pommer, V., Keppert, M., Trník, A., Černý, R., 2021b. Physical and Chemical Characteristics of Heat Resistant Materials Based on High Alumina Cement. Kazimierz Dolny, Poland, 020004. https://doi.org/10.1063/5.0069565.
Koňáková, D., Pommer, V., Jerman, M., Keppert, M., Černý, R., Vejmelková, E., 2022a. Utilization of ceramic powder, calcined shale and sintered mullite as partial replacements of calcium aluminate cement. Construct. Build. Mater. 326, 126824 https://doi.org/10.1016/j.conbuildmat.2022.126824.
Koňáková, D., Pommer, V., Šádková, K., Keppert, M., Černý, R., Vejmelková, E., 2022b. Impact of plasticizers' types on the performance of calcium aluminate cement. J. Mater. Res. Technol. 20, 1512–1523. https://doi.org/10.1016/j.jmrt.2022.07.155.
Lewis, R., 2017. The role of microsilica in sustainable concrete. MATEC Web Conf 120, 02011. https://doi.org/10.1051/matecconf/201712002011.
Li, Y., Liu, X., Niu, X., Song, L., 2007. Influence of minor oxides on formation and decomposition of mineral calcium sulfoaluminate ($3CaO{\cdot}3Al_2O_3{\cdot}CaSO_4$). Mater. Res. Innovat. 11, 92–94. https://doi.org/10.1179/143307507X196644.
Luhar, S., Cheng, T.-W., Luhar, I., 2019a. Incorporation of natural waste from agricultural and aquacultural farming as supplementary materials with green concrete: a review. Compos. B Eng. 175, 107076 https://doi.org/10.1016/j.compositesb.2019.107076.
Luhar, S., Cheng, T.-W., Nicolaides, D., Luhar, I., Panias, D., Sakkas, K., 2019b. Valorisation of glass wastes for the development of geopolymer composites – durability, thermal and microstructural properties: a review. Construct. Build. Mater. 222, 673–687. https://doi.org/10.1016/j.conbuildmat.2019.06.169.
Madej, D., 2016. PREPARATION OF Al_2O_3-$CaAl_{12}O_{19}$-ZrO_2 COMPOSITE CERAMIC MATERIAL BY THE HYDRATION AND SINTERING OF $Ca_7ZrAl_6O_{18}$-REACTIVE ALUMINA MIXTURE. Ceramics 27–33. https://doi.org/10.13168/cs.2016.0004.
Martins, D.J., Correia, J.R., De Brito, J., 2016. The effect of high temperature on the residual mechanical performance of concrete made with recycled ceramic coarse aggregates: residual performance of concrete with recycled ceramic aggregates. Fire Mater. 40, 289–304. https://doi.org/10.1002/fam.2287.
Martins, A.C.P., Franco De Carvalho, J.M., Costa, L.C.B., Andrade, H.D., De Melo, T.V., Ribeiro, J.C.L., Pedroti, L.G., Peixoto, R.A.F., 2021. Steel slags in cement-based composites: an ultimate review on characterization, applications and performance. Construct. Build. Mater. 291, 123265 https://doi.org/10.1016/j.conbuildmat.2021.123265.
Massazza, F., 2003. Pozzolana and pozzolanic cements. In: LEA's Chemistry of Cement and Concrete, pp. 471–635.
Nejat, P., Morsoni, A.K., Jomehzadeh, F., Behzad, H., Saeed Vesali, M., Majid, M.Z.Abd, 2013. Iran's achievements in renewable energy during fourth development program in comparison with global trend. Renew. Sustain. Energy Rev. 22, 561–570. https://doi.org/10.1016/j.rser.2013.01.042.
Nowacka, M., 2017. Effect of metakaolin on early hydration of calcium aluminate cement Wpływ metakaolinu na wczesną hydratację cementu glinowo-wapniowego. CHEMICAL REVIEW 1, 72–76. https://doi.org/10.15199/62.2017.4.14.
Okoronkwo, M.U., Glasser, F.P., 2016. Stability of stratlingite in the CASH system. Mater. Struct. 49, 4305–4318. https://doi.org/10.1617/s11527-015-0789-x.
Papatzani, S., Paine, K., 2020. A step by step methodology for building sustainable cementitious matrices. Appl. Sci. 10, 2955. https://doi.org/10.3390/app10082955.
Popovics, S., 1992. Concrete Materials: Properties, Specifications, and Testing, second ed. Noyes Publications, Park Ridge, N.J.
Ptáček, P., Opravil, T., Šoukal, F., Havlica, J., Holešinský, R., 2013. Kinetics and mechanism of formation of gehlenite, Al–Si spinel and anorthite from the mixture of kaolinite and calcite. Solid State Sci. 26, 53–58. https://doi.org/10.1016/j.solidstatesciences.2013.09.014.
Rajabi Mashhadi, Z., Naghizadeh, R., 2021. Effects of temperature and duration of anorthite synthesis from mixtures of kaolin and calcite. J. Inst. Eng. India Ser. E 102, 227–238. https://doi.org/10.1007/s40034-021-00212-6.
Rashad, A.M., 2013. PROPERTIES OF ALKALI-ACTIVATED FLY ASH CONCRETE BLENDED WITH SLAG, p. 10.
Reig, L., Soriano, L., Borrachero, M.V., Monzó, J., Payá, J., 2016. Influence of calcium aluminate cement (CAC) on alkaline activation of red clay brick waste (RCBW). Cement Concr. Compos. 65, 177–185. https://doi.org/10.1016/j.cemconcomp.2015.10.021.
Rivas Mercury, J.M., Turrillas, X., De Aza, A.H., Pena, P., 2006. Calcium aluminates hydration in presence of amorphous SiO2 at temperatures below 90°C. J. Solid State Chem. 179, 2988–2997. https://doi.org/10.1016/j.jssc.2006.05.017.
Šádková, K., Koňáková, D., Pommer, V., Černý, R., Vejmelková, E., 2023. Application of secondary calcined shale in the design of low-cement binder for thermal-resistant composites. Ceram. Int. 49, 13452–13468. https://doi.org/10.1016/j.ceramint.2022.12.220.
Sadrmomtazi, A., Gashti, S.H., Tahmouresi, B., 2020. Residual strength and microstructure of fiber reinforced self-compacting concrete exposed to high temperatures. Construct. Build. Mater. 230, 116969 https://doi.org/10.1016/j.conbuildmat.2019.116969.
Salomao, R., Kawamura, M.A., Emilio, A.B.V., Sakihama, J., Segadaes, A.M., 2021. Calcium aluminate cement in castable alumina: from hydrate bonding to the in situ formation of calcium hexaluminate. Ceram. Int. 47, 15082–15093. https://doi.org/10.1016/j.ceramint.2021.02.066.
K.L. Scrivener, Calcium Aluminate Cements, (n.d.).
Siddique, R., Klaus, J., 2009. Influence of metakaolin on the properties of mortar and concrete: a review. Appl. Clay Sci. 43, 392–400. https://doi.org/10.1016/j.clay.2008.11.007.
Snellings, R., Machner, A., Bolte, G., Kamyab, H., Durdzinski, P., Teck, P., Zajac, M., Muller, A., De Weerdt, K., Haha, M.B., 2022. Hydration kinetics of ternary slag-limestone cements: impact of water to binder ratio and curing temperature. Cement Concr. Res. 151, 106647 https://doi.org/10.1016/j.cemconres.2021.106647.
Song, F., Yu, Z., Yang, F., Liu, Y., Lu, Y., 2014. Stratlingite and calcium hemicarboaluminate hydrate in belite-calcium sulphoaluminate cement. Ceramics 58, 269–274.
Srinivas, D., Ramagiri, K.K., Kar, A., Adak, D., Noroozinejad Farsangi, E., Dutta, S., 2021. Experimental characterization of quaternary blended mortar exposed to marine environment using mechanical strength, corrosion resistance and chemical composition. J. Build. Eng. 42, 102822 https://doi.org/10.1016/j.jobe.2021.102822.
Stutzman, P., 2004. Scanning electron microscopy imaging of hydraulic cement microstructure. Cement Concr. Compos. 26, 957–966. https://doi.org/10.1016/j.cemconcomp.2004.02.043.
Teng, Y., Li, K., Pan, W., Ng, T., 2018. Reducing building life cycle carbon emissions through prefabrication: evidence from and gaps in empirical studies. Build. Environ. 132, 125–136. https://doi.org/10.1016/j.buildenv.2018.01.026.
Trnik, A., Medved, I., Cerny, R., 2012. Measurement of linear thermal expansion coefficient of concrete at high temperatures: a comparison of isothermal and non-isothermal methods. CEMENT WAPNO BETON 17, 363-+.
Vejmelková, E., Koňáková, D., Kulovaná, T., Keppert, M., Žumár, J., Rovnaníková, P., Keršner, Z., Sedlmajer, M., Černý, R., 2015. Engineering properties of concrete containing natural zeolite as supplementary cementitious material: strength, toughness, durability, and hygrothermal performance. Cement Concr. Compos. 55, 259–267. https://doi.org/10.1016/j.cemconcomp.2014.09.013.
Vejmelková, E., Koňáková, D., Doleželová, M., Scheinherrová, L., Svora, P., Keppert, M., Reiterman, P., Černý, R., 2018a. Effect of calcined Czech claystone on the properties of high performance concrete: microstructure, strength and durability. Construct. Build. Mater. 168, 966–974. https://doi.org/10.1016/j.conbuildmat.2018.02.204.
Vejmelková, E., Koňáková, D., Čáchová, M., Záleská, M., Svora, P., Keppert, M., Rovnaníková, P., Černý, R., 2018b. High-strength concrete based on ternary binder with high pozzolan content. Struct. Concr. 19, 1258–1267. https://doi.org/10.1002/suco.201700173.
Wang, H., De Leon, D., Farzam, H., 2014. C(4)AF reactivity-chemistry and hydration of industrial cement. ACI Mater. J. 111, 201–210.
Wang, Y., Li, X., Chen, P., Zhu, B., 2018. Matrix microstructure optimization of alumina-spinel castables and its effect on high temperature properties. Ceram. Int. 44, 857–868. https://doi.org/10.1016/j.ceramint.2017.10.010.
Wi, K., Lee, H.-S., Lim, S., Song, H., Hussin, M.W., Ismail, M.A., 2018. Use of an agricultural by-product, nano sized Palm Oil Fuel Ash as a supplementary cementitious material. Construct. Build. Mater. 183, 139–149. https://doi.org/10.1016/j.conbuildmat.2018.06.156.
Xie, T., Ozbakkaloglu, T., 2015. Behavior of low-calcium fly and bottom ash-based geopolymer concrete cured at ambient temperature. Ceram. Int. 41, 5945–5958. https://doi.org/10.1016/j.ceramint.2015.01.031.
Yun-Fei, F., Bo-Quan, Z., Xiang-Cheng, L., Ping-An, C., 2017. Synthesis and Rheological Property of Calcium Aluminate Cement Containing MgAl$lt;inf$gt;2$lt;/inf$gt;O$lt;

inf$gt;4$lt;/inf$gt; Spinel. J. Inorg. Mater. 32, 884. https://doi.org/10.15541/jim20160582.
Yüzer, N., Akoz, F., Oztürk, L.D., 2004. Compressive strength–color change relation in mortars at high temperature. Cement Concr. Res. 34, 1803–1807. https://doi.org/10.1016/j.cemconres.2004.01.015.
Zapata, J., Azevedo, A., Fontes, C., Monteiro, S., Colorado, H., 2022. Environmental impact and sustainability of calcium aluminate cements. Sustainability 14, 2751. https://doi.org/10.3390/su14052751.
Zhang, D., Li, C., Jiang, N., Gao, J., Touzo, B., Yuan, W., 2018. Influence of powder characteristics of reactive alumina on properties of alumina-spinel castables. Ceram. Int. 44, 9984–9990. https://doi.org/10.1016/j.ceramint.2018.03.056.
Zhang, P., Li, N., Luan, J., Gao, S., Ye, G., 2020. Relationship between the strength and microstructure of CAC-bonded castables under intermediate temperatures. Ceram. Int. 46, 888–892. https://doi.org/10.1016/j.ceramint.2019.09.046.
Zhang, K., Shen, P., Yang, L., Rao, M., Nie, S., Wang, F., 2021. Development of high-ferrite cement: toward green cement production. J. Clean. Prod. 327, 129487 https://doi.org/10.1016/j.jclepro.2021.129487.
Zhu, B., Song, Y., Li, X., Chen, P., Ma, Z., 2015. Synthesis and hydration kinetics of calcium aluminate cement with micro MgAl2O4 spinels. Mater. Chem. Phys. 154, 158–163. https://doi.org/10.1016/j.matchemphys.2015.01.060.

4.3.4 The role of ceramic powder in sustainable thermal-resistant cement-based composites

D. Koňáková, K. Šádková, R. Vaníčková, V. Pommer, M. Keppert, E. Vejmelková
Construction and Building Materials 487 (2025) 142095 [64]
https://doi.org/10.1016/j.conbuildmat.2025.142095

This study contributes to the development of sustainable, thermally resistant cementitious composites by systematically evaluating ceramic powder and reactive alumina as partial replacements for CAC. Addressing both sustainability goals and performance requirements, the research systematically investigates how these materials can substitute up to 60% of CAC. The designed ternary binder systems were optimised in terms of both mechanical and thermal performance. A comprehensive evaluation of hydration kinetics, phase development, microstructure, and mechanical properties of the two most promising mixtures was carried out before and after exposure to extreme temperatures (up to 1400 °C).

Ceramic powder alone increased early porosity and reduced strength due to its filler effect, but in combination with reactive alumina, it enhanced the formation of stable hydrates, reduced metastable phases, and promoted a denser, thermally stable microstructure. Optimised ternary blends (A15-C15 and A15-C30) demonstrated compressive strengths exceeding 100 MPa and superior retention of mechanical properties after high-temperature exposure. These blends outperformed pure CAC in both residual strength and porosity stability.

The main findings of this study include:

- Proposing ceramic powder as a viable SCM for refractory binders
- Demonstrating the synergistic effect of reactive alumina and ceramic powder
- Optimising binder compositions, targeting both mechanical strength and refractory performance, while reducing cement consumption.

In summary, this study identifies ternary CAC–ceramic powder–reactive alumina binders as sustainable, high-performance alternatives for thermal-resistant cementitious composites, with a clear potential for application in high-temperature construction environments.

Construction and Building Materials 487 (2025) 142095

Contents lists available at ScienceDirect

Construction and Building Materials

journal homepage: www.elsevier.com/locate/conbuildmat

The role of ceramic powder in sustainable thermal-resistant cement-based composites

Dana Koňáková *, Kateřina Šádková, Romana Vaníčková, Vojtěch Pommer, Martin Keppert, Eva Vejmelková

Department of Materials Engineering and Chemistry, Faculty of Civil Engineering, Czech Technical University in Prague, Thákurova 7, Prague 166 29, Czech Republic

ARTICLE INFO

Keywords:
Cement-based composites
Ceramic powder
Reactive alumina
Supplementary cementitious materials
Thermal resistance
Mixture optimization

ABSTRACT

This study investigates the potential of substituting calcium aluminate cement (CAC) with ceramic powder (CP) and reactive alumina (RA) to create thermally resistant and sustainable cement-based composites. A total of 14 mixes were designed with varying admixture ratios up to 60 % of CAC were evaluated, with two ternary systems (A15-C15 and A15-C30) selected for detailed analysis. While CP alone increased porosity and reduced strength, its combination with RA significantly improved performance. The A15-C15 and A15-C30 mixtures achieved compressive strengths of 107.6 MPa and 93.5 MPa, respectively, with reduced porosity and enhanced thermal resistance up to 1400 °C. Calorimetry showed that A15-C15 maintained high hydration activity (280 J/g), while A15-C30 followed an altered hydration path. Phase and thermal analyses revealed altered phase composition with reduced metastable hydrates and calcium aluminosilicate hydrates. Aging confirmed the long-term durability of studied composites.

1. Introduction

Many industrial and manufacturing processes cannot operate without exposure to high temperatures. It is, therefore, necessary to choose a suitable material for constructing structures such as furnaces or chimneys that are resistant to such thermal stresses. Concrete may appear to be such a material as it is inherently non-flammable. Commonly used Portland cement (PC) based concretes are suitable for applications up to temperatures not exceeding 700 °C. At 1000 °C, some of the concrete components start to melt, leading to destruction [1–6]. For high-temperature applications, it is better to use concrete with aluminous cement (CAC), which can withstand temperatures up to 1600 °C and is more resistant to aggressive environments [7,8]. However, before its application in the structure, it is necessary to take into account the conversion process, which is caused by the conversion of the unstable calcium aluminates hydrates CAH_{10} and C_2AH_8 to the thermodynamically stable katoite C_3AH_6 and gibbsite AH_3, which can lead to the deformation of the structure [9–11].

In parallel with the need for high-performance materials, growing environmental concerns further intensify the search for more sustainable alternatives. In general, the production of cement is a significant environmental burden as it requires very high temperatures and thus a large amount of fuel to be burned, leading to a large production of greenhouse gases and a large consumption of non-renewable resources [12–15]. CO_2 emissions from cement production account for 8 % of total CO_2 emissions [16]. The solution to this problem is to find other materials that can serve as supplementary cementitious materials (SCMs) and replace cement as much as possible. Portland cement (PC) substitution has been tested many times in the past. Most often, PC is currently replaced by one of the industrial byproducts such as slag [17,18], fly ash [19,20], microsilica [21,22] or other industrial wastes [23,24]. However, with increasing pressure to adopt environmentally friendly practices and align with zero-waste ideology, the use of many conventional SCMs faces limitations in reduced availability. Moreover, industrial wastes also have many uses in other industries, so there is a constant need to look for other possible alternatives for concrete admixtures.

One promising candidate for suitable pozzolana is ceramic waste, which is readily available as a by-product of construction, demolition, and ceramic manufacturing processes. In China, for example, around 13 million tonnes of ceramic waste are generated every day and have no further use [25–27]. Regarding the pozzolanic properties, when the ceramic waste is ground to a fine powder, it shows an excellent pozzolanic activity, as it contains significant amounts of silica SiO_2 and alumina Al_2O_3. On that account waste, ceramic powder has great

* Corresponding author.
E-mail address: dana.konakova@fsv.cvut.cz (D. Koňáková).

https://doi.org/10.1016/j.conbuildmat.2025.142095
Received 31 March 2025; Received in revised form 22 May 2025; Accepted 1 June 2025
Available online 4 June 2025
0950-0618/© 2025 Elsevier Ltd. All rights are reserved, including those for text and data mining, AI training, and similar technologies.

potential to replace both PC and CAC in concrete [22,28]. Brazilian research shows that if 20 % of PC were replaced by ceramic waste, the amount of CO_2 produced would be reduced by 10 % [29]. Another research reported that a 20 % replacement of cement with waste ceramic dust would lead to an economic saving of 9.6 % in cement production, and the energy consumption spent on cement production would decrease by 6.7 % [25]. In addition to reducing price and emissions, ceramic dust could also improve the properties of the resulting cement composite.

There are many experiments dealing with the combination of PC and ceramic waste from roof tiles [30–34], floor tiles [35], and bricks [36–40]. Although concrete with brick dust admixture initially had lower strength than mixtures without admixture, after 90 days, its strength was comparable or even higher [41]. Brick dust acted more like a filler in the initial setting phase. The pozzolanic properties became apparent in the later stage of solidification when its pozzolanic activity started to consume calcium hydroxide partially and promoted the formation of hydrated calcium aluminates [42,43]. Researches showed that 20 % PC replacement improved composite durability with minimal loss of strength [43,44]. If more waste ceramic dust was added to the concrete, all the ceramic dust would not react, and this residue would act as filler. For example, when 60 % of ceramic waste is added to the mix, about 20 % acts only as a packing material [45]. Most studies agree that the smaller the particle size of ceramic dust, the more reactive and effective it is [25,46].

Beyond room-temperature performance, several studies have also explored the behavior of cementitious composites with ceramic waste under high-temperature conditions. For example, concrete incorporating ceramic aggregate has shown good resistance to compressive and abrasive forces up to 1000 °C [47]. The inclusion of ceramic waste also enhanced the residual strength of concrete after high-temperature exposure, although in some cases, samples experienced explosive spalling [48].

In addition to examining the performance of ceramic waste as aggregate, attention has also been given to its role as a partial replacement for thermal-resistant calcium aluminate cement. Research on replacing aluminate cement with waste brick dust can also be found. For example, When recycled refractory brick aggregate (RRBA) was used to replace cement in varying proportions (0, 25, 50, 75, and 100 %), the resulting composites exhibited higher compressive strength at temperatures exceeding 800 °C compared to the reference mixes. Additionally, concretes with higher RRBA content (75 and 100 %) demonstrated lower weight losses when exposed to 800 and 1000 °C [49]. In further studies, 5 % and 15 % of CAC were substituted with ceramic dust, metashale, and sintered mullite, and the samples were exposed to temperatures up to 1400 °C. The blended cement pastes exhibited improved performance both at ambient conditions and under thermal loading. Brick dust, in particular, had a significant impact on the phase composition, increasing the degree of hydration, reducing porosity, and enhancing compressive strength. The most favourable results were achieved with a 5 % CAC replacement by brick dust [50].

Previous studies and literature reviews have demonstrated the applicability of ceramic waste as a partial cement replacement. However, while many works [28–39] focusing primarily on ambient or early-age performance, limited attention has been given to their behaviour under extreme conditions exceeding 1000 °C. Some studies have reported promising high-temperature resistance with ceramic aggregates or refractory brick dust [48–51], but systematic evaluations involving fine ceramic powder at high temperatures (up to 1400 °C) remain scarce. Furthermore, the long-term durability of such composites after prolonged curing and thermal exposure is not well documented. Building on this foundation, the present study aims to further evaluate the potential of ceramic waste powder in combination with calcium aluminate cement. In contrast to earlier works, not only were blended cements examined, but primarily, ternary binder systems incorporating reactive alumina powder were investigated. This admixture was chosen to enhance pozzolanic reactivity and overall material performance [51–53]. There exists a critical gap in understanding the synergistic effect of ceramic powder and activated alumina on phase evolution, microstructure densification, and thermomechanical integrity in refractory applications. To address this, several mix designs were tested with replacement levels up to 60 %, followed by an in-depth analysis of the two most promising systems. These were characterised in terms of phase composition, microstructure, and residual properties after exposure to temperatures as high as 1400 °C. The objective was to assess the effectiveness of these alternative materials in producing sustainable, thermally resistant cement-based composites.

2. Experimental methods and materials

2.1. Analytical methods

The elemental composition of the samples was analysed using energy-dispersive X-ray fluorescence (ED-XRF). A QUANT'X benchtop spectrometer was utilised, capable of performing both qualitative and quantitative assessments on various sample forms, including solids, powders, and liquids. This method covers a broad range of elements, from sodium to uranium. The instrument's typical accuracy for major constituents falls within ± 0.5–1.5 %, depending on the calibration quality and the sample preparation technique.

Mineralogical composition was assessed using X-ray diffraction (XRD), conducted on a PANalytical Aeris diffractometer fitted with a conventional CoKα radiation source operating at 40 kV. To enable quantification of amorphous content, an internal standard method was employed, incorporating 20 wt% of highly crystalline zinc oxide (ZnO) into the samples. The diffraction data were interpreted using Profex software [54], which applies Rietveld refinement for phase identification and quantification. This approach generally yields an accuracy within ± 1–3 % for major crystalline phases, while uncertainties may be higher for minor or poorly crystalline components.

Isothermal calorimetry was employed to evaluate the reactivity of designed binders by monitoring the heat evolution during hydration. Measurements were conducted using an 8-channel TAM Air calorimeter (TA Instruments) under isothermal conditions at 20 °C. The water/binder ratio was 0.5 in order to ensure proper homogenization. At lower ratios (0.3 as used in composites), the mix within the ampoule was too stiff, preventing uniform mixing and leading to incomplete hydration. The calorimeter provides a repeatability of ± 2 % for total heat release under controlled conditions, ensuring reliable assessment of the reactivity of individual admixtures.

Simultaneous thermal analysis (STA) was carried out using the STA 449 Jupiter instrument (NETZSCH), which integrates differential scanning calorimetry (DSC) and thermogravimetric analysis (TG). Measurements were conducted under an inert argon atmosphere with a controlled flow rate of 40 mL/min. Samples were heated at a constant rate of 10 °C/min up to 1400 °C. Data were evaluated using Proteus Thermal Analysis software. The system offers temperature accuracy of ± 0.3 °C, heat flow (enthalpy) accuracy of approximately 1 %, and balance resolution of 0.1 μg.

2.2. Basic physical properties

Particle size distribution was determined using laser diffraction analysis with a Bettersizer S3 Plus instrument. This device offers a wide measurement range from 0.01 μm to 3500 μm, enabling accurate assessment of both fine and coarse fractions. The system provides high resolution, with a typical size accuracy of ± 1 % for D50 values and less than 3 % variability for broader distributions.

The density of the studied materials was measured using helium pycnometry with a Pycnomatic ATC EVO device (Thermo Scientific). The instrument, equipped with interchangeable measurement cells ranging from 4 to 100 cm^3 , enables accurate analysis of both fine

powders and solid materials. The method provides high precision with a measurement accuracy of ± 0.01 g/cm^3 .

The bulk density of studied composites was determined using a standard gravimetric method based on the ratio of a sample's mass to its bulk volume. The accuracy of bulk density determination is typically within ± 0.02 g.cm^{-3} for compacted materials. The obtained bulk density values were subsequently combined with density data (measured by helium pycnometry) to calculate the total open porosity of the samples using the standard relation.

For more detailed information about pore size distribution, composites were analysed using mercury intrusion porosimetry (MIP), specifically with a PASCAL 140 + 440 porosimeter (Thermo Fisher Scientific Inc.). The MIP technique is based on measuring the pressure required to intrude non-wetting mercury into the pore system of a material. The used apparatus enables the characterisation of pores within a radius range of approximately 10 nm to 100 µm. The measurement offers typical accuracy in pore size determination within ± 2 % for mesopores and macropores and a cumulative porosity accuracy of ± 1–3 %, depending on sample properties and preparation.

2.3. Mechanical parameters

The mechanical properties of the composites, namely compressive strength and flexural strength, were evaluated in accordance with the applicable standards [55]. Flexural strength was assessed using three prismatic specimens (40 × 40 × 160 mm) on an MTS 100 loading device, following a standard three-point bending configuration with a span length of 100 mm. Subsequently, compressive strength was determined on the broken halves of the flexural specimens using the EU40 testing machine. During compression testing, each fragment was placed between two steel loading plates measuring 40 × 40 mm.

Prior to mechanical testing, the dynamic modulus of elasticity was determined using ultrasonic pulse velocity measurements [56]. A Proceq PunditLab+ device equipped with a 54 kHz pulse transducer was employed to measure the ultrasonic wave velocity. The testing was conducted in a one-dimensional configuration, with the dimensionality coefficient assumed to be 1.

2.4. Thermal characteristics

Thermal conductivity and volumetric heat capacity were measured using the ISOMET 2114 on three cubic samples (70 × 70 × 70 mm). This device uses a dynamic method based on the temperature response to heat flow pulses induced by a powered probe. The accuracy of the measurement is ± 5 % for thermal conductivity and ± 10 % for volumetric heat capacity. Afterwards, values of specific heat capacity were calculated by dividing the volumetric heat capacity by the bulk density of the composites.

Thermal strain as a function of temperature was measured using a horizontal linear dilatometer (CLASIC CZ s. r. o.). The device operates on a comparative method, where the expansion of the tested specimen is evaluated against a corundum reference standard. The specimen is placed inside a corundum tube, fixed on one side and in contact with a pull-rod on the other, which transmits length changes to a displacement sensor. Data were recorded using the "Dilatometer 1.3" software to calculate thermal strain and the temperature-dependent linear thermal expansion coefficient.

2.5. Raw materials characterisation

Studied materials contain three kinds of binder components: calcium aluminate cement, ceramic powder and reactive alumina. They were firstly characterised by means of determination of their chemical and phase composition and their basic physical and granulometric properties. The summary of their chemical composition can be found in Table 1, while the cumulative particle size distribution is presented in Fig. 1.

The reference type of binder was calcium aluminate cement (CAC) with a medium alumina content above 70 %. Specifically, Secar® 71, manufactured in Kerneos S.A., was used in all test specimens. According to its data sheet, it is guaranteed to have a minimum compressive strength of 31.7 MPa after 24 hours and a minimum initial strength of 8.6 MPa after 6 hours of setting. Mineralogically, this cement contained 55 % krotite (CA, $CaO.Al_2O_3$), 36 % grossite (CA_2, $CaO.2Al_2O_3$), and about 5 % amorphous matter. It also contained trace amounts of corundum (Al_2O_3), mayenite ($C12A7$, $12CaO.7Al_2O_3$). Regarding the physical properties, it has a specific gravity of 2 890 kg.m^{-3} and the average particle diameter (D_{50}) of 8.6 µm.

Ceramic powder (CP), which is produced during the grinding of HELUZ brick blocks, specifically in the production plant in Libochovice, Cech Republic, was used in the mixture design. This dust is either taken to a landfill or returned to production as a sharpening agent. Table 1 shows the chemical composition compatible with the desired applicability as supplementary cementitious materials, as it exceeded the limit of 70 % for hydraulic oxides [57]. Regarding the mineralogical composition, the ceramic powder contained 38 % of the amorphous phase, 31 % quartz (SiO_2), 11 % illite ($Al_4KO_{12}Si_2$), and 7 % orthoclase ($K(AlSi_3O_8)$). The remaining observed phases (calcite ($CaCO_3$), biotite ($K(Mg,Fe)_3AlSi_3O_{10}(OH)_2$), microcline ($K(AlSi_3O_8)$), albite ($Na(AlSi_3O_8)$), muscovite ($KAl_2(AlSi_3O_{10})(OH)_2$) and hematite ($Fe_2O_3$)) were presented in the amount below 3 %. The specific gravity of the used ceramic powder was 2489 kg.m^{-3}. When focusing on granulometric properties, it is visible that, with the average particle diameter (D_{50}) of 17µm, it is slightly coarser compared to calcium aluminate cement.

As was mentioned in the introduction, reactive alumina was supplemented into the mixture design in order to improve the reactivity of designed binders. Namely, super reactive alumina Nabalox No 713 from Nablatec AG was employed. This reactive alumina (RA) was chosen mainly to add more alumina (Al_2O_3) into the mixture and because of its high reactivity, homogeneous microstructure, and low sodium oxide (Na_2O) content. Regarding the physical properties, it has a higher specific gravity of 3943 kg.m^{-3} and the finest granulometry with the

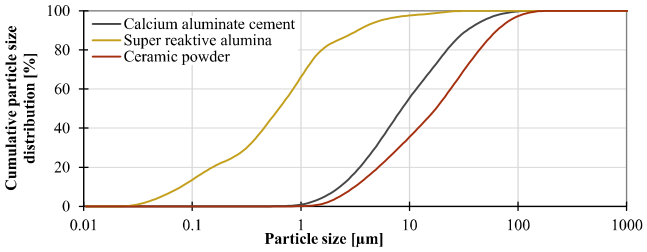

Fig. 1. Particle size distribution of binder components.

Table 1
Chemical composition of binders [%].

	Al_2O_3	SiO_2	Fe_2O_3	CaO	MgO	TiO_2	K_2O	Na_2O
Calcium aluminate cement	70.7	0.4	0.1	28.2	0.1	-	0.06	-
Ceramic powder	20.0	51.3	6.0	11.5	4.5	0.8	3.2	1.3
Reactive alumina	99.7	0.05	0.03	-	-	-	-	0.10

average particle diameter of 0.7 μm.

For the production of the thermal resistant composites, fireclay aggregate from the manufacturer České lupkové závody a.s. was used. Thanks to its high content of alumina content and low fusible impurities, it can withstand high temperatures. In order to achieve the standard grain size curve [58] aggregate was mixed from the following 4 fractions: 0/0.5, 0.5/1, 1/2, and 1/3 of A 111 VHR in the ratio of 11:6:10:5. The last component, apart from tap water, was a superplasticizer used in order to improve the workability of fresh mixtures. Based on previous research dealing with the compatibility of varying types of plasticizers for calcium aluminate cement, a modified polycarboxylates base was chosen [59]. Specifically, Sika ViscoCrete 2700 was used.

3. Mix design and optimisation

In the first phase of the experiments, finding the optimal amount of CAC replacement by waste ceramic powder and reactive alumina was necessary. A total of 14 different cement composite formulations and one reference mixture were proposed, from which the two with the best resulting properties were chosen for the next phase of the research aiming at a more detailed characterisation of the properties and monitoring changes in structure.

3.1. Design and production of studied composites

The studied composite contained a ternary binder composed of varying proportions of calcium aluminate cement, ceramic powder and reactive alumina. The maximum replacement level for alternative materials was set at 60 %, and incremental steps at 15 %. With this logic, a total of 14 mixtures were designed. Specific binder ratios are shown in the phase diagram in Fig. 2. The labelling of mixtures corresponds to their compositions: 'A' means reactive alumina and 'C' for ceramic powder. The following number in the mixtures' names indicates the percentage of the ingredient in the mixture. A total of 4 mixes were produced in which CAC was replaced only by brick dust (C15 - C60). In another 4 mixtures, CAC was replaced solely by reactive alumina (A15 - A60). These were included primarily for comparative purposes, as the main objective was to determine the effect of brick dust on refractory composites. The remaining 6 mixtures combined both admixtures in different proportions (A15-C15, A15-C30, A30-C15, A15-C45, A30-C30, A45-C15). In addition, the reference sample FR containing only CAC was prepared for the sake of comparison. Fig. 3

The overall composite composition can be found in Table 2. Each mixture, therefore, contained 500 g of binder, 1600 g of filler, and 5 g of plasticizer. For characterization purposes of phase composition, in the second stage of the research, pastes with no aggregate were produced as well. However in both cases, the water coefficient was chosen to be the same for all mixtures - 0.3. Regarding the production process, it took place in the laboratory condition 20 ± 1 °C and relative humidity 25–30 %). For testing purposes, samples of standard dimensions of 40 × 40 × 160 mm were produced. The raw materials were weighed to an accuracy of ± 2 g and then thoroughly mixed in an electric mixer. After their proper homogenization, the dosage of water mixed with plasticizer was poured into the mix. When the mixture showed no signs of lumps, impurities, or unwetted parts of cement or other additives after mixing, it was placed in pre-cleaned and greased moulds (prisms with 40x40x160 mm) and leveled using a spatula. After filling, the moulds were compacted on a vibrating table to remove any air bubbles that may have formed in the mortar during deposition.

Finally, the samples were aligned along the edges of the mould and covered by plastic film to prevent water evaporation and consequent microcracking. These samples were stored at the laboratory (20 ± 1 °C, RH of 25–30 %) for one day. After that, they were demoulded and placed in a climate chamber set at 20 °C and 50 % R.H. for 28 days. Controlled temperature was important in order to prevent the hydration process from being adversely affected by the ambient environment. After 28 days of curing, one set of samples was examined without temperature loading. The second set was fired at 1400 °C before further investigation. In order to prevent explosive spalling, these samples were initially dried for one day at 105°C. Then they were put into the electric furnace where heating rate was set at 10 °C/min and exposure of maximal temperature was 3 hours. After firing, the samples were allowed to cool down spontaneously.

3.2. Evaluation of composites performance

3.2.1. Basic physical properties

Among the basic physical properties, the porosity of the investigated samples had the most significant impact on the performance of other physical properties and, therefore, played a fundamental role in assessing the optimal replacement level. Determined values of porosities can be found in Fig. 4. At ambient temperature, porosity ranged from 12 % for reference material FR to as high as 39 % for material C60 with 60 % of ceramic powder. The observed behaviour clearly indicated that ceramic powder application led to a substantial increase in porosity. On the contrary, samples with reactive alumina content showed porosity within a narrower range, from 13 % to 15 %, with values quite close to the reference FR. On that account, it can be concluded that reactive alumina helped maintain lower baseline porosity. Regarding the combinations of admixtures, such samples generally showed porosity often comparable to or lower than those of the individual composites with solely ceramic powder or reactive alumina. Such performance suggested a synergistic effect of used admixtures in controlling initial pore development.

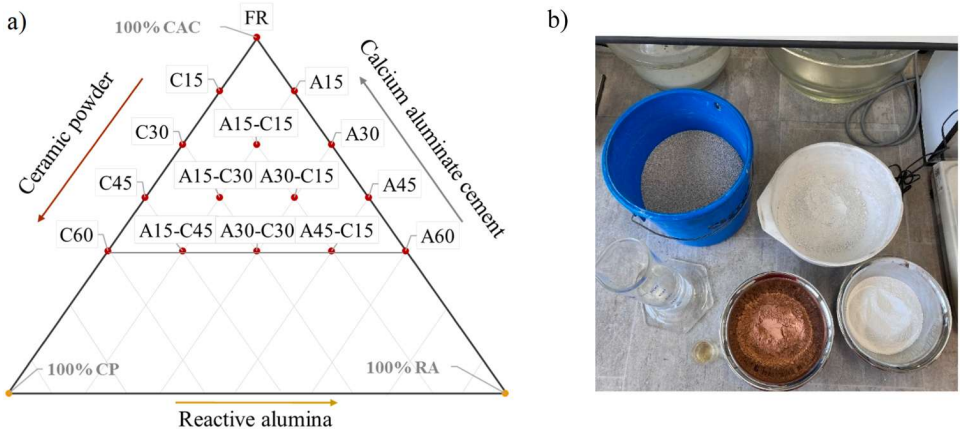

Fig. 2. a) Phase composition of designed binder, b) Raw materials.

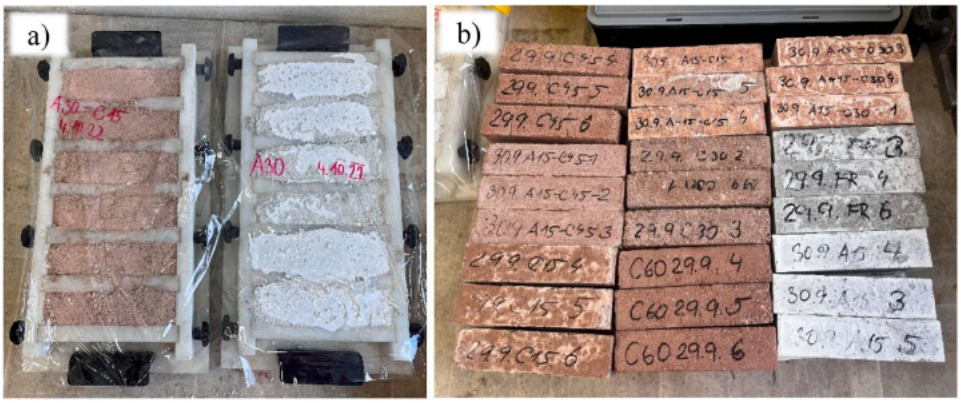

Fig. 3. Prepared samples of designed composites a) in mould, b) before testing.

Table 2
Composition of the mixtures.

Material	Dosage [kg]
Blended binder (CAC+CP+RA)	500
Fireclay (A114 VHR 0–0.5)	550
Fireclay (A114 VHR 0.5–1)	300
Fireclay (A114 VHR 1–2)	500
Fireclay (A114 VHR 1–3)	250
Plasticizer (Sika ViscoCrete 2700)	5
Water	150

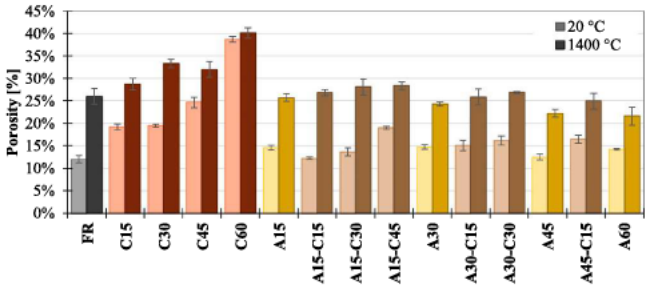

Fig. 4. Porosity of designed composites at 28 days.

When focused on performance after the temperature exposure, due to the continuous phase changes (such as dehydration, recrystallization or partial sintering), the residual porosity went up in all cases of studied composites. The reference composite FR exhibited a high increase in residual porosity of 116 %. On the contrary, samples with ceramic powder, despite having higher residual porosity, showed a substantially lower growth of the values. Composite C60 with 60 % of ceramic powder reached only a 4 % increase, suggesting densification or sintering at high temperature. Alumina powder showed a comparable impact, lowering of porosity growth, but the modification was less pronounced. Composite A60 with 60 % of reactive alumina showed the growth of residual porosity of 52 %. Ternary systems containing both admixtures displayed more varied behavior, but generally, their porosity increases remained lower than that of the reference composite.

3.2.2. Mechanical properties

The most determining mechanical property for building materials is, indisputably, compressive strength. Therefore, in this stage of research, only their values are presented (see Fig. 5). At room temperature, it is evident that increasing the amount of ceramic powder had a detrimental effect on the resulting compressive strength. The C60 mixture performed the worst, which is consistent with its high porosity. Such an observation was somehow assumed, considering the high replacement levels and

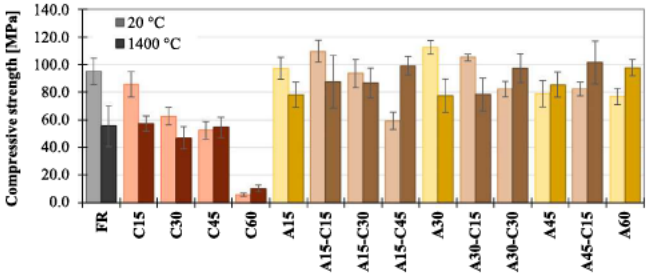

Fig. 5. Compressive strength of designed composites at 28 days.

previous research [50] where a 5 % dosage of ceramic powder was found to be optimal. In the case of the sole reactive alumina, its application resulted in the improvement of compressive strength only when its content did not exceed 30 %. Once this threshold was exceeded, compressive strength began to decline, indicating a possible oversaturation effect at higher dosages. Ternary systems that combine ceramic powder and reactive alumina generally maintained remarkably higher strength, suggesting a synergic effect of both admixtures. The best compressive strengths at room temperature were achieved by samples A15-C15. Their compressive strengths supressed the reference mixture FR by an average of 10 %.

After exposure to 1400 °C, the compressive strength of all samples changed significantly, reflecting the influence of thermal exposure on microstructural stability. The reference mixture (FR) experienced a considerable strength reduction of approximately 42 %, indicating limited resistance to high-temperature degradation. Such a pronounced decrease was not observed for any other mix. When ceramic powder was used, the deterioration of compressive strength was reversed, and at higher dosage, the residual values even went up. This phenomenon corresponded with the reduced porosity fall caused probably by partial sintering and densification of the structure. When focused on reactive alumina, these composites showed improved thermal stability, with lower strength losses or even gains at higher dosage. The A60 sample, for example, recorded a 27 % increase in residual compressive strength. This highlighted the beneficial effect of alumina content at elevated temperatures. Ternary systems confirmed the synergistic effect of used admixtures, as they proposed the highest values of the residual compressive strengths, between 41 % and 83 % higher compared to the residual compressive strength of the reference material FR. Interestingly, the higher the CAC replacement level was, the better residual compressive strength exhibited after exposure to 1400 °C.

3.2.3. Discussion and optimization criterion

The measurements revealed that using ceramic powder alone was not very suitable. With a higher dosage of ceramics, the porosity of the

material increased, which led to lower mechanical strengths at room temperature. After firing, the mechanical properties were slightly higher but still did not reach the desired values. However, the combination of brick dust with reactive alumina proved to be very suitable. Most of the samples showed mechanical properties at room temperature comparable to the reference mixture. After firing, most of the composites with combined admixtures achieved better compressive strengths than the reference sample. It is very promising that up to 60 % of aluminate cement was replaced with good results.

To guide further development of thermally resistant composites, an optimization criterion was established to evaluate overall material performance. The approach integrates three key parameters: 1) impact of admixtures on the compressive strength at ambient temperature, 2) impact of admixtures on the residual compressive strength, and 3) dosage of used admixtures. The main aim was to maximize mechanical performance while minimizing degradation and, of course, optimizing the use of ceramic powder and reactive alumina. To reflect the relative importance of each factor, the weighting coefficients were set to 2:1:2. Based on these principles, an evaluation function was formulated to calculate Composite Performance Index (CPI) as follows:

$$CPI \quad 2 \bullet \frac{f_c}{f_c^{FR}} + \frac{f_{cr}}{f_{cr}^{FR}} + 2 \bullet (C \quad A)$$

CPI…composite performance index [-]

f_c…compressive strength at ambient temperature [MPa]

f_c^{FR}…compressive strength of reference material at ambient temperature [MPa]

f_{cr}…residual compressive strength [MPa]

f_{cr}^{FR}…residual compressive strength of reference material [MPa]

C…the percentage of ceramic powder in the binder [-]

A…the percentage of reactive alumina in the binder [-]

After evaluating the composite performance with the help results of CPI (Fig. 6), the best-performing composites were clearly those combining reactive alumina with ceramic powder. Composites A15-C15 and A15-C30 achieved the highest CPI values, both exceeding 3.6, confirming their balanced performance in both mechanical strength and material optimization. These ternary systems outperformed the reference as well as most single-admixture samples. On the other hand, mixtures with high ceramic powder content alone, such as C60, showed significantly lower CPI values due to poor strength at room temperature, despite partial recovery after firing and desired admixtures dosages. Based on this analysis, the two most promising mixtures (A15-C15 and A15-C30) were selected for detailed characterisation and a broader determination of their physical properties.

4. Composites characterisation and performance

As was mentioned above, the composites for further detailed investigation were those with the most promising results of preliminary optimisation, namely samples A15-C15, A15-C30. The reference composite FR was also included in the study. However, it served solely as a benchmark material for comparative purposes. At this stage, additional specimens were produced to enable a more comprehensive evaluation of material properties not only after 28 days but also after 1 year. Furthermore, the temperature exposure regime was expanded to include more steps: specifically, temperatures were set to 20 °C, 400 °C, 1000 °C, and 1400 °C, allowing for a broader assessment of thermal resistance. Temperature treatment followed the same procedure as in the previous stage: Initial drying at 105 °C, followed by high-temperature exposure with the heating rate of 10 °C/min, a 3-hour holding period at the target temperature, and subsequent spontaneous cooling.

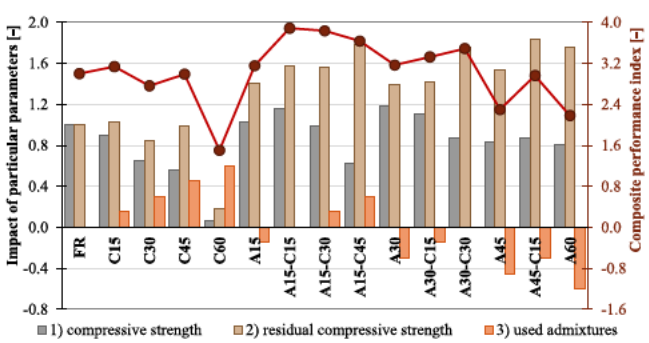

Fig. 6. Composite performance index.

4.1. Hydration mechanism

The hydration mechanism was described through the view of hydration heat released during the 60 hours with the help of isothermal calorimetry. The results of isothermal calorimetry are presented in Fig. 7. All studied binders exhibited a typical hydration performance for calcium aluminate cement, which can be divided into three stages: initial, latent and the main hydration period. The first initial period is characterized by a sharp peak in the first 20 minutes. During this time, the CA and CA_2 phases dissolute upon contact with water, releasing Ca^{2+} and $Al(OH)_4^-$ ions, generating an immediate heat release. When admixtures were added into the binders, a higher amount of heat was released during the first period, although the time remained unchanged. This effect can be attributed primarily to the impact of ceramic powder, as the reactive alumina is generally considered insoluble in water under normal conditions. It can undergo surface hydration (generating hydroxyl groups on the surface), but the release heat of this is relatively low [60]. On the contrary, ceramic powder, containing 38 % of amorphous (and thus reactive) phases, can partially dissolve in the alkaline solution, generating silica and alumina ions, which contribute to heat evolution during the initial period.

Following the initial exothermic peak, all samples entered the latent period. This stage corresponds to the time when the dissolution of CA and CA_2 slows down while the solution remains saturated with Ca^{2+} and $Al(OH)_4^-$ ions. During this dormant phase, only limited hydrate formation occurs, and thermal activity is minimal. The reference sample exhibited a latent period lasting approximately 3.5 hours. In the case of admixture application, this time was remarkably shortened. Both A15-C15 and A15-C30 showed an earlier onset of the main hydration reaction, as the latent period took only 1 hour for A15-C15 and even 45 minutes for A15-C30. This behaviour can be attributed to increased concentration of aluminate and silicate ions, which accelerated the supersaturation. Alongside, reactive alumina and insoluble grains of ceramic powder acted as nucleation sites for the progression of the main hydration phase, which further contributed to the shortening of the latent period.

The last main hydration period corresponds to the rapid precipitation of hydration phases. In the case of CAC, this included mainly CAH_{10}, C_2AH_8, C_3AH_6 and AH_3. During their formation, the majority of the total heat was released. In the case of the reference binder FR, the heat released was sharp, and the time of the main hydration period lasted approximately 10 hours. The impact of the alternative admixtures was also substantial in this phase. The main hydration period was somewhat prolonged, and the peak value of heat flow was reduced. The reason for such a performance can be of two kinds. Firstly, the replacement of cement with less reactive ceramic powder may reduce the quantity of available ions and limit overall reaction enthalpy. Secondly, the nature of the hydration products themselves may influence the thermal response as well. In systems where C-S-H or C-A-S-H gels are formed, as is typical in Portland cement-based binders, the heat released is substantially lower, and the hydration process tends to be more prolonged and gradual. Therefore, the observed reduction in heat evolution does not necessarily reflect only lower reactivity but rather a change in the hydration mechanism and product composition. This assumption was supported by the total hydration heat evolved in 60 days (see Fig. 7b),

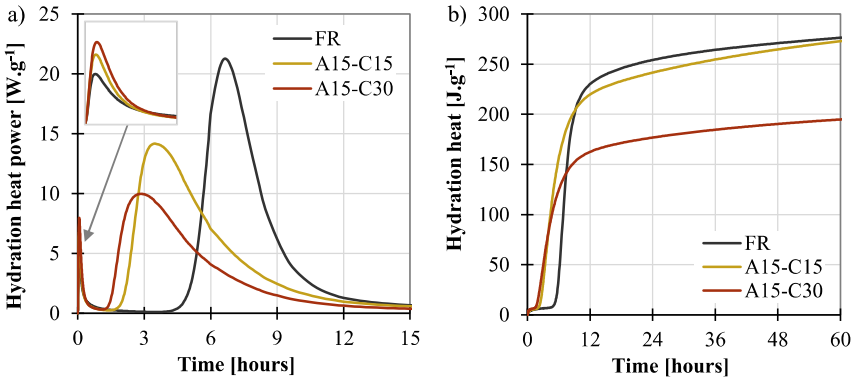

Fig. 7. Results of isothermal calorimetry.

which reached comparable values for the reference composite FR and the ternary binder-based one A15-C15. On the other hand, A15-C30, which contains a higher amount of ceramic powder, exhibited a noticeably lower total heat release, indicating reduced reactivity or a more fundamentally altered hydration pathway.

4.2. Microstructure and phase composition

4.2.1. Microstructure of studied composites

For monitoring the microstructure, the scanning electron microscope was used. In Fig. 8, SEM pictures of all three composites after 28 days can be found. The micrograph of the reference composite FR reveals a more porous and fragmented structure with pronounced surface cracking and irregularly distributed particles. These features suggest weak matrix cohesion and insufficient densification, which may negatively affect the composite's durability and mechanical integrity. In contrast, the A15-C15 composite exhibits a noticeably more compact microstructure. Cracks are less frequent and narrower, and the overall matrix appears more homogenous. The finer particle distribution and improved bonding between phases indicate a positive effect of the additives on the matrix structure, likely contributing to enhanced thermal and mechanical performance. The A15-C30 composite demonstrates the most consolidated microstructure among the three. While some cracking is still present, it is less pronounced and more localized. The matrix shows dense packing with minimal porosity and well-integrated phases.

Scanning electron microscopy performed after exposure to 1400 °C revealed the most significant differences in the microstructure of the studied composites Fig. 9. All samples exhibited evidence of sintering, accompanied by a generally higher porous structure (compared to ambient temperature). However, notable differences in homogeneity and phase distribution were observed among the composites. At first sight, it is visible that the reference composite FR exhibited the most heterogeneous microstructure, characterized by distinct regions of crystalline phases and irregular morphology. In contrast, the A15-C15 composite exhibited reduced crystallinity, though some crystalline domains remained identifiable. Despite the presence of localized cracking, the matrix maintained a relatively compact and cohesive structure. The A15-C30 composite demonstrated the highest degree of sintering, with a dense and continuous matrix, however, some microcracks were observed as well in this case.

4.2.2. Phase development

For a first elucidation of the phase development, the STA was employed. The results of the studied composites at the age of 28 days, as well as after 1 year, can be found in Fig. 10. Reference sample FR showed a typical performance of calcium aluminate cement at 28 days. Dehydration range up to 400 °C contained several steps of phase dehydration: namely dehydration of amorphous AH_3 (60–120 °C), CAH_{10} (100–160 °C), and C_2AH_8 (140–240 °C), followed by dehydration of gibbsite AH_3 (210–320 °C) and katoite C_3AH_6 (240–370 °C) [50]. The subsequent range between approximately 400–900 °C can be called a steady state where no substantial changes in material occurred. This is followed by the recrystallization area, where re-new phases of calcium aluminates (like krotite CA and grossite CA_2) were formed. Finally, after exposure to 1200 °C the material begins to sinter, leading to the development of so-called ceramic bonds—robust interparticle connections that significantly enhance compressive strength and thermal resistance. During the analysis of evolved gas, the most visible ion current was observed for water molecule (as presented in Fig. 10d), and no other significant signals were found.

With the application of a blended binder, the amount of water bounded in the hydrates was lower by 1.9 % for A15-C15 and by 4.7 % for A15-C30. This indicates that the admixtures influenced the hydration either by suppressing the formation of conventional calcium aluminate

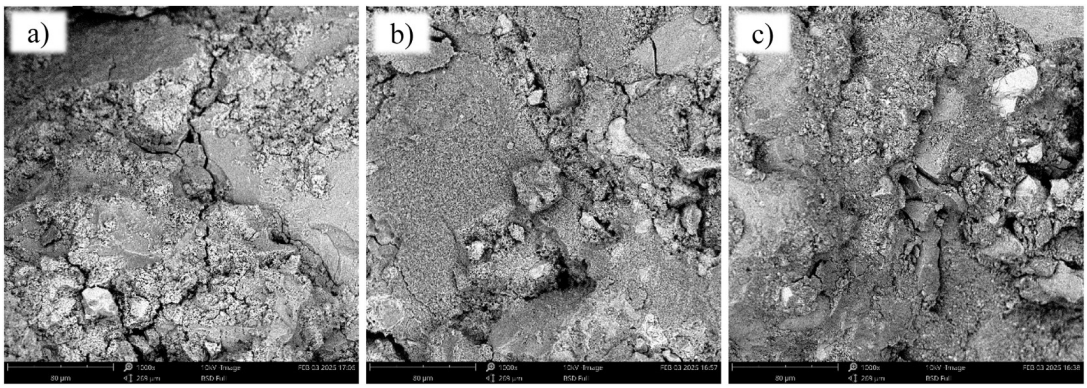

Fig. 8. SEM at ambient temperature – 1000x magnification: a) FR, b) A15-C15, c) A15-C30.

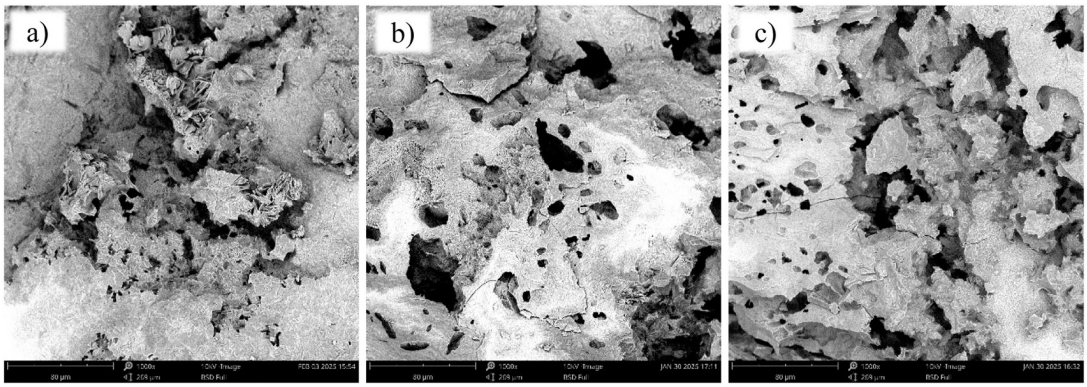

Fig. 9. SEM images after exposure to 1400 °C – 1000x magnification: a) FR, b) A15-C15, c) A15-C30.

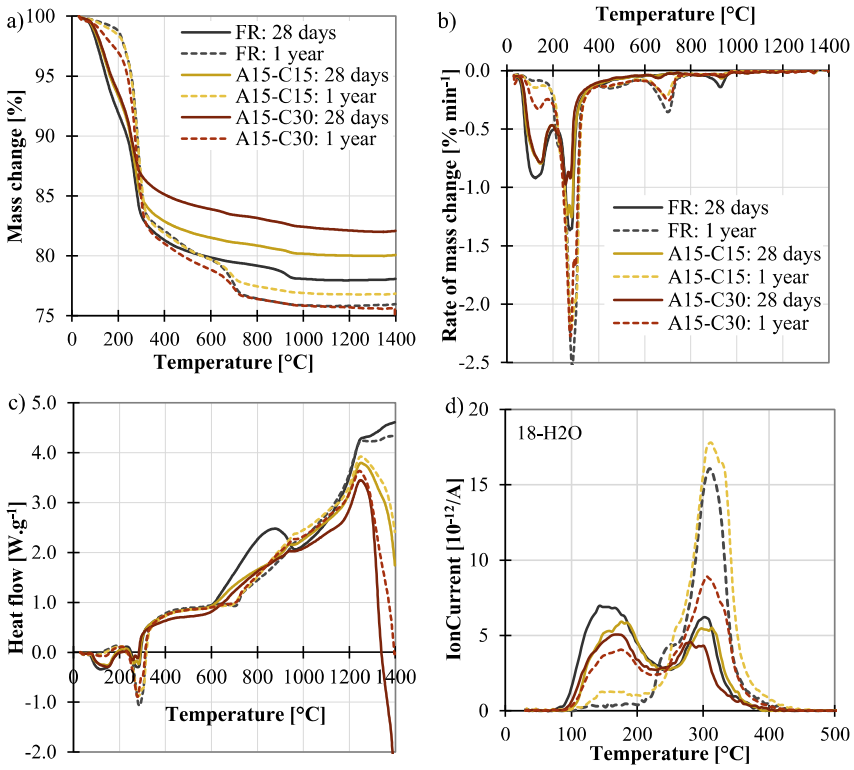

Fig. 10. Results of STA: a) TG, b) DTG, c) DSC, d) ion current of H_2O.

hydrates (C-A-H) or by promoting the formation of alternative phases such as calcium aluminosilicate hydrates (C-A-S-H). Considering the phase modification, several possibilities, such as stratlingite C_2ASH_8 (with stepwise dehydration in several steps of 130 °C, 170 °C and 240 °C [61]) or gismondine CAS_4H_9 (with multiple overlapping dehydration peaks at 105°C, 125°C 155°C and 240 °C [62]) came into consideration [50]. The second distinctive variation was observed in the sintering range, where substantial modification was observed due to the application of an alternative admixture. The presence of ceramic powder accelerated or intensified melting. This could be due to the formation of low-melting eutectic compositions or increased glassy phase content introduced by the ceramic powder. Specifically, the used ceramic powder contained a noticeable portion of fluxing phases (e.g., clay, micas or feldspars), which can reduce the local melting point and promote viscous flow at extreme temperatures. At 1400 °C, these components may partially melt and form transient liquid phases, which act as sintering aids by filling voids, enhancing particle packing, and promoting ceramic bonding. Thus, rather than delaying melting, the admixtures seemed to promote earlier or more complete fusion, which may play a role in developing ceramic bonding and densification at high temperatures. Such observations are consistent with SEM analysis after 1400 °C.

When focused on the development of phase during the time, the most visible modifications were observed in the dehydration range as well. The first peak corresponding to the dehydration of metastable CAH_{10} considerably diminished or disappeared, while the second double peak attributed to decomposition of katoite C_3AH_6 and gibbsite AH_3 decomposition become distinctively dominant. This evolution is also supported by the mass spectrometry results, which showed a decrease in H_2O release between 100–200 °C, consistent with reduced bound water in low-temperature hydrates, by approximately 1 % in the case of reference composite FR. This phenomenon is known as the conversion process, an inevitable phenomenon in calcium aluminate cement systems. However, when focused on the ternary binder-based composites, there were still observable peaks at a temperature of approximately 170 °C, which further support the possibility of phase modification toward more

stable phases (such as C-A-S-H). In addition, after 1 year of curing, the amount of fixed water in the hydration phases remarkably increased due to the application of alternative binders. This time, the A15-C15 and A15-C30 showed even by 0.2 % and 1.3 % higher amount of fixed water compared to the reference FR. This finding further supports the assumption that hydration was, due to the ceramic powder and reactive alumina application, noticeably slower, as was observed in the results of isothermal calorimetry (Fig. 7). Another distinctive difference was observed in the temperature range of 650–720 °C. Regarding the possible component, this can be attributed to the remarkably higher amount of katoite C_3AH_6 in the mixtures. This hydrate, during dehydration, can form intermediate phase $C_{12}A_7H$, which exhibits a decomposition temperature of 690–750 °C [63], closely aligning with the observed thermal range. To complement the description of the results after 1 year, it should be noted that the ternary binder-based composites showed a less pronounced endothermic peak after 1200 °C, indicating a more advanced degree of pre-sintering or phase consolidation occurring during long-term hydration.

4.2.3. Phase composition

To support the assumption from STA, the phase compositions of studied composite after varying temperature treatments and in time were determined using XRD. The results of phase composition at the age of 28 days are summarized in Fig. 11. Reference composite FR at ambient temperature proved to have a not-converted composition, as it contained a noticeable amount of metastable CAH_{10}. It also contained C_2AH_8, but this phase had no well-defined structure, and thus it was not possible to quantify it by Retvieled refinement [59]. Katoite C_3AH_6 was also present, but it was not a dominant hydration product. In addition, the studied paste was somewhat carbonated as it contained not non-negligible amount of monocarboaluminate. Regarding the aluminate hydrates, apart from amorphous AH_3, the paste contained about 6 % of gibbsite. However, a substantial amount of cement (about 57 %) remained unhydrated.

When ceramic powder and reactive alumina replaced the calcium aluminate cement in the mixtures, the nature of C-A-H phases remained unchanged, but their amount was reduced accordingly, while the amount of aluminate hydrate A-H remained equal. Nevertheless, a substantial change was observed in the case of unhydrated grains of CAC, whose amount went down remarkably. The decrease is much greater than what could be attributed solely to the lower amount of grossite CA_2 and krotite CA in the mixtures (by average on 55 % for CA_2 and 33 % for CA). This observation indicates that the used admixtures enhanced the hydration degree of calcium aluminate, probably also providing more nucleation sites at the beginning of the main hydration reaction. Regarding the other components, when reactive alumina was used, about 10 % of it remained unchanged. Contrary ceramic powder confirmed its contribution to the previously described phase modification, as the ternary binder-based composite contained a noticeable amount of stratlingite C_2ASH_8 and gismondine CAS_4H_9 in addition also much higher amount of amorphous matter.

As the temperature increased, the hydration-related phases, such as CAH_{10}, katoite C_3AH_6, monocarboaluminate $CA\hat{C}H$, and gibbsite AH_3, gradually disappeared, confirming their thermal instability. Similarly, phases like stratlingite C_2ASH_8 and gismondine CAS_4H_9, which formed at ambient conditions, diminished and were eliminated at higher temperatures, indicating limited thermal durability. In the case of katoite C_3AH_6, two varying partial dehydration products were identified after 400 °C, namely $C_{12}A_7H$ and C_4A_3H, while the other hydrates proved to be completely dehydrated. In contrast, high-temperature stable phases such as grossite CA_2 and krotite CA increased sharply with heating. In the case of reactive alumina application, a higher amount of alumina seemed to modify the equilibrium at higher temperatures, as a substantial amount of hibonite CA_6 recrystallised at the expense of krotite CA. When focused on ceramic powder, it provided an amount of silica, which led to the formation of gehlenite C_2AS, wollastonite CS, and mullite A_2S, signifying solid-state reactions and recrystallization. Meanwhile, amorphous and non-identified phases generally decreased with temperature loading, dropping from 26 % to 41 % at 20 °C to as low as 9–19 % at 1000 °C. With further temperature growth to 1400 °C,

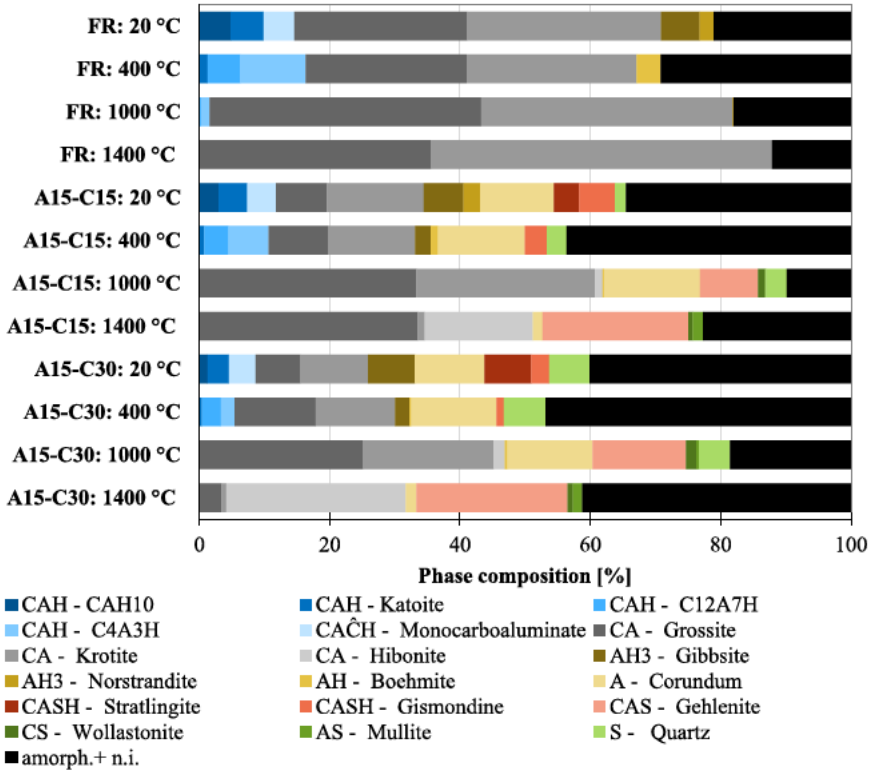

Fig. 11. Summary of phase composition of studied binders at 28 days.

the amorphous matter continued to fall only in the case of reference composite FR. In the case A15-C15 and A15-C30, likely due to the partial melting and fusion, the amount of amorphous matter increased significantly, reaching 22 % and 42 %, respectively.

After 1 year, samples were also undertaken for the temperature exposure and subsequent phase analyses. The results are summarized in Fig. 12. At ambient temperature, all studied systems (FR, A15-C15 and A15-C30) showed a significant increase in the amount of hydration products and a decrease in calcium aluminates, which correspond to the continuous hydration. In addition, as the CAH_{10} disappeared, while the amount of katoite C_3AH_6 and crystal AH_3 (in the form of gibbsite and nordstrandite) went up, the matrices seemed to be completely converted, containing only thermodynamically stable phases. At 400 °C, a key difference was the greater presence of intermediate dehydration products after 1 year. $C_{12}A_7H$ and C_4A_3H appeared in higher amounts in aged samples. This can be explained by a higher amount of more structured hydrates, which then decomposed into well-defined intermediates upon heating. Despite these changes, the higher temperature exposure to 1000 °C and 1400 °C showed only minor modification of the amount of observed phases and thus they can be considered as negligible.

4.3. Basic physical properties

Bulk density and matrix density belong to the fundamental basic physical properties together with porosity or, more precisely, pore structure. The reached values of densities are presented in Fig. 13. When focused firstly on the bulk density, it is visible that the reference composite reached the highest values, and the application of ceramic powder and reactive alumina caused a minor fall of this property by 0.5 % and 1.7 % for A15-C15 and A15-C30, respectively. Regarding the impact of temperature loading, with increasing temperature loading, residual bulk densities progressively decreased. The biggest difference was observed between 1000 °C and 1400 °C, which corresponded with the biggest changes in the phase composition and structure of the composites. During the time values of bulk density did not change significantly.

Concerning the matrix densities, they showed a reverse trend; reference composite FR reached the lowest values among the studied materials. This can be directly linked with the specific gravity of observed phases, where calcium aluminate hydrates C-A-H have, in general, lower gravity than aluminate hydrates A-H and calcium aluminate silicate hydrates C-A-S-H [50]. Regarding the impact of temperature, continuous dehydration led to the formation of denser dehydrated phase, which caused the residual matrix density increase, on average by 6 % up to 1000 °C. Beyond this point, at higher temperatures, sintering and partial melting processes caused matrix density values to decrease by approximately 2 % in the case of the reference composite FR, and by about 4 % when alternative admixtures were used.

The results of porosity are presented in Fig. 14a. It is visible, that at 20 °C, porosity ranged from 11 % to 14 %, with the reference composite FR exhibiting the lowest values and A15-C30 showing slightly higher porosity, likely due to the incorporation of fine ceramic powder and reactive alumina, which influenced early-stage microstructure. Concerning temperature treatment, all composites showed a progressive increase in porosity from 20 °C to 1400 °C. At 400 °C, porosity values rose by 64 % for FR and by 46 % for A15-C30, primarily due to the dehydration of hydration products. Following the results of the STA (Fig. 10), the mass decrease in this temperature range correlated well with the rise of porosity; more specifically, the higher the mass loss was, the bigger the increase in porosity composite showed. This phenomenon highlighted the direct relationship between dehydration intensity and microstructural opening. After exposure to 1400 °C, residual porosity reached the maximum values despite the occurrence of sintering. However, the extent of porosity growth was much lower in the case of ternary binder-based systems: reference composite FR reached by 137 % higher residual porosity (compared to ambient temperature), while composite A15-C15 showed the growth by 105 % and A15-C30 even by only 89 %. This suggested that ceramic admixtures enhanced sintering behaviour and limited porosity growth at extreme temperatures.

When comparing samples after 1 year of curing to their 28-day

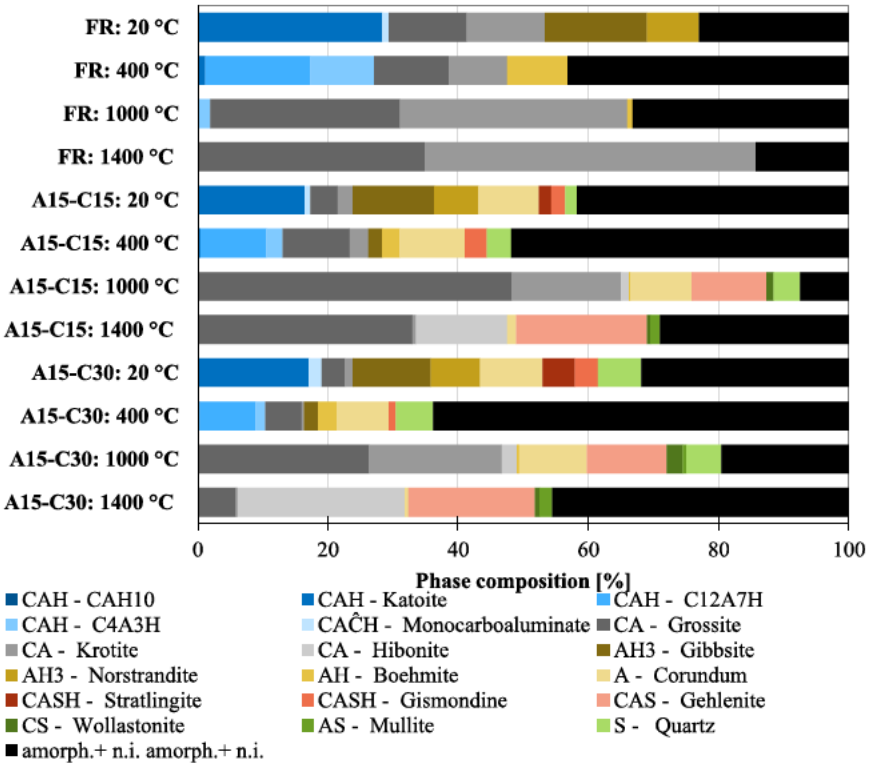

Fig. 12. Summary of phase composition of studied binders at 1 year.

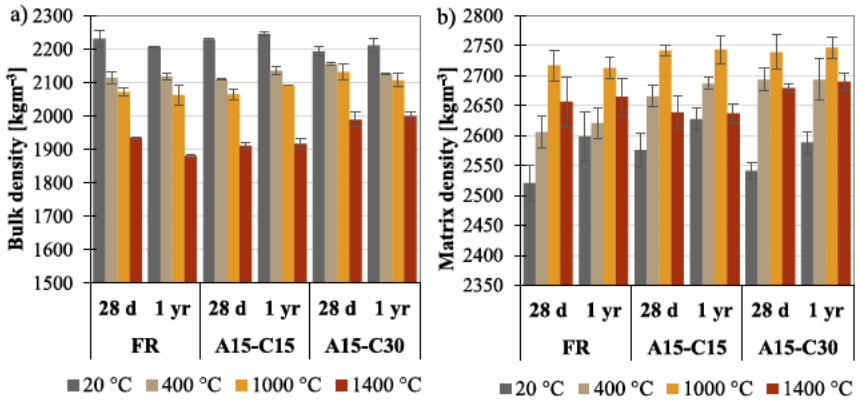

Fig. 13. Densities of studied composites: a) bulk density, b) matrix density.

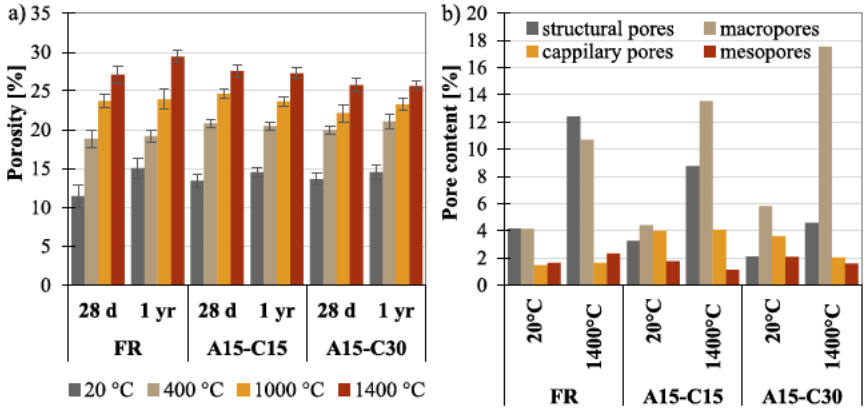

Fig. 14. Porosity of studied composites: a) overall porosity in time, b) structure of pores for selected composites.

counterparts, porosity values showed a modest increase across all temperatures. At 20 °C, long-term curing led to an increase of porosity by approximately 31 % in the case of reference composite FR. This was likely due to the conversion process, which is known by porosity growth. In accordance with the presented results of STA and XRD, the ceramic powder and reactive alumina decrease the degree of conversion, or, more precisely, the amount of metastable hydrates in the matrix. Therefore, the porosity growth in time was, in the case of ternary binder-based composites, much lower; specifically by 8 % for A15-C15 and by 7 % for A15-C30. At elevated temperatures, the effect of aging became evident in the case of reference composite FR. This material reached by 8 % higher value of residual porosity after 1 year (compared to the value at 28 days), suggesting that the changes in microstructure at ambient temperatures also somewhat affected the structure after exposure to high temperatures. On the contrary, for the composites containing ceramic powder and reactive alumina, the effect of aging was much less pronounced. When comparing residual porosities after 1400 °C at 28 days and 1 year, they differ only by 1 % and 0.5 % for A15-C15 and A15-C30, respectively. Such a variation fell within the accuracy of the measurement. This indicates that while aging modifies the microstructure, thermal exposure remains the dominant factor influencing porosity evolution in ternary binder-based composites

In general, the more important parameter, that only the value of total porosity is distribution and characteristics of the pore structure itself. On that account, MIP was conducted on selected composites FR, A15-C15, and A15-C30 at 28 days at ambient conditions (20 °C) and after thermal exposure to 1400 °C. Fig. 14b provide a summary of pore structure refinement, while in following Fig. 15, there are presented the pore size

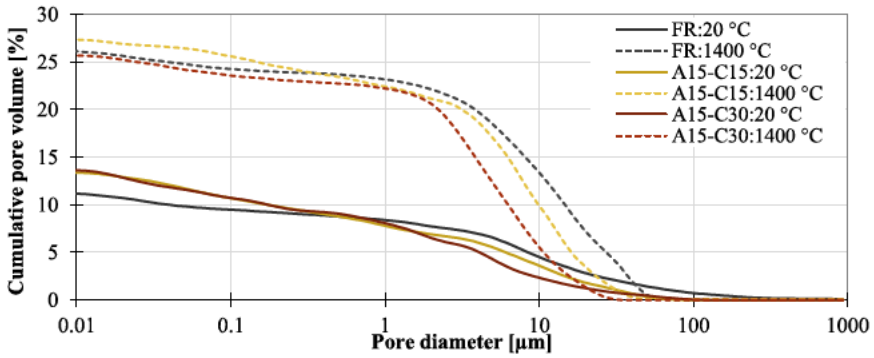

Fig. 15. Pore structure of selected composites at 28 days.

distributions curves. At 20 °C, all samples exhibited a similar overall shape in their cumulative pore volume curves. However, composite A15-C30 displayed the lowest content of structural pores and cracks (with a diameter over 10 μm), followed by A15-C15 and FR. This confirms the beneficial role of ceramic powder in promoting finer microstructure as observed also by SEM (Fig. 8). Conversely, in the range of smaller pores, this tendency was reversed. The composites with alternative admixtures exhibited slightly higher cumulative volumes of macropores (1–10 μm) and significantly higher content of capillary pores (0.05–1 μm), suggesting higher permeability of ternary binder-based composites. When focused specifically on mesopores (2–50 nm), their content appeared relatively comparable among all studied composites, indicating that the admixtures had a limited impact on the development of the finest pore network.

Thermal exposure had an immense impact on the pore structure of all studied composites. With increasing temperature, the cumulative pore volume curves shifted toward larger pore diameters, indicating progressive coarsening of the microstructure. This shift was most pronounced in the reference composite FR, where a substantial increase of approximately 197 % in the volume of macropores and structural voids (above 10 μm) and of 157 % in the case of large macropores (1–10 μm) was observed. In contrast, the composites incorporating ceramic powder and reactive alumina (A15-C15 and A15-C30) exhibited a markedly finer pore structure even after high-temperature exposure. Not only that, the increase of structural pores and macropores was lower (by 169 % for A15-C15 and by 1147 % for A15-C30), but they also showed a smaller maximal diameter of pores; specifically, 135 μm for FR contrary to 45 μm for A15-C15 and 34 μm for A15-C30. When focused on capillary pores and mesopores, some pore enlargement occurred in the case of reference composite. Contrary, in the case of ternary-binders, the decrease of the content of these pores was observed, indicating effective sintering and phase consolidation. The reduced pore coarsening in these ternary systems can be attributed to the formation of high-temperature crystalline phases such as gehlenite, mullite, and hibonite, which provided thermal stability and structural rigidity.

4.4. Mechanical parameters

The evolution of compressive strength over time and under various thermal conditions further emphasised the benefits of ternary binder systems incorporating ceramic powder and reactive alumina. As shown in Fig. 16a, at 28 days, the reference composite FR reached quite a high compressive strength of 95 MPa, falling into the scope of high-performance concretes. However, mixture A15-C15 outperformed it significantly, gaining by approximately 13 % higher value. This confirmed the beneficial effect of combining ceramic powder and reactive alumina in enhancing early-age mechanical performance. On the other hand, A15-C30, containing a high dosage of admixtures, initially showed slightly lower strength (by 2 % lower compared to reference FR), likely due to its increased porosity and altered hydration dynamics.

When subjected to elevated temperatures, the ternary binder-based composites demonstrated superior residual compressive strength compared to the reference. The FR mixture experienced continuous degradation with rising temperatures, decreasing by 28 % at 400 °C and further by 42 % after exposure to 1400 °C. When ceramic powder and reactive alumina were used, a similar trend of residual compressive reduction was observed within the temperature range up to 1000 °C, but the decreases were generally somewhat less pronounced. Remarkably, after exposure to 1400 °C the performance of the ternary-blended binders significantly improved due to sintering and partial fusion of phases. In these cases, compressive strength values recovered and approached their original levels. Specifically, the residual compressive strength at 1400 °C was only by 19 % and even by 7 % lower for A15-C15 and A15-C30 respectively (compared to their values at ambient temperature)

With prolonged curing to 1 year, the impact of aging on compressive strength varied depending on the composition. In the case of FR, the conversion process resulted in slight strength losses at all temperatures, with residual strength at 1400 °C falling even by 52 %. Contrary, composite A15-C15 exhibited minimal changes over time, retaining its strength remarkably well (1 % variation at 20 °C and 20 % decrease after exposure to 1400 °C), suggesting hydration stabilization and microstructural consistency. Interestingly, A15-C30 showed the most significant strength gains over time, reaching by 13 % higher value at ambient temperature. This confirmed the slower hydration process of composites with alternative admixtures. Regarding the residual compressive strength of the A15-C30, also in this case, the composites proved to perform well, as the fall was compared to the ambient temperature of only 4 %.

The analysis of flexural strength Fig. 16b) further complemented the findings observed in compressive strength tests, highlighting both the benefits and limitations of the ternary binder systems under thermal and aging effects. At ambient temperature, the composites FR and A15-C15 mixtures reached a comparable value of flexural strength varied only by 1 %, while composites A15-C30 showed a moderately lower value by about 14 % compared to the reference FR, consistent with its slightly lower early-age compressive strength and increased porosity.

When exposed to elevated temperatures, the differences among the mixtures became more evident. The FR composite showed a moderate decline in strength at 400 °C (by 44 %) and further increased (by 11 % compared to ambient temperature) after exposure to 1400 °C. Interestingly, the residual flexural strength did not follow the same trend as the residual compressive strength, which remained low after 1400 °C. Despite that, this performance is not common; it can be explained by surface sintering. High temperature exposure caused the formation of

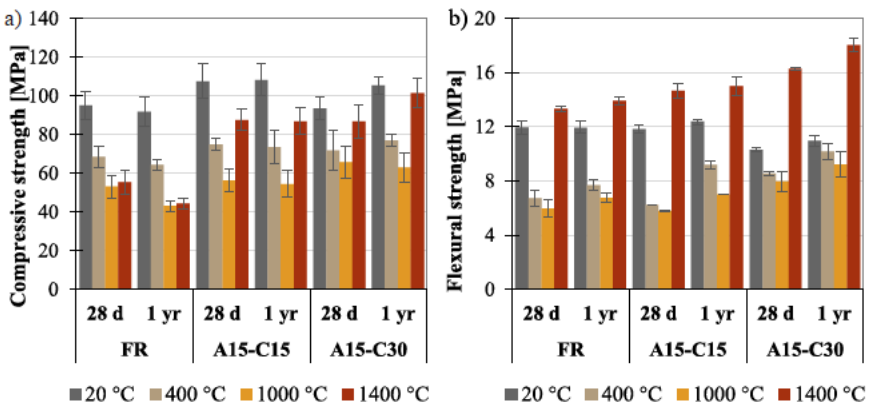

Fig. 16. Mechanical strength of studied composites: a) compressive strength, b) flexural strength.

dense, glassy or partially melted phases near the outer zones of the sample. This is accompanied by the healing of surface microcracks, closing pores, and improving tensile load transfer, consequently leading to higher flexural strength (which is more surface-sensitive). Contrary, in the case of compressive strength, bulk material (not just the surface) matters more. If the core remains porous, cracked, or thermally damaged, the compressive strength may still be low. Composite A15-C15 followed a similar thermal trend as the reference FR, decreasing by 47 % at 400 °C but increasing by 24 % after 1400 °C. In contrast, A15-C30 displayed markedly superior thermal resistance, with values falling only by 17 % at 400 °C and growing by 58 % at 1400 °C, showing the maximal observed flexural strength. This behaviour mirrored its performance in compressive strength tests and indicated enhanced sintering and phase bonding at high temperatures.

Focusing on the development of flexural strength in time, prolonged curing to 1 year further emphasized the advantages of the ternary systems. The FR composite remained largely stable over time, while A15-C15 showed slight improvement across all temperatures. A15-C30 demonstrated the most notable long-term development, with its flexural strength increasing by 6 % at ambient temperature and peaking at 65 % higher value of residual flexural strength at 1400 °C. This confirmed the continued hydration and phase consolidation over time, which contributed to superior mechanical integrity. As with compressive strength, the flexural performance strongly supported the effectiveness of ceramic powder and reactive alumina in producing thermally resilient and mechanically durable composites.

The last studied mechanical property was the dynamic modulus of elasticity, whose results are presented in Fig. 17. At ambient temperature after 28 days, the reference composite FR reached the highest value. In contrast, ternary binder-based composites reached by 7 % and 13 % lower dynamic modulus. This reduction can be attributed to the initial dilution effect of replacing cement with reactive alumina and ceramic powder, which may slightly reduce early stiffness due to slower reactivity and microstructural refinement, resulting in higher porosity at this age.

Regarding the temperature exposure, the residual dynamic modulus of elasticity followed the trend observed in other mechanical parameters: a significant decrease up to 1000 °C and a subsequent growth at the exposure to 1400 °C. This again corresponded well with the progressive dehydration and microstructural destabilization confirmed by STA (Fig. 10) and porosity (Fig. 14). Regarding the highest temperature 1400 °C, as previously mentioned, the dynamic modulus partially recovered, especially in the case of A15-C30. This composite reached only by 12 % lower value compared to the ambient temperature, surpassing all other formulations.

After 1 year, A15-C30 exceeded the initial modulus of the reference mix and showed the highest increase in the dynamic modulus. Specifically, the growth was by 6 %, while composites FR and A15-C30 exhibited a decrease of 3 % during the aging. This increase suggests long-term pozzolanic activity of the used admixtures together with the filler effect of the ceramic powder, leading to the formation of additional hydrates and a denser microstructure. These results highlight that while reactive alumina–ceramic blends may compromise early-age stiffness, they contribute positively to long-term mechanical performance.

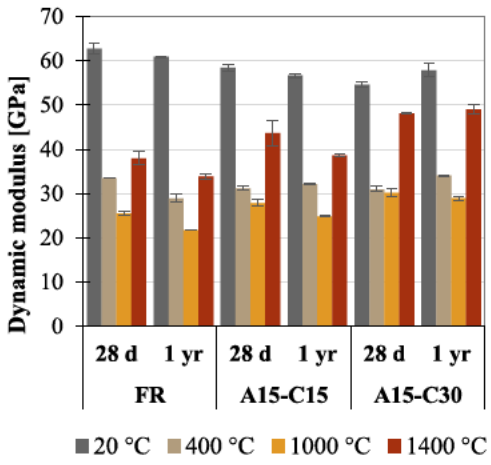

Fig. 17. Dynamic modulus of elasticity of studied composites.

4.5. Thermal characteristics

4.5.1. Thermophysical properties

Thermal conductivity and specific heat capacity belong among investigated thermophysical properties. Their values can be found in Fig. 18a. Thermal conductivity was evaluated to assess the heat transfer capacity of the studied composites under various thermal conditions. At 20 °C and 28 days, the reference composite FR reached the highest value of thermal conductivity, while composite A15-C15 exhibited by 13 % and A15-C30 by 14 % lower values. This variation reflects the influence of the admixture composition on microstructure, particularly on porosity and phase composition. Specifically, the application of ceramic powder and reactive alumina led to the reduction of crystalline phases (having generally a higher thermal conductivity) and porosity growth, which consequently influenced the reduced thermal conductivity.

As temperature increased, all composites showed a decrease in thermal conductivity up to 1000 °C, followed by a partial recovery at 1400 °C. This pattern corresponds to progressive dehydration, increased porosity, and eventual sintering, as described also in mechanical performance. Regarding the difference between particular materials, all studied composites showed similar rates of the residual thermal conductivity changes, falling into the scope of the accuracy of used measurement methods.

When comparing the values after 1 year, only minor changes were observed. Specifically, a negligible decrease of approximately 1 % occurred at lower temperatures, while slight increases were recorded at higher temperatures, such as 2 % at 1400 °C. Generally speaking, from the point of view of thermal conductivity, there was no distinctive difference between ternary binder-based composites, as both A15-C15 and A15-C30 reached comparable values.

Specific heat capacity was also examined to evaluate the thermal energy storage potential of the composites at various temperatures. The measured values are presented in Fig. 18b. At 20 °C and 28 days, the lowest specific heat capacity was recorded for composite FR, followed by A15-C15 and A15-C30. This ranking suggests that admixtures based on reactive alumina and ceramic powder can enhance the composite's ability to store thermal energy. The increased specific heat in A15-C30 and A15-C15 likely results from the higher content of amorphous phases and fine particles, which raise internal surface area and thermal inertia. In contrast, FR, composed primarily of crystalline hydrates, exhibited the lowest heat capacity, in line with its denser and more structured matrix.

As temperature increased, the specific heat capacity of all composites initially rose, peaking at 1000 °C and then after 1400 °C, they showed a moderate increase or remained steady. Interestingly, FR showed the highest values at elevated temperatures and the highest growth of 21 %, while A15-C15 and A15-C30 displayed lower values at both 1000 °C and 1400 °C and lower increase by 6 % and 1 %, respectively. This behaviour could be attributed to the early onset of structural transformations and dehydration in ternary binders, which may reduce the heat storage capacity relative to the matrix of FR.

After 1 year of curing, similarly to thermal conductivity, only moderate changes in specific heat capacity were observed across all temperatures. These results suggest that long-term hydration and structural stabilization have only a limited impact on the specific heat capacity, with most changes governed by high-temperature phase behaviour rather than aging.

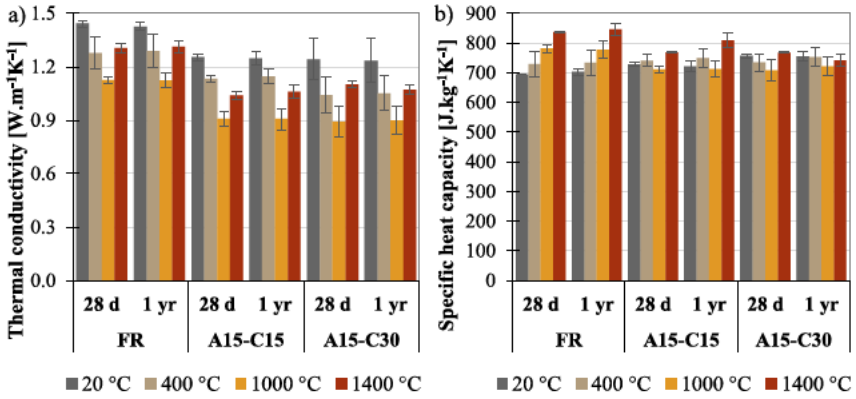

Fig. 18. Thermal properties of the studied composites.

4.5.2. Thermomechanical deformation

The thermal strain behaviour of the investigated materials reveals distinct responses linked to their compositional differences and corresponding phase transformations. At ambient temperature, reference composite FR showed the highest thermal expansion coefficient, as shown in Table 3, and ceramic powder and reactive alumina decrease this value. During the temperature exposure, all three samples (FR, A15-C30, and A15-C15) exhibit an initial thermal expansion comparable (Fig. 19), with notable divergences emerging up to 400 °C affected by dehydration processes (Fig. 10). The reference sample (FR) demonstrates the steepest thermal strain profile, attributed to the higher amount of hydrated phases (Fig. 11). A similar trend was observed in A15-C15, which showed similar but slightly lower values of thermal strain. On the contrary, composite A15-C30 with the lower amount of hydration products showed noticeably lower values of thermal strain. During the further temperature increase from 400 to about 900 °C, all composites showed constant growth of thermal strain and equal value of thermal expansion coefficient. At approximately 900 °C the recrystallization of the thermally stable phases (such as krotite CA and grossite CA_2 or gehlenite C_2AS) caused a minor drop of thermal strain. Continuous temperature growth caused further thermal strain up to 1200 °C. This temperature appears to be critical for the studied composites, as it marks the onset of more profound microstructural evolution. Beyond 1200 °C, particularly in the A15-C30 composite, a significant drop in thermal strain was observed, likely due to viscous sintering or the formation of a transient liquid phase in regions rich in amorphous or metastable phases. In contrast, the FR and A15-C30 samples maintained more stable strain values, indicating the formation of well-crystallized, high-temperature phases that reinforce structural integrity. These findings highlight the essential role of composition, particularly the balance of cement and ceramic additives, in governing the thermal stability and phase evolution of alumina-based refractory composites.

Table 3
Thermal expansion coefficient [10^6 K ^{1}].

State	FR		A15-C15		A15-C30	
	28 d	1 yr	28 d	1 yr	28 d	1 yr
Ambient temperature (20 °C)	7.7	5.9	6.7	4.6	5.2	4.5
Dehydration range max (60–400 °C)	11.8	7.4	11.4	5.0	8.5	5.1
Dehydration range min (60–400 °C)	−4.7	−3.7	−4.6	−5.8	−5.0	−6.1
Steady state (400–800 °C)	5.1	5.3	5.7	5.3	5.1	5.2
1st recrystallisation (900 °C)	−1.2	−0.3	0.2	−1.2	1.0	−1.3
Before sintering and melting (1200 °C)	8.9	10.2	9.7	9.4	11.8	10.9
Maximal temperature (1400 °C)	46.0	84.5	70.2	87.6	53.2	42.4

When focused on the impact of aging, up to 1200 °C, the performance remain comparable, with only minor modifications. However, after this threshold temperature, the promoted microstructural reorganization, phase stabilization, and densification proved to have an immense influence on the thermal response. In the aged samples, a noticeable reduction in thermal strain drop in the sintering and melting range values was observed compared to the unaged counterparts. Overall, aging improves the thermal stability and reduces the thermal strain of the composites, especially in systems enriched with ceramic additives, by fostering the formation of a robust and well-crystallized microstructure capable of withstanding high-temperature service conditions.

5. Conclusion

This study explored the influence of partial replacement of calcium aluminate cement (CAC) with ceramic powder and reactive alumina on the thermal, physical, and mechanical performance of refractory composites. The results demonstrated that while high levels of ceramic powder alone led to increased porosity and reduced compressive strength at ambient temperature, its combination with reactive alumina produced a synergistic effect, enhancing both initial and residual mechanical properties. Notably, ternary systems A15-C15 and A15-C30 achieved compressive strengths comparable or superior to the reference mix and exhibited great performance also after thermal exposure up to 1400 °C.

The characterization data revealed that while ceramic powder reduced the reactivity and delayed hydration onset, reactive alumina effectively promoted more complete and structured hydration. These differences were evident in isothermal calorimetry, where the total heat evolution in A15-C15 closely matched that of the reference mix (FR), while A15-C30 showed significantly reduced heat release, suggesting a fundamentally altered hydration pathway.

Thermal analysis revealed that the incorporation of ceramic powder modified the hydration mechanism, promoting the formation of calcium aluminosilicate hydrates and reducing the extent of metastable hydrate conversion. Furthermore, phase analysis showed that ternary composites facilitated more complete hydration, higher amorphous content, and enhanced high-temperature phase formation, contributing to improved structural integrity. Long-term aging confirmed the durability of these composites with stable phase evolution.

In terms of physical and mechanical properties, the use of ceramic powder slightly reduced bulk and matrix densities but contributed to the refinement of the pore structure and thermal insulation ability. Importantly, high-temperature exposure revealed that composites with ceramic and alumina additives experienced lower porosity growth and, therefore also better mechanical performance. Particularly, A15-C15 demonstrated the best balance between early hydration and

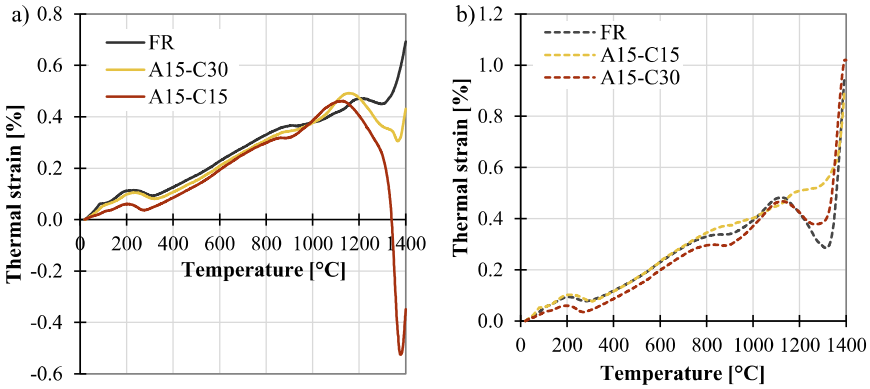

Fig. 19. Thermal strain of studied composites: a) at 28 days, b) after 1 year.

mechanical durability, while A15-C30 excelled in high-temperature strength due to a more sintered and densified microstructure.

Overall, the study confirmed that up to 60 % of CAC can be successfully replaced by a blend of ceramic powder and reactive alumina without compromising, and in some cases even enhancing, mechanical and thermal performance. This approach not only improves sustainability by utilizing waste materials but also yields high-performance composites suitable for demanding thermal applications.

CRediT authorship contribution statement

Kateřina Šádková: Writing – original draft, Investigation. **Romana Vaníčková:** Investigation, Data curation. **Dana Koňáková:** Writing – original draft, Data curation, Conceptualization. **Eva Vejmelková:** Writing – review & editing, Resources, Data curation. **Vojtěch Pommer:** Supervision, Investigation, Data curation. **Martin Keppert:** Validation, Investigation.

Declaration of Competing Interest

The authors declare that they have no known competing financial interests or personal relationships that could have appeared to influence the work reported in this paper

Acknowledgement

This research has been supported by the Czech Science Foundation under project No 23–04772S, and by the Czech Technical University under project SGS25/116/OHK1/3T/11.

Data availability

Data will be made available on request.

References

[1] O. Arioz, Effects of elevated temperatures on properties of concrete, Fire Saf. J. 42 (2007) 516–522, https://doi.org/10.1016/j.firesaf.2007.01.003.
[2] K.D. Hertz, Concrete strength for fire safety design, Mag. Concr. Res. (2005) 445–453 (n.d.).
[3] G.A. Khoury, C.E. Majorana, F. Pesavento, B.A. Schrefler, Modelling of heated concrete, Mag. Concr. Res. (2002) (n.d.).
[4] A. Sadrmomtazi, S.H. Gashti, B. Tahmouresi, Residual strength and microstructure of fiber reinforced self-compacting concrete exposed to high temperatures, Constr. Build. Mater. 230 (2020) 116969, https://doi.org/10.1016/j.conbuildmat.2019.116969.
[5] N. Yüzer, F. Akoz, L.D. Oztürk, Compressive strength–color change relation in mortars at high temperature, Cem. Concr. Res. 34 (2004) 1803–1807, https://doi.org/10.1016/j.cemconres.2004.01.015.
[6] D. Koňáková, V. Pommer, K. Šádková, R. Černý, E. Vejmelková, High-temperature resistance of cement composites with randomly distributed aluminium silicate fibers, Cem. Concr. Compos. 145 (2024) 105339, https://doi.org/10.1016/j.cemconcomp.2023.105339.
[7] 13 - Calcium Aluminate Cements, in: Lea's Chemistry of Cement and Concrete, n.d.: pp. 713–782.
[8] S.R. Klaus, J. Neubauer, F. Goetz-Neunhoeffer, Hydration kinetics of CA2 and CA—Investigations performed on a synthetic calcium aluminate cement, Cem. Concr. Res. 43 (2013) 62–69, https://doi.org/10.1016/j.cemconres.2012.09.005.
[9] A. Koehler, C. Roßler, J. Neubauer, F. Goetz-Neunhoeffer, Phase and porosity changes in a calcium aluminate cement and alumina system under hydrothermal conditions, Ceram. Int. 49 (2023) 4659–4667, https://doi.org/10.1016/j.ceramint.2022.09.353.
[10] X. Shang, G. Ye, Y. Zhang, H. Li, D. Hou, Effect of micro-sized alumina powder on the hydration products of calcium aluminate cement at 40 °C, Ceram. Int. 42 (2016) 14391–14394, https://doi.org/10.1016/j.ceramint.2016.06.005.
[11] E. Vejmelková, D. Koňáková, L. Scheinherrová, M. Doleželová, M. Keppert, R. Černý, High temperature durability of fiber reinforced high alumina cement composites, Constr. Build. Mater. 162 (2018) 881–891, https://doi.org/10.1016/j.conbuildmat.2018.01.076.
[12] M. Schneider, M. Romer, M. Tschudin, H. Bolio, Sustainable cement production—present and future, Cem. Concr. Res. 41 (2011) 642–650, https://doi.org/10.1016/j.cemconres.2011.03.019.
[13] S. Popovics, Concrete Materials - Properties, Specifications and Testing (2nd Edition), 2nd ed., William Andrew Publishing/Noyes, San Diego, n.d.
[14] K.L. Scrivener, V.M. John, E.M. Gartner, Eco-efficient cements: potential economically viable solutions for a low-CO2 cement-based materials industry, Cem. Concr. Res. 114 (2018) 2–26, https://doi.org/10.1016/j.cemconres.2018.03.015.
[15] Y. Geng, Z. Wang, L. Shen, J. Zhao, Calculating of CO2 emission factors for Chinese cement production based on inorganic carbon and organic carbon, J. Clean. Prod. 217 (2019) 503–509, https://doi.org/10.1016/j.jclepro.2019.01.224.
[16] D.-Y. Oh, T. Noguchi, R. Kitagaki, W.-J. Park, CO2 emission reduction by reuse of building material waste in the Japanese cement industry, Renew. Sustain. Energy Rev. 38 (2014) 796–810, https://doi.org/10.1016/j.rser.2014.07.036.
[17] A.C.P. Martins, J.M. Franco De Carvalho, L.C.B. Costa, H.D. Andrade, T.V. De Melo, J.C.L. Ribeiro, L.G. Pedroti, R.A.F. Peixoto, Steel slags in cement-based composites: an ultimate review on characterization, applications and performance, Constr. Build. Mater. 291 (2021) 123265, https://doi.org/10.1016/j.conbuildmat.2021.123265.
[18] E. Ozbay, M. Erdemir, H.I. Durmuş, Utilization and efficiency of ground granulated blast furnace slag on concrete properties – a review, Constr. Build. Mater. 105 (2016) 423–434, https://doi.org/10.1016/j.conbuildmat.2015.12.153.
[19] P.R. Da Silva, J. De Brito, Experimental study of the porosity and microstructure of self-compacting concrete (SCC) with binary and ternary mixes of fly ash and limestone filler, Constr. Build. Mater. 86 (2015) 101–112, https://doi.org/10.1016/j.conbuildmat.2015.03.110.
[20] O. Kayali, M. Sharfuddin Ahmed, Assessment of high volume replacement fly ash concrete – concept of performance index, Constr. Build. Mater. 39 (2013) 71–76, https://doi.org/10.1016/j.conbuildmat.2012.05.009.
[21] N.K. Lee, K.T. Koh, S.H. Park, G.S. Ryu, Microstructural investigation of calcium aluminate cement-based ultra-high performance concrete (UHPC) exposed to high temperatures, Cem. Concr. Res. 102 (2017) 109–118, https://doi.org/10.1016/j.cemconres.2017.09.004.
[22] E. Vejmelková, D. Koňáková, M. Čáchová, M. Záleská, P. Svora, M. Keppert, P. Rovnaníková, R. Černý, High-strength concrete based on ternary binder with high pozzolan content, Struct. Concr. 19 (2018) 1258–1267, https://doi.org/10.1002/suco.201700173.
[23] I. Pundiene, V. Antonovič, R. Stonys, M. Aleknevičius, I. Demidova-Buiziniene, A. Gailius, The effect of deflocculants on the structure and physical-mechanical properties of fireclay refractory castables, Ms 18 (2012) 390–395, https://doi.org/10.5755/j01.ms.18.4.3103.
[24] R. García, R. Vigil de la Villa, I. Vegas, M. Frías, M.I. Sánchez de Rojas, The pozzolanic properties of paper sludge waste, Constr. Build. Mater. 22 (2008) 1484–1490, https://doi.org/10.1016/j.conbuildmat.2007.03.033.
[25] L. Li, W. Liu, Q. You, M. Chen, Q. Zeng, Waste ceramic powder as a pozzolanic supplementary filler of cement for developing sustainable building materials,

J. Clean. Prod. 259 (2020) 120853, https://doi.org/10.1016/j.jclepro.2020.120853.
[26] X.W. Tan, A.P.P. Perera, A. Tan, D. Tan, K.A. Khor, R.W. Beuerman, J.S. Mehta, Comparison of Candidate Materials for a Synthetic Osteo-Odonto Keratoprosthesis Device, Invest. Ophthalmol. Vis. Sci. 52 (2011) 21, https://doi.org/10.1167/iovs.10-6186.
[27] L. Li, W. Liu, Q. You, M. Chen, Q. Zeng, C. Zhou, M. Zhang, Relationships between microstructure and transport properties in mortar containing recycled ceramic powder, J. Clean. Prod. 263 (2020) 121384, https://doi.org/10.1016/j.jclepro.2020.121384.
[28] M.I. Sánchez De Rojas, M. Frías, E. Sabador, E. Asensio, J. Rivera, C. Medina, Use of ceramic industry milling and glazing waste as an active addition in cement, J. Am. Ceram. Soc. 101 (2018) 2028–2037, https://doi.org/10.1111/jace.15355.
[29] R.D. Toledo Filho, J.P. Gonçalves, B.B. Americano, E.M.R. Fairbairn, Potential for use of crushed waste calcined-clay brick as a supplementary cementitious material in Brazil, Cem. Concr. Res. 37 (2007) 1357–1365, https://doi.org/10.1016/j.cemconres.2007.06.005.
[30] M.C. Bignozzi, S. Bonduà, Alternative blended cement with ceramic residues: Corrosion resistance investigation on reinforced mortar, Cem. Concr. Res. 41 (2011) 947–954, https://doi.org/10.1016/j.cemconres.2011.05.001.
[31] A.E. Lavat, M.A. Trezza, M. Poggi, Characterization of ceramic roof tile wastes as pozzolanic admixture, Waste Manag. 29 (2009) 1666–1674, https://doi.org/10.1016/j.wasman.2008.10.019.
[32] F. Puertas, I. García-Díaz, A. Barba, M.F. Gazulla, M. Palacios, M.P. Gómez, S. Martínez-Ramírez, Ceramic wastes as alternative raw materials for Portland cement clinker production, Cem. Concr. Compos. 30 (2008) 798–805, https://doi.org/10.1016/j.cemconcomp.2008.06.003.
[33] M.I. Sánchez De Rojas, F.P. Marín, M. Frías, J. Rivera, Properties and performances of concrete tiles containing waste fired clay materials, J. Am. Ceram. Soc. 90 (2007) 3559–3565, https://doi.org/10.1111/j.1551-2916.2007.01944.x.
[34] L.A. Pereira-de-Oliveira, J.P. Castro-Gomes, P.M.S. Santos, The potential pozzolanic activity of glass and red-clay ceramic waste as cement mortars components, Constr. Build. Mater. 31 (2012) 197–203, https://doi.org/10.1016/j.conbuildmat.2011.12.110.
[35] N. Ay, M. Ünal, The use of waste ceramic tile in cement production, Cem. Concr. Res. 30 (2000) 497–499, https://doi.org/10.1016/s0008-8846(00)00202-7.
[36] H. Binici, S. Kapur, J. Arocena, H. Kaplan, The sulphate resistance of cements containing red brick dust and ground basaltic pumice with sub-microscopic evidence of intra-pore gypsum and ettringite as strengtheners, Cem. Concr. Compos. 34 (2012) 279–287, https://doi.org/10.1016/j.cemconcomp.2011.10.001.
[37] M. Bediako, Pozzolanic potentials and hydration behavior of ground waste clay brick obtained from clamp-firing technology, Case Stud. Constr. Mater. 8 (2018) 1–7, https://doi.org/10.1016/j.cscm.2017.11.003.
[38] A. Naceri, M.C. Hamina, Use of waste brick as a partial replacement of cement in mortar, Waste Manag. 29 (2009) 2378–2384, https://doi.org/10.1016/j.wasman.2009.03.026.
[39] F. Bektas, K. Wang, H. Ceylan, Effects of crushed clay brick aggregate on mortar durability, Constr. Build. Mater. 23 (2009) 1909–1914, https://doi.org/10.1016/j.conbuildmat.2008.09.006.
[40] P.O. Awoyera, J.M. Ndambuki, J.O. Akinmusuru, D.O. Omole, Characterization of ceramic waste aggregate concrete, HBRC J. 14 (2018) 282–287, https://doi.org/10.1016/j.hbrcj.2016.11.003.
[41] B.B. Sabir, S. Wild, J. Bai, Metakaolin and calcined clays as pozzolans for concrete: a review, Cem. Concr. Compos. 23 (2001) 441–454, https://doi.org/10.1016/S0958-9465(00)00092-5.
[42] V.F. Rahhal, M.A. Trezza, A. Tironi, C.C. Castellano, M. Pavlíková, J. Pokorný, E. F. Irassar, O. Jankovský, Z. Pavlík, Complex characterization and behavior of waste fired brick powder-portland cement system, Materials 12 (2019) 1650, https://doi.org/10.3390/ma12101650.
[43] X. Chen, D. Zhang, S. Cheng, X. Xu, C. Zhao, X. Wang, Q. Wu, X. Bai, Sustainable reuse of ceramic waste powder as a supplementary cementitious material in recycled aggregate concrete: mechanical properties, durability and microstructure assessment, J. Build. Eng. 52 (2022) 104418, https://doi.org/10.1016/j.jobe.2022.104418.
[44] F. Pacheco-Torgal, S. Jalali, Reusing ceramic wastes in concrete, Constr. Build. Mater. 24 (2010) 832–838, https://doi.org/10.1016/j.conbuildmat.2009.10.023.
[45] V. Tydlitát, J. Zákoutský, P. Volfová, R. Černý, Hydration heat development in blended cements containing fine-ground ceramics, Thermochim. Acta 543 (2012) 125–129, https://doi.org/10.1016/j.tca.2012.05.022.
[46] T. Santos, V.V.S. Machado, O.H. Borges, V.R. Salvini, C. Parr, V.C. Pandolfelli, Calcium aluminate cement aqueous suspensions as binders for Al2O3-based particle stabilised foams, Ceram. Int. 47 (2021) 8398–8407, https://doi.org/10.1016/j.ceramint.2020.11.204.
[47] A. Halicka, P. Ogrodnik, B. Zegardlo, Using ceramic sanitary ware waste as concrete aggregate, Constr. Build. Mater. 48 (2013) 295–305, https://doi.org/10.1016/j.conbuildmat.2013.06.063.
[48] D.J. Martins, J.R. Correia, J. De Brito, The effect of high temperature on the residual mechanical performance of concrete made with recycled ceramic coarse aggregates, Fire Mater. 40 (2016) 289–304, https://doi.org/10.1002/fam.2287.
[49] A. Baradaran-Nasiri, M. Nematzadeh, The effect of elevated temperatures on the mechanical properties of concrete with fine recycled refractory brick aggregate and aluminate cement, Constr. Build. Mater. 147 (2017) 865–875, https://doi.org/10.1016/j.conbuildmat.2017.04.138.
[50] D. Koňáková, V. Pommer, M. Jerman, M. Keppert, R. Černý, E. Vejmelková, Utilization of ceramic powder, calcined shale and sintered mullite as partial replacements of calcium aluminate cement, Constr. Build. Mater. 326 (2022) 126824, https://doi.org/10.1016/j.conbuildmat.2022.126824.
[51] D. Koňáková, V. Pommer, K. Šádková, M. Záleská, M. Bohm, M. Keppert, E. Vejmelková, Heat-resistant composites based on ternary binders with a low cement content: characterization and performance, Dev. Built Environ. 18 (2024) 100400, https://doi.org/10.1016/j.dibe.2024.100400.
[52] D. Koňáková, K. Šádková, V. Pommer, E. Vejmelková, R. Černý, Characterization of low-cement heat resistant binder with high alumina content, in: Stavropol, Russia, 2023: p. 030016. https://doi.org/10.1063/5.0147154.
[53] K. Šádková, D. Koňáková, E. Vejmelková, V. Pommer, W.-T. Lin, R. Černý, Effect of heating temperature on the properties of low-cement heat resistant composites, in: Stavropol, Russia, 2023: p. 030005. https://doi.org/10.1063/5.0146714.
[54] N. Dobelin, R. Kleeberg, Profex: a graphical user interface for the Rietveld refinement program BGMN, (2015).
[55] ČSN E.N. 1015-11 (722400):. Methods of Test for Mortar for Masonry - Part 11: Determination of Flexural and Compressive Strength of Hardened Mortar, (2020).
[56] ČSN 73 1370 - Non-destructive testing of concrete - Ultrasonic pulse method for testing concrete, n.d.
[57] ASTM C618. Standard specification for fly ash and raw or calcined natural pozzolan for use as a mineral admixture in Portland cement concrete, (2003).
[58] ČSN EN 206+A2 (732403) Concrete - Specifications, properties, production and conformity, (n.d.).
[59] D. Koňáková, V. Pommer, K. Šádková, M. Keppert, R. Černý, E. Vejmelková, Impact of plasticizers' types on the performance of calcium aluminate cement, J. Mater. Res. Technol. 20 (2022) 1512–1523, https://doi.org/10.1016/j.jmrt.2022.07.155.
[60] Y. Yue, G. Melani, H. Kirsch, A. Paarmann, P. Saalfrank, R.K. Campen, Y. Tong, Structure and Reactivity of α-Al_2 O_3 (0001) Surfaces: How Do Al–I and Gibbsite-like Terminations Interconvert? J. Phys. Chem. C. 126 (2022) 13467–13476, https://doi.org/10.1021/acs.jpcc.2c03743.
[61] M.U. Okoronkwo, F.P. Glasser, Stability of stratlingite in the CASH system, Mater. Struct. 49 (2016) 4305–4318, https://doi.org/10.1617/s11527-015-0789-x.
[62] M.U. Okoronkwo, S.K. Mondal, B. Wang, H. Ma, A. Kumar, Formation and stability of gismondine-type zeolite in cementitious systems, J. Am. Ceram. Soc. 104 (2021) 1513–1525, https://doi.org/10.1111/jace.17572.
[63] M.C. Ball, The thermal dehydroxylation of C3AH6, Cem. Concr. Res. 6 (1976) 419–420, https://doi.org/10.1016/0008-8846(76)90107-1.

5 Fibre reinforcement

The incorporation of fibres into cementitious composites is a well-established method for enhancing mechanical performance, particularly tensile strength, toughness, and crack resistance. When fibres are applied to calcium aluminate cement (CAC) systems, the role and demands on fibre reinforcement become significantly more complex than in the case of PC. This complexity arises from the unique thermal and chemical environment associated with CAC applications, which frequently involve exposure to elevated temperatures, rapid heating, thermal cycling or an aggressive environment. In these conditions, fibres are not only expected to enhance mechanical properties during the initial curing and ambient temperature service life but must also retain their reinforcing capabilities after thermal exposure.

5.1 The role of fibres in high-temperature resistant materials

In fire-resistant concretes and composites, fibres fulfil two essential functions: preventing explosive spalling during thermal shock and enhancing fracture energy following high-temperature exposure.

The first group of fibres addresses the critical problem of explosive spalling, primarily caused by the rapid build-up of vapour pressure within the cement matrix during heating. This process is driven by the evaporation of both free and chemically bound water. While water vapour near the surface can escape readily, vapour trapped in deeper layers generates significant internal pressure, which may exceed the tensile strength of the material. In addition to moisture-related mechanisms, explosive spalling is further influenced by the thermomechanical behaviour of the composite under thermal gradients. Uneven heating causes differential thermal expansion and contraction among the material's constituents. Typically, aggregates expand when heated, whereas the dehydrated cement paste may shrink. This disparity induces internal shear stresses and progressively weakens the interfacial bonds between the matrix components. Moreover, rapid or uneven temperature rises within the composite can create significant thermal strain differentials, further contributing to internal stress accumulation. When the combined effects of vapour pressure and thermally induced stresses surpass the material's mechanical limits, sudden delamination of the surface layer may occur. This failure manifests as explosive spalling, resulting in violent fragmentation, which poses both safety risks and structural damage.

To mitigate this risk, fibres with low decomposition or melting temperatures below 200 – 300 °C are employed. Organic fibres are the most common representatives in this context, as their molecular decomposition temperature falls below 250 °C. These fibres are generally short (under 12 mm in length) and fine (with a diameter of about 20 µm). They are applied in relatively small quantities, typically between 0.02% and 0.1% by volume [39]. During heating, these fibres degrade, leaving behind channels that facilitate the release of vapour and thus prevent the accumulation of critical pore pressures. Beyond their primary function, these channels also enhance the transport of vapour and gases within the microstructure, marginally improving heat transfer. This improved permeability can help to moderate the temperature gradient between the heated surface and the cooler interior layers, thereby reducing the severity of thermally induced stresses. Nevertheless, it is important to emphasise that the overall thermal conductivity of fibre-reinforced cementitious composites remains relatively low, with heat transfer still dominated by conduction through the solid matrix. Consequently, the impact of these channels on reducing thermal gradients is secondary to their principal role in preventing vapour pressure accumulation.

The second group of fibres reinforces the cementitious matrix by enhancing its mechanical performance, both under ambient conditions and after exposure to elevated temperatures. These fibres primarily increase the fracture toughness, flexural strength, and energy absorption capacity of the composite, limiting the growth and propagation of microcracks and improving post-crack load-bearing behaviour. They also contribute to the residual mechanical strength of the material following thermal exposure, where the matrix alone may suffer from strength degradation. Compared to vapour-release fibres, these ones are larger (lengths up to 30 mm, diameters up to 0.4 mm) and are used in higher dosages, sometimes exceeding 6% by volume [39]. The choice of fibre type, geometry, and dosage depends on the specific mechanical performance requirements and the anticipated service temperature of the application. For high-temperature environments, such as industrial furnaces or refractory linings operating at temperatures up to 1200 °C, heat-resistant metallic fibres are commonly employed.

The most effective strategy for enhancing the fire resistance and mechanical performance of calcium aluminate cement composites appears to be the use of hybrid fibre reinforcement, combining fibres from both functional groups. This complementaryaction addresses both primary failure mechanisms: low-melting-point

organic fibres serve as a sacrificial phase that mitigates vapour pressure accumulation and prevents explosive spalling during the early stages of thermal exposure. Simultaneously, thermally stable metallic or mineral materials provide structural reinforcement, improving fracture toughness, crack bridging, and load-bearing capacity both before and after fire exposure. Such hybrid reinforcement allows for optimisation of the overall fibre dosage, balancing mechanical performance, spalling prevention, and processing workability.

5.2 Material basement

A wide variety of fibre materials has been studied for these applications, including organic polymers, metals, and inorganic minerals. Each class of fibres offers distinct physical and chemical properties such as thermal resistance, melting or decomposition temperature, mechanical strength, and chemical durability in alkaline environments. The balance between these characteristics determines the fibres' suitability for use in fire-resistant or mechanically demanding applications. Table 8 summarises the most commonly used fibres in CAC composites, highlighting their physical properties.

Table 8 Properties of some fibres used as concrete reinforcement [39,40]

Material	Density [kg.m^{-3}]	Average tensile strength [GPa]	Elastic Modulus [GPa]	Elongation at break [%]	Softening temp. [ºC]	Melting / decomposing temp. [ºC]
Carbon	1760	3.5	235	1.2	-	3500
Steel	7800	0.62	207	23	450-600	1440
Basalt	2700	4.84	110	3.1	800	1260
Glass	2580	3.445	76	4.8	700-750	846
PET	1500	1.2	14	8.5	230	260
Nylon	1140	0.47	3	30	190-220	241
PVA	1260	1.25	22	7.5	180-200	225
Coir	150	0.174	2.3	32	-	200
Bagasse	550	0.23	1.7	8.7	-	180
Flax	1450	0.7	6.7	2	-	165
PP	910	0.475	4.1	25	130-150	160
Hemp	1250	0.255	9.5	2.2	-	150
PE	920	0.103	130	45	90-110	120

5.2.1 Low melting point organic fibres

Polypropylene (PP) fibres belong among the most widely used reinforcements in cement-based composites which are supposed to be accidentally thermally loaded. These fibres typically exhibit lengths ranging from 6 to 12 mm and diameters of approximately 10 to 20 μm, with dosage levels generally between 0.02% and 0.1%. The decomposition of PP fibres occurs at relatively low temperatures (160 – 170 °C), at which point they thermally degrade and contribute to the reduction of the risk of explosive spalling. The dosage of 0.075 % by mass mitigates the intensity of spalling, while the higher dosage of about 0.1% by mass led to its prevention [41]. Quantitative studies have shown that PP fibres not only enhance fire resistance but also influence the mechanical performance of CAC at ambient temperatures. CAC composites with 1% by volume of PP showed 1.9%, 20% and 16.7 % of compressive, direct tensile, and flexural strengths increase at 28 days. However, these fibres caused a significant reduction in workability, and over 2% dosage of PP caused a significant decrease in mechanical strength [42]. It has been demonstrated that the incorporation of PP fibres significantly improves also the residual mechanical properties of CAC composites, confirming their essential role in fire resistance [43].

Polyethene (PE) fibres are also employed in fire-resistant cement-based composites, although they are less common than PP. These fibres are typically shorter (4 to 10 mm in length) and finer (diameters of 10 – 15 μm), and are applied in similar dosages ranging from 0.02% to 0.1% by volume. PE fibres decompose at lower temperatures (110 – 130 °C), making them effective in initiating early vapour release during the initial stages of heating. Experimental studies on CAC–GGBFS mortars reinforced with PE fibres revealed that these fibres improved strain-hardening behaviour and post-cracking performance at ambient conditions. 1% vol. of PE fibres in CAC-GGBFS mortar caused by 21% increase in compressive strength and by 26% higher tensile strength [44]. In addition, such material proved to have higher durability to sulfuric acid attack [45]. However, PE fibres were found to have a more pronounced negative effect on fresh mix workability due to their hydrophobic surface.

In conclusion, polymer fibres play a crucial role in enhancing the fire resistance and mechanical performance of calcium aluminate cement composites. Polypropylene (PP) fibres are the most widely used for spalling prevention, creating vapour-release channels upon thermal decomposition and improving both fire resistance and residual strength. However, their influence on mechanical properties at ambient temperature is

limited, and excessive dosages negatively affect workability. Polyethene (PE) fibres, though less common, similarly contribute to vapour release but at lower decomposition temperatures. They also enhance mechanical performance and chemical durability, but tend to reduce workability more significantly.

5.2.2 Thermally stable fibres

The most common representative of fibres used for the improvement of mechanical properties is steel fibres (SF). They typically have lengths ranging from 25 to 35 mm and diameters between 0.3 and 0.5 mm, and are applied at dosages from 1% to 6% by volume. SF are available in various forms, including straight, hooked-end, and crimped geometries, with hooked-end fibres being particularly effective in enhancing crack-bridging capacity. Their chemical composition, often chromium- or nickel-alloyed steel, is chosen to resist oxidation and maintain mechanical properties at elevated temperatures. SF preserve their structural integrity up to approximately 600 °C. At temperatures beyond 600 – 650 °C, they exhibit a pronounced reduction in yield strength and elastic modulus, although they continue to contribute to crack bridging and load transfer. For service temperatures approaching 1000 – 1200 °C, alloyed steels containing chromium or nickel are preferred, as they offer improved oxidation resistance and mechanical retention. Quantitative studies have shown that 1 vol.% SF resulted in notable enhancements of approximately 19.7%, 68%, and 26.4% in compressive, direct tensile, and flexural strengths [42]. Another study confirmed the positive effect, as 2 vol.% of SF increased the compressive strength of CAC-blended mixtures by 11% at ambient temperature, and by 38% after exposure to 1000 °C [43].

Basalt fibres (BF) have emerged as a thermally stable alternative for reinforcing calcium aluminate cement composites. Derived from natural volcanic rock, BF possess a softening temperature of approximately 800 °C and a melting point exceeding 1000 °C. BF are typically applied in lengths of 10 to 30 mm and dosages ranging from 0.5% to 3% by volume. Their primary functions are enhancing tensile strength, fracture energy, and resistance to thermal cracking. Regarding some quantitative studies, only a few investigations have been conducted in which BF were used in combination with CAC. However, it was reported that CAC-based foam concrete with 2% vol. of BF has slightly reduced workability, improved compressive strength by 9%, and flexural strength by 55%. In addition, application of BF leads to the reduction of drying shrinkage and a decrease in sorptivity by 41% [46].

Carbon fibres (CF) represent a high-performance reinforcement for CAC, particularly in applications where high strength and thermal stability are required. These fibres, typically applied in lengths of 6 to 12 mm and at dosages from 0.5% to 2% by volume, exhibit exceptional tensile strength and stiffness, while remaining thermally stable up to 3500 °C in inert environments. However, in air, carbon fibres begin to oxidise at temperatures as low as 400 – 600 °C, limiting their durability in oxidising high-temperature conditions unless protected by coatings or inert atmospheres. It was presented that the application of carbon fibres reduces the induction period of CAC hydration. When 0.6 mass% of CF was employed, cement pastes showed 23% higher compressive strength, and even 73% of flexural strength [47]. In the case of CAC mortar, 1% vol. of fibres led to a twofold increase in bending strength, and it was also reported that volume shrinkage during the hardening process was significantly reduced [48].

It is visible that the selection of fibres for CAC-based composites must balance mechanical reinforcement with thermal stability. Steel fibres remain the most effective for enhancing strength and toughness, though their performance diminishes beyond 600 °C without alloying. Basalt fibres offer a thermally stable alternative that improves tensile strength and crack resistance while maintaining integrity at temperatures above 800 °C. Carbon fibres, despite their superior mechanical properties and thermal stability in inert environments, face limitations in oxidising atmospheres due to their susceptibility to oxidation at elevated temperatures. Each fibre type offers distinct advantages, and their careful selection enables the design of CAC composites tailored for demanding fire-resistant and structural applications.

5.3 Author contribution – selected papers

In the field of fibre reinforcement, most research in high-temperature composites has been concentrated on PC matrices and conventional fibres such as steel or polypropylene, with limited attention given to CAC. Consequently, recent research has focused on evaluating fibre reinforcement strategies tailored specifically for CAC, aiming to enhance its mechanical stability, limit thermal strain, and improve residual properties after exposure to elevated temperatures. Particular emphasis has been placed on basalt and aluminino-silicate fibres, whose thermal stability makes them promising candidates for refractory and fire-resistant applications.

5.3.1 High-temperature resistance of concretes produced from two different cements

D. Koňáková, M. Čáchová, M. Doleželová, L. Scheinherrová, E. Vejmelková, R. Černý, Cement, Wapno, Beton 2016(5) (2016) 295-309 [49]

The selected paper contributes to the understanding of the durability and residual performance of CAC and PC composites exposed to elevated temperatures, with a particular focus on the influence of cement type and basalt fibre reinforcement. The research systematically compared four cement composites, examining the interplay between matrix composition and fibre reinforcement through the view of evaluation of a broad set of physical, mechanical, hygric, and thermal characteristics after exposure to 400 °C and 1000 °C.

Key findings demonstrated that CAC composites exhibited significantly higher thermal stability, maintaining up to 23% of their initial compressive strength after exposure to 1000 °C, compared to near-complete strength loss in PC systems. Basalt fibres contributed positively to mechanical performance and slightly mitigated thermal strain, although their effect on porosity and workability was modest.

Beyond mechanical strengths, the study provided valuable insights into hygric transport and thermal properties after high-temperature exposure, showing that CAC composites had higher open porosity but better resistance to deterioration of water transport and thermal conductivity. The research also analysed residual pore structures, thermal strain, and phase changes in both cement types.

This work advances the understanding of:

- The comparative fire resistance and durability of CAC vs. PC composites
- The role of basalt fibres in improving residual strength

The findings provide practical guidelines for selecting binder systems and fibre reinforcements in high-temperature structural and refractory concretes, contributing valuable data for both academic research and fire-safe design.

MIĘDZYNARODOWE CZASOPISMO NAUKOWE
POŚWIĘCONE ZAGADNIENIOM CHEMII
I TECHNOLOGII MATERIAŁÓW WIĄŻĄCYCH I BETONU

ROK XXI/LXXXIII
WRZESIEŃ – PAŹDZIERNIK 2016 r.
Nr 5

cement wapno beton

Czasopismo dostępne w wersji elektronicznej na stronie www.cementwapnobeton.pl

Dana Koňáková, Monika Čáchová, Magdalena Doleželová, Lenka Scheinherrová, Eva Vejmelková, Robert Černý

Department of Materials Engineering and Chemistry, Faculty of Civil Engineering, Czech Technical University in Prague, Czech Republic

Odporność na wysoką temperaturę betonów otrzymanych z dwóch różnych cementów

High-temperature resistance of concretes produced of two different cements

Słowa kluczowe: kompozyty cementowe, cement portlandzki, cement glinowy, włókna trwałe termicznie, wysokie temperatury, pozostałe właściwości

Keywords: cement composites, Portland cement, calcium aluminate cement, thermally stable fibers, high temperatures, residual properties

1. Wstęp

Beton jest materiałem o dużej odporności w stosunku do swojego otoczenia, szeroko stosowanym w budownictwie. Jednakże, istnieje duże prawdopodobieństwo wystąpienia uszkodzeń w ekstremalnych warunkach. Typowym przykładem takich warunków jest pożar i działanie wysokich temperatur. Do czynników, które mają duży wpływ na stopień uszkodzenia betonu w wysokich temperaturach, należą: szybkość wzrostu temperatury, maksymalny jej poziom, czas ekspozycji, szybkość chłodzenia z maksymalnej temperatury, warunki panujące po ochłodzeniu oraz poziom przenoszonego obciążenia (1, 2). Pomimo dużego wpływu wymienionych czynników, w rzeczywistości otaczające warunki mogą być trudne do przewidzenia, lub bardziej precyzyjnie, trudne do kontroli.

Innym ważnym czynnikiem wpływającym na odporność konstrukcji na pożar lub działanie wysokich temperatur jest skład betonu (3). W odróżnieniu od warunków temperaturowych, skład betonu można dostosować do wymaganej odporności termicznej. Problem projektowania cementowych materiałów kompozytowych, odpornych na działanie wysokich temperatur, jest złożony. Należy wziąć

1. Introduction

Concrete, in regards to its surroundings, is a highly resistant material widely used in the building industry. However, there is a high probability of damage l kely to occur when it is exposed to extreme conditions. A typical example of such situation is fire and the exposure to high temperatures. The parameters of heating, which has major impact on the degree of concrete damage, are the rate of heating, maximum attained temperature, duration of exposure, method of cooling after reaching the maximum temperature, post-cooling treatment and the level of applied load (1, 2). Despite the major impact of mentioned factors, in a real structure the surrounding conditions can be hardly predicted or, more precisely, they can be hardly influenced.

The specific composition of a cement composite is another important parameter affecting the resistance of a structure to fire or high temperatures (3). In a comparison with the parameters of heating, the composition can be optimized with respect to thermal resistance demands. The problem of designing cement composite materials resistant to high temperatures is a complex and in-depth

pod uwagę dwa główne aspekty: odporność stosowanych składników na podwyższoną temperaturę oraz zgodność ich właściwości w wysokiej temperaturze. Beton jest materiałem składającym się z wielu składników, głównie z matrycy cementowej, kruszywa, porów (wypełnionych powietrzem i roztworem o różnym stężeniu jonów), a także różnego rodzaju zbrojeniem. Defekty w betonie, takie jak pęknięcia, rozwarstwienia, osłabienie lub przerwanie wiązania między matrycą cementową a zbrojeniem lub odspojenie części warstw powierzchniowych wywołanych ogrzewaniem, są spowodowane głównie rozkładem uwodnionych faz, niezgodnością termiczną właściwości kruszywa i zaczynu cementowego oraz ciśnieniem powstającym w porach zaczynu cementowego (4).

W celu otrzymania betonu odpornego na wysokie temperatury, należy rozważyć zastosowanie cementu glinowego, o dużej zawartości Al_2O_3 (5). Oczywiście należy wziąć pod uwagę, że ze względu na przemianę fazową produktów hydratacji (6), betony z cementu glinowego mogą stracić około 30% do 50% swojej wytrzymałości. Dobrze znane jest zniszczenie kilku budynków w latach 1970 i 1980, w wyn ku czego zastosowanie betonu z ego cementu do wykonywania konstrukcji przenoszących obciążenia zostało zabronione. Niemniej jednak, beton z cementu glinowego, zachowuje się korzystnie w kontakcie z ogniem i wysokimi temperaturami, co jest nadal jego zaletą. W porównaniu z cementem portlandzkim, cement glinowy różni się zasadniczo składem fazowym: główną fazą jest glinian monowapniowy CA, obok którego, w przypadku dużej zawartości glinu, występuje dwuglinian wapnia CA_2 i $C_{12}A_7$ (7). Ta ostatnia faza jest prawie zawsze obecna w cemencie glinowym. Głównymi produktami hydratacji glinianów wapnia są nietrwałe gliniany wapnia: dziesięciowodny glinian wapnia CAH_{10}, ośmiowodny glinian C_2AH_8 oraz termodynamicznie trwały sześciowodny glinian trójwapniowy C_3AH_6 (8) i wodorotlenek glinu AH_3. Wiadomo, że proces hydratacji zależy w dużym stopniu od temperatury.

Kiedy zaczyn z cementu glinowego jest wystawiony na działanie podwyższonych temperatur, ulega on dużym zmianom (9). W temperaturze około 110°C odparowuje woda powierzchniowa i woda odparowywalna oraz usuwana jest woda związana w amorficznym żelu AH_3. W około 150°C rozpoczyna się proces dehydratacji uwodnionych glinianów wapniowych, a w 300°C zachodzi rozkład krystalicznego gibbsytu AH_3. W temperaturze 500°C, rozpoczyna się powstawanie fazy $C_{12}A_7$. Ze wzrostem temperatury przechodzi ona w glinian wapnia CA, a także w dwuglinian wapnia CA_2. W temperaturze wyższej od 1400°C powstaje CA_6.

Wzmocnienie betonu włóknami ma ważne znaczenie. Włókna są stosowane z ki ku powodów, przede wszystkim w celu zwiększenia wytrzymałości betonu na rozciąganie, zginanie i odporności na uderzenia, odporności na mróz, a także zmniejszenia skurczu oraz kruchości betonu. Wybór rodzaju włókien: ze stali, szkła, węgla lub organiczne, głównie polipropylenowe, zależy od oczekiwanych właściwości kompozytu. Należy wziąć pod uwagę, które właściwości będą w rozpatrywanym przypadku najważniejsze. W przypadku betonów odpornych na ogień, ważną właściwością będzie zmniejszenie łuszczenia się warstw powierzchniowych

issue with two main aspects: the temperature resistance of utilized components and their compatibility in high temperature conditions. Concrete is a multiphase material mainly composed of the cement matrix, aggregate, pores (filled with air and solution with different ions concentration) and nowadays usually also of various types of reinforcement. The defects in concrete, such as cracks, delamination, weakening or disruption of bonds between cement matrix and reinforcement, or peeling off parts of the surface layers due to heating are caused mainly by dehydration of hydrated phases, thermal incompatibility between the aggregates and cement paste, and the pore pressure within the cement paste (4).

The application of calcium aluminate cements rich in Al_2O_3 can be considered a beneficial factor for achieving the concrete resistance to high temperatures (5). Obviously, one has to take into account that, due to the conversion of hydration products (6), calcium aluminate cement based concretes can lose about 30% to 50% of their strength. It is a well known fact that after several collapses of structures in the 1970s and 1980s its use for load bearing concrete was forbidden. Nevertheless, it performs suitably when in contact with fire and high temperatures where its utilization still has its advantages. In a comparison with Portland cement, calcium aluminate cement fundamentally differs in its phase composition; the main phase is monocalcium aluminate CA, which in the case of higher alumina content is accompanied by calcium dialuminate CA_2 and dodecacalcium heptaaluminate $C_{12}A_7$ (7). The last one is nearly always present in calcium aluminate cements. The main products of hydration of calcium aluminates are metastable calcium aluminate decahydrate CAH_{10} and dicalcium aluminate octahydrate C_2AH_8, thermodynamically stable tricalcium aluminate hexahydrate C_3AH_6 (8), and aluminum hydroxide AH_3; the hydration process is known to strongly depend on temperature.

When hydrated calcium aluminate cement is exposed to elevated temperatures, the following changes occurs (9). Temperature about 110°C is necessary for evaporating of surface and unbound moisture and also bound water of amorphous AH_3 gel is removed. At about 150°C the dehydration process of calcium aluminate hydrates begins, and at 300°C decomposition of crystalline gibbsite AH_3 starts. After temperature is increased to 500°C, the formation of dodecacalcium heptaaluminate $C_{12}A_7$ is initiated. With growing temperature it is then converted back to calcium aluminate CA and further also to calcium dialuminate CA_2. At the temperatures higher than 1400°C monocalcium hexaaluminate CA_6 is formed.

Fiber reinforcement is an essential part of most cement composite designs. Fibers are utilized for several reasons, such as increasing the toughness of concrete, tensile, flexural and shear strength, impact resistance, frost resistance, restraining the shrinkage, preventing the brittle behavior of concrete. The choice of fibers (steel, glass, synthetic, organic, etc.) depends on the desired properties of the composite and has also to take into account where the improvement is exactly sought. For fire resistant composites, an important characteristic is the ability of fibers to lessen the spalling of the surface layer and also to increase the fracture energy after heating. Basalt fibers seem to be a suitable choice for a high tem-

i wzrost energii pękania w podwyższonej temperaturze. Włókna bazaltowe wydają się być odpowiednim wyborem dla betonów odpornych na wysokie temperatury, dzięki ich trwałości w szerokim zakresie temperatur od -200ºC do +800°C (10). Co więcej, są one przyjazne dla środowiska i nieszkodliwe, mają dobrą odporność na działanie środków chemicznych i są dostępne na rynku (11). Chociaż włókna bazaltowe zmniejszają urabialność świeżej mieszanki betonowej, to poprawiają wytrzymałość na zginanie i na rozciąganie, twardość, odporność na ścieranie, wytrzymałość zmęczeniową oraz przenoszenie pewnych obciążeń po wystąpieniu spękań oraz zmniejszają zdolność do odkształceń (12). Stwierdzono również, że obecność włókien bazaltowych znacznie zmniejsza skurcz suszenia zaczynu cementowego lub zaprawy oraz zwiększa wytrzymałość i właściwości wiążące zaczynu w pierwszych dniach hydratacji (13).

W wyniku ogrzewania betonu, właściwości mechaniczne, jak również inne parametry fizyczne ulegają znacznemu pogorszeniu (14, 15). Stopień degradacji zależy od wielu czynn ków. Jednym z nich jest zawartość wilgoci. Działanie wysokiej temperatury w połączeniu z dużą zawartością wody w porach może prowadzić do niebezpiecznego łuszczenia się i odpryskiwania warstw powierzchniowych (16). Niebezpieczeństwo tych zmian, nie biorąc pod uwagę dalszego pogorszenia właściwości materiału, jest dwojakie: ryzyko zranienia osób lub uszkodzenia innych obiektów w pobliżu spowodowane odpryskami ostrych kawałków betonu oraz zmniejszenie przekroju elementu konstrukcyjnego, ograniczające jego nośność. Przepuszczalność kompozytów cementowych ma również wielkie znaczenie. W przypadku bardziej zwartego materiału, jest utrudniony transport pary wodnej, co powoduje wzrost ciśnienia w porach i dodatkowe naprężenia w materiale. Inną bardzo ważną cechą jest zdolność rozchodzenia się ciepła, zależna od przewodności cieplnej, współczynnika dyfuzji cieplnej oraz pojemności cieplnej betonu (17). Mniejsza zdolność rozchodzenia się ciepła w przypadku dużych gradientów temperatury w materiale, może zwiększać wstrząs termiczny, a więc również ryzyko łuszczenia. Jest to tylko kilka przykładów powodów, dla których należy zbadać zachowanie się betonów cementowych w wysokich temperaturach oraz podejść do tego problemu jako zagadnienia złożonego z wielu problemów.

W niniejszym artykule, przeanalizowano odporność na wysokie temperatury betonu w oparciu o badania szerokiego zakresu właściwości fizycznych. Podstawowe właściwości fizyczne a mianowicie: wytrzymałość mechaniczna, transport wody i pary wodnej oraz właściwości termiczne, oceniono po poddaniu betonu działaniu trzech różnych temperatur, a mianowicie: 105°C, 400°C i 1000°C. Badania przeprowadzono na czterech kompozytach cementowych, różniących się składem. Zostały one zaprojektowane i wykonane z dwóch cementów: portlandzkiego i glinowego. Zbadano również wpływ przypadkowo rozproszonych włókien bazaltowych.

perature resistant composite, due to their good stability in a wide range of temperatures from -200ºC to +800°C (10). Moreover, they are environmentally friendly and non-hazardous, have a good resistance to chemical attack and are commercially available (11). Although basalt fibers somehow reduce workability of fresh concrete, they improve bending and tensile strength, toughness, abrasion resistance, fatigue strength, deformation capability, and load bearing capacity after cracking (12). It was also observed that the presence of basalt fibers significantly reduces drying shrinkage of cement paste or mortar and increases the strength and bond properties of cement paste in early ages (13).

Due to the effects of heating, mechanical properties, as well as the other physical parameters, are significantly deteriorated (14, 15). The degree of deterioration is dependent on many factors. One of them is the moisture content. High temperature exposure in a combination with the high amount of water present in the pore system can result in dangerous spalling and explosive cracking of the surface layer (16). The danger of this phenomenon, when not considering the further deterioration of the material, is twofold; the risk of hurting people or damaging other objects nearby due to the flying sharp pieces and the reduction in cross-section decreasing the load bearing capacity of the structural element. The permeability of cement composite is also of a great importance. In the case of more compact material, generated pressurized water vapor has very little possible ways how to escape, and causes additional stresses within the structure. Another strongly influencing characteristic is the ability of heat propagation, affected mainly by thermal conductivity, thermal diffusivity and specific heat capacity (17). A lesser propagation of heat results in higher temperature gradients in the material that can increase thermal stress, thus also the risk of spalling. These are just a few examples of the variety of reasons for studying the behavior of cement composites in high temperature conditions as a complex problem with many aspects.

In this paper the high-temperature resistance of cement composites is analyzed using the measurement of a wide range of physical properties. Basic physical characteristics, mechanical strength, water and water vapor transport parameters, and thermal properties are determined after exposure to the temperatures of 105°C, 400°C, and 1000°C. The experiments are performed on four cement composites, differing by the used raw materials. They are designed using the ordinary Portland cement and calcium aluminate cement; the effect of randomly distributed basalt fibers is investigated as well.

2. Materials and heating conditions

The composition of the four studied composite mixes is presented in Table 1. Calcium aluminate cement Secar 71 was used as the main binder. It was produced by the French company Kerneos, SA, its specific surface area was 380 m^2kg^{-1}. Portland cement CEM I 52.5R was chosen as the second studied binder, for the reference purpose. It was produced by Lafarge, a.s., Čížkovice, its specific surface area was 390 m^2kg^{-1}. Chemical composition of both ce-

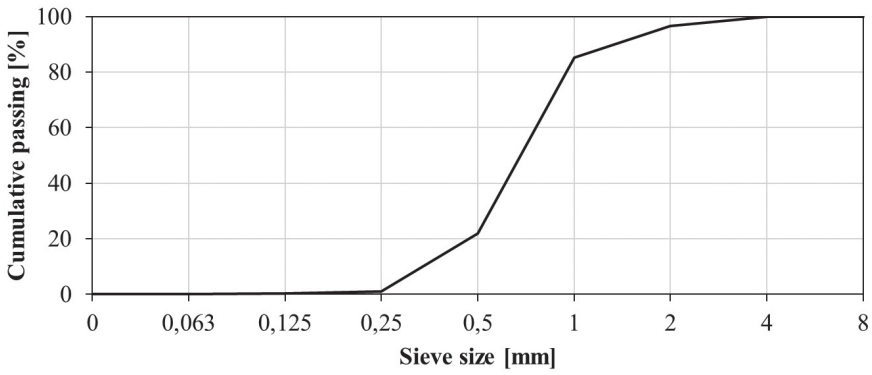

Rys. 1. Krzywa przesiewu piasku kwarcowego

Fig. 1. Grading curve of silica sand

Tablica 1 / Table 1

SKŁAD BETONÓW [kg m^{-3}]

COMPOSITION OF CONCRETES [kg m^{-3}]

Składnik \ mieszanka kompozytowa Component \ composite mixture	PS0	PSF	CS0	CSF
Cement glinowy / Calcium aluminate cement	-	-	900	900
Cement portlandzki / Portland cement	900	900	-	-
Kruszywo krzemionkowe / Silica aggregate 0.1/0.6 mm	465	465	465	465
Kruszywo krzemionkowe / Silica aggregate 0.3/0.8 mm	297	297	297	297
Kruszywo krzemionkowe / Silica aggregate 0.6/1.2 mm	234	234	234	234
Kruszywo krzemionkowe / Silica aggregate 1.0/4.0 mm	168	168	168	168
Włókna bazaltowe / Basalt fibers	-	14.5	-	14.5
Woda / Water	225	225	225	225

2. Materiały i warunki poddania próbek działaniu wysokich temperatur

Skład czterech badanych mieszanek betonowych przedstawiono w tablicy 1. Głównym spoiwem był cement glinowy Secar 71, produkowany przez francuską firmę Kerneos, SA. Powierzchnia właściwa cementu wynosiła 380 m^2kg^{-1}. Drugim spoiwem, a zarazem referencyjnym, wybrano cement portlandzki CEM I 52.5R produkowany przez Lafarge, a.s., Čížkovice. Powierzchnia właściwa tego cementu wynosiła 390 m^2kg^{-1}. Skład chemiczny obu cementów podano w tablicy 2. Kruszywo stanowiły cztery rodzaje piasku kwarcowego, pochodzące z kamieniołomu Sklopísek STRELEC, a. s.. Ich kumulacyjną krzywą przesiewu przedstawiono na rysunments is shown in Table 2. Four gradings of silica sand taken from the quarry of Sklopísek Střeleč, a. s., were used as aggregate. Their cumulative grading curve is presented in Fig. 1; they contained at least 99.2% of silica and less than 0.04% of iron oxide. Basalt fibers of 12 mm length were produced by Basaltex, a. s., their chemical composition is shown in Table 2. The amount of fibers was chosen using an empirical optimization process aimed at the achievement of satisfactory bending strength. Plasticizer Sika ViscoCrete-1035CZ was added for the improvement of workability of the mixes. The amount of water and plasticizer was set experimentally considering the attainment of the consistency F3 according to the standard (18).

In the sample preparation process dry components (aggregate and cement) were properly mixed at first. Then a portion of water containing plasticizer was added. After a few minutes of additional mixing, fibers were gradually added. Finally, the remaining water was poured in. The resulting fresh mixture was then placed into a specific mold where it was cured for 24 h at temperature (22 ± 1)°C and relative humidity (50 ± 5)%. Specimens after demolding were left in the same laboratory conditions for 28 days.

The suitable temperatures for the thermal treatment were chosen according to the results obtained for both hydrated cements by differential scanning calorimetry and ther-

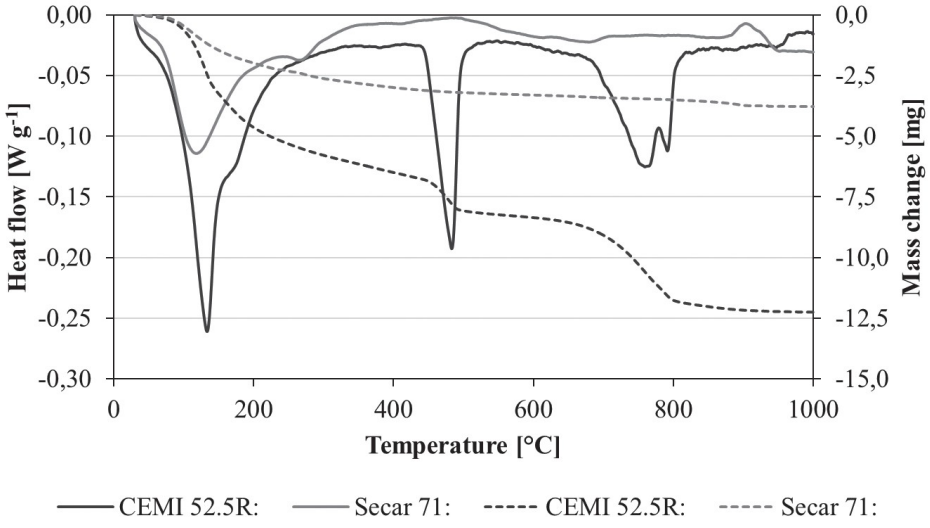

Rys. 2. Wyniki różnicowej kalorymetrii skaningowej i termograwimetrii zhydratyzowanych cementów

Fig. 2. Differential scanning calorimetry and thermogravimetry of hydrated cements

Tablica 2 / Table 2

SKŁAD CHEMICZNY CEMENTU I WŁÓKIEN BAZALTOWYCH, OKREŚLONY METODĄ FLUORESCENCJI RENTGENOWSKIEJ

CHEMICAL COMPOSITION OF CEMENTS AND BASALT FIBERS AS DETERMINED BY THE X-RAY FLUORESCENCE METHOD

Materiał / tlenek Material / oxide	CaO	Al_2O_3	K_2O	Na_2O	SiO_2	MgO	Fe_2O_3
Cement glinowy / Calcium aluminate cement	27.50	70.80	0.06	0.27	0.58	0.21	0.42
Cement portlandzki / Portland cement	64.90	6.40	1.20	0.30	18.10	1.00	2.40
Włókna bazaltowe / Basalt fibers	8.92	17.60	1.66	2.66	54.39	3.62	9.77

ku 1. Zawierają one co najmniej 99% krzemionki i mniej niż 0,04% tlenku żelaza. Zastosowano włókna bazaltowe o długości 12 mm, produkowane przez Basaltex, a. s.. Ich skład chemiczny podano w tablicy 2. Dodatek włókien dobrano doświadczalnie, tak aby zapewnić zadowalającą wytrzymałość na zginanie. W celu poprawy urabialności mieszanek betonowych zastosowano plastyfikator Sika ViscoCrete-1035CZ. Ilość wody i plastyfikatora ustalono doświadczalnie, biorąc pod uwagę osiągnięcie konsystencji F3, zgodnie z normą (18).

W procesie przygotowania próbek, w pierwszej kolejności zmieszano suche składniki (kruszywa i cement), a następnie dodano wodę zawierającą plastyfikator. Po kilku minutach mieszania stopniowo dodawano włókna. Na koniec dodano pozostałą wodę. Otrzymaną świeżą mieszankę umieszczono w formach, w których przebywała przez 24 godziny w temperaturze 22 ± 1 °C i wilgotności względnej 50 ± 5 %. Próbki po rozformowaniu przechowywano w tych samych warunkach przez 28 dni.

Temperatury, odpowiednie do przeprowadzenia doświadczeń, wybrano na podstawie wyn ków badań za pomocą różnicowej kalorymetrii skaningowej oraz termograwimetrii, zaczynów z obu cementów. Rysunek 2 pokazuje, że procesy zachodzące poniżej temperatury 250°C były związane głównie z utratą wolnej wody z porów kapilarnych i wody związanej w hydratach (C-S-H w przypadku cementu portlandzkiego oraz C-A-H i AH_3 w przypadku cementu glinowego). Pierwszą wybraną temperaturą było 105°C. Zastosowano ją w celu odróżnienia wpływu wody odparowywalnej od nieodparowywalnej. W przypadku cementu portlandzkiego, rozkład wodorotlenku wapniowego zachodzi w 450°C, zatem druga wybrana temperatura wynosiła 400°C. Inny pik na krzywej DTA zaczynu cementowego zarejestrowano w zakresie 700-800°C. Jest on związany z dekarbonatyzacją $CaCO_3$. W przypadku cementu glinowego wystąpił mały pik endotermiczny w temperaturze 300ºC, w której rozkłada się C_3AH_6. Inny główny pik występował w temperaturze około 900°C. Powinien on odpowiadać tworzeniu się glinianu monowapniowego. Trzecią wybraną temperaturą jest 1000 °C. W temperaturze tej procesy rozkładu składników zaczynu są zakończone.

Wstępne oddziaływanie podwyższonej temperatury na beton przeprowadzono w następujący sposób. Najpierw próbki wysuszono przetrzymując je w suszarce w 105°C, przez 24 godziny, które traktowano jako próbki odniesienia. Próbki ogrzewano w piecu elektrycznym, zamykanym od góry, z szybkością 0,5°C

mogravimetry. Fig. 2 shows that processes up to the temperature of 250°C were mostly connected with the loss of free water in capillary pores and bound water in hydrates (C-S-H in the case of Portland cement and C-A-H and AH_3 in the case of calcium aluminate cement). The first temperature was thus selected as 105°C, in order to distinguish between the evaporable and non-evaporable water. In the case of Portland cement, calcium hydroxide decomposition occurred at about 450°C and therefore, the second loading temperature was chosen at 400°C. Another peak on DTA curve of Portland cement was recorded at the temperature range of 700-800°C which corresponded to $CaCO_3$ decomposition. In the case of calcium aluminate cement a small endothermic peak was observed at about 300ºC where C_3AH_6 was decomposed. Another minor peaks were found at about 900°C, which should correspond with the formation of monocalcium aluminate. The third temperature for thermal loading was chosen as 1000°C where most decomposition processes were supposed to be completed.

The thermal pre-treatment was performed as follows. At first, the specimens were dried in an oven at 105°C for 24 hours which presented the first, reference state for the comparisons. The exposure to 400°C and 1000°C was done in an electric top-cover furnace with the heating rate of 0.5°C per min. After reaching the final temperature (400°C or 1000°C), samples were exposed at that temperature for 3 hours. Cooling was slow and took place in the furnace.

3. Experimental methods

3.1. Basic physical properties

Bulk density, matrix density, and open porosity were measured using the water vacuum saturation method (19) for nine samples (three for every temperature), with the dimensions of 50 x 50 x 50 mm. The samples were dried in an oven at 105°C at first to remove the evaporable water and their mass was determined. Then they were placed into a desiccator with de-aired water. During three hours air was evacuated with a vacuum pump from the desiccator. The samples were then immersed in water not less than 24 hours. After removing the samples from the desiccator, their mass was measured both on the air and after immersion in water. In this way, the volume can be determined which made possible to calculate bulk density, matrix density, and open porosity.

na minutę. Po osiągnięciu temperatur maksymalnych (400°C lub 1000°C), próbki przetrzymano w tej temperaturze przez 3 godziny. Po zakończeniu ogrzewania, próbki chłodzono powoli, w piecu.

3. Metody badań

3.1. Podstawowe właściwości fizyczne

Gęstość pozorną, gęstość rzeczywistą oraz porowatość otwartą zmierzono posługując się metodą próżniowego nasycania wodą (19). Zbadano 9 próbek (po trzy dla każdej temperatury) o wymiarach 50 x 50 x 50 mm. Próbki najpierw wysuszono w suszarce w 105°C, aby usunąć odparowywalną wodę i określono ich masę. Następnie, umieszczono je w eksykatorze próżniowym wypełnionym wodą. Przez trzy godziny z eksykatora usuwano powietrze za pomocą pompy próżniowej. Próbki pozostawiono zanurzone w wodzie, przez czas nie krótszy niż 24 godziny. Po wyjęciu z eksykatora próbki zważono w powietrzu oraz hydrostatycznie.

Strukturę porowatości zmierzono za pomocą porozymetrii rtęciowej. Rozmiar porów obliczono na podstawie zmierzonego ciśnienia, stosując równanie Washburna. Badania przeprowadzono posługując się porozymetrem rtęciowym PASCAL 140 i 440 (Thermo Scientific). Zakres stosowanego ciśnienia odpowiada wielkości porów o średnicach od 10 nm do 100 μm.

3.2. Wytrzymałość

Wytrzymałość na ściskanie i zginanie wyznaczono zgodnie z normą (20). Badanie przeprowadzono na dziewięciu próbkach (po trzy dla każdej temperatury) o wymiarach 40 x 40 x 160 mm. Zastosowano zginanie trzypunktowe, a odległość pomiędzy punktami podparcia wynosiła 100 mm. Obciążanie próbek kontynuowano do momentu złamania. Zanotowano maksymalną wartość przyłożonej siły. Na podstawie oceny maksymalnego momentu zginającego oraz wskaźnika przekroju, obliczono wytrzymałość na zginanie. Wytrzymałość na ściskanie zmierzono na próbkach pozostałych po pomiarze wytrzymałości na zginanie. Dlatego, w tym przypadku zbadano osiemnaście próbek (po sześć dla każdej temperatury). Podczas próby ściskania próbki umieszczono pomiędzy dwoma stalowymi płytkami o wymiarach 40 x 40 mm, zwracając szczególną uwagę na osiowe obciążanie próbek. Podobnie jak w przypadku badania wytrzymałości na zginanie, zanotowano maksymalną siłę niszczącą.

3.3. Transport wody i pary wodnej

Transport pary wodnej mierzono suchą oraz mokrą metodą miseczkową (21). Pomiary przeprowadzono na dziewięciu cylindrycznych próbkach (po trzy dla każdej temperatury) o średnicy 115 mm i wysokości 20 mm. Pomiary te prowadzi się w dwóch środowiskach, różniących się ciśnieniem parcjalnym pary wodnej. W suchej metodzie miseczkowej stosuje się pojemniki z żelem krzemionkowym, w celu utrzymania 5% wilgotności względnej. Aby wywołać jednokierunkowy transport pary wodnej przez próbki, ich ściany boczne są izolowane. Zamknięte pojemniki z próbkami umieszCharacterization of the pore structure was done by the mercury intrusion porosimetry. The pore size is then calculated from the measured pressure using Washburn's equation. The experiments were carried out using instruments PASCAL 140 and 440 (Thermo Scientific). The range of applied pressure corresponded to the pore diameters from 10 nm to 100 μm.

3.2. Strength

Compressive and bending strength were determined according to the standard (20). Bending strength was measured using an MTS 100 loading device for nine samples (three for each temperature) with the dimensions of 40 x 40 x 160 mm. The experiment was arranged as a three-point bending test with 100 mm span length. Loading was continued until the breaking point, and the ultimate force was noted. By evaluating the maximum bending moment and the known section modulus, the bending strength was calculated. To determine the compressive strength the loading device EU40 was employed. Remainders of the samples left over after the measurement of bending strength were used. Therefore, eighteen samples (six for every temperature) were examined in this case. In the actual experiment samples were put between two steel pressure plates with the dimensions of 40 x 40 mm. Since only simple compression should be involved, special emphasis was given to the centering of the arrangement. The ultimate force was noted as in the case of bending strength. The compressive strength was calculated using the value of the active force and the known loading area.

3.3. Water and water vapor transport parameters

Water vapor transport parameters were measured by the dry-cup and wet-cup methods (21). Nine cylindrical samples (three for every temperature) with a diameter of 115 mm and 20 mm height were used for the experiment. The principle of this measurement consisted in the establishment of two environments with different partial pressure of water vapor. In the dry-cup arrangement cups contained silica gel, which simulated 5% relative humidity. Specimens were water- and vapor proof insulated on four lateral sides. The purpose of this insulation was to achieve water vapor transport in only one dimension. Then, the samples were fixed at the upper part of the cups containing silica gel and sealed. The cups were then placed in a climatic chamber with the temperature of 25°C and relative humidity of 50%. For two weeks the cups were periodically weighed. The steady state values of mass gain or mass loss determined by linear regression over the last five readings were used to determine the water vapor diffusion resistance factor. After two weeks of measurement the cups were remade to the wet-cup arrangement. This entailed silica gel being exchanged for water, consequently simulating a relative humidity of 95%. Otherwise, conducting the experimental process of wet-cup measurement was the same as in the case of dry-cup experiment.

The liquid water transport was characterized by the water absorption coefficient. For the experimental measurement nine samples (three for every temperature) with the dimensions of

czono w komorze klimatycznej w temperaturze 25°C i wilgotności względnej 50%. Przez dwa tygodnie pojemniki z próbkami były regularnie ważone. Przyrost lub ubytek masy próbek, wyznaczone metodą regresji liniowej na podstawie pięciu ostatnich odczytów, posłużyły do wyznaczenia współczynn ka oporu dyfuzyjnego pary wodnej. Po dwóch tygodniach pomiarów układ dostosowano do warunków mokrej metody miseczkowej. W tym celu, w miejsce żelu krzemionkowego do pojemników wprowadzono wodę, zapewniając wilgotność względną równą 95%. Pomiary przeprowadzano tak samo jak w przypadku suchej metody miseczkowej.

Parametry transportu wody oceniono na podstawie analizy współczynników absorpcji wody. Do ich wyznaczenia użyto dziewięciu próbek (po trzy dla każdej temperatury) o wymiarach 50 x 50 x 50 mm. Tak jak w przypadku oceny transportu pary wodnej, izolowano ściany boczne badanych próbek. Następnie, powierzchnię próbki zanurzano w wodzie na głębokość 1 - 2 mm. Przez cały czas badania utrzymywano stały poziom wody w zbiorniku, stosując butelkę Mariotta, z dwoma rurkami kapilarnymi. Jedną z nich, o średnicy wewnętrznej 2 mm, zanurzono w wodzie. Druga o średnicy wewnętrznej 5 mm, znajdowała się powyżej poziomu wody i rejestrowano wzrost masy próbek. Współczynnik absorpcji wody obliczano z krzywej sorpcji (22), wynikającej z danych pomiarowych. Pozorną dyfuzję wody wyznaczono metodą Kumarana, ze współczynnika absorpcji (23).

3.4. Właściwości termiczne

Przewodność cieplną i ciepło właściwe określono stosując aparat ISOMET 2104. Pomiary przeprowadzono na dziewięciu próbkach (po trzy dla każdej temperatury) o wymiarach 70 x 70 x 70 mm. Isomet 2104 jest urządzeniem wykorzystującym dynamiczną metodę pomiaru, stąd czas pomiaru wynosi mniej niż pół godziny. Pomiar polegał na analizie odpowiedzi termicznej materiału na impuls cieplny. Ciepło wytwarzane jest przez elektryczny opornik. Następnie rejestrowana jest temperatura materiału i oceniana na podstawie regresji wielomianowej. Ze względu na zależność przewodności cieplnej oraz pojemności cieplnej od obecności wody w materiale, pomiary zostały wykonane zarówno w stanie suchym jak i w stanie nasycenia wodą.

Pomiar odkształceń termicznych w zależności od temperatury zmierzono za pomocą dylatometru (24), na trzech próbkach o wymiarach 15 x 15 x 160 mm. Pomiar został przeprowadzony metodą porównawczą. Rzeczywisty współczynnik rozszerzalności cieplnej został określony przez porównanie analizowanej próbki z materiałem odniesienia. W tym celu, zastosowano rurkę korundową (o znormalizowanych właściwościach), w której umieszczano 50 x 50 x 50 mm were used. Specimens had to be insulated, as in the case of water vapor transport, on four lateral sides. Then the face side of the specimens was immersed 1 - 2 mm in the water. A constant water level in the tank was achieved by a Mariotte bottle with two capillary tubes. One of them, with an inside diameter of 2 mm, was submerged under the water level. The second one, with an inside diameter of 5 mm, remained above water level. The automatic balance allowed recording of the increase in mass to the specimen. The water absorption coefficient was calculated from the sorptivity plot (22) which was taken from measured data. Apparent moisture diffusivity was calculated from water absorption coefficient using the method proposed by Kumaran (23).

3.4. Thermal properties

Using an ISOMET 2104 device, thermal conductivity and specific heat capacity were determined. Measurement was performed for nine samples (three for each temperature) with the dimensions of 70 x 70 x 70 mm. ISOMET 2104 is a commercial device which applies a dynamic measurement method, so that the time it takes to make a measurement is reduced to less than half an hour. The measurement process is based on an analysis of a temperature response of an analyzed material to heat flow impulses. The heat flow is induced by a resistor heater. The temperature is then recorded and evaluated from the polynomial regression. Because of the impact of the water presence on thermal conductivity, as well as on specific heat capacity, both studied characteristics were measured in both dry state and water saturated state.

The measurement of thermal strain depending on temperature was performed by a linear thermal horizontal dilatometer (24) for three samples with the dimensions of 15 x 15 x 160 mm. The device utilizes a comparative method; the real thermal expansion is determined by comparing the analyzed specimen with a standard. For that purpose, corundum having standardized properties was employed in the form of a tube where the measured specimen was placed. One side of the specimen was placed against the fixed

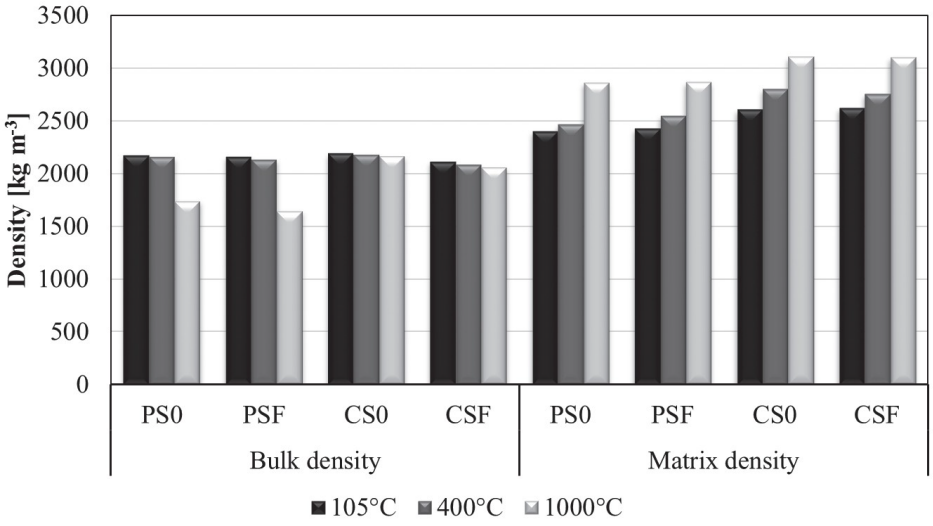

Rys. 3. Gęstość pozorna i gęstość matrycy betonów ogrzewanych w różnych temperaturach

Fig. 3. Bulk density and matrix density of concretes heated at different temperature

czono badaną próbkę. Jedna strona próbki stykała się z nieruchomą ścianą rurki, a druga strona próbki stykała się z cięgłem, połączonym ze wskaźnikiem zmian długości. Szybkość ogrzewania próbek wynosiła 1°C na minutę, a temperatura maksymalna wynosiła 800°C.

4. Wyniki i dyskusja

4.1. Podstawowe właściwości fizyczne

Wpływ obu cementów oraz włókien na gęstość pozorną po wysuszeniu w 105°C był niewielki [rysunek 3]. Maksymalna różnica gęstości pozornej wynosiła 3%. Wygrzanie próbek w 400°C również nie miało prawie żadnego wpływu na gęstość pozorną. Zmniejszyła się ona o około 1% w przypadku wszystkich betonów. Wygrzewanie próbek w 1000°C, spowodowało zmniejszenie gęstości pozornej betonów z cementu portlandzkiego o 22%, a kompozytów z cementu glinowego o mniej niż 2%. Betony z włóknami miały nieco mniejszą gęstość pozorną niż bez nich dodatku.

Hydratacja cementu glinowego spowodowała, że gęstość matrycy cementowej była o około 8% większa niż gęstość matrycy z cementu portlandzkiego [rysunek 3]. Wpływ dodatku włókien bazaltowych na gęstość matrycy był bardzo niewie ki; otrzymane wartości różniły się o mniej niż 1%. Podczas ekspozycji w wysokich temperaturach nastąpił rozkład hydratów i powstawanie bezwodnych faz o większej gęstości. W związku z tym, gęstość matrycy cementowej we wszystkich betonach wzrosła średnio o około 5% po ogrzewaniu w temperaturze 400°C i o 16% w przypadku ogrzewania w temperaturze 1000°C.

Betony z cementu glinowego miały średnio o 42% większą porowatość otwartą niż kompozyty z cementu portlandzkiego [rysunek 4]. Mniejszy wpływ na porowatość otwartą miał dodatek włókien. W tym przypadku wzrosła ona o około 15%. Ogólnie wpływ ekspozycji w wysokich temperaturach był ogromny. Jest to związane ze zmianami zachodzącymi w matrycy cementowej, związanej z powstawaniem bezwodnych faz o większej gęstości, a także z przemianami dotyczącymi kruszywa. Po wygrzewaniu w temperaturze 400°C porowatość otwarta we wszystkich betonach wzrosła o około 26%. Tendencja ta utrzymywała się ze wzrostem temperatury, jednak po wygrzewaniu próbek w 1000°C, betony z cementu glinowego wykazały lepszą odporność termiczną. Średni wzrost porowatości otwartej betonów z cementu portlandzkiego wyniósł około 75%, podczas gdy w przypadku kompozytów z cementu glinowego wyniósł około 45%.

Pomiary rozkładu wie kości porów w próbkach odniesienia wykazały, że w betonach z cementu portlandzkiego jest najwięcej porów o średnicy około 0,1 µm [rysunek 5]. Pory

wall and the second side touched a pull-rod which was connected to the length change indicator. The heating rate of the dilatometer was set at 1 °C per min and the maximum temperature of measurement was 800°C.

4. Results and discussion

4.1. Basic physical properties

In the reference state the influence of both cement and fibers on the bulk density was low (Fig. 3); it varied only up to 3%. The thermal loading at 400°C had almost no effect as well; the bulk densities decreased by about 1% for all studied cement composites. After the temperature exposure to 1000°C, the decrease of bulk densities of materials based on Portland cement was about 22%, but for composites containing calcium aluminate cement the change of bu k densities was less than 2%. The composites with fibers showed a little higher bulk densities than those without reinforcement.

The hydration of calcium aluminate cement led to somewhat heavier matrix; the values of matrix densities of composites from that cement were about 8% higher than when ordinary Portland cement was used (Fig. 3). The influence of basalt fibers on matrix densities of final composites was very low; the obtained values varied by less than 1%. Due to the temperature exposure material transformations occurred; hydrates were decomposed and more dense anhydrous phases were formed. Therefore, the residual matrix densities of all studied composites increased, in average by about 5% after exposure to 400°C and by 16% in the case of heating at 1000°C.

Composites based on calcium aluminate cement reached (in average) 42% higher values of open porosities that with Portland cement (Fig. 4). A lower impact on porosity could be observed in the case of fiber utilization. Open porosity was increasing by about 15% when fibers were added. Anyhow, the influence

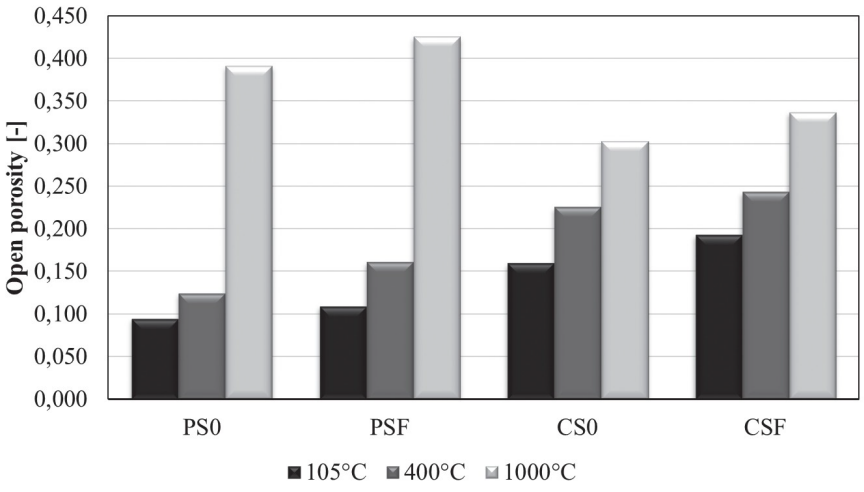

Rys. 4. Porowatosć otwarta betonów

Fig. 4. Open porosity of concretes

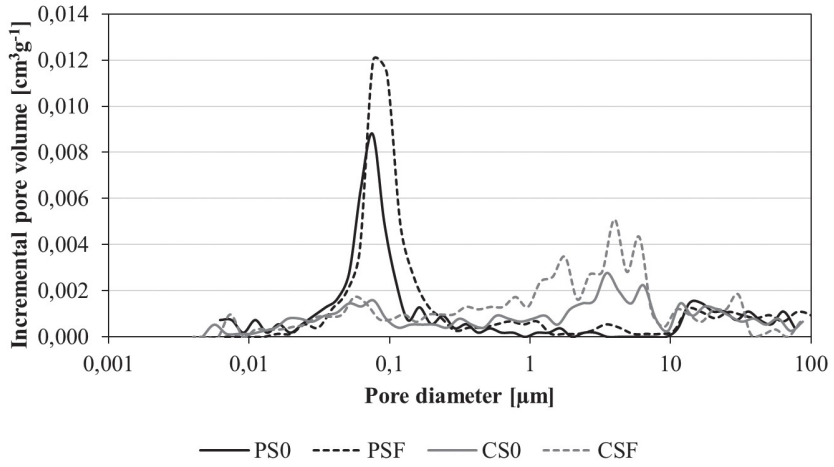

Rys. 5. Krzywa rozkładu wielkości porów w betonach z cementu portlandzkiego i cementu glinowego

Fig. 5. Pore size distribution curves of concretes from Portland and calcium aluminate cements

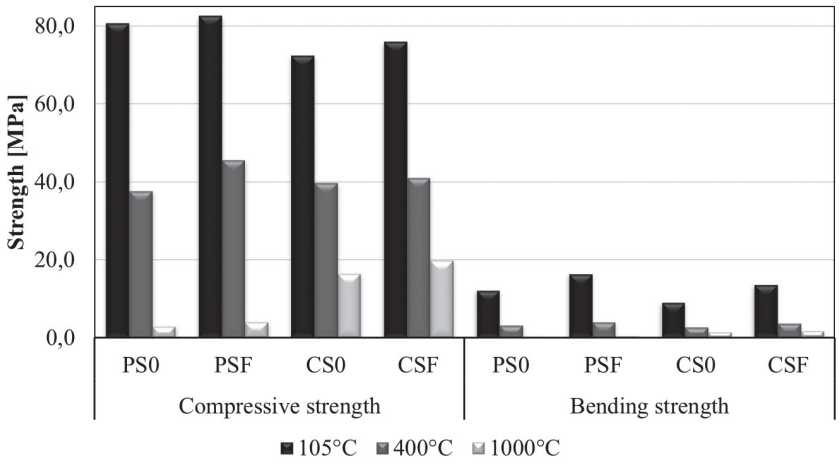

Rys. 6. Wytrzymałość na ściskanie i zginanie betonów wygrzewanych w różnych temperaturach

Fig. 6. Compressive and bending strength of concretes heated at different temperature

te są mniejsze niż w przypadku betonów z cementu glinowego, w których maksimum porów przypadało pomiędzy 1 a 10 µm. Można więc przyjąć, że kompozyty z cementu glinowego, powinny mieć znacznie większą zdolność transportu wody. Dodatek włókien spowodował wzrost średniej średnicy porów. Uzyskane wyniki były zgodne z pomiarami porowatości otwartej.

4.2. Wytrzymałość

W normalnych warunkach betony z cementu portlandzkiego osiągnęły wytrzymałość na ściskanie wyższą o około 9% niż kompozyty z cementu glinowego [rysunek 6]. Wyniki te są zgodne z pomiarami porowatości otwartej [rysunek 4]. Dodatek włókien spowodował wzrost wytrzymałości na ściskanie o około 4%. Stwierdzono zatem, że obecność włókien kompensuje wzrost porowatości otwartej spowodowany ich dodatkiem, ale nie powoduje znacznej poprawy wytrzymałości. Ogrzewanie w temperaturze 400°C, spowodowało spadek wytrzymałości na ściskanie, średnio

of high-temperature exposure was huge. It was associated with matrix changes (formation of denser dehydrated phases), as well as with aggregate transformations. When composites had been exposed to the temperature of 400°C the open porosities of all studied material increased by about 26%. This trend continued with increasing thermal loading but after pre-heating at 1000°C composites based on calcium aluminate cement exhibited better thermal resistance. The growth of open porosity was for Portland cement composites about 75% while for the those with calcium aluminate cement it was only 45%, in average.

The pore size distribution measurements in the reference state showed that composites from Portland cement had the maximum content of pores at about 0.1 µm (Fig. 5). Their pore structure was finer than of the composites with calcium aluminate cements which had their maxima between 1 and 10 µm. Therefore, it could be assumed that the composites with calcium aluminate cement should have considerably bigger ability of water transport. The influence of fiber utilization was reflected in the increase of the observed maxima, in particular. The achieved results were in conformity with the measurements of open porosity.

4.2. Strength

In the reference state the composites of Portland cement reached about 9% higher compressive strength than those based on calcium aluminate cement (Fig. 6). This was in a basic accordance with the open porosity measurements (Fig. 4). The influence of fiber addition was slightly positive; the compressive strength of reinforced composites was about 4% higher. Therefore, the presence of fibers was able to compensate for the increase of open porosity caused by their application in the mix but did not bring a substantial strength improvement. The exposure to 400°C led to a fall of compressive strength which was similar in all cases, about 47% in average. However, substantial differences were observed when the heating temperature was 1000°C. While the decrease of compressive strength for Portland cement composites was about 96%, regardless fiber utilization, for the materials based on calcium aluminate cement it was 77% for the samples without reinforcement and 74% when fibres were used. This was, apparently, in a good qualitative agreement with the thermal decomposition reactions, observed in the particular cement matrices by differential scanning calorimetry and thermogravimetry (Fig. 2).

o około 47% wszystkich próbek. Jednakże, znaczne różnice stwierdzono, po ogrzaniu próbek do temperatury 1000°C. Podczas, gdy spadek wytrzymałości na ściskanie betonów z cementu portlandzkiego wynosił około 96%, bez i z dodatkiem włókien, to w przypadku kompozytów z cementu glinowego wynosił 77% dla próbek bez włókien i 74% z ich dodatkiem. Wyn ki te są zgodne z reakcjami rozkładu termicznego, zachodzącymi w tych matrycach cementowych, stwierdzonych na podstawie różnicowej kalorymetrii skaningowej i termograwimetrii [rysunek 2].

Pomiary wytrzymałości na zginanie wykazały ogólną tendencję podobną do wytrzymałości na ściskanie [rysunek 6]. W normalnych warunkach, wytrzymałość na zginanie betonów z cementu portlandzkiego była o około 21% większa, niż kompozytów z cementu glinowego. Efekt wzmocnienia matrycy włóknami był wyraźniejszy niż w przypadku wytrzymałości na ściskanie i wzrosła ona średnio o około 29%. Uzasadnia to również zastosowanie włókien jako składnika betonów, eksploatowanych w normalnych warunkach. W każdym przypadku, poddanie betonów działaniu temperatury wynoszącej 400°C spowodowała spadek wytrzymałości na zginanie, średnio o 72%. Po wygrzewaniu w temperaturze 1000°C, spadek wytrzymałości na zginanie wyniósł 97% w przypadku betonów z cementu portlandzkiego i 85% dla kompozytów z cementu glinowego.

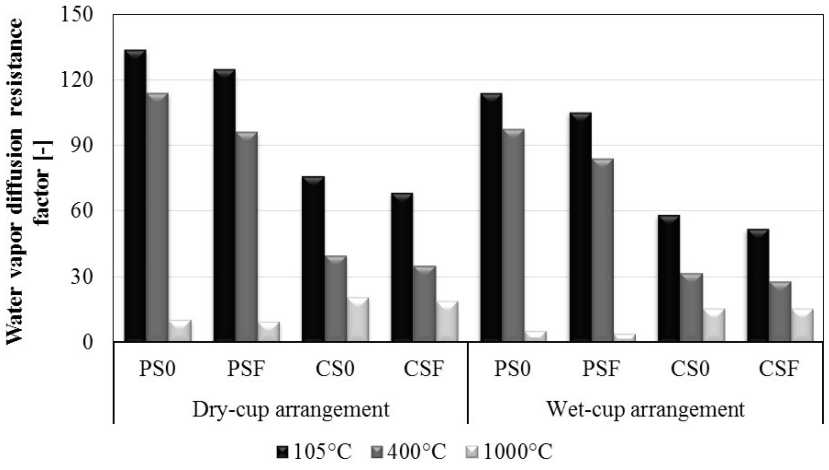

Rys. 7. Współczynnik oporu dyfuzyjnego pary wodnej betonów ogrzewanych w różnych temperaturach

Fig. 7. Water vapor diffusion resistance factor of concretes heated at different temperature

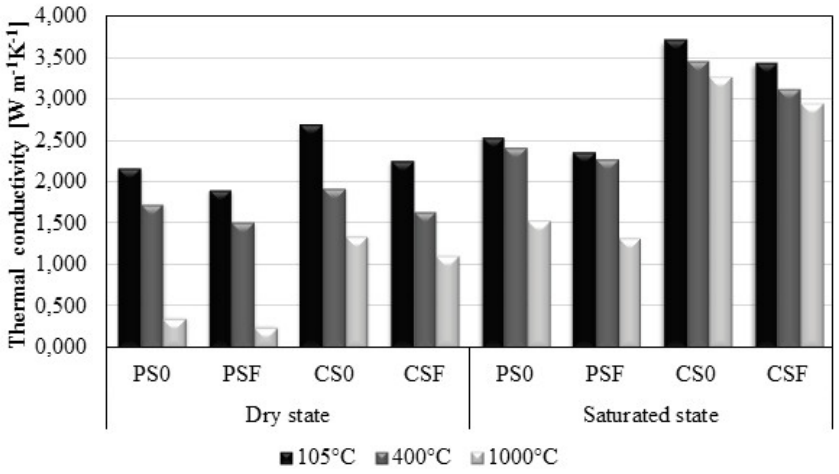

Rys. 8. Przewodność cieplna betonów ogrzewanych w różnych temperaturach

Fig. 8. Thermal conductivity of concretes heated at different temperature

4.3. Transport wody i pary wodnej

W warunkach normalnych betony z cementu portlandzkiego wykazały współczynnik oporu dyfuzyjnego pary wodnej o około 47% większy niż kompozyty z cementu glinowego, w obu metodach doświadczalnych [rysunek 7]. Wykorzystanie włókien spowodowało zmniejszenie współczynn ka oporu dyfuzyjnego pary wodnej o około 9%, w obu metodach. Wyniki te są zgodne z pomiarami porowatości [rysunek 4]. Współczynnik oporu dyfuzyjnego pary wodnej zmniejsza się wraz ze wzrostem temperatury ekspozycji. W przypadku ogrzewania w 400°C jego spadek wyniósł około 18% dla kompozytów z cementu portlandzkiego i około 47% dla betonów z cementu glinowego. Zwiększenie temperatury do 1000°C spowodowało prawie 94% spadek współczynnika oporu dyfuzyjnego pary wodnej betonów z cementu portlandzkiego i 72% spadek w przypadku betonów z cementu glinowego. Tendencja ta była zgodna z rosnącą porowatością otwartą [rysunek 4]. Wpływ dodatku włókien na zmiany współczynnika oporu dyfuzyjnego pary wodnej w zależności od temperatury był bardzo mały. Należy

For bending strength the overall tendency was similar to the compressive strength (Fig. 6). In the reference state the utilization of Portland cement resulted in about 21% higher bending strengths than when calcium aluminate cement was used. The positive effect of fiber reinforcement was more pronounced than for the compressive strength; an about 29% increase was observed, in average. This justified well their application in the mix in normal conditions. Regarding the impact of thermal loading, the temperature of 400°C caused a similar decrease of bending strength of all studied cement composites, the average decrease was about 72%. For the heating at 1000°C, the reduction of bending strength was almost 97% in the case of Portland cement composites and 85% for calcium aluminate cement composites; the effect of fibers was not evidenced.

zauważyć, że pomiary dwoma metodami miseczkowymi suchą i mokrą dały różne współczynniki oporu dyfuzyjnego pary wodnej. Wyn ki otrzymane suchą metodą były zawsze większe od otrzymanych mokrą metodą miseczkową. Jest to jednak dobrze znane zjawisko, które obserwowano również w przypadku innych materiałów. Jest ono prawdopodobnie spowodowane przez częściowe podciąganie kapilarne skondensowanej pary wodnej, w warunkach dużej wilgotności względnej (25).

Współczynnik absorpcji wody zależał głównie od rodzaju użytego cementu [tablica 3]. Betony z cementu portlandzkiego cechowały się niższymi o około 41% współczynnikami od kompozytów z cementu glinowego. Jest to zgodne z rozkładem wielkości porów [rysunek 5]. W tym przypadku czynnikiem decydującym, była zawartość porów kapilarnych w przedziale od 1 do 10 µm w betonie z cementu glinowego. Wpływ zawartości włókien był niekorzystny w obu przypadkach – spowodował wzrost współczynnika absorpcji wody. Można to uzasadnić zmianami w rozkładzie wielkości porów [rysunek 5]. Ogrzewanie spowodowało znaczny wzrost zdolności transportowych wody w betonach. Wygrzewanie betonów w temperaturze 400**°C**, spowodowało wzrost współczynnika absorpcji wody w zakresie od 30% do 53%. W przypadku temperatury 1000**°C** współczynniki absorpcji wody w przypadku betonów z cementu portlandzkiego wzrosły o 97%; podczas gdy dla betonów z cementu glinowego wzrost ten wynosił 88%. Wartości wilgotności nasycenia miały większy wpływ na pozorną dyfuzję wody w betonach [tablica 3] niż współczynniki absorpcji wody. W związku z tym otrzymane wyniki nie są przekonywające, tak samo jak pod względem zdolności materiału do transportu wody. Jednak należy zauważyć, że założenie stałej dyfuzji wody przyjętej w obliczeniach jest uproszczeniem, o ograniczonej możliwości zastosowania (26).

4.4. Właściwości termiczne

Betony z cementu portlandzkiego miały po wysuszeniu w 105°C przewodnictwo cieplne mniejsze o 18% od betonów z cementu glinowego. W stanie nasycenia wodą różnica ta wynosiła 31%. Jest to sprzeczne z wynikami porowatości otwartej [rysunek 4]. Jednakże, należy wziąć pod uwagę inny skład matrycy, wynikający ze stosowania różnych rodzajów cementu oraz inne czynniki, które mają prawdopodobnie różny wpływ. Kolejnym czynnikiem, mającym wpływ na przewodność cieplna, może być inna, w przypadku obu rodzajów betonów, struktura porowatości, na którą wskazują różnice w rozkładzie wielkości porów [rysunek 5]. Zatem, nie ma prostej metody znalezienia związków przewodności cieplnej z innymi właściwościami betonów. Wpływ dodatku włókien na przewodność cieplną jest nieznaczny. Ich dodatek zmniejsza ją o 14% w próbkach suchych i o 7% w stanie nasycenia wodą. W tym przypadku wyniki były zgodne z wynikami porowatości otwartej

4.3. Water and water vapor transport parameters

In the reference state composites based on Portland cement showed about 47% higher values of water vapor diffusion resistance factor than the materials with calcium aluminate cement, in both experimental arrangements (Fig. 7). Utilization of fibers led to a decrease of water vapor diffusion resistance factor, the fall was about 9% (for both environments). These findings were in accordance with the porosity data (Fig. 4). The water vapor diffusion resistance factor decreased with the increasing temperature exposure. In the case of heating at 400°C the decrease was of about 18% for Portland cement composites and about 47% for concrete from calcium aluminate cement. Heating at 1000°C caused an almost 94% drop of water vapor diffusion resistance factor of concretes prepared from Portland cement and 72% drop for those of calcium aluminate cement. This tendency was, once again, in accordance with growing open porosities (Fig. 4). The influence of random fiber reinforcement on the changes of water vapor diffusion resistance factor due to the temperature exposure was very low. It should be noted that both experimental arrangements (dry-cup and wet cup) showed different values of residual water vapor diffusion resistance factor; the achieved results obtained in the case of dry-cup arrangement were always higher than the wet-cup values. It is, however, a well-known phenomenon, which was observed also in the case of other materials. It is caused probably by a partial transport of capillary condensed water at higher relative humidity (25).

Water absorption coefficients in the reference state were influenced mainly by the used cements (Table 3). Concretes of Portland cement exhibited about 41% lower values than those from calcium aluminate cement. This was in a clear relation to the pore distribution (Fig. 5). The presence of capillary pores within the range of 1 to 10 µm in concrete from calcium aluminate cement was the decisive factor in that respect. The impact of fiber reinforcement was negative in all cases, the water absorption coefficient always increased when fibers were added. This could be explained by the changes in pore distribution (Fig. 5), once again. Heating

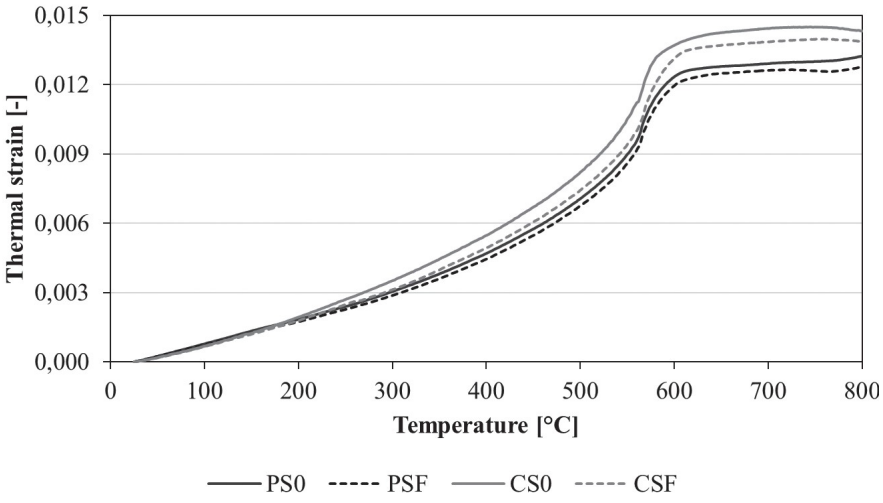

Rys. 9. Odkształcenia termiczne betonów z cementu portlandzkiego i cementu glinowego

Fig. 9. Thermal strain of concretes from Portland cement and calcium aluminate cement

Tablica 3 / Table 3

PARAMETRY TRANSPORTU WODY

LIQUID WATER TRANSPORT PARAMETERS

Typ kompozytu Composite type	Współczynnik absorpcji wody Water absorption coefficient [kg $m^{-2}s^{-1/2}$]			Pozorna dyfuzja wilgoci Apparent moisture diffusivity [m^2s^{-1}]		
	105 °C	400 °C	1000 °C	105 °C	400 °C	1000 °C
PS0	0.0075	0.0128	0.2469	6.80E-09	9.94E-09	4.42E-07
PSF	0.0081	0.0172	0.2949	4.88E-09	1.12E-08	4.66E-07
CS0	0.0120	0.0184	0.1041	4.55E-09	9.47E-09	1.51E-07
CSF	0.0143	0.0203	0.1111	5.54E-09	1.33E-08	1.81E-07

[rysunek 4]. Potwierdziły one znaczny wpływ rodzaju matrycy na przewodność cieplną betonów.

Zależność przewodności cieplnej od poddania betonów działaniu wysokich temperatur, potwierdziła zgodność z wcześniej analizowanymi właściwościami. Przewodność cieplna betonów z cementu portlandzkiego uległa zmniejszeniu po wygrzewaniu w temperaturze 400°C o około 20% w stanie suchym oraz o 4% w stanie nasycenia wodą. W przypadku betonów z cementu glinowego, spadek ten wynosił około 28% w stanie suchym i około 8% w próbkach nasyconych wodą. Betony z cementu portlandzkiego ogrzewane do 1000°C miały mniejszą aż o 86% przewodność cieplną w stanie suchym i niższą o 42%, w stosunku do próbek nasyconych wodą. Przewodność cieplna betonów z cementu glinowego ogrzanych do 1000°C, była mniejsza o 50% w stanie suchym oraz o 13% w stanie nasycenia próbek wodą, w stosunku do próbek dojrzewających w warunkach normalnych. Dodatek włókien we wszystkich przypadkach zmniejszał nieznacznie przewodność cieplną próbek. Również w próbkach betonów o tym samym rodzaju matrycy, ważnym czynnikiem wpływającym na przewodność cieplną jest porowatość otwarta.

Ciepło właściwe betonów z cementu portlandzkiego, po wysuszeniu w 105°C, jest mniejsze o 8% i o 16% w stanie nasycenia próbek wodą od ciepła właściwego betonów z cementu glinowego [tablica 4]. Wpływ dodatku włókien na ciepło właściwe był bardzo mały. W wyniku poddania betonów działaniu wysokich temperatur ciepło właściwe próbek nieznacznie wzrosło. Wygrzanie próbek betonów z cementu portlandzkiego w 400°C spowodowało wzrost ciepła właściwego o około 6% w stanie suchym i o 9% w stanie nasycenia wodą. W przypadku betonów z cementu glinowego wzrost ciepła właściwego wynosił około 3% w obu przypadkach. Poddanie próbek działaniu temperatury wynoszącej 1000°C prowadziła do stopniowego wzrostu właściwej pojemności cieplnej. W przypadku betonów z cementu portlandzkiego wzrost ten był większy o 11% w stanie suchym i prawie o 40% w stanie nasycenia próbek wodą. Beton z cementu glinowego, po wygrzewaniu w temperaturze 1000°C wykazał mniejszy wzrost ciepła właściwego. Wynosił on 5% w przypadku próbek suchych oraz około 7% po nasyceniu wodą. Zmiany pojemności cieplnej korespondują ze zmianami składu fazowego, spowodowanymi działaniem wysokiej temperevoked a significant increase of water transport ability of studied materials. When the concretes were heated at the temperature of 400°C, the increase of water absorption coefficients ranged from 30% to 53%. In the case of temperature exposure at 1000°C the values of water absorption coefficient of the concretes from Portland cement grew by 97%; when calcium aluminate cement was used the increase was about 88%. The apparent moisture diffusivities of concretes (Table 3) were affected by the values of saturation moisture content in a more significant way than by the water absorption coefficients. Therefore, the obtained results were not convincing, as for the capability of liquid moisture transport of the materials under consideration. However, it should be noted that the assumption of constant moisture diffusivity involved in its calculation is a clear oversimplification with a limited applicability (26).

4.4. Thermal properties

Composites of Portland cement had in the reference state after drying 18% lower thermal conductivity than those based on calcium aluminate cement; when they were saturated by water the difference was higher than 31%. This was contradictory to the open porosity data (Fig. 4). However, the different matrix composition resulting from the application of different types of cement was another factor which had to be taken into account in that respect; it acted probably in an opposite way. The third factor could be the different topology of the pore space of both composite types which was indicated by the substantial differences in the pore distribution (Fig. 5). Therefore, there was not any simple way how to relate the thermal conductivity values to the other parameters. The influence of fibers was relatively low; their utilization lowered the values of thermal conductivity by 14% in dry state and by 7% in water saturated state. In this case the results were in a qualitative agreement with the open porosity (Fig. 4) which confirmed the significant effect of the matrix type on the thermal conductivity of studied materials.

Regarding the effect of high-temperature exposure, the tendency was in conformity with the other parameters analyzed before. Thermal conductivity of concretes from Portland cement decreased due to the exposure at 400°C by about 20% in dry state and by 4% in water saturated state. When calcium aluminate cement was used, the decrease was about 28% for dry materials and about 8% when samples were saturated by water. Concretes heated at 1000 °C showed another drop of thermal conductivities. Concrete from Portland cement had almost 86% lower values of thermal conductivity in dry state and 42% lower in water saturated state. The concretes of calcium aluminate cement, when heated at the extreme temperature of 1000°C, showed thermal conductivity about 50% lower in dry state and about 13% lower in water saturation conditions. The influence of fiber utilization was the same in all cases; their presence always slightly decreased the

ratury [rysunek 2]. Betony z cementu portlandzkiego, wykazują mniejszą odporność na takie zmiany, co jest zgodne z ich mniejszą odpornością na wysokie temperatury.

Działanie temperatury do 400°C powodowało nieznaczne odkształcenia termiczne próbek betonów. Różnice w przypadku betonów z różnych cementów były relatywnie małe. Dodatek włókien spowodował nieznaczny spadek rozszerzalności cieplnej. W zakresie temperatur 570-600°C odnotowano znaczny wzrost odkształceń termicznych, spowodowany przez piasek zawarty w betonach. W 573°C β-kwarc przechodzi w odmianę polimorficzną α. Ta przemiana powoduje rozszerzalność cieplną.

Tablica 4 / Table 4

CIEPŁO WŁAŚCIWE

SPECIFIC HEAT CAPACITY

Typ kompozytu Composite type	Ciepło właściwe – stan suchy Specific heat capacity – dry state [J kg^{-1}K^{-1}]			Ciepło właściwe – stan nasycenia wodą Specific heat capacity – water saturated state [J kg^{-1}K^{-1}]		
	105 °C	400 °C	1000 °C	105 °C	400 °C	1000 °C
PS0	698	722	767	835	910	1357
PSF	691	754	800	898	1027	1469
CS0	751	775	791	1003	1035	1114
CSF	757	782	798	1061	1082	1105

5. Podsumowanie

Zbadano odporność na wysokie temperatury czterech betonów z cementu portlandzkiego i cementu glinowego. Do dwóch, spośród badanych kompozytów, dodano włókna bazaltowe, które są trwałe w wysokich temperaturach. Zaczyny cementowe zbadano za pomocą różnicowej kalorymetrii skaningowej i termograwimetrii, w celu wyznaczenia temperatur charakterystycznych, w których przygotowane próbki powinny być wygrzewane. Następnie, po ogrzaniu próbek do wybranych temperatur (105°C, 400°C i 1000°C) wyznaczono podstawowe właściwości fizyczne, parametry transportu wody i pary wodnej oraz właściwości cieplne.

Wyniki badań pokazały, że w stanie odniesienia – po wysuszeniu próbek w suszarce w 105°C w ciągu 24 godzin, betony z cementu portlandzkiego (PCC) miały lepsze właściwości niż betony z cementu glinowego (CAC). Może to być spowodowane przez rozkład AH_3. Porowatość otwarta PCC oraz zdolność transportu wody i pary wodnej były mniejsza, a wytrzymałość na ściskanie i wytrzymałość na zginanie większa. Dodatek włókien bazaltowych, rozmieszczonych przypadkowo, spowodował znaczny wzrost wytrzymałości na zginanie dla obu rodzajów kompozytów po wysuszeniu w 105°C, ale nieznaczny wzrost wytrzymałości na ściskanie. Jest to spowodowane głównie przez zwiększenie porowatości otwartej, w wyn ku dodatku włókien do mieszanki.

Oba rodzaje betonów PCC i CAC były w stopniu zadawalającym odporne na wygrzewanie w temperaturze 400°C. Pogorszenie ich właściwości było stosunkowo małe, a pozostałe właściwości były akceptowalne dla ich ograniczonego zastosowania jako materiałów konstrukcyjnych. Po wygrzewaniu w temperaturze 1000°C beton CAC zachował około 25% swojej wytrzymałości, dzięki czemu może on mieć bardzo ograniczone zastosowanie jako materiał konstrukcyjny, to właściwości betonu PCC pogorszyły się niemal całkowicie. Dwa najważniejsze czynniki wpływające na właściwości badanych kompozytów to rozkład C-S-H i $Ca(OH)_2$ w betonach

thermal conductivity. The effect of open porosity was, thus for the same matrix type, governing also in this case.

Specific heat capacities of concretes from Portland cement showed in the reference state lower values (8% in dry state and 16% in water saturated state) than those of calcium aluminate cement (Table 4). Influence of fiber addition was very low. Due to the high-temperature exposure the specific heat capacity was slightly higher. In the case of heating at 400°C the increase of specific heat capacity of Portland cement concrete was about 6% in dry state and 9% in water saturated state. When calcium aluminate cement was used the increase was about 3% in both cases. The exposure at 1000°C led to progressive growth of the values of specific heat capacity. In the case of Portland cement concrete the growth was higher (11% in dry state and almost 40% in water saturated state). Composites of calcium aluminate cement exposed to the extreme temperature of 1000°C showed a lower increase of specific heat capacity. When the materials were dry the growth was about 5%, in the case of water saturation it was about 7%. The variations in specific heat capacity reflected well the changes in composition of the particular composites, caused by the change of phase composition induced by heating at high temperature (Fig. 2). Composites of Portland cement were, apparently, more susceptible to such changes which was in accordance with their lower high-temperature resistance.

High-temperature thermal strain of all composites was moderate up to approximately 400°C. The differences between the concretes with different cement matrices were relatively low, the presence of fibers slightly decreased the thermal expansion. The steep increase of thermal strain in the temperature range of 570-600°C was caused by the silica aggregate in the mixtures. At 573°C β-quartz was transformed to α-polymorph, which was accompanied with expansion.

5. Conclusions

The resistance to high temperature of four concretes from Portland cement and calcium aluminate cement were analyzed. Two of the studied mixes were provided with randomly distributed basalt

PCC i wszystkich uwodnionych glinianów wapniowych w betonach CAC w temperaturze około 450°C, objętościowe zmiany krzemionki w 573°C spowodowane przez przemianę polimorficzną kwarcu β → α w obu betonach: PCC i CAC. Nie stwierdzono żadnego znacznego wpływu trwałych termicznie włókien na właściwości badanych betonów wygrzanych w temperaturach 400°C i 1000°C, niezależnie od rodzaju matrycy cementowej.

Podziękowania

Niniejsze badania to zostało sfinansowane przez Czeską Fundację Nauki, w ramach projektu nr P104 / 12/0791 oraz Ministerstwo Edukacji, Młodzieży i Sportu Republiki Czeskiej, w ramach projektu nr SGS16 / 199 / OHK1 / 3T / 11.

Literatura / References

1. D. N. Crook, M. J. Murray, Regain of strength after firing of concrete. Mag. Conc. Res., **22**, 149-154 (1970).

2. A. Petzold, M. Röhrs, Concrete for High Temperatures. London: Maclaren and Sons Ltd., 1970.

3. P. K. Metha, P. J. M. Monreiro, Concrete: Structure, Properties, and Materials. Englewood Cliffs, New Jersey: Prentice Hall College Div., 1986.

4. S. Mindess, J. F. Young, D. Darwin, Concrete. Engelwood Cliffs, New Jersey: Prentice-Hall, Inc., 1981.

5. C. M. George, Industrial Aluminous Cements, Chapter 9, ed. P. Baru-es, Structure and Preformance of Cements, Applied Science Publishers, London, New York.

6. W. Khaliq, H. A. Khan, High temperature material properties of calcium aluminate cement concrete. Constr. Build. Mat. **94**, 475-487 (2015).

7. A. Smith, T. Chotard, N. Gimet-Breart, D. Fargeot, Correlation between hydration mechanism and ultrasonic measurements in an aluminous cement: effect of setting time and temperature on the early hydration. J. of the European Ceramic Society **22**, 1947-1958 (2002).

8. N. Ukrainczyk, T. Matusinović, Thermal properties of hydrating calcium aluminate cement pastes. Cem. Concr. Res. **40**, 128-136 (2010).

9. V. Antonovič, J. Keriene, R. Boris, M. Aleknevičius, The Effect of Temperature on the Formation of the Hydrated Calcium Aluminate Cement Structure. Procedia Engineering **57**, 99-106 (2013).

10. V. Fiore, G. Di Bella, A. Valenza, Glass–basalt/epoxy hybrid composites for marine applications. Materials and Design **32**, 2091-2099 (2011).

11. V. Dhand, G. Mittal, K. Y. Rhee, S.-J. Park, D. Hui, A short review on basalt fiber reinforced polymer composites. Composites Part B: Engineering **73**, 166-180 (2015).

12. C. Jiang, K. Fan, F. Wu, D. Chen, Experimental study on the mechanical properties and microstructure of chopped basalt fibre reinforced concrete. Materials and Design **58**, 187-193 (2014).

13. N. Kabay, Abrasion resistance and fracture energy of concretes with basalt fiber. Constr. Build. Mat. **50**, 95-101 (2014).

14. L. Domagała, I. Hager, Influence of high temperature on compressive strength of structural lightweight concrete. Cement Wapno Beton **79**, 138-143 (2012).

fibers which are supposed to be thermally stable in the high-temperature range. The matrices of the investigated hardened mixes were analyzed at first using differential scanning calorimetry and thermogravimetry, in order to identify the characteristic temperatures at which the prepared specimens should be heated. Then, the basic physical properties, water and water vapor transport parameters, and thermal properties were determined after heating to the temperatures of 105°C, 400°C, and 1000°C, which were found the most appropriate.

Experimental results showed that in the reference state representing the specimens dried in an oven at 105 °C for 24 hours the Portland-cement concretes (PCC) exhibited overall better properties than the calcium aluminate cement concretes (CAC) which could be at least partially affected by the possible AH_3 decomposition. The open porosity of PCC was lower, compressive and bending strengths higher, the capability of water and water vapor transport lower. The application of basalt fibers led in the reference state to a substantial increase in bending strength for both composite types but the compressive strength was improved only slightly, mainly because of the increase of open porosity induced by the incorporation of fibers in the cement matrices.

Both PCC and CAC were able to resist to the heating at 400°C in a satisfactory way; the deterioration of their properties was relatively low and the residual properties were still acceptable for their limited use in a structure. The situation after exposure to 1000°C was different. While CAC retained about 25% of its strength, thus it was still capable of some (though very limited) use, the properties of PCC were deteriorated almost completely. The two most important factors affecting the properties of the analyzed composites were, apparently, the decomposition of C-S-H and $Ca(OH)_2$ in PCC and all calcium aluminate hydrates in CAC at approximately 450°C and the volumetric changes of silica aggregates at 573°C caused by the quartz β → α transition for both PCC and CAC. The effect of randomly distributed thermally stable basalt fibers was not found to have any substantial effect on the properties of the analyzed composites subjected to both 400°C and 1000°C, regardless of the matrix type.

Acknowledgements

This research has been supported by the Czech Science Foundation, under project No P104/12/0791, and Ministry of Education, Youth and Sports of the Czech Republic, under project No SGS16/199/OHK1/3T/11.

15. I. Hager, T. Tracz, K. Krzemień, Usefulness of selected destructive and non-destructive methods in the assessment of concrete after fire. Cement Wapno Beton **81**, 145-151 (2014).

16 V. K. R. Kodur, L. Phan, Critical factors governing the fire performance of high strength concrete systems. Fire Safety Journal **42**, 482-488 (2007).

17. D. R. Flynn, Response of High Performance Concrete to Fire Conditions: Review of Thermal Property Data and Measurement Techniques. Milwood, USA: National Institute of Standards and Technology, 1999.

18. ČSN EN 206 - Concrete – Specification, performance, production and conformity. Prague: Czech Standardization Institute, 2014.

19. S. Roels, J. Carmeliet, H. Hens, O. Adan, H. Brocken, R. Černý, Z. Pavlík, C. Hall, K. Kumaran, L. Pel, R. Plagge, Interlaboratory Comparison of Hygric Properties of Porous Building Materials. J. of Thermal Envelope and Building Science **27**, 307-325 (2004).

20. ČSN EN 1015: Methods of test for mortar for masonry - Part 11: Determination of flexural and compressive strength of hardened mortar. Prague: Czech Standardization Institute, 2000.

21. ČSN 72 7031: Determination of water vapour diffusion coefficient of building materials by method without temperature gradient. Prague: Czech Standardization Institute, 2001.

22. E. Vejmelková, M. Pavlíková, M. Jerman, R. Černý, Free water intake as means of material characterization. J. of Building Physics **33**, 29-44 (2009).

23. M. K. Kumaran, Moisture diffusivity of building materials from water absorption measurements. J. of Thermal Envelope and Building Science **22**, 349-355 (1999).

24. A. Trník, I. Medveď, R. Černý, Measurement of linear thermal expansion coefficient of concrete at high temperatures: A comparison of isothermal and non-isothermal method. Cement Wapno Beton **79**, 363-372 (2012).

25. R. Černý, P. Rovnaníková, Transport processes in concrete. London: Spon Press, 2002.

26. T. Korecký, M. Keppert, J. Maděra, R. Černý, Water transport parameters of autoclaved aerated concrete: Experimental assessment of different modeling approaches. J. of Building Physics **39**, 170-188 (2015).

5.3.2 High temperature durability of fibre reinforced high alumina cement composites

E. Vejmelková, D. Koňáková, L. Scheinherrová, M. Doleželová, M. Keppert, R. Černý, Construction and Building Materials 162 (2018) 881–891 [50]
https://doi.org/10.1016/j.conbuildmat.2018.01.076

This paper presents a significant advancement in the understanding of the high-temperature durability of CAC composites, particularly those reinforced with basalt fibres. While previous research addressed the varying matrices and the general impact of basalt fibres. This work is aimed more specifically at the hydration and thermal resistance of CAC, including varying ratios of basalt fibres. The study offers comprehensive evaluations of fibre-reinforced CAC composites exposed to temperatures up to 1000 °C, covering not only basic physical and mechanical characteristics but also thermal and hygric transport properties.

The research systematically analysed CAC hydration (rich in Al_2O_3), confirming the coexistence of metastable (CAH_{10}, C_2AH_8) and stable (C_3AH_6, AH_3) hydrates during early curing. Thermal and mineralogical analyses (XRD, STA, TG) clarified the dehydration and recrystallisation processes critical for CAC's thermal performance.

The use of basalt aggregates and fibres significantly improved CAC durability. The optimal composite, combining longer and shorter fibres (90:10 ratio), retained 50% compressive and 34% bending strength after 1000 °C exposure. It also exhibited the lowest porosity, highest water and vapour resistance, and minimal thermal strain, maintaining near-linear thermal expansion from 20 to 1000 °C. Beyond, the study provided novel insights into moisture transport, sorption, and thermal conductivity under extreme heat, showing how basalt fibres limit microstructural degradation.

Key contributions include:

- Comprehensive analysis of CAC phase evolution under thermal loading
- Evidence of basalt fibres influencing mechanical retention and thermal strain
- Optimising fibre content and formulation for refractory applications

The work presents a major step toward developing durable basalt fibre reinforced CAC composites for structural and refractory applications by assessing a wide scope of properties.

Construction and Building Materials 162 (2018) 881–891

Contents lists available at ScienceDirect

Construction and Building Materials

journal homepage: www.elsevier.com/locate/conbuildmat

Virtual Special Issue
Durability of Innovative Construction Materials and Structures

High temperature durability of fiber reinforced high alumina cement composites

Eva Vejmelková, Dana Koňáková, Lenka Scheinherrová, Magdaléna Doleželová, Martin Keppert, Robert Černý *

Department of Materials Engineering and Chemistry, Faculty of Civil Engineering, Czech Technical University in Prague, Thákurova 7, 166 29 Prague 6, Czech Republic

HIGHLIGHTS

- High temperature durability of high alumina cement fiber reinforced composites was studied.
- Simultaneous presence of CAH_{10}, C_2AH_8, C_3AH_6, and AH_3 was found after 2 28 days hydration.
- Basalt aggregates and basalt fibers improved significantly high temperature durability.
- Residual compressive and bending strengths were up to 50% and 34% after 1000 °C exposure.
- Thermal strain was almost linear within the whole 20 1000 °C range.

ARTICLE INFO

Article history:
Received 22 May 2017
Received in revised form 8 January 2018
Accepted 13 January 2018

Keywords:
Cement composites
High alumina cement
Basalt fibers
Durability
High temperatures

ABSTRACT

The effect of high temperature exposure on the durability of fiber reinforced composite materials based on high alumina cement is studied. A combination of X ray diffraction and thermal analyses of hydrated phases shows a simultaneous presence of all principal hydrates (CAH_{10}, C_2AH_8, C_3AH_6, AH_3) in significant amounts during the whole 2 28 days hydration period. The application of basalt aggregates and basalt fibers is found to improve significantly the high temperature durability, in a comparison with the cement paste. The residual values of compressive and bending strength of the most successful mix with the com bination of longer and shorter basalt fibers in a 90:10 ratio are 50% and 34%, respectively, after 1000 °C exposure. The fiber reinforced composite material with the most favorable mechanical properties exhi bits also the highest resistance to water and water vapor transport and the lowest water vapor adsorption after 1000 °C pre heating, which correlates well with its lowest amount of pores bigger than 100 nm. The thermal conductivity and specific heat capacity of all analyzed composites show a significant increase with the increasing moisture content; the differences between the values in dry and water saturated state are up to 100% and 65%, respectively. The thermal strain of all studied materials is almost linear within the whole 20 1000 °C range, with the basalt fibers being able to decrease it by up to 7% at 1000 °C.

© 2018 Elsevier Ltd. All rights reserved.

1. Introduction

Durability of concrete is mainly governed by its permeation properties and the harshness of the environment [1,2]. Transport of water, soluble salts, and gases in concrete presents the basic pre requisite for concrete deterioration because of their possible inter actions with concrete components, which can affect the integrity of the cement matrix, aggregates, interfacial transition zone, or the steel reinforcement [3]. Therefore, water transport in concrete became a subject of many research studies to date. For example, Guimaraes et al. [4] tried to develop a numerical program for pre diction of water absorption in porous media. Bao et al. [5] focused on the investigation of the influence of effects of short term sus tained uniaxial compressive or tensile loadings on water transport. Smyl et al. [6] studied isothermal unsaturated moisture transport and simulated moisture ingress in damaged mortar and concrete. Very frequent were also investigations of salt transport in cement composites.

Wang et al. [7] simulated water and chlorides transport in cracked unsaturated concrete. Chloride transport coupled with simulation of fracture mechanics in cracked concrete was

* Corresponding author.
E-mail address: cernyr@fsv.cvut.cz (R. Černý).

https://doi.org/10.1016/j.conbuildmat.2018.01.076
0950-0618/© 2018 Elsevier Ltd. All rights reserved.

described in the study of Tavares et al. [8], while Real et al. [9] investigated corrosion induced by the presence of chlorides in structural lightweight aggregate concrete. Similarly to the pres ence of chlorides, also sulfates can induce degradation processes. For example Najjar et al. [10] investigated damage mechanisms caused by both chemical and physical sulfate attack. Modeling of this kind of attack was also the matter of the study performed by Cefis et al. [11]. Among other kind of chemicals, for example min eral and organic acid attack was studied by Beddoe [12] and Dyer [13].

The external conditions acting negatively on concrete elements in building structures can be represented mainly by the marine environment, ground water, gas environment, or the freeze/thaw cycles. Bo et al. [14] proposed probabilistic durability assessment of concrete structures in marine environments. Du et al. [15] ana lyzed inhibitory effects of chloride ions on concrete sulfate attack in the marine conditions. Ghobadi et al. [16] studied ground water effect on concrete lining of tunnels. In addition to ordinary envi ronments, concrete can be used also in some specific application, which can harmfully affected its structure. Voefel et al. [17] inves tigated the mechanisms of concrete deterioration in biogas diges ter. Yu et al. [18] formulated an equation for determining freeze thaw fatigue damage in concrete. Freeze thaw loadings can though act together with some previously mentioned degradation pro cesses. For example, Chen et al. [19] assessed the effects of simul taneous sulfate attack and freeze thaw cycle damage of cement based material, while Wang et al. [20] studied concrete under chloride salt freeze thaw cycles.

High temperature durability of concrete is mostly understood in terms of its fire resistance. Current research can be divided into two groups. The first is focused on the behavior of structural ele ments, such as concrete filled steel plate composite walls (Wei et al. [21]), or concrete filled steel tubular columns (Shekaste hband et al. [22], Song et al. [23]), under fire. The second group deals with residual properties of cement composites. Concrete based on Portland cement (PC) was probably the most often ana lyzed material in that respect. Tan et al. [24], in a characteristic example of such studies, analyzed the influence of high tempera tures up to 600 °C on residual properties of PC based foamed con crete and reported a decrease of compressive strength at maximal temperature exposure by about 50 70%. Cementitious composites based on blended cement (PC with fly ash) with hybrid PVA and steel fibers were examined by Liu et al. [25]. They presented a decrease of compressive strength after exposure to 800 °C by about 50%, despite the use of silica sand and Portland cement, which was probably due to the positive effect of pozzolanic fly ash and PVA fibers. Bodnárová et al. [26] investigated behavior of blended cement (PC with pozzolan) based composites with polypropylene or steel fibers and basalt or lightweight aggregate and reported a decrease of compressive strength in the range of 42% 65% due to the loading by 800 °C. In general, it can be concluded that PC does not resist to high temperatures very well. Thermal behavior of PC depends on temperature decomposition range of particular cement phases, specifically of calcium silicate hydrates (CSH), portlandite, and calcium carbonate, and of the content of bound water [27]. Dehydration of CSH begins at about 100 °C [27 29], which is accompanied by decomposition of ettringite and other sulfoalumi nates at 100 °C 200 °C [29]. Another important reactions are port landite decomposition occurring in the temperature range of 400 °C 600 °C [27 29] and decomposition of calcite from 500 °C to 920 °C [27,29]. All mentioned processes are accompanied by big mass losses. The material transformation is often manifested in explosive spalling (up to about 300 °C) and crack formation.

Calcium aluminate cement (CAC) rich in Al_2O_3 may present an alternative to PC in high temperature applications. Its utilization may seem controversial, in general. Because of the loss of long term strength, which led to collapse and defects of buildings in the second half of 20th century, CAC was forbidden in 1970s for construction of load bearing structures. However, on the other hand, its overall suitability for a production of concrete elements and composites exposed to temperatures even above 1000 °C was never infirmed. In a comparison with PC, CAC fundamentally differs in phase composition; calcium silicates are not present. The main phase of calcium aluminate cement is monocalcium alu minate (CA), which in the case of higher alumina cement is accom panied by dicalcium aluminates (CA_2) and dodecacalcium heptaaluminate ($C_{12}A_7$) [30]. Minor phases which calcium alumi nate cement can contain are gehlenite (C_2AS), brownminilerrite (C_4AF) and dicalcium silicate (C_2S) [30]. The hydration process is widely influenced by phase composition. However, in contrast to the hydration of calcium silicate compounds (the formed hydrates are similar for temperatures up to 100 °C), the process of CAC hydration is strongly dependent on temperature. The main prod ucts are calcium aluminate decahydrate (CAH_{10}), occurring mainly at temperatures under 22 °C, followed by dicalcium aluminate octahydrate (C_2AH_8), arising primarily from 20 °C to 30 °C [31]. Both mentioned phases are hexagonal and metastable. The last most common product is cubic and stable tricalcium aluminate hexahydrate (C_3AH_6), which is usually present in paste when hydration temperature is above 30 °C or due to the conversion pro cess [32]. In addition to the mentioned calcium aluminate hydrates (CAH), also aluminum hydroxide (AH_3), either in the form of amor phous phase or as crystalline gibbsite, is present in hydrated CAC pastes. Similarly to PC, also CAC thermal decomposition begins at about 100 °C, with the amorphous AH_3 in this case [33]. The dehy dration of CAH phases takes place in a wider temperature range, from 100 °C to 370 °C [29,33,34], or actually up to 750 °C taking into the account the final dehydration of $C_{12}AH_7$ [34]. At higher temperatures, 900 °C 1000 °C, the recrystallization process of $C_{12}A_7$ to CA and CA_2 occurs [33,34]. In a comparison with PC, the mass changes are generally lower and CAC is able to withstand even temperatures above 1400 °C [35].

Current practical applications of CAC are mainly connected with designing refractory castables. Wang et al. [35] investigated a material composed of tabular alumina, reactive alumina, CAC and dispersant agent and reported mechanical strengths growth at temperatures above 1000 °C, which was caused by the sintering process and densifying effect of recrystallization of calcium alumi nate phases. Klaus et al. [36] studied a similar refractory castable but they focused on the influence of specific surface area of alu mina filler on the hydration kinetics of CAC. Regarding the high temperature under 1000 °C, Khaliq et al. [37] studied the difference between the behavior of concretes based on CAC and PC. They con firmed higher compressive strength of concrete based on CAC in the temperature range of 20 °C 800 °C, as well as higher elastic modulus and compressive toughness. Zhang et al. [38] compared the temperature dependence of thermal diffusivity of cement pastes based on these two kinds of cement. Alonso et al. [39] proved in their study the applicability of CAC blended with blast furnace slag in the conditions of long term repeated thermal load ing up to 550 °C.

One of the most common possibilities how to improve the per formance of cement composites is reinforcing them by fibers. Specifically, the fibers application can lead to increasing the tough ness of concrete, tensile, flexural, and shear strength, impact resis tance, frost resistance, or restraining the shrinkage. The choice of fibers (steel, glass, synthetic, organic fibers) depends on the required properties, and where the improvement is desired. For fire resistant concrete, an important characteristic is the ability of fibers to lessen the spalling of the surface layer and also to increase the fracture energy after heating. Basalt fibers can be con sidered as a very suitable choice in that respect, which is due to

their high temperature resistance up to 1255 °C [40]. In a comparison with glass fibers, they exhibit lower mass changes due to the high temperature exposure [41]. Basalt fibers also have one of the highest tensile strength among the most common kinds of fibers, higher elastic modulus than glass fibers, they are lighter in comparison with steel fibers, and their elongation at break is lower than of glass and steel fibers. Basalt fibers shows somehow weaker properties in a comparison with carbon fibers, but they are cheaper [42].

The application of basalt fibers in concrete production was mostly investigated in concrete based on PC to date. Jiang et al. [43] reported that although basalt fibers somehow reduced workability of fresh concrete, they improved bending and tensile strength, toughness, abrasion resistance, fatigue strength, deformation capability, and load bearing capacity after cracking when used with blended cement. Kabay [44] studied abrasion resistance and fracture energy of PC based concrete. They confirmed the flexural strength and fracture energy to increase due to the basalt fibers. Their utilization also led to an improvement of abrasion resistance and reduction of drying shrinkage of cement paste or mortar. Jalasutram et al. [45] investigated mechanical properties of fiber reinforced concrete and found out, that the basalt fibers up to 2% of volume led to almost no difference in compressive strength. However, the splitting strength and flexural strength was improved due to the reinforcement, and flexural toughness as well. Ren et al. [46] dealt with the influence of basalt fibers on concrete based on blended cement exposed to elevated temperatures and reported that their application led to improvement of strength performance, deformation capacity, and energy absorption of concrete also after temperature exposure up to 800 °C.

Table 1
Chemical composition of raw materials.

Material	Al_2O_3	CaO	Na_2O	SiO_2	MgO	Fe_2O_3	K_2O
CAC	70.7	28.2	0.4	0.4	0.1	0.1	0.1
Basalt aggregate	17.2	12.8	4.2	41.9	7.2	11.0	0.9
Basalt fibers	17.6	8.9	2.7	54.4	3.6	9.8	1.7

The studies dealing with fiber reinforcement of concrete based on CAC were relatively rare until now, the type of fibers notwithstanding. For example, Boris et al. [47] reported a positive effect of carbon fibers utilization on early hydration and microstructure of CAC pastes. Garcés et al. [48] investigated carbon fibers in CAC mortars and found that carbon fibers improved the mortars strength but increased their porosity at the same time. Frantsis et al. [49] studied the bonding ability of steel fibers in CAC. References dealing with the application of basalt fibers in CAC based composites were not found in common literature sources.

In this paper, the high temperature durability of fiber reinforced composite materials based on calcium aluminate cement rich in Al_2O_3 is studied. At first, the course of hydration of high alumina cement is monitored by a combination of qualitative and quantitative X ray diffraction and thermal analysis. The response of high alumina cement pastes to high temperature exposure is analyzed by thermogravimetry and differential scanning calorimetry, and by the measurement of mechanical properties. Then, several different fiber reinforced composite mixes based on high alumina cement are designed and their properties are determined as functions of previous thermal load up to 1000 °C. The high temperature induced changes of the wide range of investigated parameters, namely porosity, pore size distribution, compressive strength, bending strength, water absorption coefficient, apparent moisture diffusivity, water vapor diffusion resistance factor, sorption isotherms, thermal conductivity, specific heat capacity, and thermal strain, are discussed in a relation to the type and dosage of applied fibers, and the most successful composite mixes are identified.

2. Materials and mix design

The calcium aluminate cement (CAC) Secar 71 produced by Kerneos, Inc., was used for the preparation of cement composites in this study. This material with a content of aluminum oxide of about 70% belongs to high alumina cements. A detailed chemical composition of Secar 71, as determined by the X-ray fluorescence spectrometry (a Thermo ARL 9400 XP device, data evaluation by the standardless software UniQuant 4), can be found in Table 1. The qualitative X-ray diffraction (XRD) analysis performed using a PANalytical X'Pert PRO system (Fig. 1) showed

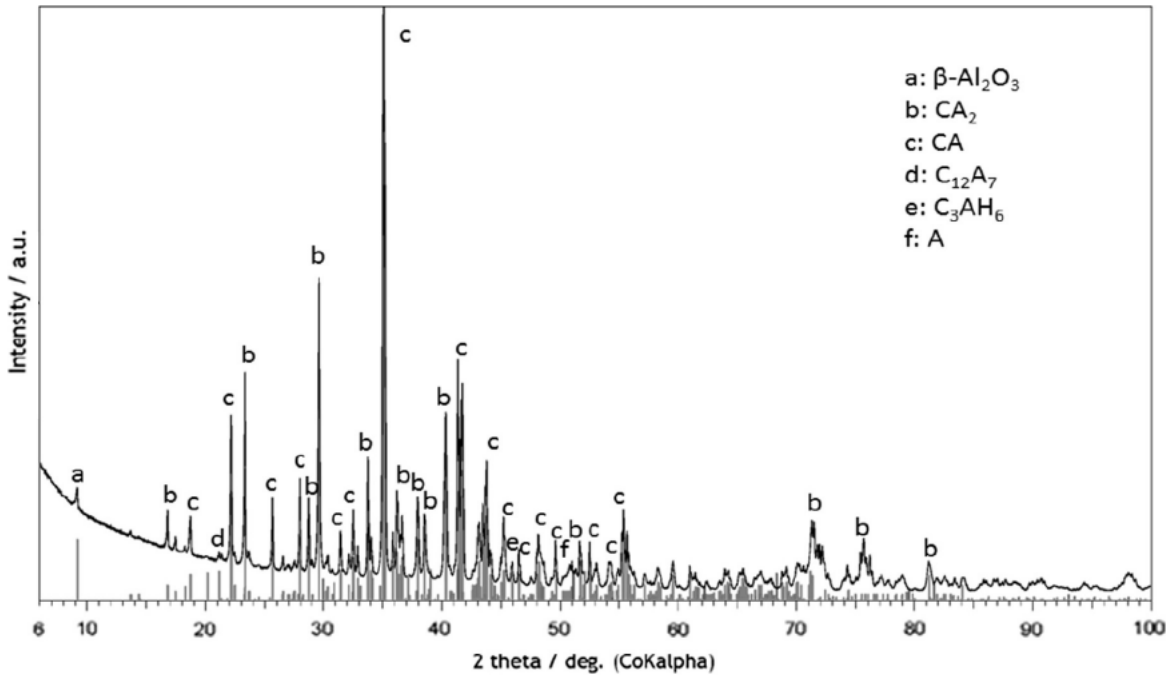

Fig. 1. XRD pattern of CAC.

Table 2
Mineralogical composition of CAC.

CA	CA_2	$C_{12}A_7$	A	β-Al_2O_3	Amorphous
54.7	38.1	0.5	0.8	1.4	4.5

krotite (calcium aluminate CA) and grossite (calcium di-aluminate, CA_2) as the main phases; the minor phases were corundum (A), β-Al_2O_3 (or possibly $NaAl_{11}O_{17}$), and mayenite ($C_{12}A_7$). A small amount of katoite (C_3AH_6) was detected as well; it indicated a partial hydration of CAC already before the samples were produced.

The results of quantitative XRD analysis (Rietveld method, 20% of ZnO as internal standard, evaluation by the TOPAS software) of the high alumina cement in Table 2 revealed, besides the crystalline phases mentioned before, also a certain amount of amorphous phases which, on the basis of mass balance, contained mainly Al_2O_3. The specific surface area of Secar 71 was 381 m^2 kg^{-1} (Blaine), its grain size distribution curve had the maximum at 11 μm (Fig. 2). The initial and final setting times were determined as 255 min and 285 min, respectively.

Two grades (0/4 and 2/5 mm) of crushed basalt originating from Dobkovičky quarry (Kámen Zbraslav, a. s.) were used as aggregates. The basalt was composed mainly of pyroxene (specifically, clinopyroxene, augite and, in lower amount, diopside), succeeded by analcime, anorthite, muscovite, and, in lower amount, by nepheline. The chemical composition, as determined by XRF, is given in Table 1, the grain size distribution of the aggregates is shown in Fig. 3, density of basalt aggregates is 3086 kg m^{-3}.

The third main component of cement composites were basalt fibers. They were produced by Basaltex, a.s., and their chemical composition can be found in Table 1, while Table 3 summarized their physical properties. Two different fiber lengths were used, specifically 12 and 6 mm. The remaining components of composite mixes were polycarboxylate ether based superplasticizer Sika ViscoCrete-1035CZ and tap water.

The cement pastes used for the analysis of the course of hydration and of the basic response to high-temperature exposure, had the water/cement ratio of 0.25. The composition of the analyzed fiber-reinforced composites is summarized in Table 4. The free parameter of the mix design was the ratio between the longer (12 mm) and shorter (6 mm) fibers, which was 100:0, 90:10 and 80:20 for the mixtures denoted as CB0, CB1 and CB2, respectively. A reference composite without any fibers, CBR, was studied as well, for the sake of comparison.

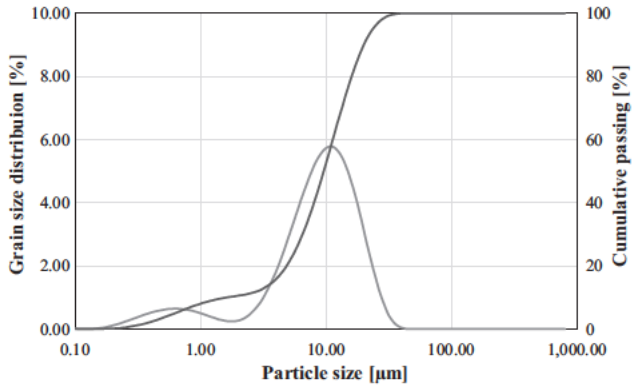

Fig. 2. Grain size distribution of CAC.

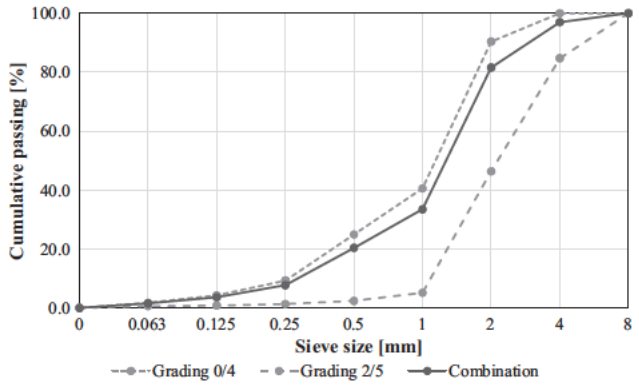

Fig. 3. Grain size distribution of basalt aggregates.

Table 3
Physical properties of used basalt fibers.

Property	Value
Density [kg m^{-3}]	2900
Melting temperature [°C]	1350
Softening temperature [°C]	950
Water absorption capacity [%]	0.5
Modulus of elasticity in tension [GPa]	100
Tensile strength [GPa]	1.85–2.15
Compressive strength [MPa]	300
Thermal conductivity [W m^{-1} K^{-1}]	0.027–0.033
Electrical resistivity [Ω m]	1012

Table 4
Composition of studied composites (kg/m^3).

Component	CBR	CB0	CB1	CB2
CAC	900	900	900	900
Basalt aggregates 0/4	880	880	880	880
Basalt aggregates 2/5	220	220	220	220
Basalt fibers 12 mm	–	14.5	13.05	11.6
Basalt fibers 6 mm	–	0	1.45	2.9
Superplasticizer	13.5	13.5	13.5	13.5
Water	225	225	225	225

In the sample preparation process dry components (aggregate and cement) were mixed at first. Then, a portion of water containing superplasticizer was added. After a few minutes of additional mixing, fibers were gradually added. Finally, the remaining water was poured in. The resulting fresh mixtures were put into specific moulds. The specimens were cured in laboratory conditions, the temperature was (20 ± 1) °C, the relative humidity 25–30%. The experimental measurements were started after 28 days of curing.

As the main aim of research work in this paper was to study the high temperature durability of designed composites, a part of specimens was exposed to high temperatures before testing and the residual values of the particular parameters were determined. Before the thermal pre-treatment, the specimens were dried at 105 °C for 24 h, in order to exclude the effects of fast free water evaporation. Then, they were put in an electric top-cover furnace and heated to the chosen temperature with a rate of 0.5 °C per min. After reaching the predetermined temperature, the samples were left in the fumace for 3 h in isothermal conditions. The subsequent cooling was natural and was realized in the furnace as well. The loading temperatures were selected, according to the results of thermal analysis, as 400 °C and 1000 °C, one set of specimens served as a reference.

3. Experimental methods

3.1. Cement paste

The main purpose of the experiments on cement paste was to monitor the course of hydration of high alumina cement during the first 28 days period and to get basic information on the response of the paste to high temperature exposure.

The hydration process was analyzed by a combination of qual itative and quantitative XRD and thermal analyses. XRD measure ments were done using the same method as described in Section 2. The simultaneous thermal analysis (STA) consisted in monitoring the heat flow (power) and the mass changes during heating simul taneously, i.e., differential scanning calorimetry (DSC) and thermo gravimetry (TG) were used at the same time. The experiments were carried out using a Labsys Evo (Setaram) device in the tem perature range of 20 1000 °C in an argon atmosphere with a flow rate of 40 mL min^{-1}. The heating rate was 5 °C min^{-1}.

The response of high alumina cement pastes to high tempera ture exposure was analyzed by STA and by the measurement of mechanical properties. The compressive strength and bending strength were determined according to the EN standard for mor tars [50]. Measurement of bending strength was performed on three samples (40 × 40 × 160 mm), using an MTS 100 loading device in three point bending tests with 100 mm length span. Compressive strength was then determined on fragments of the

samples used in the bending strength measurement. An EU40 loading device was employed and in the actual experiment the samples were put between two steel pressure plates with dimensions of 40 × 40 mm. Great emphasis was given to the centering of the arrangement, because only simple compression should act in this case.

3.2. Fiber reinforced composites

The fiber reinforced composites were analyzed using a wide set of experimental methods, in order to get a complex view of the high temperature induced effects. The measurements included the parameters of the pore space, basic physical properties, mechanical parameters, hygric and thermal properties, and thermomechanical parameters.

Characterization of the pore structure was performed by mercury intrusion porosimetry (MIP). Pore size distribution curves were obtained using Pascal 140 and 440 (Thermo Scientific) instruments in the range of pore radii of 3 nm 100 μm.

Bulk density, matrix density, and open porosity were the studied basic physical properties. The water vacuum saturation method [51] was used, which is based on the principle of Archimedes mass. Three samples (50 × 50 × 50 mm) were dried at 105 °C at first, so that the majority of physically bound water was removed. Then they were placed into a desiccator with boiled distilled water and air was evacuated during 3 h with a vacuum pump. The samples were kept under water not less than 24 h.

Compressive and bending strength of fiber reinforced composites were measured using the same methods, as described in Section 3.1 for cement paste. The number and dimensions of the specimens were the same as well.

The liquid water transport ability was characterized using a water absorption experiment. Three samples (50 × 50 × 50 mm) insulated on four lateral sides were immersed 2 mm in water and their mass changes in time were recorded by an automatic balance. Water absorption coefficient was then determined from the sorptivity plot [52] and the apparent moisture diffusivity was calculated according to Ref. [53].

Cup methods [54] were used for the characterization of water vapor transport, which were based on establishing two environments with different partial water vapor pressures. Three cylindrical samples (diameter 115 mm, height 15 mm) were insulated and fixed in cups containing silica gel (dry cup) or water (wet cup), which simulated the relative humidity of 5% or 95%, respectively. The experiment took place in a climatic chamber with the relative humidity of 50%. Steady state values of the mass gain or the mass loss, respectively, determined by the linear regression over the last five readings were used for the calculation of water vapor diffusion resistance factor.

The water vapor adsorption isotherms were determined to describe the moisture storage ability of the analyzed composites. In the experiments, 14 samples (30 × 30 × 10 mm) were used. The measurements took place in a climatic chamber where the relative humidity was increased in 20% steps.

Thermal conductivity and specific heat capacity were determined using an Isomet 2104 device. The measurement process was based on an analysis of temperature response of the analyzed sample to heat flow pulses. Because of the known high impact of water presence on thermal conductivity and specific heat capacity of most building materials, both studied thermal characteristics were measured in dry and water saturated state on three samples (70 × 70 × 70 mm).

The measurement of thermal strain depending on temperature was performed by a horizontal dilatometer [55] for three samples with the dimensions of 15 × 15 × 160 mm. The applied device utilized a comparative method; the real thermal expansion was determined by comparing the analyzed specimen with a reference corundum tube. One side of the specimen was placed against a fixed wall and the second side touched a pull rod which was connected to the length change indicator. The heating rate of the dilatometer was set to 1 °C per min and the maximum temperature of measurement was 1000 °C.

4. Results and discussion

4.1. Cement paste

The qualitative XRD analysis of CAC pastes detected the presence of CAH_{10}, C_2AH_8, C_3AH_6, and AH_3, as well as of unreacted CA and CA_2, over the whole analyzed time period of 2 28 days

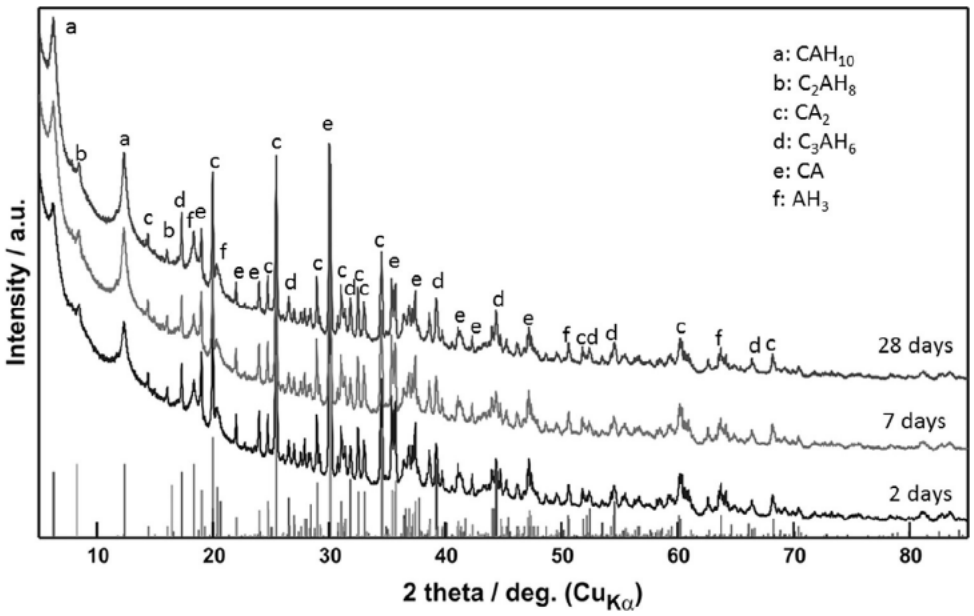

Fig. 4. X-ray diffractograms of CAC pastes.

(Fig. 4). Unfortunately, the quantitative analysis of this system could not be done in a common way because the structure of C_2AH_8 is not known.

The results of thermal analysis of CAC pastes are presented in Figs. 5 and 6. The loss of mass up to 120 °C [34] was connected with the loss of free water in capillary pores and bound water in the AH_3 gel. The first endothermic peak at about 120 °C corresponded with the dehydration of CAH_{10}. Decomposition temperature of this hydrate was found to range from 100 °C to 160 °C before [29,33]. There was not observed any significant peak at the decomposition temperature of C_2AH_8 which is known to dehydrate in the range of 140 °C 240 °C [29,33,34]. Its presence could though be hidden by the major peak of CAH_{10} and the multiple one of gibbsite (210 °C 320 °C [29,34]) and C_3AH_6 (240 °C 370 °C [33,34]). Gibbsite and C_3AH_6 may be products of CAC hydration but they may also be present as secondary products of the decomposition of thermodynamically unstable hydrates CAH_{10} and C_2AH_8. C_3AH_6 dehydration gave rise to $C_{12}A_7H$ that was supposed to decompose at about 750 °C [34]. However, Fig. 6 shows that this reaction occurred earlier, at about 690 °C. Its product, $C_{12}A_7$, appeared as a renewed dehydrated phase, which later, at temperatures over 900 °C, recrystallized to CA and CA_2. The raw CAC showed only one visible peak, in the temperature range of 240 °C to 300 °C (Fig. 6), which corresponded to C_3AH_6 thermal decomposition [34]; the raw cement contained 1.3% of this hydrate.

It should be noted that the quantification of the components of CAC systems by thermal analysis appeared as a very complex task for two basic reasons. First, the thermal decomposition processes, where water was released from the material, were overlapping. Second, the individual hydrates could be generated not only at the CAC hydration or conversion but also "in situ" during the thermal analysis, e.g., CAH_{10} decomposed during the measurement as

$$3CAH_{10} \rightarrow C_3AH_6 + 2AH_3 + 18H \quad (1)$$

Therefore, the common quantification procedures used for some other materials, such as Portland cement paste, could not be utilized for most components in this case.

As any of the applied experimental techniques (TG, DSC, XRD) itself did not enable a direct quantification of components present in the studied system, a specific procedure based on their combination was proposed for the identification of changes in CAC paste composition over time during the first 28 days of hydration.

A simplified system, consisting only of CA and CA_2 as the unreacted CAC components and the principal hydrates, CAH_{10}, C_2AH_8, C_3AH_6, and AH_3, was considered. The quantification procedure was based on the mass balance of Ca, Al and H (as elements), where two parameters were used as input values:

a) the amount of chemically bound water; it corresponded to the total mass loss obtained from TG; the free water was eliminated by gentle (50 °C, 2 h) drying of powder sample prior to the TG analysis,
b) the mass of CAC mixed in the paste.

Balancing of the three mentioned elements allowed to draw up three equations where on the left side were the sources (the known amounts of CAC and bound water) and on the right side the products, i.e., CAH_{10}, C_2AH_8, C_3AH_6, AH_3 and unreacted CAC (five unknowns). The intensity of X ray diffractions of CA_2 in time (Fig. 4) did not change what indicated that its rate of hydration was negligible; this observation was in accord with the previous findings [34,56]. Therefore, CA was assumed as the sole reacting part of CAC and CA_2 was not taken into the balance. Mayenite ($C_{12}A_7$) reaction was also omitted in the balance because of its low content (Table 2) in the used CAC even though this phase is highly reactive [34]. In order to reduce the number of unknowns in the balance, the following steps were done:

a) the content of CAH_{10} was calculated from TG using the mass loss between 110 and 160 °C (Fig. 5) where only a small overlap with other processes could be assumed [33,34],
b) the amount on unreacted CA was estimated from the intensities of its main diffraction at $2\theta = 30°$ (Fig. 4).

In this way, three sets (2, 7, and 28 days) of three equations for three unknowns, namely the mass fractions of C_2AH_8, C_3AH_6, and AH_3 in the paste, were obtained.

The results of the proposed quantification procedure are presented in Table 5. The rest to 100% was CA_2, A, β Al_2O_3, and the amorphous phase of CAC consisting mainly of alumina. The degree of conversion of CA reached 33.6% after 28 days. The simultaneous presence of all principal hydrates (CAH_{10}, C_2AH_8, C_3AH_6, AH_3) during the whole analyzed 2 28 days hydration period showed that the commonly accepted reaction scheme [57,58], where the forma

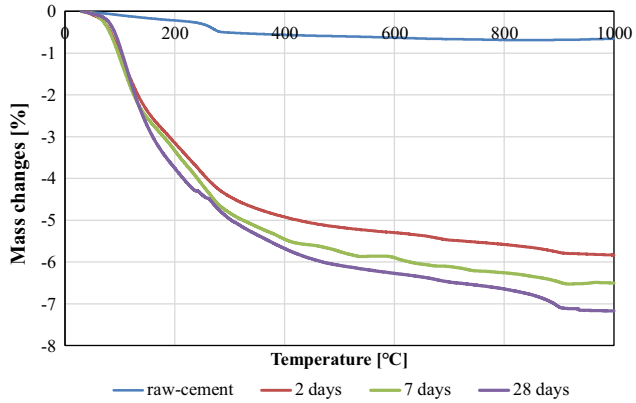

Fig. 5. Thermogravimetry of raw CAC and CAC pastes.

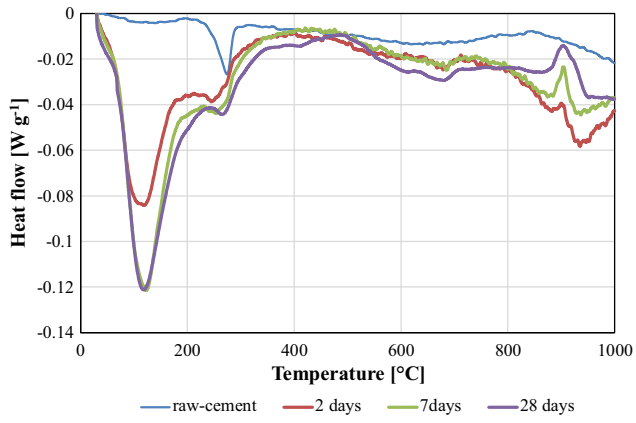

Fig. 6. Differential scanning calorimetry of CAC and CAC pastes.

Table 5
Mass fractions of hydration products and residual CA (in %).

Component	2 days	7 days	28 days
CAH_{10}	4.3	4.3	6.2
C_2AH_8	4.4	5.4	4.5
C_3AH_6	3.2	7.9	8.9
AH_3	2.4	5.8	5.2
Residual CA	41.4	34.6	33.7
Degree of CA conversion	19.6	32.3	33.6

tion of a specific hydrate depends strictly on the reaction temper ature, can be considered as only indicative.

The time development of both compressive and bending strength of cement paste was very fast (Fig. 7). After the first two days, the compressive strength reached 70% of its 28 days value, for the bending strength it was even 92%. This confirmed the fast hydration process which is typical for calcium aluminate cements.

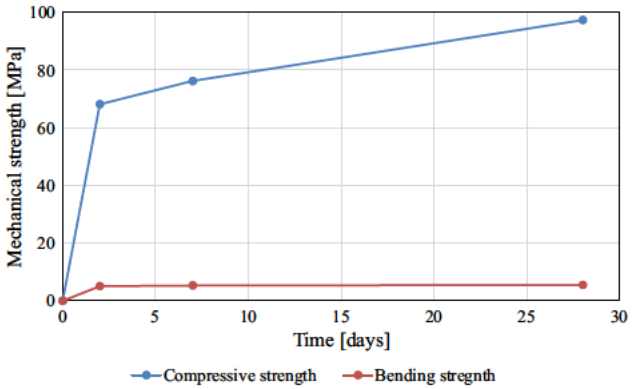

Fig. 7. Mechanical strength development of cement paste.

Table 6
Mechanical properties of cement paste after high-temperature exposure.

Compressive strength [MPa]			Bending strength [MPa]		
Ref	400 °C	1000 °C	Ref	400° C	1000 °C
97.4	86.7	49.8	5.5	2.1	0.7

The residual mechanical parameters of cement paste after the thermal pre treatment described in Section 2 are shown in Table 6. Apparently, the high temperature exposure had a relatively low deteriorating effects on the compressive strength; after heating to 400 °C its value decreased by about 11%, for 1000 °C the fall of compressive strength was 49%. However, in the case of bending strength the situation was worse; the decrease was 62% for 400 °C and 87% for 1000 °C. The calcium aluminate cement alone was thus not able to provide sufficient high temperature durability.

The observed decrease of strength was caused by thermal decomposition of the above quantified hydrates (Table 5), which was accompanied by volume changes. The diffractogram of CAC paste thermally treated at 1000 °C (Fig. 8) indicated that only anhydrous phases were present.

The Rietveld analysis, including the determination of the amount of amorphous matter (35.5%), was possible for the 1000 °C pre heated specimens, since they did not contain C_2AH_8. Table 7 summarizes the content of crystalline phases in the reference state and after pre heating at 1000 °C. As each of the present phases has a known specific volume (reciprocal of density), the theoretical specific volume and density of crystalline portion of both states could be calculated on basis of materials' composition and specific volumes of crystalline components (Table 7). Generally, hydrates had higher specific volume than anhydrous phases and thus dehy dration was accompanied with volume shrinkage causing the decrease of strength. A comparison of the calculated and experi mentally determined values of density showed that the latter were lower. It was caused by the presence of amorphous matter in stud ied materials; amorphous matter has generally a lower density than crystalline matter of the same chemical composition.

4.2. Fiber reinforced composites

The cumulative pore volume curves obtained by MIP (Fig. 9) show that in the reference conditions (without thermal pre

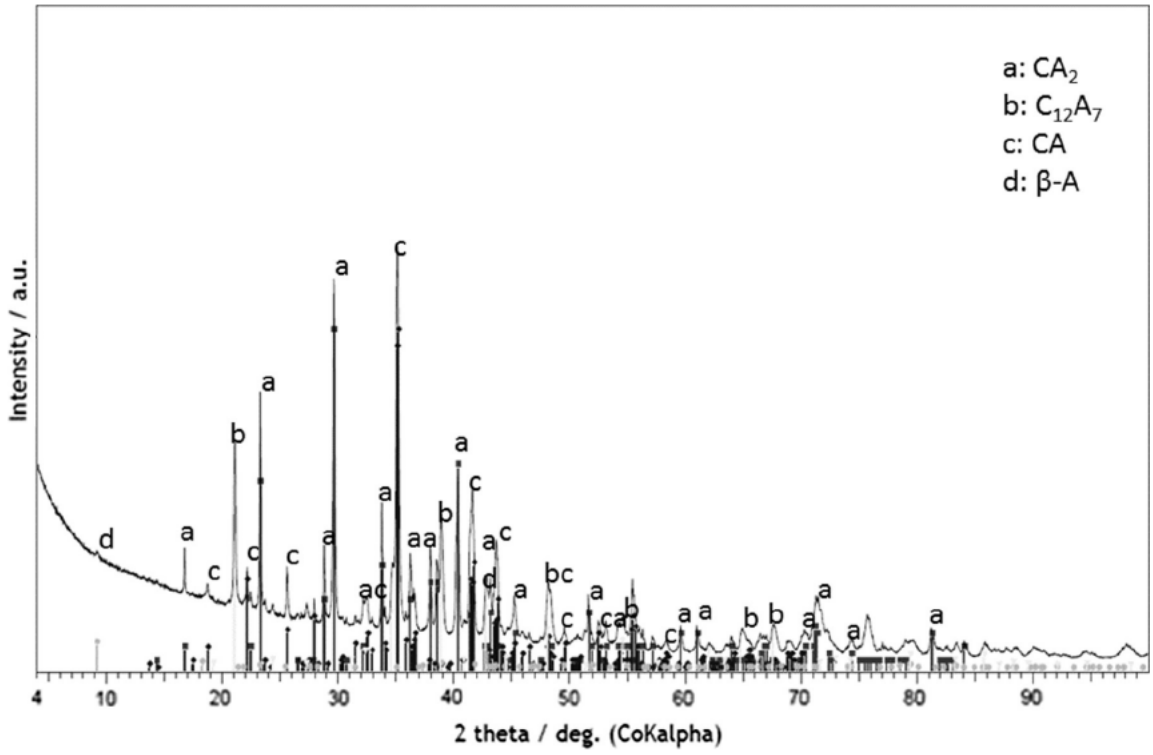

Fig. 8. XRD of CAC paste thermally treated at 1000 °C.

Table 7
Comparison of phase composition of CAC paste in reference state and thermally treated at 1000 °C.

	Phase composition (wt%)		Specific volume of the phase ($cm^3\ g^{-1}$)
	Ref	1000 °C	
CAH_{10}	6.2	–	0.575
C_2AH_8	4.5	–	0.513
C_3AH_6	8.9	–	0.397
AH_3	5.2	–	0.427
CA	33.7	45.6	0.336
CA_2	35.4	39.2	0.347
$C_{12}A_7$	0.4	13.3	0.372
Theoretical specific volume ($cm^3\ g^{-1}$)	0.354	0.339	–
Theoretical density ($g\ cm^{-3}$)	2.826	2.952	–
Measured density ($g\ cm^{-3}$)	2.762	2.904	–

treatment) the lowest porosity exhibited the reference composite CBR without fiber reinforcement. The other materials reached somewhat higher porosity but differed only slightly each other. The major difference between the reference material and the fiber

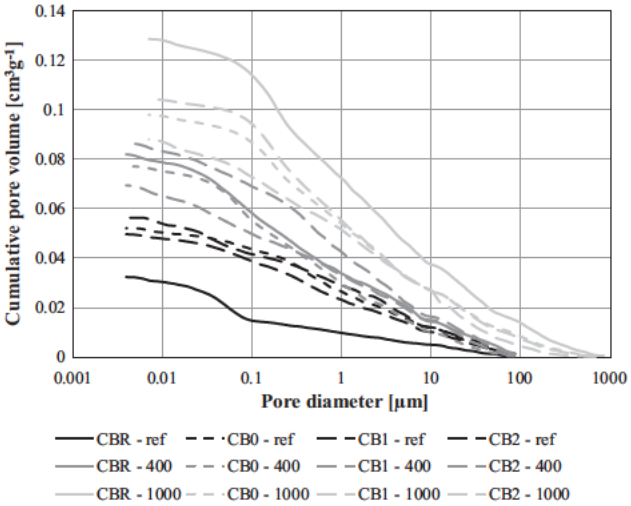

Fig. 9. Cumulative pore volume of composites.

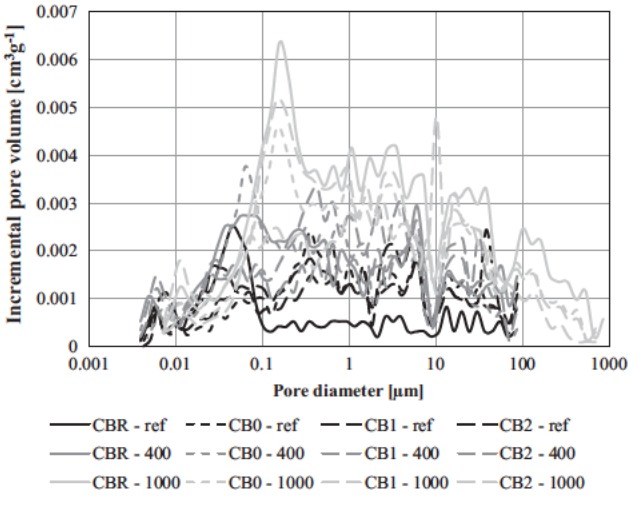

Fig. 10. Pore size distribution curves of composites.

Table 8
Basic physical properties of composites.

	Open porosity [–]			Matrix density [$kg\ m^{-3}$]			Bulk density [$kg\ m^{-3}$]		
	Ref	400 °C	1000 °C	Ref	400 °C	1000 °C	Ref	400 °C	1000 °C
CBR	0.201	0.286	0.370	2936	3257	3588	2347	2326	2259
CB0	0.219	0.281	0.345	2950	3198	3487	2304	2300	2282
CB1	0.214	0.265	0.323	2937	3140	3408	2309	2308	2306
CB2	0.222	0.291	0.355	2963	3235	3528	2306	2295	2276

reinforced composites was in the range of 100 nm 10 μm (Fig. 10). The tendency observed for the composites not affected by high temperature exposure was though considerably changed after the thermal pre treatment. Heating to 400 °C resulted in the poros ity of the reference material being comparable with the fiber rein forced composites, and in the case of 1000 °C the reference material reached even the highest porosity within the 100 nm 1 mm range. Regarding the influence of fibers, the best behavior, i.e., the lowest porosity, was observed for the composite CB1 with the longer shorter fiber ratio of 90:10.

The open porosity of studied composites measured for bigger specimens by the water vacuum saturation method (Table 8) increased by up to 85% in the case of the reference material but only up to 50% for CB1, due to the high temperature loading. The results were in a qualitative agreement with the MIP results in Fig. 8. The matrix densities reached for all materials very similar values in the reference conditions, 2950 $kg\ m^{-3}$ in average, and systematically increased, by up to 22%, with the increasing pre treatment temperature (Table 8), which was a result of decompo sition processes in the cement matrix described in Section 4.1. The bulk density showed an opposite tendency to the open porosity (Table 8). The reference material exhibited the highest bulk density in the reference conditions but also its biggest fall with the increas ing temperature. The fiber reinforced composite CB1, on the other hand, showed a very slow decrease of bulk density, only 1% after heating to 1000 °C.

The combination of longer and shorter fibers in the 90:10 ratio in the material CB1 appeared as the most successful solution also in the case of mechanical properties (Table 9), which was in a good agreement with the MIP experiments (Figs. 9 and 10) and with the measurements of basic physical properties (Table 8). After heating to 1000 °C, CB1 still retained 50% compressive strength and 34% bending strength, which could be considered as a good result. The positive effect of basalt fibers on both compressive and bend ing strengths was observed already in the reference conditions without any thermal pre treatment (Table 9); the difference between the reference material CBR and CB1 was 23% for compres sive strength and 12% for bending strength. Obviously, the thermal pre treatment magnified the role of fiber reinforcement; for 1000 °C the compressive strength of CB1 was 2.6 times higher and the bending strength 1.6 times higher than CBR.

The water absorption coefficient of analyzed composites was in the reference state very low and increased only moderately after

Table 9
Mechanical properties of composites.

	Compressive strength [MPa]			Bending strength [MPa]		
	Ref	400 °C	1000 °C	Ref	400 °C	1000 °C
CBR	84.4	48.4	19.6	12.87	5.46	2.98
CB0	95.9	65.4	39.5	13.40	6.60	4.30
CB1	103.6	80.6	51.8	14.45	7.97	4.89
CB2	88.8	54.3	24.5	13.06	6.03	3.71

Table 10
Liquid water transport properties of composites.

	Water absorption coefficient [kg m $^{-2}$ s $^{-1/2}$]			Apparent moisture diffusivity [m^2 s $^{-1}$]		
	Ref	400 °C	1000 °C	Ref	400 °C	1000 °C
CBR	0.014	0.029	0.151	7.53E−09	1.59E−08	2.22E−07
CB0	0.019	0.023	0.098	9.50E−09	1.03E−08	1.12E−07
CB1	0.016	0.020	0.079	7.44E−09	9.56E−09	8.55E−08
CB2	0.019	0.027	0.114	8.93E−09	1.33E−08	1.45E−07

Table 11
Water vapor transport properties of composites.

	Water vapor diffusion resistance factor: dry-cup [–]			Water vapor diffusion resistance factor: wet-cup [–]		
	Ref	400 °C	1000 °C	Ref	400 °C	1000 °C
CBR	67.8	30.1	16.9	58.33	24.98	12.07
CB0	58.3	30.3	19.2	51.60	24.34	15.54
CB1	57.5	32.4	21.4	51.41	26.69	17.68
CB2	58.8	28.8	18.1	53.42	24.04	14.86

the 400 °C pre heating (Table 10). However, for the 1000 °C expo sure its fast increase was observed for all four materials and also the difference between particular composites became more con siderable; CBR without fiber reinforcement reached about two times higher value of water absorption coefficient than CB1 with the basalt fibers ratio of 90:10. The apparent moisture diffusivity followed similar trends as the water absorption coefficient. The obtained results were in a good qualitative agreement with the open porosity (Table 8) and with the pore size distribution mea surements (Fig. 10). The amount of capillary pores in the range of 1 100 μm was, apparently, the most important factor deciding about the liquid water transport capability of studied materials.

The highest resistance against water vapor transport in the ref erence conditions showed the reference material CBR (Table 11) which was in accordance with its lowest open porosity (Table 8). The composites containing basalt fibers reached by about 14% lower values in the dry cup arrangement, and by about 11% in the case of wet cup. This tendency was though reversed after high temperature exposure, when composites without fiber reinforce ment achieved either comparable (for 400 °C) or higher (for 1000 °C) values of the water vapor diffusion resistance factor. After the thermal pre treatment at 1000 °C, the difference between CBR and CB1, which showed the best results, was 27% in the dry cup and 46% in the wet cup experiment.

The water vapor adsorption capability of all composites was rel atively high, in particular for the relative humidity over 60% (Fig. 11). In the reference conditions the lowest values of moisture content reached CBR, i.e., the composite without fiber reinforce ment. Its ability to moisture storage was, however, strongly increased as a result of high temperature exposure. This was caused primarily by the presence of recrystallized CA and CA_2 (Fig. 8) which were able to react with the surface phase of water adsorbed on the pore walls. After the pre treatment at 1000 °C, the lowest water vapor adsorption showed CB1, i.e., the fiber rein forced composite with 90:10 ratio of longer and shorter fibers.

The highest thermal conductivity in dry state showed the com posite without fiber reinforcement in reference conditions, the lowest the same material after 1000 °C pre heating (Fig. 12). The decrease was very substantial, under 50% of the reference value, which was related to the changes in open porosity (Table 8). The fiber reinforced composites exhibited similar trend but the differ ences in thermal conductivity caused by high temperature expo

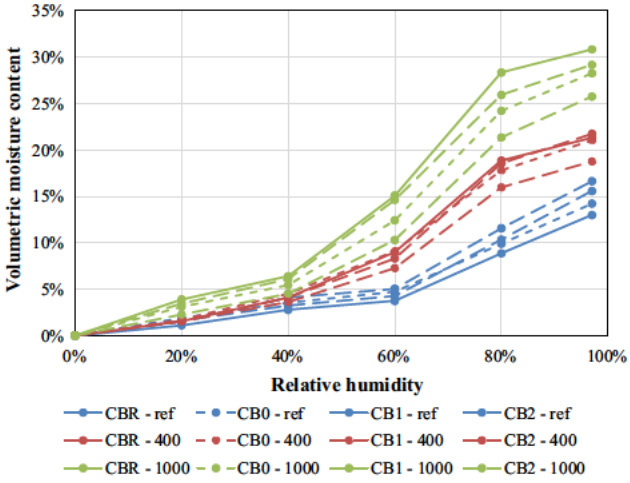

Fig. 11. Adsorption isotherms of composites.

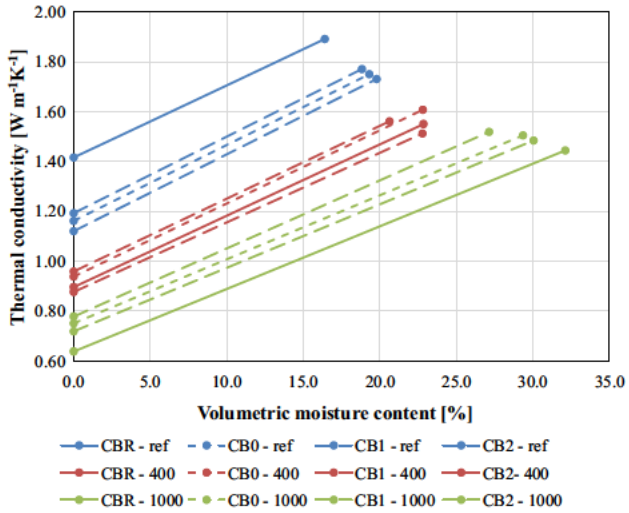

Fig. 12. Thermal conductivity of composites.

sure were lower. The thermal conductivities of all analyzed materials exhibited a significant dependence on moisture content; their values in water saturated state were up to two times higher than in the dry state.

The specific heat capacity in dry state was similar for all com posites; the differences were within the error range of the applied method (Fig. 13). The influence of moisture content was more remarkable, due to the very high specific heat capacity of water; the observed increase was up to 65%.

All studied composites exhibited an almost linear dependence of thermal strain on temperature (Fig. 14), which was a very posi tive result. Apparently, the favorable properties of basalt aggre gates in high temperature conditions presented the most essential factor in that respect. The differences between particular composites were negligible up to 120 °C. Then, the effects of decomposition of calcium aluminate hydrates in the cement matrix gained on importance and the positive effect of fiber rein forcement could be observed. The lowest strain over the whole temperature range of 20 1000 °C was found for the material CB1 with the longer shorter fiber ratio of 90:10; at 1000 °C it was by 7% lower than for the reference CBR.

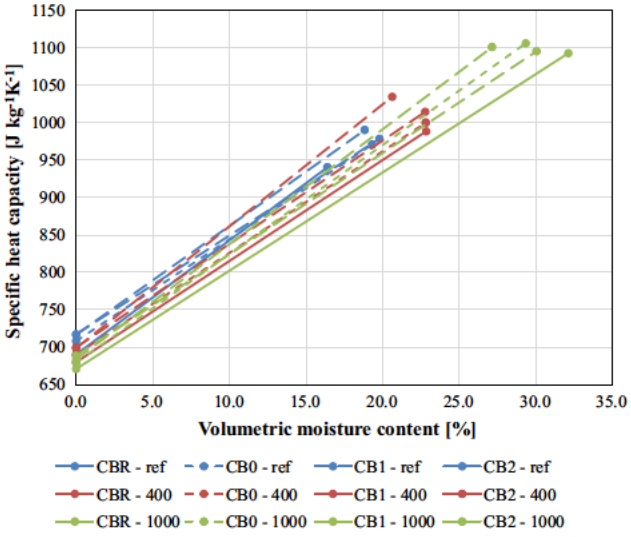

Fig. 13. Specific heat capacity of composites.

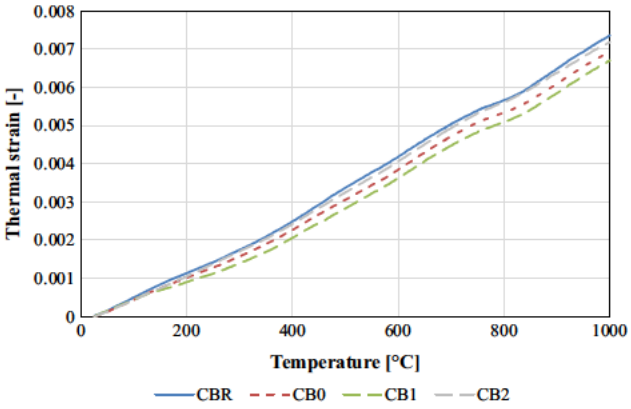

Fig. 14. Thermal strain of composites.

5. Conclusions

The high temperature durability of fiber reinforced composite materials based on calcium aluminate cement rich in Al_2O_3 was studied, using a wide set of methods for materials characterization and identification of material parameters. The main experimental findings can be summarized as follows:

- XRD analysis of cement pastes detected the presence of CAH_{10}, C_2AH_8, C_3AH_6, and AH_3, as well as of unreacted CA and CA_2, over the whole analyzed time period of 2 28 days.
- Thermal analysis of cement pastes identified the dehydration of CAH_{10} at 110 160 °C, C_3AH_6 at 240 300 °C, $C_{12}A_7H$ at 690 °C, and recrystallization of CA and CA_2 at 900 °C.
- A novel procedure based on the combination of XRD and thermal analysis was proposed for the quantification of components present in the hydrated calcium aluminate cement. A simultaneous presence of all principal hydrates (CAH_{10}, C_2AH_8, C_3AH_6, AH_3) in significant amounts during the whole analyzed 2 28 days hydration period was observed, confirming that the commonly accepted reaction scheme where the formation of a specific hydrate depends strictly on the reaction temperature, is only indicative.
- The calcium aluminate cement alone was not found capable to provide a sufficient high temperature durability. The residual compressive strength of cement paste after heating to 1000 °C was still 51% but in the case of bending strength it was only 13%.
- The application of basalt aggregates and basalt fibers improved significantly the high temperature durability of calcium aluminate cement based materials. In the most successful mix CB1 with the combination of longer and shorter fibers in the 90:10 ratio, the residual values of compressive and bending strength were, after exposure to 1000 °C, 50% and 34%, respectively.
- The fiber reinforced composite CB1 achieved also the highest resistance to water and water vapor transport and the lowest water vapor adsorption after 1000 °C pre heating, which correlated well with its lowest amount of pores bigger than 100 nm.
- The thermal conductivity and specific heat capacity of all analyzed materials exhibited a significant dependence on moisture content; the thermal conductivity in water saturated state was up to two times higher than in the dry state, for the specific heat capacity the observed increase was up to 65%.
- The thermal strain of all studied composites was almost linear within the whole 20 1000 °C range, which was primarily due to the positive effects of basalt aggregates. The basalt fibers were found to decrease the thermal strain even more, by up to 7% for CB1 at 1000 °C.

Acknowledgment

This research was supported by the Czech Science Foundation, under project No P105/12/G059.

References

[1] P.C. Aitcin, The durability characteristics of high performance concrete: a review, Cem. Concr. Compos. 25 (2003) 409–420.
[2] L. Basheer, J. Kropp, D.J. Cleland, Assessment of the durability of concrete from its permeation properties: a review, Constr. Build. Mater. 15 (2001) 93–103.
[3] R. Černý, P. Rovnaníková, Transport Processes in Concrete, Spon Press, London, 2002.
[4] A.S. Guimarães, I.M. Ribeiro, V.P. de Freitas, A tool to predict water absorption in porous building materials, J. Porous Media 20 (2) (2017) 127–141.
[5] J. Bao, L. Wang, Effect of short-term sustained uniaxial loadings on water absorption of concrete, J. Mater. Civ. Eng. 29 (3) (2017). a.n. 04016234.
[6] D. Smyl, F. Ghasemzadeh, M. Pour-Ghaz, Modeling water absorption in concrete and mortar with distributed damage, Constr. Build. Mater. 125 (2016) 438–449.
[7] L. Wang, J. Bao, T. Ueda, Prediction of mass transport in cracked-unsaturated concrete by mesoscale lattice model, Ocean Eng. 127 (2016) 144–157.
[8] F. Tavares, C. Andrade, B. Capra, Coupled simulation of fracture mechanics and transport of chlorid in cracked concrete submitted to permanent loading, in: Proceedings of the 8th International Conference on Fracture Mechanics of Concrete and Concrete Structures, Toledo, Spain, 2013, pp. 1884–1892.
[9] S. Real, J.A. Bogas, B. Ferrer, Service life of reinforced structural lightweight aggregate concrete under chloride-induced corrosion, Mater. Struct. 50 (2) (2017). a.n. 101.
[10] M.F. Najjar, M.L. Nehdi, A.M. Soliman, T.M. Azabi, Damage mechanisms of two-stage concrete exposed to chemical and physical sulfate attack, Constr. Build. Mater. 137 (2017) 141–152.
[11] N. Cefis, C. Comi, Chemo-mechanical modelling of the external sulfate attack in concrete, Cem. Concr. Res. 93 (2017) 57–70.
[12] R.E. Beddoe, Modelling acid attack on concrete: Part II. A computer model, Cem. Concr. Res. 88 (2016) 20–35.
[13] T. Dyer, Influence of cement type on resistance to organic acids, Mag. Concr. Res. 69 (4) (2017) 175–200.
[14] Y. Bo, N. Chao-lie, L. Bing, Probabilistic durability assessment of concrete structures in marine environments: reliability and sensitivity analysis, China Ocean Eng. 31 (1) (2017) 63–73.
[15] J. Du, J. Ye, G. Li, Inhibitory effects of chloride ions on concrete sulfate attack in the marine adsorption environment, Marine Georesour. Geotechnol. 35 (3) (2017) 371–375.
[16] M.H. Ghobadi, M. Firuzi, E. Asghari-Kaljahi, Relationships between geological formations and groundwater chemistry and their effects on the concrete lining of tunnels (case study: Tabriz metro line 2), Environ. Earth Sci. 75 (12) (2016). a.n. 987.
[17] C. Voegel, A. Bertron, B. Erable, Mechanisms of cementitious material deterioration in biogas digester, Sci. Total Environ. 571 (2016) 892–901.

[18] H. Yu, H. Ma, K. Yan, An equation for determining freeze-thaw fatigue damage in concrete and a model for predicting the service life, Constr. Build. Mater. 137 (2017) 104–116.
[19] J. Chen, R. Bharata, T. Yin, Q. Wang, H. Wang, T. Zhang, Assessment of sulfate attack and freeze–thaw cycle damage of cement-based materials by a nonlinear acoustic technique, Mater. Struct. 50 (2) (2017). a. n. 105.
[20] Y. Wang, M.Z. An, Z.R. Yu, S. Han, W.Y. Ji, Durability of reactive powder concrete under chloride-salt freeze-thaw cycling, Mater. Struct. 50 (1) (2017). a. n. 18.
[21] F. Wei, Ch. Fang, B. Wu, Fire resistance of concrete-filled steel plate composite (CFSPC) walls, Fire Saf. J. 88 (2017) 26–39.
[22] B. Shekastehband, A. Taromi, K. Abedi, Fire performance of stiffened concrete filled double skin steel tubular columns, Fire Saf. J. 88 (2017) 13–25.
[23] T.-Y. Song, Z. Tao, A. Razzazzadeh, L.-H. Han, K. Zhou, Fire performance of blind bolted composite beam to column joints, J. Constr. Steel Res. 132 (2017) 29–42.
[24] X. Tan, W. Chen, J. Wang, D. Yang, Y. Qi, Y. Ma, X. Wang, S. Ma, Ch. Li, Influence of high temperature on the residual physical and mechanical properties of foamed concrete, Constr. Build. Mater. 135 (2017) 203–211.
[25] J.-Ch. Liu, K.H. Tan, Fire resistance of strain hardening cementitious composite with hybrid PVA and steel fibers, Constr. Build. Mater. 135 (2017) 600–611.
[26] L. Bodnárová, J. Hroudová, J. Brožovský, J. Zach, J. Valek, Behaviour of cement composites with lightweight and heavyweight aggregates at high temperatures, Period. Polytech. Civ. Eng. 61 (2) (2017) 272–281.
[27] Q. Zhang, G. Ye, Dehydration kinetics of Portland cement paste at high temperature, J. Therm. Anal. Calorim. 110 (1) (2012) 153–158.
[28] H. Sabeur, G. Platret, J. Vincent, Composition and microstructural changes in an aged cement pastes upon two heating–cooling regimes, as studied by thermal analysis and X-ray diffraction, J. Therm. Anal. Calorim. 126 (3) (2016) 1023–1043.
[29] N.C. Collier, Transition and decomposition temperatures of cement phases - a collection of thermal analysis data, Ceramics – Silikaty 60 (4) (2016) 338–343.
[30] A. Smith, T. Chotard, N. Gimet-Breart, D. Fargeot, Correlation between hydration mechanism and ultrasonic measurements in an aluminous cement: effect of setting time and temperature on the early hydration, J. Eur. Ceram. Soc. 22 (2002) 1947–1958.
[31] N. Ukrainczyk, T. Matusinović, Thermal properties of hydrating calcium aluminate cement pastes, Cem. Concr. Res. 40 (1) (2010) 128–136.
[32] H.G. Midgley, A. Midgley, The conversion of high alumina cement, Mag. Concr. Res. 27 (91) (1975) 59–77.
[33] V. Antonovič, J. Kerienė, R. Boris, M. Aleknevičius, The effect of temperature on the formation of the hydrated calcium aluminate cement structure, Procedia Eng. 57 (2013) 99–106.
[34] M.-A. Maaroufi, A. Lecomte, C. Diliberto, O. Francy, P. Le Brun, Thermo-hydrous behavior of hardened cement paste based on calcium aluminate cement, J. Eur. Ceram. Soc. 35 (2015) 1637–1646.
[35] Y. Wang, X. Li, B. Zhu, P. Chen, Microstructure evolution during the heating process and its effect on the elastic properties of CAC-bonded alumina castables, Ceram. Int. 42 (2016) 11355–11362.
[36] S.R. Klaus, F. Goetz-Neunhoeffer, J. Neubauer, Influence of the specific surface area of alumina fillers on CAC hydration kinetics, Adv. Cem. Res. 28 (1) (2016) 62–70.
[37] W. Khaliq, H.A. Khan, High temperature material properties of calcium aluminate cement concrete, Constr. Build. Mater. 94 (2015) 475–487.
[38] Q. Zhang, D.M. Yan, Temperature dependence of thermal diffusivity of OPC and CAC cement paste, Adv. Cem. Res. 28 (9) (2016) 576–582.
[39] M.C. Alonso, J. Vera-Agulo, L. Guerreiro, V. Flor-Laguna, M. Sanchez, M. Collares-Pereira, Calcium aluminate based cement for concrete to be used as thermal energy storage in solar thermal electricity plants, Cem. Concr. Res. 82 (2016) 74–86.
[40] V. Dhand, G. Mittal, K.Y. Rhee, S.-J. Park, D. Hui, A short review on basalt fiber reinforced polymer composites, Compos. Part B 73 (2015) 166–180.
[41] V. Fiore, T. Scalici, G. Di Bella, A. Valenza, A review on basalt fibre and its composites, Compos. Part B 74 (2015) 74–94.
[42] A. Anandamurthy, V. Guna, M. Ilangovan, N. Reddy, A review of fibrous reinforcements of concrete, J. Reinf. Plast. Compos. 36 (7) (2017) 519–552.
[43] C. Jiang, K. Fan, F. Wu, D. Chen, Experimental study on the mechanical properties and microstructure of chopped basalt fibre reinforced concrete, Mater. Des. 58 (2014) 187–193.
[44] N. Kabay, Abrasion resistance and fracture energy of concretes with basalt fiber, Constr. Build. Mater. 50 (2014) 95–101.
[45] S. Jalasutram, D.R. Sahoo, V. Matsagar, Experimental investigation of the mechanical properties of basalt fiber-reinforced concrete, Struct. Concr. 36 (7) (2017) 519–552.
[46] W. Ren, J. Xu, H. Su, Dynamic compressive behavior of basalt fiber reinforced concrete after exposure to elevated temperatures, Fire Mater. 40 (5) (2016) 738–755.
[47] R. Boris, V. Antonovic, J. Keriene, R. Stonys, The effect of carbon fiber additive on early hydration of calcium aluminate cement, J. Therm. Anal. Calorim. 125 (3) (2016) 1061–1070.
[48] P. Garcés, E. Zornoza, E.G. Alcocel, Ó. Galao, L.G. Andión, Mechanical properties and corrosion of CAC mortars with carbon fibers, Constr. Build. Mater. 34 (2012) 91–96.
[49] P. Frantzis, R. Baggott, Bond between reinforcing steel fibres and magnesium phosphate/calcium aluminate binders, Cem. Concr. Compos. 22 (2000) 187–192.
[50] ČSN EN 1015, Methods of Test for Mortar for Masonry – Part 11: Determination of Flexural and Compressive Strength of Hardened Mortar, Czech Standardization Institute, Prague, 2000.
[51] S. Roels, J. Carmeliet, H. Hens, O. Adan, H. Brocken, R. Černý, Z. Pavlík, C. Hall, K. Kumaran, L. Pel, R. Plagge, Interlaboratory comparison of hygric properties of porous building materials, J. Therm. Envelope Build. Sci. 27 (4) (2004) 307–325.
[52] E. Vejmelková, M. Pavlíková, M. Jerman, R. Černý, Free water intake as means of material characterization, J. Build. Phys. 33 (2009) 29–44.
[53] M.K. Kumaran, Moisture diffusivity of building materials from water absorption measurements, J. Therm. Envelope Build. Sci. 22 (1999) 349–355.
[54] ČSN 72 7031, Determination of Water Vapour Diffusion Coefficient of Building Materials by Method Without Temperature Gradient, Czech Standardization Institute, Prague, 2001.
[55] A. Trník, I. Medved', R. Černý, Measurement of linear thermal expansion coefficient of concrete at high temperatures: a comparison of isothermal and non-isothermal method, Cement Wapno Beton 79 (2012) 363–372.
[56] J. Bensted, J.R. Smith, High alumina cements – some important aspects, Cement Wapno Beton 82 (2015) 215–223.
[57] K.L. Scrivener, J.-L. Cabiron, R. Letourneux, High-performance concretes from calcium aluminate cements, Cem. Concr. Res. 29 (1999) 1215–1223.
[58] T.J. Chotard, A. Smith, M.P. Boncoeur, D. Fargeot, C. Gault, Characterisation of early stage calcium aluminate cement hydration by combination of non-destructive techniques: acoustic emission and X-ray tomography, J. Eur. Ceram. Soc. 23 (2003) 2211–2223.

5.3.3 High-temperature resistance of cement composites with randomly distributed aluminium silicate fibres

D. Koňáková, V. Pommer, K. Šádková, R. Černý, E. Vejmelková,
Cement Concrete Composite 145 (2024) 105339 [51]
https://doi.org/10.1016/j.cemconcomp.2023.105339

This study advances the field of high-temperature-resistant cement composites by evaluating aluminium silicate fibres as a novel reinforcement material, addressing a gap where most prior work focused on steel, carbon, or basalt fibres. The research systematically examined the influence of these fibres on the mechanical, hygric, and thermal properties of both PC and CAC composites, before and after exposure to extreme temperatures (up to 1000 °C).

The findings showed that randomly dispersed aluminium silicate fibres (optimal dosage 1 vol.%) improved bending and compressive strengths, reduced thermal strain (particularly in CAC matrices), and stabilised porosity growth after thermal loading. Unlike steel or glass fibres, aluminium silicate fibres retained their structure without softening up to 1000 °C. Their overall performance closely resembled that of basalt fibres, but with potential cost and chemical stability advantages.

Beyond mechanical reinforcement, the study provided insights into water and vapour transport and thermal conductivity, confirming that aluminium silicate fibres positively influence these parameters after heat exposure. Particularly in CAC systems with basalt aggregates, the fibre-reinforced composites maintained superior integrity across mechanical and transport properties.

This work advances the state of the art by:

- Introducing aluminium silicate fibres as a viable, thermally stable reinforcement for fire-resistant cement composites
- Providing detailed comparisons between CAC and PC matrices
- Offering practical guidance on fibre dosage and matrix selection

In summary, this work expands the range of high-performance fibre reinforcements for cementitious composites, demonstrating that aluminium silicate fibres offer a durable, thermally stable alternative to conventional fibres in fire-resistant and structural applications.

Cement and Concrete Composites 145 (2024) 105339

Contents lists available at ScienceDirect

Cement and Concrete Composites

journal homepage: www.elsevier.com/locate/cemconcomp

High-temperature resistance of cement composites with randomly distributed aluminium silicate fibbers

Dana Koňáková *, Vojtěch Pommer, Kateřina Šádková, Robert Černý, Eva Vejmelková

Department of Materials Engineering and Chemistry, Faculty of Civil Engineering, Czech Technical University in Prague, Thákurova 7, 166 29, Prague 6, Czech Republic

ARTICLE INFO

Keywords:
C. Mechanical properties
C. Transport properties
D. Calcium aluminate cement
D. Portland cement
E. Fibre reinforcement

ABSTRACT

Aluminium silicate fibres are known for their low thermal conductivity and specific heat capacity, high thermal shock resistance, low weight and excellent corrosion resistance. However, their use in cement-based composites for high-temperature applications has been very limited. In this paper, the effect of randomly dispersed alumina-silicate fibres on the high-temperature resistance of cement composites is analysed as a function of the mix composition. The measurement of the basic physical, mechanical, hygric and thermal properties shows the most favourable results for the composites containing calcium aluminate cement and basalt aggregates, the fibre dosage of 1 % being an optimal solution. A comparison with the results reported by other researchers shows that in the temperature range up to 1000 °C, aluminium silicate fibres perform better than steel, glass and carbon fibres for both Portland cement and calcium aluminate cement matrices, and their effect is similar to that of basalt fibres.

1. Introduction

The investigation of a high-temperature impact on building materials caused by fire or industrial machinery has become increasingly important in recent decades. With the development of industry and technology, the demands on the performance of building materials are rising as well. Simultaneously, the fire hazard grows as well as often the maximal loading temperature goes up (both in fire scenarios and in technological processes). Concrete as one of the most commonly used load-bearing materials can resist well to elevated temperatures. However, the range of temperature resistance of various types of concrete differs from case to case. The factors influencing its performance include cement composition, water-to-binder ratio, moisture content, type of used aggregate, supplementary cementitious materials application, and the type and amount of fibre reinforcement.

In the event of a fire or a high-temperature exposure in general, concrete does not release any toxic substances, but it comes to forming microcracks and changing the structure. The level of damage depends on the severity and duration of the fire. At temperatures above 100 °C the physically bound and free water evaporates. This process is partially reversible but it can lead to explosive spalling, which can be dangerous. In the temperature range of 95 °C–200 °C AFm, AFt and gypsum dehydrate; simultaneously the dehydration of calcium silicate hydrates is initiated (100 °C–150 °C) [1,2]. Calcium aluminate hydrates decompose at the temperatures of 120–320 °C, similarly to alumina hydrates (120 °C and 210 °C–320 °C for amorphous and crystal forms, respectively) [1,3]. As a consequence of the mentioned processes, small micro-cracks form, and strength decreases by about 10 % [4]. The temperature loading above 300 °C gives rise to wider cracks. In the case of Portland cement (PC), at temperatures of 450 °C–500 °C [1–3,5] portlandite decomposes. In general, the chemical bonds in hydrated cement collapse at about 625 °C [6] and in the temperature range between 500 °C and 800 °C the strength sharply decreases. When quartz is presented (as one of the most common aggregates), its α to β transition occurs at 573 °C, being accompanied by volumetric changes and thus an additional remarkable strength decrease. Another important process takes place in the temperature range from 700 °C to 800 °C when calcium carbonate (in the form of calcite, vaterite, aragonite or with the amorphous structure [5,7]) is decomposed. For calcium aluminate cement (CAC) application, there is another important transformation: At 750 °C $C_{12}A_7$ is formed which is later, at temperatures over 900 °C, recrystallized to CA and CA_2 [1–3,8]. At ~1200 °C sintering of calcium aluminate matrix takes place. Consequently, the porosity decreases, and the mechanical strength goes up. Such composites can be useable up to 1700 °C [6]. Apart from the chemical transformation, the described processes can also cause changes in the physical properties of

* Corresponding author.
E-mail address: dana.konakova@fsv.cvut.cz (D. Koňáková).

https://doi.org/10.1016/j.cemconcomp.2023.105339
Received 4 January 2021; Received in revised form 26 April 2023; Accepted 15 October 2023
Available online 19 October 2023
0958-9465/© 2023 Elsevier Ltd. All rights reserved.

temperature-loaded concrete. The main issues are a decrease in bulk density, a reduction of toughness, an increase in porosity, a decrease in thermal conductivity, and a growth of water vapour permeability. As a result, the mechanical performance is significantly weakened. From the point of view of load-bearing capacity, one of the most significant impacts has indisputably the explosive spalling [9–11].

The negative effects of concrete's high-temperature exposure can be successfully reduced by fibre application. There are two main reasons why dispersed fibres are suitable as reinforcement in concrete composites. Firstly, they improve the mechanical performance, e.g., by increasing the toughness of concrete, tensile, flexural and shear strength, impact resistance, frost resistance, and restraining shrinkage [12]. Secondly, some types of fibres can help in the elimination of spalling effect. Such fibres have low melting or decomposition temperature (below 200–300 °C [13].), the most common representatives being polymeric fibres. The decomposition temperature of chemical bonds in organic substances is mostly below 250 °C. Therefore, during the heating polymeric fibres are decomposed and create "channels" in the structure so that vapour can be released without growing the inner pressure. The length of these fibres is usually ~10 mm and the diameter is ~20 μm [6]. Their amount in concrete mixture ranges from 0.02 to 0.1 %. Despite that the main idea of these fibres is the elimination of explosive spalling, they can propose beneficial performance also at ambient temperature. They can improve mechanical properties and impact resistance of composite [14].

Regarding the first group of fibres, they help to improve the performance of thermally resistant materials in a similar way as in the case of composites without temperature loading. These fibres are usually bigger in comparison with the low-melting-point fibres; the length is up to 30 mm and the diameter is up to 0.4 mm [6]. In addition, their amount is usually higher, up to 6 %. The particular choice of fibres depends on their mechanical properties as well as on their temperature resistance. The most common fibres are made from steel, glass, basalt, or carbon [14]. Unfortunately, steel, glass and carbon are not suitable for temperatures above ~600 °C. Basalt fibres can be applied up to 950 °C. For higher temperatures above 1200 °C also chromium or nickel-containing steel alloys can be used [15]. For the practical reasons of synergic improvement, quite often it is suitable to use hybrid fibres, more precisely combinations of fibres. The most common combination of steel with other materials; it can be named for example steel-polymeric fibre reinforcement [16], steel-glass fibres [17], or steel-basalt hybrid reinforcement [18].

As it is visible, the choice of materials which can be used as fibre reinforcement at high temperatures is rather small. The most perspective from the point of view of physical properties was asbestos fibres. They showed excellent chemical resistivity, electrical non-conductivity, high strength and flexibility, and especially great thermal resistance and non-combustibility. After widespread use in the second half of the 20th century, in 1984 it was proven that asbestos belong to the carcinogenic agents. As a consequence, its utilization has been prohibited worldwide. Even though there has been considerable effort and investment in finding appropriate substitutes for these fibres, very few suitable materials have been found and this matter is still worth addressing.

Ceramics, which can be fiberized by melting alumina and silica in a suitable ratio, present prospective materials with potential use in high-temperature-resistant cement-based composites. The aluminium silicate-based continuous fibres are made by sol-gel process, while short fibres are prepared by melt-spinning route [19]. The aluminium silicate fibres have low thermal conductivity, low heat capacity, great thermal shock resistance, low weight, and excellent corrosion resistance. They can be applied in the temperature range up to 1480–1750 °C [6,19]. Moreover, compared to basalt fibres, they are less expensive. Currently, there are plenty of forms of ceramic fibre products, e.g., blankets, felts, bulk fibres, vacuum-formed or cast shapes, or textiles. They are most often used in automotive- and aerospace heat-resistant applications, such as fire barriers or thermal insulations [19].

The applicability of aluminium silicate fibres for investment casting was studied by Lü et al. [20]. They successfully improved the silicon sol shell for the casting process by introducing aluminium silicate and polypropylene fibres into a slurry. Similarly, Lu et al. [21] studied the effect of aluminium silicate fibres on the crack resistance of a ceramic mould. In both cases, the studied fibres exhibited a beneficial performance. Miao et al. [22] focused their research on the ceramic matrix as well. They found 600 °C to be the optimal temperature for using an aluminium silicate fibres-based ceramic filter element. The combination of aluminium silicate fibres with alloy matrix was studied by Rathod et al. [23] but their composite suffered from a relatively higher coefficient of friction, wear rate and frictional heating as compared to the alloys. In contrast, Nath and Singh [24] reported an increase in the hardness and rate of age hardening of a reinforced alloy. Another application of aluminium silicate fibres can be found in the work of Zhu et al. [25]. They prepared an aluminium silicate refractory fibreboard with a resistance of up to 1200 °C.

The application of aluminium silicate fibres in cement-based composites was not very frequent until now. Su et al. [26] studied the mechanical properties of ceramic fibre-reinforced concrete based on blended cement. According to their research, an increasing volume fraction of fibres led to compressive, tensile, and bending strength increases. The rate of deformation was more pronounced as the volume fraction of ceramic fibres increased. The addition of ceramic fibres to the concrete improved its dynamic strength, critical stress, and energy absorption as well. The energy absorption was even better than for the carbon fibre-reinforced concrete. Moreover, in their other study, Su et al. [27] also noted the positive effect of the addition of 0.1 %, 0.2 %, and 0.3 % ceramic fibres on dynamic load resistance.

Aluminium silicate fibres seem to have great potential as concrete reinforcement. However, their utilization in cement-based composites in high-temperature applications has not been studied yet in detail. In this paper, an analysis of the impact of randomly distributed aluminium silicate fibres on the high-temperature resistance of cement-based composites of varying composition is presented. Contrary to the other research this article is focused not only on the impact of fibres on mechanical properties, but a wide range of material parameters of the composites is determined. Studied parameters include the basic physical, mechanical, hygric and thermal properties both at room temperature and after high-temperature exposure. The effect of aluminium silicate fibre utilization in different types of cement matrix is then assessed by comparison with other types of fibres.

2. Experimental methods

2.1. Material characterization

The elementary composition of raw materials was determined by X-ray fluorescence (XRF) spectrometry. A Thermo ARL 9400 XP device was used. The acquired data were evaluated by UNIQUANT 4 software.

The phase composition of raw materials was studied by X-ray diffraction (XRD) using a PANalytical Aeris system with a CoK_{α} tube. The quantification of the present phases was performed by Rietveld analysis with internal standard (20 % of ZnO); the evaluation was done by the HighScore and Profex software [28].

Simultaneous thermal analysis (STA), consisting of differential scanning calorimetry (DSC) and thermogravimetry (TG), was carried out using a LABSYS EVO DTA/DSC (SETARAM Inc.). The experiments were done in the temperature range from 30 °C to 1000 °C with a heating rate of 5 °C min^{-1}, in an argon atmosphere with a flow rate of 40 mL min^{-1}.

The SEM micrographs were acquired with the help of a Phenom XL desktop device equipped with a BSE detector and CeB6 source. The voltage was set as 15 kV for all measurements, and zooming was 80 μm and 10 μm.

For a determination of granulometry of fine components, the laser diffraction method was used (Bettersizer S3 Plus device). The samples

were dispersed in ethanol in order to prevent hydration and sonicated 3 min before the analysis. The fineness was also described by specific surface area, as measured by the Blaine permeability method [29].

Granulometric curves of aggregates were determined by the standard grading test [30]. The utilized sieve was set up to 8 mm because just fine aggregate was used in the mix design.

2.2. Basic physical properties

Bulk density, matrix density and open porosity were determined by the water vacuum saturation method [31] using dry mass, water-saturated mass and mass under the water level. Five samples (50 × 50 × 50 mm) were dried in a drier at 105 °C. Then they were placed into a desiccator with boiled distilled water and the air was evacuated for 3 h with a vacuum pump. Then the samples were kept under water level for 24 h.

2.3. Mechanical properties

Mechanical properties, specifically compressive strength and bending strength, were measured according to the standard [32]. Determination of the bending strength was performed on three samples (40 × 40 × 160 mm) using the loading device MTS 100. The arrangement of the measurement was a classical three-point bending test with a 100 mm span length. Compressive strength was then determined on fragment samples from the bending strength measurement. A EU40 loading device was employed and in the actual experiment, the samples were put between two steel pressure plates with the dimensions of 40 × 40 mm.

2.4. Hygric parameters

Determination of liquid water transport parameters was performed by applying the sorption experiment. Three samples (50 × 50 × 50 mm) insulated on four lateral sides were immersed in 2 mm in water and using automatic balance the mass changes in time were recorded. The water absorption coefficient was then derived from the sorptivity plot [33].

Cup methods [34] were used for the characterization of water vapour transport. Three round disc samples (diameter 115 × 15 mm) were insulated and fixed in cups. The cups contained silica gel, or water which simulated the relative humidity of 5 % or 95 %, respectively. The experiment took place in a climatic chamber with a relative humidity of 50 %. Steady-state values of the mass gain or the mass loss determined by the linear regression over the last five readings were used for the calculation of the water vapour diffusion resistance factor.

2.5. Thermal characteristics

The thermal conductivity and the specific heat capacity were determined by ISOMET 2104. The measurement process was based on an analysis of the temperature response of the analysed material to heat flow impulses. Because of the extensive impact of water presence on the thermal conductivity, the thermal characteristics were determined in dependence on moisture content on three samples (70 × 70 × 70 mm).

The measurement of thermal strain depending on temperature was performed by a linear thermal horizontal dilatometer [34,35] for three samples with the dimensions of 15 × 15 × 160 mm. The device utilized a comparative method; the thermal expansion was determined by comparing the analysed specimen with a reference corundum rod. The heating rate of the dilatometer was set as 1 °C per min and the maximal temperature of measurement was 1000 °C.

3. Materials and composite mixtures

3.1. Raw materials and their characterization

The aluminium silicate fibres had a length ranging from 5 to 15 mm, the average diameter was 6 μm, and their bulk density was 200 kg m^{-3}. According to the producer (Basaltex a.s) they were applicable up to 1260 °C. The XRF analysis of the fibres showed mainly silica and alumina (Table 1). From the mineralogical point of view, as determined by XRD, they were largely amorphous (Fig. 1). After exposure to 400 °C, the fibre composition did not exhibit any changes. However, when the temperature reached 1000 °C, some recrystallization occurred. The quantitative XRD analysis of crystalline phases after exposure to 1000 °C showed, that mullite and sillimanite were presented in equal amounts (Fig. 1). Both minerals have good thermal resistance, and their melting or transformation temperatures are above 1600 °C. For a better comprehension of phase changes, the results of STA are presented in Fig. 2. Apparently, the recrystallization of both phases took place at 955–995 °C and very low mass changes were observed in the whole temperature range. SEM pictures of fibres after exposure to different temperature treatments are presented in Figs. 3–5. It is obvious that despite the high-temperature loading, the fibres remained the same, and no negative agglomeration, sintering or fusing appeared. Also, no cracks or other damage to fibres were found. Therefore, the applied aluminium silicate fibres could be considered very suitable for high-temperature applications.

Portland cement (PC) CEM I 52.5 R was used as the reference binder. Its Blaine-specific surface area was 393 m^2 kg^{-1}. Calcium aluminate cement (CAC) containing ~ 70 % alumina oxide and belonging to medium alumina cement was selected as the second binder because of its supposed better resistance to high temperatures. Its specific surface area was 380 m^2 kg^{-1}. The chemical composition of both cements is presented in Table 1, while the mineralogical composition can be found in Table 2. The grain size distribution is shown in Fig. 6. Despite both applied binders being cements, their composition and thus also the properties of the cement mixtures, e.g. hydration process, temperature dependency, setting times, or high-temperature resistance of hydration products, is distinctively different.

Two types of aggregates were used in the cement mixtures. The silica aggregate was composed almost entirely of quartz. A proper combination of four gradings (25 % of grade 0.1/0.6 mm, 5 % of 0.3/0.8 mm, 15 % of 0.6/1.2 mm and 55 % of 1/4 mm) was selected to achieve a continuous granulometric curve. Crushed basalt was employed as the second aggregate because of its better thermal resistance. Its chemical and mineralogical composition is presented in Tables 1 and 2 Two gradings (0/4 mm and 2/5 mm) were combined in the ratio of 4:1 in this case. It should be mentioned, that not only the continuity of granulometric curves was paid attention to during the mix design, but an emphasis was laid also on the similarity of both curves (Fig. 7).

The remaining components of the designed mixtures were portable water and superplasticizer based on modified polycarboxylate-ether. The purpose of the plasticizer application was not only to improve the workability; it was also needed for a better disintegration of fibre conglomerates.

3.2. Preparation of composite mixtures and thermal loading

Three mixtures with different fibre dosages were prepared to evaluate the applicability of aluminium silicate fibres. A reference mixture without fibres was analysed as well. The mass of fibres ranged from 0 g to 30 g, volumetrically the fibre dosage corresponded to 0 %, 0.5 %. 1 % and 1.5 %. The basic composition of designed mixtures is shown in Table 3. Regarding the other components, the effect of their combinations was studied. Four sets of basic mixtures were created, each set differing in the type of cement and aggregate, giving a total of 16 mixtures studied. Their labelling was derived from the particular

Table 1
Chemical composition of raw materials (% by mass).

	CaO	Al_2O_3	Fe_2O_3	SiO_2	MgO	Na_2O	K_2O	SO_3	P_2O_5	TiO_2
Aluminium silicate fibres	0.2	45.0	0.5	53.4			0.1			0.5
Portland cement	64.9	6.4	2.4	18.1	1.0	0.3	1.2	4.9	0.2	
Calcium aluminate cement	28.2	70.7	0.1	0.4	0.1	0.4	0.1			
Silica aggregate			0.0	99.4						
Basalt aggregate	12.8	17.2	11.0	41.9	7.2	4.2	0.9		1.0	3.2

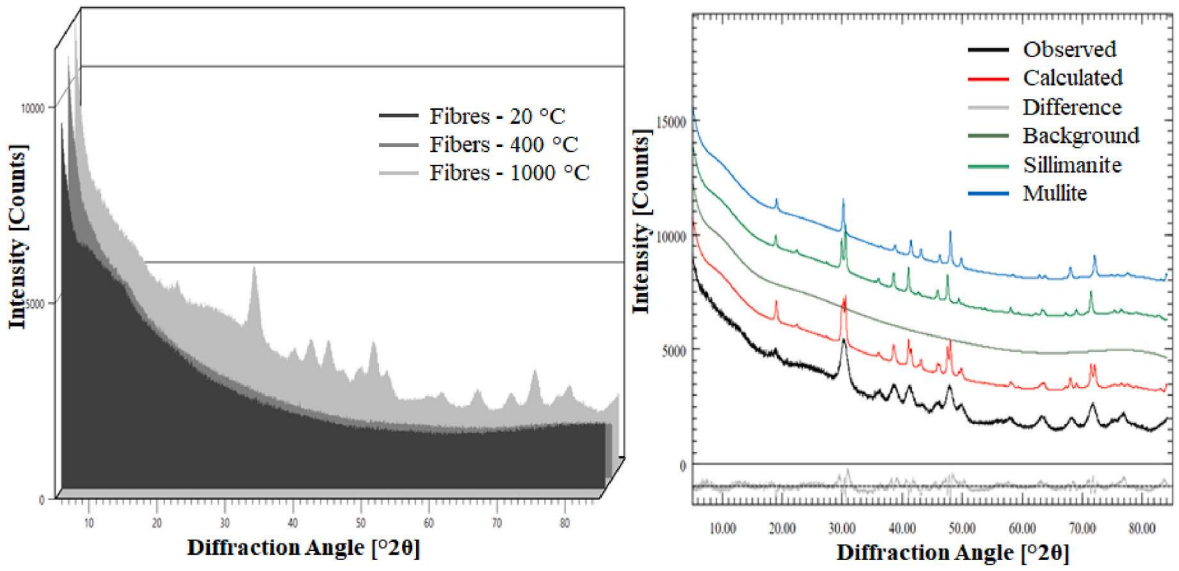

Fig. 1. Diffractograms of studied fibres exposed to different temperatures (left), Diffractogram of aluminium silicate fibres exposed to 1000 °C (right).

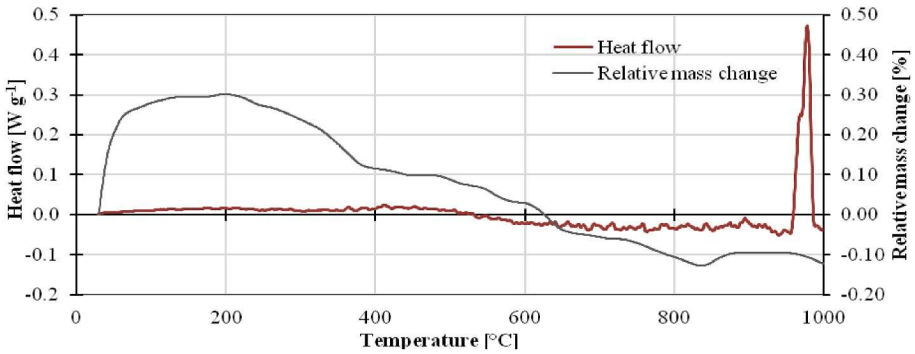

Fig. 2. STA (DSC and TG) of aluminium silicate fibres.

composition; the first letter designates the type of cement (P - Portland cement, C - calcium aluminate cement) and the second letter signifies the aggregate (S - silica aggregate, B – basalt aggregate). The last letter relates to fibre dosage, as it can be found in Table 3. Table 4 shows the complete list of studied mixtures.

The preparation process was the same for all mixtures. At first, dry components (aggregate and cement) were properly mixed. Then a portion of water containing the plasticizer was poured. After a few minutes of additional mixing, fibres were gradually added. Finally, the remaining water was supplemented. The resulting fresh mixtures were put into moulds. The specimens were made and cured in laboratory conditions, at 20 ± 1 °C and 25–30 % relative humidity.

After 28 days of curing, the samples were exposed to different thermal loadings. Taking into consideration the well-known changes occurring in cement composites during temperature exposure, three different conditions were chosen. One-third of the samples were taken as a reference with no temperature loading. The second third was heated to 400 °C, where the passed processes include releasing of free and physically bounded water, dehydration of calcium aluminate hydrates or calcium silicate hydrates, and decomposition of AFm and AFt phases. The last third of specimens were exposed to 1000 °C when the most important recrystallization and decomposition processes are done but the raw materials are not melted yet and cement composites are not disintegrated. In the case of calcium aluminate cement utilization, the sintering process (which causes a subsequent improvement in the mechanical performance of the composite) does not begin yet.

The temperature exposure took place in an electrical top-cover furnace. Before the thermal loading, the specimens were dried in an oven at 105 °C for 24 h. The main aim was to evaporate free water from the inner structure and prevent thus explosive spalling during the thermal load. The actual thermal loading was performed continuously with the temperature rate increase of 0.5 °C min^{-1}. After reaching the

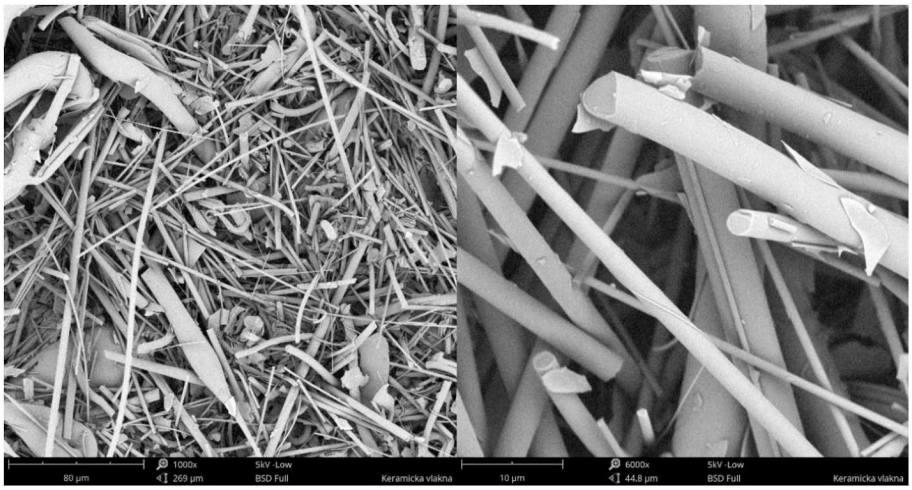

Fig. 3. SEM of aluminium silicate fibres at room temperature.

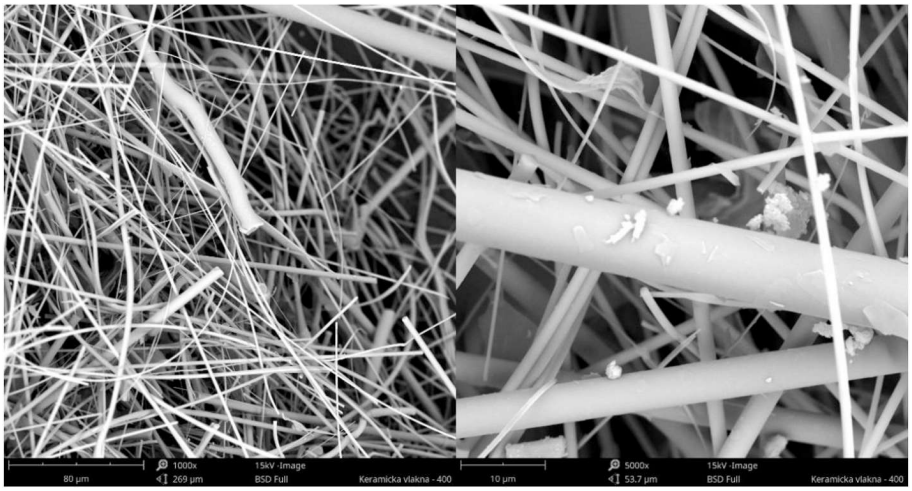

Fig. 4. SEM of aluminium silicate fibres after heating to 400 °C.

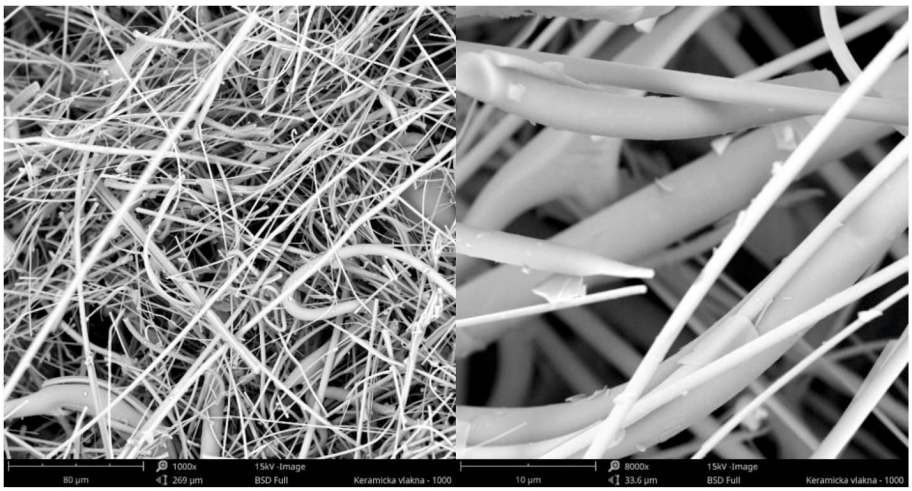

Fig. 5. SEM of aluminium silicate fibres after heating to 1000 °C.

Table 2
Mineralogical composition of raw materials.

Portland cement		Calcium aluminate cement		Basalt aggregate	
Alite	47.0	Krotite	55.1	Diopside	38.3
Belite	2.4	Grossite	35.8	Clinopyroxene	13.3
Tricalcium aluminate	12.6	Mayenite	0.4	Bytownite	11.5
Brownmillerite	6.1	Corundum	1.3	Nepheline	9.6
Gypsum	5.9	β-alumina	1.6	Augite	6.3
Amorphous	26.0	Gehlenite	0.7	Analcime	6.3
		Katoite	0.1	Muscovite	6.3
		Amorphous	5.1	Magnetite	4.5
				Anorthite	4.0

final temperature, the loading duration was 3 h. Then the specimens were left to a spontaneous cooling.

4. Experimental results

4.1. Basic physical properties

Open porosity measured by the water-vacuum saturation method is presented in Fig. 8. It is obvious that without temperature loading, the application of fibres led to the open porosity increase, regardless of the other components. The higher amount of fibre used, the bigger growth of the open porosity was observed. On average, the application of 0.5 vol % of fibres led to 9 % growth; in the case of 1 vol% the open porosity went up by about 15 % and the highest fibres amount of 1.5 vol% caused an increase by 21 % compared with the reference materials without reinforcement.

Regarding the impact of temperature loading, the values of open porosity increased significantly. An indisputable positive effect of the application of more thermally stable raw materials, which reduced the open porosity growth, could be seen. The worst performance showed the composite PSR. It reached the biggest changes at all; 400 °C caused by a 102 % higher value of the residual open porosity, and for the pre-treatment at 1000 °C even by 312 %. This deterioration was successfully lessened by the fibre reinforcement. The optimal amount seemed to be 1 %, which resulted in a growth of 68 % in the case of 400 °C, and 180 % after the exposure to 1000 °C. More thermal-resistant raw materials (CAC, basalt aggregates) showed a remarkable improvement as well but it was not so distinctive. It was caused by the much better performance of the reference mixture CBR, which exhibited a growth of 42 % for 400 °C and by 85 % when exposed to 1000 °C. As in the previously described set, the best results showed the composite with 1 % of aluminium silicate fibres.

In Fig. 9, there can be found the values of matrix densities determined by the water-vacuum saturation method. Regarding the reference

Table 3
Basic mixture composition (kg m ^{3}).

	R	1	2	3
Cement (Portland cement or Calcium aluminate cement)	900	900	900	900
Aggregate (Silica aggregate or basalt aggregate)	1100	1100	1100	1100
Aluminium silicate fibres	0	10	20	30
Superplasticizer	9	9	9	9
Portable water	225	225	225	225

Table 4
Composition of mixture sets.

Mixtures	Cement type	Aggregate type
PSR, PS1, PS2, PS3	Portland cement	Silica aggregate
PBR, PB1, PB2, PB3	Portland cement	Basalt aggregate
CSR, CS1, CS2, CS3	Calcium aluminate cement	Silica aggregate
CBR, CB1, CB2, CB3	Calcium aluminate cement	Basalt aggregate

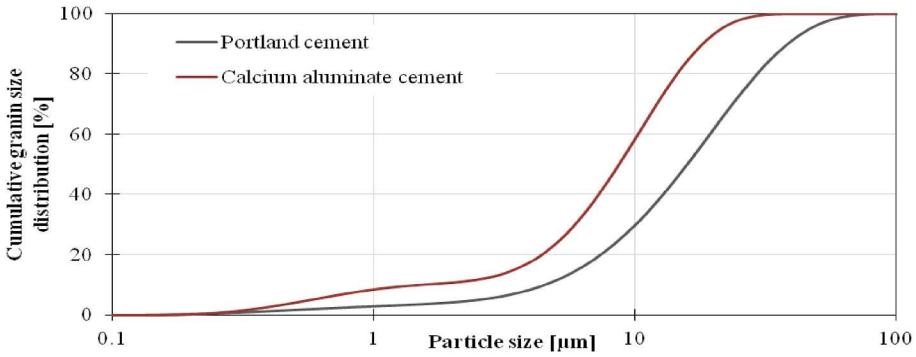

Fig. 6. Grain size distribution of used cements.

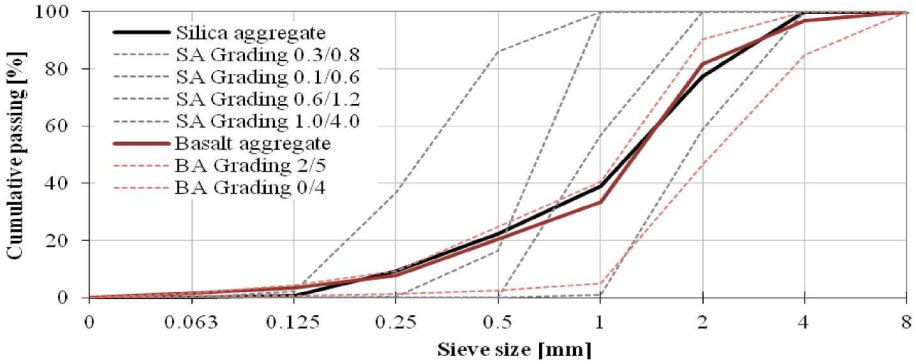

Fig. 7. Granulometry of used aggregates.

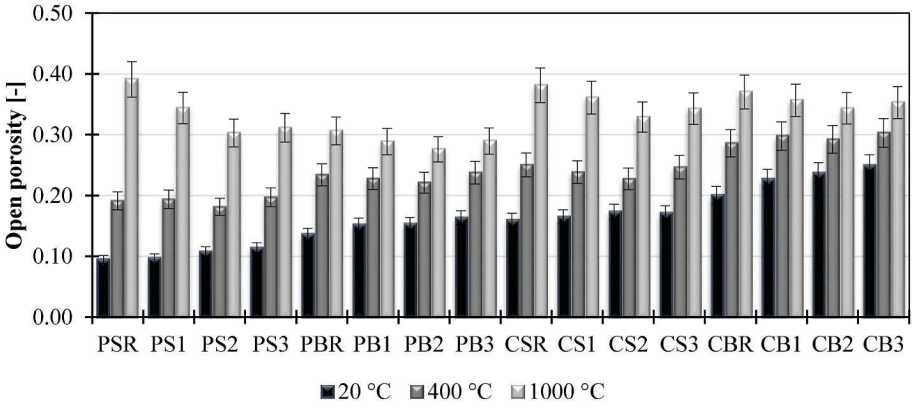

Fig. 8. Open porosity of studied composites.

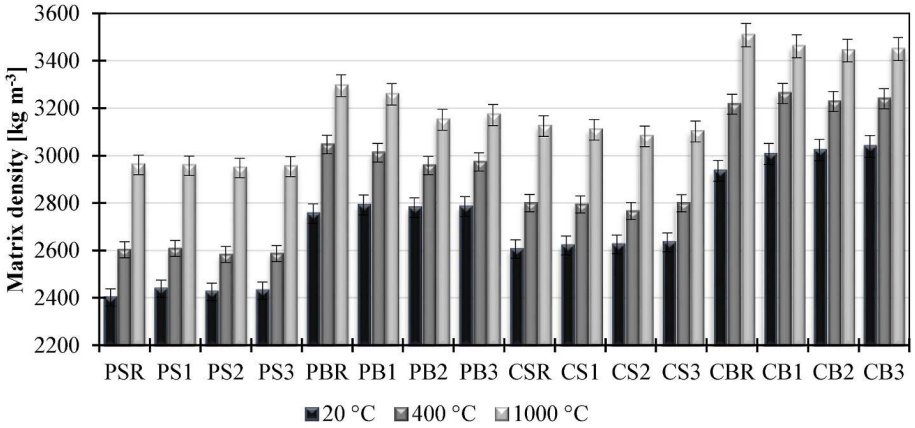

Fig. 9. Matrix density of studied composites.

state without temperature loading, by all means, the application of fibres led to a little growth of matrix density, by 1.5 % on average. However, the difference was almost equal to the accuracy of the used measurement method. The impact of temperature was in the case of matrix density also distinctive. Due to the temperature exposure material transformations occurred, e.g., hydrated phases were decomposed and denser anhydrous minerals were formed. Therefore, the residual matrix densities went up; by 7 % for 400 °C and 18 % for 1000 °C on average, regardless of the raw-materials combination. When focused on the impact of studied fibres, it was reversed to that at ambient temperature; their application led to a minor fall of residual matrix densities. The difference was 2 % on average.

The bulk density is presented in Fig. 10. Without temperature loading the composites of particular sets reached almost equal values, and thus it could be concluded, that bulk density was unaffected by the aluminium silicate fibre application. When focused on the temperature impact, the values of residual bulk density were lessened, compared to the reference state. Regarding silica-based sets, the positive impact of fibre reinforcement was indisputable. The optimal fibre dosage seemed to be 1 vol%, which was consistent with the open porosity. The bulk density after exposure to the 1000 °C was decreased by 12 % and 7 % for the sets with Portland cement and calcium aluminate cement, respectively. Speaking about the combination with basalt aggregate, also in this case the aluminium silicate fibres seemed to have a positive impact.

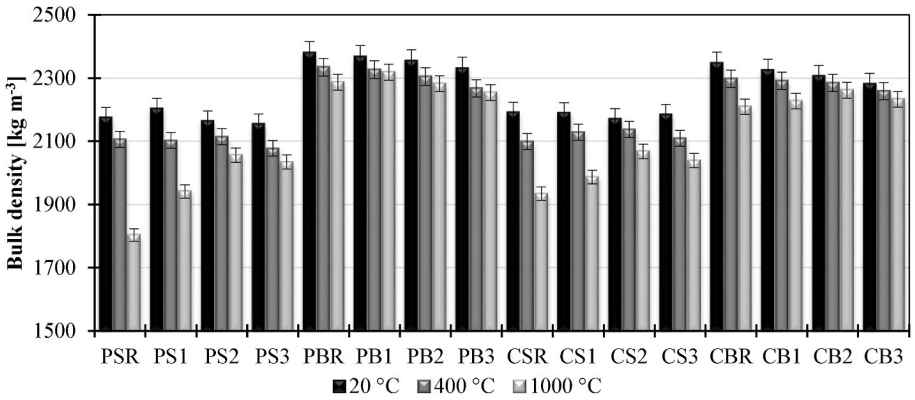

Fig. 10. Bulk density of studied composites.

However, the bulk density decrease was about 2 %, which was close to the limit of measurement accuracy.

4.2. Mechanical properties

The values of residual bending strength are shown in Fig. 11. The impact of the aluminium silicate fibres on the bending strength was positive by all means. The biggest improvement was observed when Portland cement and silica aggregate were combined. The fibre application resulted in 73 % higher values compared to the reference material. Nevertheless, also in the case of the combination of more thermally resistant raw materials, the fibre reinforcement caused a great improvement; the bending strengths went up by 41 % on average, as compared with the reference material CBR.

Regarding the influence of temperature exposure, the fall of bending strength after 400 °C pre-heating ranged from 53 to 63 % for particular reference materials. The aluminium silicate fibre reinforcement successfully reduced the fall by 10 % on average (regardless of the amount of the fibres). When focused on 1000 °C, the impact of temperature loading was substantial. Despite the improvement due to the fibre reinforcement, materials based on silica aggregate reached unapplicable values; especially when Portland cement was used; the decrease of residual bending strength was up to 96 %. The sample sets based on the basalt aggregate reached more suitable values. The lowest decrease showed the composite CB2 when the fall of bending strengths was by 74 %. In general, the sets containing basalt showed a lowering of the fall of the residual bending strength by 6 % on average.

In the reference state without temperature exposure, the compressive strength increased with the increasing fibre dosage (Fig. 12). However, the improvement was lower than in the case of flexural strength, for 0.5 % only by 3 % and for 1 % by 6 %. The higher amount of aluminium silicate fibres showed no effect.

When focused on the influence of temperature, residual properties reached remarkably lower values than in the reference state, similarly to bending strength. For 400 °C. the decrease of compressive strength was for reference materials from 53 % to 43 %, with the highest value for PSR and the lowest for calcium aluminate cement. This decrease was successfully lessened by the aluminium silicate fibres application, by 4 % for 0.5 % fibre dosage and even by 7 % for 1 %. The highest studied amount of fibres exhibited only minor improvement, by 1 % on average, which was lower than the standard deviation of the determined values. The exposure to 1000 °C caused a further decrease in residual compressive strength. As expected, the highest deterioration showed the set based on PC. Similarly to the bending strength, the aluminium silicate fibres could not provide any noticeable improvement, and all materials showed a decrease of 96 % for the set with silica aggregate and 83 % for the basalt aggregate. The best performance had the set based on calcium aluminate cement and basalt aggregate. This matrix was strong and solid enough, and thus also fibre reinforcement could provide an appropriate improvement. The fall of residual compressive strength was thanks to the application of aluminium silicate fibres reduced by 12 %.

4.3. Hygric parameters

Concerning fire safety, water is still one of the most often used firefighting mediums, thus it is important to include the water transport ability of thermally resistant composites in the complex research. Moreover, hygric properties belong to the decisive parameters necessary for the durability assessment.

The water absorption coefficient as a representative of liquid water transport parameters is presented in Fig. 13. In the reference samples, the use of fibre reinforcement led to moderate growth of water absorption coefficient, namely by 20 %, 27 % and 29 % for 0.5 %, 1 % and 1.5 % fibre dosage, respectively.

The temperature exposure caused a more remarkable increase in the water absorption coefficient, which was in accordance with the growing open porosity of studied materials. After 400 °C the residual water absorption coefficient reached ~1.6 times higher values than in the reference state, on average. However, the influence of the reinforcement was reversed. The presence of aluminium silicate fibres caused a minor decrease in the residual water absorption coefficient, as compared with the reference composites. This decreasing tendency continued to grow also after exposure to 1000 °C. Nevertheless, at such high temperatures, the ability of water transport was significantly increased, and the residual absorption coefficient reached, on average, 10 times higher values than at room temperature. It was caused not only by the growth of open porosity as such, but a crucial role had also the different pore size distribution. It can be assumed that after high-temperature exposure, the pore size diameter grows significantly and the composites contain a bigger amount of capillary pores [36].

Fig. 14 shows the water vapour diffusion resistance factor for dry-cup and wet-cup arrangements. As is common for building materials, wet-cup values were always somewhat lower than in the dry-cup arrangement. Nevertheless, in the reference state, the application of aluminium silicate fibres led to a decrease in the water vapour diffusion resistance factor. Somewhat bigger changes were observed for the sets with basalt aggregate. In general, the use of the reinforcement led to a fall by 6 %, 11 % and 14 % for 0.5 %, 1 % and 1.5 % fibre dosage, respectively.

Similarly to the liquid water transport, also the water vapour transport ability grew with temperature exposure as the open porosity increased. However, in this case, more significant was the temperature loading by 400 °C. For the reference mixtures, the fall of water vapour diffusion resistance factors ranged, on average, from 46 % to 56 %. Apparently, in this temperature range, a higher amount of small micropores appeared, as the matrix was transformed due to the chemical decomposition reactions. When focused on the impact of fibre reinforcement, the presence of aluminium silicate fibres application led to a decrease of the fall of residual water vapour diffusion resistance factor

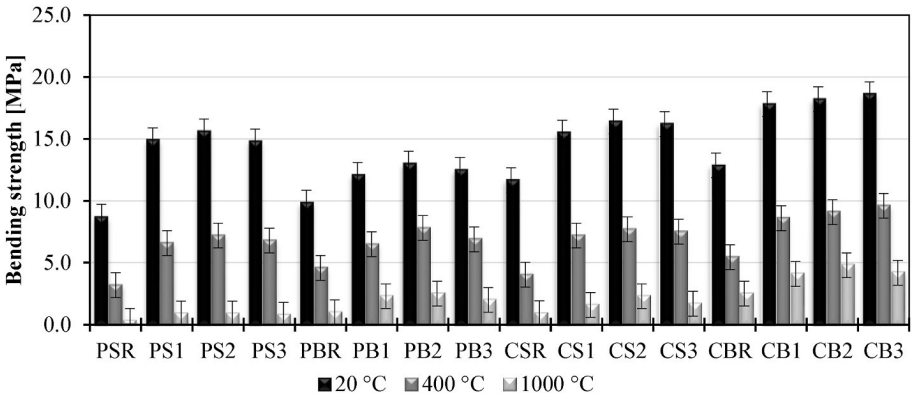

Fig. 11. Bending strength of studied composites.

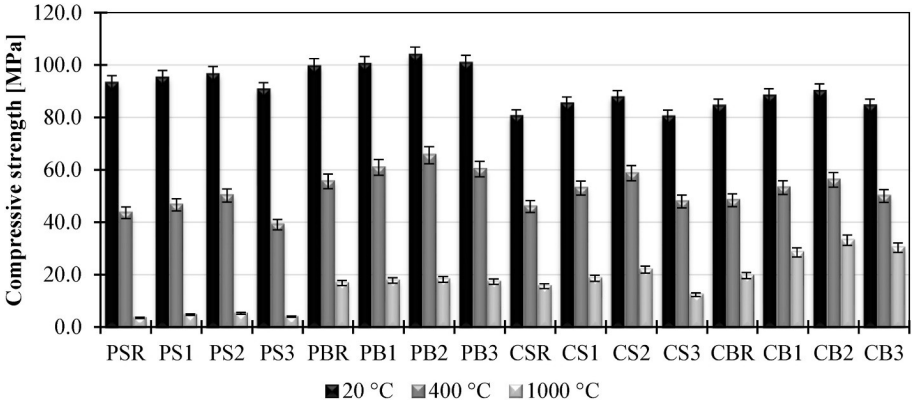

Fig. 12. Compressive strength of studied composites.

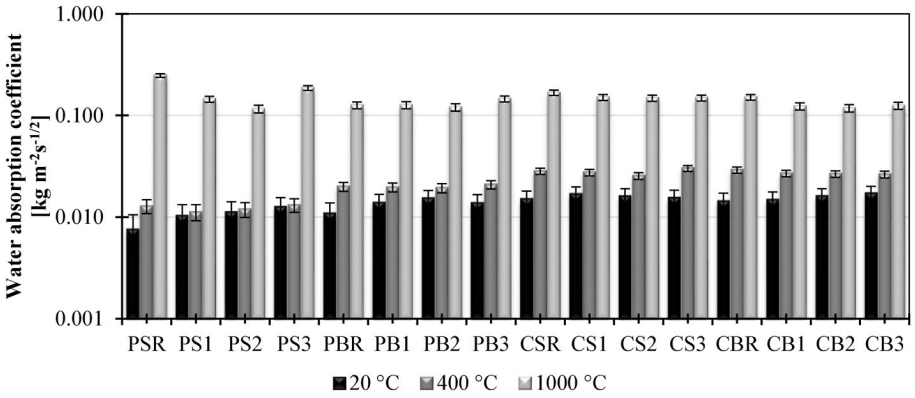

Fig. 13. Water absorption coefficient of studied composites.

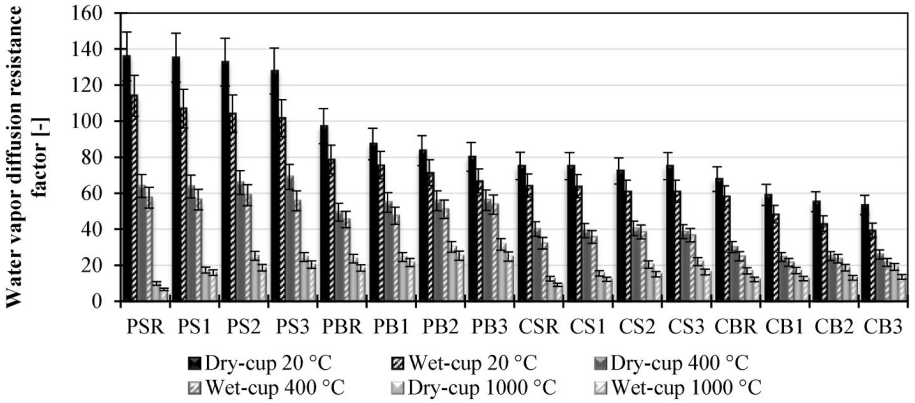

Fig. 14. Water vapour diffusion resistance factor of studied composites.

by 4 %, 11 % and 12 % for 0.5 %, 1 % and 1.5 %, respectively. This tendency could be observed also after the 1000 °C exposure.

4.4. Thermal characteristics

Thermal conductivity in dependence on moisture content is presented in Figs. 15–17. The results are organized according to particular temperature loadings, for better clarity. At room temperature, the application of aluminium silicate fibres led to a remarkable decrease in thermal conductivity. This was caused not only by the higher porosity of reinforced composites but also by the relatively low thermal conductivity of used fibres. The higher dosage was used, the higher fall was observed. Specifically, the application of 0.5 %, 1 % and 1.5 % of fibres resulted in 12 %, 15 % and 19 % lower values.

When focused on thermal exposure, the residual thermal conductivities decreased compared to the reference state. Regarding the impact of aluminium silicate fibres, after 400 °C pre-heating the reinforced composites showed still lower values of the residual thermal conductivity than the reference materials, but the decrease was lower than at room temperature. It ranged from 2 % to 9 %, on average, for particular fibres dosage. For the temperature loading of 1000 °C, the tendency was reversed, and the residual thermal conductivity of reinforced composites exhibited higher values than the reference materials. The growth was by 8 %, 17 % and 19 %, on average, for fibre dosage of 0.5 %, 1 % and 1.5 %, respectively. It could be attributed not only to the lower residual porosity of reinforced composites, but a potential effect could have also

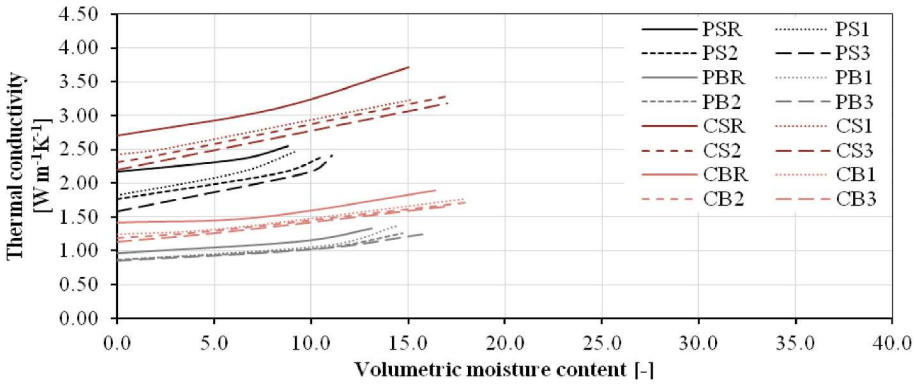

Fig. 15. Thermal conductivity of studied composites at ambient temperature.

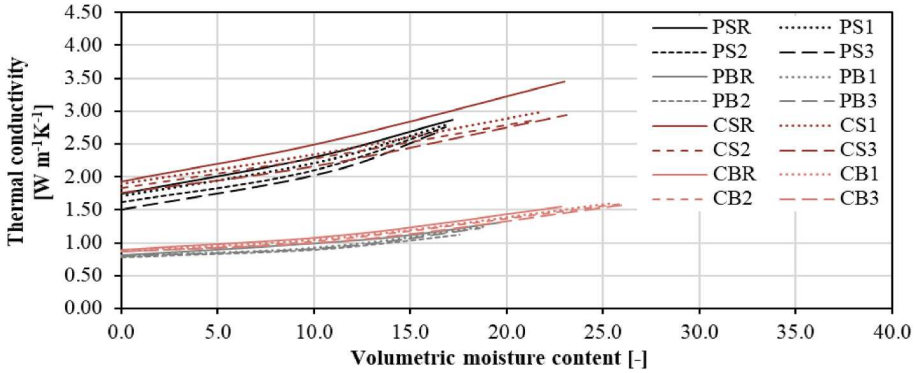

Fig. 16. Thermal conductivity of studied composites after 400 °C pre-heating.

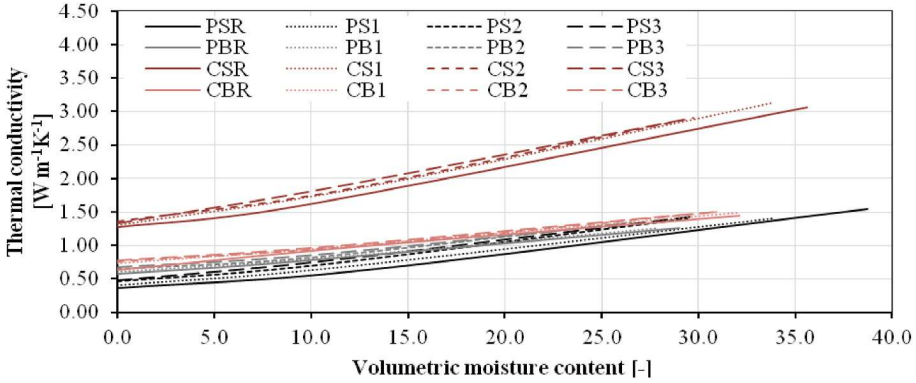

Fig. 17. Thermal conductivity of studied composites after 1000 °C pre-heating.

the partial recrystallization of fibres, which can lead to the growth of their thermal conductivity.

Specific heat capacities in the dry state are shown in Fig. 18. At room temperature, the use of fibre reinforcement always led to the fall of specific heat capacity. Bigger changes were observed for Portland cement-based sets, especially in combination with the silica aggregate. A 4.3 %–9.7 % decrease was observed for the fibre dosage of 0.5 %–1.5 %. On the contrary, for the set based on calcium aluminate cement and basalt aggregate a maximal decrease of only 1.3 % was found.

The exposure to higher temperatures led to the fall of residual specific heat capacity in both applied pre-treatments. For all studied materials the changes were very similar; after 400 °C the decrease was 3 % on average, while loading by 1000 °C caused a drop of 5 %. The impact of fibres remained similar as in the case of room temperature.

The thermal strain in the temperature range up to 1000 °C is presented in Fig. 19, and the values of the linear thermal expansion coefficient are shown in Fig. 20. The mixtures containing silica aggregate reached twice higher values of thermal strain due to the recrystallization of quartz at 573 °C. At that temperature, their thermal expansion coefficients showed 90 % higher values. Regarding the impact of the fibre, in the case of the Portland cement application, the presence of aluminium silicate fibres caused somewhat higher values of thermal strain. The observed elongation was remarkably increased for temperatures higher than 800 °C, in particular. On the other hand, for calcium aluminate cement-based composites the use of reinforcement led to a thermal strain reduction. The best performance was achieved for the 1 % fibre dosage.

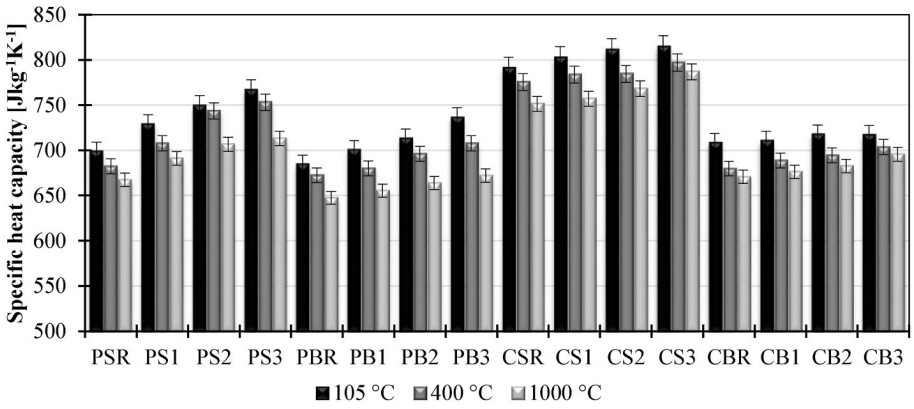

Fig. 18. Specific heat capacity of studied composites in the dry state.

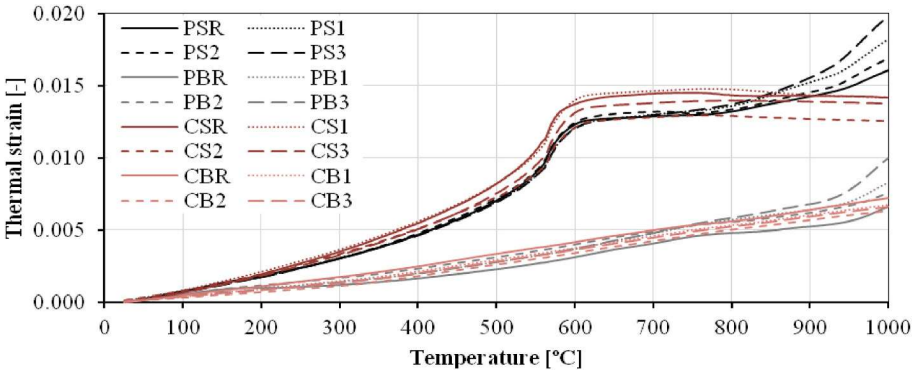

Fig. 19. Thermal strain of studied composites.

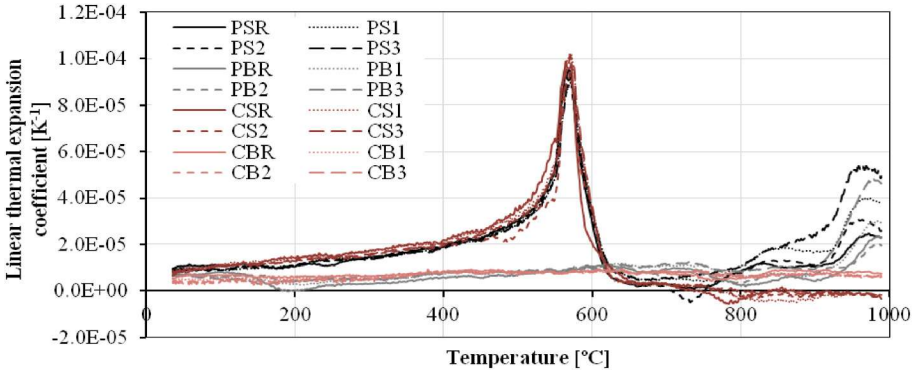

Fig. 20. Linear thermal expansion coefficient of studied composites.

5. Discussion

The application of randomly distributed aluminium silicate fibres for cement-based composites was studied relatively rarely until now. Therefore, their effect on the properties of various cement matrices deserves a detailed comparison with other, more frequently used, types of fibres. In Table 5, there are summarized basic physical properties of fibres used in cement composites [6,15,16,36,37]. Apparently, from the point of view of a possible utilization for improving the performance of thermally resistant materials only five types of fibres (including aluminium silicate) show a sufficiently high softening temperature and can thus be considered as prospective candidates.

The most common fibres used for concrete reinforcement are steel fibres. In the current research, this kind of fibre is usually investigated in combination with some organic fibres, and almost entirely with the PC matrix. Bodnárová et al. [38] investigated the behaviour of blended cement-based composites with steel and polypropylene fibres, and basalt or lightweight clay-based aggregate. They reported a positive effect of dispersed steel reinforcement up to 400 °C, especially on flexural strength. Compared to the aluminium silicate fibres analysed in this paper, the improvement due to the steel fibres was higher but it could be influenced by the increase of mechanical strengths after exposure to 200 °C for all mixtures regardless of the fibre type.

In contrast to the research of Bodnárová et al. [38], Ding et al. [39] presented a decreasing tendency of mechanical strengths due to temperature exposure. Nevertheless, they confirmed the positive effect of steel fibres in the whole temperature range they studied. Up to 600 °C the fibre-reinforced self-compacting concrete based on PC, seemed to be useable, chiefly when the steel fibre was combined with polypropylene fibres. The impact of steel fibres on residual compressive strength was

Table 5
Basic physical properties of common fibres.

Fibres	Density [kg m ^{3}]	Tensile strength [GPa]	Elastic modulus [GPa]	Linear thermal expansion coefficient [10 ^{6} K ^{1}]	Elongation at break [%]	Softening temperature [°C]
Aluminium silicate	2700	1.700	150	0.4	2.0	1260
Steel	7800	0.620	207.0	10.8	23.0	1440
E-glass	2580	3.445	76.0	5.4	4.8	846
S2-glass	2460	4.890	97.0	2.9	5.4	1056
Carbon	1760	3.500	235.0	0.36	1.2	3500
Basalt	2700	4.840	89	8.0	3.15	950
PP	910	0.475	4.1	150.0	25.0	160
PVA	1260	1.250	22.0	0.1	7.5	225
Nylon	1140	0.470	3.0	80	30.0	241
PET	1500	1.200	14.0	60	8.5	260
PE	920	0.103	130	180	45	120
Hemp	1250	0.255	9.5	–	2.2	150
Cellulose	1200	0.400	10	–	–	–
Jute	1400	0.600	19.8	–	1.8	–
Coir	150	0.174	2.3	–	32.0	200
Bagasse	550	0.230	1.7	–	8.7	180
Flax	1450	0.700	6.7	0.5	2.0	165

found to be comparable with the results obtained in this paper by the application of aluminium silicate fibres.

Steel fibres combined with polyvinyl alcohol fibres and improved calcium carbonate whiskers were studied by Li et al. [40]. Their investigation was focused, among other issues, on structural changes in steel fibres. They concluded that the maximum temperature for their application was 800 °C when their mechanical performance due to the fibre oxidation decreased sharply. In contrast, in this paper, it was proved that the aluminium silicate fibres remained unaffected by temperature exposure in the whole studied range up to 1000 °C. Li et al. [40] also reported a positive effect of hybrid fibres on the mechanical performance of composite containing PC, fly ash and silica sand up to 500 °C. However, this could be influenced by the utilization of silica sand, which is not suitable for temperatures above 550 °C due to the recrystallization of quartz. A similar conclusion can be found also in the study performed by Liu et al. [41], who presented hybrid steel and polyvinyl alcohol fibres suitability in similar raw-material composition up to 600 °C.

Sultan et al. [42] focused their study on the varying reinforcement as well. They investigated the behaviour of concrete made from blended cement and fine silica sand. Regarding the fibre's kind, they studied steel, glass, polypropylene fibres, and also steel combined with polypropylene. Compared to the aluminium silicate fibres used in this paper, sole steel fibres provided a higher improvement in the case of compressive strength at ambient temperature; on average by 14 %. Nevertheless, according to their results, sole steel and glass fibres did not inhibit the devastating spalling of concrete, which restricted their use to 400 °C or 300 °C for steel or glass fibres, respectively. Although the softening temperature of steel fibres is quite high (about 1440 °C), they can be used effectively in a much lower temperature range, their high linear thermal expansion coefficient and fibre degradation being the main obstacles.

According to the studies presented above, steel fibres seem to be appropriate for the application up to 600 °C only. At room temperature, steel fibres are more suitable than aluminium silicate fibres but for higher temperatures, the ceramic fibres show a much better performance in cement-based composites.

Glass fibres present another type of frequently used fibres for concrete reinforcement. When focused on their physical properties, they show higher tensile strength, lower linear thermal expansion coefficient, but also lower softening temperature compared to steel fibres. However, when focused on the current research, only a few studies dealing with their application in a high-temperature range can be found. Raza et al. [43] examined steel and glass fibres, and their possible combination as well, in the temperature range of 25 °C–800 °C. In contrast with [44], they reported a beneficial effect of explosive spalling elimination in both cases of used fibres. This could be attributed to the different fibre dosages. A more likely explanation could though be the different curing conditions, more precisely different moisture content, thus Sultan's [42] concrete should be more predisposed to explosive spalling. In general, Raza et al. [43] concluded, that both fibres are suitable for temperatures up to 800 °C but steel fibres showed a more beneficial performance. At 400 °C, a comparison with the aluminium silicate fibres used in this paper could be performed. 3 vol% of sole glass fibres increased residual compressive strength by 2 %, while the optimal amount of aluminium silicate fibres provided a 5 % improvement. Regarding the bending strength, aluminium silicate fibres were more suitable as well, the growth was in the case of the glass fibres 8 %, while when the aluminium silicate fibres were employed, it was 10 %.

A comparison between steel and glass fibres can be found also in the work of Moghadam et al. [44]. The temperature range of the experimental program was up to 800 °C, the matrix was PC cement, and they used calcareous aggregate. They reported a positive effect of both fibre types. Nevertheless, in accordance with Raza's work [43], steel fibres exhibited better performance compared to glass. Glass fibres showed some limit at about 500 °C, and higher temperature exposure led to a decrease in shear strength. Besides the mechanical properties, they determined durability characteristics as well and reported their improvement in all temperature stages. In contrast to our results, the water absorption ability at room temperature went down due to the fibre reinforcement. But the growing tendency caused by temperature exposure was in conformity with the results in this work.

A deeper study of glass fibre effects was performed by Wang et al. [45], who dealt with glass fibres dosage and their length as well. Regarding the dosage, in the case of short fibre, the optimal value was 0.5 % of cement weight, while longer glass fibres were suitable for up to 1 %. They studied temperature exposure up to 1000 °C and reported that at such a high-temperature glass fibres had no impact on residual performance of concrete. On the contrary, the aluminium silicate fibres studied in this paper showed a beneficial effect even at 1000 °C.

Glass fibre in 0.5 % dosage seemed to be adequate also according to the comparative study of Cavdar et al. [46]. They investigated cement mortar based on PC reinforced by polypropylene, polyvinyl chloride, glass or carbon fibres. The impact of all fibres on the compressive strength was not positive, but an improvement of flexural strength due to the use of glass fibre reinforcement was observed in the temperature range up to 450 °C. Glass fibres caused a much bigger decrease of bulk density compared to the impact of aluminium silicate fibres in this paper.

Taking into account the above-surveyed research, it can be concluded that glass fibres seem to have a lower potential for high-

temperature applications than aluminium silicate fibres.

Carbon fibres show not only good thermal resistance but also have a great mechanical performance and one of the lowest linear thermal expansion coefficients (taking into account common fibres, see Table 5). However, their performance at high-temperature exposure strongly depends on the particular environment. In the oxidizing atmosphere, they start to oxidize above 500 °C [47]. Cavdar et al. [46] found in their study that the bulk density of cement mortar went down due to the carbon fibres utilization more distinctively compared to the aluminium silicate fibres analysed in this paper. Nevertheless, they reported an improvement in flexural strength due to the carbon fibre application at temperatures from 100 °C to 650 °C for all fibre dosages, while at room temperature the use of carbon fibres was not beneficial. On the other hand, the compressive strength was almost entirely lost. When comparing the mechanical performance, the aluminium silicate fibres investigated in this paper were found to be more suitable than carbon fibres.

Carbon fibres in cement composites were also examined by Tanyildzi [48]. He employed them up to the amount of 8 kg m^{-3}. The best carbon fibre dosage was found to be 0.5 vol% for PC, and 1 vol% for blended cement and the fall of residual compressive strengths was marginal between 600 and 800 °C. This conclusion was confirmed by Akbar et al. [49]. Their blended cement pastes (silica fume and PC based) also showed the best performance in the case of 1 % of carbon fibres in the mix. According to the XRD, TG and SEM measurements, Akbar et al. [49] reported that at 600 °C the fibres were separated from the matrix, at 800 °C they were partially degraded, and at 900 °C they were completely burnt out. On the contrary, the aluminium silicate fibres analysed in this paper showed good stability up to 1000 °C and thus seemed to be more useful for such conditions.

Boris et al. [50] studied the applicability of carbon fibres up to 0.6 % by mass in CAC-based pastes. They found a positive effect of fibres on both compressive and bending strengths at room temperature. However, regarding the higher temperatures, they studied the mortars only using thermal analysis. Contrary to Akbar et al. [49], they reported the threshold temperature for carbon fibres as 600 °C, when these fibres burnt out, and thus they could provide no beneficial effect after exceeding this temperature.

The reinforcement of cement composites by carbon fibres seems to be a better option for high-temperature applications, as compared to steel or glass fibres. However, the aluminium silicate fibres used in this paper showed a much better performance of designed composites from the points of view of both residual mechanical properties and high-temperature stability.

During the last century, asbestos fibres were a widely used reinforcement in cement-based composites. They were considered one of the best solutions for concrete resistant to high temperatures. Unfortunately, asbestos was proven to be harmful to human health, in 1984 it was put on the list of proven carcinogenic agents and its use was prohibited.

Basalt fibres appeared as one of the promising possibilities for asbestos substitution already in the last decades of the 20th century. Although they have similar chemical composition to asbestos, they are non-hazardous to human health (due to the different morphology and surface properties) [51]. The application of basalt fibres was studied, e.g., by Ren et al. [52]. Their mixtures were composed of blended cement, crushed limestone, and basalt fibres up to 0.3 % of volume. The temperature loading was performed up to 800 °C, in contrast with some previous studies the cooling was done by water spraying. Ren et al. [52] reported that the application of basalt fibres led to an improvement in strength performance, deformation capacity and energy absorption of concrete also after temperature exposure in the whole temperature range. The optimal fibre volume was found to be 0.2 %. Higher fibre dosage was studied by Jalasutram et al. [53], who investigated the mechanical properties of fibre-reinforced concrete based on PC. They presented that the use of basalt fibres up to 2 % of volume led to almost no difference in compressive strength. However, the splitting strength and flexural strength were improved due to the reinforcement, as well as the flexural toughness. Yonggui et al. [54] dealt with basalt fibres as well. Concrete containing PC, nano-silica, river sand and gravel or crushed recycled concrete with fibre dosage up to 3 kg m^{-3} was investigated in the temperature range up to 600 °C. At both room temperature and higher temperatures, the application of basalt fibres was found beneficial for the splitting tensile strength and compressive strength, the improvement was generally increased as the basalt fibre content grew. The use of basalt fibres in combination with CAC was studied by Vejmelková et al. [55] who observed a positive effect of basalt fibres in the temperature range up to 1000 °C. Comparing the effect of basalt fibres in Vejmelková et al. [55] and aluminium silicate fibres in this paper, the composites with basalt fibres exhibited somewhat higher values of compressive strength but higher bending strengths were achieved when aluminium silicate fibres were employed. When focused on the thermal strain, the biggest differences were found in the different matrices. For *P*C-based composites, the basalt fibres seemed to be more advantageous, while for CAC the aluminium silicate fibres showed lower strain.

Taking into account the properties of basalt fibres (high softening temperature, high tensile strength, and low thermal strain in particular) they are, apparently, more suitable for high-temperature applications than steel-, glass- or carbon fibres as their thermal stability is much better. When comparing basalt fibres to aluminium silicate ones, both kinds have their advantages and seem to be beneficial as reinforcing materials for high-temperature-resistant cement-based composites.

6. Conclusions

The applicability of randomly distributed aluminium silicate fibres for cement composites was analysed in the paper. As the studied fibres have good thermal resistance, also their impact on the composite performance at high temperatures was investigated. The experimental results showed the good potential of aluminium silicate fibres for application in cement-based composites in the temperature range of up to 1000 °C. The main findings can be summarized as follows.

- The fibres remained unaffected in the temperature range up to 1000 °C and no negative agglomeration, sintering, fusing, or other damage was observed.
- The open porosity of the analysed composites at room temperature increased due to the use of fibre reinforcement. After high-temperature exposure, this tendency was reversed and the presence of fibres led to a decrease in residual open porosity.
- The application of aluminium silicate fibres led to a considerable increase in bending and compressive strengths both at room temperature and after pre-heating up to 1000 °C, as compared to the reference composites. The fibre dosage of 1 % appeared as the optimal solution as no substantial improvement was achieved by a further increase of fibre amount in the mixes.
- The water- and water vapour transport ability of the studied composite materials at room temperature increased due to the application of aluminium silicate fibres. This tendency was reversed after high-temperature exposure, which was in accordance with the changes in open porosity.
- The room-temperature thermal conductivity of fibre-reinforced composites substantially decreased, as compared with the reference materials. After the exposure to 400 °C, the difference between reference and reinforced composites was diminished, and after 1000 °C pre-heating the presence of aluminium silicate fibres led to an increase of thermal conductivity. The specific heat capacity increased due to the fibre reinforcement for all studied materials and conditions.

- The use of aluminium silicate fibres led to a thermal strain reduction of up to 1000 °C for calcium aluminate cement-based composites only. The best performance was achieved for 1 % fibre dosage.
- The composites containing calcium aluminate cement and basalt aggregates showed the best performance among the studied mixes in the whole high-temperature range up to 1000 °C.
- The comparison of material parameters determined for the fibre-reinforced cement composites in this paper with the results reported by other investigators for different types of fibres showed that the aluminium silicate fibres performed at high temperatures better than steel-, glass-, and carbon fibres and their effect were similar to basalt fibres for both Portland cement and calcium aluminate cement matrices.

Based on the presented conclusions, it can be stated, that the use of aluminium silicate fibres in the field of high-temperature resistant composites is not only appropriate but advantageous as well. The optimal fibre dosage was found to be 1 % regardless of the matrix types. The promising factor of this study is the possibility of filling the gap in the field of fibre-reinforcing materials suitable also for high temperatures, which has been an issue worth addressing for more than twenty years.

Declaration of competing interest

The authors declare that they have no known competing financial interests or personal relationships that could have appeared to influence the work reported in this paper.

Data availability

Data will be made available on request.

Acknowledgement

This research has been supported by the Czech Science Foundation, under project No. 21-00800S and by the Grant Agency of the Czech Technical University in Prague, grant No. SGS22/137/OHK1/3T/11.

References

[1] N.C. Collier, Transition and decomposition temperatures of cement phases - a collection of thermal analysis data, Ceram. - Silik. (2016) 338–343, https://doi.org/10.13168/cs.2016.0050.
[2] Q. Zhang, G. Ye, Dehydration kinetics of Portland cement paste at high temperature, J. Therm. Anal. Calorim. 110 (2012) 153–158, https://doi.org/10.1007/s10973-012-2303-9.
[3] M.-A. Maaroufi, A. Lecomte, C. Diliberto, O. Francy, P. Le Brun, Thermo-hydrous behavior of hardened cement paste based on calcium aluminate cement, J. Eur. Ceram. Soc. 35 (2015) 1637–1646, https://doi.org/10.1016/j.jeurceramsoc.2014.11.029.
[4] M. Soutsos, Concrete Durability: a Practical Guide to the Design of Durable Concrete Structures, Thomas Telford, London, 2010.
[5] K. Scrivener, R. Snellings, B. Lothenbach (Eds.), A Practical Guide to Microstructural Analysis of Cementitious Materials, CRC Press, Boca Raton, FL, 2016.
[6] R. Sarkar, REFRACTORY TECHNOLOGY: Fundamentals and Applications, CRC PRESS, S.l., 2020.
[7] S. Ortaboy, J. Li, G. Geng, R.J. Myers, P.J.M. Monteiro, R. Maboudian, C. Carraro, Effects of CO $_2$ and temperature on the structure and chemistry of C–(A–)S–H investigated by Raman spectroscopy, RSC Adv. 7 (2017) 48925–48933, https://doi.org/10.1039/C7RA07266J.
[8] D. Koňáková, V. Pommer, K. Šádková, M. Keppert, R. Černý, E. Vejmelková, Impact of plasticizers' types on the performance of calcium aluminate cement, J. Mater. Res. Technol. 20 (2022) 1512–1523, https://doi.org/10.1016/j.jmrt.2022.07.155.
[9] J. Piasta, Z. Sawicz, L. Rudzinski, Changes in the structure of hardened cement paste due to high temperature, Mater. Construcción 17 (1984) 291–296, https://doi.org/10.1007/BF02479085.
[10] M. Abid, X. Hou, W. Zheng, R.R. Hussain, High temperature and residual properties of reactive powder concrete – a review, Construct. Build. Mater. 147 (2017) 339–351, https://doi.org/10.1016/j.conbuildmat.2017.04.083.
[11] Q. Ma, R. Guo, Z. Zhao, Z. Lin, K. He, Mechanical properties of concrete at high temperature—a review, Construct. Build. Mater. 93 (2015) 371–383, https://doi.org/10.1016/j.conbuildmat.2015.05.131.
[12] V. Afroughsabet, L. Biolzi, T. Ozbakkaloglu, High-performance fiber-reinforced concrete: a review, J. Mater. Sci. 51 (2016) 6517–6551, https://doi.org/10.1007/s10853-016-9917-4.
[13] D. Zhang, A. Dasari, K.H. Tan, On the mechanism of prevention of explosive spalling in ultra-high performance concrete with polymer fibers, Cement Concr. Res. 113 (2018) 169–177, https://doi.org/10.1016/j.cemconres.2018.08.012.
[14] D.-Y. Yoo, N. Banthia, Impact resistance of fiber-reinforced concrete – a review, Cem. Concr. Compos. 104 (2019), 103389, https://doi.org/10.1016/j.cemconcomp.2019.103389.
[15] A. Anandamurthy, V. Guna, M. Ilangovan, N. Reddy, A review of fibrous reinforcements of concrete, J. Reinforc. Plast. Compos. 36 (2017) 519–552, https://doi.org/10.1177/0731684416685168.
[16] H.R. Pakravan, M. Latifi, M. Jamshidi, Hybrid short fiber reinforcement system in concrete: a review, Construct. Build. Mater. 142 (2017) 280–294, https://doi.org/10.1016/j.conbuildmat.2017.03.059.
[17] V. Aruchamy, V. Ramasamy, S. Venkatraman, A novel strength behavior prediction model of self-compacting concrete with foundry sand and hybrid fibers, Struct. Concr. 23 (2022) 2313–2321, https://doi.org/10.1002/suco.202100091.
[18] K. Cao, G. Liu, H. Li, Z. Huang, Mechanical properties and microstructures of Steel-basalt hybrid fibers reinforced Cement-based composites exposed to high temperatures, Construct. Build. Mater. 341 (2022), 127730, https://doi.org/10.1016/j.conbuildmat.2022.127730.
[19] E. Yalamaç, M. Sutcu, S.B. Basturk, Ceramic fibers, in: Fiber Technol. Fiber-Reinf. Compos., Elsevier, 2017, pp. 187–207, https://doi.org/10.1016/B978-0-08-101871-2.00009-6.
[20] K. Lü, X. Liu, Z. Du, Y. Li, Properties of hybrid fibre reinforced shell for investment casting, Ceram. Int. 42 (2016) 15397–15404, https://doi.org/10.1016/j.ceramint.2016.06.188.
[21] D. Lu, Z. Wang, Y. Jiang, R. Zhou, Effect of aluminum silicate fiber modification on crack-resistance of a ceramic mould, China Foundry 9 (2012) 322–327.
[22] L. Miao, X. Wu, Z. Ji, F. Chen, Effects of heat-treatment conditions in the preparation of aluminum silicate fiber-based ceramic filter element for hot-gas filtration, Ceram. Int. 46 (2020) 18193–18199, https://doi.org/10.1016/j.ceramint.2020.04.141.
[23] S. Rathod, A. Raghubanshi, Y. Srivastava, V.R. Kiragi, D.P. Mondal, Dry sliding wear behaviour study of alumina-silicate short fiber reinforced AA2014-Al alloy composite, Mater. Today Proc. 18 (2019) 3445–3453, https://doi.org/10.1016/j.matpr.2019.07.272.
[24] D. Nath, V. Singh, Ageing characteristics of aluminium alloy aluminosilicate discontinuous fibre reinforced composites, Scripta Mater. 40 (1999) 791–794, https://doi.org/10.1016/S1359-6462(99)00019-6.
[25] Q. Zhu, C.S. Zhao, J.J. Pang, Preparation of new alumina silicate refractory fiberboard and study on its performance, Adv. Mater. Res. 236–238 (2011) 1347–1350. https://doi.org/10.4028/www.scientific.net/AMR.236-238.1347.
[26] H. Su, J. Xu, Dynamic compressive behavior of ceramic fiber reinforced concrete under impact load, Construct. Build. Mater. 45 (2013) 306–313, https://doi.org/10.1016/j.conbuildmat.2013.04.008.
[27] H. Su, J. Xu, W. Ren, Mechanical properties of ceramic fiber-reinforced concrete under quasi-static and dynamic compression, Mater. Des. 57 (2014) 426–434, https://doi.org/10.1016/j.matdes.2013.12.061.
[28] N. Doebelin, R. Kleeberg, *Profex* : a graphical user interface for the Rietveld refinement program *BGMN*, J. Appl. Crystallogr. 48 (2015) 1573–1580, https://doi.org/10.1107/S1600576715014685.
[29] ČSN EN 196-6, Methods of Testing Cement – Part 6, Determination of fineness, 2019, 722100.
[30] ČSN EN 933-1, Zkoušení Geometrických Vlastností Kameniva - Část 1, Stanovení zrnitosti - Sítový rozbor, 2012, 721193.
[31] S. Roels, J. Carmeliet, H. Hens, O. Adan, H. Brocken, R. Cerny, Z. Pavlik, C. Hall, K. Kumaran, L. Pel, R. Plagge, Interlaboratory comparison of hygric properties of porous building materials, J. Therm. Envelope Build. Sci. 27 (2004) 307–325, https://doi.org/10.1177/1097196304042119.
[32] ČSN EN 1015-11, Methods of Test for Mortar for Masonry - Part 11: Determination of Flexural and Compressive Strength of Hardened Mortar, 2020, 722400.
[33] E. Vejmelková, M. Pavlíková, M. Jerman, R. Černý, Free water intake as means of material characterization, J. Build. Phys. 33 (2009) 29–44, https://doi.org/10.1177/1744259109104069.
[34] R. Černý, Complex System of Methods for Directed Design and Assessment of Functional Properties of Building Materials: Assessment and Synthesis of Analytical Data and Construction of the System, Czech Technical University, Prague, 2010.
[35] A. Trnik, I. Medved, R. Cerny, Measurement of linear thermal expansion coefficient of concrete at high temperatures: a comparison of isothermal and non-isothermal methods, Cem. WAPNO BETON. 17 (2012) 363. -+.
[36] M. Keppert, E. Vejmelkova, S. Svarcova, P. Bezdicka, R. Cerny, Microstructural changes and residual properties of fiber reinforced cement composites exposed to elevated temperatures, Cem. WAPNO BETON. 17 (2012) 77. -+.
[37] V. Dhand, G. Mittal, K.Y. Rhee, S.-J. Park, D. Hui, A short review on basalt fiber reinforced polymer composites, Composites, Part B 73 (2015) 166–180, https://doi.org/10.1016/j.compositesb.2014.12.011.
[38] L. Bodnarova, J. Hroudova, J. Brozovsky, J. Zach, J. Valek, Behaviour of cement composites with lightweight and heavyweight aggregates at high temperatures, Period. Polytech. Civ. Eng. (2016), https://doi.org/10.3311/PPci.9365.
[39] Y. Ding, C. Azevedo, J.B. Aguiar, S. Jalali, Study on residual behaviour and flexural toughness of fibre cocktail reinforced self compacting high performance concrete

after exposure to high temperature, Construct. Build. Mater. (2011), https://doi.org/10.1016/j.conbuildmat.2011.04.058. S095006181100198X.
[40] L. Li, D. Gao, Z. Li, M. Cao, J. Gao, Z. Zhang, Effect of high temperature on morphologies of fibers and mechanical properties of multi-scale fiber reinforced cement-based composites, Construct. Build. Mater. 261 (2020), 120487, https://doi.org/10.1016/j.conbuildmat.2020.120487.
[41] J.-C. Liu, K.H. Tan, Fire resistance of strain hardening cementitious composite with hybrid PVA and steel fibers, Construct. Build. Mater. 135 (2017) 600–611, https://doi.org/10.1016/j.conbuildmat.2016.12.204.
[42] H.K. Sultan, I. Alyaseri, Effects of elevated temperatures on mechanical properties of reactive powder concrete elements, Construct. Build. Mater. 261 (2020), 120555, https://doi.org/10.1016/j.conbuildmat.2020.120555.
[43] S.S. Raza, L.A. Qureshi, B. Ali, A. Raza, M.M. Khan, H. Salahuddin, Mechanical properties of HybridSteel–glass fiber-reinforced reactive powder concrete AfterExposure to elevated temperatures, Arabian J. Sci. Eng. 45 (2020) 4285–4300, https://doi.org/10.1007/s13369-020-04435-4.
[44] M. Abdi Moghadam, R.A. Izadifard, Effects of steel and glass fibers on mechanical and durability properties of concrete exposed to high temperatures, Fire Saf. J. 113 (2020), 102978, https://doi.org/10.1016/j.firesaf.2020.102978.
[45] W.-C. Wang, H.-Y. Wang, K.-H. Chang, S.-Y. Wang, Effect of high temperature on the strength and thermal conductivity of glass fiber concrete, Construct. Build. Mater. 245 (2020), 118387, https://doi.org/10.1016/j.conbuildmat.2020.118387.
[46] A. Çavdar, A study on the effects of high temperature on mechanical properties of fiber reinforced cementitious composites, Composites, Part B 43 (2012) 2452–2463, https://doi.org/10.1016/j.compositesb.2011.10.005.
[47] A. Vinci, L. Zoli, E. Landi, D. Sciti, Oxidation behaviour of a continuous carbon fibre reinforced ZrB 2 –SiC composite, Corrosion Sci. 123 (2017) 129–138, https://doi.org/10.1016/j.corsci.2017.04.012.
[48] H. Tanyildizi, Prediction of the strength properties of carbon fiber-reinforced lightweight concrete exposed to the high temperature using artificial neural network and support vector machine, Adv. Civ. Eng. 2018 (2018) 1–10, https://doi.org/10.1155/2018/5140610.
[49] A. Akbar, K.M. Liew, Influence of elevated temperature on the microstructure and mechanical performance of cement composites reinforced with recycled carbon fibers, Composites, Part B 198 (2020), 108245, https://doi.org/10.1016/j.compositesb.2020.108245.
[50] R. Boris, V. Antonovič, J. Keriene, R. Stonys, The effect of carbon fiber additive on early hydration of calcium aluminate cement, J. Therm. Anal. Calorim. 125 (2016) 1061–1070, https://doi.org/10.1007/s10973-016-5312-2.
[51] E. Quagliarini, F. Monni, S. Lenci, F. Bondioli, Tensile characterization of basalt fiber rods and ropes: a first contribution, Construct. Build. Mater. 34 (2012) 372–380, https://doi.org/10.1016/j.conbuildmat.2012.02.080.
[52] W. Ren, J. Xu, H. Su, Dynamic compressive behavior of basalt fiber reinforced concrete after exposure to elevated temperatures: behavior of Basalt Fiber Reinforced Concrete, Fire Mater. 40 (2016) 738–755, https://doi.org/10.1002/fam.2339.
[53] S. Jalasutram, D.R. Sahoo, V. Matsagar, Experimental investigation of the mechanical properties of basalt fiber-reinforced concrete: JALASUTRAM et al, Struct. Concr. 18 (2017) 292–302, https://doi.org/10.1002/suco.201500216.
[54] W. Yonggui, L. Shuaipeng, P. Hughes, F. Yuhui, Mechanical properties and microstructure of basalt fibre and nano-silica reinforced recycled concrete after exposure to elevated temperatures, Construct. Build. Mater. 247 (2020), 118561, https://doi.org/10.1016/j.conbuildmat.2020.118561.
[55] E. Vejmelková, D. Koňáková, L. Scheinherrová, M. Doleželová, M. Keppert, R. Černý, High temperature durability of fiber reinforced high alumina cement composites, Construct. Build. Mater. 162 (2018) 881–891, https://doi.org/10.1016/j.conbuildmat.2018.01.076.

6 Conclusion

This habilitation thesis has explored the multifaceted potential of calcium aluminate cement-based composites in addressing some of the pressing challenges in the construction materials sector related to material base, durability, high-temperature resistance, and environmental sustainability. Through an in-depth investigation into the hydration mechanisms and microstructural analysis of CAC and a further assessment of a wide scope of physical properties (including basic physical, mechanical, thermal and hygric characteristics), the research confirms that CAC represents a viable and high-performance alternative to traditional Portland cement in specialised applications.

The integration of suitable chemical additives, particularly plasticisers, has proven to be crucial in refining the rheological and mechanical properties of CAC systems. Modified polycarboxylates emerged as the most promising class, balancing workability and strength while mitigating adverse effects such as excessive porosity or hydration retardation.

The incorporation of supplementary cementitious materials presents an essential advancement in reducing the clinker content of CAC composites by up to 60%, significantly lowering their carbon footprint. These SCMs not only serve ecological goals but also enhance the hydration dynamics and long-term durability of the cement matrix. The most promising approach was revealed to be the combination of SCMs in ternary binder systems, which, through synergistic interactions, help to improve the properties of the designed composites. Among the investigated materials, the most effective SCMs were waste calcined shale and ceramic waste combined with alumina-based admixtures.

Further, fibre reinforcement, carefully chosen to complement the thermal and chemical characteristics of CAC, was demonstrated to enhance composite integrity under extreme thermal loading. These fibres, such as basalt or aluminium silicate fibres, contribute not only to crack resistance but also to improved thermal resistance and mechanical stability at temperatures exceeding 1000 °C.

Altogether, the findings validate CAC composites as highly adaptable materials suited for both structural and refractory applications, particularly where Portland cement's limitations in chemical and thermal stability are pronounced. The research contributes substantially to both academic knowledge and industrial practice, bridging the performance-sustainability gap in high-performance cementitious systems.

6.1 Possibility of further investigation

Building upon the insights gained from this habilitation thesis, several directions for future research have emerged. These issues aim not only to deepen the understanding of calcium aluminate cement-based systems but also to advance their industrial applicability, environmental performance, and material optimisation under extreme conditions:

- Synergistic design of fibre reinforced ternary binder-based composites: Systematic studies are needed to assess how the interplay between fibre type (e.g. ceramic, basalt, polypropylene), fibre dosage, and fibre-matrix interface interacts with SCM-induced modifications in hydration kinetics and microstructure.
- Advanced hydration modelling and phase evolution: Further investigation into the kinetics of hydration and long-term phase stability is essential, particularly for ternary CAC-SCM systems.
- Durability under combined degradation mechanisms: While individual degradation mechanisms (conversion, carbonation, thermal exposure, and alkaline hydrolysis) have been well characterised, their synergistic or competitive effects remain unexplored.
- Life cycle assessment of CAC-based composite systems: As sustainability becomes a central criterion in materials engineering, future research must incorporate comprehensive life cycle assessment (LCA) to evaluate the environmental impacts of CAC-based composites throughout their production, use, and end-of-life stages.

References

[1] H. Pollmann, Calcium Aluminate Cements - Raw Materials, Differences, Hydration and Properties, Reviews in Mineralogy and Geochemistry 74 (2012) 1–82. https://doi.org/10.2138/rmg.2012.74.1.

[2] J. Kopanda, G. MacZura, Production Processes, Properties and Applications for Calcium Aluminate Cements. Alumina Chemicals Science and Technology Handbook, LD Hard Editor, 171, Amer. Ceram. Soc., Inc., Westerwille, Ohio (1990).

[3] L.D. Hart, E. Lense, eds., Alumina chemicals: science and technology handbook, American Ceramic Society, Westerville, Ohio, 1990.

[4] J. Bied, Le ciment alumineux, Rev. Met. Paris 19 (1922) 759–764. https://doi.org/10.1051/metal/192219120759.

[5] K. Scrivener, A. Capmas, Calcium aluminate cements, Advanced Concrete Technology 3 (2003) 1–31.

[6] L. Svoboda, Stavební hmoty, 1. české vyd. (dotisk), Jaga, Bratislava, 2004.

[7] D.G. Altenpohl, J.G. Kaufman, D.G. Altenpohl, D.G. Altenpohl, Aluminum: technology, applications, and environment: a profile of a modern metal, 6. ed., rev.expanded English version, reprinted 1999, Aluminium Association [u.a.], Washington, D.C, 1999.

[8] Mindat.org, (n.d.). https://www.mindat.org/ (accessed August 29, 2024).

[9] P. Hewlett, Lea's Chemistry of Cement and Concrete, 4th ed., Elsevier Science & Technology, n.d.

[10] X. Pan, J. Liu, D. Zhang, H. Yu, Formation and transition of calcium aluminate and calcium silicate compounds from pre-synthesized mullite in low-calcium system by solid-state reaction, Ceramics International 46 (2020) 16583–16589. https://doi.org/10.1016/j.ceramint.2020.03.230.

[11] M. Ilatovskaia, O. Lonski, M. Löffler, L. Blenau, A. Charitos, O. Fabrichnaya, Phase Relations in the CaO-Nd2O3-Al2O3 System in Application for Rare Earth Recycling, JOM 75 (2023) 1993–2002. https://doi.org/10.1007/s11837-023-05731-8.

[12] I. Odler, Special Inorganic Cements, 0 ed., CRC Press, 2003. https://doi.org/10.1201/9781482271942.

[13] D.I. https://www.datamintelligence.com, Calcium Aluminate Cement: Growth & Key Player Insights, DataMIntelligence (n.d.). https://www.datamintelligence.com/research-report/calcium-aluminate-cement-market (accessed August 29, 2024).

[14] J. Zapata, A. Azevedo, C. Fontes, S. Monteiro, H. Colorado, Environmental Impact and Sustainability of Calcium Aluminate Cements, Sustainability 14 (2022) 2751. https://doi.org/10.3390/su14052751.

[15] A. Intiso, F. Rossi, A. Proto, R. Cucciniello, The fascinating world of mayenite (Ca12Al14O33) and its derivatives, Rend. Fis. Acc. Lincei 32 (2021) 699–708. https://doi.org/10.1007/s12210-021-01025-w.

[16] S.R. Klaus, J. Neubauer, F. Goetz-Neunhoeffer, Hydration kinetics of CA2 and CA—Investigations performed on a synthetic calcium aluminate cement, Cement and Concrete Research 43 (2013) 62–69. https://doi.org/10.1016/j.cemconres.2012.09.005.

[17] V. Antonovič, J. Kerienė, R. Boris, M. Aleknevičius, The Effect of Temperature on the Formation of the Hydrated Calcium Aluminate Cement Structure, Procedia Engineering 57 (2013) 99–106. https://doi.org/10.1016/j.proeng.2013.04.015.

[18] A. Koehler, J. Neubauer, F. Goetz-Neunhoeffer, How C12A7 influences the early hydration of calcium aluminate cement at different temperatures, Cement and Concrete Research 162 (2022) 106972. https://doi.org/10.1016/j.cemconres.2022.106972.
[19] M. Taylor, C. Tam, D. Gielen, Energy Efficiency and CO2 Emissions from the Global Cement Industry, (n.d.).
[20] J. Chen, C. Liang, B. Li, E. Wang, G. Li, X. Hou, The effect of nano-γAl 2 O 3 additive on early hydration of calcium aluminate cement, Construction and Building Materials 158 (2018) 755–760. https://doi.org/10.1016/j.conbuildmat.2017.10.071.
[21] C. Sweegers, H.C. de Coninck, H. Meekes, W.J.P. van Enckevort, I.D.K. Hiralal, A. Rijkeboer, Morphology, evolution and other characteristics of gibbsite crystals grown from pure and impure aqueous sodium aluminate solutions, Journal of Crystal Growth 233 (2001) 567–582. https://doi.org/10.1016/S0022-0248(01)01615-3.
[22] M.P. Adams, J.H. Ideker, Influence of aggregate type on conversion and strength in calcium aluminate cement concrete, Cement and Concrete Research 100 (2017) 284–296. https://doi.org/10.1016/j.cemconres.2017.07.007.
[23] B. Pacewska, M. Nowacka, Studies of conversion progress of calcium aluminate cement hydrates by thermal analysis method, J Therm Anal Calorim 117 (2014) 653–660. https://doi.org/10.1007/s10973-014-3804-5.
[24] M.-A. Maaroufi, A. Lecomte, C. Diliberto, O. Francy, P. Le Brun, Thermo-hydrous behavior of hardened cement paste based on calcium aluminate cement, Journal of the European Ceramic Society 35 (2015) 1637–1646. https://doi.org/10.1016/j.jeurceramsoc.2014.11.029.
[25] K. Berent, S. Komarek, R. Lach, W. Pyda, The Effect of Calcination Temperature on the Structure and Performance of Nanocrystalline Mayenite Powders, Materials 12 (2019) 3476. https://doi.org/10.3390/ma12213476.
[26] V. Šatava, PHASE TRANSFORMATIONS DURING HYDROTHERMAL HEATING OF TRICALCIUM ALUMINATE IN LIQUID WATER, Ceramics - Silikaty 37 (1993) 76–78.
[27] M. Soutsos, Concrete durability: a practical guide to the design of durable concrete structures, Thomas Telford, London, 2010.
[28] L. Fernández-Carrasco, F. Puertas, M.T. Blanco-Varela, T. Vázquez, Carbonatación de pastas de cemento de aluminato de calcio, Mater. Construcc. 51 (2001) 127–136. https://doi.org/10.3989/mc.2001.v51.i263-264.358.
[29] L. Fernández-Carrasco, J. Rius, C. Miravitlles, Supercritical carbonation of calcium aluminate cement, Cement and Concrete Research 38 (2008) 1033–1037. https://doi.org/10.1016/j.cemconres.2008.02.013.
[30] S.M. Park, J.G. Jang, H.M. Son, H.K. Lee, Stable conversion of metastable hydrates in calcium aluminate cement by early carbonation curing, Journal of CO2 Utilization 21 (2017) 224–226. https://doi.org/10.1016/j.jcou.2017.07.002.
[31] E. García Alcocel, P. Garcés, S. Chinchón, General study of alkaline hydrolysis in calcium aluminate cement mortars under a broad range of experimental conditions, Cement and Concrete Research 30 (2000) 1689–1699. https://doi.org/10.1016/S0008-8846(00)00396-3.
[32] Y. Wang, L. Lei, J. Liu, Y. Ma, Y. Liu, Z. Xiao, C. Shi, Accelerators for normal concrete: A critical review on hydration, microstructure and properties of cement-based materials, Cement and Concrete Composites 134 (2022) 104762. https://doi.org/10.1016/j.cemconcomp.2022.104762.

[33] T. Dorn, O. Blask, D. Stephan, Acceleration of cement hydration – A review of the working mechanisms, effects on setting time, and compressive strength development of accelerating admixtures, Construction and Building Materials 323 (2022) 126554. https://doi.org/10.1016/j.conbuildmat.2022.126554.
[34] H. Xie, X. Liu, Y. Zheng, B. Chi, J. Guo, X. Dai, Z. Zhang, M. Sun, L. Duan, Z. Wang, S. Cui, Effect of complexation of alkanolamine in accelerators on the initial stage of cement hydration, Construction and Building Materials 393 (2023) 132105. https://doi.org/10.1016/j.conbuildmat.2023.132105.
[35] Admixture Interactions in Concrete, in: Concrete Admixtures Handbook, Elsevier, 1996: pp. 95–136. https://doi.org/10.1016/b978-081551373-5.50007-6.
[36] P.I. Nwaichi, N. Ridzuan, E.O. Nwaichi, C. Umunnawuike, A. Agi, Recent advances and prospects on retarder application in oilwell cement: A review, Geoenergy Science and Engineering 241 (2024) 213103. https://doi.org/10.1016/j.geoen.2024.213103.
[37] K.G. Fikeni, X. Pang, Y. Yu, X. Xia, F. Sun, H. Wang, K. Lv, J. Sun, An overview of oil well cement retarders and the retardation mechanisms, Geoenergy Science and Engineering 241 (2024) 213116. https://doi.org/10.1016/j.geoen.2024.213116.
[38] D. Koňáková, V. Pommer, K. Šádková, M. Keppert, R. Černý, E. Vejmelková, Impact of plasticizers' types on the performance of calcium aluminate cement, Journal of Materials Research and Technology 20 (2022) 1512–1523. https://doi.org/10.1016/j.jmrt.2022.07.155.
[39] R. SARKAR, REFRACTORY TECHNOLOGY: fundamentals and applications, CRC PRESS, S.l., 2020.
[40] A. Anandamurthy, V. Guna, M. Ilangovan, N. Reddy, A review of fibrous reinforcements of concrete, Journal of Reinforced Plastics and Composites 36 (2017) 519–552. https://doi.org/10.1177/0731684416685168.
[41] A. Kudžma, V. Antonovič, R. Stonys, V. Gribniak, Refractory castables cured at low temperatures—Spalling risks and testing, Case Studies in Construction Materials 22 (2025) e04701. https://doi.org/10.1016/j.cscm.2025.e04701.
[42] T.T. Win, L. Prasittisopin, P. Jongvivatsakul, S. Likitlersuang, Investigating the role of steel and polypropylene fibers for enhancing mechanical properties and microstructural performance in mitigating conversion effects in calcium aluminate cement, Construction and Building Materials 430 (2024) 136515. https://doi.org/10.1016/j.conbuildmat.2024.136515.
[43] A. Sharma, A.B.D. Roy, P.P. Bansal, Enhancing the residual performance of concrete using calcium aluminate cement composites, Magazine of Concrete Research 77 (2025) 667–687. https://doi.org/10.1680/jmacr.24.00294.
[44] W. Fan, Y. Zhuge, X. Ma, C.W.K. Chow, N. Gorjian, Strain hardening behaviour of PE fibre reinforced calcium aluminate cement (CAC) – Ground granulated blast furnace (GGBFS) blended mortar, Construction and Building Materials 241 (2020) 118100. https://doi.org/10.1016/j.conbuildmat.2020.118100.
[45] W. Fan, Y. Zhuge, X. Ma, C.W.K. Chow, N. Gorjian, J.-A. Oh, W. Duan, Durability of Fibre-Reinforced Calcium Aluminate Cement (CAC)–Ground Granulated Blast Furnace Slag (GGBFS) Blended Mortar after Sulfuric Acid Attack, Materials 13 (2020) 3822. https://doi.org/10.3390/ma13173822.
[46] O.Y. Bayraktar, G. Yarar, A. Benli, G. Kaplan, O. Gencel, M. Sutcu, M. Kozłowski, M. Kadela, Basalt fiber reinforced foam concrete with marble waste and calcium aluminate cement, Structural Concrete 24 (2023) 1152–1178. https://doi.org/10.1002/suco.202200142.

[47] R. Boris, V. Antonovič, J. Kerienė, R. Stonys, The effect of carbon fiber additive on early hydration of calcium aluminate cement, J Therm Anal Calorim 125 (2016) 1061–1070. https://doi.org/10.1007/s10973-016-5312-2.
[48] P. Beroll, S. Schmalzl, D. Volkmer, Influence of surface-modification, length and volume fraction of carbon short fibers on the mechanical properties of calcium aluminate cement systems, Materials Today Communications 25 (2020) 101704. https://doi.org/10.1016/j.mtcomm.2020.101704.
[49] D. Koňáková, M. Čáchová, M. Doleželová, L. Scheinherrová, E. Vejmelkova, R. Černý, High-temperature resistance of concretes produced of two different cements, Cement, Wapno, Beton 2016 (2016) 295–309.
[50] E. Vejmelková, D. Koňáková, L. Scheinherrová, M. Doleželová, M. Keppert, R. Černý, High temperature durability of fiber reinforced high alumina cement composites, Construction and Building Materials 162 (2018) 881–891. https://doi.org/10.1016/j.conbuildmat.2018.01.076.
[51] D. Koňáková, V. Pommer, K. Šádková, R. Černý, E. Vejmelková, High-temperature resistance of cement composites with randomly distributed aluminium silicate fibers, Cement and Concrete Composites 145 (2024) 105339. https://doi.org/10.1016/j.cemconcomp.2023.105339.
[52] M. Collepardi, S. Monosi, P. Piccioli, The influence of pozzolanic materials on the mechanical stability of aluminous cement, Cement and Concrete Research 25 (1995) 961–968. https://doi.org/10.1016/0008-8846(95)00091-P.
[53] Microstructure of the system calcium aluminate cement-silica fume: application in waste immobilization, in: Studies in Surface Science and Catalysis, Elsevier, 2007: pp. 1617–1628. https://doi.org/10.1016/s0167-2991(07)81039-1.
[54] Y. Zhou, Y. Chen, Z. Wang, Z. Zhu, L. Xu, Potential of sodium chloride solution as mixing water in calcium aluminate cement modified with siliceous minerals, Advances in Cement Research 36 (2024) 293–305. https://doi.org/10.1680/jadcr.23.00009.
[55] S. Zokaei, H. Siad, M. Lachemi, O. Mahmoodi, E. Ozcelikci, M. Şahmaran, Mechanical, physical and durability performance of engineered cementitious composites prepared with calcium aluminate cement, Advances in Cement Research 37 (2025) 371–383. https://doi.org/10.1680/jadcr.24.00050.
[56] T.T. Win, C. Panwisawas, P. Jongvivatsakul, W. Pansuk, L. Prasittisopin, Effects of Fly Ash Composition to Mitigate Conversion of Calcium Aluminate Cement Composites, Buildings 13 (2023) 2453. https://doi.org/10.3390/buildings13102453.
[57] T.T. Win, L. Prasittisopin, P. Jongvivatsakul, S. Likitlersuang, Investigating the synergistic effect of graphene nanoplatelets and fly ash on the mechanical properties and microstructure of calcium aluminate cement composites, Journal of Building Engineering 78 (2023) 107710. https://doi.org/10.1016/j.jobe.2023.107710.
[58] M. Idrees, O. Ekincioglu, M.S. Sonyal, Hydration behavior of calcium aluminate cement mortars with mineral admixtures at different curing temperatures, Construction and Building Materials 285 (2021) 122839. https://doi.org/10.1016/j.conbuildmat.2021.122839.
[59] C. Aswin Karthik, M. Sathishraj, B. Panda, P. Muthukumar, Evaluation of Thermal and Mechanical Properties of Concrete With Ground Granulated Blast Furnace Slag and Calcium Aluminate Cement for High-Temperature Thermal Energy Storage Applications, Energy Storage 7 (2025). https://doi.org/10.1002/est2.70164.

[60] H.J. Yang, K.Y. Ann, M.S. Jung, Development of Strength for Calcium Aluminate Cement Mortars Blended with GGBS, Advances in Materials Science and Engineering 2019 (2019) 1–12. https://doi.org/10.1155/2019/9896012.
[61] D. Koňáková, V. Pommer, M. Jerman, M. Keppert, R. Černý, E. Vejmelková, Utilization of ceramic powder, calcined shale and sintered mullite as partial replacements of calcium aluminate cement, Construction and Building Materials 326 (2022) 126824. https://doi.org/10.1016/j.conbuildmat.2022.126824.
[62] K. Šádková, D. Koňáková, V. Pommer, R. Černý, E. Vejmelková, Application of secondary calcined shale in the design of low-cement binder for thermal-resistant composites, Ceramics International 49 (2023) 13452–13468. https://doi.org/10.1016/j.ceramint.2022.12.220.
[63] D. Koňáková, V. Pommer, K. Šádková, M. Záleská, M. Böhm, M. Keppert, E. Vejmelková, Heat-resistant composites based on ternary binders with a low cement content: Characterization and performance, Developments in the Built Environment 18 (2024) 100400. https://doi.org/10.1016/j.dibe.2024.100400.
[64] D. Koňáková, K. Šádková, R. Vaníčková, V. Pommer, M. Keppert, E. Vejmelková, The role of ceramic powder in sustainable thermal-resistant cement-based composites, Construction and Building Materials 487 (2025) 142095. https://doi.org/10.1016/j.conbuildmat.2025.142095.

List of author publications

[1] Vejmelková E.; Koňáková D.; Čáchová M.; Keppert M.; Černý R., Effect of hydrophobization on the properties of lime-metakaolin plasters, Construction and Building Materials 37 (2012) 556-561. 10.1016/j.conbuildmat.2012.07.097

[2] Koňáková D.; Čáchová M.; Keppert M.; Vejmelková E.; Černý R., Hygric transport parameters of several kinds of sandstones, Applied Mechanics and Materials 621 (2014) 24-29. 10.4028/www.scientific.net/AMM.621.24

[3] Koňáková D.; Čáchová M.; Vejmelková E.; Keppert M.; Černý R., Thermal properties of selected timbers, Advanced Materials Research 982 (2014) 100-103. 10.4028/www.scientific.net/AMR.982.100

[4] Koňáková D.; Špedlová V.; Čáchová M.; Vejmelková E.; Černý R., Influence of basalt fibres and aggregates on the thermal expansion of cement-based composites, Advanced Materials Research 1054 (2014) 17-21. 10.4028/www.scientific.net/AMR.1054.17

[5] Vejmelková E.; Koňáková D.; Krojidlová A.; Hovorková V.; Čáchová M.; Reiterman P.; Černý R., Properties of cement composites containing coir pith, Advanced Materials Research 982 (2014) 136-140. 10.4028/www.scientific.net/AMR.982.136

[6] Čáchová M.; Koňáková D.; Vejmelková E.; Keppert M.; Polozhiy K.; Černý R., Heat and water vapor transport properties of selected commercially produced plasters, Advanced Materials Research 982 (2014) 90-93. 10.4028/www.scientific.net/AMR.982.90

[7] Čáchová M.; Koňáková D.; Vejmelková E.; Keppert M.; Polozhiy K.; Černý R., Pore structure and thermal characteristics of clay bricks, Advanced Materials Research 982 (2014) 104-107. 10.4028/www.scientific.net/AMR.982.104

[8] Koňáková D.; Hovorková V.; Vejmelková E.; Keppert M.; Černý R., Influence of metashale as cement replacement on the hygric transport properties of concrete, Advanced Materials Research 1054 (2014) 188-193. 10.4028/www.scientific.net/AMR.1054.188

[9] Vejmelková E.; Koňáková D.; Kulovaná T.; Hubáček A.; Černý R., Mechanical and thermal properties of moderate-strength concrete with ceramic powder used as supplementary cementitious material, Advanced Materials Research 1054 (2014) 194-198. 10.4028/www.scientific.net/AMR.1054.194

[10] Čáchová M.; Koňáková D.; Vejmelkokvá E.; Keppert M.; Reiterman P.; Černý R., The properties of innovated mortars utilizing secondary raw material, WIT Transactions on the Built Environment 137 (2014) 49-56. 10.2495/HPSM140051

[11] Čáchová M.; Koňáková D.; Vejmelková E.; Polozhiy K.; Černý R., Pore distribution and water vapor diffusion parameters of lime plasters with waste brick powder, Advanced Materials Research 1054 (2014) 205-208. 10.4028/www.scientific.net/AMR.1054.205

[12] Čáchová M.; Koňáková D.; Vejmelková E.; Keppert M.; Reiterman P.; Krojidlová A.; Černý R., Mechanical and thermal properties of composites containing waste coir pith, Advanced Materials Research 1054 (2014) 238-242. 10.4028/www.scientific.net/AMR.1054.238

[13] Koňáková D.; Vejmelková E.; Špedlová V.; Polozhiy K.; Černý R., Cement composites for high temperature applications, Advanced Materials Research 982 (2014) 154-158. 10.4028/www.scientific.net/AMR.982.154

[14] Vejmelková E.; Čáchová M.; Koňáková D.; Reiterman P.; Černý R., Lime plasters containing waste ceramic powder as partial replacement of siliceous aggregates, Advanced Materials Research 1035 (2014) 77-82. 10.4028/www.scientific.net/AMR.1035.77
[15] Vejmelková E.; Čáchová M.; Konaková D.; Keppert M.; Reiterman P.; Černý R., Differences in the properties of arenaceous marlstones from different quarries, Advanced Materials Research 982 (2014) 149-153. 10.4028/www.scientific.net/AMR.982.149
[16] Vejmelková E.; Koňáková D.; Čáchová M.; Keppert M.; Hubáček A.; Černý R., Application of zeolite as a partial replacement of cement in concrete production, Applied Mechanics and Materials 621 (2014) 30-34. 10.4028/www.scientific.net/AMM.621.30
[17] Koňáková D.; Čáchová M.; Polozhiy K.; Vejmelková E.; Keppert M.; Černý R., The high temperature resistance of a para-aramid fibre-reinforced concrete composite, WIT Transactions on the Built Environment 137 (2014) 201-212. 10.2495/HPSM140181
[18] Keppert M.; Čáchová M.; Ďurana K.; Fořt J.; Koňáková D.; Pavlík Z.; Trník A.; Černý R., Relationship between pore size distribution and mechanical properties of porous sedimentary rocks, Advanced Materials Research 905 (2014) 207-211. 10.4028/www.scientific.net/AMR.905.207
[19] Čáchová M.; Koňáková D.; Vejmelková E.; Reiterman P.; Keppert M.; Černý R., Properties of lime plasters with different ceramic powder dosage, Applied Mechanics and Materials 621 (2014) 19-23. 10.4028/www.scientific.net/AMM.621.19
[20] Koňáková D.; Vejmelková E., Reinforced cement composites – Effect of hybrid fibres on selected properties, Materials Science Forum 824 (2015) 179-183. 10.4028/www.scientific.net/MSF.824.179
[21] Koňáková D.; Čáchová M.; Vejmelková E.; Keppert M.; Černý R., Hygric properties of sandstones as a function of porosity, AIP Conference Proceedings 1648 (2015) 410009. 10.1063/1.4912638
[22] Vejmelková E.; Koňáková D.; Kulovaná T.; Keppert M.; Žumár J.; Rovnaníková P.; Keršner Z.; Sedlmajer M.; Černý R., Engineering properties of concrete containing natural zeolite as supplementary cementitious material: Strength, toughness, durability, and hygrothermal performance, Cement and Concrete Composites 55 (2015) 259-267. 10.1016/j.cemconcomp.2014.09.013
[23] Koňáková D.; Čáchová M.; Vejmelková E.; Reiterman P.; Černý R., Thermal insulating plasters and their hygric properties, AIP Conference Proceedings 1648 (2015) 410010. 10.1063/1.4912639
[24] Keppert M.; Čáchová M.; Koňáková D., Transport of liquids in porous rocks, Materials Science Forum 824 (2015) 117-120. 10.4028/www.scientific.net/MSF.824.117
[25] Vejmelková E.; Koňáková D.; Rovnaníková P., Properties of concrete with lower amount of SCM, Materials Science Forum 824 (2015) 65-69. 10.4028/www.scientific.net/MSF.824.65
[26] Koňáková D.; Koťátková J.; Vejmelková E., Influence of cracks on the properties of self-compacting concrete, Materials Science Forum 824 (2015) 139-143. 10.4028/www.scientific.net/MSF.824.139
[27] Koňáková D.; Vejmelková E.; Čáchová M.; Siddique J.A.; Polozhiy K.; Reiterman P.; Keppert M.; Černý R., Treated Coconut Coir Pith as Component of Cementitious Materials, Advances in Materials Science and Engineering 2015 (2015) 264746. 10.1155/2015/264746

[28] Špedlová V.; Koňáková D., Behavior of cement composites loaded by high temperature, Materials Science Forum 824 (2015) 121-125. 10.4028/www.scientific.net/MSF.824.121
[29] Koťátková J.; Koňáková D.; Vejmelková E.; Reiterman P.; Siddique J.A., Mechanical and water transport properties of HSC with different SCMs, Materials Science Forum 824 (2015) 105-110. 10.4028/www.scientific.net/MSF.824.105
[30] Koňáková D.; Vejmelková E., Thermal expansion of aluminate cement-based composite containing basalt fibres with different length, Key Engineering Materials 675-676 (2016) 675-678. 10.4028/www.scientific.net/KEM.675-676.675
[31] Čáchová M.; Koňáková D.; Vejmelková E.; Keppert M.; Cerný R., Moisture properties of the lightweight brick body, AIP Conference Proceedings 1738 (2016) 280009. 10.1063/1.4952069
[32] Čáchová M.; Koňáková D.; Vejmelková E.; Keppert M.; Cerný R., Mechanical and thermal properties of the Czech marbles, AIP Conference Proceedings 1738 (2016) 280010. 10.1063/1.4952070
[33] Čáchová M.; Vejmelková E.; Koňáková D.; Žumár J.; Keppert M.; Reiterman P.; Černý R., Application of ceramic powder as supplementary cementitious material in lime plasters, Medziagotyra 22 3 (2016) 440-444. 10.5755/j01.ms.22.3.7433
[34] Vejmelková E.; Kot'átková J.; Čáchová M.; Koňáková D., Comparison of the effects of different pozzolana on the properties of self-compacting concrete, Key Engineering Materials 677 (2016) 103-107. 10.4028/www.scientific.net/KEM.677.103
[35] Keppert M.; Čáchová M.; Koňáková D., Durability assessment of stones for renovation of historic buildings, CESB 2016 - Central Europe Towards Sustainable Building 2016: Innovations for Sustainable Future (2016) 1133-1136.
[36] Koňáková D.; Čáchová M.; Vejmelková E., Influence of moisture content on the thermal properties of concrete containing agricultural waste materials, Key Engineering Materials 677 (2016) 241-245. 10.4028/www.scientific.net/KEM.677.241
[37] Čáchová M.; Koťátková J.; Koňáková D.; Vejmelková E.; Bartoňková E.; Černý R., Hygric Properties of Lime-cement Plasters with the Addition of a Pozzolana, Procedia Engineering 151 (2016) 127-132. 10.1016/j.proeng.2016.07.403
[38] Čáchová M.; Vejmelková E.; Šestáková K.; Reiterman P.; Keppert M.; Koňáková D.; Černý R., Basic physical and mechanical properties of composites based on three different cements, Key Engineering Materials 677 (2016) 186-190. 10.4028/www.scientific.net/KEM.677.186
[39] Koňáková D.; Čáchová M.; Doleželová M.; Scheinherrová L.; Vejmelková E.; Černý R., High-temperature resistance of concretes produced of two different cements; [Odporność na wysoką temperaturę betonów otrzymanych z dwóch różnych cementów], Cement, Wapno, Beton 2016 5 (2016) 295-309.
[40] Koňáková D.; Kočí V.; Zumár J.; Keppert M.; Holčapek O.; Vejmelková E.; Cerný R., Effect of heat and moisture transport and storage properties of building stones on the hygrothermal performance of historical building envelopes, AIP Conference Proceedings 1790 (2016) 150011. 10.1063/1.4968750
[41] Keppert M.; Žumár J.; Čáchová M.; Koňáková D.; Svora P.; Pavlík Z.; Vejmelková E.; Černý R., Water Vapor Diffusion and Adsorption of Sandstones: Influence of Rock Texture and Composition, Advances in Materials Science and Engineering 2016 (2016) 8039748. 10.1155/2016/8039748
[42] Kočí V.; Maděra J.; Jerman M.; Žumár J.; Koňáková D.; Čáchová M.; Vejmelková E.; Reiterman P.; Černý R., Application of waste ceramic dust as a ready-to-use

replacement of cement in lime-cement plasters: an environmental-friendly and energy-efficient solution, Clean Technologies and Environmental Policy 18 6 (2016) 1725-1733. 10.1007/s10098-016-1183-2
[43] Čachová M.; Koňaková D.; Čechmánek R.; Vejmelková E.; Keppert M., Sustainable composites for fire protection of building structures, CESB 2016 - Central Europe Towards Sustainable Building 2016: Innovations for Sustainable Future (2016) 1044-1048.
[44] Koťátková J.; Čáchová M.; Koňáková D.; Vejmelková E., Hygric properties of HPC with natural pozzolana, Key Engineering Materials 677 (2016) 93-97. 10.4028/www.scientific.net/KEM.677.93
[45] Čáchová M.; Koťátková J.; Koňáková D.; Vejmelková E.; Keppert M.; Reiterman P.; Žumár J.; Černý R., Monitoring the damage of exterior renders caused by the environment, International Journal of Sustainable Development and Planning 12 2 (2017) 342-351. 10.2495/SDP-V12-N2-342-351
[46] Čáchová M.; Koňáková D.; Vejmelková E.; Vyšvařil M., Ternary binder based plasters with improved thermal insulating ability, IOP Conference Series: Materials Science and Engineering 251 1 (2017) 12008. 10.1088/1757-899X/251/1/012008
[47] Keppert M.; Fořt J.; Trník A.; Koňáková D.; Vejmelková E.; Pokorný J.; Svora P.; Pavlík Z.; Černý R., Behavior of Sandstones Under Heat Treatment, International Journal of Thermophysics 38 4 (2017) 60. 10.1007/s10765-017-2191-0
[48] Čáchová M.; Koňáková D.; Vejmelková E.; Koťátková J.; Černý R., The comparison of water, water vapour transport properties and mechanical characterization of two commercial plasters on market in the Czech Republic, Key Engineering Materials 722 KEM (2017) 357-361. 10.4028/www.scientific.net/KEM.722.357
[49] Koňáková D.; Čáchová M.; Vejmelková E.; Keppert M.; Jerman M.; Bayer P.; Rovnaníková P.; Černý R., Lime-based plasters with combined expanded clay-silica aggregate: Microstructure, texture and engineering properties, Cement and Concrete Composites 83 (2017) 374-383. 10.1016/j.cemconcomp.2017.08.005
[50] Kotátková J.; Čáchová M.; Koňáková D.; Vejmelková E.; Reiterman P., Mechanical and thermal properties of HSC with fine natural pozzolana as SCM, AIP Conference Proceedings 1863 (2017) 290004. 10.1063/1.4992441
[51] Koňáková D.; Kotátková J.; Čáchová M.; Vejmelková E.; Čechmánek R.; Reiterman P.; Černý R., The influence of high temperatures on selected properties of calcium aluminous composites, AIP Conference Proceedings 1863 (2017) 150008. 10.1063/1.4992330
[52] Kočí V.; Vejmelková E.; Čáchová M.; Koňáková D.; Keppert M.; Maděra J.; Černý R., Effect of Moisture Content on Thermal Properties of Porous Building Materials, International Journal of Thermophysics 38 2 (2017) 28. 10.1007/s10765-016-2164-8
[53] Čáchová M.; Koňáková D.; Vejmelková E.; Bartoňková E.; Keppert M.; Černý R., Properties of lime-cement plasters incorporating ceramic powder, International Journal of Computational Methods and Experimental Measurements 5 2 (2017) 144-153. 10.2495/CMEM-V5-N2-144-153
[54] Koňáková D.; Čáchová M.; Doleželová M.; Kočí V.; Vejmelková E.; Černý R., Mechanical, hydric and thermal properties of fine-grained high performance concrete, AIP Conference Proceedings 1809 (2017) 20029. 10.1063/1.4975444
[55] Černý R.; Čáchová M.; Koňáková D.; Vejmelková E.; Konvalinka P., Effect of ambient conditions on the properties of concrete containing waste materials as partial portland cement replacement, International Multidisciplinary Scientific

GeoConference Surveying Geology and Mining Ecology Management, SGEM 17 62 (2017) 131-138. 10.5593/sgem2017/62/S26.017
[56] Vejmelková E.; Koňáková D.; Čáchová M.; Záleská M.; Svora P.; Keppert M.; Rovnaníková P.; Černý R., High-strength concrete based on ternary binder with high pozzolan content, Structural Concrete 19 5 (2018) 1258-1267. 10.1002/suco.201700173
[57] Čáchová M.; Koňáková D.; Vejmelková E.; Vyšvařil M.; Rovnaníková P., Lightweighted plasters using perlite, lime and recycled finely ground brick powder, International Multidisciplinary Scientific GeoConference Surveying Geology and Mining Ecology Management, SGEM 18 6.4 (2018) 461-470. 10.5593/sgem2018V/6.4/S09.058
[58] Vejmelková E.; Koňáková D.; Doleželová M.; Scheinherrová L.; Svora P.; Keppert M.; Reiterman P.; Černý R., Effect of calcined Czech claystone on the properties of high performance concrete: Microstructure, strength and durability, Construction and Building Materials 168 (2018) 966-974. 10.1016/j.conbuildmat.2018.02.204
[59] Fořt J.; Vejmelková E.; Koňáková D.; Alblová N.; Čáchová M.; Keppert M.; Rovnaníková P.; Černý R., Application of waste brick powder in alkali activated aluminosilicates: Functional and environmental aspects, Journal of Cleaner Production 194 (2018) 714-725. 10.1016/j.jclepro.2018.05.181
[60] Čáchová M.; Koňáková D.; Vejmelková E.; Vyšvařil M.; Bayer P., Hygric and mechanical parameters of ternary binder based plasters lightweighted by expanded perlite, IOP Conference Series: Materials Science and Engineering 379 1 (2018) 12004. 10.1088/1757-899X/379/1/012004
[61] Kočí V.; Čáchová M.; Koňáková D.; Vejmelková E.; Jerman M.; Keppert M.; Maděra J.; Černý R., Heat and Moisture Transport and Storage Parameters of Bricks Affected by the Environment, International Journal of Thermophysics 39 5 (2018) 63. 10.1007/s10765-018-2383-2
[62] Vejmelková E.; Koňáková D.; Scheinherrová L.; Doleželová M.; Keppert M.; Černý R., High temperature durability of fiber reinforced high alumina cement composites, Construction and Building Materials 162 (2018) 881-891. 10.1016/j.conbuildmat.2018.01.076
[63] Čáchová M.; Koňáková D.; Vejmelková E.; Záleská M.; Vyšvařil M.; Bayer P., Hygric parameters of ternary binder based plasters lightweighted by expanded perlite, AIP Conference Proceedings 1978 (2018) 250010. 10.1063/1.5043885
[64] Vejmelková E.; Konáková D.; Doleželová M.; Pommer V.; Scheinherrová L., Basic physical and mechanical properties of alkali-activated aluminosilicates with different ceramic waste fineness, International Multidisciplinary Scientific GeoConference Surveying Geology and Mining Ecology Management, SGEM 19 6.3 (2019) 269-276.
[65] Vejmelková E.; Koňáková D.; Scheinherrová L.; Pommer V.; Černý R., Thermal characteristics of bentonite cement based composites, AIP Conference Proceedings 2133 (2019) 20039. 10.1063/1.5120169
[66] Vejmelková E.; Koňáková D.; Kobetičová K.; Pommer V.; Konvalinka P., Varying sorption admixture for concrete casing for radionuclide protection barriers: Mechanical properties, International Multidisciplinary Scientific GeoConference SGEM 19 4.1 (2019) 17-24. 10.5593/sgem2019/4.1/S16.003
[67] Vejmelkova E.; Pommer V.; Kobeticova K.; Konakova D.; Scheinherrova L.; Konvalinka P.; Keppert M.; Medved I.; Cerny R., Enhancement of sorption capacity to Sr and Cs of a cement composite by addition of brick powder, IOP

Conference Series: Materials Science and Engineering 549 1 (2019) 12046. 10.1088/1757-899X/549/1/012046
[68] Scheinherrová L.; Vejmelková E.; Konáková D.; Rovnaniková P.; Cerný R., Characterization of ceramic-based alkali activated aluminosilicate composites, AIP Conference Proceedings 2293 (2020) 190002. 10.1063/5.0026800
[69] Koňáková D.; Vejmelková E.; Pommer V.; Černý R., Properties of CAC paste with varying alumina based admixtures, AIP Conference Proceedings 2429 (2021) 20017. 10.1063/5.0070338
[70] Pommer V.; Vejmelková E.; Koňáková D.; Scheinherrová L.; Keppert M.; Kočí V., Impact of precursor granulometry on mechanical properties of geopolymers activated by potassium silicate, AIP Conference Proceedings 2429 (2021) 20042. 10.1063/5.0069630
[71] Doleželová M.; Koňáková D.; Vejmelková E., Influence of aluminosilicate fibers on mechanical properties of composite based on Portland cement exposed to high temperatures, AIP Conference Proceedings 2343 (2021) 30011. 10.1063/5.0047863
[72] Keppert M.; Pommer V.; Koňáková D.; Vejmelková E.; Černý R., Influence of metakaolin on pH of cement paste, AIP Conference Proceedings 2429 (2021) 20012. 10.1063/5.0069758
[73] Kočí V.; Koňáková D.; Pommer V.; Keppert M.; Vejmelková E.; Černý R., Exploiting advantages of empirical and optimization approaches to design alkali activated materials in a more efficient way, Construction and Building Materials 292 (2021) 123460. 10.1016/j.conbuildmat.2021.123460
[74] Jogl M.; Koňáková D.; Pommer V.; Vejmelková E.; Konvalinka P., Application of expanded glass granulate and basalt fibers in the formation of lightweight cement-based refractory composite, AIP Conference Proceedings 2322 (2021) 20025. 10.1063/5.0042065
[75] Koňáková D.; Vejmelková E.; Pommer V.; Keppert M.; Trník A.; Černý R., Physical and chemical characteristics of heat resistant materials based on high alumina cement, AIP Conference Proceedings 2429 (2021) 20004. 10.1063/5.0069565
[76] Koňáková D.; Pommer V.; Jerman M.; Keppert M.; Černý R.; Vejmelková E., Utilization of ceramic powder, calcined shale and sintered mullite as partial replacements of calcium aluminate cement, Construction and Building Materials 326 (2022) 126824. 10.1016/j.conbuildmat.2022.126824
[77] Kočí V.; Koňáková D.; Pommer V.; Vejmelková E.; Cerný R., Optimization of low-cement high-temperature resistant composite mixtures, AIP Conference Proceedings 2611 (2022) 40002. 10.1063/5.0119373
[78] Konakova D.; Pommer V.; Sadkova K.; Keppert M.; Cerny R.; Vejmelkova E., Impact of plasticizers' types on the performance of calcium aluminate cement, Journal of Materials Research and Technology 20 (2022) 1512-1523. 10.1016/j.jmrt.2022.07.155
[79] Pommer V.; Sádková K.; Scheinherrová L.; Koňáková D.; Keppert M.; Vejmelková E., On the Composition of Sodium Silicate - Sodium Hydroxide Activator for the Waste Ceramics Recycling, AIP Conference Proceedings 2425 (2022) 150010. 10.1063/5.0082452
[80] Šádková K.; Konáková D.; Vejmelková E.; Pommer V.; Lin W.-T.; Cerný R., Effect of Heating Temperature on the Properties of Low-Cement Heat Resistant Composites, AIP Conference Proceedings 2801 1 (2023) 30005. 10.1063/5.0146714

[81] Keppert M.; Pommer V.; Konáková D.; Vejmelková E.; Cerný R., Hydration Kinetics of Blended Cements for Application With Basalt Reinforcement, AIP Conference Proceedings 2801 1 (2023) 30011. 10.1063/5.0146767
[82] Koňáková D.; Vejmelková E.; Pommer V.; Kočí V.; Černý R., Material Properties of Low-Cement Heat Resistant Composites Containing Ceramic Powder, AIP Conference Proceedings 2849 1 (2023) 170002. 10.1063/5.0162266
[83] Koňáková D.; Šádková K.; Vejmelková E.; Pommer V.; Černý R., Thermal Properties of Heat Resistant Composites Based on Calcium Aluminate Cement: The Effect of Plasticizers, AIP Conference Proceedings 2918 1 (2023) 20010. 10.1063/5.0170862
[84] Šádková K.; Koňáková D.; Pommer V.; Černý R.; Vejmelková E., Application of secondary calcined shale in the design of low-cement binder for thermal-resistant composites, Ceramics International 49 9 (2023) 13452-13468. 10.1016/j.ceramint.2022.12.220
[85] Vejmelková E.; Pommer V.; Šádková K.; Konáková D., The nature of kaolinitic clays and their impact on the performance of SCM, Journal of Physics: Conference Series 2628 1 (2023) 12032. 10.1088/1742-6596/2628/1/012032
[86] Vejmelková E.; Pommer V.; Šádková K.; Konáková D., The possibility of thermal activation of bentonitic clays: Impact of temperature, Journal of Physics: Conference Series 2628 1 (2023) 12013. 10.1088/1742-6596/2628/1/012013
[87] Kočí V.; Vejmelková E.; Koňáková D.; Pommer V.; Grzeszczyk S.; Matuszek-Chmurowska A.; Mordak A.; Černý R., Basic physical, mechanical, thermal and hygric properties of reactive powder concrete with basalt and polypropylene fibers after high-temperature exposure, Construction and Building Materials 374 (2023) 130922. 10.1016/j.conbuildmat.2023.130922
[88] Konáková D.; Šádková K.; Pommer V.; Vejmelková E.; Černý R., Characterization of Low-Cement Heat Resistant Binder With High Alumina Content, AIP Conference Proceedings 2801 1 (2023) 30016. 10.1063/5.0147154
[89] Keppert M.; Pommer V.; Šádková K.; Botnari A.; Vejmelková E.; Koňáková D., Blended lime plasters with biomass ash and natural fibres reinforcement, Journal of Physics: Conference Series 2792 1 (2024) 12004. 10.1088/1742-6596/2792/1/012004
[90] Keppert M.; Koňáková D.; Pommer V.; Vejmelková E.; Černý R., Reactivity of precursors for geopolymerization studied by isothermal calorimetry, Journal of Thermal Analysis and Calorimetry 149 19 (2024) 10619-10631. 10.1007/s10973-024-13492-y
[91] Keppert M.; Pommer V.; Šádková K.; Krejsová J.; Vejmelková E.; Černý R.; Koňáková D., Thermal activation of illitic-kaolinitic mixed clays, Journal of Thermal Analysis and Calorimetry 149 19 (2024) 10533-10544. 10.1007/s10973-024-13342-x
[92] Šádková K.; Pommer V.; Vejmelková E.; Koňáková D., Mechanical properties of blended cements affected by impurities in thermally activated clays, Journal of Physics: Conference Series 2792 1 (2024) 12005. 10.1088/1742-6596/2792/1/012005
[93] Vejmelková E.; Pommer V.; Šádková K.; Koňáková D., Preliminary study of thermal activation of brick clays used as supplementary cementitious materials, AIP Conference Proceedings 3030 1 (2024) 70006. 10.1063/5.0193115
[94] Holeček P.; Kliková K.; Koňáková D.; Stiborová H.; Nežerka V., Ureolytic bacteria-assisted recycling of waste concrete fines, Powder Technology 434 (2024) 119310. 10.1016/j.powtec.2023.119310

[95] Pommer V.; Šádková K.; Vejmelková E.; Maděra J.; Koňáková D., On hygric properties of blended plasters for building renovation, AIP Conference Proceedings 3030 1 (2024) 70001. 10.1063/5.0193082
[96] Brejcha V.; Kobetičová K.; Pommer V.; Koňáková D.; Böhm M., Analysis of porosity and abrasion resistance of composite material based on flax fiber and bio-epoxy resin with corundum additive, AIP Conference Proceedings 3030 1 (2024) 70004. 10.1063/5.0193118
[97] Pommer V.; Šádková K.; Sellnerová K.; Vejmelková E.; Koňáková D., Design of concrete mixtures with calcined brick soil, Journal of Physics: Conference Series 2911 1 (2024) 12027. 10.1088/1742-6596/2911/1/012027
[98] Keppert M.; Pommer V.; Krejsová J.; Gill L.; Breníková M.; Urbanová M.; Vejmelková E.; Konáková D., Mechanical Properties of Acid Activated Metakaolin, Advances in Transdisciplinary Engineering 59 (2024) 75-80. 10.3233/ATDE240529
[99] Maděra J.; Vejmelková E.; Pommer V.; Šádková K.; Rovnaníková P.; Koňáková D., Design of blended plasters for building renovation with improved thermal insulating ability, AIP Conference Proceedings 3030 1 (2024) 70002. 10.1063/5.0193065
[100] Keppert M.; Pommer V.; Kulhavá K.; Koňáková D.; Vejmelková E.; Černý R., Residual physical properties of thermally loaded alkali activated slag, Journal of Physics: Conference Series 2911 1 (2024) 12028. 10.1088/1742-6596/2911/1/012028
[101] Šádková K.; Pommer V.; Keppert M.; Vejmelková E.; Koňáková D., Difficulties in Determining the Pozzolanic Activity of Thermally Activated Lower-Grade Clays, Materials 17 20 (2024) 5093. 10.3390/ma17205093
[102] Akir S.; Lontio Fomekong R.; Chacko L.; Děkanovský L.; Mazánek V.; Sturala J.; Koňáková D.; Sofer Z., Nanoengineering bismuth-modified vanadium carbide MXene for enhanced electrochemical performance in neutral electrolyte: A pathway toward high-performance supercapacitors, Journal of Energy Storage 85 (2024) 110962. 10.1016/j.est.2024.110962
[103] Pommer V.; Sellnerová K.; Keppert M.; Vejmelková E.; Konáková D., Performance of Calcined Brick Soils on Mechanical Properties of Blended Cement, Advances in Transdisciplinary Engineering 59 (2024) 194-201. 10.3233/ATDE240545
[104] Šádkova K.; Pommer V.; Vejmelková E.; Parashar A.; Cerný R.; Konvalinka P.; Koňáková D., Impact of waste materials on hygric transport parameters of low-cement heat-resistant composites, AIP Conference Proceedings 3030 1 (2024) 70005. 10.1063/5.0195901
[105] Wu B.; Li M.; Mazánek V.; Liao Z.; Ying Y.; Oliveira F.M.; Dekanovsky L.; Jan L.; Hou G.; Antonatos N.; Wei Q.; Pal B.; He J.; Koňáková D.; Vejmělková E.; Sofer Z., In Situ Vanadium-Deficient Engineering of V2C MXene: A Pathway to Enhanced Zinc-Ion Batteries, Small Methods 8 9 (2024) 2301461. 10.1002/smtd.202301461
[106] Koňáková D.; Pommer V.; Šádková K.; Krejsová J.; Černý R.; Maděra J.; Vejmelková E., Phase development of lime-based plasters blended with waste calcined shale, Journal of Thermal Analysis and Calorimetry 149 19 (2024) 10521-10532. 10.1007/s10973-024-13246-w
[107] Krejsová J.; Koňáková D.; Pommer V.; Poláková L.; Černý R.; Maděra J.; Vejmelková E., Valorization of waste wood fly ash in environmentally friendly lime-based plasters with enhanced strengths for renovation purposes, Journal of Building Engineering 87 (2024) 109056. 10.1016/j.jobe.2024.109056

[108] Koňáková D.; Pommer V.; Šádková K.; Černý R.; Vejmelková E., High-temperature resistance of cement composites with randomly distributed aluminium silicate fibbers, Cement and Concrete Composites 145 (2024) 105339. 10.1016/j.cemconcomp.2023.105339
[109] Koňáková D.; Pommer V.; Šádková K.; Vejmelková E.; Parashar A.; Kočí V.; Černý R., Analysis of Physical and Chemical Aspects of Using Calcium Aluminate Cement for the Preparation of Low-Cement Heat-Resistant Composites, AIP Conference Proceedings 3094 1 (2024) 120004. 10.1063/5.0211101
[110] Koňáková D.; Pommer V.; Šádková K.; Záleská M.; Böhm M.; Keppert M.; Vejmelková E., Heat-resistant composites based on ternary binders with a low cement content: Characterization and performance, Developments in the Built Environment 18 (2024) 100400. 10.1016/j.dibe.2024.100400
[111] Papavasileiou A.V.; Děkanovský L.; Chacko L.; Wu B.; Luxa J.; Regner J.; Paštika J.; Koňáková D.; Sofer Z., Unraveling the Versatility of Carbon Black – Polylactic Acid (CB/PLA) 3D-Printed Electrodes via Sustainable Electrochemical Activation, Small Methods (2025). 10.1002/smtd.202402214
[112] Böhm M.; Jerman M.; Keppert M.; Kobetičová K.; Koňáková D.; Pavlíková M.; Černý R., Alkaline Treatment of Straw for Composite Material Production and Its Impact on Water Vapor Adsorption Characteristics, Journal of Renewable Materials 13 2 (2025) 363-383. 10.32604/jrm.2024.056984
[113] Koňáková D.; Vejmelková E.; Pommer V.; Krejsová J.; Poláková L.; Maděra J., Applicability of Natural Fibres as a Reinforcement for Lime-Based Plasters, AIP Conference Proceedings 3269 1 (2025) 30001. 10.1063/5.0247506
[114] Klikova K.; Holecek P.; Nezerka V.; Prosek Z.; Konakova D.; Demnerova K.; Stiborova H., Application of Sporosarcina pasteurii for the biomineralization of calcite in the treatment of waste concrete fines, Environmental Science and Pollution Research (2025) 100004. 10.1007/s11356-025-36102-2
[115] Koňáková D.; Šádková K.; Vaníčková R.; Pommer V.; Keppert M.; Vejmelková E., The role of ceramic powder in sustainable thermal-resistant cement-based composites, Construction and Building Materials 487 (2025) 142095. 10.1016/j.conbuildmat.2025.142095
[116] Pommer V.; Šádková K.; Keppert M.; Vejmelková E.; Koňáková D., Performance of thermally activated lower-grade clays – The impact of phase composition, Journal of Building Engineering 106 (2025) 112685. 10.1016/j.jobe.2025.112685
[117] Kliková K.; Holeček P.; Koňáková D.; Stiborová H.; Nežerka V., Exploiting Bacillus pseudofirmus and Bacillus cohnii to promote CaCO3 and AFt phase formation for stabilizing waste concrete fines, Cement and Concrete Composites 155 (2025) 105839. 10.1016/j.cemconcomp.2024.105839